Database-informed analysis of sedimentary systems at the marine shelf-to-slope transition

Laura Henrika Bührig

Submitted in accordance with the requirements for the degree of
Doctor of Philosophy

The University of Leeds
Institute of Applied Geosciences
School of Earth and Environment

September, 2023

The candidate confirms that the work submitted is her own, except where work which has formed part of jointly-authored publications has been included. The contribution of the candidate and the other authors to this work has been explicitly indicated below. The candidate confirms that appropriate credit has been given within the thesis where reference has been made to the work of others.

The three data chapters (Chapters 3, 4 and 5) were conceptualised and written with the aim of publication. Both Chapters 3 and 4 are already published as jointly-authored publications; Chapter 5 is in preparation for submission to a journal at the time of the submission of the thesis. The contributions of the candidate and each co-author are as follows:

Chapter 3: published

Bührig, L.H., Colombera, L., Patacci, M., Mountney, N.P., & McCaffrey, W.D. 2022a. A global analysis of controls on submarine-canyon geomorphology. *Earth-Science Reviews*. 233, 104150. doi:10.1016/j.earscirev.2022.104150

Bührig**,** L.H.: Main author; conceptualisation, data collection, data processing, data analysis and interpretation, figure illustrations and writing of manuscript.

Colombera, L.: Specialist technical guidance and advice for the interpretation of the data and application of statistical analyses, in-depth discussion and manuscript review.

Patacci, M.: Specialist technical guidance and advice for the interpretation of the data and application of statistical analyses, in-depth discussion and manuscript review.

Mountney, N.P.: Specialist technical guidance and advice for the interpretation of the data and application of statistical analyses, in-depth discussion and manuscript review.

McCaffrey, W.D.: Specialist technical guidance and advice for the interpretation of the data and application of statistical analyses, in-depth discussion and manuscript review.

Chapter 4: published

Bührig, L.H., Colombera, L., Patacci, M., Mountney, N.P., & McCaffrey, W.D. 2022b. Tectonic influence on the geomorphology of submarine canyons: implications for deep-water sedimentary systems. *Frontiers in Earth Science*. 10:836823. doi:10.3389/feart.2022.836823

Bühri**g,** L.H.: Main author; conceptualisation, data collection, data processing, data analysis and interpretation, figure illustrations and writing of manuscript.

Colombera, L.: Specialist technical guidance and advice for the interpretation of the data and application of statistical analyses, in-depth discussion and manuscript review.

Patacci, M.: Specialist technical guidance and advice for the interpretation of the data and application of statistical analyses, in-depth discussion and manuscript review.

Mountney, N.P.: Specialist technical guidance and advice for the interpretation of the data and application of statistical analyses, in-depth discussion and manuscript review.

McCaffrey, W.D.: Specialist technical guidance and advice for the interpretation of the data and application of statistical analyses, in-depth discussion and manuscript review.

Chapter 5: in preparation for submission

Bührig, L.H., Colombera, L., Mountney, N.P., & McCaffrey, W.D. *In preparation.* Controls on the geometry of shelf-edge deltas.
Bühri**g,** L.H.: Main author; conceptualisation, data collection, data processing, data analysis and interpretation, figure illustrations and writing of manuscript.

Colombera, L.: Specialist technical guidance and advice for the interpretation of the data and application of statistical analyses, in-depth discussion and manuscript review.

Mountney, N.P.: Specialist technical guidance and advice for the interpretation of the data and application of statistical analyses, in-depth discussion and manuscript review.

McCaffrey, W.D.: Specialist technical guidance and advice for the interpretation of the data and application of statistical analyses, in-depth discussion and manuscript review.

This copy has been supplied on the understanding that it is copyright material and that no quotation from the thesis may be published without proper acknowledgement.

The right of Laura Henrika Bührig to be identified as Author of this work has been asserted by her in accordance with the Copyright, Designs and Patents Act 1988.

© 2023 The University of Leeds and Laura Henrika Bührig

Acknowledgements

Firstly, my biggest thank you and my deepest gratitude to my wonderful team of supervisors Nigel Mountney, Luca Colombera, Marco Patacci, and Bill McCaffrey, who gave me the opportunity to continue doing what I love during my time as a postgraduate researcher at the University of Leeds. Learning about Earth and the amazing ways it functions as a geodynamic system still brings me so much joy every day!! Every one of you has contributed in your own way to my journey over these past years and my continuing growth as a person and a researcher. Thank you for your guidance, encouragement, and for all of your support throughout my PhD. I have learnt so much from you through your thoughtful and thorough feedback, our discussions, and your invaluable insights. Thank you for all the effort and dedication you always put into your work and for always being available when I had a question, problem, or an upcoming deadline!!

I would also like to thank the sponsors and partners of both the Fluvial, Eolian & Shallow-Marine Research Group and the Turbidites Research Group, as well as the PGR Pandemic Support Fund of the University of Leeds, for their financial support that has enabled my research.

When I started my PhD project I would never have imagined that I would spend a large part of my time conducting my research within my own four walls in home office while the World was battling a major pandemic and later recovering from it. So many big and small ways of showing kindness helped Everyone to get through this difficult time. I am very thankful for our amazing community of geoscientists which provided support to us Early Career Researchers during these years by organising online webinars and conferences where we could participate and present our work and receive feedback. These small islands of social interaction and communication meant a lot to me!!

I loved my time in Leeds and West Yorkshire, and I will always be thankful for the wonderful friendships I made there. Especially thank you to Adriana, Antonio, Chaz, Daniela, Dave, Daz, Ezekiel, Giacomo, Iz, Kaixuan, Lisa,

Lucia, Marina, Soma, Sonia, Caroline and Gill, for all the laughter and fun times we spent together!!

My special thank you to my family – Äiti and Isä, and Jan – thank you for your unconditional love and always supporting my dreams and aspirations.

Lizzy, Pauli and Happy, thank you for always cheering me up when I needed it and just being your furry selves.

Last but not least, Julius, thank you for everything. I could not wish for a better partner in life. Sharing this journey with you makes me so happy and I cannot wait to start our next adventure together!!

Abstract

Submarine canyons and shelf-edge deltas are important elements of continental margins, which influence sediment transport dynamics across shelves and slopes to deep-water basins, and the storage of sediment. However, the factors that control their evolution and their relative importance remain poorly understood. Via three separate metastudies this thesis presents a quantitative, global study of submarine canyons and shelf-edge deltas in the context of (i) their physiographic setting, (ii) their associated source-to-sink (S2S) system, and (iii) their environmental setting, resulting in a novel quantitative characterisation of submarine canyons and shelf-edge deltas. The principal findings of this project are as follows: (i) Overall, scaling relationships of submarine canyons and shelf-edge deltas with descriptors of their physiographic setting and environment are weak, which reflects the complex influence of multiple factors, both allogenic and autogenic, on their geomorphologies, and how these factors might amplify, weaken or overprint a scaling relationship. (ii) Despite the complex and variable geomorphologies demonstrated for studied examples of submarine canyons and shelf-edge deltas, some morphometric attributes of both sedimentary system types do differ between environmental settings, indicating a greater genetic influence of certain individual environmental variables over others. (iii) Moderate and strong scaling of morphometric attributes in submarine canyons and shelf-edge deltas with each other, and with variables of the physiographic setting and associated S2S system, suggest that the geomorphologies of submarine canyons and shelf-edge deltas can be predicted to some degree, based on knowledge of their environmental setting, and vice versa. The findings from this project help to clarify the complex influence of multiple factors on the geomorphologies of submarine canyons and shelf-edge deltas, providing a framework for the prediction of their geomorphologic characteristics across environmental settings and for the integration of submarine canyons and shelf-edge deltas into S2S system analyses.

Table of Contents

Acknowledgements ..... **v**
Abstract ..... **vii**
Table of Contents ..... **viii**
List of Tables ..... **xvii**
List of Figures ..... **xix**
1 Introduction **1**
1.1 Rationale 5
1.2 Aim and Objectives 11
1.3 Methodology 11
1.4 Thesis outline 15
1.4.1 Chapter 2: Background 15
1.4.2 Chapter 3: A global analysis of controls on submarine-canyon geomorphology 15
1.4.3 Chapter 4: Tectonic influence on the geomorphology of submarine canyons: implications for deep-water sedimentary systems 16
1.4.4 Chapter 5: Sedimentary characteristics of shelf-edge deltas in a source-to-sink context 16
1.4.5 Chapter 6: Discussion 17
1.4.6 Chapter 7: Conclusions 17
2 Background **19**
2.1 Introduction 20
2.2 Controlling factors of submarine canyons 21
2.2.1 Submarine canyon definition 21
2.2.2 Submarine canyon evolution 23
2.2.2.1 Processes influencing canyon evolution 24
2.2.2.2 Canyon-physiographic setting 26
2.2.2.3 Environmental variables 28
2.2.3 Submarine canyon studies 31
2.2.3.1 Research bias in submarine canyon studies 31
2.2.3.2 Evaluation of aspects of submarine-canyon geomorphology in quantitative studies 32
2.2.4 Conceptual models of submarine canyons 41
2.2.4.1 Conceptual models of submarine canyon evolution 41

2.2.4.2 Submarine canyons as parts of source-to-sink (S2S) systems 44
2.2.5 Submarine canyon classification schemes 44
2.2.5.1 Seafloor lithology, tectonic-margin type, sediment transport mechanism and complexity of canyon configuration 45
2.2.5.2 Canyon longitudinal profile shape, environmental controls and sedimentary and hydrodynamic processes 45
2.2.5.3 Tectonic-margin type 45
2.2.5.4 Position of the canyon head relative to the shelf break, source type and lithology, intra-canyon processes, cross-sectional shape, lithology of canyon fill and association with distal deep-water deposits 46
2.2.5.5 Position of the canyon head relative to the shelf break, canyon morphometric characteristics and canyon spacing 46
2.3 Controlling factors of shelf-edge deltas 53
2.3.1 Shelf-edge delta definition 53
2.3.2 Shelf-edge delta evolution 56
2.3.2.1 Processes influencing shelf-edge delta evolution 56
2.3.3 Shelf-edge delta studies 57
2.3.3.1 Research bias in shelf-edge delta studies 57
2.3.3.2 Evaluation of aspects of shelf-edge delta geomorphology in quantitative studies 58
2.3.4 Conceptual models of shelf-edge deltas 60
2.3.5 Shelf-edge delta classification schemes 61
2.3.5.1 Hydrodynamic-process regime 61
2.3.5.2 Delta & margin stability 62
2.3.5.3 Sea level dynamics, physiographic setting, delta characteristics and processes 62
2.3.5.4 Sea level dynamics, shelf width, magnitude of sediment supply, and delta characteristics 63
2.4 Source-to-sink (S2S) research 68
2.4.1 Definitions 68
2.4.1.1 The source-to-sink (S2S) system 68
2.4.1.2 The sediment-routeing system 69
2.4.1.3 Source areas 70

2.4.1.4 Sinks 70
2.4.1.5 Source-to-sink (S2S) system segments 71
2.4.2 Source-to-sink (S2S) system models 75
2.4.2.1 Representation of submarine canyons and shelf-edge deltas in conceptual models of source-to-sink (S2S) systems 75
2.4.2.2 Representation of sediment transport pathways and marine hydrodynamic processes in conceptual models of source-to-sink (S2S) systems 78
2.4.2.3 Complexity of sediment routeing systems 80
2.4.3 Source-to-sink (S2S) system classifications 80
2.4.3.1 Intra- vs. extra-basinal sediment sources 81
2.4.3.2 Morphological characteristics of source-to-sink (S2S) systems 81
2.4.3.3 Efficiency of signal propagation across a source-to-sink (S2S) system 81
2.4.3.4 Hierarchical relationships between source-to-sink (S2S) systems 82
2.4.3.5 Sediment connection between source-to-sink (S2S) systems 82
2.5 Sedimentary systems at the shelf-to-slope transition: The importance of shelf-edge deltas and submarine canyons as controls on continental-margin evolution 87
2.5.1 Influence of submarine canyons and shelf-edge deltas on the evolution of continental margins 87
2.5.2 Influence of submarine canyons and shelf-edge deltas on source-to-sink (S2S) systems 89
2.5.2.1 Size and extent of source-to-sink (S2S) systems 89
2.5.2.2 Evolution of younger source-to-sink (S2S) systems 89
2.6 Summary 90
3 A global analysis of controls on submarine-canyon geomorphology 91
3.1 Introduction 92
3.2 Background 95
3.2.1 Controls on submarine canyon evolution 95
3.2.2 Submarine canyon studies 97
3.3 Dataset and methodology 102
3.3.1 Study parameters 112

3.3.1.1 Canyon morphometric parameters 112
3.3.1.2 Environmental parameters and external controls .. 113
3.3.2 Statistical analyses 118
3.3.3 Limitations of the study 119
3.4 Scaling relationships between canyon morphometrics 121
3.4.1 Observations 121
3.4.2 Interpretations 122
3.4.2.1 Sedimentary processes 123
3.4.2.2 Hydrodynamic processes 124
3.4.2.3 Structural controls 126
3.4.2.4 Biogenic processes 126
3.5 Relationships between canyon morphometric parameters and attributes of the physiographic setting 131
3.5.1 Distance between canyon and shoreline (Dis_{min}) 132
3.5.1.1 Observations 132
3.5.1.2 Interpretations 132
3.5.2 Canyon bathymetry 133
3.5.2.1 Observations 133
3.5.2.2 Interpretations 134
3.5.3 Latitudinal position of the canyon apex (Lat_{abs}) 137
3.5.3.1 Observations 138
3.5.3.2 Interpretations 138
3.6 Scaling relationships between canyon morphometric parameters and source-to-sink (S2S) system attributes 143
3.6.1 Terrestrial catchment (L_{fls}, Q_{fls}, A_{flsc}, H_{flsc}) 146
3.6.1.1 Observations 146
3.6.1.2 Interpretations 146
3.6.2 Continental shelf (W_{sh}, G_{sh}, D_{sh}) 150
3.6.2.1 Observations 150
3.6.2.2 Interpretations 151
3.6.3 Continental slope (W_{sl}, G_{sl}, D_{sl}) 158
3.6.3.1 Observations 158
3.6.3.2 Interpretations 158
3.7 Variations in canyon morphometric parameters across classes of environments 161

3.7.1 Canyon-apex location relative to the shelf break 163
3.7.1.1 Observations 163
3.7.1.2 Interpretations 164
3.7.2 Continental-margin type 167
3.7.2.1 Observations 167
3.7.2.2 Interpretations 168
3.7.3 Source-to-sink (S2S) system setting 171
3.7.3.1 Observations 171
3.7.3.2 Interpretations 171
3.7.4 Oceanographic environment 175
3.7.4.1 Observations 175
3.7.4.2 Interpretations 175
3.7.5 Latitudinal zones 178
3.7.5.1 Observations 178
3.7.5.2 Interpretations 178
3.7.6 Width-to-depth ratios 181
3.7.6.1 Observations 181
3.7.6.2 Interpretations 181
3.8 Summary and conclusions 183
4 Tectonic influence on the geomorphology of submarine canyons: implications for deep-water sedimentary systems 191
4.1 Introduction 192
4.2 Dataset and methods 194
4.2.1 Dataset 194
4.2.2 Methods 201
4.2.2.1 Canyon definition 202
4.2.2.2 Study parameters 202
4.2.3 Statistical analyses 205
4.2.4 Limitations of the study 206
4.3 Results 207
4.3.1 Scaling between canyon morphometric parameters and the tectonic setting 207
4.3.1.1 Continental-margin type 207
4.3.1.2 Active-margin plate-boundary type 211

4.3.2 Scaling in submarine canyons in active versus passive margins 214
4.3.2.1 Canyon dimensions 214
4.3.2.2 Maximum canyon sidewall steepness versus maximum canyon width and -depth 214
4.3.3 Scaling between canyon morphometric parameters and characteristics of their physiographic setting in active versus passive margins 216
4.3.3.1 Seafloor depth at the canyon apex (SD_{min}) 217
4.3.3.2 Minimum canyon-shoreline distance (Dis_{min}) 217
4.3.4 Scaling between canyon morphometry and characteristics of the source-to-sink (S2S) system 221
4.3.4.1 Terrestrial catchment (L_{fls}, Q_{fls}, A_{flsc}; H_{flsc}) 221
4.3.4.2 Shelf-break depth (D_{sh}) 222
4.3.4.3 Slope width (W_{sl}) 222
4.3.5 Characterization of canyon source-to-sink (S2S) system and physiographic setting by tectonic setting 226
4.3.5.1 Attributes of the canyon geological contexts and their variations across margin types 226
4.3.5.2 Scaling between attributes of the source-to-sink (S2S) systems of active and passive margins 227
4.4 Discussion 230
4.4.1 Tectonic influence on controlling factors on submarine-canyon geomorphology 230
4.4.1.1 Intra-canyon sedimentary processes 231
4.4.1.2 Sediment connection to fluvial and littoral sources 233
4.4.1.3 Sediment supply to shelf margins 235
4.4.1.4 Structural controls 235
4.4.2 Canyon geomorphology and associated characters of deep-water systems 237
4.4.3 Implications of the findings and future work 239
4.5 Conclusions 240
5 Controls on the geometry of shelf-edge deltas 242
5.1 Introduction 243
5.2 Dataset and methods 246
5.2.1 Dataset 246
5.2.2 Studied variables 249

5.2.2.1 Deltaic elements 250
5.2.2.2 Source-to-sink (S2S) system attributes 253
5.2.2.3 Environmental attributes 255
5.2.3 Statistical analyses 259
5.2.4 Limitations of the study 260
5.3 Results 262
5.3.1 Shelf-edge delta geometry 263
5.3.1.1 Frequency distributions of shelf-edge deltaic elements 263
5.3.1.2 Scaling relationships of geometric parameters in shelf-edge deltas 265
5.3.2 Scaling relationships of delta geometric parameters with environmental variables 268
5.3.2.1 Terrestrial catchment (L_{fls}, Q_{fls}, A_{flsc}, H_{flsc}) 268
5.3.2.2 Shelf width (W_{sh}) 270
5.3.2.3 Palaeolatitude (Lat_{abs}) 271
5.3.3 Delta geometries versus environmental controls 272
5.3.3.1 Hydrodynamic-process regime 272
5.3.3.2 Fluvial feeder-system type 273
5.3.3.3 Source-to-sink (S2S) system setting 274
5.3.3.4 Oceanographic environment 275
5.3.3.5 Palaeolatitudinal zone 276
5.4 Discussion 277
5.4.1 Variability in geometric characteristics of shelf-edge deltas 277
5.4.2 Controlling factors on shelf-edge delta geometry 278
5.4.2.1 Hydrodynamic-process regime 278
5.4.2.2 Terrestrial catchment 279
5.4.2.3 Margin configuration 280
5.4.2.4 Source-to-sink (S2S) setting 281
5.4.2.5 Oceanographic environment 281
5.4.2.6 Palaeolatitude 281
5.4.2.7 Shelf-edge delta architecture 283
5.5 Conclusions 284

6 Discussion 287

6.1 Controlling factors of morphometric characteristics of submarine canyons and shelf-edge deltas: implications for conceptual and semi-quantitative models 288

6.1.1 Continental-margin configuration 290

6.1.1.1 Accommodation and bypass of sediment 290

6.1.1.2 Shelf- and slope gradients as drivers of autogenic and allogenic sedimentary processes in submarine canyons and shelf-edge deltas 291

6.1.1.3 Co-relationships of continental-margin configuration with morphometric attributes of submarine canyons and shelf-edge deltas 292

6.1.2 Terrestrial catchment characteristics 300

6.1.3 Marine hydrodynamic processes: oceanographic environment and hydrodynamic-process regime 312

6.1.4 Tectonic setting 319

6.1.5 Latitude 327

6.2 Influence of morphometric characteristics of shelf-edge deltas and submarine canyons on sediment delivery across shallow and deep-water environments 332

6.2.1 Submarine-canyon geomorphology 332

6.2.2 Shelf-edge delta geometry 337

6.3 Scaling relationships of shelf-edge delta- and submarine canyon geomorphologies: applications and limitations 341

6.3.1 Reconstruction of characteristics of submarine canyons, shelf-edge deltas, and their associated source-to-sink (S2S) systems in outcrop and subsurface 341

6.3.1.1 Applications 341

6.3.1.2 Limitations 343

6.3.2 Implications for industrial applications 346

6.3.3 Planning and conducting of field surveys, experimental- and modelling studies 347

7 Conclusions 348

7.1 Overarching conclusions of this project 349

7.2 Future research 353

7.2.1 Prospective study variables for future quantitative analyses of submarine canyons and shelf-edge deltas 354

7.2.1.1 Morphometric attributes of submarine canyons and shelf-edge deltas 354

7.2.1.2 Architectural elements of submarine canyons and shelf-edge deltas 354

7.2.1.3 Environmental factors and processes 355

7.2.2 Genetic links of submarine canyons and shelf-edge deltas with other sedimentary systems within the source-to-sink (S2S) system 356

7.2.3 Re-evaluation of scaling relationships seen in submarine canyons and shelf-edge deltas from larger datasets in the future 357

7.2.4 Application of other statistical techniques 358

7.2.5 Submarine canyons and shelf-edge deltas as repositories for the storage of carbon dioxide 358

7.2.6 Application of findings to extraterrestrial planetary source-to-sink (S2S) systems 358

List of References 360

List of Abbreviations 412

Appendix A List of study variables and their definitions 413

Appendix B Datasets 1, 2 and 3 416

Appendix C Published versions of chapters 3 and 4 417

List of Tables

Table 2.1 Overview table of examples of regional, continental and global scale studies addressing submarine canyon research presented in ascending order by year of publication. min. = minimum; av. = average. **41**

Table 2.2 Overview table of examples of submarine canyon classification schemes in the literature presented in ascending order by year of publication (see also Figure 2.4a-d). **53**

Table 2.3 Overview table of examples of shelf-edge delta classification schemes in the literature presented in ascending order by year of publication (see also Figure 2.8a-c). n.a. = not addressed. **68**

Table 2.4 Examples of source-to-sink system segments distinguished in conceptual models in the literature presented in ascending and alphabetical order by year of publication (see also Figure 2.11a-e) and this study. **75**

Table 2.5 Overview of marine hydrodynamic processes, their capabilities to transport grain-size fractions and their order of duration. **79**

Table 2.6 Overview of classification schemes of source-to-sink (S2S) systems in the literature sorted in ascending and alphabetical order by year of publication (see also Figure 2.14a-f). **86**

Table 3.1 Overview of the 96 case studies and associated 135 literature data sources of the present study. Numbers in brackets refer to channel forms termed as submarine ‘gullies’ by the authors. See Figure 3.1 for locations. **111**

Table 3.2 Overview and definition of the study parameters that have been considered in this work. Three asterisks (***) denote values that have been calculated. Two asterisks (**) denote values that have been obtained either from the literature, as reported by the original authors, measured or calculated. A single asterisk (*) denotes values that have been retrieved from the literature, as stated by the original authors. **118**

Table 4.1 Summary of the 97 case studies considered in this study. The numbers of canyons reported in brackets indicate channel forms that were termed as ‘submarine gullies’ by the authors of the original data sources. **201**

Table 4.2 Overview of the parameters investigated in the study and their definitions. **205**

Table 5.1 Overview of the 39 case studies of the study (for their geographic location see also Figure 5.1). No. of elements = numbers of deltaic elements investigated; c = delta complex; l = delta lobe; u = unclassified hierarchical level of the deltaic element; Fm. = formation. **249**

Table 5.2 Study parameters considered in this study. A single asterisk (*) denotes values that have been retrieved from the literature as stated by the authors. Two asterisks (**) denote values that have been obtained either from the literature, as reported by the original authors, from open-source bathymetry, or have been calculated, or a combination thereof. **259**

Table A Overview and definition of the study variables that have been considered in this project. Three asterisks (***) denote values that have been calculated. Two asterisks (**) denote values that have been obtained either from the literature, as reported by the original authors, from open-source bathymetry, or have been calculated, or a combination thereof. A single asterisk (*) denotes values that have been retrieved from the literature, as stated by the original authors. **415**

List of Figures

Figure 1.1 Schematic figure of a shelf-edge delta and submarine canyon within the context of a source-to-sink system and overview of key study variables considered in the research project. (SC1), (SC2) and (SED) refer to which of the external controls were investigated in the three different metastudies in data chapters 3, 4 and 5, respectively: SC1 = Submarine-canyon study 1 (Chapter 3) SC2 = Submarine-canyon study 2 (Chapter 4) SED = Shelf-edge delta study (Chapter 5). **12**

Figure 1.2 Schematic overview of the overarching workflow of this research project. DMAKS = Deep-Marine Architecture Knowledge Store (e.g. Cullis et al., 2019); SMAKS = Shallow-Marine Architecture Knowledge Store (e.g. Colombera et al., 2016). **14**

Figure 2.1a&b A. High-resolution bathymetric map of an example of a submarine canyon on the modern seafloor: Ipala Canyon offshore W Mexico (Urías Espinosa et al., 2016). B. High-resolution bathymetric map depicting a canyon system constituting of several canyons: Cook Strait Canyon system, New Zealand (Micallef et al., 2014). Added text in blue. **23**

Figure 2.2a-e (continued). **37**

Figure 2.2a-e Selected analyses of scaling relationships of canyon morphometric attributes with environmental variables and sedimentary systems in the literature sorted in ascending order by year of publication. A. Scatterplots and results of statistical analyses of canyon morphometric attributes with submarine fan volume from the global investigation of 29 source-to-sink systems by Sømme et al. (2009). B. Results of the statistical evaluation of differences in mean values of studied morphometric attributes in submarine canyons as a function of the tectonic-margin type from the global study of 5,849 submarine canyons by Harris & Whiteway (2011). Statistically significant differences in mean values at 95% confidence intervals are underlaid in yellow. C. Scatterplots of average canyon sinuosity versus latitudinal position of the submarine canyon from the global study by Harris & Whiteway (2011). D. Boxplots of centreline length (CL) and sinuosity (Sn) in submarine canyons in general (All) and for blind/slope-confined (BC) and shelf-incising (SIC) canyons from the continental study of 713 submarine canyons offshore Australia by Huang et al. (2014; see their full Figure 14 for the entirety of boxplots). E. Boxplots of canyon characteristics vs. the tectonic setting from the global study of 52 source-to-sink systems by Nyberg et al. (2018b). **38**

Figure 2.3a&b Examples of conceptual models of submarine-canyon evolution in the literature sorted in ascending order by year of publication. **43**

Figure 2.4a-e (continued). **49**

Figure 2.4a-e (continued). **50**

Figure 2.4a-e Examples of submarine-canyon classification schemes in the literature sorted in ascending an alphabetic order by year of publication (see also Table 2.2). Added text in blue. **51**

Figure 2.5a&b Examples of schematic models of main subenvironments within a shelf-edge delta. A. Edwards (1981). B. Schwartz & Graham (2015). Added text in blue. **55**

Figure 2.6a&b A. Overview of key characteristics of different types of deltas and some of their controls (Porębski & Steel, 2003). Red box: Compilation of information on shelf-edge deltas and aspects of their environmental setting (modified from Porębski & Steel, 2003). B. Summary characteristics of shelf-edge deltas of Pleistocene ages from four different geographic regions (partial table of Porębski & Steel, 2003). **60**

Figure 2.7a-c (continued). **65**

Figure 2.7a-c Examples of graphic visualisations of shelf-edge delta classification schemes in the literature sorted in ascending order by year of publication. Added text in blue (see also Table 2.3). **66**

Figure 2.8 Schematic model of a source-to-sink system and some of its environmental controls (Blum & Hattier-Womack, 2009). **69**

Figure 2.9a-d Examples of different types of sediment routeing systems from A. simple to B.-D. more complex configurations. S1-S3: Sediment source areas. D1-3: Depositional sink. A.-C. Modified after Figure 1.5 of Allen (2017). D. Source-to-sink system comprising multiple source areas and one sink (based in part on Allen, 2017). **70**

Figure 2.10a-e Examples of major segments of source-to-sink systems recognised in conceptual models in the literature sorted in ascending and alphabetical order by year of publication (see also Table 2.4). **75**

Figure 2.11a&b Examples of source-to-sink system models with shelf-edge deltas in their configuration in ascending order by year of publication. **77**

Figure 2.12a-e (continued). **84**

Figure 2.12a-e Graphic visualisations of classification schemes for source-to-sink systems in the literature sorted in ascending and alphabetical order by year of publication (see also Table 2.6). **85**

Figure 3.1a&b A. Overview map of distribution of the 96 case studies. B. Geographic distribution of the 96 case studies and 282 submarine canyons (World map from freevectormaps.com). **103**

Figure 3.2a&b A. Attributes of the source-to-sink system and physiographic setting investigated in the study. 1. Terrestrial catchment: fluvial system length, average annual fluvial discharge, catchment size, maximum elevation. 2. Shelf configuration: width, depth, average gradient. 3. Slope configuration: width, depth, average gradient. 4. Canyon-apex location relative to the shelf break. 5. Minimum distance to shoreline. 6. Seafloor depth at the top of the canyon. 7. Seafloor depth at the canyon mouth. B. Key canyon morphometric parameters considered in the study: L = canyon length along thalweg; L_{en} = canyon length along endpoints; W_{max} = maximum canyon width; D_{max} = maximum canyon depth; SI_{av} = average canyon sinuosity index; thG_{av} = average canyon thalweg gradient; SW_{max} = maximum canyon sidewall steepness. **116**

Figure 3.3 Heat maps of correlations of canyon morphometric parameters with each other for canyons of the study displaying values of Pearson's correlation coefficient r and Spearman's rank correlation coefficient r_s, and their respective p-values. L = canyon length; W_{max} = maximum canyon width; W_{av} = average canyon width; D_{max} = maximum canyon depth; D_{av} = average canyon depth; SI_{av} = average canyon sinuosity index; thG_{av} = average canyon thalweg gradient; SW_{max} = maximum canyon sidewall steepness. n.e.d. = not enough data to facilitate statistical analyses. **127**

Figure 3.4a-q (continued). **129**

Figure 3.4a-q (continued). **130**

Figure 3.4a-q A.-O. Scatterplots of canyon morphometric parameters for studied submarine canyons. P.&Q. Scatterplots of canyon length with width (P) and average depth (Q) plotted from the dataset of Harris et al. (2014b) with an overlay of data from this study for comparison. N = number of observations; r = Pearson's correlation coefficient; r_s = Spearman's rank correlation coefficient. **131**

Figure 3.5 Heat maps for correlations of canyon morphometrics with the physiographic setting displaying values of Pearson's correlation coefficient r and Spearman's rank correlation coefficient r_s, and their respective p-values. L = canyon length; W_{max} = maximum canyon width; W_{av} = average canyon width; D_{max} = maximum canyon depth; D_{av} = average canyon depth; SI_{av} = average canyon sinuosity index; thG_{av} = average canyon thalweg gradient; SW_{max} = maximum canyon sidewall steepness; Dis_{min} = minimum distance between the canyon and shoreline; SD_{min} = minimum seafloor depth at the canyon; SD_{max} = maximum seafloor depth at the canyon; Lat_{abs} = absolute value of the latitude of the canyon apex. **131**

Figure 3.6a-f Scatterplots of minimum canyon-shoreline distance and canyon morphometric parameters. N = number of correlations; r = Pearson's correlation coefficient; r_s = Spearman's rank correlation coefficient. **133**

Figure 3.7a-f Scatterplots of seafloor depth at the top of the canyon and canyon morphometric parameters. N = number of correlations; r = Pearson's correlation coefficient; r_s = Spearman's rank correlation coefficient. **136**

Figure 3.8a-f Scatterplots of seafloor depth at the canyon mouth and canyon morphometric parameters. N = number of correlations; r = Pearson's correlation coefficient; r_s = Spearman's rank correlation coefficient. **137**

Figure 3.9a-f Scatterplots of absolute values of latitude of the canyon apex and canyon morphometric parameters. N = number of correlations; r = Pearson's correlation coefficient; r_s = Spearman's rank correlation coefficient. **142**

Figure 3.10a-c Heat maps for correlations of canyon morphometrics with parameters of the associated source-to-sink system displaying values of Pearson's correlation coefficient r and Spearman's rank correlation coefficient r_s, and their respective p-values. A. Terrestrial catchment. B. Continental shelf. C. Continental slope. *L* = canyon length; W_{max} = maximum canyon width; W_{av} = average canyon width; D_{max} = maximum canyon depth; D_{av} = average canyon depth; SI_{av} = average canyon sinuosity index; thG_{av} = average canyon thalweg gradient; SW_{max} = maximum canyon sidewall steepness; L_{fls} = fluvial system length; Q_{fls} = average annual fluvial discharge; A_{flsc} = size of the catchment; H_{flsc} = maximum elevation in the catchment area; W_{sh} = shelf width; D_{sh} = shelf-break depth; G_{sh} = average shelf gradient. 4. Slope configuration: W_{sl} = slope width; D_{sl} = slope-break depth; G_{sl} = average slope gradient. *** indicates scarcity of data (N<15). **145**

Figure 3.11 Heat maps for correlations of parameters of the source-to-sink system specific to studied submarine canyons displaying values of Pearson's correlation coefficient r and Spearman's rank correlation coefficient r_s, and their respective p-values. L_{fls} = fluvial system length; Q_{fls} = average annual fluvial discharge; A_{flsc} = size of the catchment; H_{flsc} = maximum elevation in the catchment area; W_{sh} = shelf width; D_{sh} = shelf-break depth; G_{sh} = average shelf gradient. 4. Slope configuration: W_{sl} = slope width; D_{sl} = slope-break depth; G_{sl} = average slope gradient. *** indicates scarcity of data (N<15). **145**

Figure 3.12a-t Scatterplots between attributes of terrestrial catchments and canyon morphometric parameters. N = number of correlations; r = Pearson's correlation coefficient; r_s = Spearman's rank correlation coefficient. **150**

Figure 3.13a-r Scatterplots between attributes of the continental shelf and canyon morphometric parameters. N = number of correlations; r = Pearson's correlation coefficient; r_s = Spearman's rank correlation coefficient. **156**

Figure 3.14a-f Boxplots of frequency distributions of canyon morphometric parameters for studied submarine canyons distinguished based on shelf-break depth thresholds of 120 m at the canyon. Tabulated statistics refer to canyons grouped based on shelf-break thresholds of 120 m and 130 mbsl, respectively. N = number of readings; min = minimum value; mean = mean value; StDev = standard deviation; median = median value; max = maximum value. **157**

Figure 3.15a-r Scatterplots between attributes of the continental slope and canyon morphometric parameters. N = number of correlations; r = Pearson's correlation coefficient; r_s = Spearman's rank correlation coefficient. **161**

Figure 3.16a-f Boxplots of frequency distributions of the investigated canyon morphometric parameters. *L* = canyon length; W_{max} = maximum canyon width; W_{av} = average canyon width; D_{max} = maximum canyon depth; D_{av} = average canyon depth; SI_{av} = average canyon sinuosity index; thG_{av} = average canyon thalweg gradient; SW_{max} = maximum canyon sidewall steepness; N = number of readings; min = minimum value; mean = mean value; StDev = standard deviation; median = median value; max = maximum value. **163**

Figure 3.17a-j A.-H. Boxplots of frequency distributions of canyon morphometric parameters for studied canyons classified on the location of the canyon apex relative to the shelf break into slope-confined (N=99) and shelf-incising canyons (N=154). I.&J. Boxplots of canyon length (I) and average depth (J) and results of statistical analyses plotted from the dataset of Harris et al. (2014b) for calibration. *L* = canyon length; W_{max} = maximum canyon width; W_{av} = average canyon width; D_{max} = maximum canyon depth; D_{av} = average canyon depth; SI_{av} = average canyon sinuosity index; thG_{av} = average canyon thalweg gradient; SW_{max} = maximum canyon sidewall steepness; N = number of readings; min = minimum value; mean = mean value; StDev = standard deviation; median = median value; max = maximum value. Results of Two-Sample T-test: DF = degrees of freedom. **167**

Figure 3.18a-h Boxplots of frequency distributions of canyon morphometric parameters for studied canyons classified based on the continental-margin type into active-margin (N=153) and passive-margin canyons (N=129) (classification after Harris et al., 2014b). See Figure 3.17 for legend. **171**

Figure 3.19a-h Boxplots of frequency distributions of canyon morphometric parameters for studied submarine canyons classified based on the source-to-sink setting into continental-margin (N=189) and insular canyons (N=57). *** denotes data paucity. See Figure 3.17 for legend. **175**

Figure 3.20a-h Boxplots of frequency distributions of canyon morphometric parameters for studied submarine canyons classified based on the oceanographic environment into submarine canyons associated with open seas (N=162) and semi-enclosed and enclosed seas (N=120). See Figure 3.17 for legend.**.. 178**

Figure 3.21a-h Boxplots of frequency distributions of canyon morphometric parameters for studied submarine canyons classified based on latitudinal zones into tropical (N=116), temperate (N=149) and polar canyons (N=16). * indicates that Two-Sample-T-tests have been conducted for submarine canyons in tropical versus temperate latitudinal zones. N = number of readings; min = minimum value; mean = mean value; StDev = standard deviation; median = median value; max = maximum value. Results of Welch's ANOVA test: DF 1 = degrees of freedom numerator; DF 2 = degrees of freedom denominator. Results of Two-Sample T-test: DF = degrees of freedom. *** denotes data paucity. **181**

Figure 3.22a-f Boxplots of frequency distributions of maximum-width-to-maximum depth (wdmax) ratios in studied submarine canyons A. for the dataset and B.-F. across classes of environments. * indicates that Two-Sample-T-tests have been conducted for submarine canyons in tropical versus temperate latitudinal zones. See Figure 3.21 for legend.**..... 183**

Figure 3.23a&b Summary tables displaying relationships of canyon morphometric parameters A. with each other and B. with environmental parameters for results of the correlation analyses and hypothesis testing with a statistical significance ($p \leq 0.1$) and $N \geq 15$ for each parameter and canyon group. *L* = canyon length; W_{max} = maximum canyon width; W_{av} = average canyon width; D_{max} = maximum canyon depth; D_{av} = average canyon depth; SI_{av} = average canyon sinuosity index; thG_{av} = average canyon thalweg gradient; SW_{max} = maximum canyon sidewall steepness; L_{fls} = fluvial system length; Q_{fls} = average annual fluvial discharge; A_{flsc} = size of the catchment; H_{flsc} = maximum elevation in the catchment area; W_{sh} = shelf width; D_{sh} = shelf-break depth; G_{sh} = average shelf gradient. 4. Slope configuration: W_{sl} = slope width; D_{sl} = slope-break depth; G_{sl} = average slope gradient; Dis_{min} = minimum distance between the canyon and shoreline; SD_{min} = minimum seafloor depth at the canyon; SD_{max} = maximum seafloor depth at the canyon; Lat_{abs} = absolute value of the latitude of the canyon apex; *cnh. location* = canyon-apex location relative to the shelf break; *margin type* = continental-margin type; *ocean. env.* = oceanographic environment; *lat.* = latitude at the canyon apex; *sh. depth* = shelf-break depth at the canyon. *** denotes datasets that were deemed too small for statistical analyses. **189**

Figure 3.24a&b Schematic diagrams summarising controlling factors of submarine-canyon geomorphology recognised in the literature and whose statistical signature has been evaluated in this study. **190**

Figure 4.1a&b A. Overview map of the distribution of the 97 case studies and their associated margin-type setting. Continental-margin classification after Harris et al. (2014b) (World map from freevectormaps.com). B. Key parameters investigated in the study: 1. Submarine canyon: *L* = canyon length along thalweg; L_{en} = canyon length along endpoints; W_{max} = maximum canyon width; D_{max} = maximum canyon depth; SI_{av} = average canyon sinuosity index; thG_{av} = average canyon thalweg gradient; SW_{max} = maximum canyon sidewall steepness. 2. Terrestrial catchment: L_{fls} = fluvial system length; Q_{fls} = average annual fluvial discharge; A_{flsc} = catchment size; H_{flsc} = maximum catchment elevation. 3. Shelf configuration: W_{sh} = shelf width; D_{sh} = shelf-break depth; G_{sh} = average shelf gradient. 4. Slope configuration: W_{sl} = slope width; D_{sl} = slope-break depth; G_{sl} = average slope gradient. 5. Canyon-physiographic setting: SD_{min} = seafloor depth at canyon apex; SD_{max} = seafloor depth at canyon mouth. Dis_{min} = minimum distance of canyon to shoreline. **196**

Figure 4.2a-h Stacked histograms of morphometric values in studied submarine canyons in active (a) vs. passive (p) margins. N = number of readings; μ = mean value; η = median value; DF = degrees of freedom. **210**

Figure 4.3a-c Stacked histograms of aspect ratios in studied submarine canyons in active (a) vs. passive (p) margins. N = number of readings; μ = mean value; η = median value; DF = degrees of freedom. **211**

Figure 4.4a-i Dot plots of morphometric values and aspect ratios for the studied submarine canyons from active margins, classified on plate-boundary type. N = number of readings; min = minimum value; mean = mean value; StDev = standard deviation; median = median value; max = maximum value. Results of Welch's ANOVA test: DF Num = degrees of freedom numerator; DF Den = degrees of freedom denominator. Games-Howell post hoc test: Dmean = difference of means; SE = standard error. **213**

Figure 4.5a-g Results of the correlation analyses of canyon morphometric parameters and aspect ratios with parameters of the physiographic setting at the canyon in active vs. passive margins. A.&B. Overview of results presented as heat maps. C.-G. Scatter plots of results. *L* = canyon length; W_{max} = maximum canyon width; W_{av} = average canyon width; D_{max} = maximum canyon depth; D_{av} = average canyon depth;SI_{av} = average canyon sinuosity index; thG_{av} = average canyon thalweg gradient; SW_{max} = maximum canyon sidewall steepness; *** = correlations not reported due to small dataset size. **216**

Figure 4.6a&b Results of the correlation analyses of canyon morphometric parameters and aspect ratios with parameters of the physiographic setting at the canyon in active vs. passive margins presented as heat maps. *L* = canyon length along thalweg; L_{en} = canyon length along endpoints; W_{max} = maximum canyon width; D_{max} = maximum canyon depth; SI_{av} = average canyon sinuosity index; thG_{av} = average canyon thalweg gradient; SW_{max} = maximum canyon sidewall steepness; *lwmax* = length-to-maximum width ratio; *wdmax* = maximum width-to-maximum depth ratio; *ldmax* = length-to-maximum depth ratio; SD_{min} = seafloor depth at canyon apex; SD_{max} = seafloor depth at canyon mouth. Dis_{min} = minimum distance of canyon to shoreline; *** = correlations not reported due to small dataset size. **219**

Figure 4.7a-h Scatterplots of attributes of the canyon-physiographic setting with canyon morphometric parameters for submarine canyons of the study in active vs. passive margins. W_{av} = average canyon width; D_{max} = maximum canyon depth; D_{av} = average canyon depth; SI_{av} = average canyon sinuosity index; SW_{max} = maximum canyon sidewall steepness; *wdmax* = maximum width-to-maximum depth ratio; SD_{min} = seafloor depth at canyon apex; Dis_{min} = minimum distance of canyon to shoreline; N = number of readings; r = Pearson's correlation coefficient; rs = Spearman's rank correlation coefficient. **220**

Figure 4.8a-r Scatterplots of attributes of the terrestrial catchment, shelf and slope with canyon morphometric parameters for submarine canyons of the study in active vs. passive margins. L = canyon length; W_{max} = maximum canyon width; SI_{av} = average canyon sinuosity index; thG_{av} = average canyon thalweg gradient; SW_{max} = maximum canyon sidewall steepness; L_{fls} = fluvial system length; Q_{fls} = average annual fluvial discharge; A_{flsc} = catchment size; H_{flsc} = maximum catchment elevation; D_{sh} = shelf-break depth; W_{sl} = slope width; N = number of readings; r = Pearson's correlation coefficient; rs = Spearman's rank correlation coefficient. **225**

Figure 4.9a&b Results of the correlation analyses of canyon morphometric parameters and aspect ratios with parameters of the A. shelf and B. slope at the canyon in active vs. passive margins presented as heat maps. L = canyon length; W_{max} = maximum canyon width; D_{max} = maximum canyon depth; SI_{av} = average canyon sinuosity index; thG_{av} = average canyon thalweg gradient; SW_{max} = maximum canyon sidewall steepness; lwmax = length-to-maximum width ratio; wdmax = maximum width-to-maximum depth ratio; ldmax = length-to-maximum depth ratio; W_{sh} = shelf width; D_{sh} = shelf-break depth; G_{sh} = average shelf gradient; W_{sl} = slope width; D_{sl} = slope-break depth; G_{sl} = average slope gradient; *** = correlations not reported due to small dataset size. **226**

Figure 4.10a-n Boxplots of frequency distributions of attributes of source-to-sink systems and of the canyon-physiographic setting linked to submarine canyons of active and passive margins. N = number of readings; min = minimum value; mean = mean value; StDev = standard deviation; median = median value; max = maximum value; DF = degrees of freedom. **229**

Figure 4.11a&b Results of the correlation analyses of attributes of the source-to-sink system in active vs. passive margins presented as heat maps. L_{fls} = fluvial system length; Q_{fls} = average annual fluvial discharge; A_{flsc} = catchment size; H_{flsc} = maximum catchment elevation; W_{sh} = shelf width; D_{sh} = shelf-break depth; G_{sh} = average shelf gradient; W_{sl} = slope width; D_{sl} = slope-break depth; G_{sl} = average slope gradient; *** = correlations not reported due to small dataset size. **230**

Figure 5.1 Overview map of distribution of the 39 case studies and survey type (World map from freevectormaps.com). **247**

Figure 5.2a&b A. Conceptual model of a shelf-edge delta in context of the main segments of a source-to-sink system. 1 = Terrestrial catchment; 2 = Continental shelf (emerged); 3 = Continental slope. B. Main depositional subenvironments within a shelf-edge delta. Depicted shelf-edge delta evolution during lowstand conditions. **252**

Figure 5.3 Schematic illustration of hierarchical relationships between deltaic elements and of value types of measurements and their definitions in this study. *L* = length; *W* = width; *T* = thickness; *A* = area. **253**

Figure 5.4a-d Boxplots of frequency distributions of geometries observed in studied shelf-edge deltas for deltaic elements (N=112), overall and separately for delta lobes (N=46) and lobe complexes (N=23). *L* = length; *W* = width; *T* = thickness; *A* = area; max = maximum value; true = true value; p&u = partial or unlimited value; N = number of readings; min = minimum value; mean = mean value; StDev = standard deviation; median = median value; max = maximum value. **265**

Figure 5.5a-f Scatterplots of deltaic element geometric parameters with each other. *L* = length; *W* = width; *T* = thickness; *A* = area; max = only maximum values; all = maximum, true, partial and unlimited values; W_{sh} = modern shelf width at the delta location; r = Pearson's correlation coefficient; rs = Spearman's rank correlation coefficient; N = number of observations; * = not enough data for statistical analyses. **268**

Figure 5.6a-f Scatterplots of data on terrestrial catchment attributes and the width of deltaic elements A.-D. Late Quaternary examples of shelf-edge deltas in the study. E&F. All shelf-edge deltas independent of their age. All catchment values were obtained from the modern counterpart of the fluvial system or -systems the shelf-edge delta was associated with during its evolution. *W* = width; max = only maximum values; all = maximum, true, partial and unlimited values; *lq* = Late Quaternary examples; A_{flsc} = catchment size; H_{flsc} = maximum catchment elevation; L_{fls} = fluvial system length; Q_{fls} = average annual fluvial discharge; r = Pearson's correlation coefficient; rs = Spearman's rank correlation coefficient; N = number of observations. **270**

Figure 5.7a-d Scatterplots of data on modern shelf widths and deltaic element geometric parameters for the studied Late Quaternary shelf-edge deltas. *L* = length; *W* = width; *T* = thickness; *A* = area; max = only maximum values; all = maximum, true, partial and unlimited values; W_{sh} = modern shelf width at the delta location; r = Pearson's correlation coefficient; rs = Spearman's rank correlation coefficient; N = number of observations; * = not enough data for statistical analyses. **271**

Figure 5.8a-d Scatterplots of data on the absolute palaeolatitude of shelf-edge deltas and deltaic element geometric parameters. *L* = length; *W* = width; *T* = thickness; *A* = area; *max* = only maximum values; *all* = maximum, true, partial and unlimited values; Lat_{abs} = absolute latitudinal position of the shelf-edge delta; r = Pearson's correlation coefficient; rs = Spearman's rank correlation coefficient; N = number of observations. **272**

Figure 5.9a-d Boxplots of frequency distributions of geometries seen in deltaic elements of shelf-edge deltas associated with fluvial-dominated (N=28) and mixed-process regimes (N=27) as interpreted in the literature. *L* = length; *W* = width; *T* = thickness; *A* = area; N = number of readings; min = minimum value; mean = mean value; StDev = standard deviation; median = median value; max = maximum value. **273**

Figure 5.10a-d Boxplots of frequency distributions of geometries seen in deltaic elements of shelf-edge deltas associated with single rivers (N=48) and multiple fluvial systems (N=6). *L* = length; *W* = width; *T* = thickness; *A* = area; N = number of readings; min = minimum value; mean = mean value; StDev = standard deviation; median = median value; max = maximum value. **274**

Figure 5.11a-d Boxplots of frequency distributions of geometries seen in deltaic elements of shelf-edge deltas associated with continental (N=70) and insular (N=4) source-to-sink settings. *L* = length; *W* = width; *T* = thickness; *A* = area; N = number of readings; min = minimum value; mean = mean value; StDev = standard deviation; median = median value; max = maximum value..... **275**

Figure 5.12a-d Boxplots of frequency distributions of geometries seen in deltaic elements of shelf-edge deltas associated with open seas (N=9) and semi-enclosed seas (N=77). *L* = length; *W* = width; *T* = thickness; *A* = area; N = number of readings; min = minimum value; mean = mean value; StDev = standard deviation; median = median value; max = maximum value. **276**

Figure 5.13a-d Boxplots of frequency distributions of geometries seen in deltaic elements of shelf-edge deltas associated with tropical (0° to 23.5° degrees; N=20), temperate (23.5° to 66.5° degrees; N=87) and polar (> 66.5° degrees; N=2) latitudinal zones. *L* = length; *W* = width; *T* = thickness; *A* = area; N = number of readings; min = minimum value; mean = mean value; StDev = standard deviation; median = median value; max = maximum value..... **277**

Figure 5.14 Schematic diagram summarising controlling factors of shelf-edge delta geometry recognised in the literature and whose global significance is indicated from the results in this study..... **286**

Figure 6.1a-e (continued). **296**

Figure 6.1a-e (continued). **297**

Figure 6.1a-e (continued). **298**

Figure 6.1a-e Conceptual models of morphometric attributes in submarine canyons and shelf-edge deltas and their scaling with end-members of shelf- and slope configuration in a source-to-sink system. A. length, average canyon thalweg gradient and maximum sidewall steepness in a submarine canyon vs. slope configuration. B. Maximum width and -depth in a submarine canyon vs. slope width. C. Length, maximum width and -thickness in a shelf-edge delta element vs. shelf configuration. D. Length in a submarine canyon vs. shelf-break depth. E. Maximum sidewall steepness in a submarine canyon vs. shelf width. **299**

Figure 6.2a-f (continued). **306**

Figure 6.2a-f (continued). **308**

Figure 6.2a-f (continued). **309**

Figure 6.2a-f (continued). **310**

Figure 6.2a-f Conceptual models of morphometric attributes in shelf-edge deltas and submarine canyons and their scaling with end-members of terrestrial catchment characteristics in a source-to-sink system. A. Shelf-edge delta element width vs. size and maximum elevation of the terrestrial catchment. B. Shelf-edge delta element dimensions and area vs. fluvial feeder-system type. C. Length and average sinuosity in a submarine canyon vs. average annual fluvial discharge. D. Length, maximum width and average sinuosity in a submarine canyon vs. maximum catchment elevation. E. Maximum depth in a submarine canyon vs. fluvial system length. F. Maximum width and depth in a submarine canyon vs. terrestrial catchment size. **311**

Figure 6.3a&b Conceptual models of morphometric attributes in submarine canyons and shelf-edge deltas and their scaling with end-members of the oceanographic environment of a source-to-sink system. A. Maximum depth and sidewall steepness in a submarine canyon vs. the oceanographic environment. B. Length, width and area in shelf-edge deltaic elements vs. the oceanographic environment. **317**

Figure 6.4 Conceptual models of morphometric attributes in shelf-edge deltas and their scaling with end-members of the hydrodynamic-process regime in a source-to-sink system at the terrestrial to marine transition. Width and thickness in a shelf-edge deltaic element vs. the hydrodynamic-process regime. **318**

Figure 6.5a&b Conceptual models of morphometric attributes in submarine canyons and their scaling with end-members of the tectonic setting. A. Maximum canyon sidewall steepness vs. the margin type. B. Maximum canyon width vs. the plate-boundary type. **325**

Figure 6.6a&b A. Conceptual, semi-quantitative model of incised-valley fill geometries along passive and active margins in Wang et al. (2019; their Figure 16). In contrast to this research, which comprised transform margins with convergent margins under the class of active margins, Wang et al. (2019) grouped transform margins and passive margins together. B. Extended S2S system model from Wang et al. (2019) with integrated findings from this project for shelf-edge delta geometry. Modifications of the original figure by Wang et al. (2019) comprise added text in yellow boxes and shelf-edge delta elements in orange colour. **..... 327**

Figure 6.7a&b Conceptual models of morphometric attributes in submarine canyons and shelf-edge deltas and their scaling with the latitudinal setting of a source-to-sink system. A. Average canyon thalweg gradient vs. the latitudinal zone. B. Length and maximum width in a shelf-edge delta vs. the latitudinal zone. **..... 331**

Figure 6.8a-e Conceptual models of relationships between aspects of submarine-canyon geomorphology and sediment routeing to deep-water environments as a function of environmental variables. A. Shallow submarine canyons. B. Deep submarine canyon. C. Low-sinuosity submarine canyon. D. High-sinuosity submarine canyon. E. Along continental margins characterised by high intra-slope relief variability, sediment transport across slope might be inhibited in shallow and high-sinuosity submarine canyons. **..... 337**

Figure 6.9a-c Conceptual models of relationships between shelf-edge delta size and sediment routeing to deep-water environments as a function of environmental variables. A. Short and small shelf-edge delta. B. Long and large shelf-edge delta. C. Along continental margins characterised by high-energetic longshore currents and/or storm waves, sediment transport across slope might be inhibited in long and large deltas. **..... 341**

Figure 7.1 Schematic diagram summarising some of the key findings of this project regarding controlling factors of the geomorphologies of submarine canyons and shelf-edge deltas recognised in the literature and indicated from the results in this study. **..... 353**

1 Introduction

The dynamics of sediment transport from shallow-marine to deep-water environments and genetic linkages between sedimentary environments within continental shelves and slopes are not well understood. Source-to-sink (S2S) research facilitates the investigation of landscape evolution over time, with focus on the study of sediment transport dynamics and their erosional and depositional products as a function of autogenic and allogenic controls. As such, it forms a powerful framework to increase understanding of the spatial and temporal evolution of sedimentary systems. By utilising field surveys of ancient and modern sedimentary environments (e.g. Anderson et al., 2015; Bhattacharya et al., 2016; Kuehl et al., 2016, and references therein; Liu et al., 2018; Snedden et al., 2018; Chen et al., 2020), and from their investigation in experimental (e.g. Kim et al., 2013; Lai et al., 2016; Straub, 2019), numerical (e.g. Gong et al., 2021; Wan et al., 2021) and quantitative studies (e.g. Wetzel, 1993; Sømme et al., 2009; Nyberg et al. 2018b; Pettinga et al., 2018; Wang et al., 2019; 2020), S2S research has facilitated insights into genetic relationships of sedimentary and morphologic characteristics of sedimentary systems with their physiographic setting and environmental controls.

Prior global-scale, quantitative analyses of sedimentary systems have identified the existence of general scaling relationships of their morphometric attributes with various variables of their environmental setting. Many of these studies have focused on submarine fans (e.g. Wetzel, 1993; Sømme et al., 2009; Nyberg et al., 2018b; Pettinga et al., 2018) and fluvial systems (e.g. Sømme et al., 2009; Nyberg et al., 2018a&b); more recently the research focus has also included fluvial environments and subenvironments, such as incised valleys (e.g. Wang et al., 2019; 2020) and Gilbert-type deltas (e.g. Budai et al., 2021), as well as aeolian systems (e.g. Cosgrove et al., 2021).

Some of the environmental factors that have been shown to scale with morphometric aspects of sedimentary systems include – but are not limited to – morphometric characteristics of the associated terrestrial catchment (e.g. fluvial systems, Sømme et al., 2009; Nyberg et al., 2018a&b; incised-valley fills, Wang et al., 2019; submarine fans, Snedden et al., 2018), continental shelf (e.g. fluvial systems, Sømme et al., 2009; incised-valley

fills, Wang et al., 2019) and slope (e.g. fluvial systems, Sømme et al., 2009), fluvial discharge rates (e.g. in relation to submarine fans, Wetzel, 1993), rate of sediment deposition (e.g. submarine fans, Wetzel, 1993; Sømme et al., 2009), mean tidal range at the shoreline (e.g. incised-valley fills, Wang et al., 2020), and bathymetric depth (e.g. submarine fans, Sømme et al., 2009).

In addition, studies have shown the existence of scaling relationships between geometric attributes of sedimentary systems. These include Gilbert-type deltas (Budai et al., 2021), submarine fans (e.g. Sømme et al., 2009; Nyberg et al., 2018b; Snedden et al., 2018), and their lower-hierarchy components submarine fan-channels and -lobes (Pettinga et al., 2018). The recognition of scaling relationships between morphometric attributes of a sedimentary system suggests that they are coevally influenced by one or several controls.

Moreover, scaling relationships of morphometric characteristics have been demonstrated for connected sedimentary environments and sub-environments, as is the case between fluvial systems and submarine fans (e.g. Nyberg et al., 2018b; Snedden et al., 2018), channels and their distally connected lobes in submarine fans (see Pettinga et al., 2018), and submarine canyons and submarine fans (e.g. Sømme et al., 2009). This indicates that the coeval influence of an environmental control can be traced across different sedimentary systems within a S2S system, or that characteristics of a relatively more proximally located sedimentary environment exert influence on the morphology of a more distally located one.

Such insights aid the interpretation of ancient sedimentary systems and reconstruction of palaeoenvironmental conditions during their time of activity (e.g. Nyberg et al., 2018b); for example, by providing first-order estimates of original geometries of sedimentary environments in outcrop- and subsurface studies (e.g. Martinsen et al., 2010; Xu et al., 2017; Snedden et al., 2018; Liu et al., 2019; Wang et al., 2020) and by linking geometries of sedimentary environments to palaeoenvironmental factors, such as the continental-margin type (e.g. Wang et al., 2019), and the climatic setting as a function of latitude (e.g. Cosgrove et al., 2021). Moreover, knowledge of boundary

conditions and their effect on morphologies of sedimentary systems can inform laboratory and modelling studies (Nyberg et al., 2018b), by contributing to more accurate interpretation of the depositional record of ancient sedimentary environments and to prediction of the evolution of modern ones. Therefore, S2S research constitutes an important tool to provide solutions to today's societal, economic and ecological challenges, including the following:

(i) The evolution of modern sedimentary systems such as rivers, deltas and submarine canyons is influenced by both environmental and anthropogenic influences. By unravelling the relative impact of the diverse natural and anthropogenic controls on their sedimentary and morphological evolution, it will be possible to develop and improve strategies for their preservation (e.g. Syvitski et al., 2009; Fernandez-Arcaya et al., 2017).

(ii) Sedimentary systems constitute key parts of subsurface resource systems. For example, the continued need for procurement of hydrocarbons (e.g. Bhattacharya et al., 2016) during the transition to a carbon-free energy grid (e.g. Davies & Simmons, 2021) and in light of geopolitical crises causing regional shortages, requires predictive tools which can aid in the identification of new hydrocarbon plays.

(iii) Moreover, sedimentary systems are important subsurface resource plays for the energy transition in context of carbon capture and storage (e.g. Bachu & McEwen, 2011;Teng & Zhang, 2018; Callas et al., 2022), geothermal energy production (e.g. Moeck, 2014), and for hydrogen (e.g. Muhammed et al., 2022) and radioactive waste material storage (e.g. Bachu & McEwen, 2011).

(iv) Research efforts on Mars aim to assess environmental conditions for the formation and viability of life on other planets (e.g. McLennan et al., 2019, and references therein). Insights gained from Terrestrial S2S systems might be used to assess the transferability of geological processes on Earth to Martian S2S

systems, aid in the reconstruction of palaeoenvironments and deciphering of the geologic record on Mars (e.g. Grotzinger et al., 2013; Hayden et al., 2021).

1.1 Rationale

The transport of sediment from terrestrial and intra-shelf source areas to deep-water environments is notably influenced by the presence of geostrophic currents along the margins of continental shelves (e.g. Allen & Durrieu de Madron, 2009 and references therein) and along wider shelves where the mouths of rivers are far removed from the shelf edge (e.g. Normark et al., 2009). Hence, both submarine canyons and shelf-edge deltas constitute important sedimentary systems at the shelf-to-slope transition because they enable sediment transport across this domain.

Shelf-edge deltas and submarine canyons have a crucial role for the evolution of continental margins in the following ways: (i) their role as key facilitators of sediment dispersal from terrestrial and intra-shelf environments to continental slopes and basin floors (shelf-edge deltas, e.g. Steel et al., 2003; Dixon et al., 2012; Gong et al., 2016; submarine canyons, e.g. Normark et al., 2009; Fildani, 2017); and (ii) their ability to achieve significant sizes and to form large-scale sediment sinks and longer-term archives of palaeoenvironmental conditions (shelf-edge deltas, e.g. Suter & Berryhill, 1985; Porębski & Steel, 2003; Schwartz & Graham, 2015; submarine canyons, e.g. Normark & Carlson, 2003; Anderson et al., 2006; Harris & Whiteway, 2011; Harris et al., 2014b). Moreover, the capability of submarine canyons to intercept sediment from margin-parallel currents (e.g. Patsch & Griggs, 2006; Covault et al., 2007; Smith et al., 2018; Wang et al., 2018) delimits sediment budgets transported along continental margins and the supply of sediment to S2S systems in a down-current direction (e.g. Patsch & Griggs, 2006). As such, shelf-edge deltas and submarine canyons comprise important parts of S2S systems from their control on the spatial extent and scale of S2S systems.

However, although shelf-edge deltas and submarine canyons are well-studied sedimentary systems, genetic linkages between their

geomorphologies and allogenic controls have thus far received relatively little attention compared to other sedimentary systems, despite the relevance of their morphometric characteristics in various regards.

For example, the size of a shelf-edge delta affects the geomorphology of a shelf margin (e.g. Bart & Anderson, 2004). Also, the progradation of a continental margin is driven by sediment discharge rates from rivers and the development of shelf-edge deltas (e.g. Morton & Suter, 1999; Carvajal et al., 2009). Thus, delta size might aid in estimating the order of magnitude of fluvial sediment supply to a margin. Moreover, the geometries of shelf-edge deltas may exert influence on their evolution; in larger shelf-edge deltas, autogenic processes are thought to be more influential compared to allogenic controls as sea-level fluctuations (e.g. Straub, 2019 and references therein). Furthermore, larger shelf-edge deltas with steeper surface gradients have been proposed to be more likely to promote triggering of sediment gravity flows and delta-front failure (see Sylvester et al., 2012).

Analogously, the morphology and bathymetric depth range of a submarine canyon impacts not only the local seafloor relief of a continental margin, but also the efficiency of sediment routeing to deep-water environments. Deep canyons are more likely to contain sediment transported along-canyon by intra-canyon flows and across-canyon margin-parallel currents within the confines of the canyon, although this also depends on the magnitude of the flow (e.g. Allin et al., 2016). Like shelf-edge deltas, submarine canyons exert control on the local hydrodynamic regime from their ability to focus waves and currents related to tides (e.g. Shepard, 1976; Lee et al., 2009; Waterhouse et al., 2017), storms (e.g. Shepard et al., 1977; Palanques et al., 2006a; Sequeiros et al., 2019), internal waves (e.g. Shepard et al., 1974; Hotchkiss & Wunsch, 1982; Ruiz-Angulo & Zavala-Hidalgo, 2016) and tsunami waves (e.g. Aranguiz & Shibayama, 2013; Iglesias et al., 2014), and to facilitate upwelling of water masses (e.g. Waterhouse et al., 2009 and references therein).

Results from numerical and stratigraphic forward modelling experiments indicate that canyon geomorphology exerts control on hydrodynamic processes within and adjacent to a canyon. For example, the distribution of

maximum wave heights and magnitude of run-ups of tsunamis appears to be controlled by the size of a submarine canyon, with longer and deeper canyons promoting lower run-ups (e.g. Aranguiz & Shibayama, 2013), whereas canyon width seems to variably affect both the former process and wave height patterns (e.g. Iglesias et al., 2014). In their modelling experiments, Wan et al. (2021) found that coarser sediment is more efficiently transported along shallow canyons and those with low-sinuosity compared to their deep and high-sinuosity counterparts. This indicates that the depth and sinuosity of a canyon exert control on basinward sediment transport.

Moreover, findings from the study of modern canyons suggest that their morphometric aspects including dendricity, sinuosity (e.g. Fanelli et al., 2018) and size (e.g. Santora et al., 2018) affect the biodiversity and abundance of faunal assemblages.

Since they facilitate sediment transport to slope and basin-floor environments, both submarine canyons (e.g. Nyberg et al., 2018b) and shelf-edge deltas (e.g. Porębski & Steel, 2003; Dixon et al., 2012; Gong et al., 2016) are also indicators for the presence of submarine fans. Because sand-rich delta subenvironments such as the delta plain and delta front (e.g. Covault et al., 2009; Schwartz & Graham, 2015; Gomis-Cartesio et al., 2017), and coarse-grained submarine-canyon fills (e.g. Anderson et al., 2006; Jobe et al., 2011) constitute reservoirs for hydrocarbons (shelf-edge deltas, e.g. Roberts et al., 2000; Cummings & Arnott, 2005; submarine canyons, e.g. Anderson et al., 2006), sedimentary deposits of such subenvironments possess porosities that are suitable for carbon sequestration to aid in mitigating the impact of anthropogenically induced climate change (e.g. Callas et al., 2022). Hence their sizes and geometries are relevant criteria for estimating the feasibility and efficiency of production and storage, respectively.

Nevertheless, despite the (i) suggested influence of morphologic attributes of submarine canyons and shelf-edge deltas on the evolution of continental margins and deep-water basins in view of their influence on local hydrodynamic conditions and sediment routeing to deep-water

environments, (ii) the economic relevance of canyon- and delta geometries in reservoir prospection, and (iii) the importance of submarine canyons for the thriving of marine faunal communities, the exploration of genetic linkages of the geomorphologies of shelf-edge deltas and submarine canyons with variables of their environmental setting have thus far received little attention in the literature. Although the two types of sedimentary systems have been the subject of many local- and regional-scale studies, global-scale studies are rare and have commonly focussed on only a modest subset of study variables, with limited attention towards their geomorphologies (submarine canyons, e.g. Nelson et al., 1970; Harris & Whiteway, 2011; shelf-edge deltas, e.g. Dixon et al., 2012; Gong et al., 2016). Similarly, few experimental and modelling studies exist that have explored the efficiency in routeing sediment to deep-water environments as a function of their morphometric characteristics (e.g. Wan et al., 2021) and environmental variables (e.g. Straub, 2019; Wan et al., 2021). As a consequence, the factors that control the morphologies of shelf-edge deltas and submarine canyons and their morphological variabilities, and their relative importance, are still not well understood.

Therefore, given the importance of shelf-edge deltas and submarine canyons as components of S2S systems and their economic and ecologic relevance, knowledge of controls on their morphometries would aid in (i) assessing the likelihood of sediment dispersal to deep-water environments and development of intra-slope or basin-floor depositional systems, (ii) reconstructing and predicting their geomorphologies, and (iii) identifying margins and stratigraphic intervals where boundary conditions existed that promoted the development of large shelf-edge deltas and canyons; in turn, (iv) information on palaeoenvironmental characteristics of their associated continental margins and external controls can be inferred from their morphometric attributes. Such insights would be particularly valuable in geographic regions where it is challenging to reconstruct the spatial extent, configuration and geomorphic characteristics of entire S2S systems and their subenvironments due to limited subsurface coverage, scarcity and spatial limitations of outcrops, and where the original configuration of

palaeoenvironments is fragmented due to tectonic activity, and for the modelling of ancient and future margin environments from sedimentary-system to margin scale.

Based on the above incentive and the existing research gaps, the following three research questions have been identified as a framework for this project:

- **Research Question 1:** *How variable are morphometric attributes in shelf-edge deltas and submarine canyons in general and as a function of environmental controls?*

Research question 1 addresses the limited knowledge of variability of morphometries in the two sedimentary-system types both in general and as a function of specific environmental attributes as a result of the scarcity of both regional-scale (e.g. Huang et al., 2014) and global-scale (e.g. Nelson et al., 1970; Harris & Whiteway, 2011; Harris et al., 2014b) quantitative studies of submarine canyons that have considered attributes of canyon geomorphology, and the lack of quantitative shelf-edge delta studies that have evaluated their morphometric characteristics (see Chapter 2).

- **Research Question 2:** *Is it possible to reliably reconstruct or predict the original geomorphologies of both shelf-edge deltas and submarine canyons, respectively, based on outcrop and subsurface data that provide (i) partial knowledge of values of their morphometric attributes, and (ii) information on variables of their physiographic- and environmental setting?*
- **Research Question 3:** *By having knowledge of such linkages, can boundary conditions for the development of certain morphotypes of shelf-edge deltas and submarine canyons be identified?*

Research questions 2 and 3 are founded on the limited knowledge of controlling factors of morphometric characteristics of both shelf-edge deltas and submarine canyons, and as a result the paucity of conceptual and numerical models of their morphologies on both sedimentary-system and S2S system scale. Shelf-edge deltas tend to be underrepresented in conceptual models of S2S systems, whereas submarine canyons are

commonly represented but with only limited consideration of their geomorphology (e.g. Sømme et al., 2009; Nyberg et al., 2018b). Moreover, existing conceptual (e.g. Jobe et al., 2011; Micallef et al., 2014) and numerical models (e.g. Wan et al., 2021), which address aspects of submarine-canyon geomorphology, are commonly based on regional studies tied to specific sets of environmental controls, or are derived from global studies but limited to the evaluation of few morphometric characteristics and/or environmental controls (e.g. Harris & Whiteway, 2011). These circumstances raise the question of whether these models are universally applicable. For shelf-edge deltas, no conceptual models presently exist that are based on quantitative analyses of their morphologies (see Chapter 2).

Thus, answering the three research questions posed herein has important implications for the validation and improvement of existing conceptual models of shelf-edge deltas and submarine canyons and their associated S2S systems, and understanding of the geomorphologic evolution of continental margins.

The quantitative, global scale investigation of submarine canyons and shelf-edge deltas constitutes a useful means to address these research questions because it allows for the assessment of their morphometric characteristics across diverse environmental settings. Due to their often-large scale, with widths and depths of the orders of several kilometres (e.g. Harris & Whiteway, 2011; Harris et al., 2014b), the preserved fills of large canyons tend to be only partially exposed in outcrop (Anderson et al., 2006), which impedes the study of their geomorphology from ancient examples. Hence, the widespread presence of submarine canyons with present-day expression on the seafloor (e.g. Harris & Whiteway, 2011; Harris et al., 2014b) provides a valuable prerequisite for the quantitative study of these systems in modern environments; such features provide a good spatial control of the S2S system and its characteristics. In contrast, the relative rareness of modern examples of shelf-edge deltas (e.g. Daniell et al., 2020) requires a different approach: their study requires examination of the depositional record but with acknowledgement that information on their environmental setting is likely to be more limited.

1.2 Aim and Objectives

The aim of this research is to develop understanding of factors that control the geomorphologies of sedimentary systems at the shelf-to-slope transition. To realise this aim, morphometric characteristics of (i) submarine canyons and (ii) shelf-edge deltas have been quantitatively investigated on a global scale, utilising a relational-database approach.

Specific research objectives of this work for the overall project are as follows:

(I) To evaluate the variability of morphometric attributes in (i) submarine canyons and (ii) shelf-edge deltas, respectively, on a global scale, both in general and as a function of different environmental variables.

(II) To assess the existence and nature of scaling relationships of morphometric attributes with each other in (i) submarine canyons and (ii) shelf-edge deltas, respectively, and with variables of their physiographic setting and associated S2S systems.

(III) To revise and extend existing conceptual models of (i) submarine canyons and (ii) shelf-edge deltas, respectively, in context of their superordinate S2S systems and accommodating continental margins.

(IV) To establish causal links between the environmental setting (at the scale of both individual S2S systems and entire continental margins) and the efficiency of sediment routeing to deep-water environments via (i) submarine canyons and (ii) shelf-edge deltas, respectively, as a function of their morphometries.

An overview of key variables investigated in this research project is provided in Figure 1.1.

1.3 Methodology

To achieve the aim of this project and to fulfil the specific related research objectives, this work has conducted quantitative, statistical analyses of morphometric attributes of submarine canyons, shelf-edge deltas and their

associated physiographic- and environmental settings in a source-to-sink framework. To enable this, high-resolution datasets from field-, seafloor- and subsurface studies in peer-reviewed publications and government agency sources, as well as open-source worldwide bathymetry (GEBCO 2019 NOAA NCEI Visualization; Google Earth) were utilised to extract information on the variables under investigation.

The research project is organised into three individual studies, with each focussing on a particular subset of research objectives and study variables. For each of the three studies, a catalogue of study parameters tailored towards the aim and specific research objectives has been developed (Fig. 1.1).

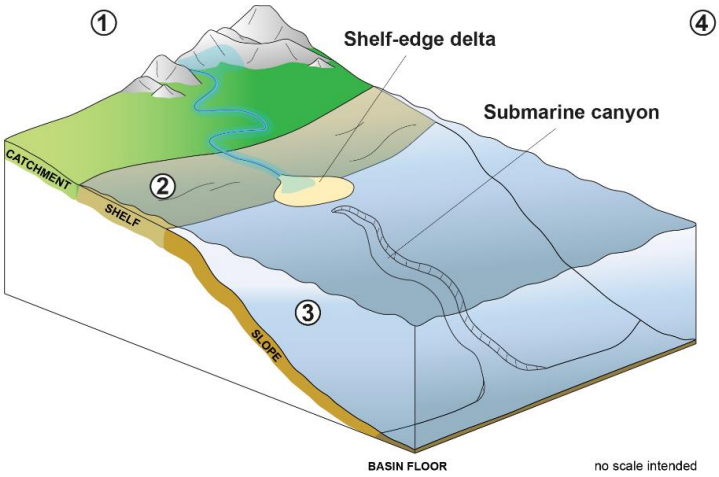

SHELF-EDGE DELTA	SUBMARINE CANYON	CATCHMENT	SHELF	SLOPE	EXTERNAL CONTROLS
Geomorphology: *delta-element dimensions; area*	**Geomorphology:** *dimensions; av. canyon sinuosity; av. canyon thalweg gradient; canyon sidewall steepness*	**Fluvial system:** *length; average annual fluvial discharge; feeder-system type*	**Geomorphology:** *width; depth; average gradient*	**Geomorphology:** *width; depth; average gradient*	**Tectonic setting**
					S2S system setting
					Oceanographic environment
Physiographic setting: *latitude*	**Physiographic setting:** *canyon bathymetry; distance to shoreline; latitude*	**Terrestrial catchment:** *area; maximum elevation* ①	②	③	**Hydrodynamic-process regime** ④

Figure 1.1 Schematic figure of a shelf-edge delta and submarine canyon within the context of a source-to-sink system and overview of key study variables considered in the research project. (SC1), (SC2) and (SED) refer to which of the external controls were investigated in the three different metastudies in data chapters 3, 4 and 5, respectively: SC1 = Submarine-canyon study 1 (Chapter 3) SC2 = Submarine-canyon study 2 (Chapter 4) SED = Shelf-edge delta study (Chapter 5).

Each individual study is based on a global dataset:

(i) *Dataset 1* constitutes a global compilation of submarine-canyon geomorphology and comprises 282 submarine canyons with expression on the present-day seafloor based on 135 literature data sources.

(ii) *Dataset 2* is an extension of dataset 1 and holds information on 294 modern submarine canyons with data derived from 136 literature sources.

(iii) *Dataset 3* was obtained from 50 literature sources and consists of 112 shelf-edge deltaic elements of Permian to Late Quaternary age.

To minimise bias arising from an imbalanced study selection, the shelf-edge deltas and submarine canyons were chosen with the aim to compile datasets that were representative of a wide range of geographic distributions and environmental settings.

For the digitisation of the datasets, the data have been coded in compliance with the database standards of two relational databases developed by the Sedimentology Group of the University of Leeds: (i) the *Deep-Marine Architecture Knowledge Store* (DMAKS) (datasets 1 & 2); and (ii) the *Shallow-Marine Architecture Knowledge Store* (SMAKS) (dataset 3). Both databases enable the storage of data on sedimentary systems from system- to facies-scale, following a hierarchical approach (see Colombera et al., 2016; Cullis et al., 2019). To achieve the aim and research objectives set for the overall project and its individual parts, both existing attributes already used in the SMAKS and DMAKS databases and an extensive number of newly defined attributes – created in alignment with the existing database standards – have been utilised. In the course of the project, the database schemes and the contained data populations have been further developed.

In the analysis of the available data, the following types of statistical methods have been applied to characterise scaling within shelf-edge deltas and submarine canyons and to explore scaling relationships with attributes of their associated S2S system and environmental setting:

(i) *Descriptive statistics* quantitatively characterise frequency distributions of studied parameters in terms of minimum, mean, median and maximum values;

(ii) *Hypothesis testing* allows to investigate statistical differences in mean values of studied parameters as a function of different physiographic and environmental factors;

(iii) *Correlation analysis* assesses the existence, strength and nature of scaling relationships between two study parameters.

An overview of the workflow of this project is given in Figure 1.2. The different types of statistical analyses, and the extent to which they have been applied in each study, are discussed in detail in chapters 3, 4 and 5.

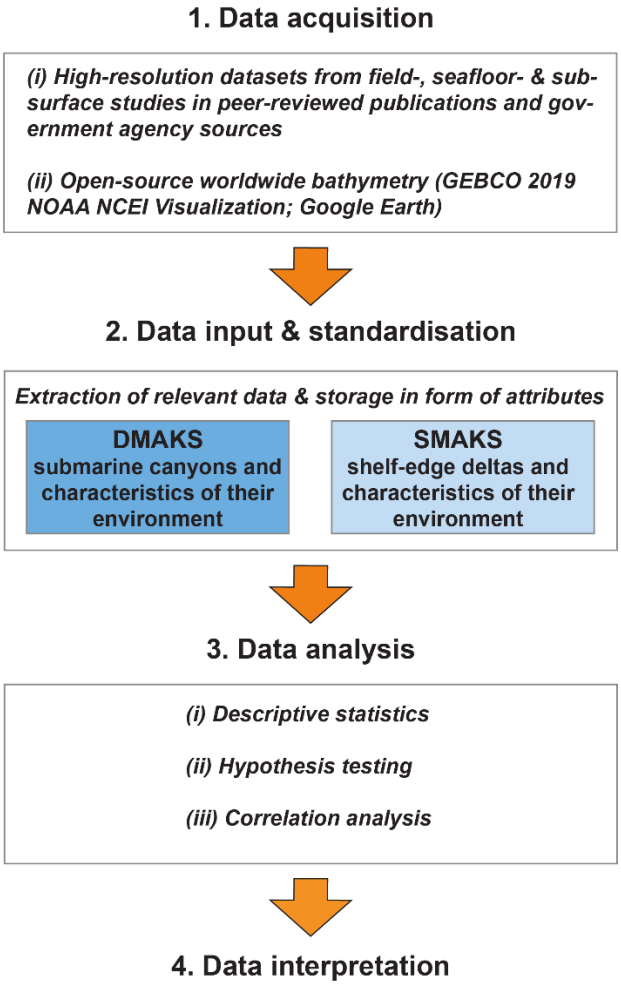

Figure 1.2 Schematic overview of the overarching workflow of this research project. DMAKS = Deep-Marine Architecture Knowledge Store (e.g. Cullis et al., 2019); SMAKS = Shallow-Marine Architecture Knowledge Store (e.g. Colombera et al., 2016).

1.4 Thesis outline

The thesis is organised into seven chapters, including a background chapter (Chapter 2), three data chapters corresponding to the three research studies (Chapters 3, 4 & 5) and a discussion chapter (Chapter 6), which integrates findings from the three studies and addresses the overarching research objectives of this work. Chapter 7 gives a summary of the key insights and identifies potential areas of research for future work.

A complete list of the study variables investigated in each study, and their definitions, are provided in Appendix A. Appendix B contains the raw datasets used in the three studies. Appendix C comprises the two published versions of data chapters 3 and 4, respectively.

The following sections constitute an overview of the chapters of this thesis.

1.4.1 Chapter 2: Background

This chapter presents a review of the literature relevant to this project, providing in-depth background on controls on the evolution of submarine canyons and shelf-edge deltas that have been identified from their studies, and an assessment of the role of their morphologies in existing conceptual models and classification schemes. Moreover, Chapter 2 provides an overview of the S2S system and its configuration and introduces key terms and their definitions. The complexity of S2S systems is highlighted, which contrasts with the current state of conceptual S2S system models in the literature, which tend to be oversimplified. Despite this, a diverse range of classification schemes of S2S systems exists. Furthermore, the importance of submarine canyons and shelf-edge deltas for the evolution of continental margins and deep-water systems is highlighted. Lastly, the key research gaps that were identified from the review and which formed the framework for this project are summarised.

1.4.2 Chapter 3: A global analysis of controls on submarine-canyon geomorphology

The role of possible controlling factors in influencing the geomorphology of submarine canyons has been investigated using a database of 282 globally distributed modern examples collated from the literature and open-source

worldwide bathymetry. Canyon geomorphology has been characterised quantitatively in terms of maximum and average canyon dimensions, canyon sinuosity, average canyon thalweg gradient, and maximum canyon sidewall steepness. An assessment is made of how geomorphological characteristics vary with respect to the position of the canyon apex relative to the shelf break, continental-margin type, terrestrial source-to-sink system setting, oceanographic environment, and latitude. Scaling relationships between canyon morphometric parameters, and correlations between these and attributes of the canyon-physiographic settings, terrestrial catchments, and continental shelves and slopes, have been quantified.

1.4.3 Chapter 4: Tectonic influence on the geomorphology of submarine canyons: implications for deep-water sedimentary systems

This chapter presents a database-informed metastudy of 294 globally distributed submarine canyons has been conducted with the aim of elucidating the role of tectonic setting on submarine-canyon geomorphology. To achieve this, data from seafloor and subsurface studies derived from 136 peer-reviewed publications and from open-source worldwide bathymetry datasets have been statistically analysed. In particular, relationships between margin type (active vs. passive) or plate-boundary type (convergent vs. transform vs. complex) have been assessed for key morphometric parameters of submarine canyons, including: streamwise length, maximum and average width and depth, canyon sinuosity, average canyon thalweg gradient, and maximum canyon sidewall steepness. In addition, possible scaling relationships between canyon morphometric parameters and characteristics of the associated terrestrial catchment, continental shelf and slope, and of the broader physiographic setting for canyons along both active and passive margins have been evaluated.

1.4.4 Chapter 5: Sedimentary characteristics of shelf-edge deltas in a source-to-sink context

Despite their important role in sediment dispersal to marine environments, and their influence on the geomorphology and hydrodynamic setting of continental margins, shelf-edge deltas are commonly overlooked in source-

to-sink models, perhaps because few are developed during present-day highstand conditions. In subsurface and outcrop, their recognition can be difficult where information on the physiographic context is limited. Moreover, it has yet to be determined in detail whether specific architectural and geometric characteristics of accumulated deposits of these deltaic systems can be linked to specific attributes of their environmental setting.

To address these issues, a comparative, global scale metastudy of the sedimentology and geomorphology of 112 Permian to late Quaternary delta lobes and delta complexes has been undertaken to increase the understanding of factors that govern the geometric characteristics of deltaic architectural elements and of relationships between delta geometry (length, width, thickness and area) and attributes of their palaeoenvironmental setting (characteristics of the associated terrestrial catchment and shelf, latitudinal position).

1.4.5 Chapter 6: Discussion

In Chapter 6, the novel findings from the three metastudies are used to introduce new holistic end-member models of morphologic attributes of shelf-edge deltas and submarine canyons as a function of attributes of their superordinate S2S systems and environmental settings. Moreover, the results are discussed and compared with those of other quantitative meta-analyses of sedimentary systems. Furthermore, their implications for the efficiency of sediment dispersal to deep-water environments in S2S systems comprising a shelf-edge delta and/or submarine canyon in their configuration are addressed. In addition, scientific and industrial applications of the identified scaling relationships are highlighted, and limitations of this approach.

1.4.6 Chapter 7: Conclusions

Chapter 7 summarises the key findings of the three metastudies and their discussion within the framework of the aim and research objectives of the overarching project (see section 1.2). This chapter revisits and answers the research questions that have motivated this project (see section 1.1). In

addition, implications of the insights gained for future studies are discussed, and potential routes of future research are identified.

2 Background

2.1 Introduction

This chapter provides a literature review of the current state of research on controls of the evolution and geomorphologies of submarine canyons and shelf-edge deltas, and an overview of key definitions and concepts in source-to-sink (S2S) research and existing conceptual models, which led to the identification of the current gaps in research knowledge that this project seeks to address.

The geomorphology of any sedimentary system is the result of the combined influence of a set of dynamic processes, autogenic and allogenic controls, characteristics of the accommodation, and the nature (type and rate) of sediment supply over time. As sedimentary systems at the interface between different sedimentary environments, the morphologic evolution of submarine canyons and shelf-edge deltas is influenced by a multitude of factors. Sections 2.2 and 2.3 review controlling factors of the evolution of submarine canyons and shelf-edge deltas and their resulting geomorphologies, respectively, and compare how the current state of knowledge of the two system types translates to their conceptual models and classification schemes.

Section 2.4 provides an overview of the source-to-sink (S2S) concept in sedimentary research – including definitions of key terms which are used in this project – and addresses the limitations of existing conceptual models and classification schemes of S2S systems in the literature.

Section 2.5 examines the important roles of submarine canyons and shelf-edge deltas for the evolution of continental margins and their associated deep-water environments. It highlights the stark contrast between the acknowledged important influence of the two sedimentary system types on sediment transport dynamics within marine parts of S2S systems, and the lack of consideration of shelf-edge deltas and only limited consideration of submarine canyons in conceptual models and classification schemes of S2S systems in the literature.

Section 2.6. provides a short summary of the key research gaps that have emerged from the literature review in sections 2.2 to 2.5, which themselves have inspired this research project.

2.2 Controlling factors of submarine canyons

2.2.1 Submarine canyon definition

Submarine canyons are channel forms located within the slopes of continental margins (Fig. 2.1a). The criteria used by authors in the definition of a submarine canyon and to differentiate it from other geomorphologic features (e.g. fan valleys; Shepard, 1972; submarine gullies; Gales et al., 2013) vary in the literature, sometimes significantly. Submarine canyons have been variably defined based on their (i) genetic origin (e.g. Shepard, 1972), (ii) physiography (e.g. minimum dimensions, e.g. Harris & Whiteway, 2011; cross-sectional shape type (e.g. Shepard, 1972; Huang et al., 2014), and (iii) bathymetric setting (e.g. Harris & Whiteway, 2011), amongst other factors. These variations in definition are important with regard to quantitative studies of submarine canyons because they can significantly influence or alter the outcomes of the analyses. For example, the chosen criteria affect the number of canyons that might be recognised in a certain geographical area, or the representation of canyons with certain characteristics in a sample size.

In addition, where two or more canyons are interconnected with each other, the term ‘canyon system’ has been applied in the literature (e.g. Mountjoy et al., 2009; Bernhardt et al., 2015) (Fig. 2.1b).

This study defines a submarine canyon as a single, predominantly erosional channelform incised into the continental slope. This has been done for the following reasons:

(i) The definition specifies “predominantly erosional” to acknowledge that, although erosional processes such as sediment gravity flows and slope failure constitute processes commonly associated with canyon formation (e.g. Pratson et al., 2007), the channelform of a submarine canyon can also incorporate preexisting seafloor relief

with little or no downcutting involved (e.g. Twichell et al., 2000; Urías Espinosa et al., 2016) and can become enlarged through aggradation along its margins (e.g. Armitage et al., 2010; Soulet et al., 2016).

(ii) Because submarine gullies are thought to constitute channelforms in the early stage of canyon formation (e.g. Amblas et al., 2017), and smaller-scale channelforms on the slope have been variably referred to as submarine canyons and gullies (e.g. Alonso & Ercilla, 2003; Gervais et al., 2004; 2006; Chen et al., 2017; Susanth et al., 2021), the chosen definition disregards canyon dimensions and bathymetric setting, itself related to the length of a canyon.

(iii) Given that submarine canyons can evolve from the co-occurrence and interplay of various processes, including sedimentary, hydrodynamic, structural and biogenic processes (see section 2.2.2.1) the definition does not consider the genetic origin as a factor.

The landward part of a submarine canyon is referred to in the literature as “canyon head” (e.g. Harris & Whiteway, 2011; Smith et al., 2018; Bernhardt & Schwanghardt, 2021). In this project the term “canyon apex” is used *sensu stricto* for the point of the shallowest bathymetry along the canyon apex, whereas the term “canyon head” is used *sensu lato* for the proximal area in a submarine canyon. The canyon mouth is defined here as the most distal point of the canyon along its axis, where the canyon cross-sectional profile is no longer distinguishable from the surrounding seafloor.

A.

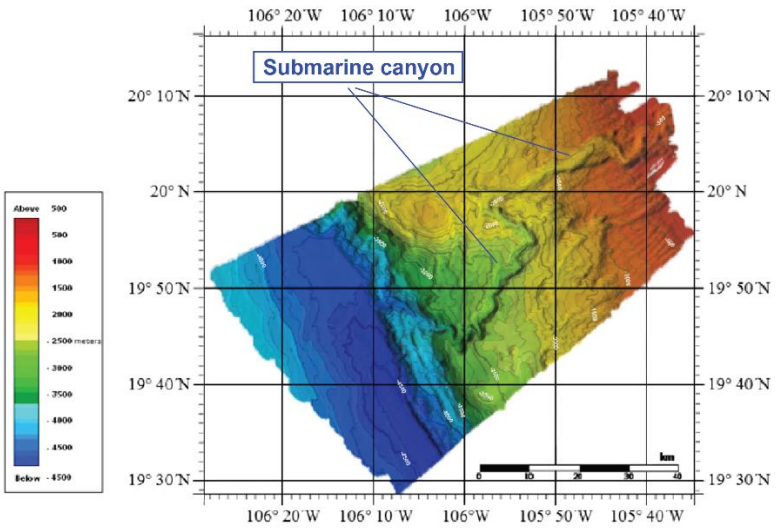

Urías Espinosa et al. (2016)

B.

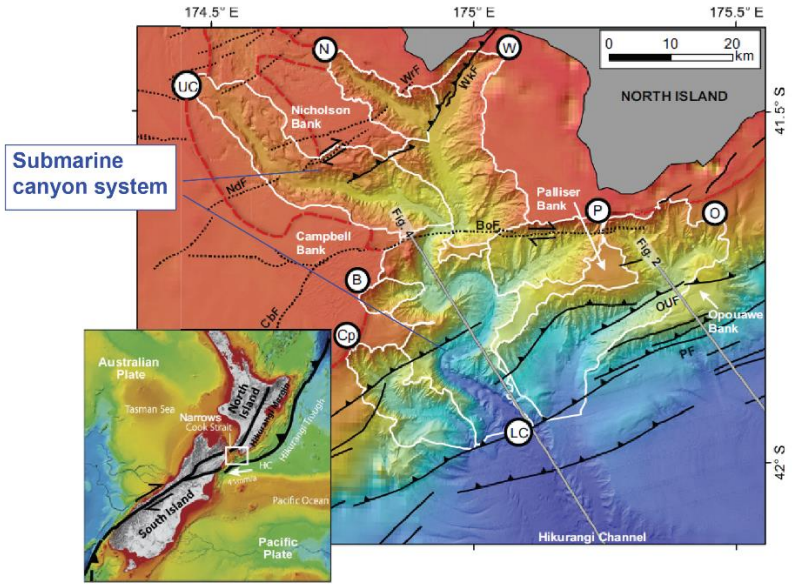

Micallef et al. (2014)

Figure 2.1a&b A. High-resolution bathymetric map of an example of a submarine canyon on the modern seafloor: Ipala Canyon offshore W Mexico (Urías Espinosa et al., 2016). B. High-resolution bathymetric map depicting a canyon system constituting of several canyons: Cook Strait Canyon system, New Zealand (Micallef et al., 2014). Added text in blue.

2.2.2 Submarine canyon evolution

Although submarine canyons are generally well studied sedimentary systems (e.g. Matos et al., 2018), the genesis and long-term evolution of

submarine canyons remains a topic of ongoing debate (e.g. Pratson et al., 2007 and references therein; Smith et al., 2017, 2018).

This is despite technological advances in data acquisition and processing throughout the last decades, which allowed for more precise observations of flow processes in submarine canyons (e.g. Shepard, 1981; Xu, 2011; Paull et al., 2018) and analyses of their deposits (e.g. Maier et al., 2019).

2.2.2.1 Processes influencing canyon evolution

An important consideration for the evaluation of controlling factors of submarine canyon and shelf-edge delta geomorphologies is the identification of the processes that influence their evolution. A review of the literature on submarine canyons shows that they can evolve from a variety of processes related to (i) sedimentary, (ii) hydrodynamic, (iii) biogenic, and (iv) tectonic processes, which themselves are influenced by environmental factors.

Erosional and aggradational sedimentary processes

The erosion of seafloor by (i) slope failure and (ii) sediment gravity flows are considered the two main mechanisms that facilitate the initiation of submarine canyons and promote their evolution by retrogressive erosion at the canyon apex and down-slope growth by erosive intra-canyon flows that extend beyond the mouth of the canyon (e.g. Shepard, 1972; 1981; Pratson et al., 2007; Lai et al., 2016). The morphologic evolution of a canyon can also be governed by aggradational processes related to sediment deposition within its channel and onto its margins from intra-canyon sediment gravity flows (e.g. Straub & Mohrig, 2009; Armitage et al., 2010; Soulet et al., 2016), margin-parallel currents (e.g. Rona, 1970), and hemipelagic fallout (e.g. Armitage et al., 2010; Jobe et al., 2011).

Marine hydrodynamic processes

Marine hydrodynamic processes are important processes for the evolution of submarine canyons due to their ability to transport sediment to submarine canyons, for example via longshore currents (e.g. Covault et al., 2011b), slope currents (e.g. Warratz et al., 2019), tidal currents and waves (e.g. Mountjoy et al., 2014), storm currents and waves (e.g. Sequeiros et al., 2019), and dense shelf water cascading (e.g. Gaudin et al., 2006; Palanques

et al., 2006a). Moreover, where water masses flow across a submarine canyon, as margin-parallel currents (e.g. Wang et al., 2018), or along the canyon axis, as tidal currents (e.g. Mountjoy et al., 2014; Mulder et al., 2012), internal waves (e.g. Wang et al., 2022b), else as upwelling (e.g. Huhn et al., 2007; Brun et al., 2023) or downwelling (e.g. Palanques et al., 2006a) water masses, these processes might promote intra-canyon erosion and both counteract or enhance sediment transport dynamics within a submarine canyon. However, despite their importance, the interplay of bottom currents, down-canyon flows, and canyon morphology are still little understood and require further research (e.g. Mencaroni et al., 2021).

Biogenic processes

Another factor that has been invoked as a potential control on canyon evolution is the biogenic activity of organisms and their products. Where reef systems have developed along a margin, their presence might influence canyon evolution from their impact on the strength (e.g. Oiwane et al., 2011) and topography (e.g. Puga-Bernabéu et al., 2011) of seafloors, and their function as a sediment source to canyons from their production of carbonate (e.g. Shepard, 1972). Moreover, the colonization of canyon walls by organisms might variably increase or decrease the stability of canyon margins (e.g. Shepard, 1981; Eittreim et al., 1982).

Tectonic processes

Tectonic processes can affect the evolution of submarine canyons in multiple and complex ways. Along margins with tectonic activity canyons can occupy seafloor topography created by faulting and extensional tectonics, and might preferably form along fault lines where the substrate is weakened and topographic lows are created (e.g. Shepard, 1981; Greene et al., 1991; Algan et al., 2002; Urías Espinosa et al., 2016; Serra et al., 2020). Developing faults can also cut off a submarine canyon from sediment sources (e.g. Chiang et al., 2012), function as a sediment source from their promotion of seafloor erosion (e.g. Han et al., 2010), and modify the geomorphology of a submarine canyon. For example, strike-slip faults can increase canyon width by shifting the canyon thalweg and focus of erosion of intra-canyon flows (e.g. Micallef et al., 2014). Where canyons incorporate

topographic lows created by faults, the orientation of faults at a high angle to the margin can significantly increase their overall sinuosity (e.g. Urías Espinosa et al., 2016). The association of narrow shelves with margin convergence creates favourable conditions for the sediment connection of submarine canyons with rivers and littoral cells along active convergent margins (e.g. Bernhardt & Schwanghart, 2021).

Salt movement

Salt tectonics linked to the movement of salt and the impact of salt diapirs on seafloor topography are factors that can influence the evolution of a submarine canyon from their control on sediment transport pathways (e.g. Cumberpatch et al., 2021 and references therein) and where canyons occupy seafloor relief modified by salt movement (e.g. Twichell et al., 2020).

2.2.2.2 Canyon-physiographic setting

From its control on the ability of a submarine canyon to intercept sediment, the physiographic setting of a submarine canyon constitutes a crucial factor for its geomorphologic evolution.

Location of the canyon head relative to the shelf break

The spatial extent of a submarine canyon along a continental margin determines, to some degree, the range of processes and source areas it potentially has access to. Within the continental slope, submarine canyons can receive sediment from slope-parallel currents (e.g. Warratz et al., 2019; Serra et al., 2020) and from localised slope failure along their margins (e.g. Serra et al., 2020). Retrogressive erosion within a submarine canyon from intra-canyon failure at the canyon apex constitutes an autogenic process that is perceived to be particularly important for the evolution of slope-confined canyons due to their limited access to terrestrial and intra-shelf sediment sources (e.g. Farre et al., 1983; Pratson et al., 2007); some authors even consider it as the sole facilitator of evolution in slope-confined canyons (e.g. Harris & Whiteway, 2011). However, findings from canyon studies challenge this perception suggesting that within the continental slope, sediment supply by (i) slope-parallel currents (e.g. Warratz et al., 2019; Serra et al., 2020; Rodrigues et al., 2022), and (ii) hemipelagic fallout

(e.g. Armitage et al., 2010; Jobe et al., 2011) can be important drivers of canyon evolution. Moreover, fluvial discharge and intra-shelf sediments can also be distributed to a slope-confined canyon given the canyon is located within runout distance of sediment gravity flows (e.g. Cronin et al., 2005).

It has been suggested that many of the present-day submarine canyons that are incised into modern shelves had established sediment connections with fluvial systems during past sea-level lowstands when rivers had prograded onto the shelf margin (e.g. May et al., 1983), highlighting the importance of fluvial sediment discharge on the evolution of a submarine canyon. As such, fluvial discharge is considered to be an important evolutionary mechanism for shelf-incised canyons (see section 2.2.2.2). Shelf-incising canyons also potentially have access to sediment from intra-shelf source areas such as unconsolidated shelf deposits (e.g. Piper & Normark, 2009; Pierau et al., 2011) and littoral cells (e.g. Normark et al., 2009; Covault et al., 2007; 2011b). In addition to, or absence of fluvial transport, terrestrial sediment can be supplied to submarine canyons by unconfined flows related to catastrophic events, as volcanic eruptions (e.g. Klaus & Taylor, 1991), aeolian transport, as fallout from volcanic eruptions (e.g. Klaus & Taylor, 1991) and fine-grained sediment transported by winds (e.g. Pierau et al., 2010; 2011), and by the erosion of cliffs and coastlines (e.g. Noda & Tuzino, 2010; Parra et al., 2012). It is also important to stress that the connection of a submarine canyon to the shelf might also be controlled by high sediment supply and depositional rates in its proximal part (e.g. Smith et al., 2005), which can cause the progradation of the canyon head onto the continental slope (e.g. Mauffrey et al., 2015).

Distance of the canyon to fluvial outlets and littoral cells

Independent of the type of sediment transport processes that are active along a continental margin – such as sediment gravity flows, longshore drift and tidal currents, to name a few – and the source areas that are present, the efficiency of sediment dispersal to a submarine canyon is ultimately controlled by the available volume of sediment and distance of the canyon to the sediment source. The dependency of transport radii of grain fractions from grain size from a point source was demonstrated in a global analysis of deposits within submarine canyons associated with margins with fluvial

outlets and littoral cells by Sweet & Blum (2016). The authors identified transport threshold distances for gravel-sized sediment of ≤ 500 m, sand between 1 km and 5 km, and silt and clay of up to 40 km, which demonstrates the importance of the distance of a canyon to shorelines and associated fluvial outlets, and to littoral cells.

2.2.2.3 Environmental variables

The occurrence of processes, and their magnitude, that influence the evolution of a submarine canyon (section 2.2.2.1), and the canyon-physiographic setting (section 2.2.2.2) are influenced by a multitude of environmental variables, some of which are discussed in the following sections.

Climate

Climate, principally through precipitation, influences erosion rates within terrestrial catchments (e.g. Milliman & Farnsworth, 2011; Clift, 2020). This in turn controls terrestrial sediment supply to submarine canyons including fluvial sediment discharge and coastal erosion. In arid regions sediment can be supplied to canyons by aeolian transport or where aeolian dunes formed during sea-level lowstand on emerged shelves and are subsequently eroded during later rising of sea level (e.g. Henrich et al., 2010; Pierau et al., 2010). Furthermore, the latitudinal position of a canyon can determine the availability of sediment type and dominant transport process in canyon evolution. In low-latitudinal regions, carbonate sediments from reef systems can constitute a significant sediment source (e.g. Tournadour et al., 2017), whereas in high-latitudinal regions, submarine canyons can receive sediment transported by glacial processes (e.g. Armitage et al., 2010; Gales et al., 2021). In addition, seasonal variability in the magnitude of hydrodynamic processes as dense shelf-water cascading (e.g. Palanques et al., 2006a) and surface currents (e.g. Li et al., 2022) can exert control on the volume of sediment distributed to a submarine canyon.

Sea level

Another factor that exerts influence the evolution of submarine canyons is sea level, via its control on sediment connection of canyons with intra-shelf

and terrestrial sediment sources. During lowering of sea-level and lowstands, fluvial sediment supply to a canyon is promoted where rivers have cut into emerged shelves and their mouths reach the shelf margin (e.g. Mauffrey et al., 2017), and littoral cells are pushed basinward in vicinity of canyon heads (e.g. Covault et al., 2007). In the course of the subsequent transgression and highstand phases, the sediment connection tends to be lost due to the retreat of the shoreline, unless the shelf is sufficiently narrow and/or the canyon is retrograded in front of the river mouth (e.g. Covault et al., 2007; Normark et al., 2009; Sweet & Blum, 2016). However, throughout the transgression, wave ravinement of shelf deposits, including of intra-shelf and shelf-edge deltas (e.g. Ferro et al., 1999; Yoo et al., 2017), might function as a local source of sediment supply to a canyon. The sediment connection of some canyons with rivers during present-day sea level highstand via longshore current transport (e.g. Covault et al., 2007; 2011b), and where canyons have retrograded in front of rivers along very narrow shelves (e.g. SW Taiwan margin, Liu et al., 2016), demonstrates that sediment connection of a canyon with terrestrial and intra-shelf source areas is not necessarily linked to lowstand conditions (e.g. Posamentier et al., 1991).

Configuration of shelves and slopes

Morphologic characteristics of shelves and slopes can exert influence on canyon evolution from their role as accommodation, and their control on sediment transport pathways. Narrow shelves are advantageous for sediment connection of submarine canyons with rivers, littoral cells, and intra-shelf source areas, because they facilitate short distances both for the across-shelf transport of sediment and for the retrogradation of canyons to the shoreline. However, along margins with wide and shallow shelves the shelf area that emerges during phases of sea level regression is larger compared to that of narrow shelves; this might provide significant locally sourced sediment to a canyon from the incision and excavation of shelf substrate by incised valleys (e.g. Blum & Hattier-Womack, 2009) and the erosion of intra-shelf deposits both during regressive and transgressive phases (e.g. Pierau et al., 2010). Also, land-detached canyons can remain

active during highstand conditions by sediment supply from within the shelf (e.g. Whittard Canyon; Heijnen et al., 2022).

The widths of the continental shelf and slope inherently delimit the length of a submarine canyon. Moreover, steep gradients within both subenvironments promote seafloor failure and the runout distance of sediment gravity flows; both are important processes for canyon evolution (see section 2.2.2.1). Furthermore, where continental slopes are characterised by rugose intra-slope relief, such depressions can retain sediment, decreasing the strength and runout distance of intra-canyon flows (e.g. Hsiung et al., 2014). Submarine canyons that incorporate intra-slope basins in their pathways may depart from simple geomorphic profiles, for example by locally increasing canyon width where the canyon crosses the basin (e.g. Twichell et al., 2000).

Terrestrial catchment characteristics

Fluvial sediment supply is considered an important factor for the evolution of submarine canyons. In particular, hyperpycnal flows developed at river mouths related to flooding events facilitate the transport of fluvial sediments across shelves into canyon heads (e.g. Puig et al., 2014 and references therein) and can achieve great runout lengths where they transition into turbidity currents (e.g. Zhao et al., 2018; Talling et al., 2022). Hence, the size of a drainage basins from its direct control on source area size and its influence on fluvial discharge rates (e.g. Sømme et al., 2009; Milliman & Farnsworth, 2011) constitutes a control on sediment dispersal to submarine canyons in front of rivers and canyons connected with a river via longshore current transport.

Lithology of source sediment and substrate

The lithology of source sediment might affect canyon evolution by influencing both sediment transport dynamics within a gravity flow, and the degree of erosion of the flow. For example, cohesive sediment gravity flows tend to have shorter runout distances compared to non-cohesive flows (e.g. Baker et al., 2017). Furthermore, substrate lithology of the shelf and slope affects the erodibility of the seafloor (e.g. Oiwane et al., 2011) and in turn the

ability of a canyon to increase in size. Another factor that influences the runout distance of marine sediment gravity flows, and their ability to reach canyon heads and fully traverse a canyon beyond its mouth, is the magnitude of a sediment gravity flow (e.g. Talling et al., 2022).

The above discussion identifies a great variety in sediment sources, sediment transport processes and pathways. The recognition of many controls highlights the complex influence of factors on the evolution of submarine canyons.

2.2.3 Submarine canyon studies

2.2.3.1 Research bias in submarine canyon studies

Submarine canyons are ubiquitous features along modern continental margins, as documented in the global inventories by Harris & Whiteway (2011) and Harris et al. (2014b), who identified 5,849 and 9,477 submarine canyons worldwide, respectively. The abundance of published studies on submarine canyons has been quantified by an epistemic study of the scientific literature on submarine canyons conducted by Matos et al. (2018), who recorded 1,968 publications published between 1929 and 2016 on this topic.

However, despite this large number of publications, which suggest that submarine canyons are well studied sedimentary systems, the results by Matos et al. (2018) revealed several examples of bias in canyon research. The authors identified a regionalisation of canyon studies, with the literature covering less than 10% of the worldwide recognised canyons by Harris et al. (2014b) and almost half of the 1,968 publications referring to only 11 submarine canyons. Regarding the understanding of controlling factors of submarine canyons, this is problematic: it demonstrates that many of the findings in the literature are derived from specific geographic areas with specific sets of environmental conditions on both local and regional scale. Hence, the applicability of such insights to submarine canyons and regions with different controls is uncertain, and due to the paucity of global-scale studies with focus on submarine canyons (e.g. De Pippo et al., 1999; Harris & Whiteway, 2011), is difficult to assess.

2.2.3.2 Evaluation of aspects of submarine-canyon geomorphology in quantitative studies

Although submarine canyons have been comparatively investigated in prior studies in a global (e.g. Shepard, 1981; De Pippo et al., 1999; Harris & Whiteway, 2011; Harris et al., 2014b), continental (e.g. Huang et al., 2014), and regional context (e.g. Jipa & Panin, 2020), only a few of these studies have quantitatively assessed aspects of their geomorphologies (e.g. Nelson et al., 1970; Harris & Whiteway, 2011; Harris et al., 2014b; Huang et al., 2014). An overview of selected studies and their key findings are summarised in the following sections, in ascending order by year of publication, and in Figure 2.2a-e and Table 2.1.

Sømme et al. (2009)

The first global study that investigated scaling relationships between morphometric characteristics of submarine canyons and variables of their environment as part of source-to-sink (S2S) system studies is that of Sømme et al. (2009). In their dataset of 29 modern source-to-sink systems with submarine fan-configuration, Sømme et al. (2009) found that submarine canyons along active margins were generally characterised by smaller dimensions with overall shorter lengths, smaller widths and depths when compared to canyons accommodated on passive margins. The fact that studied canyons along passive margins displayed greater lengths compared to their counterparts along active margins was interpreted by Sømme et al. (2009) as a co-relationship from continental slopes in active-margin settings tending to be shorter and having steeper gradients than continental slopes along passive margins. The authors also showed that width-to-depth ratios in canyons displayed weak scaling with the volume of their associated submarine fans whereas canyon length correlated moderately with fan volume (their Figure 12 and Fig. 2.2a, this study). Sømme et al. (2009) linked the latter relationship to slope physiography, with passive-margin slopes being characterised by larger fans, greater slope lengths and lower gradients.

Covault et al. (2011a)

In their investigation of 20 submarine canyon-channel profiles Covault et al. (2011a) distinguished three types of composite profiles – convex, slightly concave, and very concave – for which the authors identified relationships with characteristics of the margin type and depositional architecture of slope- and basin floor environments (see their Figure 9).

Harris & Whiteway (2011)

As the first global inventory of submarine canyons the quantitative study by Harris & Whiteway (2011), which considered 5,849 submarine canyons with present-day expression on the seafloor, produced valuable insights into the variability of frequency distributions of canyon length, average canyon sinuosity, the average canyon thalweg gradient, dendricity and depth range among other variables; differences were seen to arise as a function of environmental variables and the geographic region. Moreover, the authors evaluated differences between frequency distributions of above morphometric attributes in canyons along active versus passive margins, which revealed for their dataset that canyons were on average shorter and steeper along active margins, whereas average canyon sinuosity only differed marginally between the two margin types (Fig. 2.2b). In addition, Harris & Whiteway (2011) conducted correlation analyses for average sinuosity in shelf-incising canyons versus the latitudinal position of the canyon, which did not reveal a relationship (Fig. 2.2c). However, the study has various limitations. First, the study only considered submarine canyons that were resolved in the one arc minute resolution of the ETOPO1 bathymetry grid, which excluded features that are observable at a finer scale of resolution. Second, based on the criteria Harris & Whiteway (2011) chose to adapt for the definition of a submarine canyon, the study only considered canyons of a minimum size and depth range (see their Table 1 and Tab. 2.1, this study). In addition, the study only distinguished active and passive margin settings, and did not take into consideration a more comprehensive classification of the tectonic setting into sub-settings. However, the investigation of submarine canyons across different types of tectonic settings, such as rift settings (e.g. Oiwane et al., 2011), strike-slip settings

(e.g. Normark et al., 2009) and complex tectonic settings with different types of plate boundaries and directions of motion (e.g. Micallef et al., 2014), reveal a complex picture of sediment transport mechanisms and sets of environmental controls, which has not been addressed in a global context yet.

Harris et al. (2014b)

Building on the dataset published in 2011, Harris et al. (2014b) compiled a global inventory of submarine canyons which applied the criteria for the definition of a submarine canyon from the study by Harris & Whiteway (2011) but was based on higher-resolution data, which resulted in the identification of 9,477 submarine canyons, including 80.5% of the canyons identified by Harris & Whiteway (2011). The authors compared mean values of canyon length, depth and area for the studied submarine canyons in general and grouped into geographic regions and as a function of the position of the canyon head relative to the shelf margin. Their findings showed that shelf-incising canyons were on average longer and covered a greater area than canyons confined to the continental slope, by a factor of 1.47 and 2.07, respectively, whereas slope-confined canyons are characterised by a mean depth more than twice than seen in shelf-incising canyons, by a factor of 2.12. Their analysis also revealed the highest mean values for canyon length and area were grouped in the geographic regions in the Arctic and Southern oceans, which indicates an influence of the latitudinal position of a submarine canyon on its evolution (see text in Harris et al., 2014b and their Table 9).

Huang et al. (2014)

To date, the only continental-scale study of submarine canyons is the one by Huang et al. (2014), who conducted a comprehensive analysis of 713 submarine canyons along the Australian margin. By statistically evaluating a large number of variables describing aspects of the morphology, physiographic setting and spacing of submarine canyons (see their Tables 1 & 2 and Fig. 2.2d, this study), the authors demonstrated that aspects of canyon morphology can differ greatly on a continental scale.

Nyberg et al. (2018b)

Like Sømme et al. (2009), Nyberg et al. (2018b) investigated scaling relationships in source-to-sink systems with submarine fan configuration. Aspects of submarine-canyon geomorphology were only marginally considered in their analysis. Their evaluation was based on 52 S2S systems, which allowed the authors a re-assessment of the results by Sømme et al. (2009) from a larger dataset. Nyberg et al. (2018b) examined frequency distributions of canyon heads as a function of the tectonic-margin type and canyon length distribution across different tectonic settings. The dataset of Nyberg et al. (2018b) demonstrates a higher frequency of canyon heads along active margins and different ranges in length values for canyons in different tectonic environments, corroborating the previous findings by Harris & Whiteway (2011) that the tectonic setting constitutes a control on canyon evolution (their Figure 11b and Fig. 2.2e, this study).

A.

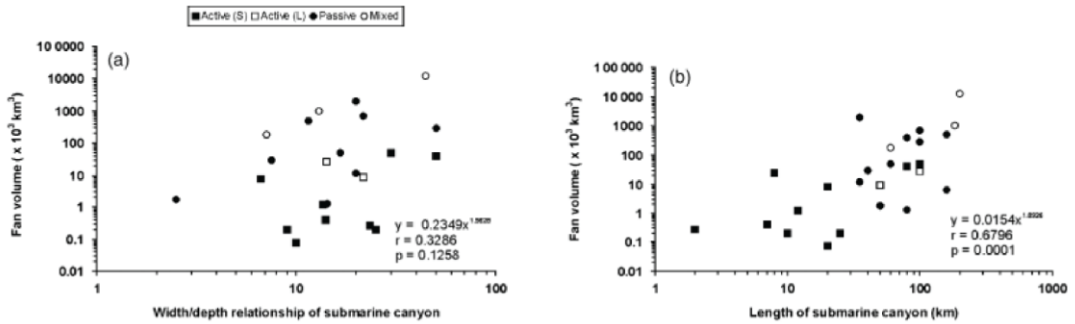

Sømme et al. (2009)

B.

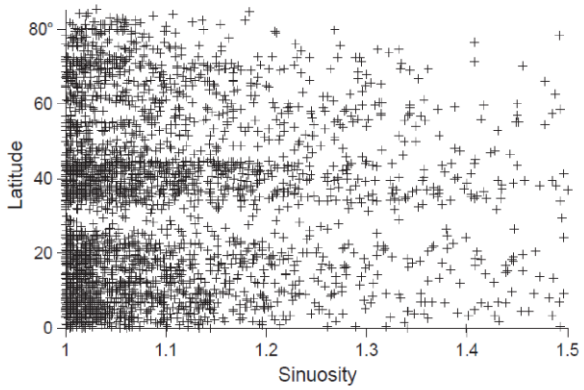

Harris & Whiteway (2011)

C.

		Active Margins	Passive Margins
	Canyon Occurrence (number)	2,586	2,244
	Type 1 Occurrence (number)	118	34
Mean values	Slope (Degrees)	5.4 ± 3.5	3.8 ± 2.7
	Spacing (km)	26.5± 21.5	39.2 ± 38.2
	Length (km)	39.9± 34.0	53.7 ± 40.8
	Dendricity (per 100,000 km²)	7.2 ± 6.6	3.3 ± 4.1
	Sediment thickness (m)	944 ± 1120	2,624 ± 2549
	Depth Range (m)	2,003 ± 878	1,984 ± 842
	Sinuosity	1.133 ± 0.183	1.102 ± 0.127
	Cumulative Length (km)	114,913	121,000

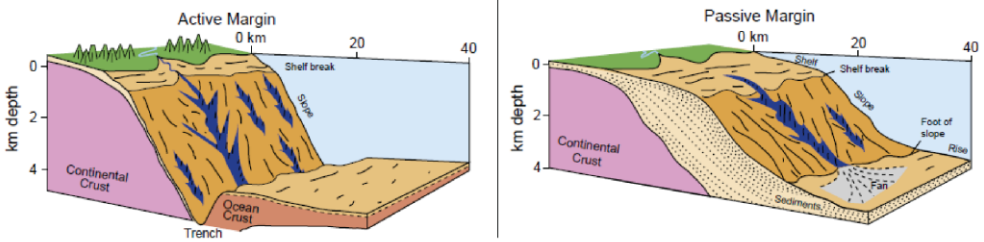

Harris & Whiteway (2011)

D.

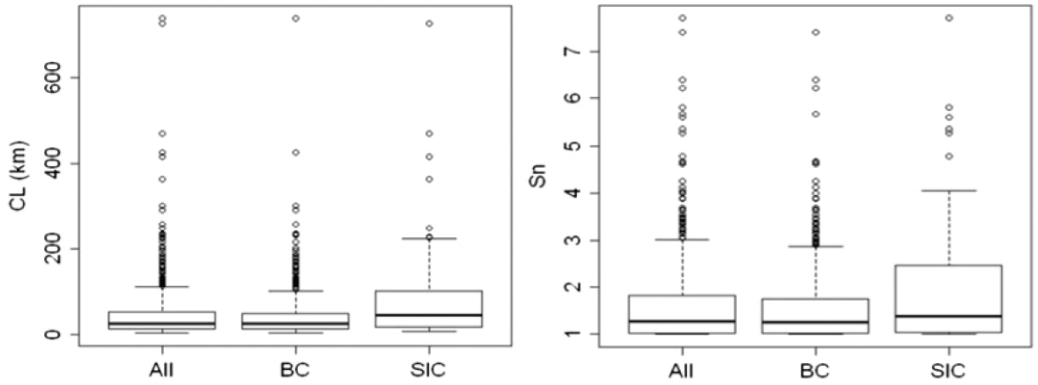

Huang et al. (2014)

E.

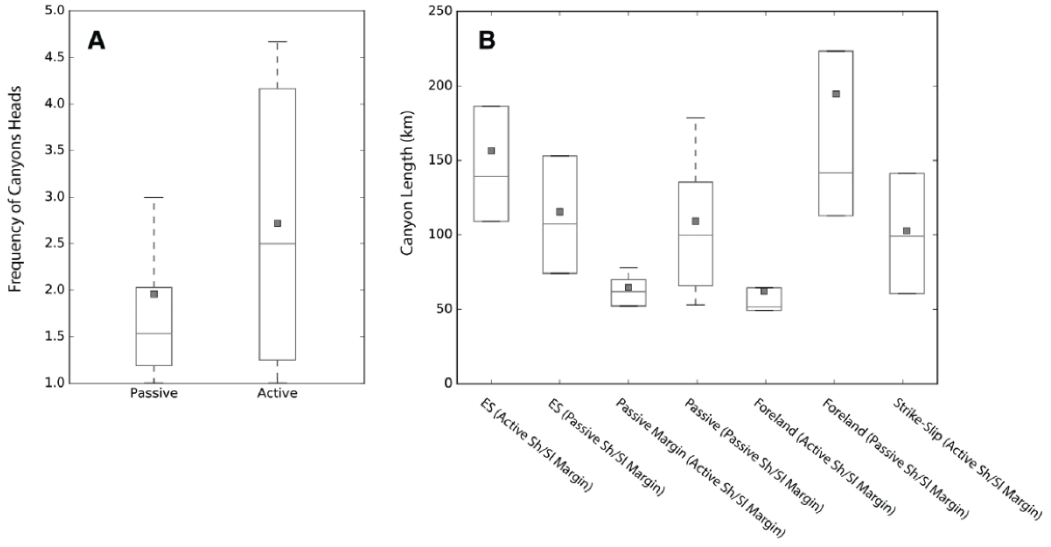

Nyberg et al. (2018b)

Figure 2.2a-e (continued).

Figure 2.2a-e Selected analyses of scaling relationships of canyon morphometric attributes with environmental variables and sedimentary systems in the literature sorted in ascending order by year of publication. A. Scatterplots and results of statistical analyses of canyon morphometric attributes with submarine fan volume from the global investigation of 29 source-to-sink systems by Sømme et al. (2009). B. Results of the statistical evaluation of differences in mean values of studied morphometric attributes in submarine canyons as a function of the tectonic-margin type from the global study of 5,849 submarine canyons by Harris & Whiteway (2011). Statistically significant differences in mean values at 95% confidence intervals are underlaid in yellow. C. Scatterplots of average canyon sinuosity versus latitudinal position of the submarine canyon from the global study by Harris & Whiteway (2011). D. Boxplots of centreline length (CL) and sinuosity (Sn) in submarine canyons in general (All) and for blind/slope-confined (BC) and shelf-incising (SIC) canyons from the continental study of 713 submarine canyons offshore Australia by Huang et al. (2014; see their full Figure 14 for the entirety of boxplots). E. Boxplots of canyon characteristics vs. the tectonic setting from the global study of 52 source-to-sink systems by Nyberg et al. (2018b).

Authors	Study scale	Data type	Geographic region	Study population
Nelson et al. (1970)	Global	Literature-derived; bathymetric data	Africa; N America; Asia; Europe	12
De Pippo et al. (1999)	Global	Obtained by the authors (not specified)	Africa; N & S America; Asia; Europe	56
Sømme et al. (2009)	Global	Literature-derived; SRTM30PLUS digital elevation models; online databases	Africa; N & S America; Asia; Europe	29
Covault et al. (2011a)	Global	Literature-derived; bathymetric data	Africa; N & S America; Asia; Europe	20
Harris & Whiteway (2011)	Global	ETOPO1 bathymetry dataset	Africa; N & S America; Antarctica; Arctic; Asia; Europe	5,849
Harris et al. (2014b)	Global	Modified SRTM_30 PLUS dataset; Australian bathymetric model of Whiteway (2009); EMODNet 2013 data	Africa; N & S America; Antarctica; Arctic; Asia; Europe	9,477
Huang et al. (2014)	Continental	3 bathymetric datasets with differing resolution	Australia	713
Nyberg et al. (2018b)	Global	Literature-derived; datasets of Harris et al. (2014) & Harris & Whiteway (2011)**; Global Terrestrial Sink Catchment dataset; SRTM v4.1 & GMTED2010 digital elevation models	Africa; N & S America; Antarctica; Arctic; Asia; Europe	52
Jipa & Panin (2020)	Regional	Literature-derived; bathymetric data	Black Sea	10's of canyons

Authors	Canyon parameters
Nelson et al. (1970)	Length; average canyon thalweg gradient
De Pippo et al. (1999)	Length; degree of canyon sinuosity (linear vs. sinuous); average canyon thalweg gradient; canyon cross-sectional shape
Sømme et al. (2009)	Length; width; depth
Covault et al. (2011a)	Canyon-channel longitudinal profile shape & normalised length across slope
Harris & Whiteway (2011)	Length; average canyon sinuosity; average canyon thalweg gradient; canyon dendricity; canyon spacing (focal variety & nearest neighbour)
Harris et al. (2014b)	Length; area; depth
Huang et al. (2014)	Canyon polygon parameters (planar area; perimeter; centreline length; min. bounding rectangle width, length & orientation); length-to-width ratio; border index; compactness; number of branches (sub-canyons); canyon volume; canyon head to foot distance; canyon sinuosity; head incision depth; gradient (av. gradient; range of gradient; head-to-foot gradient; % of canyon area with slope gradients >15°); canyon surface area; canyon rugosity; average canyon incision depth into shelf break; canyon area incising into shelf break
Nyberg et al. (2018b)	Length; frequency of canyon heads
Jipa & Panin (2020)	Canyon dendricity; present-day activity

Table 2.1 (continued).

Authors	Canyon-physiographic setting	Environmental variables
Nelson et al. (1970)	Water depth at canyon head & -mouth	---
De Pippo et al. (1999)	Water depth at canyon head & mouth; longitudinal & latitudinal position of canyon; canyon orientation	---
Sømme et al. (2009)	Water depth at canyon head; position of canyon head relative to a fluvial outlet	Tectonic-margin type; submarine fan volume
Covault et al. (2011a)	Latitude (> 40° vs. < 40°)	Tectonic-margin type; glacial influence (latitude> 40°); fluvial sediment load; grain size
Harris & Whiteway (2011)	Position of canyon head relative to shelf break; bathymetric depth range; latitudinal position	Tectonic-margin type; latitude; sediment connection with river; sediment discharge; geographic region
Harris et al. (2014b)	Position of canyon head relative to shelf break	Geographic region
Huang et al. (2014)	Position of canyon head relative to shelf break; Euclidian distance canyon to shelf break & mouth of nearest permanent river; Euclidian distance of canyon to nearest canyon; number of neighbouring canyons within a nominated proximity; water depth at canyon head & mouth; baythmetric depth range	Geographic region
Nyberg et al. (2018b)	Distance to river mouth	Tectonic-margin type; tectonic regime
Jipa & Panin (2020)	---	Shelf width; energy relief; connectivity canyon head to river mouth; fluvial feeder system type; geographic region

Table 2.1 Overview table of examples of regional, continental and global scale studies addressing submarine canyon research presented in ascending order by year of publication. min. = minimum; av. = average.

2.2.4 Conceptual models of submarine canyons

2.2.4.1 Conceptual models of submarine canyon evolution

As discussed in sections 2.2.2 and 2.2.3 the number of factors that have been invoked as influences on the geomorphologic evolution of a submarine canyon are multiple. Reflecting the limited numbers of global studies of

submarine canyons, existing models of submarine canyon evolution are largely based on the study of individual submarine canyons or canyon systems in a regional context (e.g. Jobe et al., 2011; Micallef et al., 2014) for which specific sets of controlling conditions apply. Thus, the universal applicability of these models has to be questioned. Because these models commonly focus on processes, with limited consideration of submarine-canyon geomorphology, they also do not consider the variable impact of a control or co-influence of several factors on a canyon morphometric attribute (Fig. 2.3a&b).

A.

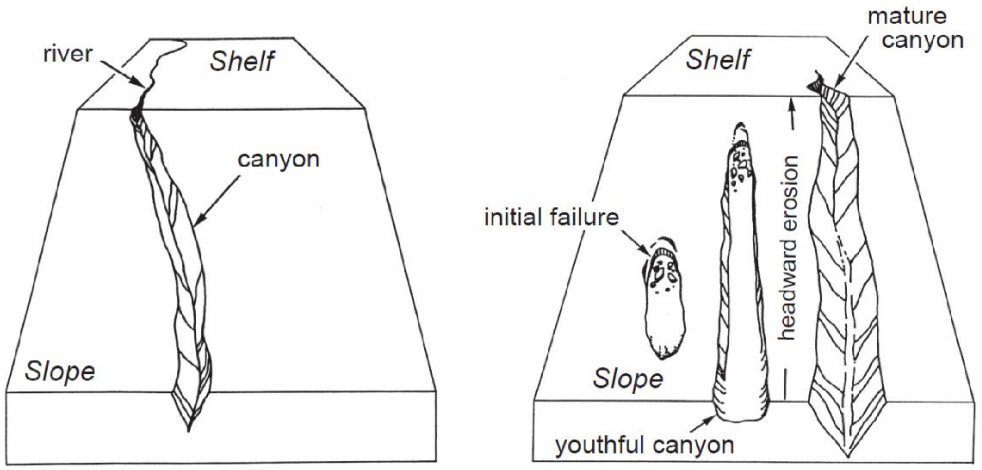

Pratson et al. (2007)

B.

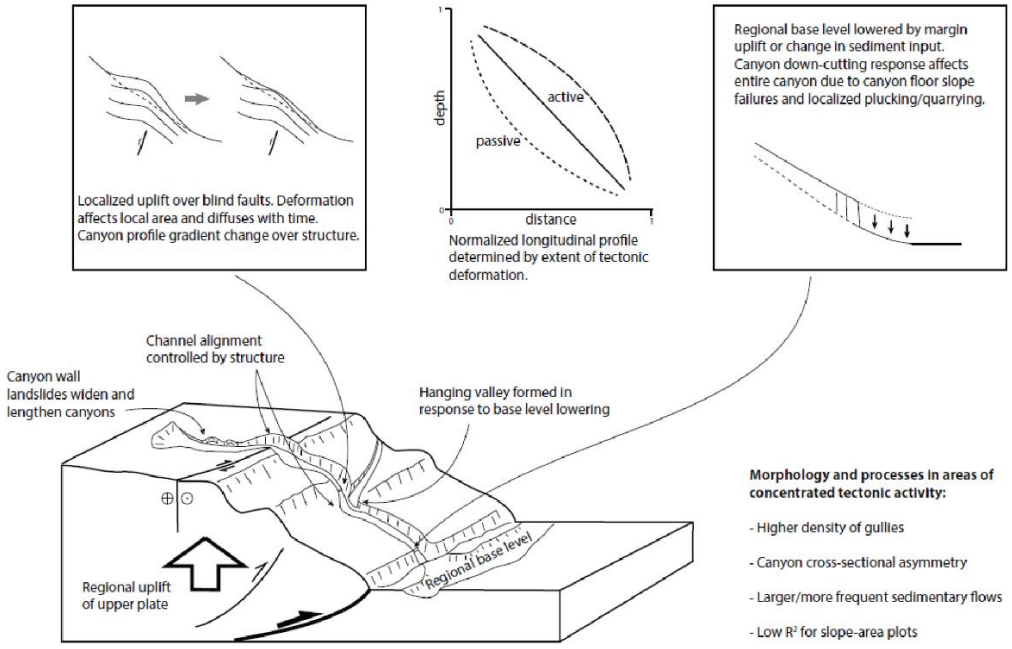

Micallef et al. (2014)

Figure 2.3a&b Examples of conceptual models of submarine-canyon evolution in the literature sorted in ascending order by year of publication.

2.2.4.2 Submarine canyons as parts of source-to-sink (S2S) systems

In many conceptual models of S2S systems, the presence of a shelf-incising submarine canyon is linked to the presence of a fluvial system (see section 2.4.2), which mirrors how various submarine canyons worldwide are interpreted to have been predominantly controlled by fluvial systems during their evolution (e.g. Antobreh & Krastel, 2006; Popescu et al., 2015). However, examples of shelf-incising canyons with signs of more recent activity without any sediment connection to a fluvial source (e.g. Mountjoy et al., 2014) and the sediment connection of canyons to intra-shelf and intra-slope sources (see section 2.2.2) demonstrate the importance of bringing other S2S models within the remit of this research. Also, a number of present-day submarine-canyon systems are considered in-part active and in-part inactive (e.g. Bernhardt et al., 2015; Smith et al., 2018), demonstrating that various sediment sources can supply different parts of the same canyon system at different times. Such activities demonstrate the existence of sediment routeing pathways (e.g. Noda et al., 2008, Bernhardt et al., 2015) that are more complex than those depicted as sediment transport routes along the S2S system axis in simple models (see section 2.4.2 and Fig. 2.12a-e).

2.2.5 Submarine canyon classification schemes

Currently, no unifying classification scheme for submarine canyons exists in the literature. Instead, submarine canyons have been variably classified based on different criteria. These include the physiographic setting of the canyon (e.g. location of the canyon head relative to the shelf break; Harris & Whiteway, 2011; Jobe et al., 2011; Huang et al., 2014), characteristics of the continental margin (e.g. terrestrial catchment and shelf physiography; Sømme et al., 2009; Jipa & Panin, 2018), sediment connection of the canyon to a fluvial system (e.g. Harris & Whiteway, 2011), the substrate type of the seafloor (e.g. Sømme et al., 2009), and the canyon-longitudinal profile shape (e.g. Covault et al., 2011a).

The following sections comprise an overview of different canyon classification schemes that are based on global-, continental- or regional-scale studies (see also Figure 2.4a-e & Table 2.2).

2.2.5.1 Seafloor lithology, tectonic-margin type, sediment transport mechanism and complexity of canyon configuration

Based on the study of 29 “sub-modern” source-to-sink systems with submarine canyon configuration, Sømme et al. (2009) distinguished two main types of submarine canyons. Type 1 canyons are commonly associated with small S2S systems along active margins that are characterised by a narrow shelf. This canyon type is incised into bedrock and forms complex canyon networks. Sediment transport occurs predominantly by bottom currents and surface plumes. Type 2 canyons are parts of larger S2S systems along passive margins, erode into unconsolidated or partially consolidated sediments on the seafloor and constitute single channel-forms. In this type of canyon sediment transport is predominantly facilitated by waves and currents (Fig. 2.4a).

2.2.5.2 Canyon longitudinal profile shape, environmental controls and sedimentary and hydrodynamic processes

From their global-scale investigation of 20 submarine-canyon channel profiles, Covault et al. (2011a) identified three main types of combined canyon-channel profiles: (i) slightly concave, (ii) convex, and (iii) very concave. The authors genetically linked each of the three longitudinal shapes to one main control, namely (i) pre-existing depositional relief, (ii) tectonic uplift, and (iii) erosional sedimentary processes, respectively. Covault et al. (2011a) suggested for the three shape types the prevalence of specific sets of controls, detailed in Fig. 2.4b.

2.2.5.3 Tectonic-margin type

Similar to the classification scheme by Covault et al. (2011a), Harris & Whiteway (2011) also focused on one singular control in their classification scheme. These authors statistically evaluated frequency distributions of the 5,849 submarine canyons in their global database as a function of the tectonic-margin type grouped into active-margin and passive-margin canyons. Harris & Whiteway (2011) found that submarine canyons along active margins had on average steeper thalweg gradients, shorter lengths, higher dendricity, lower sediment thickness and marginally greater depth

range and overall sinuosity compared to their counterparts along passive margins (Fig. 2.4c).

2.2.5.4 Position of the canyon head relative to the shelf break, source type and lithology, intra-canyon processes, cross-sectional shape, lithology of canyon fill and association with distal deep-water deposits

Like Sømme et al. (2009), Jobe et al. (2011) differentiated two main types of submarine canyons in their classification scheme. Based on the study of modern submarine canyons and of an ancient canyon system along the continental margin of Equatorial Guinea they used the following criteria: position of the canyon head relative to the shelf break, grain size of source sediment, presence or absence of distal deep-water deposits, cross-sectional shape, lithology of canyon fill, intra-canyon processes. Type 1 canyons are incised into the shelf, supplied by coarse-grained sediment from fluvial systems and/or littoral cells and associated with large submarine fan-channel systems. The predominant processes within Type 1 canyons are sandy turbidity currents and mass failures. Type 1 canyons are characterised by v-shaped cross-sectional shapes and sand-rich canyon fills. Type 2 canyons are slope-confined and due to the lack of sediment connection with rivers or longshore currents sediment supply is low and fine-grained related to hemipelagic fallout. Consequently, intra-canyon processes are predominantly depositional, and Type 2 canyons lack association with a distal depositional system. As opposed to Type 1 canyons Type 2 canyons have u-shaped cross-sections and a mud-rich fill (Fig. 2.4d).

2.2.5.5 Position of the canyon head relative to the shelf break, canyon morphometric characteristics and canyon spacing

Huang et al. (2014) presented a novel classification scheme of submarine-canyon geomorphology from their study of 713 submarine canyons along the Australian margin. On the basis of an extensive number of canyon morphometric and physiographic attributes and spacing between canyons (see Tab. 2.1), these authors developed a four-level hierarchical classification scheme based on the following criteria (in descending order): (i) position of the canyon head relative to the shelf break, (ii) steepness of

canyon margins and canyon gradient, (iii) canyon volume versus size of canyon head incision, (iv) spacing to adjacent canyons (Fig. 2.4e).

As seen for submarine canyon models (section 2.2.4), existing submarine-canyon classification schemes have commonly focused on specific variables of the canyon-physiographic and environmental setting and have only partially considered morphometric characteristics of submarine canyons (see Tab. 2.2). In addition, some of the classification schemes are based on continental-scale (e.g. Huang et al., 2014) or regional-scale studies (e.g. Jobe et al., 2011; Jipa & Panin, 2020).

From this, several problems arise:

(i) Without a systematic evaluation of the multitude of factors that have been proposed in the literature to govern canyon evolution (see section 2.2.2) it remains unclear to which extent a factor influences different morphometric attributes in a submarine canyon, and whether different factors can generate the same morphologic signature.

(ii) Without an overall assessment of canyon geomorphology, it remains unclear to which extent different canyon morphometric attributes are controlled by individual controls.

(iii) Continental-scale and regional-scale studies investigate submarine canyons in context of a specific set of controls that are particular to the geographic region. Hence, for classification schemes derived from insights from continental- and regional-scale studies the general applicability of these schemes has to be questioned.

A.

Type 1 canyons: commonly associated with small tectonically active systems with narrow shelves; sediment transport predominantly by bottom currents & surface plumes; canyon networks incised into bedrock; long-lived systems

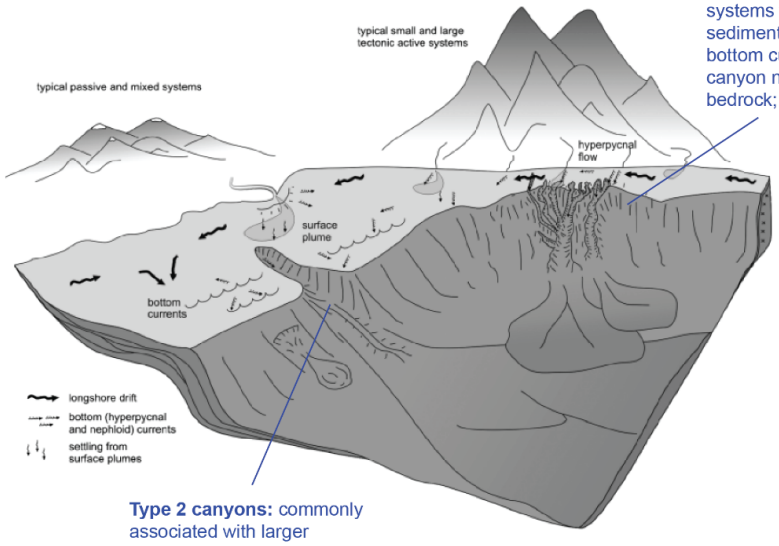

Type 2 canyons: commonly associated with larger passive-margin systems; sediment transport predominantly by wave & current

Sømme et al. (2009)

B.

Slightly concave canyon-channel longitudinal profile: appreciable pre-existing depositional relief; mature margin-driven nepheloid flows during highstand conditions; canyons incise into semi-unconsolidated substrate where thick shallow-marine deposits exist; potentially more short-lived systems bottom currents & surface plumes; canyon networks incised into bedrock; long-lived systems

Convex canyon-channel longitudinal profile: tectonic uplift & deformation in convergent margins & gravity-driven along passive margins

Very concave canyon-channel longitudinal profile: enhanced erosion from sediment gravity flows; young & underfilled margins with narrow shelves & steep slopes & nearby source areas; associated coarse-grained submarine fan

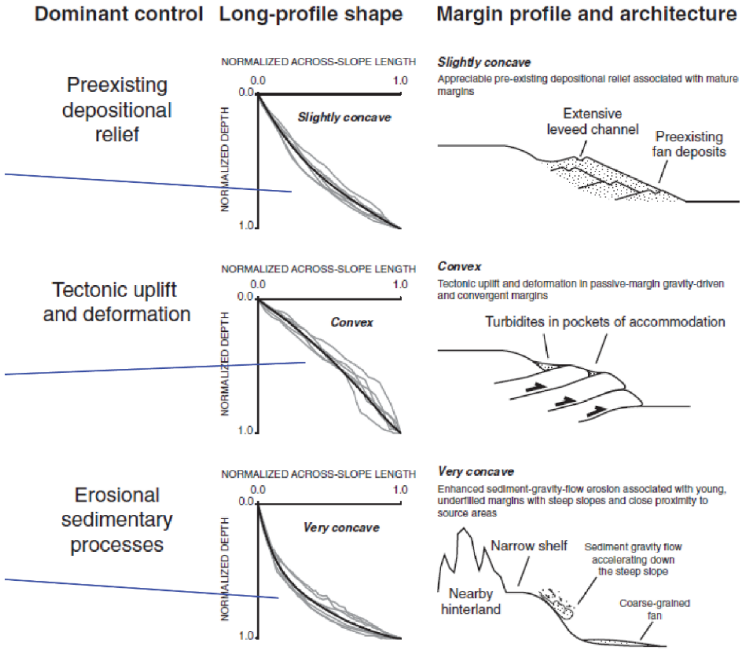

Covault et al. (2011a)

C.

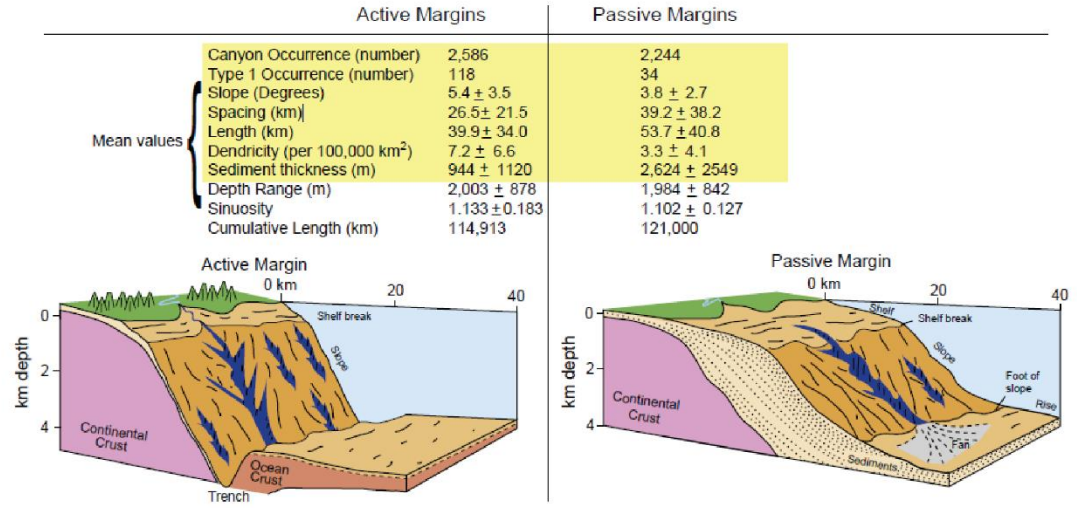

Harris & Whiteway (2011)

D.

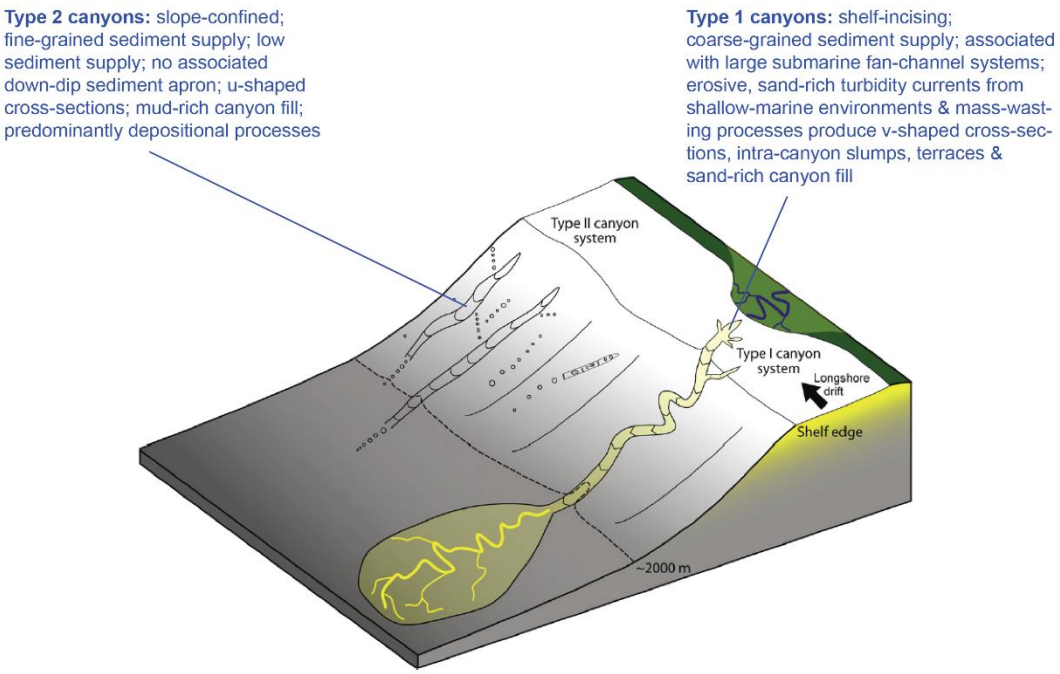

Jobe et al. (2011)

Figure 2.4a-e (continued).

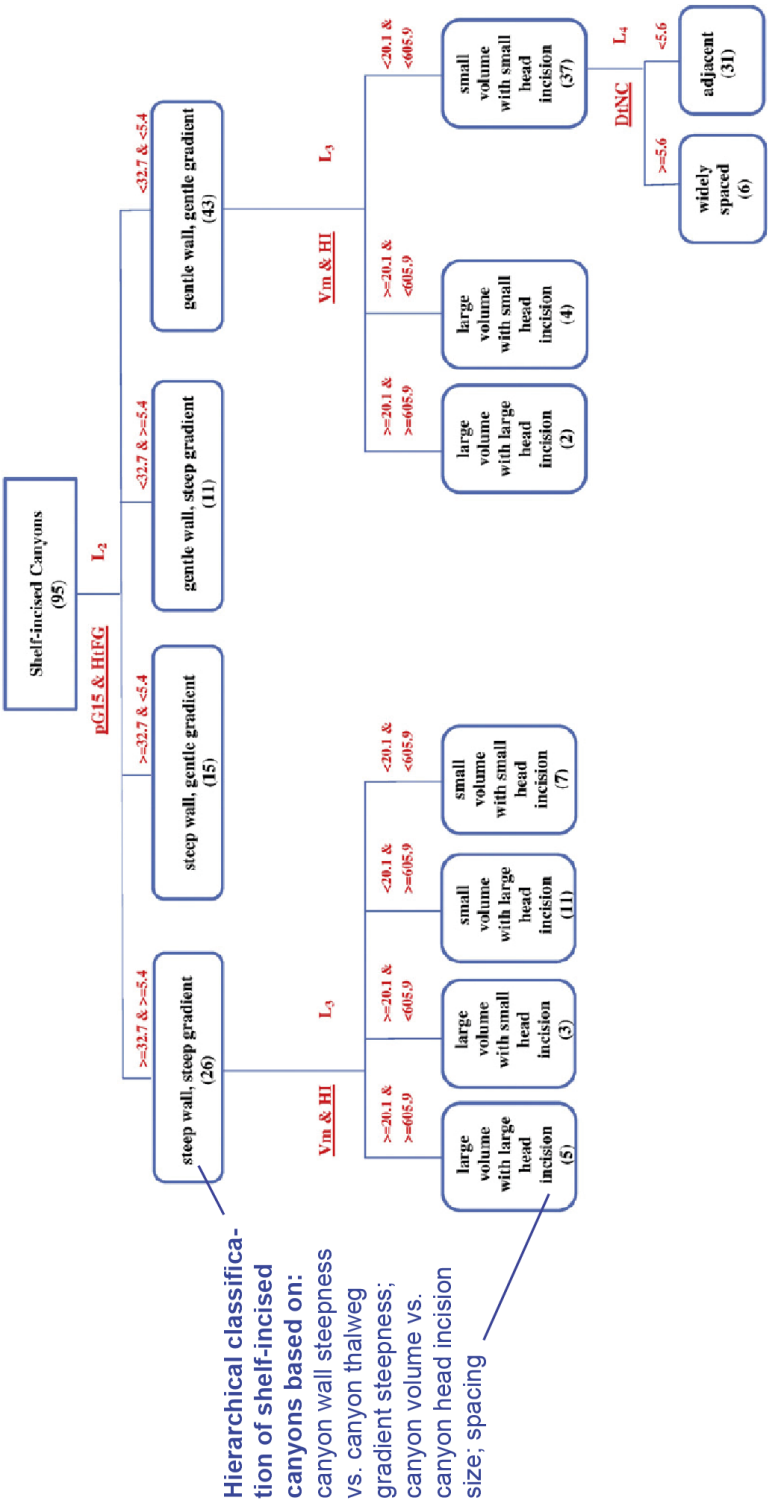

E

Figure 2.4a-e (continued).

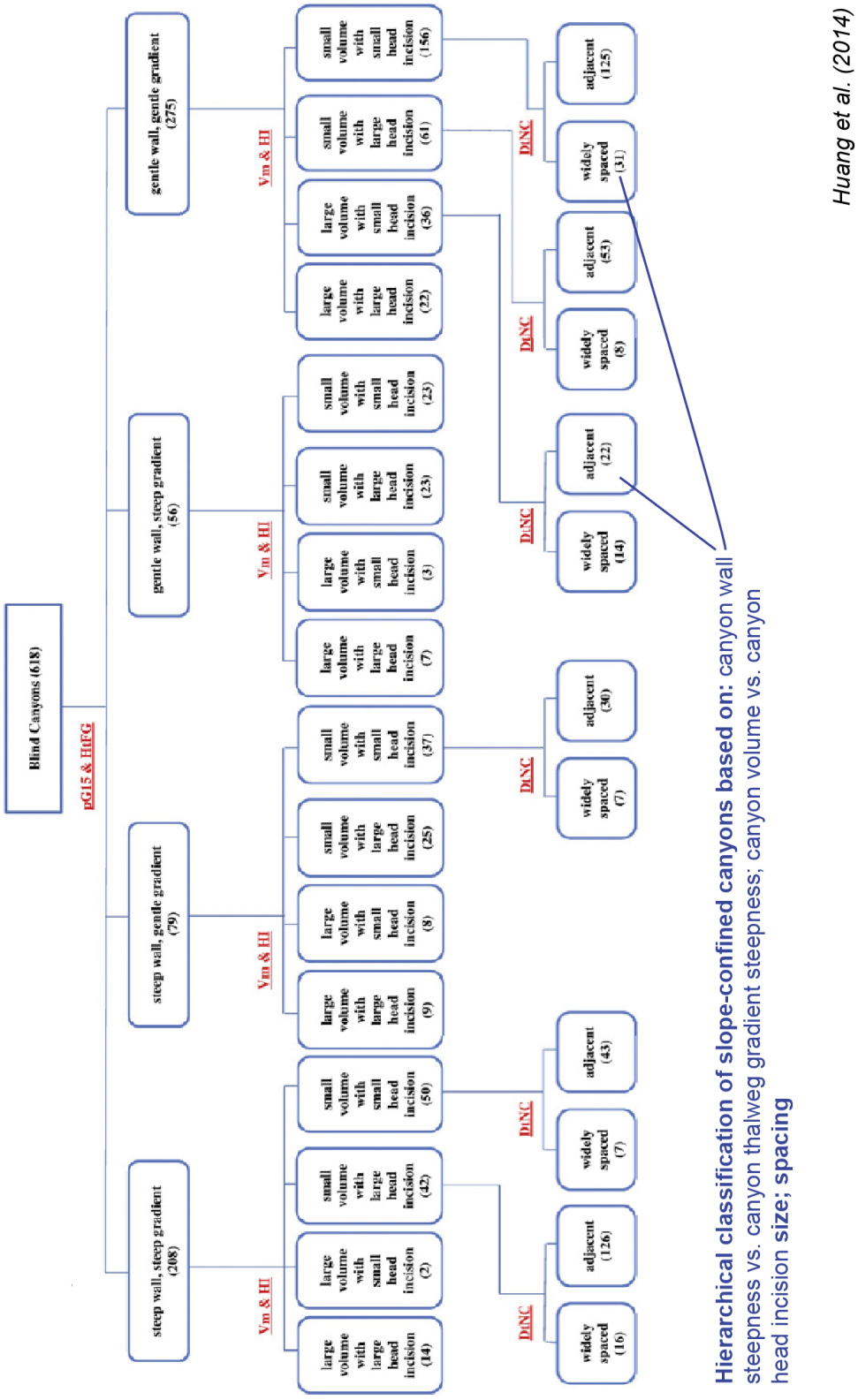

Figure 2.4a-e Examples of submarine-canyon classification schemes in the literature sorted in ascending an alphabetic order by year of publication (see also Table 2.2). Added text in blue.

Criterion / Criteria	Canyon classes	Definition	Canyon geomorphology	Reference
Seafloor lithology, tectonic-margin type; sediment transport mechanisms; canyon dendricity	Type 1	Incises into bedrock; canyon system; small S2S systems along active margins	Canyon dendricity (single canyon vs. canyon system)	*Sømme et al. (2009)*
	Type 2	Incises into unconsolidated & partially consolidated sediments; single channel-form		
Canyon-channel longitudinal profile shape & normalised length across slope*	Slightly concave	Appreciable pre-existing depositional relief; mature margin	Normalised canyon length; canyon thalweg gradient	*Covault et al. (2011a)*
	Convex	Tectonic uplift & deformation in convergent margins & gravity-driven along passive margins		
	Very concave	Enhanced erosion from gravity flows; young,underfilled margins; narrow shelves & steep slopes; near source areas; distal coarse-grained fan		
Tectonic-margin type	Active margin	Short; high average canyon thalweg gradient	Canyon length; average canyon thalweg gradient; canyon dendricity	*Harris & Whiteway (2011)*
	Passive margin	Long; low average canyon thalweg gradient; low dendricity		
Source type and lithology, intra-canyon processes, cross-sectional shape, lithology of canyon fill and association with distal deep-water deposits	Type 1	Shelf-incising; coarse-grained fluvial & littoral sed. supply; sandy turbidity currents & mass failure; v-shaped cross section; sand-rich fill; large fan-channel system	Cross-sectional shape	*Jobe et al. (2011)*
	Type 2	Slope-confined; no connection to rivers & littoral cells; hemipelagic fallout deposition; u-shaped cross section; mud-rich fill; no distal depositional system		
Canyon head location relative to shelf break; canyon wall steepness; canyon thalweg gradient; canyon volume; head incision size; canyon spacing	Shelf-incising	Four-level hierarchical classification: (i) canyon head location relative to shelf-break; (ii) steepness of canyon margins & canyon gradient; (iii) canyon volume vs. size of canyon head incision; (iv) spacing to adjacent canyons	Canyon thalweg gradient; canyon margin steepness	*Huang et al. (2014)*
	Slope-confined			

* Canyon- & channel parameters not differentiated by the authors

Table 2.2 Overview table of examples of submarine canyon classification schemes in the literature presented in ascending order by year of publication (see also Figure 2.4a-d).

2.3 Controlling factors of shelf-edge deltas

2.3.1 Shelf-edge delta definition

Deltas constitute the terminal deposits of fluvial systems debouching into bodies of standing water. Based on their physiographic position along continental margins, different delta types are distinguished in the literature, including bayhead deltas, inner-shelf, mid-shelf and shelf-edge deltas (e.g. Porębski & Steel, 2003; 2006). For shelf-edge deltas (e.g. Edwards, 1981; Porębski & Steel, 2003; Sylvester et al., 2012; Peng et al., 2017), also termed shelf-margin deltas (e.g. Suter & Berryhill, 1985; Morton & Suter, 1999; Porębski & Steel, 2003), lowstand wedge deltas (e.g. DiBona & von der Borch, 1993) or lowstand wedges (e.g. Algan et al., 2002), which are the focus of this research, two definitions exist in the literature:

(i) *Sensu stricto*, authors have defined shelf-edge deltas as deltas that physically extend across the shelf margin onto the continental slope (e.g. Almeida Junior et al., 2020).

(ii) Some authors also consider deltas as shelf-edge deltas *sensu lato*, where the delta does not physically reach the shelf edge but is located in vicinity of the shelf margin (e.g. Sanchez et al., 2012b).

With the focus of this work being sedimentary systems at the shelf-to-slope transition, and the shelf break constituting an important boundary where (i) the presence of geostrophic currents tends to inhibit sediment transport onto the continental slope (e.g. Allen & Durrieu de Madron, 2009), and (ii) an abrupt change in seafloor gradient occurs along most continental margins (e.g. Harris & Macmillan-Lawler, 2016), the first definition is applied in this thesis. Where shelf-edge deltas are referred to in the text, this relates to shelf-edge deltas in a narrow sense.

The common distinction of a delta into the three different subenvironments delta plain, delta front and prodelta (e.g. Galloway, 1975; Reading & Collinson, 1996) is also applied to shelf-edge deltas (e.g. Edwards, 1981; Schwartz & Graham, 2015) (Fig. 2.5a&b).

Shelf-edge deltas are building blocks of continental margin successions (e.g. Porębski & Steel, 2003; Steel et al., 2003). In 2D cross section in seismic and outcrop datasets, morphometric characteristics of their surfaces and sediment bodies, which are also referred to as clinoforms and clinothems, respectively, have been used to differentiate shelf-edge deltas from other clinoform and clinothem types within a continental margin (e.g. Steel et al., 2003; Patruno et al., 2015; Patruno & Helland-Hansen, 2018). Shelf-edge delta clinoforms have heights of the order of hundreds of meters and display steep gradients that in comparison to the clinoforms of other delta types are significantly greater, which reflects the increase in accommodation and seafloor gradient on the upper slope (e.g. Porębski & Steel, 2003; 2006; Patruno et al., 2015). Trajectories of shelf-edge delta clinoform successions have been utilised as diagnostic criteria for the reconstruction of sea-level changes and sediment supply across shallow-marine and deep-water environments (e.g. Gong et al., 2015).

Shelf-edge deltas display their maximum thickness in the basinward vicinity of the shelf edge where the accommodation is greater than on the shelf due to steeper seafloor gradients, growth faulting, and compaction of the underlying margin strata (e.g. Suter & Berryhill, 1985 and references therein; Porębski & Steel, 2006).

A.

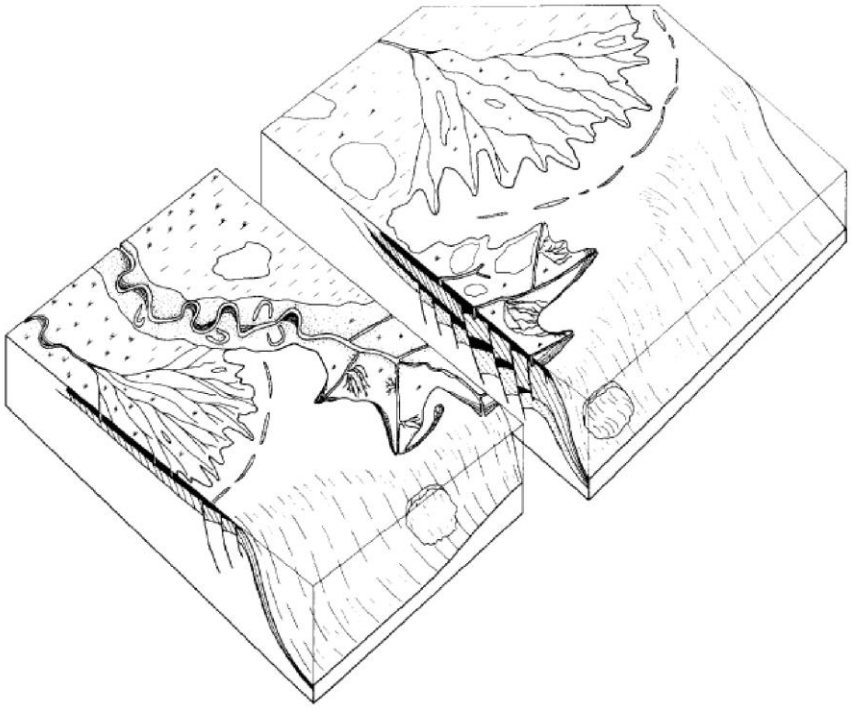

FIG. 3—Schematic block diagram showing inferred depositional patterns for deep upper Wilcox of south Texas. On cross sections, inclined lines represent prodelta muds, and black areas represent delta-plain and delta-front sands.

Edwards (1981)

B.

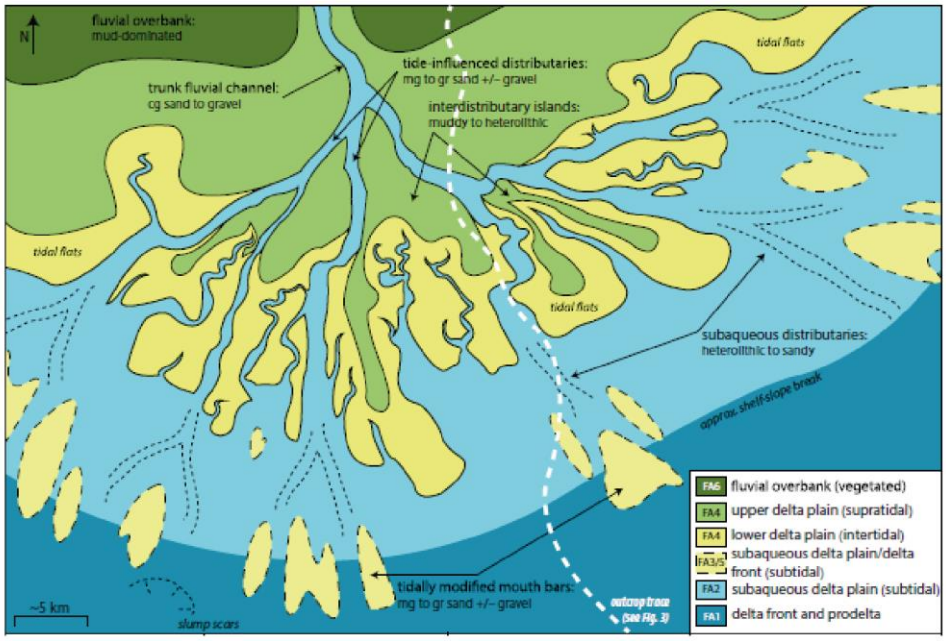

Schwartz & Graham (2015)

Figure 2.5a&b Examples of schematic models of main subenvironments within a shelf-edge delta. A. Edwards (1981). B. Schwartz & Graham (2015). Added text in blue.

2.3.2 Shelf-edge delta evolution

As in any delta type, the development of a shelf-edge delta is genetically linked to the accumulation of fluvial sediment in front of a river mouth, but with the deposits associated with the location of the shelf margin. The development of a delta at the shelf edge can be facilitated by two mechanisms: (ii) where rivers traverse across emerged shelves during phases of lowering sea-level (‘forced regression’, e.g. Steel et al., 2003; Porębski & Steel, 2006); and (ii) where fluvial sediment supply is sufficiently high and/or the shelf narrow enough that the delta can advance to the shelf break (‘normal regression’, e.g. Porębski & Steel, 2006; Uroza & Steel, 2008).

2.3.2.1 Processes influencing shelf-edge delta evolution

Depositional and erosional sedimentary processes

In addition to the deposition of sediment transported by fluvial discharge, shelf-edge deltas can receive sediment from longshore currents (e.g. Gong et al., 2016 and references therein), which might also redistribute sediments within the delta (e.g. Yoo et al., 2017). Although shelf-edge deltas are depositional sedimentary bodies, their evolution is also shown to be influenced by erosional processes. For example, the progradation of distributary channels from younger stages of delta evolution across older ones are effective in eroding delta plain and -front deposits (e.g. Steel et al., 2003). Delta fronts are sensitive to erosion related to various processes, including delta-front failure, which can be related to oversteepening of delta slopes (e.g. Dixon et al., 2012) but also to wave erosion during transgression (e.g. Santra et al., 2013; Zecchin et al., 2019), and the retrogradation of submarine canyons onto shelves (e.g. Dasgupta & Buatois, 2015).

Marine hydrodynamic processes

As sedimentary systems at the terrestrial to marine boundary, the evolution of shelf-edge deltas has been suggested to be influenced by various marine hydrodynamic processes including tidal currents and waves (e.g. Cummings et al. 2006; Almeida Junior et al., 2020), margin-parallel currents (e.g. Yoo et al., 2017), and storm waves (e.g. Bowman & Johnson, 2014), which might

supply sediment to shelf-edge deltas and rework their deposits. The redistribution of delta sediments and reworking of delta fronts by waves (e.g. Suter & Berryhill, 1985; Anderson, 2005) and longshore currents (e.g. Yoo et al., 2017) is considered an important control that facilitates the widening of a shelf-edge delta. Wave ravinement during sea-level transgression promotes the erosion of delta plains and fronts and by this a shortening and thinning of deltas post-deposition (e.g. Ferro et al., 1999; Yoo et al., 2017).

2.3.3 Shelf-edge delta studies

2.3.3.1 Research bias in shelf-edge delta studies

In contrast to submarine canyons, for which various studies have investigated their morphological aspects (see section 2.2.3.2), the morphology of shelf-edge deltas remains understudied. A review of the literature on shelf-edge deltas for this project has revealed that few studies thus far have focused on the comparative analysis of morphometric characteristics of this delta type (e.g. Porębski & Steel, 2003; Steel et al., 2003). This might be related to various factors: (i) the relative youth of the research field of shelf-edge deltas with the first reported example of a shelf-edge delta study ascribed to McMaster et al. (1970a & 1970b), who studied shelf-edge deltas offshore the coasts of Guinea-Bissau, Guinea and Sierra Leone, West Africa (Yoo et al., 2017); (ii) the paucity of fully preserved examples in the literature (see Chapter 5); (iii) the overall relatively low number of shelf-edge deltas that have been investigated (e.g. Table 1 of Dixon et al., 2012), and specifically the few examples preserved on the modern seafloor (e.g. Daniell et al., 2020). Also, the recognition of a shelf-edge delta in subsurface and outcrop studies is tied to the identification of the shelf margin and/or the water depth during deposition, which is often hampered. For example, the reconstruction of palaeoenvironments might be difficult in geographic regions with a history of tectonic fragmentation, and where information on the bathymetry of the deposits is limited. Moreover, given the inference of a narrow shelf width, sea-level lowstand and high sediment supply as factors driving their genesis, the frequency of shelf-edge delta formation in Earth’s history in comparison to other delta types might be

lower due to the reduced probability of co-occurrence of the three factors both geographically and at certain points in time for their development.

The relatively low number of studied shelf-edge deltas worldwide, and the focus of studies on specific regions such as the Gulf of Mexico (see Fig. 5.1) inherently creates a thematic bias as discussed in section 2.2.3.1 because of the limited number of sets of environmental conditions evaluated. The preferred study of shelf-edge deltas within the Gulf of Mexico can be explained by the economic interest in this region for hydrocarbon exploration (e.g. Suter & Berryhill, 1985; Lore et al., 1999).

2.3.3.2 Evaluation of aspects of shelf-edge delta geomorphology in quantitative studies

Only a small number of studies have evaluated summary characteristics of shelf-edge deltas and their physiographic settings (e.g. Porębski & Steel, 2003). The geomorphology of shelf-edge deltas has not been statistically investigated in detail in prior quantitative studies. Instead, the focus of quantitative studies has been on factors which promote the distribution of sediment from and across shelf-edge deltas to deep-water environments, with focus on shelf-edge trajectories, sea level direction movement, magnitude of sediment supply and the hydrodynamic-process regime (e.g. Porębski & Steel, 2003; Dixon et al., 2012; Gong et al., 2016).

Porębski & Steel (2003)

An overview of key characteristics of different types of deltas, including shelf-edge deltas and some of their controls, was presented by Porębski & Steel (2003). The authors considered (i) planview shape, (ii) slope and height of the clinoforms, and (iii) trend of thickening of the delta as morphometric attributes. Of the environmental controls the hydrodynamic-process regime and relative changes in sea level were included. Moreover, these authors compiled summary characteristics for shelf-edge deltas based on examples of Pleistocene age from four geographic regions, including the following aspects of shelf-edge delta geometry: (i) planview shape, (ii) length, (iii) width, and (iv) maximum thickness (see Table 1 of Porębski & Steel, 2003; Fig. 2.6a&b this chapter).

A.

Table 1
Main distinctive characteristics of shelf deltas (see also Kolla et al., 2000, and references therein)

	Bayhead deltas	Inner-Shelf Deltas	Mid-Shelf Deltas	Shelf-Margin Deltas
Shape	Confined, funnel-shaped	Birdfoot, lobate to cuspate	Erosional pods common	Lobate to strike-elongate
Clinoform slope	?	Usually < 0.001*	< 0.5°, but can be as much as 8°**	Up to 8°, usually 3–6°
Clinoform height	Several meters	Few tens of meters	Few tens of meters	Several hundreds of meters
Thickening trend	Landwards	Landwards	Seawards, or no distinct trend	Seawards, with maximum near shelf break
Dominant energy flux at delta front	Fluvial; can be tide influenced	Fluvial, wave or tide	Fluvial or wave	Fluvial or wave; tide influence may become important during late lowstand
Delta-top facies	Fluvial distributaries	Delta plain with thick distributary channel sand	Thin to absent delta plain; thick distributary channel sand below incised valley systems; erosional bypass in places	No delta plain; thin fluvial distributaries where delta perches below shelf edge. Erosional bypass common
Delta-slope facies	Heterolithic, ripple-laminated foresets	Varies depending on delta front regime	Sandstone to heterolithic foresets; rare turbidite sands	Sandstone to heterolithic foresets; slumped mouth-bar sand embedded in prodelta shales; common hyperpycnal sand turbidites. Growth faults and diapirs
Updip termination	Intertonguing with paralic deposits	Intertonguing with paralic deposits	Erosional pinchout within mid-shelf shales	Erosional pinchout within outer-shelf or upper slope shales
Downdip termination	Pinchout within central estuarine-basin heteroliths	Pinchout with inner-shelf to mid-shelf shales	Pinchout within outer-shelf shales	Pinchout within slope shales
Clinoform breakpoint trajectory	Landward rising to basinward rising	Basinward rising	Horizontal to basinward falling	Basinward falling, aggraded to landward rising
Systems tract	Transgressive	Highstand	Falling stage	Falling stage to lowstand

* See Table 6.2 in Reading and Collinson (1996).
** Posamentier and Morris (2000).

Porębski & Steel (2003)

B.

Table 2
Summary characteristics of Pleistocene shelf-margin deltas

Location	Gulf of Mexico	Izmir Bay, East Mediterranean Sea	Rhône Shelf, West Mediterranean Sea	Guinea–Sierra Leone Shelf, West Africa
Delta regime	Fluvial dominated	Fluvial dominated	Wave dominated	Wave-dominated
Tectonic setting	Passive margin; basinwards downwarping due to sediment load	Active strike–slip-related extension	Passive margin; basinwards downwarping due to sediment load	Passive margin
Physiographic setting				
Shelf width	70–140 km	40–60 km	75 km	35–190 km
Shelf gradient	<0.05°		1–3°, <0.1° near the shelf edge	≤1°
Depth of shelf break	75–100 m	110–120 m	120–135 m	85–115 m
Slope gradient	0.6–1.5°, maximum 3°	Gentle	<10°	4°
Delta geometry				
Shape	Multilobate to strike-elongate	Lobate to strike-elongate	Lobate	
Length*	25–60 km	<60 km	40–50 km	30–40 km
Width	28–120 km	?		90 km and more
Maximum thickness	60–90 m, locally above 180 m	5–50 ms, controlled by syndepositional block faulting	50 m	30–95 to above 130 m
Clinoform				
Dip	3–6°, maximum 8°	4–6°	1.5°(?)	4–6°
Seismic expression	Oblique–tangential reflectors steepening basinwards, with toplap terminations below planar scour surface. Sigmoidal forms in the most seaward bundles. Offlap associated with downstepping ensued by backstep in youngest bundles. Common internal downlap surfaces. Progradation centres defined by bidirectional downlap	Oblique reflectors terminating updip by toplap and changing downwards into gently dipping shingled forms. Transparent facies in distal delta	Oblique–tangential reflectors showing downward decreasing amplitude, intercalated with hummocky reflection packages. Individual bundles separated by steeper erosional truncations of regional extent. Clinoform bounded at top by channeled surfaces with toplap terminations below. Overall downstepping to backstepping pattern in time	Offlapping stack of thinning-up clinoforms, each above major erosional unconformity with toplap. Terminations below and downlap above

Porębski & Steel (2003)

Figure 2.6a&b A. Overview of key characteristics of different types of deltas and some of their controls (Porębski & Steel, 2003). Red box: Compilation of information on shelf-edge deltas and aspects of their environmental setting (modified from Porębski & Steel, 2003). B. Summary characteristics of shelf-edge deltas of Pleistocene ages from four different geographic regions (partial table of Porębski & Steel, 2003).

2.3.4 Conceptual models of shelf-edge deltas

The relatively low number of studied examples of shelf-edge deltas and lack of consideration of delta geomorphology in their quantitative analyses (see section 2.3.3) probably contributes to the subordinate role of morphometric characteristics of shelf-edge deltas in conceptual models. A few aspects of shelf-edge delta geomorphology, including their plan-view shape and

thickness, are addressed in some of the existing classification schemes of shelf-edge deltas.

2.3.5 Shelf-edge delta classification schemes

The focus of existing classification schemes of shelf-edge deltas on associated allogenic and autogenic processes and delta facies corresponds to the little attention that shelf-edge delta geomorphology has received thus far in the literature (see section 2.3.3). Despite this, aspects of the geomorphology of shelf-edge deltas are considered to some degree (e.g. Porębski & Steel, 2003).

2.3.5.1 Hydrodynamic-process regime

Multiple authors have classified shelf-edge deltas on the hydrodynamic-process regime. Analogue to the tripartite classification scheme for hydrodynamic processes associated with deltas of Galloway (1975) and based on the hydrodynamic process that predominantly governs shelf-edge delta evolution, they have been distinguished into (i) fluvial-dominated, (ii) wave-dominated, and (iii) tide-dominated deltas (e.g. Suter & Berryhill, 1985; Cummings, 2006; Dixon et al., 2012 and references therein; Gong et al., 2016 and references therein; Almeida Junior et al., 2020). The hydrodynamic-process regime is thought to influence the characteristics of seismic clinoforms in shelf-edge deltas and their planview shape (e.g. Suter & Berryhill, 1985).

Fluvially dominated shelf-edge deltas have been suggested to be characterised by oblique parallel to complex sigmoid-oblique seismic clinoforms (e.g. Suter & Berryhill, 1985) and by a lobate shape due to the subordinate influence of waves and tides (e.g. Anderson, 2005). By contrast, the influence of waves on the redistribution of delta sediments has been proposed to generate shoreline-parallel, strike-elongated shelf-edge deltas, which are classified as wave-dominated (e.g. Suter & Berryhill, 1985; Anderson, 2005). Cummings (2006) proposed that tide-dominated deltas preferentially develop within invaginations at the shelf margin as slump scars and submarine canyon heads, where tidal influence is amplified. This author hypothesized that a strong tidal influence would lead to the deposition of

thick upward-coarsening delta successions comprising debritic and turbiditic deposits.

In addition to fluvial processes, other hydrodynamic processes such as tidal currents can be equally or more important for the delta evolution (e.g. Schwartz & Graham, 2015). It is important to highlight that the process regime of a shelf-edge delta can change over time (e.g. Roberts et al., 2000) and can have lateral variability (e.g. Carvajal & Steel, 2009; Schwartz & Graham, 2015; Laugier & Plink-Björklund, 2016). These factors, in turn, influence the geomorphology and depositional architecture of the shelf-edge delta (e.g. Carvajal & Steel, 2009; Schwartz & Graham, 2015; Laugier & Plink-Björklund, 2016), which implies the existence of more shelf-edge delta types than currently recognised in this classification scheme.

2.3.5.2 Delta & margin stability

Porębski & Steel (2003) proposed a classification of shelf-edge deltas into (i) stable and (ii) unstable deltas which emphasizes the importance of sea-level variations and sediment supply for the evolution of shelf-edge deltas and their associated continental margins. Unstable deltas develop during phases of sea-level fall below the shelf edge and are associated with significant slope accommodation and high sediment supply, the latter might be related to large fluvial systems or high erosion rates along tectonically active margins. The large accommodation and high sediment supply promotes great delta thickness up to several hundreds of meters. By contrast, stable deltas are characterised by strike-oriented lobate bodies. The development of this delta type was linked by Porębski & Steel (2003) to sea levels at the level of the shelf margin, either related to sea level fall or -rise, and small to modest fluvial feeder systems (Fig. 2.7a & Tab. 2.3).

2.3.5.3 Sea level dynamics, physiographic setting, delta characteristics and processes

Steel et al. (2003) distinguished four different shelf-edge delta types, A to D, based on a broad number of criteria including sea level dynamics as the driving force in delta development, the position of the shelf-edge delta relative to the shelf margin, its depositional (i.e. progradation vs.

aggradation) versus erosional character (i.e. incision by fluvial channels), sedimentological and architectural delta characteristics, and its ability to facilitate sediment dispersal to basin-floor environments, leading to the build-up of submarine fans (Fig. 2.7b & Tab. 2.3).

2.3.5.4 Sea level dynamics, shelf width, magnitude of sediment supply, and delta characteristics

Uroza & Steel (2008) contrasted lowstand- and highstand shelf-edge deltas as two end-member types of shelf-edge delta as a function of sea-level dynamics, highlighting the mechanism of shelf-edge delta development during episodes of rising sea level and highstand conditions subject to specific environmental conditions. These authors emphasized the importance of a narrow shelf width in facilitating shelf-edge delta formation, even if the fluvial system is characterised by a low rate of sediment supply (Fig. 2.7c & Tab. 2.3).

As discussed for classification schemes of submarine canyons (section 2.2.5), the limited consideration of morphometric attributes of shelf-edge deltas in studies of these systems has important consequences:

(i) At present, little understanding exists on the controls on shelf-edge delta geomorphology due to the paucity of quantitative studies of shelf-edge deltas and lack of consideration of their geomorphologies.

(ii) Although certain shelf-edge delta types have been tentatively assigned morphometric characteristics, in particular regarding the order of scale of delta thickness, the range and variability of morphometric attributes in shelf-edge deltas remains unknown.

(iii) None of the above presented classification schemes are based on the systematic evaluation of shelf-edge deltas; hence, the general validity of factors as the river size as controls on shelf-edge delta evolution, and consequently on shelf-edge delta geomorphology, has not yet been proven.

A.

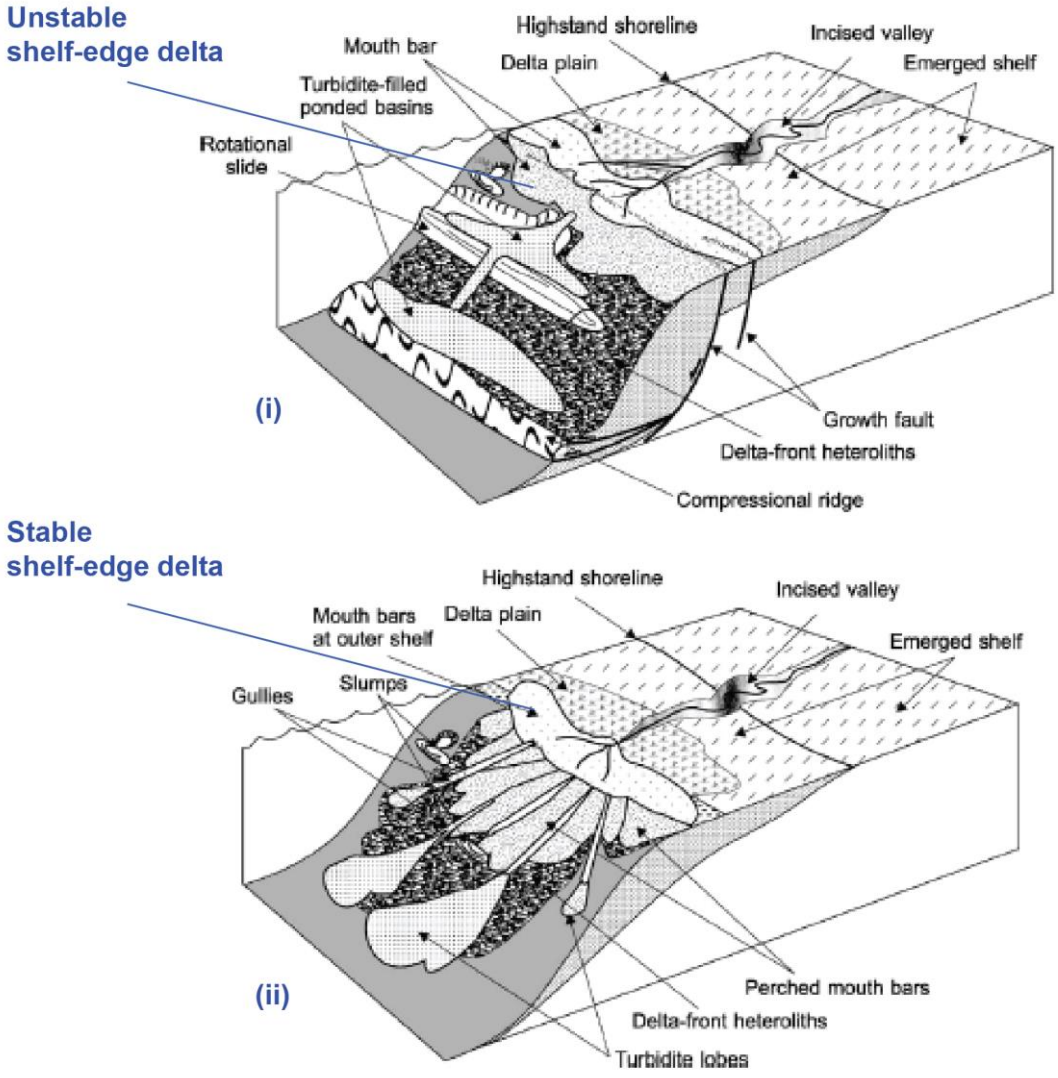

Porębski & Steel (2003)

B.

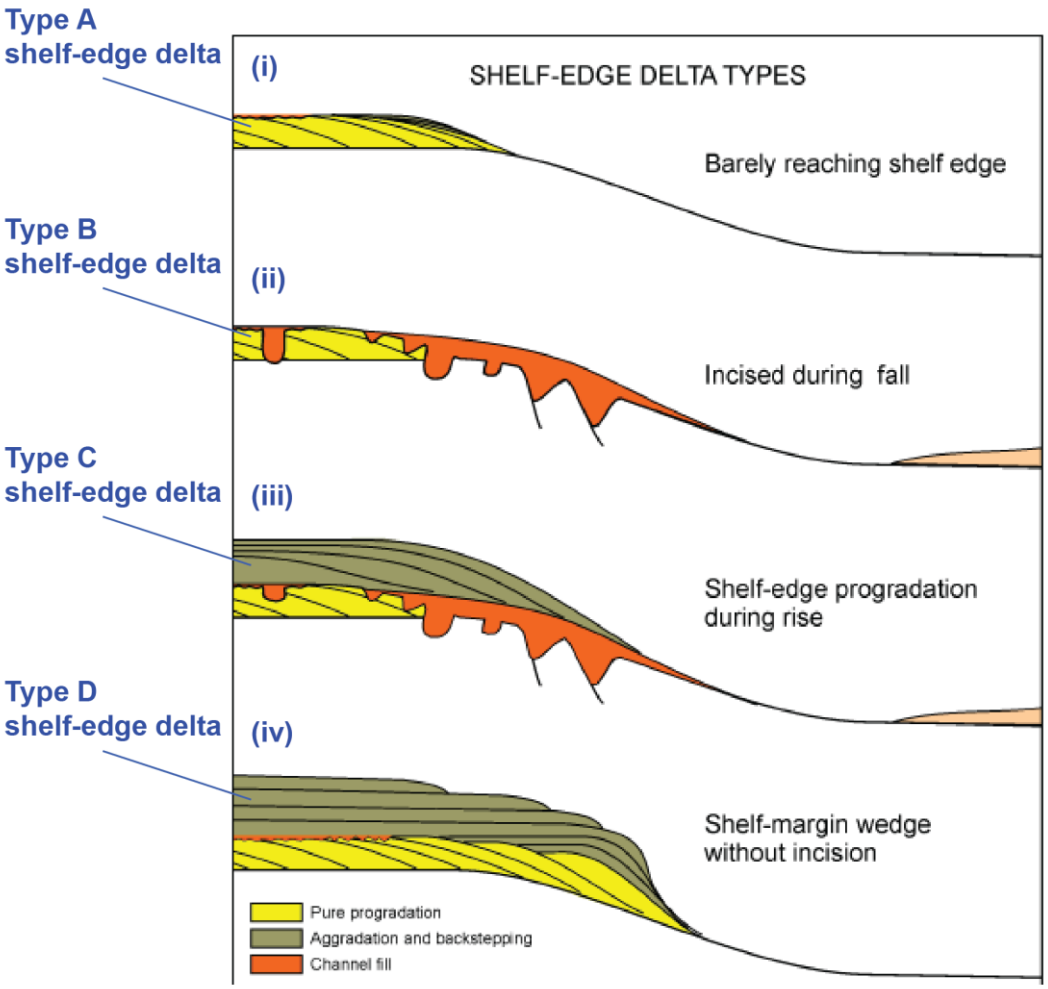

Steel et al. (2003)

Figure 2.7a-c (continued).

C.

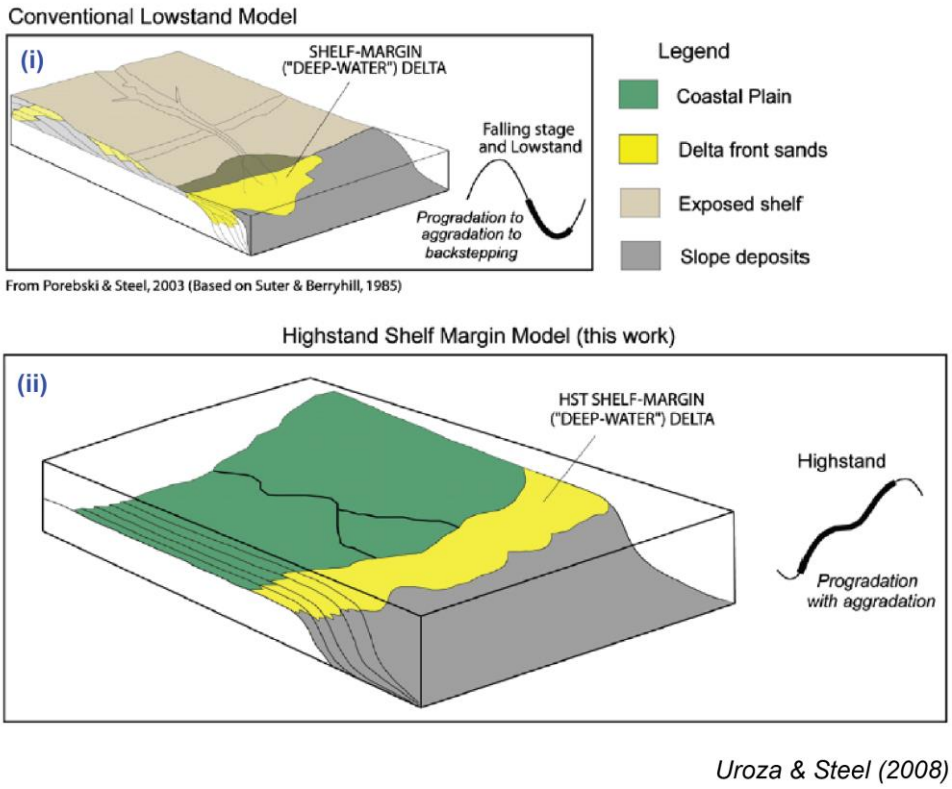

Figure 2.7a-c Examples of graphic visualisations of shelf-edge delta classification schemes in the literature sorted in ascending order by year of publication. Added text in blue (see also Table 2.3).

Criterion / Criteria	Delta classes	Definition	Delta geo-morphology	Reference(s)
Hydrodynamic process regime	Fluvial-dominated	Oblique parallel to complex sigmoid-oblique seismic clinoforms; lobate planview shape due to subordinate wave- & tidal influence	Planview shape	*e.g. Suter & Berryhill (1985); Anderson (2005); Dixon et al. (2012a) & refs. therein; Gong et al. (2016) & refs. therein*
	Wave-dominated	Redistribution of delta sediments by waves generates strike-elongated, shoreline-parallel planview shape	Planview shape	
	Tide-dominated	Develops at shelf margins within invaginations (e.g. slump scars; submarine canyon heads) where tidal influence is amplified	n.a.	
Delta stability	Unstable	Accommodation- & sediment supply driven evolution; large river or tectonically active terrestrial source area; sea-level fall below shelf margin; eroded by subsequent fluvial erosion; linked basin-floor fans; great delta thickness (100's of meters)	Delta thickness	*Porębski & Steel (2003)*
	Stable	Develops when sea level are at shelf margin depth during both regression & transgression; associated with small & modest rivers; strike-elongated lobate planview shape	Planview shape	
Sea level dynamics; position relative to shelf margin; degree of progradation; depositional characteristics; incision by fluvial channels; lithology; distribution of sediment to deep-water environments	Type A	Outer shelf to shelf edge location; develops during sea-level regression	n.a.	*Steel et al. (2003)*
	Type B	Shelf margin location; cannibalisation by subsequent fluvial erosion; forms during sea-level regression with base-level below shelf margin; sand-dominated; genetically linked basin-floor fans	n.a.	
	Type C	Shelf margin location; promote margin progradation; linked basin-floor fans rare; evolve during late transgression on older deltas & fans of same cycle; upward-coarsening & thickening units; great delta thickness (many 10's of meters)	Delta thickness	
	Type D	Shelf margin location; progradational-aggradational delta complexes of amalgamations of Types A & C; rare development of basin-floor fans; great delta thickness (many 10's of meters)	Delta thickness	
Sea level; shelf width; order of magnitude of sediment supply; depositional characteristics	Lowstand	Develops during sea-level regression & lowstand; delta architecture progradational to aggradational to backstepping	n.a.	*Uroza & Steel (2008)*
	Highstand	Forms during sea-level highstand even under low sediment supply given a sufficiently narrow shelf; delta architecture is progradational with aggradation	n.a.	

Table 2.3 Overview table of examples of shelf-edge delta classification schemes in the literature presented in ascending order by year of publication (see also Figure 2.8a-c). n.a. = not addressed.

2.4 Source-to-sink (S2S) research

2.4.1 Definitions

This section provides definitions of some of the key terms used in source-to-sink research.

2.4.1.1 The source-to-sink (S2S) system

Genetic relationships between fluvial systems, their associated deltas, submarine canyons and submarine fans were recognised as early as the late 1960s, with each of these sedimentary systems comprising individual parts within “one dynamic system” (Moore, 1969, p.2421). The first use of the term ‘source-to-sink’ (S2S) in a sedimentological context has been ascribed to Meade (1972, 1982), who investigated sediment budget distribution from the terrestrial environment to the shallow-marine environment in the context of anthropogenic influence (Helland-Hansen et al., 2016). Today, the term “source-to-sink system” is commonly applied to describe a superordinate system consisting of all genetically related sedimentary systems connected by sediment transport pathways, ranging from the most proximal source area – characterised by a predominantly erosional regime – to the ultimate sink – characterised by a dominantly depositional regime (e.g. Allen 2008, 2017; Blum & Hattier-Womack, 2009; Sømme et al., 2009; Bhattacharya et al., 2016; Helland-Hansen et al., 2016; Schattner & Lazar, 2016; Nyberg et al., 2018b; Hessler & Fildani, 2019) (Fig. 2.8).

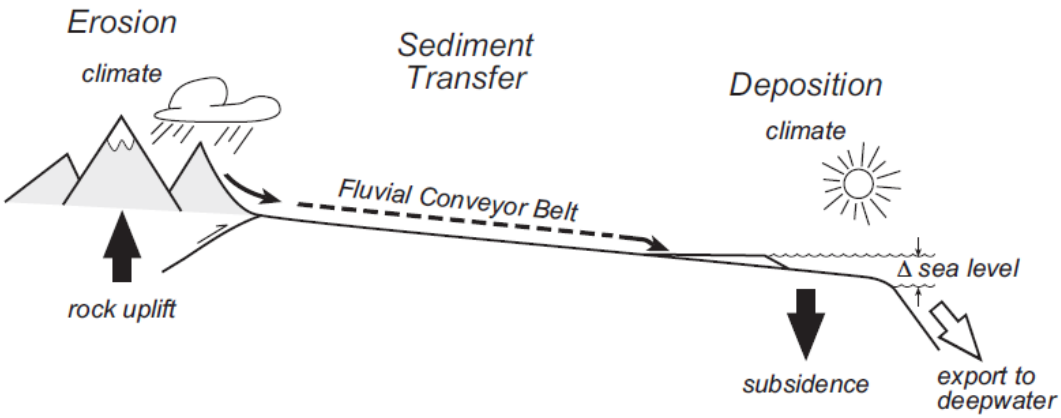

Figure 2.8 Schematic model of a source-to-sink system and some of its environmental controls (Blum & Hattier-Womack, 2009).

2.4.1.2 The sediment-routeing system

The sediment-routeing system conceptually comprises the entirety of all sediment pathways within a S2S system (e.g. Allen, 2008; 2017). The complexity of a S2S system is not only determined by the number of different processes that establish sediment pathways within it, but also by the number of source areas and sinks, and their interconnection (e.g. Allen, 2017) (Fig. 2.9a-d).

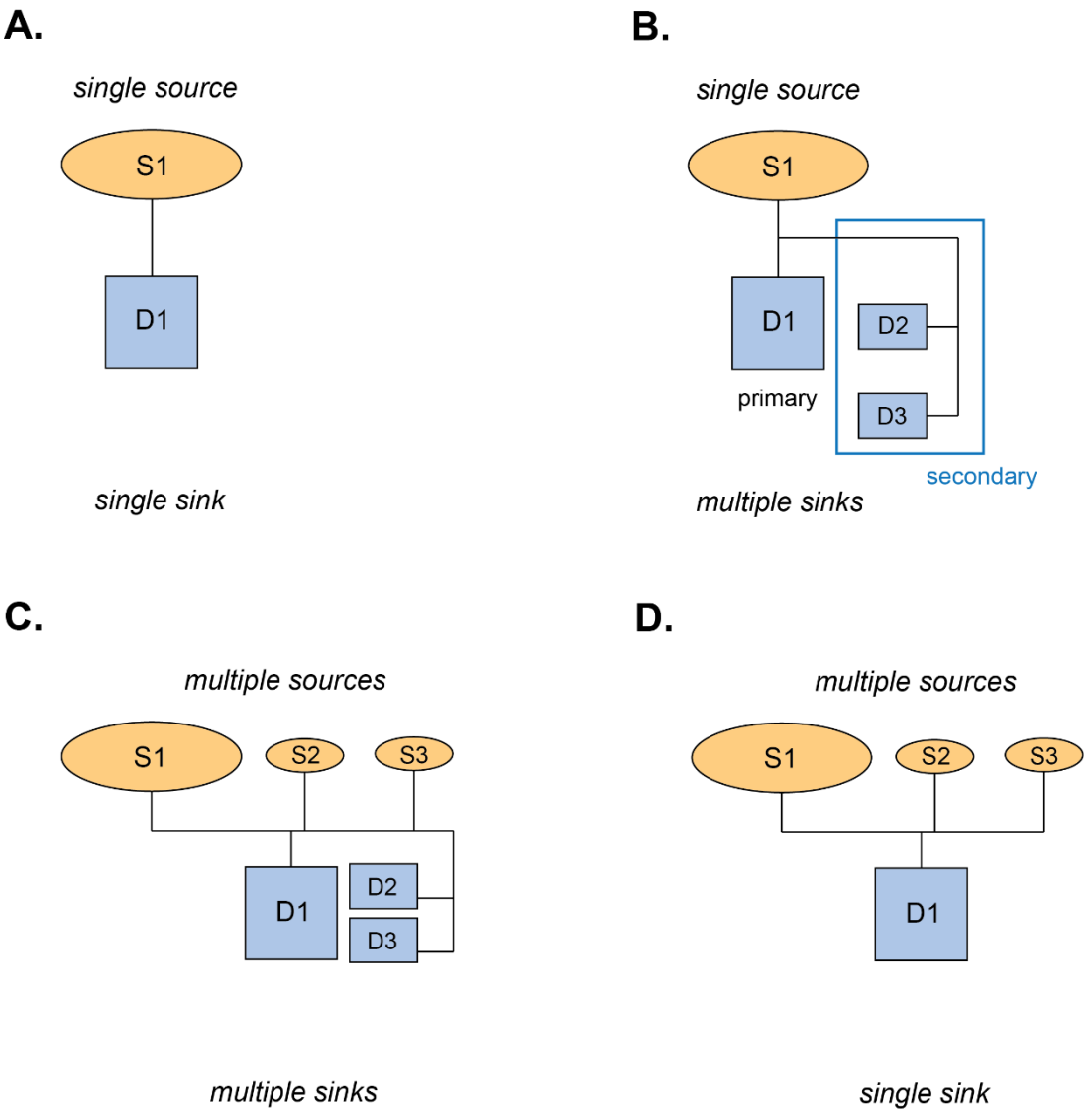

Figure 2.9a-d Examples of different types of sediment routeing systems from A. simple to B.-D. more complex configurations. S1-S3: Sediment source areas. D1-3: Depositional sink. A.-C. Modified after Figure 1.5 of Allen (2017). D. Source-to-sink system comprising multiple source areas and one sink (based in part on Allen, 2017).

2.4.1.3 Source areas

Within the S2S system a source area comprises an area characterised by a predominant erosional regime. S2S systems can be associated with single sources and with multiple sources (e.g. Allen, 2017; see also Fig. 2.9a-d).

2.4.1.4 Sinks

Sinks represent areas of accommodation where significant volumes of sediment are stored within a S2S system. Two major types of sinks, (i)

temporary or intermediate sinks and (ii) permanent or sustained sinks, can be distinguished (e.g. Bhattacharya et al., 2016; Allen, 2017):

(i) *Temporary or intermediate sinks* store sediment for a period of time during the activity of a S2S system. The sediment will undergo remobilisation at a certain point and thus be reintroduced into the sediment-routeing-system. Both submarine canyons and shelf-edge deltas can constitute intermediate sinks for sediment storage, which can be remobilised by mass failures (submarine canyons, e.g. Mountjoy et al., 2018; shelf-edge deltas, e.g. Peng et al., 2017).

(ii) *Permanent or sustained sinks* store sediment for a longer amount of time than a S2S system is active, so that the sediment is not reintroduced into the sediment-routeing system but becomes part of the depositional record, as shelf-edge delta deposits (e.g. Schwartz & Graham, 2015) and submarine canyon fills (e.g. Anderson et al., 2006). The transition of a temporary sink to a permanent sink and source area over time adds to the level of complexity S2S system models are challenged with.

The distinction between temporary and permanent sinks is ambiguous and arbitrary for modern systems due to the short window of observation and might be hampered in ancient systems with limited spatial data coverage.

2.4.1.5 Source-to-sink (S2S) system segments

Corresponding to the prevalent spatial configuration of ancient and modern clastic sedimentary systems and major geomorphologic features (e.g. Blum & Hattier-Womack, 2009), major sedimentary environments are recognised in S2S systems. The most common subdivision found in the literature and published S2S system models is the distinction into the four main segments (i) catchment, (ii) shelf, (iii) slope, and (iv) basin floor (e.g. Sømme et al., 2009; Martinsen et al., 2010; Bhattacharya et al., 2016; Helland-Hansen et al. 2016), which is also adapted in this research project. In some schemes, additional discrete segments are recognised within the four main segments as hillslope (e.g. Tofelde et al., 2021), alluvial- and coastal plains (e.g.

Nyberg et al., 2018b; Gong et al., 2021) and inner- and outer shelf environment (e.g. Gong et al., 2021) (see Figure 2.10a-e and Table 2.4).

The S2S concept has also been used to describe S2S systems confined to terrestrial environments (e.g. Nyberg et al., 2018a), including lacustrine (e.g. Liu et al., 2019) and palustrine settings (e.g. Teixeira et al., 2018). With the scope of this project being on shelf-edge deltas and submarine canyons as components of S2S systems, this chapter solely focuses on S2S systems associated with these sedimentary system types.

A.

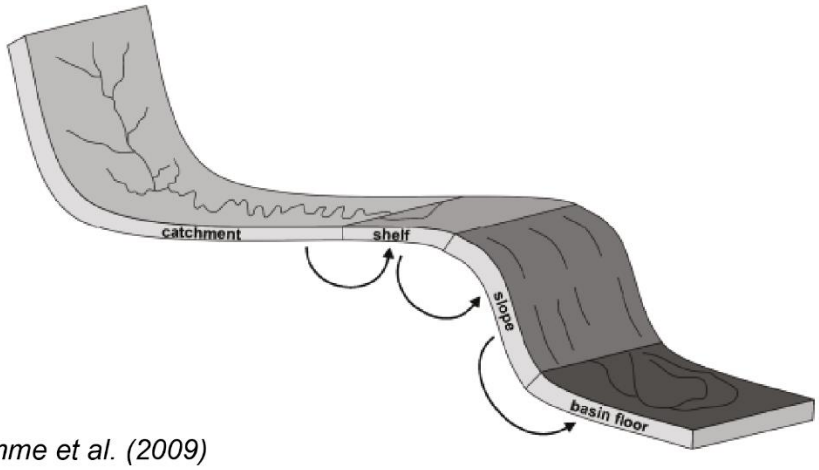

Sømme et al. (2009)

B.

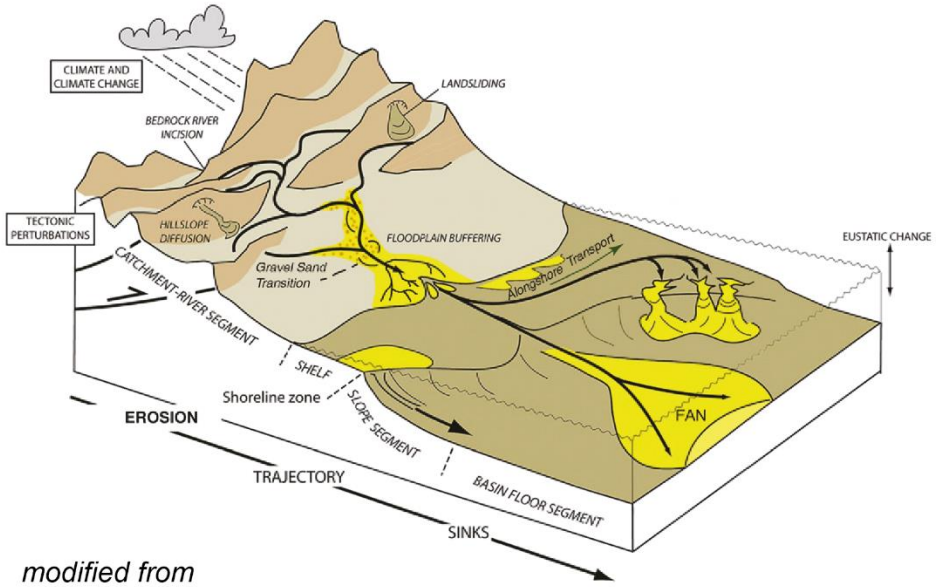

modified from
Bhattacharya et al. (2016)

C.

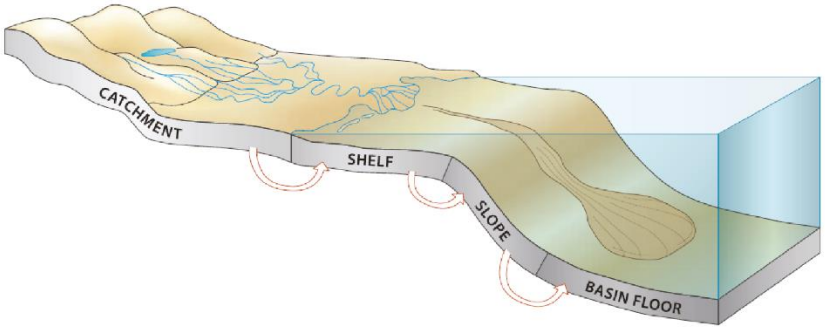

Helland-Hansen et al. (2016)

D.

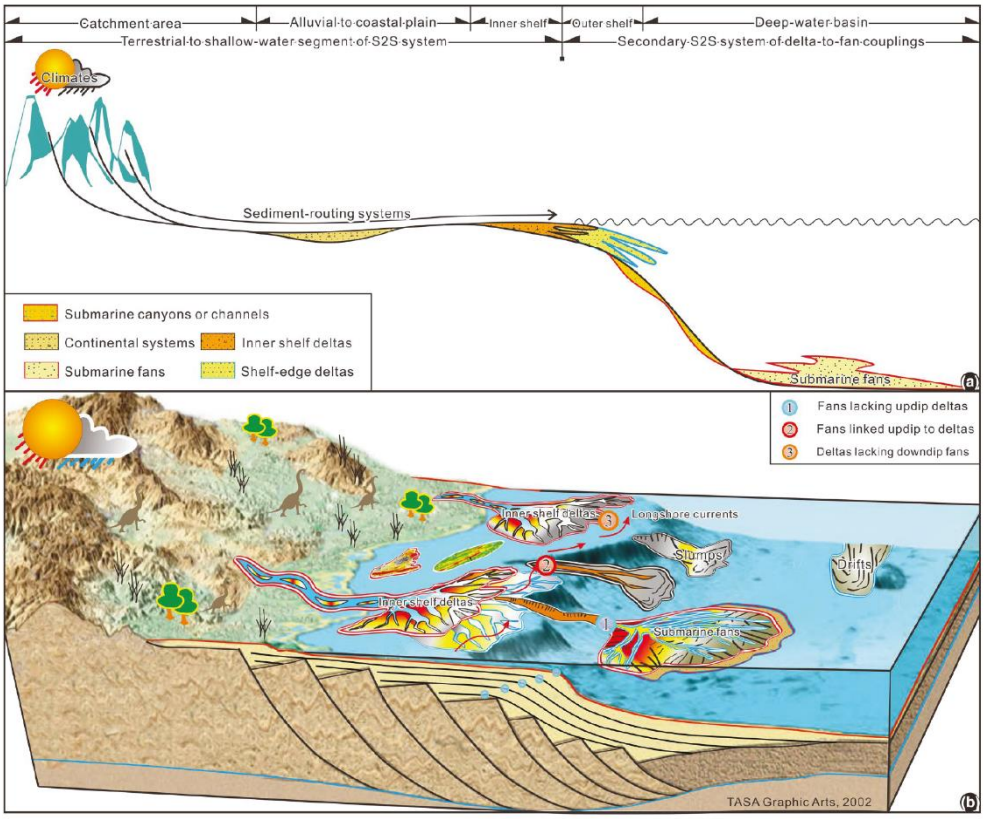

Gong et al. (2021)

E.

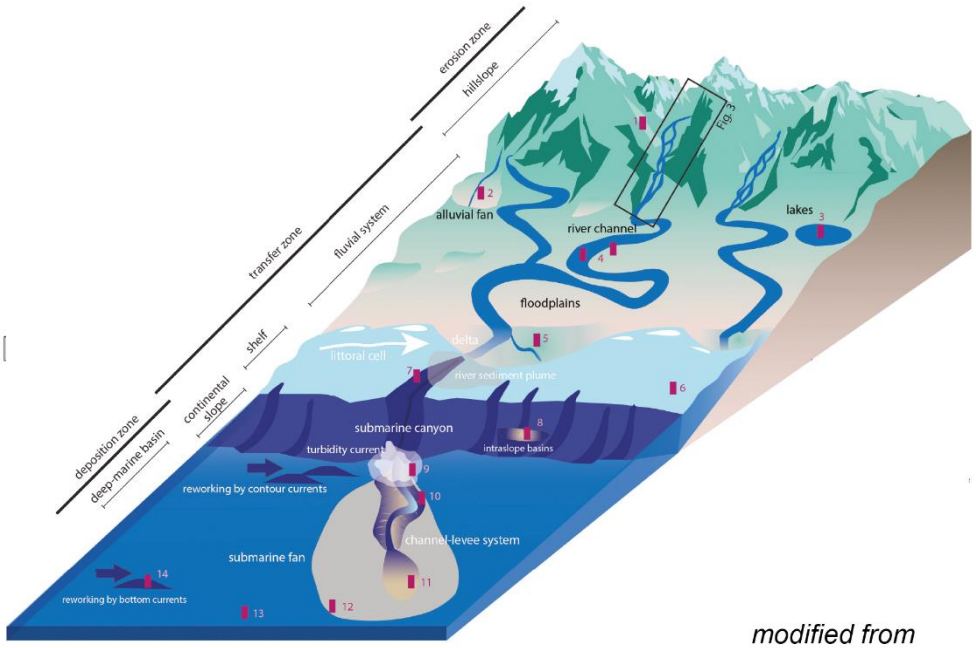

modified from Tofelde et al. (2021)

Figure 2.10a-e Examples of major segments of source-to-sink systems recognised in conceptual models in the literature sorted in ascending and alphabetical order by year of publication (see also Table 2.4).

Individual segments of S2S systems					References
Catchment	***	Shelf	Slope	Basin-floor	*Sømme et al. (2009); Bhattacharya et al. (2016); Helland-Hansen et al. (2016); **this study***
Catchment	Alluvial- & coastal plains	Shelf	Slope	Basin-floor	*Nyberg et al. (2018b)*
Catchment	Alluvial- to coastal plain	Inner shelf	Outer shelf	Deep-water basin	*Gong et al. (2021)*
Hillslope	Fluvial system	Shelf	Slope	Deep-water basin	*Tofelde et al. (2021)*

Table 2.4 Examples of source-to-sink system segments distinguished in conceptual models in the literature presented in ascending and alphabetical order by year of publication (see also Figure 2.11a-e) and this study.

2.4.2 Source-to-sink (S2S) system models

2.4.2.1 Representation of submarine canyons and shelf-edge deltas in conceptual models of source-to-sink (S2S) systems

Submarine canyons and shelf-edge deltas are important components of source-to-sink systems as (i) sediment sinks, and (ii) for the construction of deep-water systems from the routeing of sediment from source areas within the terrestrial hinterland, shelf- and slope environment to basin-floor sinks. However, despite the diverse processes acting in submarine canyons and range in potential sediment source areas that are recognised in the literature, conceptual models of S2S systems that extend across both terrestrial and marine environments are often limited to a configuration with a terrestrial hinterland catchment incised by a major fluvial system discharging onto the continental shelf. There, the fluvial sediment is captured by shelf-incising submarine canyons that extend down to the basin-floor, where a submarine fan is constructed as the ultimate long-term sediment sink (e.g. Sømme et al., 2009; Blum et al., 2013; Bhattacharya et al., 2016; Helland-Hansen et al., 2016; Nyberg et al., 2018b; Hessler & Fildani, 2019) (see Fig. 2.10a-e).

Possibly, the prevalence of this configuration in the literature – which is referred to as the “classical” S2S model in the following – is in part founded in the long-standing economic interest in sand-rich submarine-fan systems for hydrocarbon exploration (e.g. Moore, 1969; Martinsen et al., 2010; Gong et al., 2021 and references therein) and in the value of submarine fans as archives of information on the evolution of geographic regions over time, providing insights on the influence of environmental factors as climate, tectonic- and anthropogenic activity (e.g. Romans et al., 2016; Blum et al., 2018; Hessler & Fildani, 2019).

Another factor might be that this configuration of a S2S system is generally favourable for source-to-sink case studies; the vicinity of fluvial outlets to adjacent shelf-incising submarine canyons promotes stable sediment budgets across continental margins of S2S systems, with fewer loss of sediment out of the system and detectable sediment connections between the terrestrial and marine parts (e.g. Allen, 2017, and references therein).

In comparison to submarine canyons, shelf-edge deltas tend to be underrepresented in S2S system models (see Fig. 2.10a-e) and are commonly depicted in a general context of their function as major sediment distributors to deep-water environments (Fig. 2.11a&b).

A.

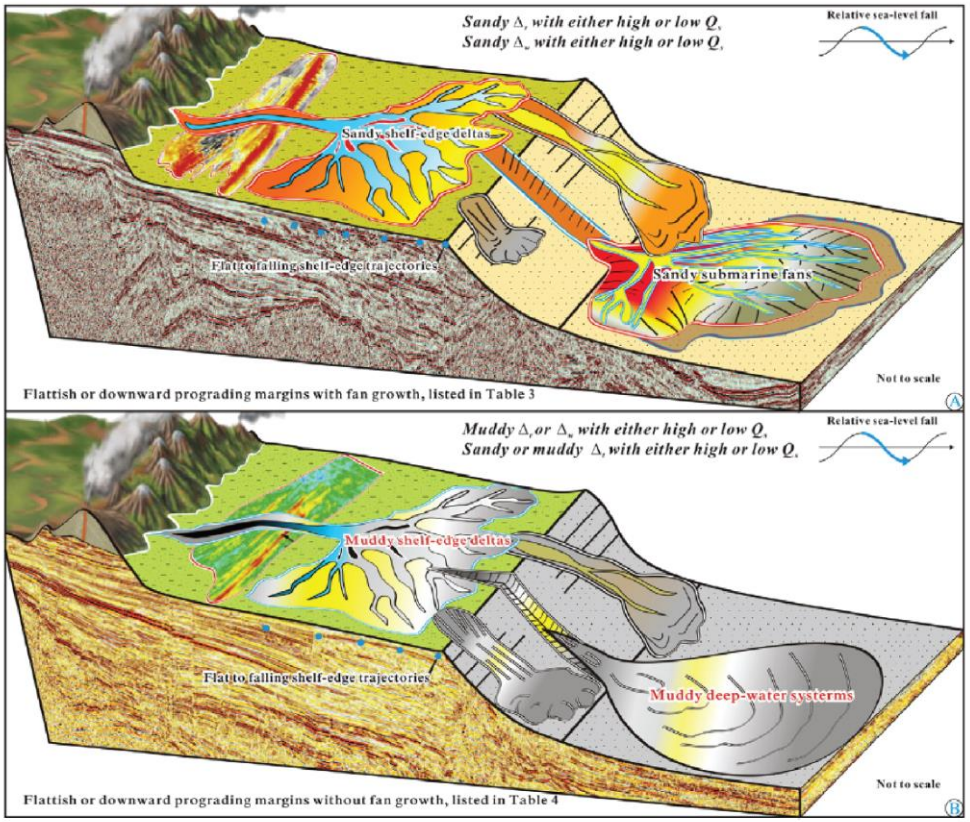

Gong et al. (2016)

B.

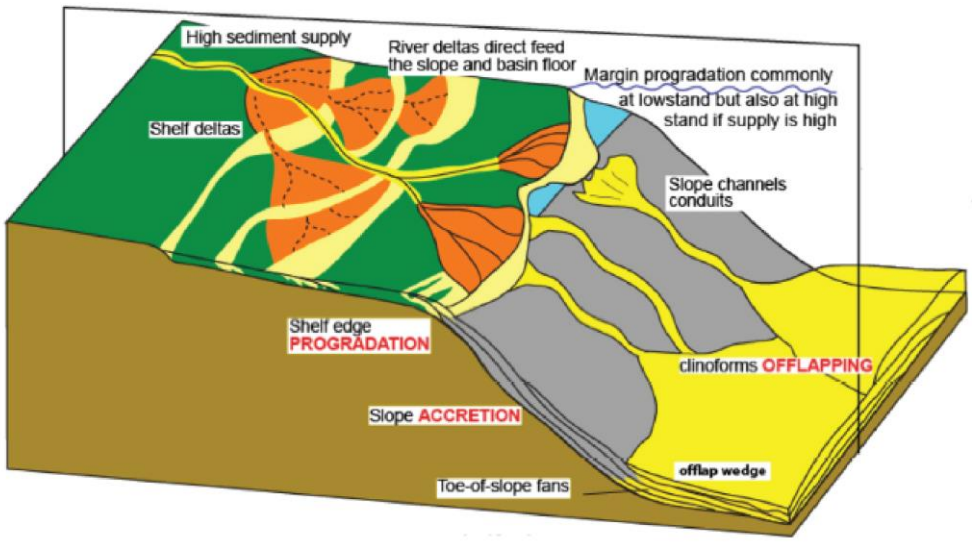

Fisher et al. (2021)

Figure 2.11a&b Examples of source-to-sink system models with shelf-edge deltas in their configuration in ascending order by year of publication.

2.4.2.2 Representation of sediment transport pathways and marine hydrodynamic processes in conceptual models of source-to-sink (S2S) systems

Sediment pathways represent the dynamic links between the various sources and sinks of a S2S system, exerting a primary control on its spatial extent. In classical S2S system models, the overall sediment transport direction is often oversimplified to a predominantly unidirectional, down-system transport from terrestrial highs to basinal lows within an overall linear sediment-routeing system along the overall gradients of continental landmasses, shelves, and slopes. In addition, off-axial sediment transport by currents along shorelines (e.g. Figure 8 of Sømme et al., 2009; Figure 1 of Bhattacharya et al., 2016; Fig. 13 of Gong et al., 2021) and continental slopes (e.g. Figure 2 of Hessler & Fildani, 2019; Figure 1 of Tofelde et al., 2021) is considered to some degree in S2S system models. By contrast, other hydrodynamic processes which affect sediment routeing within the marine environment tend to be underrepresented, despite their efficiency in transporting both coarser and finer grain-size fractions within the marine parts of S2S systems, including geostrophic currents, upwelling and downwelling, cascading of shelf waters, tidal currents and waves, internal waves, and storm waves (see Table 2.5).

Hydrodynamic process	Max. grain size transport	Order of duration	Reference(s)
Dense shelf-water cascading	Sand	Days to weeks	*Gaudin et al. (2006); Palanques et al. (2006a)*
Downwelling	Sand	Days to weeks	*Gaudin et al. (2006)*
Geostrophic currents	Sand	Long-term	*Ramsay et al. (1996)*
Longshore currents	Sand	Long-term	*Boyd et al. (2006);*
Slope currents	Sand	Long-term	*Hernández-Molina et al. (2015); Serra et al. (2020)*
Storm currents & waves	Gravel	Hours to days	*McCarroll et al. (2019); King et al. (2019)*
Tidal currents & waves	Sand	Long-term	*Mountjoy et al. (2014)*
Upwelling	Sand	Days to weeks	*Huhn et al. (2007)*

Table 2.5 Overview of marine hydrodynamic processes, their capabilities to transport grain-size fractions and their order of duration.

The scarcity of representation of marine hydrodynamic processes in S2S models might in part reflect challenges in their direct observation and quantification both in modern environments and in the depositional record, and linking such findings to sediment budgets (e.g. Carvajal & Steel, 2009). More recent advancements in the observation and measurement of interactions between marine hydrodynamic processes and sedimentary systems as submarine canyons (e.g. Puig et al., 2014 and references therein; Rodrigues et al., 2022; Wang et al., 2022b) and submarine fans

(e.g. Rodrigues et al., 2022), the influence of some of these processes on the evolution of submarine canyons and shelf-edge deltas (see sections 2.2.2.1 and 2.3.2.1, respectively), and tracking of sediment transport by oceanic currents along greater distances in regional-scale S2S studies (e.g. Boyd et al., 2008), however, emphasize the importance to consider marine hydrodynamic processes in S2S system models.

Moreover, sediment pathways established by aeolian transport (e.g. Henrich et al., 2010; Pierau et al., 2010), hemipelagic fallout (e.g. Jobe et al., 2011; Amblas et al., 2012) and glacial processes (e.g. Armitage et al., 2010; Gales et al., 2021) tend to be neglected in S2S models, although these transport mechanisms might distribute significant volumes of sediment across continental margins/to submarine canyons.

2.4.2.3 Complexity of sediment routeing systems

In classical models, the S2S system is commonly supplied by sediment from a major, most proximal terrestrial hinterland source, usually a mountain range (e.g. Allen, 2008; Blum & Hattier-Womack, 2009), in agreement with inferences made for examples of some modern (e.g. Rhône River S2S system, Normark et al., 1983; Congo River S2S system, Anka et al., 2009) and ancient S2S systems (e.g. ancestral Mississippi S2S system, Lee et al., 1996). However, for S2S systems for which (i) multiple terrestrial source areas have been identified (e.g. Clift & Giosan, 2013; Blum et al., 2018), (ii) marine source areas co-exist (e.g. Liu & Yin, 2004), or (iii) function as the main sediment source to slope systems (e.g. Boyd et al., 2008; Warratz et al., 2019; Serra et al., 2020), the classical model is not applicable. Moreover, S2S systems can also be primarily sourced via other S2S systems, as in the case of the Levant depositional system, which has been interpreted to be primarily supplied by the Nile sedimentary system (see Schattner & Lazar, 2016 & Fig. 2.14d this Chapter). These varying degrees of complexity in S2S system configuration are not captured effectively in the classical S2S system model.

2.4.3 Source-to-sink (S2S) system classifications

A unifying classification scheme for S2S systems in the literature is absent. Instead, source-to-sink systems have been variously classified based on

different criteria, including (i) intra- vs. extra-basinal sediment sources, (ii) morphological characteristics of S2S systems, (iii) efficiency of signal propagation across a S2S system, (iv) sediment connection between S2S systems, and (v) hierarchical relationships between S2S systems. The different classification schemes are summarised in sections 2.4.3.1 to 2.4.3.5 and presented in Figure 2.14a-e and Table 2.6.

2.4.3.1 Intra- vs. extra-basinal sediment sources

The duration, source type and volume of sediment supply under consideration of sea-level change have been contrasted in the “conveyor-belt” vs. “vacuum-cleaner” models developed by Blum & Törnqvist (2000; see also Blum & Hattier-Womack, 2009; Blum et al., 2013); the former is associated with long-lived sediment supply from an extra-basinal fluvial system with large catchment area and the latter with the excavation of incised valleys acting as an intra-basinal sediment source (Figure 2.12a & Tab. 2.6).

2.4.3.2 Morphological characteristics of source-to-sink (S2S) systems

Helland-Hansen et al. (2016) proposed a simplified first-order classification of S2S systems into three major end-member types based on morphological characteristics of S2S segments including widths and overall gradients of terrestrial catchments, continental shelves and slopes, basin depth and the overall length of the S2S system into (i) steep, short and deep, (ii) wide and deep, and (iii) wide and shallow systems (Figure 2.12b & Tab. 2.7). Their scheme was revised and augmented by Nyberg et al. (2018b), who discarded the class of wide and shallow systems and further differentiated the other classes based on the tectonic setting (Figure 2.12e & Tab. 2.6).

2.4.3.3 Efficiency of signal propagation across a source-to-sink (S2S) system

Based on the efficiency of propagation of environmental signals, defined as “changes in sediment production, transport, or deposition that originate from perturbations of environmental variables such as precipitation, sea level, rock uplift, subsidence, and human modifications” (p. 8, Romans et al., 2016) from terrestrial catchment source areas to deep-marine sinks,

Romans et al. (2016) categorised (i) reactive, (ii) hybrid and (iii) buffered S2S systems (Figure 2.12c & Tab. 2.6).

2.4.3.4 Hierarchical relationships between source-to-sink (S2S) systems

For S2S systems with separate sediment pathways that connect with each other, a hierarchical approach was presented by Schattner & Lazar (2016); these authors established a hierarchy between primary and secondary S2S systems based on the relative importance of sediment-routeing pathways and along-axis vs. off-axis sediment transport (Figure 2.12d & Tab. 2.6).

2.4.3.5 Sediment connection between source-to-sink (S2S) systems

Depending on whether sediment budgets within a S2S system (i) remain relatively stable or (ii) change as a consequence of external sediment supply and/or removal of sediment, S2S systems have been distinguished into ‘closed systems’ and ‘open systems’, respectively (e.g. Kuehl et al., 2016; Pechlivanidou et al., 2018) (Tab. 2.6).

A.

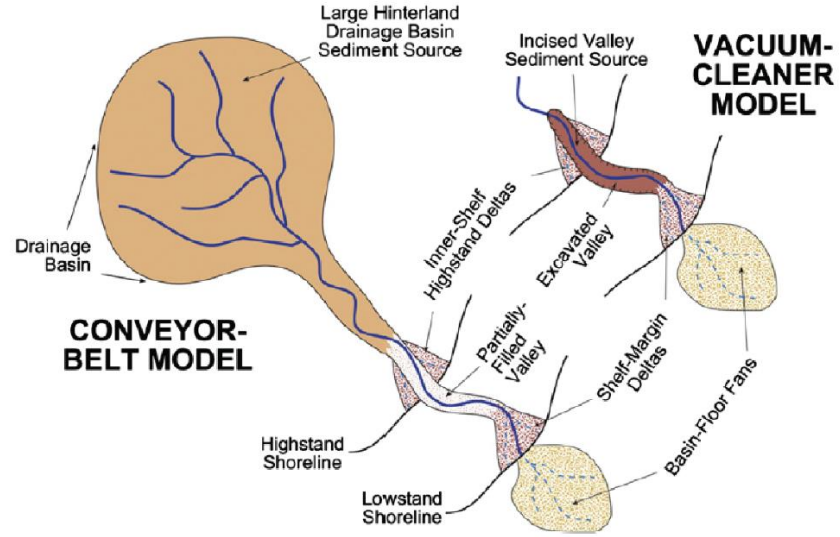

Blum et al. (2013) after Blum & Törnqvist (2000); Blum & Hattier-Womack (2009)

B.

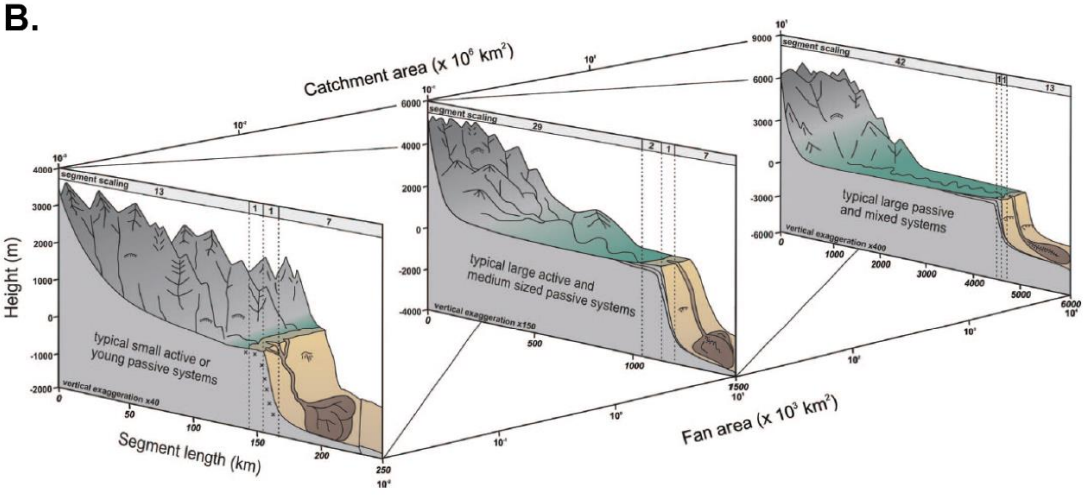

Helland-Hansen et al. (2016)

C.

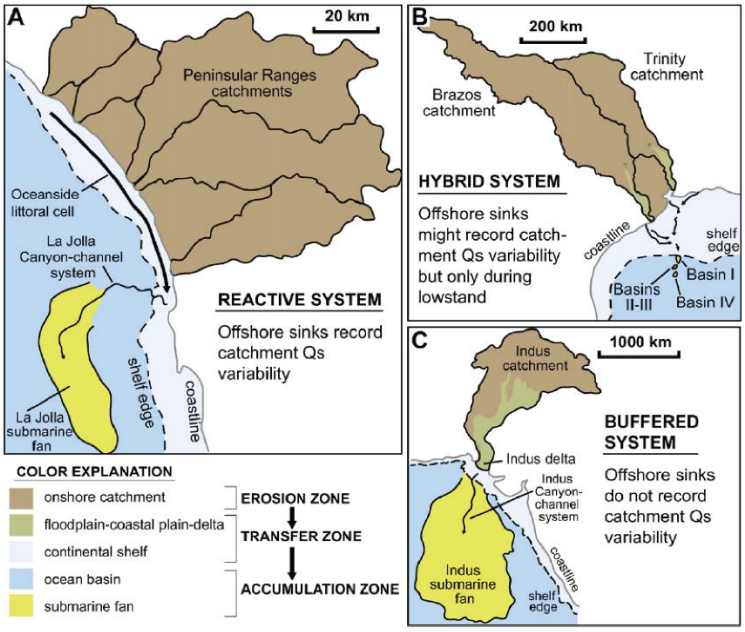

Romans et al. (2016)

D.

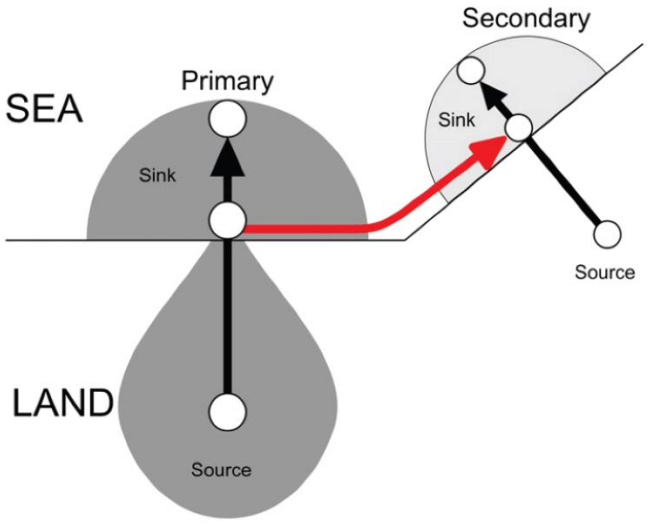

Schattner & Lazar (2016)

Figure 2.12a-e (continued).

E.

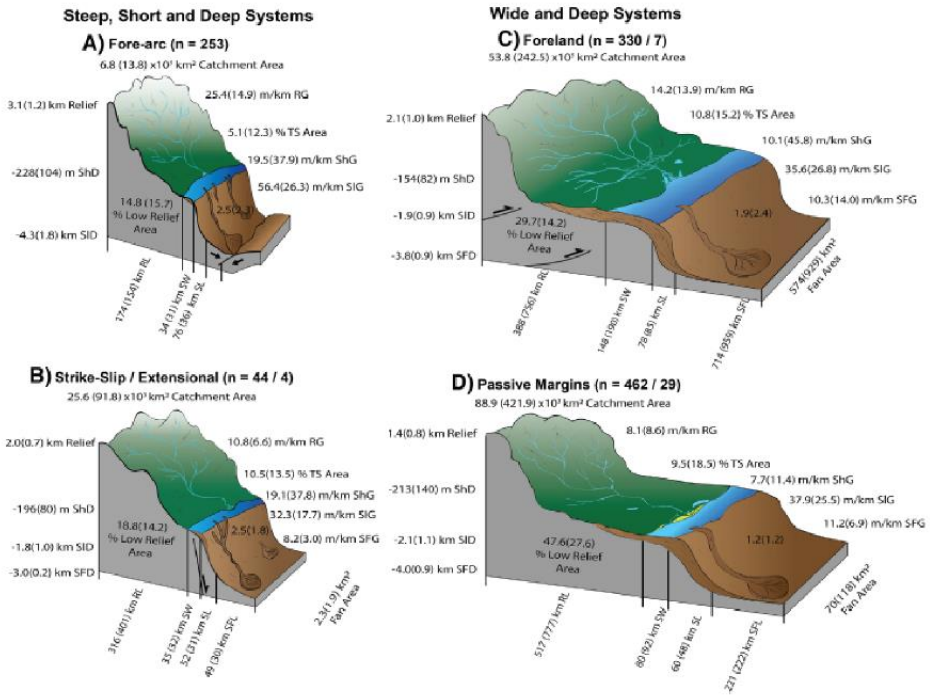

Nyberg et al., (2018b)

Figure 2.12a-e Graphic visualisations of classification schemes for source-to-sink systems in the literature sorted in ascending and alphabetical order by year of publication (see also Table 2.6).

Criterion / Criteria	S2S system classes	Reference(s)
Intra- vs. extra-basinal sediment sources	"Conveyor-belt"	*Blum & Törnqvist (2000); Blum & Hattier-Womack (2009); Blum et al. (2013)*
	"Vacuum-cleaner"	
Morphological characteristics of S2S segments	Steep, short and deep	*Helland-Hansen et al. (2016)*
	Wide and deep	
	Wide and shallow	
Efficiency of signal propagation from terrestrial catchments to deep-marine sinks	Reactive	*Romans et al. (2016)*
	Hybrid	
	Buffered	
Hierarchical relationships between different S2S systems	Primary	*Schattner & Lazar (2016)*
	Secondary	
Morphological characteristics of S2S segments; tectonic setting	Steep, short and deep (fore-arc)	*Nyberg et al. (2018b)*
	Wide and deep (strike-slip/extensional)	
	Wide and deep (foreland)	
	Wide and deep (passive margins)	
Sediment connection between different S2S systems	Closed	*e.g. Kuehl et al. (2016); Pechlivanidou et al. (2018)*
	Open	

Table 2.6 Overview of classification schemes of source-to-sink (S2S) systems in the literature sorted in ascending and alphabetical order by year of publication (see also Figure 2.14a-f).

Although all of the above schemes address important characteristics of S2S systems, these aspects remain to be integrated in one holistic classification scheme. Moreover, some factors that can have an effect on the configuration and extent of S2S systems are not considered, including (i) the accommodation of a S2S system on a continent versus an island, (ii) the oceanographic setting and whether a S2S system is associated with an open sea or a semi-enclosed or enclosed sea, and (iii) the latitudinal position or climate zone of a S2S system.

For example, in insular S2S systems, the size of the terrestrial catchment and width of the continental shelf might be inherently limited, whereas the size of the marine basin – and consequently the configuration of the slope and basin-floor segments – are naturally restricted in semi-enclosed and enclosed seas compared to open oceanic settings. Also, due to its influence on factors including precipitation, evaporation, chemical- and mechanical erosion, thermohaline currents, and surface vegetation, climate affects the transport dynamics of sediment routeing systems as well as the size of terrestrial catchments (e.g. Milliman & Farnsworth, 2011).

Moreover, genetic relationships of sedimentary systems with each other and with characteristics of the S2S system, which have been demonstrated from the investigation of scaling relationships in quantitative studies (see Chapter 1), are – if at all – only considered to a limited extend in some of the schemes.

2.5 Sedimentary systems at the shelf-to-slope transition: The importance of shelf-edge deltas and submarine canyons as controls on continental-margin evolution

2.5.1 Influence of submarine canyons and shelf-edge deltas on the evolution of continental margins

As outlined in sections 2.2 and 2.3 both submarine canyons and shelf-edge deltas are important elements of continental margins, which influence sediment transport dynamics within the shelf and slope environment.

Shelf-edge deltas can variably affect the evolution of continental margins. Where stable shelf-edge deltas are established along shelf margins, they can promote the healing of shelf margins (e.g. Steventon et al., 2020) and outbuilding of shelves given sufficiently high sediment supply (e.g. Morton & Suter, 1996; Porębski & Steel, 2003; Steel et al., 2003). Along margins where sediment is (i) bypassing the shelf edge via routeing across a shelf-margin delta to deep-water environments (e.g. Kim et al., 2013), (ii) remobilised by delta-front failure (e.g. Roberts & Sydow, 1996) or (iii) eroded by prograding distributary channels cutting into older delta sediments (e.g. Steel et al., 2003; Carvajal & Steel, 2009), margin growth can be inhibited in

the presence of shelf-edge deltas. By contrast, submarine canyons can promote margin erosion by their retrogradation across the slope and triggering of mass failures (e.g. Casalbore et al., 2018); where canyons have retrograded in front of rivers they might also counteract the growth of a continental margin by preventing the development of shelf-edge deltas by directly routeing fluvial sediment discharge to deep-water environments (e.g. Porębski & Steel 2003; Fisher et al., 2021) and eroding delta deposits (e.g. Porębski & Steel 2003).

In addition to inhibiting the evolution of deltas from the cannibalisation of their deposits, submarine canyons can also interfere with the evolution of deltas, incised valleys and submarine canyons where they intercept current-transported sediment along continental margins (e.g. Bernhardt et al., 2015). From their influence on the routeing of sediment to deep-marine environments the two sedimentary system types also exert control on the evolution of deep-water systems (shelf-edge deltas, e.g. Dixon et al., 2012; Gong et al., 2016; submarine canyons, e.g. Nelson et al., 1970; Hessler & Fildani, 2019).

Also, the presence of submarine canyons and shelf-edge deltas along a margin can affect the local hydrodynamic regime: Submarine canyons can focus waves (e.g. Smith et al., 2018) and upwelling bottom waters (e.g. Brun et al., 2023), and the presence of large-scale depressions of canyon heads within the shelf can locally modify hydrodynamic patterns within the shelf (e.g. Saldías & Allen, 2020). Similarly, where shelf-edge deltas have sufficiently prograded across continental slopes, the local creation of promontories might promote the capture of sediment transported by longshore currents, and modify the local hydrodynamic regime (e.g. Gardner et al., 2005).

Hence, both sedimentary system types are important controls on the long-term evolution of continental margins. Moreover, the ability of submarine canyons and shelf-edge deltas to facilitate sediment transport across the shelf edge to slope and basin-floor environments makes them important controls on the evolution of deep-water basins (e.g. Gong et al., 2016; Fisher et al., 2021).

2.5.2 Influence of submarine canyons and shelf-edge deltas on source-to-sink (S2S) systems

2.5.2.1 Size and extent of source-to-sink (S2S) systems

The size and extent of the marine part of a S2S system is ultimately controlled by the efficiency and distance of sediment transport across continental slopes and basin floors. For this, shelf-edge deltas and submarine canyons constitute key systems at the shelf-slope transition, because both sedimentary system types facilitate sediment transport across the shelf margin from terrestrial and intra-shelf source areas (shelf-edge deltas, e.g. Dixon et al., 2012, Gong et al., 2016; submarine canyons, e.g. Covault et al., 2011b; Puig et al., 2014 and references therein). Also, shelf-edge deltas and submarine canyons can prevent the routeing of sediment to deep-water environments by sediment storage in their sinks, either temporarily or permanently (shelf-edge deltas, e.g. Bourget et al., 2014; submarine canyons, e.g. Mountjoy et al., 2018).

2.5.2.2 Evolution of younger source-to-sink (S2S) systems

The presence of submarine canyons and shelf-edge deltas along a continental margin might also impact the evolution of subsequent, younger source-to-sink systems. Older submarine canyons can function as preferred pathways for younger canyons where their channel-forms have created negative seafloor relief and the fills of submarine canyons are more erosive compared to the surrounding substrate. Along mixed siliciclastic-carbonate margins, the presence of shelf-edge deltas may inhibit the local evolution of later clastic sediment distribution systems. This is because drowned shelf-edge deltas have been shown to constitute a suitable substrate for the development of reef systems (e.g. Droxler & Jorry, 2013 and references therein; Daniell et al., 2020), which in turn can function as barriers for sediment transport within the shelf and into the slope segment and might also prevent the retrogradation of canyons onto the shelf (e.g. Puga-Bernabéu et al., 2011).

2.6 Summary

This chapter has reviewed the scientific literature relevant to the aim and research objectives of this project (see section 1.2). The following key research gaps in the literature were identified:

(i) The understanding of controlling factors and their relative importance for the geomorphology of both submarine canyons and shelf-edge deltas is still limited, which is likely partially founded in the paucity of global-scale studies and limited consideration of variables investigated in quantitative studies. In addition, it is likely that several controls may affect individual morphometric attributes, and that single controls may variably affect several attributes; a comparative assessment is required to estimate these impacts.

(ii) This shortage in knowledge might contribute to the paucity of conceptual models and classification schemes for both sedimentary system types, and underrepresentation of shelf-edge deltas in S2S system models. Although submarine canyons are commonly considered in S2S system models with deep-water components, the representation of S2S system configurations tends to be focused on submarine canyons which are sourced by fluvial discharge, neglecting other sediment source areas and transport pathways.

(iii) Despite the existence of many classification schemes of S2S systems, none of them consider the role of submarine-canyon or shelf-edge delta geomorphologies as controls of the shallow- and deep-water parts of S2S systems.

(iv) Factors that influence the evolution of submarine canyons and shelf-edge deltas also exert influence on the evolution of the superordinate S2S system; hence, such insights will not only promote the development of conceptual models and classification schemes of submarine canyons and shelf-edge deltas, but also of S2S systems which comprise one or both of the two types of sedimentary systems.

3 A global analysis of controls on submarine-canyon geomorphology

3.1 Introduction

Submarine canyons constitute important conduits for the transfer of water masses, sediment, nutrients, organic matter and pollutants between shallow- and deep-marine environments, across continental slopes (Harris and Whiteway, 2011; Fildani, 2017). They control the sorting and segregation of sediments that are ultimately deposited in deep-marine environments, via their morphology (e.g. Soutter et al., 2021; Wan et al., 2021) and distance from fluvial outlets and littoral cells (e.g. Sweet & Blum, 2016; Sweet et al., 2020). Their ability to intercept and influence oceanic currents along shelves (e.g. Jordi et al., 2008) and slopes (e.g. Marchès et al., 2007; Voigt et al., 2013), can set hydrodynamic conditions in vicinity of their location (e.g. Allen et al., 2001; Connolly and Hickey, 2014; Saldías and Allen, 2020). Submarine canyons can impact the formation and evolution of slope systems by reducing local gradients (Orange et al., 1994), capturing and redirecting sediment pathways from adjacent canyons (e.g. Bernhardt et al., 2015), and functioning as tributaries to other canyons (e.g. Mountjoy et al., 2009). Buried canyons that are partially infilled can influence the pathways of younger ones by forming negative seafloor topography that can confine sediment transport (e.g. Pratson et al., 1994). Thus, they represent a crucial link for sediment routeing from terrestrial hinterlands, across and along shelves and slopes, to intra-slope and basin-floor sinks.

The presence of submarine canyons can also influence the formation of gas hydrates, for example in the process of canyon down-cutting by shifting the base of gas hydrate stability in underlying sediments (e.g. Davies et al., 2012; Crutchley et al., 2017). In addition, canyon fills can function as traps for hydrocarbons, which can be released by subsequent flows, and where a canyon erodes into a reservoir (e.g. Benjamin et al., 2015). Canyons can promote salt migration within the subsurface and impact the geometry of salt bodies (Fiduk, 1995), can increase the salinity of shelf waters via upwelling of deeper slope waters (e.g. Connolly and Hickey, 2014), and can tap into groundwater aquifers (e.g. Paldor et al., 2020). The association of submarine canyons with hydrocarbon-bearing deposits can promote vertical hydrocarbon migration and expulsion, which in turn can generate trains of

pockmarks in younger canyons (e.g. Benjamin et al., 2015). Pockmarks can also form atop of canyon fills as a result of sediment compaction (e.g. Jobe et al., 2011); given that these structures can reach diameters of several hundred metres and depths of tens of metres (e.g. Jobe et al., 2011; Benjamin et al., 2015), their presence might affect canyon internal flows and flow pathways on the seafloor.

Submarine canyons are also important for faunal communities, for which they provide significant habitats. Aspects of their physiography have been suggested to exert control on the biodiversity and abundance of faunal assemblages; these aspects include canyon spacing, gradient, dendricity and sinuosity (Fanelli et al., 2018), canyon size and magnitude of incision of the shelf (Santora et al., 2018). The effect of submarine-canyon geomorphology on hydrodynamic processes also impacts the spatial distribution of faunal communities like zooplankton (Allen et al., 2001).

Submarine canyons are linked to potential geohazards, due to the ability of intra-canyon slope failures to trigger tsunamis (e.g. Orange et al., 1994; Power et al., 2016), and to the influence of canyon geomorphology on tsunami propagation (e.g. Aranguiz and Shibayama, 2013; Iglesias et al., 2014). Moreover, canyon-crossing seafloor telecommunication cables are at risk of breakage from canyon-margin failure and canyon-traversing sediment gravity flows (e.g. Heezen and Ewing, 1952; Hsu et al., 2008; Carter et al., 2014). Such flows are also considered responsible for the displacement of marine pipelines (e.g. Porcile et al., 2020), hence posing a hydrocarbon leakage hazard, for example. Moreover, it has been suggested that the upslope transport of warm water currents through submarine canyons along Antarctica contributes to the acceleration of ice sheet loss, which in turn influences global sea-level rise (e.g. Morrison et al., 2020; Gales et al., 2021 and references therein).

The sedimentary fills of submarine canyons, and their linkage to down-system submarine fans (e.g. Covault, 2011b; Jobe et al., 2011) and contourite-drift systems (e.g. Wang et al., 2018; Warratz et al., 2019; Serra et al., 2020; Rodrigues et al., 2022 and references therein), make them important references and targets for hydrocarbon exploration. Canyons can

represent significant sinks for both macro- (e.g. Pierdomenico et al., 2019; Zhong and Peng, 2021) and micropollutants (e.g. Azaroff et al., 2020).

Hence, the study of submarine canyons represents a key area of interest for research linked to a broad range of scientific disciplines (Matos et al., 2018).

Source-to-sink (S2S) research investigates sediment budget dynamics and process-response relationships in both ancient and modern sedimentary systems. Scaling relationships between sedimentary systems and attributes of segments of the S2S profile are commonly established. However, the focus of such studies has been chiefly on fluvial systems and submarine fans, whereas the submarine canyons that link them remain relatively understudied (e.g. Sømme et al., 2009; Nyberg et al., 2018b).

Quantitative studies provide a means for the systematic investigation of scaling relationships across and within sedimentary environments, with consideration of environmental controls such as climate, hydrodynamic processes, or tectonic setting, which dictate sediment source areas, transport pathways and sinks (e.g. Wang et al., 2019; 2020; Budai et al., 2021; Cosgrove et al., 2021). Such studies enable an assessment of the relative importance of autogenic versus allogenic controls on aspects of the geomorphology, architecture and facies characteristics of subenvironments, and of scaling-relationships they may exhibit. Such insights can be applied to infer the geometrical characteristics of formative subenvironments based on preserved architectures seen in outcrop and subsurface studies (e.g. Martinsen et al., 2010; Xu et al., 2017), and to inform laboratory and modelling studies (Nyberg et al., 2018b). The applied usefulness of scaling relationships for the reconstruction and modelling of sedimentary systems at different scales of observations has been highlighted by various authors (e.g. Sømme et al., 2009; Martinsen et al., 2010; Helland-Hansen et al., 2016; Bhattacharya et al., 2016; Xu et al., 2017; Nyberg et al., 2018b).

Scaling relationships between aspects of canyon geomorphology and controlling factors have been identified in quantitative studies of submarine canyons at regional, continental, and global scales (see section 3.2.2). However, relationships between canyon morphometric parameters have only

been partially investigated using global datasets, and the general applicability of such relationships across environmental settings is largely unconstrained. This study addresses these knowledge gaps.

The aim of this study is to improve the understanding of controlling factors on submarine-canyon geomorphology, and of the extent to which scaling relationships of canyon morphometric parameters – mutually and with attributes of their physiographic and environmental setting – can be recognised in modern canyons. To achieve this, a global database has been built utilising datasets from published case studies of submarine canyons combined with data obtained from open-source bathymetry to support the following research objectives:

(i) to characterise morphometric parameters of submarine canyons, both generally and with consideration of the role of environmental factors (canyon-apex location relative to the shelf-break, continental-margin type, source-to-sink system setting, oceanographic environment and climate zones);

(ii) to identify and assess scaling relationships between canyon morphometric parameters;

(iii) to evaluate relationships between canyon morphometric parameters and other variables, including canyon bathymetry, distance between the canyon apex and the shoreline, parameters of the catchment, shelf and slope, and latitude of the canyon;

(iv) to identify and discuss possible causal links between observed scaling relationships and autogenic and allogenic controls, the configuration of the associated source-to-sink system, and the environmental setting.

3.2 Background

3.2.1 Controls on submarine canyon evolution

Submarine canyons are highly complex sedimentary systems whose evolution is influenced by a wide range of processes and environmental

factors (e.g. Shepard, 1936, 1981; Pratson and Coakley, 1996; Pratson et al., 2007), as demonstrated in the recent comprehensive literature reviews by Puig et al. (2014) and Amblas et al. (2017). Despite being well studied, the genesis and long-term evolution of submarine canyons remain topics of ongoing debate, and require further understanding (e.g. Pratson et al., 2007 and references therein; Baztan et al., 2005; Puig et al., 2014; Smith et al., 2017, 2018). The relative importance of controls on canyon geomorphology is still not well understood (Li et al., 2022).

Various physiographic and environmental factors are known to influence canyon evolution by exerting controls on connectivity to sediment sources, on mechanisms of sediment distribution, and on types of canyon evolutionary processes. Physiographic factors that have been invoked include the distance of the canyon to fluvial outlets and littoral cells (e.g. Sweet & Blum, 2016; Sweet et al., 2020), shelf width and gradient in the vicinity of the canyon (e.g. Covault and Graham, 2010; Gamberi et al., 2015; Jipa and Panin, 2020; Bernhardt and Schwanghart, 2021), and continental-slope gradients (e.g. McGregor, 1983; Orange et al., 1994; Lo Iacono et al., 2014). Environmental factors comprise local- and regional-scale tectonics (e.g. Ratzov et al., 2012; Micallef et al., 2014; de Almeida et al., 2015; Soutter et al., 2021), sea-level fluctuations (e.g. Rasmussen, 1994; Mitchell et al., 2007; Maier et al., 2018), and climate (e.g. Henrich et al., 2010), including glaciations (e.g. Harris et al., 2014b; Gales et al., 2021).

The oceanographic regime is also thought to influence gully formation and failures along canyon walls (e.g. Wang et al., 2022b), and is a possible cause for particular geomorphic characteristics of Arctic and Antarctic gullies (Gales et al., 2013). Also, a global study of late Quaternary incised-valley fills by Wang et al. (2020) demonstrated that the facies architecture of valley fills varies across open oceans and semi-enclosed and enclosed seas, which exhibit contrasting hydrodynamics. Considering the role of marine hydrodynamic processes in the delivery of sediment to canyons, and in intra-canyon sediment transport and erosion (see section 3.4.2.2), and given the genetic linkage between cross-shelf lowstand fluvial systems and submarine canyons (e.g. Harris and Whiteway, 2011; Maier et al., 2018), more research

is needed to establish whether and how canyon geomorphology varies as a function of the oceanographic setting.

Anthropogenic influences can also affect the evolution of modern submarine canyons, in several ways. Sediment gravity flows can be triggered by trawling (e.g. Palanques et al., 2006b; Lopez-Fernandez et al., 2013), whereas farming and deforestation (e.g. Milliman and Farnsworth, 2011), and the artificial diversion (e.g. Higgins et al., 2018) or damming of rivers (e.g. Sheng et al., 2019) may impact catchments and fluvial discharge rates, which in turn can impact sediment delivery to submarine canyons (e.g. Mazières et al., 2014; Puig et al., 2017).

3.2.2 Submarine canyon studies

Submarine canyons have been the subject of many prior studies: Matos et al. (2018) conducted a review of the scientific literature on submarine canyons published between 1929 and 2016, considering 1,968 publications. These authors identified a geographical bias in prior canyon research: less than 10% of the canyons mapped globally by Harris et al. (2014b) are covered by the literature, and almost half of the 1,968 publications concentrate exclusively on 11 intensively studied submarine canyons. Consequently, research efforts have largely been directed towards the particular environmental conditions and set of controls associated with a limited subset of canyons, depending on the thematic focus of the case study (see Matos et al., 2018). However, the rate at which studies on submarine canyons are published has further accelerated in recent years (Matos et al., 2018), due in part to technological advances in data acquisition and processing (e.g. Xu, 2011; Urías Espinosa et al., 2016; Simmons et al., 2020; Bailey et al., 2021). This section summarises examples of regional, continental, and global-scale quantitative studies of submarine-canyon geomorphology that consider the canyon physiographic and environmental setting, focussing on aspects of these studies that are relevant to the research presented in this chapter.

Canyon classification schemes based on case studies from specific regions have been proposed to be universally applicable, for example where specific

sets of controls are associated with a canyon (canyon-head location relative to the shelf break, type of intra-canyon sedimentary processes, sediment sources and sediment characteristics; cf. Jobe et al., 2011), and models for canyon evolution have been considered relevant to canyons that developed under similar external controls, as for canyons associated with active margins (e.g. Micallef et al., 2014). However, a study of 713 submarine canyons located offshore Australia by Huang et al. (2014) revealed great variability and complexity in aspects of canyon geomorphology at the continental scale, which challenges the applicability of insights generated by regional studies at a larger scale. The authors established a hierarchical classification of shelf-incising and slope-confined canyons based on the following canyon metrics: percentage of canyon area characterised by slope gradients exceeding 15°, average canyon thalweg gradient, volume subtended by the canyon channelform, canyon-head incision depth, and distance to the nearest neighbouring canyon. Their findings demonstrate a higher number of canyon classes for slope-confined canyons compared to shelf-incising ones (see Figures 6 & 7 of Huang et al., 2014).

Relationships between canyon geomorphology and the position of the canyon head relative to the shelf-break were also recognised in other regional-scale studies. In a study of 80 canyons offshore California (Santora et al., 2018), differences in frequency distributions of canyon dimensions were documented across shelf-incising versus slope-confined canyons, whereby shelf-incising canyons tend to have greater areas, lengths, widths and mean depths. Additionally, the authors found that canyon area scaled positively with canyon length and width, independently of the canyon-head location relative to the shelf-margin. Li et al. (2022) documented pronounced differences in 48 shelf-incised submarine canyons from the northwest South China Sea.

Furthermore, relationships between characteristics of S2S systems and canyon geomorphology are demonstrated in a number of regional-scale studies. For example, Jipa and Panin (2020) noted that the few submarine canyons in the N and NW region of the Black Sea were associated with continental shelves up to 200 km wide, large fluvial systems of several

thousand kilometres length and low-relief catchments of up to several hundred metres elevation. Such canyons were characterised by a single main stem and had large submarine fans as distal segments. By contrast, submarine canyons along the E and NE Black Sea margins, characterised by (i) high-elevation catchments, (ii) short feeder rivers (up to several hundred kilometres length), and (ii) shelves that are rarely wider than 15 km, tend to form dendritic drainage networks and are more closely spaced; also, their submarine fans tend to form a continuous apron-like zone. Their findings were in part corroborated by those of Fernane et al. (2022), who demonstrated that submarine canyons along the western Algerian margin display a greater degree of dendricity and incision into the shelf where they are associated with a narrow shelf configuration compared to canyons associated with wide shelf margins.

For the interpretation of autogenic and allogenic controls on canyon geomorphology, an improved understanding of the sensitivity of canyon morphometric parameters to seafloor processes and environmental factors is required. In contrast to regional studies, global-scale studies have the potential to constrain the variability in potential controls more fully in a broad range of environmental settings. Previous global-scale studies that have investigated aspects of submarine-canyon geomorphology (e.g. Nelson et al., 1970; De Pippo et al., 1999; Sømme et al. 2009; Covault et al. 2011a; Harris and Whiteway, 2011; Harris et al., 2014b; Soutter et al., 2021) and assessed the relative importance of factors promoting sediment-connection of canyons to shorelines (Bernhardt and Schwanghart, 2021) constitute important contributions to a fuller understanding of submarine canyon evolution. Nevertheless, such global investigations of the geomorphology of modern submarine canyons have been limited to individual canyon morphometric parameters and to consideration of specific environmental controls, with the datasets being limited in terms of their geographic coverage prior to the advent of a global inventory of modern submarine canyons – comprising 5,849 canyons – compiled by Harris and Whiteway (2011).

In their global study, De Pippo et al. (1999) compiled a database of selected aspects of the geomorphology of 50 submarine canyons, including canyon length, average gradient, and cross-sectional profile, together with variables describing their environmental setting (see Figure 1 of De Pippo et al., 1999). For example, the authors applied their database to tease out possible relationships between canyon geomorphology and potential controls posed by the morphological and tectonic characteristics of the associated continental margin; they additionally assessed relationships between canyon morphometric parameters, e.g. for canyon length and average canyon thalweg gradient (see Figure 5 of De Pippo et al., 1999).

Leveraging advancements in bathymetric mapping of seafloors, the study by Harris and Whiteway (2011) provided a summary of aspects of canyon geomorphology and their physiographic setting for 5,849 submarine canyons classified on geographic region, continental-margin type, location of the canyon-head relative to the shelf-break and connection to a fluvial system. The following variables were considered: canyon length, average thalweg gradient, average sinuosity, bathymetric range, spacing, and dendricity; descriptive statistics were presented for canyons classified on margin type, canyon-head location relative to the shelf break, connection to a fluvial system, and geographic region (Table 1 of Harris and Whiteway, 2011). Statistical analyses revealed that active-margin canyons are on average steeper and shorter than their counterparts along passive margins, whereas overall canyon sinuosity tends to be similar (Figure 8 of Harris and Whiteway, 2011). In addition, the authors documented relationships between mean values of canyon parameters obtained for groups of canyons classified by geographic regions and distinguished into active- and passive-margin settings. Canyons associated with an insular-margin setting were excluded from the correlation analyses. Moreover, the authors demonstrated the lack of a relationship between latitude and average canyon sinuosity for shelf-incising canyons (Figure 9 of Harris and Whiteway, 2011). The importance of fluvial sediment connection on canyon length was inferred from the observation that canyons associated with fluvial systems and incising the shelf tend to be longer than shelf-incising canyons without a river

connection and slope-confined canyons, by factors 1.60 and 2.07, respectively. In non-polar regions, Harris and Whiteway (2011) showed a positive linear relationship between the percentage of shelf-incising canyons of canyons in a geographic region and sediment discharge from rivers (Figure 10 of Harris and Whiteway, 2011).

Subsequently, Harris et al. (2014b) identified 9,477 submarine canyons utilising the first published digital geomorphic seafloor map (see Harris et al., 2014b). The significant number of newly recognised canyons reflect in part the higher resolution of seafloor data, but also the fact that canyons associated with plateaux adjoined to continental margins were also incorporated, unlike in Harris and Whiteway (2011; see Harris et al., 2014b). Harris et al. (2014b) calculated mean values of canyon area and length both for the global dataset and separately for major geographic regions. The results were further distinguished based on the location of the canyon head relative to the shelf break. In addition, the mean incision depth was reported for shelf-incising canyons in all regions (see their Table 9) and for slope-confined ones in general (text in Harris et al., 2014b). On average, canyons in the latter group display greater average depth, shorter lengths and about half the area, compared to canyons that incise the shelf. Harris et al. (2014b) also showed that submarine canyons in polar regions are, on average, about twice as large in area relative to the global average; in addition to characteristics of the slope and basin-floor environments in these settings, Harris et al. (2014b) linked these attributes to a control by sediment supply to deep-marine environments during glacial intervals of the Cenozoic. Arctic and Antarctic canyons tend to be the longest of all differentiated geographic regions, but only by a modest margin; compared to submarine canyons in the South Atlantic, for example, their average lengths are only 1.20 and 1.21 times larger. Shelf-incising canyons of the Arctic and Antarctica also tend to have the largest values of mean incision depth across all investigated regions, but on average they are only 1.035 and 1.006 times deeper than canyons in the North Atlantic. These findings, together with the low variability in mean values of average canyon sinuosity for polar and non-polar regions documented by Harris and Whiteway (2011), suggest that factors related to

latitudinal setting variably control aspects of submarine-canyon geomorphology, and that the strength in scaling might show pronounced regional variabilities.

Two global studies that have focused on the longitudinal profiles of submarine canyons are the studies by Covault et al. (2011a) and Soutter et al. (2021), who investigated the longitudinal profiles of a combination of 20 canyon and channels and of 377 submarine canyons, respectively. Covault et al. (2011a) established links between the longitudinal-profile shape – classified as convex, slightly concave or very concave – and both the margin type and the depositional architecture of deep-water environments (see their Figure 9). Soutter et al. (2021) instead investigated and discussed relationships between the Normalised Concavity Index of canyon profiles and controlling factors including attributes of the terrestrial catchment, climate and tectonic setting, as well as canyon-head location relative to the shelf break. The authors inferred a dominant tectonic control on canyon concavity, that the connection to a river is a secondary control, and that the climate of the hinterland is a relatively subordinate factor.

Collectively, these examples document the variability in canyon morphometrics but in a way that suggests that there is no individual factor or single set of overriding controls emerging from their analyses.

The quantitative global assessment of canyon geomorphology undertaken in this study with consideration of aspects of the S2S system and of the environmental and physiographic setting aims to augment the findings of these earlier studies, and the current empirical knowledge of canyon geomorphology and of its links to potential controls.

3.3 Dataset and methodology

A database was collated that stores data describing the geomorphology of submarine canyons, their environmental context and geological controlling factors. Data have been sourced from 282 globally distributed modern submarine canyons and have been grouped into 96 separate case studies, with each case study corresponding to the study of one or several

submarine canyons by a particular group of researchers (Fig 3.1. and Tab. 3.1). The database comprises literature-derived, high-resolution bathymetric surveys of the seabed and high-resolution seismic reflection datasets of the shallow subsurface, derived from 135 publications (Tab. 3.1) and open-source worldwide bathymetry datasets (GEBCO 2019 NOAA NCEI Visualization; Google Earth).

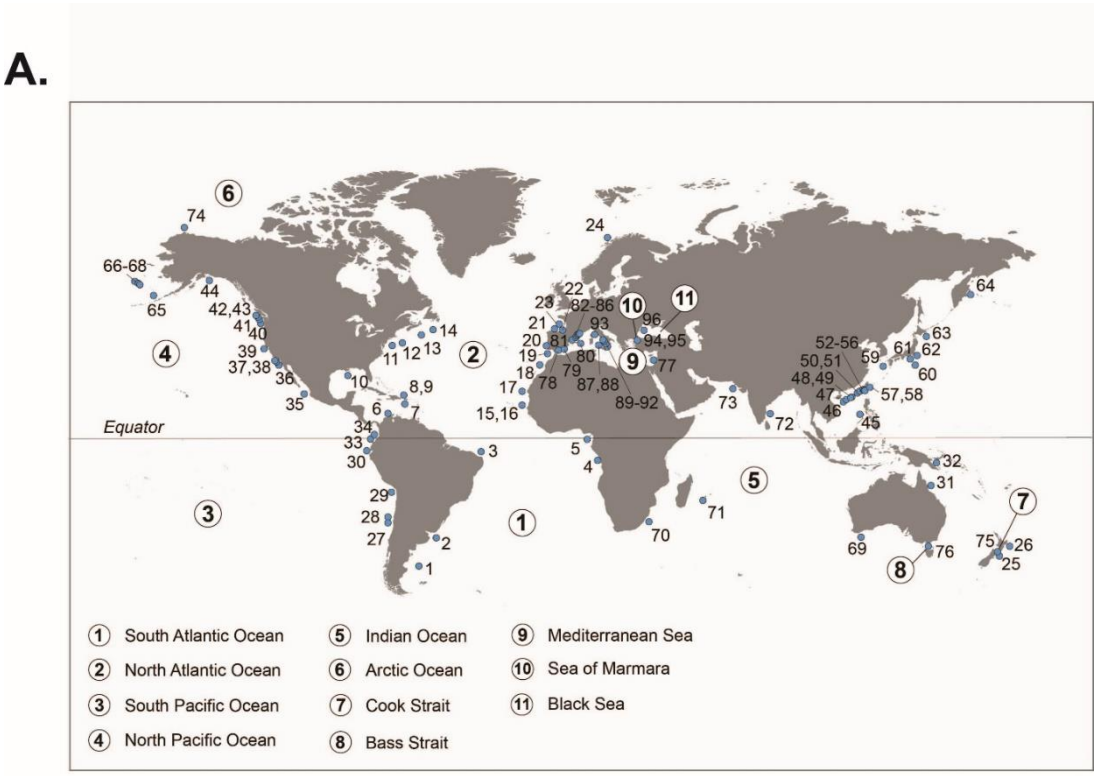

Figure 3.1a&b A. Overview map of distribution of the 96 case studies. B. Geographic distribution of the 96 case studies and 282 submarine canyons (World map from freevectormaps.com).

ID	Case study	No. of canyons	Oceanic region	Reference(s)
1	Patagonia canyons, SE Argentina	8	South Atlantic Ocean	*Lastras et al., 2011a*
2	Mar del Plata Canyon, E Argentina	1	South Atlantic Ocean	*Krastel et al., 2011; Warratz et al., 2019*
3	Potiguar Basin canyons, NE Brazil	14	South Atlantic Ocean	*de Almeida et al., 2015*
4	Congo Canyon, W Democratic Republic of Congo	1	South Atlantic Ocean	*Babonneau et al., 2002; Ferry et al., 2004*
5	Avon and Mahin canyons, SW Nigeria	2	South Atlantic Ocean	*Jimoh et al., 2018*
6	Aguja Canyon, N Colombia	1	North Atlantic Ocean (Caribbean Sea)	*Restrepo-Correa and Ojeda, 2010*
7	Guayanilla canyon system, S Puerto Rico	4	North Atlantic Ocean (Caribbean Sea)	*Trumbull and Garrison, 1973*
8	Arecibo and Quebradillas canyons, NW Puerto Rico	2	North Atlantic Ocean	*Gardner et al., 1980*
9	Mona Canyon, NW Puerto Rico	1	North Atlantic Ocean	*Mondziel et al., 2010*
10	Mississippi Canyon, S USA	1	North Atlantic Ocean (Gulf of Mexico)	*Coleman et al., 1982*
11	Hudson Canyon, NE USA	1	North Atlantic Ocean	*Rona et al., 2015*
12	Lydonia and Oceanographer canyons, NE USA	2	North Atlantic Ocean	*Valentine et al., 1980*
13	Logan Canyon, SE Canada	1	North Atlantic Ocean	*Li et al., 2019*

14	SW Grand Banks Slope canyons, SE Canada	3	North Atlantic Ocean	*Armitage et al., 2010*
15	Dakar Canyon, W Senegal	1	North Atlantic Ocean	*Pierau et al., 2010, 2011*
16	Cayar Canyon, W Senegal	1	North Atlantic Ocean	*Dietz et al., 1968*
17	Timiris Canyon, NW Mauritania	1	North Atlantic Ocean	*Krastel et al., 2004; Antobreh and Krastel, 2006*
18	Agadir Canyon	1	North Atlantic Ocean	*Ercilla et al., 1998; Wynn et al., 2002*
19	Faro and Portimao canyons, SW Portugal	2	North Atlantic Ocean (Gulf of Cadiz)	*Mulder et al., 2006*
20	Nazaré, Cascais and Setubal-Lisbon canyons, W Portugal	4	North Atlantic Ocean	*Arzola et al., 2008; Lastras et al., 2009; Allin et al., 2016*
21	Aviles Canyon system and Navia canyon, N Spain	5	North Atlantic Ocean (Bay of Biscay)	*Goméz-Ballesteros et al., 2014*
22	Capbreton Canyon, SW France	1	North Atlantic Ocean (Bay of Biscay)	*Mazières et al., 2014*
23	Audierne and Blackmud canyons, SW France	2	North Atlantic Ocean (Bay of Biscay)	*Mulder et al., 2012*
24	Lofoten-Vesterålen canyons (incl. Andøya Canyon), NW Norway	15	North Atlantic Ocean	*Rise et al., 2013*
25	Kaikoura Canyon, E New Zealand	1	South Pacific Ocean	*Lewis and Barnes, 1999*
26	Lachlan Canyon, NE New Zealand	1	South Pacific Ocean	*Walsh et al., 2007*
27	Biobío Canyon system, SW Chile	2	South Pacific Ocean	*Bernhardt et al., 2015*

28	San Antonio Canyon, NW Chile	1	South Pacific Ocean	*Hagen et al., 1996; Laursen and Normark, 2002*
29	E Arequipa Basin canyons, NW Chile	3	South Pacific Ocean	*Hagen et al., 1994*
30	Guayaquil and Santa Elena canyons, NW Equador	2	South Pacific Ocean	*Michaud et al., 2015*
31	N Great Barrier Reef canyons, NE Australia	15	South Pacific Ocean (Coral Sea)	*Puga-Bernabeu et al., 2011*
32	Solomon Sea canyons, E and SE Papua New Guinea	8	South Pacific Ocean (Solomon Sea)	*Davies et al., 1987; Galewsky and Silver, 1997*
33	Esmeraldas Canyon, NW Ecuador	1	North Pacific Ocean	*Michaud et al., 2015*
34	Mira and Patia canyons, SW Colombia	2	North Pacific Ocean	*Ratzov et al., 2012*
35	Ipala Canyon, W Mexico	1	North Pacific Ocean	*Urías Espinosa et al., 2016*
36	La Jolla and Scripps canyons, SW USA	2	North Pacific Ocean	*Le Dantec et al., 2010; Paull et al., 2013*
37	Redondo, Santa Monica and Dume canyons, SW USA	3	North Pacific Ocean	*Gardner et al., 2003; Tubau et al., 2015*
38	Mugu and Hueneme canyons, SW USA	2	North Pacific Ocean	*Piper et al., 1999;*
39	Monterey and Soquel canyons, SW USA	2	North Pacific Ocean	*Greene et al., 2002; Xu and Noble, 2009*
40	Astoria Canyon, NW USA	1	North Pacific Ocean	*Hickey, 1997; Bosley et al., 2004*
41	Quinault Canyon, NW USA	1	North Pacific Ocean	*Baker and Hickey, 1986; Carson et al., 1986*

42	Juan de Fuca Canyon, NW USA	1	North Pacific Ocean (heads in the Juan de Fuca Strait)	*Alford and MacCready, 2014*
43	Barkley Canyon, SW Canada	1	North Pacific Ocean	*Allen et al., 2001*
44	Tarr Canyon, NW USA	1	North Pacific Ocean (Gulf of Alaska)	*Carlson et al., 1990*
45	North Palawan Canyon, S China	1	North Pacific Ocean (South China Sea)	*Yin et al., 2018*
46	Modern Central Canyon, S China	1	North Pacific Ocean (South China Sea)	*Su et al., 2015*
47	3 canyons and 4 gullies, S China	3 (4)	North Pacific Ocean (South China Sea)	*Chen et al., 2017*
48	Pearl River Mouth Basin canyons, S China	17	North Pacific Ocean (South China Sea)	*Han et al., 2010; Su et al., 2020*
49	Zhujiang/Pearl River Canyon, S China	1	North Pacific Ocean (South China Sea)	*Han et al., 2010; Ding et al., 2013*
50	Dongsha Canyon	1	North Pacific Ocean (South China Sea)	*Yin et al., 2015*
51	Taiwan Canyon, SW Taiwan	1	North Pacific Ocean (South China Sea)	*Xu et al., 2014*
52	Hongtsai Canyon, SW Taiwan	1	North Pacific Ocean (South China Sea)	*Yu and Chiang, 1995*
53	Fangliao Canyon, SW Taiwan	1	North Pacific Ocean (South China Sea)	*Yu and Lu, 1995; Chiang et al., 2012*
54	Gaoping/Kaoping Canyon, SW Taiwan	1	North Pacific Ocean (South China Sea)	*Chiang and Yu, 2006; Liu et al., 2016*

55	Kaohsiung Canyon, SW Taiwan	1	North Pacific Ocean (South China Sea)	*Yu et al., 1992*
56	Penghu Canyon, SW Taiwan	1	North Pacific Ocean (South China Sea)	*Yu and Chang, 2002; Hsiung and Yu, 2011; Su et al., 2015*
57	Taitung Canyon, SE Taiwan	1	North Pacific Ocean (Philippine Sea)	*Schnuerle et al., 1998*
58	Hualien Canyon, SE Taiwan	1	North Pacific Ocean (Philippine Sea)	*Hsiung et al., 2017*
59	Goto Canyon, SW Japan	1	North Pacific Ocean (East China Sea)	*Oiwane et al., 2011*
60	Aoga Shima Canyon, SE Japan	1	North Pacific Ocean (Philippine Sea)	*Klaus and Taylor, 1991*
61	Tenryu Canyon, SE Japan	1	North Pacific Ocean	*Soh and Tokuyama, 2002*
62	Boso Canyon, SE Japan	1	North Pacific Ocean	*Soh et al., 1990*
63	Kushiro Canyon, NE Japan	1	North Pacific Ocean	*Noda et al., 2008; Noda and Tuzino, 2010; Tuzino and Noda, 2010*
64	Submarine canyons of Kamchatka, NE Russia	7	North Pacific Ocean	*Gnibidenko and Svarichevskaya, 1984*
65	Bering Canyon, Bering Sea	1	North Pacific Ocean (Bering Sea)	*Carlson and Karl, 1988; Harris and Whiteway, 2011*
66	Zhemchug, Pervenets and Navarin canyons, Bering Sea	3	North Pacific Ocean (Bering Sea)	*Carlson and Karl, 1988*
67	Middle canyon system, Bering Sea	2	North Pacific Ocean (Bering Sea)	*Carlson and Karl, 1984, 1988*

68	St. Matthew canyon system, Bering Sea	2	North Pacific Ocean (Bering Sea)	*Carlson and Karl, 1984, 1988*
69	Albany canyons, SW Australia	11	Indian Ocean	*Exon et al., 2005*
70	Tugela Canyon, E South Africa	1	Indian Ocean	*Wiles et al., 2013*
71	Saint-Etienne and Pierrefonds canyons, SW La Reunion	2	Indian Ocean	*Babonneau et al., 2013*
72	Palar Basin canyons, E India	20	Indian Ocean	*Susanth et al., 2021*
73	Indus Canyon, SE Pakistan	1	Indian Ocean (Arabian Sea)	*Von Rad and Tahir, 1997; Salmanidou et al., 2019*
74	Barrow Canyon, NW USA	1	Arctic Ocean	*Eittreim et al., 1982; Pisareva et al., 2019*
75	Cook Strait canyons, E New Zealand	9	Cook Strait	*Mountjoy et al., 2009, 2014; Micallef et al., 2014*
76	Bass canyon system, SE Australia	10	Bass Strait	*Mitchell et al., 2007*
77	Akhviz and Sour canyons, NW Israel	2	Mediterranean Sea	*Mart, 1989; Almagor, 1993*
78	Almeria, Western, Eastern and Guadiaro canyons, S Spain	4	Mediterranean Sea	*Alonso and Ercilla, 2003; Palanques et al., 2005*
79	Alías-Almanzora canyon system, SE Spain	4	Mediterranean Sea	*Puig et al., 2017*
80	Menorca Canyon, SW Menorca, Balearic Islands	1	Mediterranean Sea	*Acosta et al., 2002*
81	Orpesa Canyon, NE Spain	1	Mediterranean Sea	*Amblas et al., 2012*

82	Foix Canyon system, NE Spain	3	Mediterranean Sea	*Puig et al., 2000; Tubau et al., 2013*
83	Blanes Canyon, SE France	1	Mediterranean Sea	*Lastras et al., 2011b*
84	Palamós/La Fonera Canyon, NE Spain	1	Mediterranean Sea	*Martin et al., 2006; Palanques et al., 2006b; Lastras et al., 2011b*
85	Cap de Creus Canyon	1	Mediterranean Sea	*Baztan et al., 2005; Lastras et al., 2007; 2011b*
86	Bourcart Canyon, SE France	1	Mediterranean Sea	*Mauffrey et al., 2015*
87	Gulf of Palermo canyons, NW Sicily, Italy	7	Mediterranean Sea	*Lo Iacono et al., 2011; 2014*
88	Gulf of Castellammare canyons, NW Sicily, Italy	2	Mediterranean Sea	*Lo Iacono et al., 2014*
89	Messina Canyon, NE Sicily, Italy	1	Mediterranean Sea	*Ridente et al., 2014*
90	Petrace, Gioia and Mesima canyons, SW Italy	3	Mediterranean Sea	*Pierdomenico et al., 2016, Casalbore et al., 2018*
91	Luna and Infreschi canyons, SW Italy	2	Mediterranean Sea	*Budillon et al., 2011*
92	Dohrn Canyon, SW Italy	1	Mediterranean Sea	*Milia, 2000*
93	Golo system canyons, NE Corsica, France	4 (2)	Mediterranean Sea	*Gervais et al., 2004; 2006*
94	North İmralı Canyon, NW Turkey	1	Sea of Marmara	*Vardar, 2019*
95	Sarköy and Izmit canyons, NW Turkey	2	Sea of Marmara	*Çağatay et al., 2015*
96	Danube/Viteaz Canyon, SE Romania	1	Black Sea	*Popescu et al., 2004*

Table 3.1 Overview of the 96 case studies and associated 135 literature data sources of the present study. Numbers in brackets refer to channel forms termed as submarine ‘gullies’ by the authors. See Figure 3.1 for locations.

Submarine canyon definition

In this study, a submarine canyon is defined as a single dominantly erosional channelform incised into a continental slope. The chosen definition of submarine canyon does not consider criteria relating to bathymetric setting, minimum canyon dimensions (cf. Harris and Whiteway, 2011), genetic origin, or canyon cross-sectional shape, and is therefore inclusive of what other authors commonly refer to as 'gullies' (e.g. Field et al., 1999; Gales et al., 2013; Chen et al., 2017), ‘gulleys’ (e.g. Gulliksen, 1978; Normark et al., 2009) or ‘potential submarine canyons’ (e.g. de Almeida et al., 2015). A general definition was adopted for the following reasons: (i) submarine gullies have been considered to constitute forms at the early stage of canyon formation (e.g. Amblas et al., 2017); (ii) canyon geomorphologic attributes such as canyon size can be inherently limited by their physiographic setting; and (iii) both terms are variably used for smaller-scale erosional channel-forms on the slope. Because the broad definition applied in this study also comprises the presence of overbank deposits/levees and u-shaped channel cross-sections, the distal parts of some channelforms defined as submarine canyons might correspond to what other authors refer to as ‘submarine channels’ within the region of the lower slope and continental rise (e.g. Covault et al., 2011a and references therein; Hodgson et al., 2022).

The canyon apex is defined as the point of the shallowest bathymetry and canyon mouth as the most distal point, along a canyon axis. The term “canyon apex” has been used herein in preference to “canyon head”, the latter being a common but loosely defined term in the literature referring to the proximal part of a submarine canyon. Therefore “canyon apex” is used *sensu stricto* and “canyon head” *sensu lato*. In networks of connected channel forms, each channel-form is treated as an individual submarine canyon, whereas the network itself is termed a ‘canyon system’ (e.g. Mitchell et al., 2007; Mountjoy et al., 2009).

3.3.1 Study parameters

Data on submarine canyons, environmental setting and external controlling factors have been coded in the form of attributes recorded in the Deep-Marine Architecture Knowledge Store (DMAKS; Cullis et al., 2019). DMAKS is a relational database that allows the systematic and standardised collation of data on deep-water sedimentary systems, as originally obtained using different methods (e.g. outcrop, core, seismic, bathymetric, sonar imaging). DMAKS stores data on the architectural, geomorphological and facies characteristics of deep-water depositional systems, as well as on their external controls and depositional context (Cullis et al., 2019). Several additional bespoke attributes have been added to DMAKS to enable the present study.

The dataset for this study has been obtained from multiple sources, including the peer-reviewed literature and government agency sources. Values were extracted from the texts or manually measured or calculated. Inherent to this approach are various sources of error, including the heterogeneity of the dataset and undetected errors in the primary datasets; these limitations are discussed in section 3.3.3.

The full set of variables employed in the analyses undertaken in this study is summarised in Table 3.2.

3.3.1.1 Canyon morphometric parameters

Canyon geomorphology has been characterised by the following six morphometric parameters: (i) canyon length, (ii) canyon width (maximum and streamwise average over the full length of the canyon), (iii) canyon bankfull depth (maximum and streamwise average over the full length of the canyon), (iv) overall canyon sinuosity, (v) average canyon thalweg gradient, and (vi) maximum canyon sidewall steepness (Fig. 3.2a). Definitions of these variables are reported in Table 3.2. Values reported by authors have only been included for studies based on surveys that include bathymetric coverage of the entire canyon area. Average width and depth values were obtained from the literature for canyons surveyed by high-resolution

bathymetry and where bathymetric data was derived from 3D seismic surveys.

3.3.1.2 Environmental parameters and external controls

For the investigation of relationships between submarine-canyon geomorphology and the environmental context of the submarine canyons, attributes have been defined to record (i) canyon-physiographic setting, (ii) the configuration of the canyon terrestrial catchment, continental shelf and slope, and (iii) external controls operating at the location of the canyon (Tab. 3.2 & Fig. 3.2).

Physiographic setting

The bathymetry of the canyon is characterised by the seafloor depth at its apex and mouth (Tab. 3.2). For canyons with several tributaries at their head, the shallowest seafloor depth has been recorded. The canyons are also classified in relation to the position of their apices relative to the shelf-break as either (i) shelf-incising, where the canyon extends into the continental shelf, or (ii) slope-confined, where the apex of the canyon is situated below the shelf break (cf. Jobe et al., 2011; Huang et al., 2014).

Source-to-sink-system attributes

Relationships between the geomorphology of submarine canyons and attributes of their terrestrial catchment have been investigated only for canyons with sediment connectivity to a fluvial system at present or in the past. For these canyons, descriptors of fluvial system length, mean annual fluvial discharge, catchment area and maximum catchment area elevation (Tab. 3.2), have been recorded. Sediment connectivity of a submarine canyon with a fluvial source is defined based on the following three criteria:

(i) *The submarine canyon displays a present connection with a fluvial system*. This includes canyons fronting a river mouth, canyons for which across-shelf sediment transport from a fluvial outlet has been inferred by authors, e.g. from sedimentary structures on the seafloor as sediment waves (e.g. Puig et al., 2017), and canyons

connected to up-dip subenvironments, such as shelf channels and tributary canyons, which are physically connected with a fluvial system.

(ii) *The submarine canyon was connected to a river in the past.* This includes canyons that might not currently be connected to a fluvial system, e.g. due to present-day sea-level highstand conditions or to river-mouth shift of natural or anthropogenic cause, but that are known to have been connected in the past to a river (e.g. Sweet et al., 2020).

(iii) *The canyon apex is located within a 5 km radius of a fluvial outlet*. This criterion has been considered in view of the typical length-scale over which sand tends to be distributed to submarine canyons by rivers that lack a bathymetric connection to the canyons (see Sweet & Blum, 2016).

For canyons linked with several rivers, their cumulative length, mean annual fluvial discharge and catchment area have been recorded, to enable comparison with canyons fed by single fluvial systems. For investigation of relationships between canyon geomorphology and maximum elevation of the terrestrial catchment, the elevation above mean sea level of the highest point in the combined catchment has been recorded.

The continental shelf and slope hosting the canyons have been described in terms of width, average gradient and depth.

Continental-margin type

The source-to-sink system has been classified as being associated with either a passive or a tectonically active continental margin, the latter comprising canyons along both convergent and transform plate boundaries, following the continental-margin classification of Harris et al. (2014b; see their Figure 2).

Source-to-sink setting

The source-to-sink setting associated with the studied canyons has been classified on whether the terrestrial catchment, shelf and slope are

associated with continental landmasses (continental setting) or an island (insular setting). Canyons which could not unambiguously be assigned a setting have not been included.

Oceanographic environment

To investigate the possible controls exerted by hydrodynamic processes that vary with scale and marine water-mass confinement, and potential relationships between canyon morphometric parameters and the scale and degree of confinement of the seas where they occur, canyons are classified with respect to their oceanographic environment. To this end, two groups have been distinguished: (i) open seas, which comprise the World's oceans and experience hydrodynamic interactions with adjacent seas; they may be characterised by the occurrence of oceanic gyres; (ii) semi-enclosed and enclosed seas, which are largely bounded by landmasses and are therefore characterised by a limited hydrodynamic interaction with the oceans or seas with which they are connected; this second class includes seas, gulfs and straits.

Latitude

The latitudinal positions of canyon heads are recorded as absolute values for both hemispheres. For the investigation of latitude-related climatic influences on processes affecting canyon geomorphology, latitude values have been assigned to categories that relate to major climate belts, i.e., into tropical (corresponding to latitudes between 0° and 23.5°), temperate (between 23.5° and 66.5°), and polar zones (corresponding to latitudes higher than 66.5°). This simplified approach has been implemented for the following reasons: (i) existing climate classification schemes are commonly based on parameters of the terrestrial catchment and would therefore have limited applicability to canyons that do not receive significant fluvial discharge or none at all; moreover, climatic conditions in the marine environment are commonly not considered in these schemes; (ii) climate histories, including temperature and precipitation, would have to be reconstructed for both the present and the past to permit a consistent analysis of their impact on canyon evolution; this becomes particularly

challenging for submarine canyons associated with large source-to-sink systems; (iii) the age of inception of the majority of the canyons in the present study is poorly constrained, so that climate histories cannot be matched closely to canyon age.

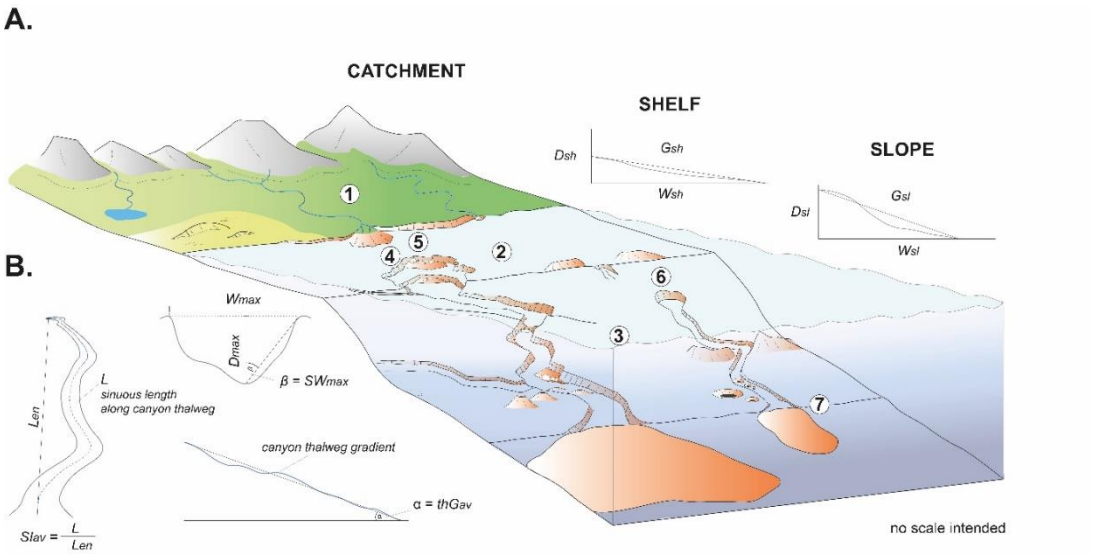

Figure 3.2a&b A. Attributes of the source-to-sink system and physiographic setting investigated in the study. 1. Terrestrial catchment: fluvial system length, average annual fluvial discharge, catchment size, maximum elevation. 2. Shelf configuration: width, depth, average gradient. 3. Slope configuration: width, depth, average gradient. 4. Canyon-apex location relative to the shelf break. 5. Minimum distance to shoreline. 6. Seafloor depth at the top of the canyon. 7. Seafloor depth at the canyon mouth. B. Key canyon morphometric parameters considered in the study: L = canyon length along thalweg; L_{en} = canyon length along endpoints; W_{max} = maximum canyon width; D_{max} = maximum canyon depth; SI_{av} = average canyon sinuosity index; thG_{av} = average canyon thalweg gradient; SW_{max} = maximum canyon sidewall steepness.

Study parameter	**Definition**
Canyon morphometrics	
L [km]**	Streamwise length of the canyon between canyon apex and canyon mouth as measured along the canyon thalweg
W_{max} [km]**	Maximum width of the canyon orthogonal to the canyon length
W_{av} [km]*	Average canyon width over the length of the entire canyon
D_{max} [m]*	Maximum depth of the canyon, i.e. depth of the canyon thalweg relative to the elevation of the canyon margins

D_{av} [m]*	Average canyon thalweg depth over the length of the entire canyon
SI_{av} [-]**	Average canyon sinuosity index, i.e. ratio between the sinuous canyon length measured along its thalweg and the straight distance between canyon apex and canyon mouth
thG_{av} [°]**	Average canyon thalweg gradient, evaluated between canyon apex and canyon mouth
SW_{max} [°]*	Maximum canyon-sidewall steepness, representing the maximum value of gradient between canyon rim and canyon bottom, evaluated along the entire length of the canyon
Physiographic setting	
canyon apex location	The location of the canyon apex relative to the shelf break, classified as 'shelf-incising' or 'slope-confined'
Dis_{min} [m]**	Minimum distance between the canyon and the shoreline
SD_{min} [m]**	Seafloor depth at the top of the canyon; for canyons with several tributaries at their head the shallowest seafloor depth has been recorded
SD_{max} [m]**	Seafloor depth at the mouth of the canyon
Canyon terrestrial catchment	
L_{fls} [km]**	Length of the river with a present-day or previous connection with the canyon, from headwater to river mouth; for canyons connected with several rivers the cumulative length has been considered
Q_{fls} [km^3/yr]*	Mean annual discharge of the fluvial system; for canyons connected with several rivers the cumulative mean annual discharge has been considered
A_{flsc} [km^2]*	Size of the catchment associated with the fluvial system; for canyons connected with several rivers the maximum area of the combined catchment has been considered
H_{flsc} [m]**	Maximum elevation of the catchment area relative to sea level; for canyons connected with several rivers the elevation of the highest peak in the combined catchment has been considered
Continental shelf	
W_{sh} [km]**	Width of the shelf at the canyon location
G_{sh} [°]**	Average shelf gradient at the canyon location

D_{sh} [m]**	Shelf-break depth at the canyon; for shelf edges with variable bathymetry, the deepest point is considered
Continental slope	
W_{sl} [km]**	Width of the slope at the canyon location
G_{sl} [°]**	Average slope gradient between the shelf break and the slope break
D_{sl} [m]**	Slope-break depth at the canyon
Other parameters	
Lat_{abs} [°]**	Absolute value of the latitude of the canyon apex
source-to-sink setting	Physiography of the source-to-sink system the canyon is associated with, classified as: (i) continental setting; (ii) insular setting; canyons situated in trenches between islands and continents have not been included
continental-margin type	For canyons located along continental margins, including canyons associated with islands: (i) active margin (including both convergent and transform settings); (ii) passive margin
oceanographic environment	(i) Open sea: canyons located in an oceanic environment with open hydrodynamic interaction with adjacent seas; exposed to oceanic gyres; (ii) Semi-enclosed and enclosed sea: canyons located in a sea which is largely bounded by landmasses and therefore has no or limited hydrodynamic interaction and connection with oceans; the definition includes seas, gulfs and straits

Table 3.2 Overview and definition of the study parameters that have been considered in this work. Three asterisks (***) denote values that have been calculated. Two asterisks (**) denote values that have been obtained either from the literature, as reported by the original authors, measured or calculated. A single asterisk (*) denotes values that have been retrieved from the literature, as stated by the original authors.

3.3.2 Statistical analyses

Relationships between canyon morphometric parameters and descriptors of physiographic setting and external controlling factors have been investigated by statistical analyses.

(i) Descriptive statistics of frequency distributions of canyon morphometric parameters are evaluated for classes of: canyon-

apex location relative to the shelf-break, continental-margin type, source-to-sink setting, oceanographic environment, and latitudinal position of the canyon apex or head. Comparisons between distributions of values in canyon groups are undertaken.

(ii) Statistical testing has been used to evaluate whether differences in mean values of canyon morphometrics between groups of canyons are statistically significant. For assessment across two groups, two-sample t-tests have been conducted, whereas differences in mean values between more than two canyon groups have been assessed by means of one-way analysis of variance (ANOVA). To test datasets with heteroscedastic distributions, Welch's t-test and Welch's ANOVA have been used throughout. Test statistics, degrees of freedom (DF) and P-values are presented for all tests. Results with p-values $\leqslant 0.01$ are reported as statistically significant. Prior to the analyses, a logarithmic variable transformation is applied to skewed frequency distributions.

(iii) Correlation analysis has been applied to investigate pairwise relationships between the studied parameters from the individual values obtained for each studied canyon. The strength and sign of correlation between two parameters is quantified by Pearson's correlation coefficient (r), to reveal linear relationships, and by Spearman's rank correlation coefficient (r_s), to reveal monotonic relationships. A correlation is considered statistically significant for p-values ≤0.01.

Although statistical analyses have been performed for any number of readings (N), the results are commonly presented and discussed when N≥15; it is explicitly stated when N<15.

All statistical analyses have been undertaken in Minitab 19.

3.3.3 Limitations of the study

Some of the key limitations of this study can be summarised as follows.

(i) In studies of submarine canyons there exists some geographic and thematic bias, as recognised by Matos et al. (2018), and some of that bias may have been inherited by this work. For example, logistic, financial and environmental challenges to investigating submarine canyons in polar regions might explain the relative scarcity of local- and regional-scale case studies of submarine canyons in the Arctic and Antarctica. Also, research efforts might be more focused on specific classes of canyons: for example, larger submarine canyons might be of particular interest for studies of marine habitats or as modern analogues for ancient systems in hydrocarbon exploration. Despite this, an effort has been made to compile a globally representative dataset of case studies of submarine canyons associated with different types of environmental settings (see Fig. 3.1 & Tab. 3.1). The study also incorporates 12 canyon studies published after 2016, which were not considered by Matos et al. (2018) in their analysis.

(ii) The scale of slope channelforms recognised in the case studies depends on data resolution, which sets the limit of the smallest mappable geomorphic features, and affects the precision of measurements. Due to heterogeneity in data types, some variability in resolution is expected.

(iii) As in any metastudy, erroneous data reported in the primary data sources may have been inadvertently included in the database. However, all reasonable measures have been taken to ensure data accuracy.

(iv) Although this study considers many environmental factors that may act as controls on canyon geomorphology, some relationships might arise from covariance of such factors with one or several parameters that have not been included in the analyses.

(v) Shelf-margin and base-of-slope depths of continental margins lacking distinct morphological breaks at the shelf-slope transition

and/or in the base-of-slope region are difficult to determine precisely. As such, these attributes may have not been reported in the literature, and have not been included in the current dataset.

(vi) Despite the ability afforded by studies of modern canyons to constrain physiographic setting, external factors and process-response relationships, measurements of the physical characteristics of canyons and their settings only represent snapshots of the temporal evolution of the studied forms.

(vii) The continental-margin type, source-to-sink setting, and oceanographic environment constitute factors that apply to the entire extent of the studied canyons, and thus allow consistent grouping. In contrast, along their length, some submarine canyons might stretch across two latitudinal zones. The position of the canyon apex relative to the shelf break can be variable over time, but incision of the shelf by the canyon does not per se represent a more mature evolutionary stage of the canyon. Some canyons that are presently slope-confined might have had a physical connection to the shelf in the past: their canyon heads and proximal parts may have been backfilled (Pratson et al., 2007) or may have prograded basinwards (Mauffrey et al., 2015). This must be considered in analyses of frequency distributions of canyon morphometrics across slope-confined and shelf-incising forms.

3.4 Scaling relationships between canyon morphometrics

3.4.1 Observations

Correlation strengths between canyon morphometric parameters are highly variable, with only some correlations being strong and statistically significant (Figs. 3.3 & 3.4a-o).

Maximum dimensions of the studied canyons are moderately correlated with each other (Fig. 3.4a-c). Strong relationships that are statistically significant exist for average canyon width with maximum width (Fig. 3.3), length (Fig. 3.4a) and maximum depth (Fig. 3.4c), and for the latter with average depth

(Fig. 3.3). In addition, modest significant scaling is demonstrated for maximum width and average depth (Fig. 3.4c). In contrast, correlations of average canyon depth with canyon length (Fig. 3.4b) and average canyon width (Fig. 3.4c) are weak and not significant. Strong correlations between length and canyon width, and no correlation between canyon length and average depth, are also observed in the dataset by Harris et al. (2014b) (Figs. 3.4p&q).

Average canyon sinuosity shows significant, respectively modest and moderate, positive correlations with canyon length (Fig. 3.4d) and average canyon depth (Fig. 3.4f), and modest correlations with maximum canyon width (Fig. 3.4e). The negative correlation between sinuosity and average canyon thalweg gradient is significant but weak (Fig. 3.4m), whereas no correlation is seen between sinuosity and maximum canyon sidewall steepness (Fig. 3.4n).

The average canyon thalweg gradient demonstrates moderate negative correlation with canyon length (Fig. 3.4g) and weak negative correlation with maximum canyon width (Fig. 3.4h), both of which are statistically significant. The positive moderate correlation between thalweg gradient and average canyon depth is not statistically significant (N = 12; Fig. 3.4i). No correlation exists between thalweg gradient and either average width (Fig. 3.4h) and maximum sidewall steepness (Fig. 3.4o).

Positive, modest and statistically significant relationships are seen between maximum canyon sidewall steepness and both maximum canyon width (Fig. 3.4k) and depth (Fig. 3.4l), whereas the maximum canyon sidewall steepness is weakly correlated with canyon length (Fig. 3.4j).

3.4.2 Interpretations

Correlations between pairs of canyon morphometric parameters suggest that these canyon characteristics may be affected by the same process or controlling factors.

In some cases, correlations may arise – either in part or fully – due to covariance with other parameters, and this may be inherent in the definition of the parameters themselves. For example, more sinuous canyons tend to

have longer streamwise canyon length for a given slope extent, whereas deeper channel forms are expected to have steeper margins.

In addition, some canyon morphometrics appear to be more strongly related to certain environmental controls; this is discussed in sections 3.5, 3.6 and 3.7.

3.4.2.1 Sedimentary processes

Because the effects of sedimentary processes on canyon evolution depend primarily on the sediment volumes they mobilise, their erosive strength and their areal extent, sedimentary processes can affect canyon morphometrics in different ways, at different locations along a canyon and even during the same event (e.g. Su et al., 2020). The ability of sediment gravity flows and slope failures to trigger one another (e.g. Pratson and Coakley, 1996; Bernhardt et al., 2015) and the common transition of the latter into the former (e.g. Puig et al., 2014) makes it difficult to differentiate between the relative importance of these processes in shaping canyon geomorphology. As a consequence, it may not be possible to establish causal links between intra-canyon-scaling relationships and sediment-transport mechanisms. Nevertheless, observed scaling between some canyon morphometric parameters suggests that the influence of one or several controlling factors tends to be prevalent, giving rise to canyon geomorphologic characteristics that are recognizable on a global scale despite specific regional or local conditions.

Canyon enlargement can be driven by active erosive processes, such as primary erosion by sediment gravity flows passing through the canyon (e.g. Li et al., 2021) or by slope failure within the canyon and on the adjacent slope (e.g. Post et al., 2022), but also by accretion of the adjacent slope or of ridges between canyons, which may be caused by along-slope currents (e.g. Rona 1970), by background sedimentation or spillover of sediment gravity flows passing through canyons (e.g. Straub and Mohrig, 2009; Armitage et al., 2010), or due to primary carbonate production (e.g. Shepard, 1972; Tournadour et al., 2017). By contrast, intra-canyon aggradation, e.g. by backfilling (Cronin et al., 2005), sediment accumulation in canyon heads

(e.g. Walsh et al., 2007) and hemipelagic sedimentation (e.g. Jobe et al., 2011) weaken the effect of erosive processes on positive scaling relationships in canyon morphometry, for example by shortening canyons and decreasing their depths.

The fact that these processes can variably modify individual canyon morphometric parameters is likely reflected in the observed scaling between maximum and average canyon dimensions. The rather strong scaling of canyon length with average canyon width may be linked to the ability of down-canyon flows to maintain their erosive behaviour beyond the canyon mouth. The moderate scaling of canyon length with maximum width might be related to the fact that lateral slope failures lead to local widening of the canyon over the excavated area, but may only increase canyon length where the mobilised sediment volume – which might also comprise intra-canyon sediment sources – is sufficient to extend the canyon beyond its present mouth. This may arise, for example, by breaching of intra-slope structural highs or by facilitating the progradation of the continental rise. Retrograde slope failures act as a primary cause of canyon lengthening (e.g. Orange et al., 1994; Pratson and Coakley, 1996; Pratson et al., 2007) and might cause the local widening of canyons in their proximal parts in correspondence of slump scars, where these are intercepted (e.g. Mulder et al., 2012). Relatively strong scaling of maximum depth with maximum and average width in the sampled canyons may in part reflect simultaneous canyon-margin aggradation and intra-canyon erosion. The positive scaling between maximum width and maximum canyon sidewall steepness can in part be explained by lateral canyon-slope failures causing a local increase in canyon width and canyon sidewall steepness, and by thalweg erosion.

3.4.2.2 Hydrodynamic processes

Marine hydrodynamic processes on the shelf and slope can variably influence canyon geomorphology: (i) by their direct effect on sedimentary processes within the canyon itself, and (ii) by exerting control on sediment supply from terrestrial, intra-shelf and -slope sources to canyons, which in turn can impact intra-canyon sedimentary processes.

Hydrodynamic processes that have been inferred to facilitate sediment supply to submarine canyons include tides (e.g. Mountjoy et al., 2014), long-lived longshore drifts (e.g. Normark et al., 2009; Smith et al., 2018), slope currents (e.g. Wang et al., 2018), high-energetic waves (e.g., solitary waves, Yin et al., 2019; storm waves, Sequeiros et al., 2019), and dense shelf-water cascading (e.g. Canals et al., 2006; Puig et al., 2014 and references therein; Gales et al., 2021). The processes are highly variable in terms of frequency, magnitude, duration and area of influence, and these factors affect both the volume and grain size of sediment sourced to canyons. Intra-canyon erosion, remobilisation and transport of sediment have been linked to tidal (e.g. Liu and Yin, 2004) and unidirectional oceanic currents (e.g. Itoh et al., 2015) passing through a canyon, and to the focussing of internal waves in both the shallower parts of shelf-incising canyons (e.g. Smith et al., 2018) and at greater water depths in canyons confined within the slope (e.g. Wang et al., 2022b). Hence, the influence of marine hydrodynamic processes on canyon geomorphology is complex and might both amplify or weaken the impact of sedimentary processes on the strength of scaling relationships between canyon morphometric attributes.

For example, canyons hosted on continental margins with strong oceanic currents might experience less frequent canyon-margin failures and reduced aggradation, due to the ability of such currents to inhibit sedimentation along canyon margins (e.g. Green, 2011). As a result, the impact of axial sediment gravity flows on scaling in canyons might be, to a lesser degree, overprinted by lateral failure in these canyons. On the contrary, currents that can lead to sediment accumulation along canyon margins may strengthen the scaling between canyon depth, width and margin slopes (see section 3.4.2.1). Moreover, the complex influence of slope currents and internal tidal waves on canyon geomorphology, related to the co-occurrence of intra-canyon erosional and depositional processes including canyon flushing and canyon-wall failure (see Wang et al., 2022b) might variably affect the strength in scaling between canyon morphometrics.

3.4.2.3 Structural controls

Structural controls might affect canyon geomorphology by their influence on pre-existing and developing seafloor topography, which might have contributed to the weakening of some of the relationships between canyon morphometric attributes. For example, where fault and diapiric structures form part of the canyon walls or are in vicinity of the canyon margin, they can steepen the canyon sidewalls (e.g. Yu and Chang, 2002; Bernhardt et al., 2015), and might overprint the effect of concurrent intra-canyon erosion by down-canyon sediment flows and canyon sidewall failure on canyon width, depth and sidewall steepness and the strength of their scaling with each other. In addition, emerging topography, generated for example by coral reef growth (e.g. Puga-Bernabéu et al., 2011) or diapiric uplift (e.g. Chiang et al., 2012), might cause flow deceleration, flow deflection, flow stripping and/or grain size segregation, which in turn might weaken the erosional effect of a flow further down-canyon. Similarly, substrate heterogeneity arising from pre-existing structural features or buried canyons might cause spatial variations in substrate erodibility. In turn, the erodibility of canyon floors or walls might be diminished or enhanced over the affected area, which can promote an overall irregular canyon geometry, and variably impact the average canyon sinuosity and canyon thalweg gradient.

3.4.2.4 Biogenic processes

The effect of the colonization of canyon walls and margins by marine fauna on canyon-wall stability has received limited attention in the literature (e.g. Shepard, 1981; Eittreim et al., 1982; Carlson and Karl, 1984; and references therein). Depending on factors such as nature of substrate, degree of bioturbation, filling and cementation, the canyon sidewall stability might be increased or decreased by bioturbation. Similarly, vegetation cover in proximal parts of canyons, specifically by marine flora in the photic zone, might reduce the erodibility of canyon slopes. The resulting variability in the erodibility of canyon walls and apices might affect the scaling relationships between canyon length, width and sidewall steepness. Thus, biogenic processes might constitute a controlling factor on scaling in canyon

morphology. Future research is needed to enhance the understanding of the impact of biota on canyon geomorphology.

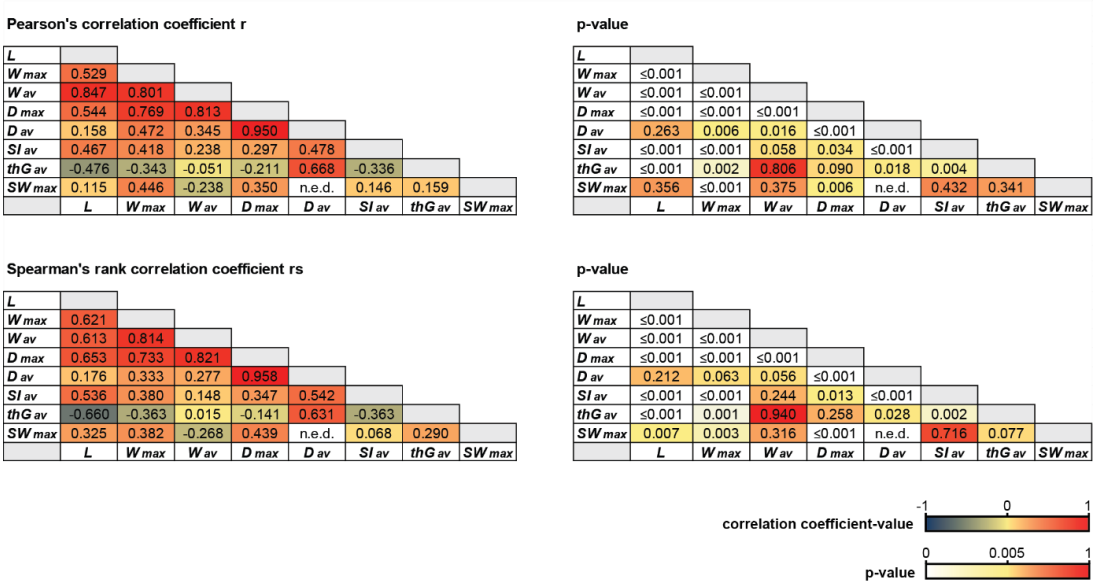

Pearson's correlation coefficient r							
L							
W max	0.529						
W av	0.847	0.801					
D max	0.544	0.769	0.813				
D av	0.158	0.472	0.345	0.950			
SI av	0.467	0.418	0.238	0.297	0.478		
thG av	-0.476	-0.343	-0.051	-0.211	0.668	-0.336	
SW max	0.115	0.446	-0.238	0.350	n.e.d.	0.146	0.159
	L	W max	W av	D max	D av	SI av	thG av

p-value							
L							
W max	≤0.001						
W av	≤0.001	≤0.001					
D max	≤0.001	≤0.001	≤0.001				
D av	0.263	0.006	0.016	≤0.001			
SI av	≤0.001	≤0.001	0.058	0.034	≤0.001		
thG av	≤0.001	0.002	0.806	0.090	0.018	0.004	
SW max	0.356	≤0.001	0.375	0.006	n.e.d.	0.432	0.341
	L	W max	W av	D max	D av	SI av	thG av

Spearman's rank correlation coefficient rs							
L							
W max	0.621						
W av	0.613	0.814					
D max	0.653	0.733	0.821				
D av	0.176	0.333	0.277	0.958			
SI av	0.536	0.380	0.148	0.347	0.542		
thG av	-0.660	-0.363	0.015	-0.141	0.631	-0.363	
SW max	0.325	0.382	-0.268	0.439	n.e.d.	0.068	0.290
	L	W max	W av	D max	D av	SI av	thG av

p-value							
L							
W max	≤0.001						
W av	≤0.001	≤0.001					
D max	≤0.001	≤0.001	≤0.001				
D av	0.212	0.063	0.056	≤0.001			
SI av	≤0.001	≤0.001	0.244	0.013	≤0.001		
thG av	≤0.001	0.001	0.940	0.258	0.028	0.002	
SW max	0.007	0.003	0.316	≤0.001	n.e.d.	0.716	0.077
	L	W max	W av	D max	D av	SI av	thG av

Figure 3.3 Heat maps of correlations of canyon morphometric parameters with each other for canyons of the study displaying values of Pearson's correlation coefficient r and Spearman's rank correlation coefficient r_s, and their respective p-values. *L* = canyon length; W_{max} = maximum canyon width; W_{av} = average canyon width; D_{max} = maximum canyon depth; D_{av} = average canyon depth; SI_{av} = average canyon sinuosity index; thG_{av} = average canyon thalweg gradient; SW_{max} = maximum canyon sidewall steepness. n.e.d. = not enough data to facilitate statistical analyses.

A.

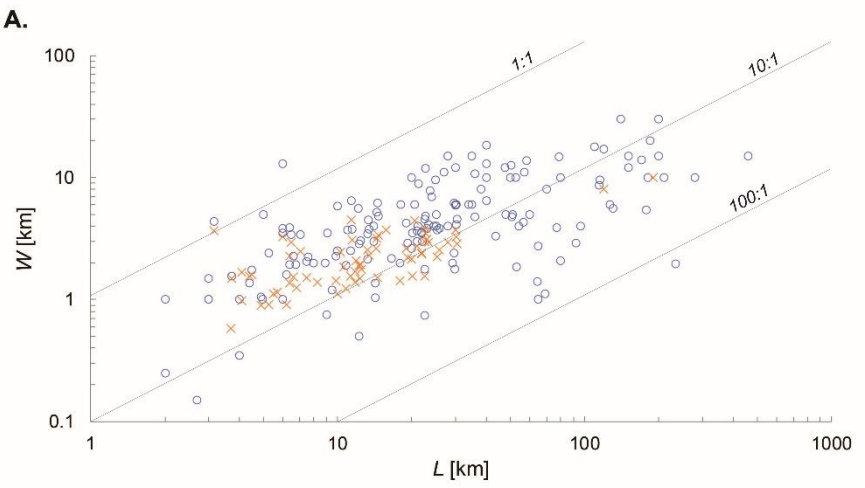

○ ***L vs Wmax:*** **N=156**	r=0.529 r_s=0.621	p≤0.001 p≤0.001	× ***L vs Wav:*** **N=66**	r=0.847 r_s=0.613	p≤0.001 p≤0.001

B.

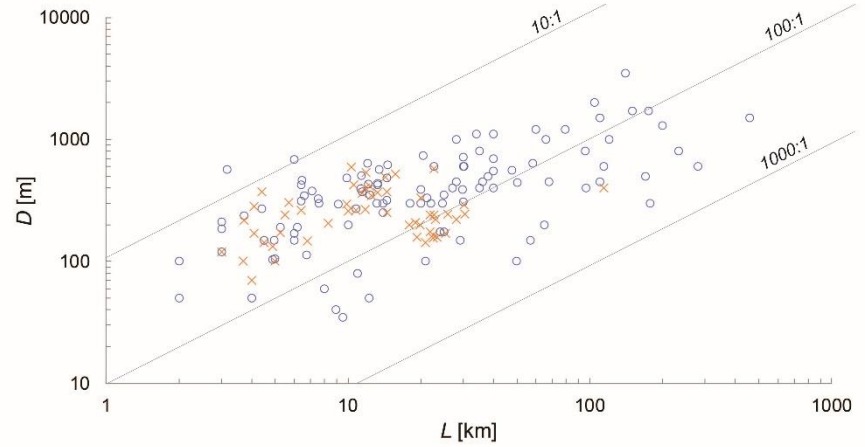

○ ***L vs Dmax:*** **N=107**	r=0.544 r_s=0.653	p≤0.001 p≤0.001	× ***L vs Dav:*** **N=52**	r=0.158 r_s=0.176	p=0.263 p=0.212

C.

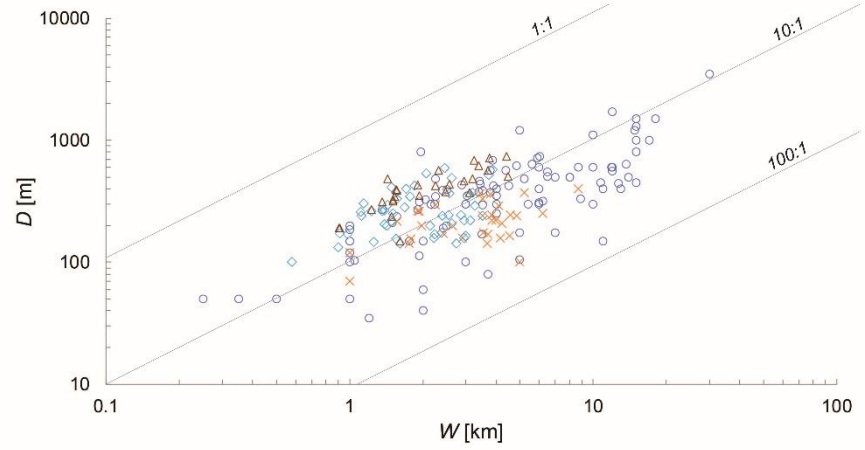

○ ***Wmax vs Dmax:*** **N=100**	r=0.769 r_s=0.733	p≤0.001 p≤0.001	△ ***Wav vs Dmax:*** **N=27**	r=0.813 r_s=0.821	p≤0.001 p≤0.001
× ***Wmax vs Dav:*** **N=32**	r=0.472 r_s=0.333	p=0.006 p=0.063	◇ ***Wav vs Dav:*** **N=48**	r=0.345 r_s=0.277	p=0.016 p=0.056

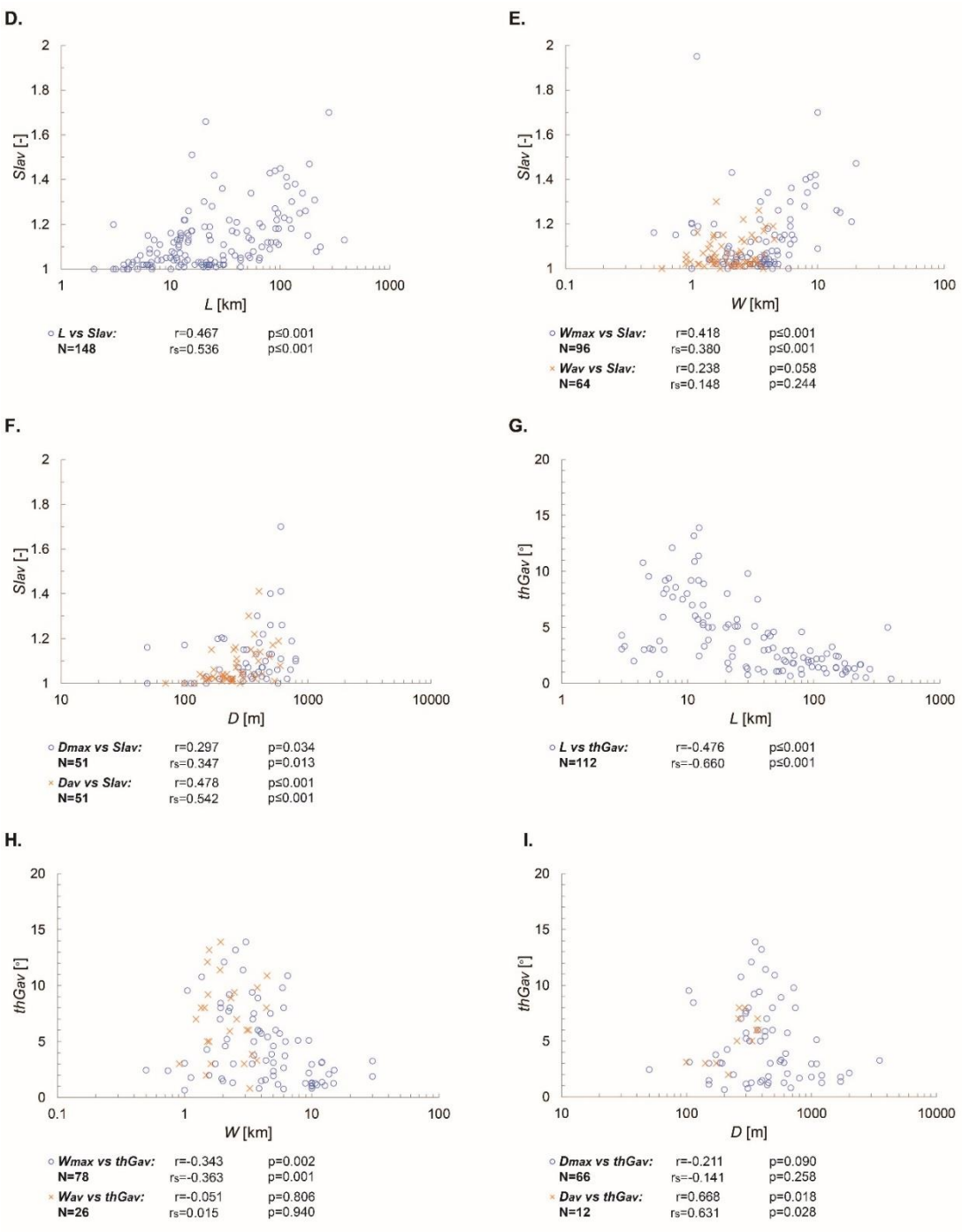

Figure 3.4a-q (continued).

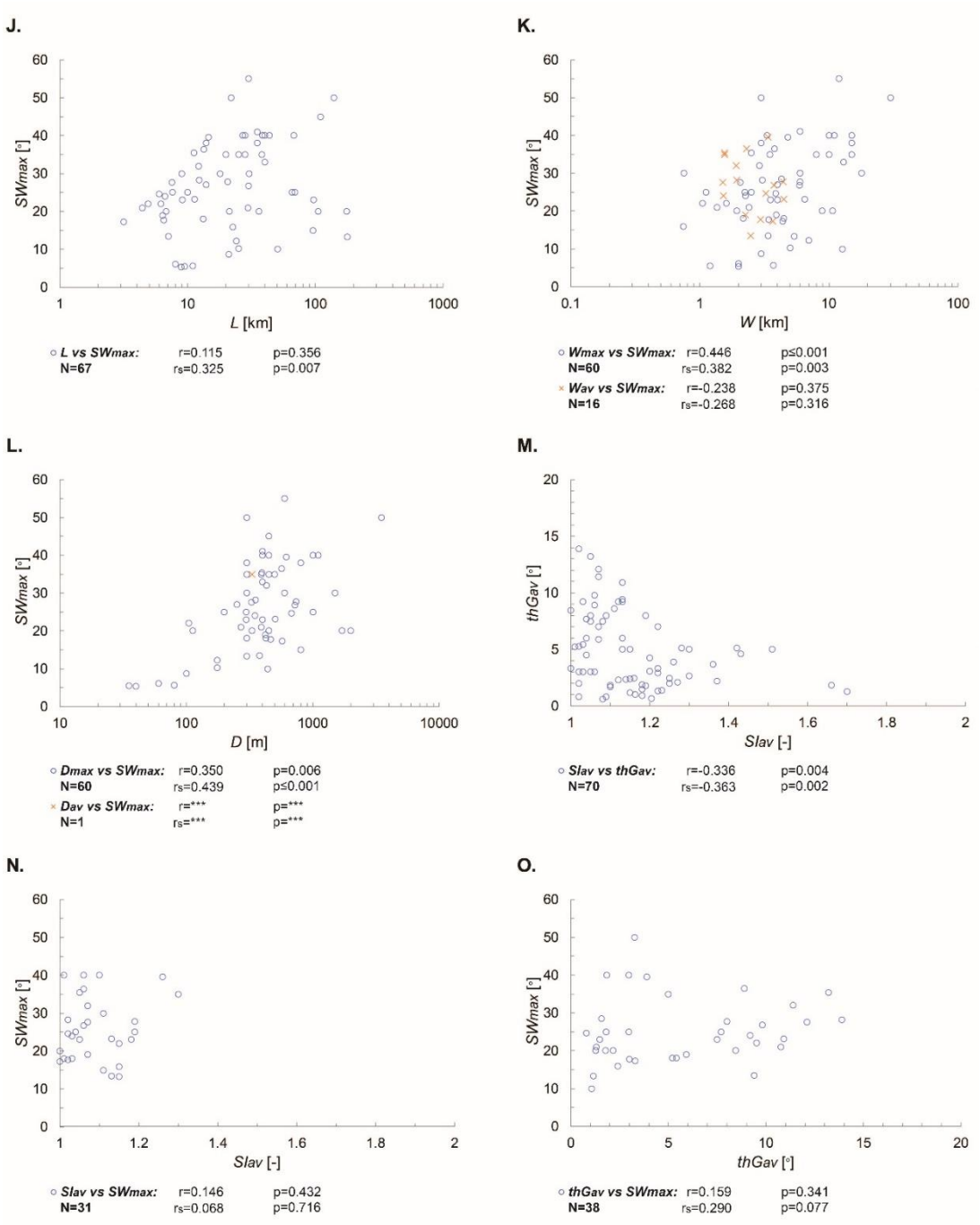

Figure 3.4a-q (continued).

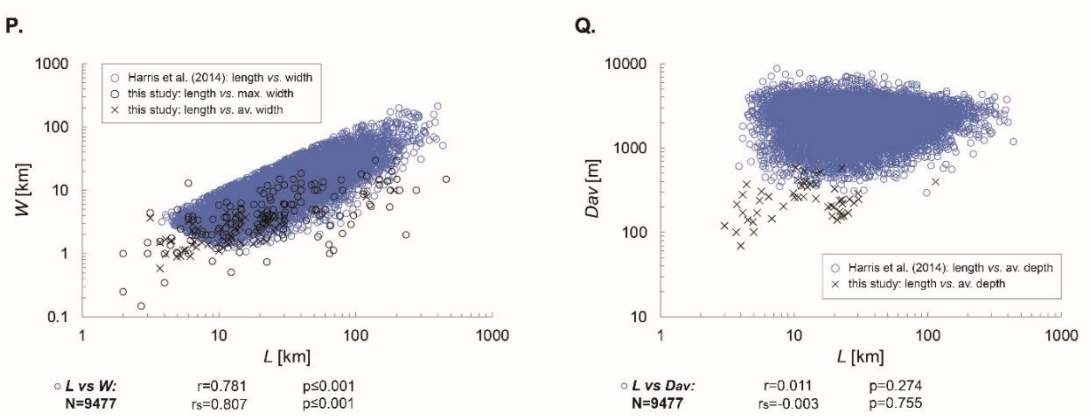

Figure 3.4a-q A.-O. Scatterplots of canyon morphometric parameters for studied submarine canyons. P.&Q. Scatterplots of canyon length with width (P) and average depth (Q) plotted from the dataset of Harris et al. (2014b) with an overlay of data from this study for comparison. N = number of observations; r = Pearson's correlation coefficient; r_s = Spearman's rank correlation coefficient.

3.5 Relationships between canyon morphometric parameters and attributes of the physiographic setting

Pearson's correlation coefficient r

L	0.097	-0.069	0.595	0.142
W max	-0.154	0.143	0.420	0.201
W av	0.171	-0.200	0.135	0.474
D max	-0.068	-0.211	0.750	0.111
D av	-0.330	-0.418	0.707	-0.398
SI av	-0.069	-0.137	0.566	0.176
thG av	-0.218	-0.056	-0.290	-0.352
SW max	-0.334	-0.101	0.364	0.465
	Dis min	*SD min*	*SD max*	*Lat abs*

p-value

L	0.129	0.342	≤0.001	0.021
W max	0.055	0.120	≤0.001	0.010
W av	0.169	0.113	0.317	≤0.001
D max	0.478	0.055	≤0.001	0.240
D av	0.017	0.002	≤0.001	0.003
SI av	0.416	0.128	≤0.001	0.031
thG av	0.021	0.577	0.004	≤0.001
SW max	0.006	0.469	0.008	≤0.001
	Dis min	*SD min*	*SD max*	*Lat abs*

Number of correlations

L	246	194	182	263
W max	155	119	108	164
W av	66	64	57	66
D max	110	83	74	113
D av	52	51	45	52
SI av	143	125	112	151
thG av	111	103	97	120
SW max	67	54	52	69
	Dis min	*SD min*	*SD max*	*Lat abs*

Spearman's rank correlation coefficient rs

L	0.037	-0.172	0.650	0.300
W max	-0.078	-0.096	0.509	0.207
W av	0.420	-0.181	-0.040	0.511
D max	-0.083	-0.353	0.776	0.123
D av	-0.095	-0.381	0.685	-0.421
SI av	-0.273	-0.277	0.460	0.218
thG av	0.011	-0.036	-0.251	-0.324
SW max	0.031	-0.129	0.365	0.415
	Dis min	*SD min*	*SD max*	*Lat abs*

p-value

L	0.566	0.017	≤0.001	≤0.001
W max	0.337	0.300	≤0.001	0.008
W av	≤0.001	0.152	0.766	≤0.001
D max	0.388	0.001	≤0.001	0.196
D av	0.501	0.006	≤0.001	0.002
SI av	0.001	0.002	≤0.001	0.007
thG av	0.905	0.719	0.013	≤0.001
SW max	0.802	0.354	0.008	≤0.001
	Dis min	*SD min*	*SD max*	*Lat abs*

correlation coefficient-value -1 0 1

p-value 0 0.005 1

Figure 3.5 Heat maps for correlations of canyon morphometrics with the physiographic setting displaying values of Pearson's correlation coefficient r and Spearman's rank correlation coefficient r_s, and their respective p-values. *L* = canyon length; W_{max} = maximum canyon width; W_{av} = average canyon width; D_{max} = maximum canyon depth; D_{av} = average canyon depth; SI_{av} = average canyon sinuosity index; thG_{av} = average canyon thalweg gradient; SW_{max} = maximum canyon sidewall steepness; Dis_{min} = minimum distance between the canyon and shoreline; SD_{min} = minimum seafloor depth at the canyon; SD_{max} = maximum seafloor depth at the canyon; Lat_{abs} = absolute value of the latitude of the canyon apex.

3.5.1 Distance between canyon and shoreline (Dis_{min})

3.5.1.1 Observations

The minimum distance between the canyon apex and the shoreline is not correlated to any of the canyon morphometric parameters except for the average canyon width (Figs. 3.5 & 3.6a-f), for which modest but statistically significant positive correlation is seen (Fig. 3.6b). However, in the assessment of a relationship with average canyon width, the average widths of canyons with a distance to a continent or island of ≤ 25 kilometres could not be evaluated.

3.5.1.2 Interpretations

Although the distance of the canyon to the shoreline plays a role in sediment distribution from fluvial sources across shelves and slopes (section 3.6.1), the results show that relationships between the distance of the canyon to the shoreline and overall canyon geomorphology are weak. It can thus be inferred that the distance to the shoreline itself is not a major factor, relative to others.

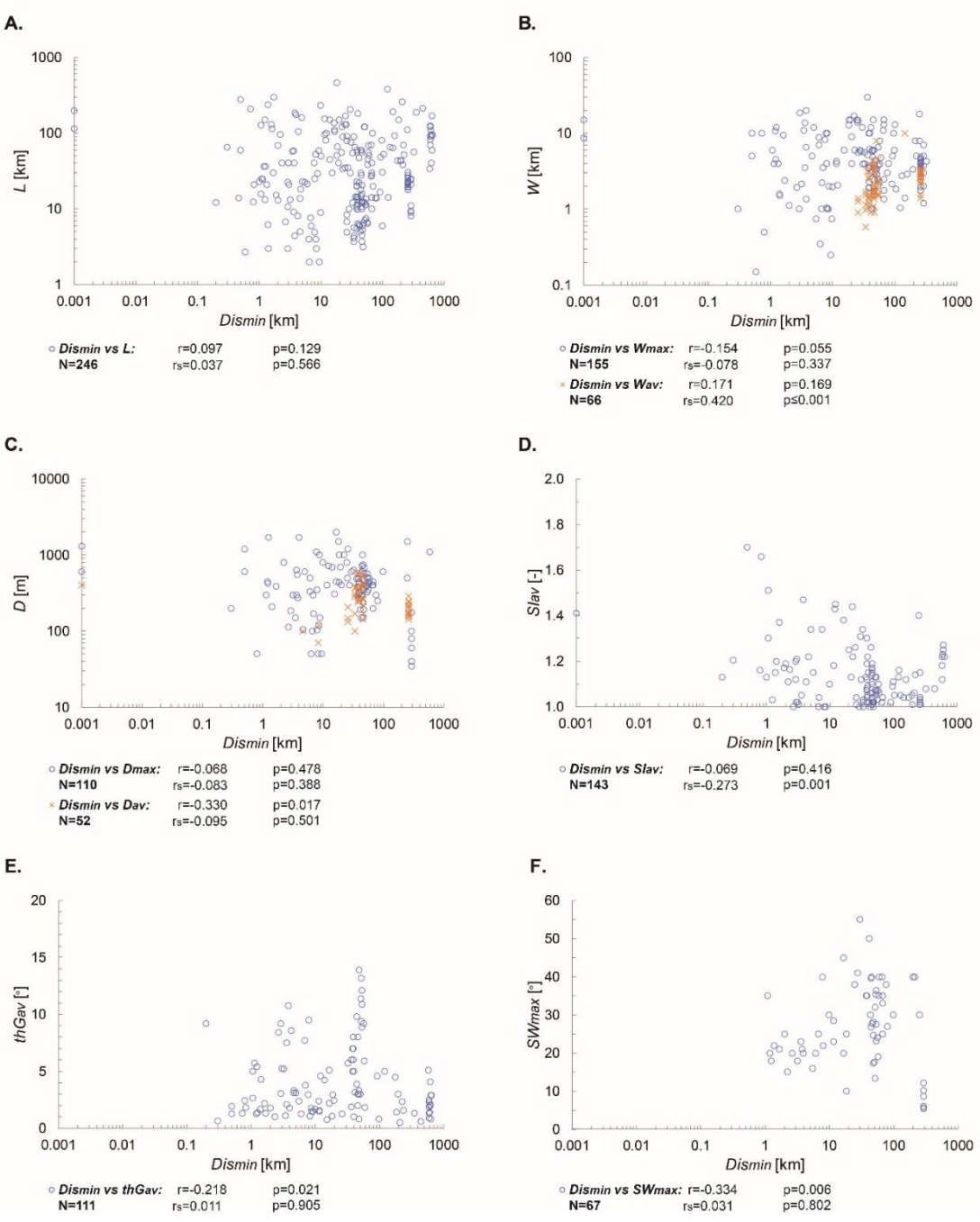

Figure 3.6a-f Scatterplots of minimum canyon-shoreline distance and canyon morphometric parameters. N = number of correlations; r = Pearson's correlation coefficient; r_s = Spearman's rank correlation coefficient.

3.5.2 Canyon bathymetry

3.5.2.1 Observations

Seafloor depth at the canyon apex (SD_{min})

Most canyon morphometrics correlate poorly with seafloor depth at the canyon apex (Figs. 3.5 & 3.7a-f). Modest negative correlations are seen with average canyon depth, and a weak negative relationship with maximum canyon depth, both of which are statistically significant (Fig. 3.7c). A weak but significant negative correlation is also displayed with average canyon sinuosity (Fig. 3.7d).

Seafloor depth at the canyon mouth (SD_{max})

The seafloor depth at the canyon mouth tends to correlate significantly with all investigated canyon morphometric parameters except for average canyon width (Figs. 3.5 & 3.8a-f). Moderate positive correlations are seen with canyon length (Fig. 3.8a), maximum canyon width (Fig. 3.8b), both maximum and average canyon depth (Fig. 3.8c), and with average canyon sinuosity (Fig. 3.8d), whereas correlations with maximum canyon sidewall steepness are weaker (Fig. 3.8f). In contrast, a weak negative correlation is seen with the average canyon thalweg gradient (Fig. 3.8e).

3.5.2.2 Interpretations

Seafloor depth at the canyon apex (SD_{min})

No clear relationships are seen between canyon geomorphology and the seafloor depth at the apex of the canyon, except for canyon depth. Data on maximum and average canyon dimensions demonstrate that large canyons can develop regardless of the seafloor depth at the canyon apex. The results indicate that the absolute canyon-apex depth does not necessarily relate to controlling factors influencing canyon geomorphology, such as a connection to sediment sources (section 3.6.1), the hydrodynamic regime (section 3.4.2.2) or structural controls (section 3.4.2.3). Although the canyon length increases with retrograde erosion at the canyon head, which leads to progressive shallowing of the canyon apex, the bathymetry of the basin ultimately determines the canyon length (section 3.6.3). The tendency of canyons to be deeper when their apex is shallower might reflect how canyon deepening may be facilitated by erosive sediment gravity flows linked to the progressive retrogradation of the canyon, which can enhance sediment delivery from terrestrial and intra-shelf sources and from sediment

remobilisation within the canyon. Weak scaling between canyon morphometric parameters and canyon-apex depth might also reflect how substrate lithology and seafloor gradients, which affect canyon morphodynamics and the magnitude and frequency of mass-wasting processes, vary systematically with depth (e.g. Harris et al., 2014b; Diesing, 2020).

Seafloor depth at the canyon mouth (SD_{max})

The results suggest that canyons reaching greater depths tend to have greater maximum dimensions and average depths, but not average widths. The observed increase in maximum canyon width and depth with increasing seafloor depth at the canyon mouth may be linked to the widening and deepening of canyons by turbidity currents in the region of the canyon mouth as a response to a decrease in slope gradient (e.g. Brunt et al., 2013). In addition, results of physical experiments suggest that, in long canyons, the upwelling of along-slope currents via the canyon mouth creates cyclonic eddies in the mouth region (Waterhouse et al., 2009). This mechanism might cause lateral erosion at the canyon margins and might promote intra-canyon erosion in the canyon-mouth area.

The results also indicate that canyons reaching into deeper waters tend to be more sinuous, which might reflect an increased impact of seafloor relief on canyon geomorphology with progressive extension of the canyon across the continental slope. For example, canyons might become more sinuous and longer where their pathways are deflected and redirected by topographic highs (e.g. Micallef et al., 2014) and intra-slope depressions (e.g. Bourget et al., 2010). The effect of seafloor topographic variability might also in part explain the positive scaling of maximum width with seafloor depth, in view of how longer canyons are more likely to have a larger number of sections displaying local widening in planform, for example where intra-slope depressions are incorporated in the canyon.

For maximum canyon sidewall steepness, the positive scaling with seafloor depth at the canyon mouth might in part reflect how the studied canyons located in open seas tend to have steeper canyon margins than those in

semi-enclosed and enclosed seas (section 3.7.4), and continental slopes in open oceanic settings reaching greater depths.

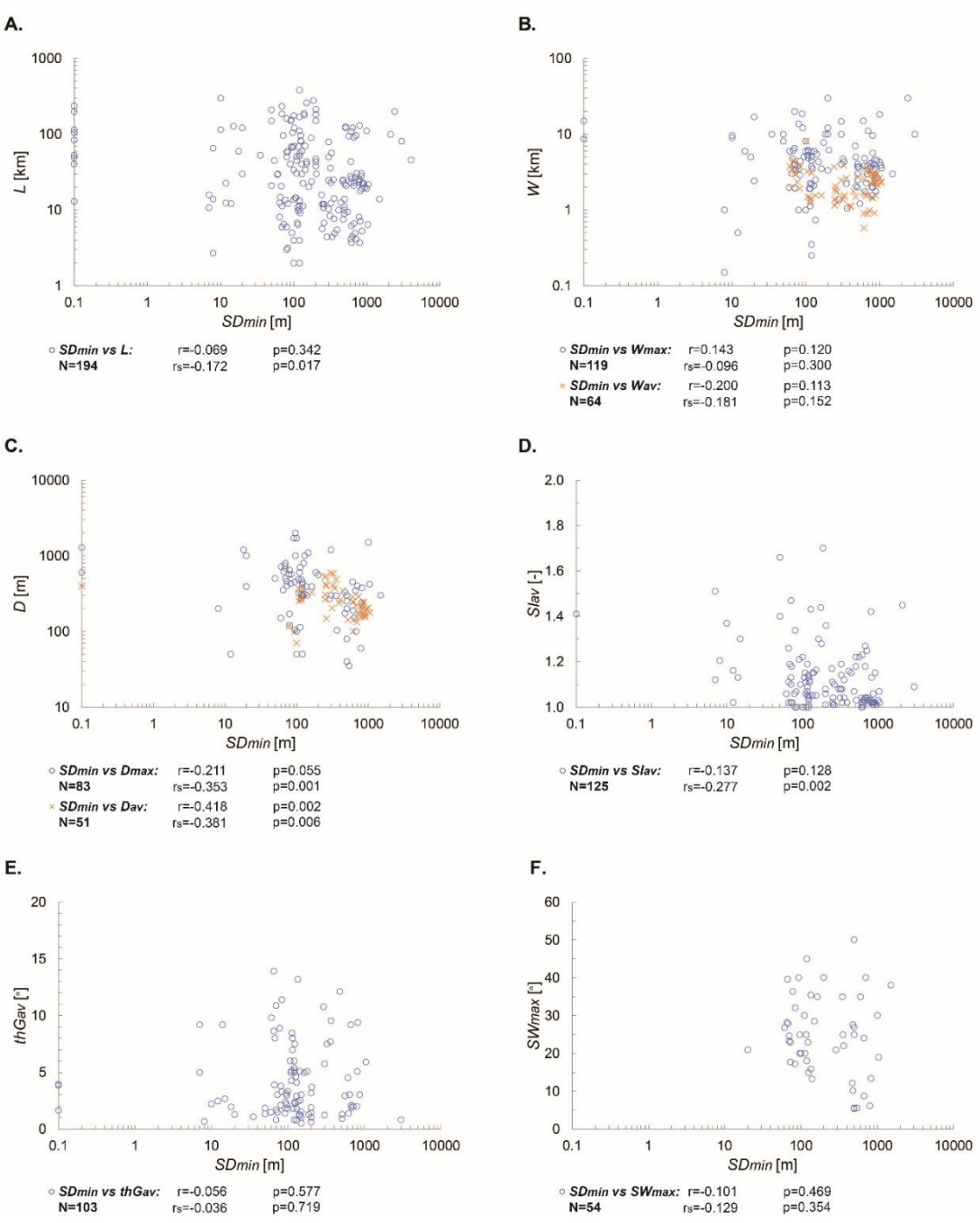

Figure 3.7a-f Scatterplots of seafloor depth at the top of the canyon and canyon morphometric parameters. N = number of correlations; r = Pearson's correlation coefficient; r_S = Spearman's rank correlation coefficient.

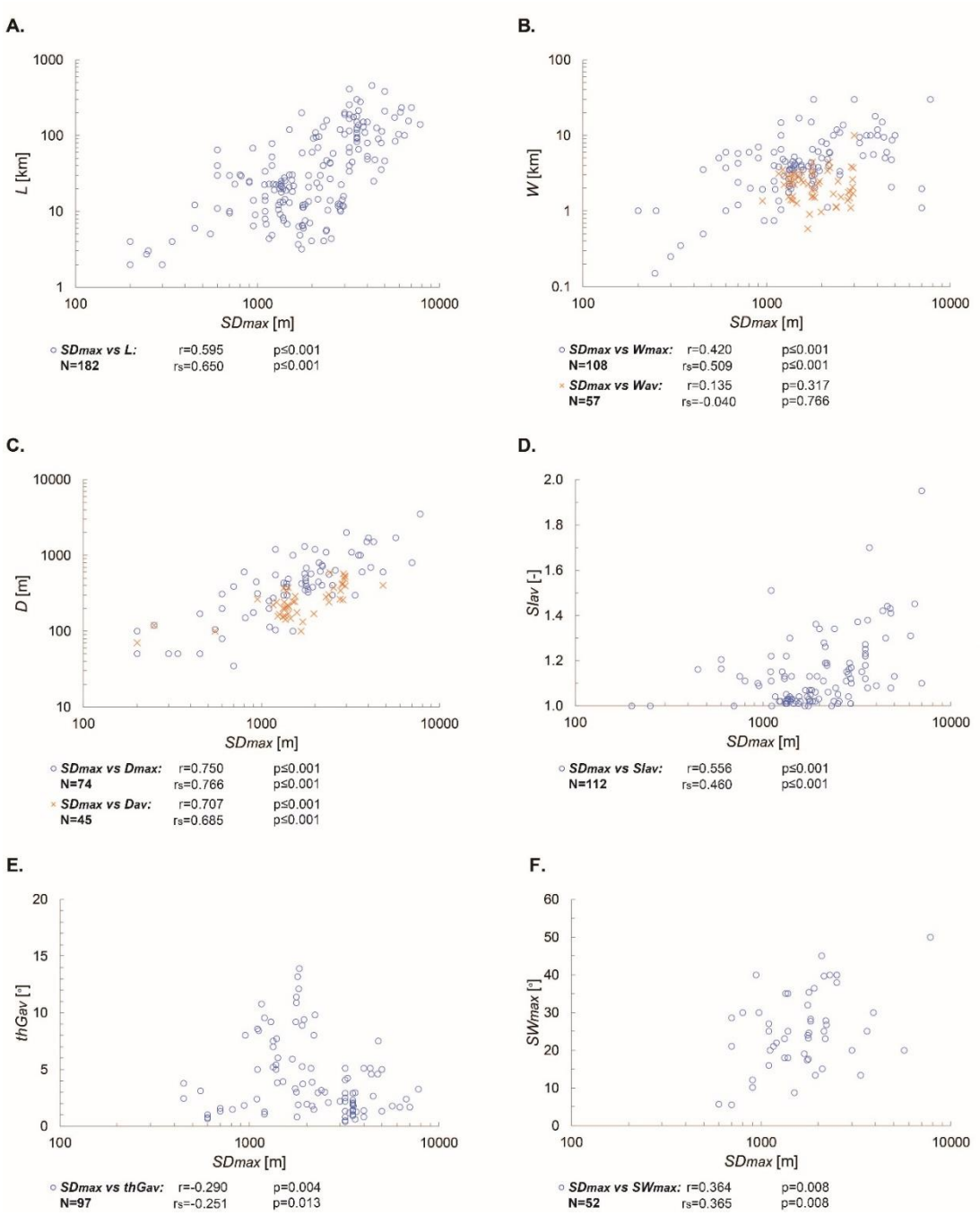

Figure 3.8a-f Scatterplots of seafloor depth at the canyon mouth and canyon morphometric parameters. N = number of correlations; r = Pearson's correlation coefficient; r_s = Spearman's rank correlation coefficient.

3.5.3 Latitudinal position of the canyon apex (Lat_{abs})

The canyons in this study cover a latitudinal range between 1° and 72° degrees. However, data on high-latitude canyons is limited to 15 examples from the NW Norwegian continental margin and the Barrow Canyon in the

NE Chukchi Sea; polar canyons along the Antarctic margin are notably lacking in the dataset (see section 3.3.3).

3.5.3.1 Observations

For absolute values of latitude of the canyon apex and canyon morphometric parameters, correlations are weak to moderate in strength (Figs. 3.5 & 3.9a-f). Moderate positive correlation exists between latitude and average canyon width (Fig. 3.9b), and modest negative correlations between latitude and both average depth (Fig. 3.9c) and maximum canyon sidewall steepness (Fig. 3.9f). Weaker but statistically significant correlations are seen for canyon length (Fig. 3.9a), average canyon sinuosity (Fig. 3.9d) and the average canyon thalweg gradient (Fig. 3.9e), which are negative for the latter and positive for the former two parameters.

3.5.3.2 Interpretations

The limited correlation between latitude and canyon morphometric parameters is interpreted to (i) arise from the complex ways in which climate can influence processes that can control canyon geomorphology (section 3.4.2); and (ii) reflect how the occurrence, frequency and magnitude of some processes vary with latitude, or are prevalent in – or even exclusive to – certain latitudinal belts.

Climate can variably influence sediment fluxes to marine environments and submarine canyons, for example by exerting controls on precipitation and subaerial erosion (e.g. Milliman and Farnsworth, 2011; Clift, 2020). Despite marked regional variations, annual precipitation rates decrease with latitude on a global scale (Milliman and Farnsworth, 2011). A general relationship between precipitation and denudation rates has been discussed in the literature (e.g. Fournier, 1949; Langbein and Schumm, 1958; Wilson, 1973; Milliman and Farnsworth, 2011; Zhang et al., 2022b). Local and regional erosion rates might vary greatly due to the impact of additional factors such as lithology, tectonic uplift and vegetation cover (e.g. Kober et al., 2015; Torres Acosta et al., 2015; Starke et al., 2020). Hence, the weakness in correlation between latitude and canyon morphometrics might reflect the complex interrelationships between these factors, variability in the degree to

which they are controlled by latitude, or that they are not important controls on submarine-canyon geomorphology.

Sediment discharge in rivers tends to peak during extreme weather events (e.g. Mulder and Syvitski, 1995), and to vary in concert with seasonal phenomena like monsoons (e.g. Clift, 2020). For example, cyclones can set the conditions that trigger hyperpycnal flows and turbidity currents at river mouths (e.g. Milliman and Kao, 2005). The passing of such cyclone-driven flows through submarine canyons is known from low-latitudinal regions including the South China Sea (e.g. Milliman and Kao, 2005; Zhang et al., 2018) and the Philippines (e.g. Sequeiros et al., 2019; Porcile et al., 2020), but cyclones also occur at temperate latitudes (e.g. Schultz et al., 2019; Son et al., 2022), and tend to preferentially occur in certain geographic regions in both hemispheres (e.g. Goni et al., 2015; Schultz et al., 2019). Storm-induced intra-canyon flows have been reported from many examples at tropical and temperate latitudes, and can also be linked to the remobilisation of shelf deposits as well as excess pore water pressure facilitating the remobilisation of surface sediments in the vicinity of canyon heads (e.g. Puig et al., 2004; 2014 and references therein).

Thus, climate-related factors that might exert control on canyon geomorphology are in many cases not tied to a certain latitudinal belt and cannot generally be captured by monotonic relationships across tropical and temperate zones.

The potential influence of glacial processes on canyon geomorphology is especially relevant to canyons in polar and mid-latitude regions that were covered by ice sheets during glacial intervals. Sediment can be supplied to slope environments by various glacial processes. The relative predominance of such processes and their importance as sediment sources to submarine canyons can vary over a glacial-interglacial cycle (e.g. Kagami et al., 1991; Gales et al., 2021; Ha et al., 2022). For example, during glacial and interglacial intervals, where ice sheets have prograded across continental shelves, sediment can be distributed to canyon heads via sediment gravity flows fed by subglacial ice streams and meltwater discharge (e.g. Kagami et al., 1991; Dowdeswell et al., 2004; Gales et al., 2021). In contrast,

glacioisostatic shelf downwarping and uplift within the shelf might cause disconnection of canyons from sediment sources, by diverting sediment pathways and creating intra-shelf sinks (e.g. Kagami et al., 1991). Moreover, ice-sheet loading along shelf margins during glacial maxima and sea-level lowstands is considered a potential trigger to mass failures on continental slopes (e.g. Mulder and Moran, 1995; Gales et al., 2021). This mechanism might contribute to intra-canyon erosion by slope failures that would trigger, or evolve into, sediment gravity flows, and cause mass failures in canyons that have reached or retrograded into glaciated shelves. In addition, sediment can be supplied to slope systems from ice-rafted debris (e.g. Gales et al., 2021; Ha et al., 2022), a process which is influenced by climate but occurs during both glacial and interglacial periods (e.g. Hemming, 2004; Alvarez-Solas et al., 2013; Ha et al., 2022). Sediment can also be transported to canyons via down-canyon cascading of dense shelf water, as seen in the Antarctic Hillary Canyon (see Gales et al., 2021).

In high-latitude settings, sediment connection of canyons to terrestrial catchments might also be affected by glacial isostatic adjustment subsequent to glacial intervals leading to river diversions (e.g. Pico et al., 2018).

An example of steep canyon margins (>40°) is reported for submarine canyons along the Labrador margin (e.g. Dowdeswell et al., 2016). One factor that might contribute to steeper margins in canyons in higher latitudes is the glaciation of continental margins. The prevalence of line sources in glacial margin settings, as opposed to point sources in low-latitudinal settings, has been suggested (e.g. Martinsen, 2005; Armitage et al., 2010): sediment can be discharged rapidly from glaciers and ice streams, and distributed sediment dispersal across the continental slope (Martinsen, 2005) can promote the aggradation of canyon margins and inter-canyon ridges due to background sedimentation and overspill from channelised flows in canyons (e.g. Armitage et al., 2010; Gales et al., 2021), which in turn increase their proneness to slope failure (Armitage et al., 2010).

Although suitable data only include submarine canyons at latitudes up to 45°, the lack of any relationships between latitude and sinuosity is in

agreement with findings by Harris and Whiteway (2011) for shelf-incising canyons (see their Figure 9). The influence of latitude-related processes on submarine-channel sinuosity has been debated: an inverse relationship between channel sinuosity and latitude, linked to influence of the Coriolis force and variations in sediment type and flow type within different latitudinal zones, has been proposed (e.g. Peakall et al., 2012); its robustness has been subsequently both challenged (e.g. Sylvester & Pirmez, 2017) and corroborated (e.g. Allen et al., 2022). The results indicate that mechanisms invoked as latitudinal controls on sinuosity for submarine channels may not be applicable to submarine canyons. This research area needs further investigation.

Regardless, these considerations must be viewed with reservation due to the limited size of the datasets for Arctic and tropical examples, and because of geographic bias. For example, canyons offshore NW Norway are accommodated on a passive margin in an open-sea setting, two environmental conditions that appear to promote steepening of canyon sidewalls; the former by promoting slope failure within canyons (section 3.7.2) and the latter by favouring canyon margin aggradation related to oceanic currents in open-sea settings (section 3.7.4).

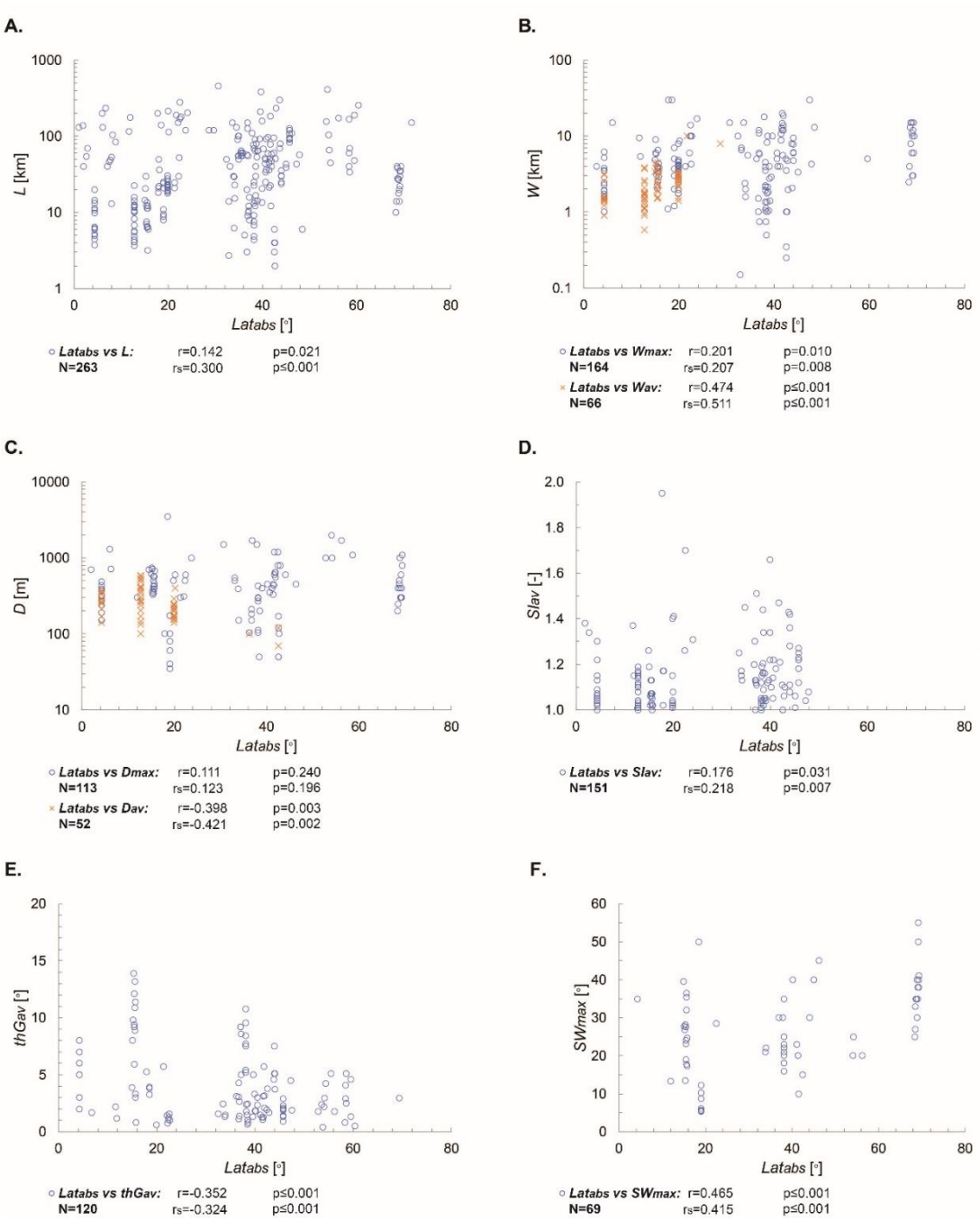

Figure 3.9a-f Scatterplots of absolute values of latitude of the canyon apex and canyon morphometric parameters. N = number of correlations; r = Pearson's correlation coefficient; r_s = Spearman's rank correlation coefficient.

3.6 Scaling relationships between canyon morphometric parameters and source-to-sink (S2S) system attributes

Scaling relationships between canyon morphometric parameters and attributes of related terrestrial catchments, continental shelves and slopes have been evaluated. For 69 submarine canyons, which represent 24% of the studied canyons, scaling relationships between canyon and terrestrial-catchment parameters have been investigated, except for maximum canyon sidewall steepness, average canyon width and depth, due to data paucity. The same applies for correlations of average canyon width and depth with slope characteristics.

An overview of the results is presented in form of heatmaps of correlation (Fig. 3.10a-c). Furthermore, relationships between attributes of canyon-associated S2S systems (Fig. 3.11) have been investigated. This has been undertaken to aid in the interpretation of controls on canyon morphometry by identifying where relationships might in part reflect covariance with one or several other factors. Correlations of canyon morphometrics with attributes of the catchment, shelf and slope are presented as scatterplots in sections 3.6.1 to 3.6.3 (Figs. 3.12-3.15), in which the findings for the individual S2S segments are discussed. In addition, canyon morphometry has been quantitatively assessed for canyons grouped based on shelf-break thresholds of 120 m and 130 m below present-day sea level at the site of the canyon (Fig. 3.14a-f).

A. Terrestrial catchment

Pearson's correlation coefficient r

L	0.184	0.244	0.210	0.387
W max	0.358	0.306	0.452	0.633
D max	0.414	***	0.372	***
SI av	-0.075	0.057	-0.089	0.586
thG av	-0.345	***	-0.273	-0.193
SW max	***	***	***	***
	L fls	*Q fls*	*A flsc*	*H flsc*

p-value

L	0.130	0.091	0.091	0.003
W max	0.056	0.232	0.014	0.001
D max	0.098	***	0.117	***
SI av	0.601	0.743	0.539	≤0.001
thG av	0.067	***	0.138	0.402
SW max	***	***	***	***
	L fls	*Q fls*	*A flsc*	*H flsc*

Spearman's rank correlation coefficient rs

L	0.107	0.666	0.137	0.636
W max	0.424	0.123	0.633	0.588
D max	0.736	***	0.737	***
SI av	-0.165	0.510	-0.127	0.602
thG av	-0.171	***	-0.106	-0.286
SW max	***	***	***	***
	L fls	*Q fls*	*A flsc*	*H flsc*

p-value

L	0.381	≤0.001	0.274	≤0.001
W max	0.022	0.639	≤0.001	0.002
D max	0.001	***	≤0.001	***
SI av	0.248	0.002	0.378	≤0.001
thG av	0.375	***	0.572	0.208
SW max	***	***	***	***
	L fls	*Q fls*	*A flsc*	*H flsc*

B. Continental shelf

Pearson's correlation coefficient r

L	0.223	0.382	-0.162
W max	0.071	0.362	-0.133
W av	0.189	0.496	0.692
D max	0.213	0.362	-0.208
D av	-0.346	***	-0.384
SI av	-0.042	0.387	0.249
thG av	-0.244	-0.348	-0.095
SW max	0.552	-0.152	-0.395
	W sh	*D sh*	*G sh*

p-value

L	0.002	≤0.001	0.082
W max	0.440	0.002	0.280
W av	0.128	0.009	≤0.001
D max	0.061	0.004	0.110
D av	0.012	***	0.157
SI av	0.620	0.001	0.035
thG av	0.012	0.002	0.404
SW max	≤0.001	0.439	0.038
	W sh	*D sh*	*G sh*

Spearman's rank correlation coefficient rs

L	0.238	0.537	-0.188
W max	0.164	0.270	-0.028
W av	0.398	0.555	0.592
D max	0.411	0.217	-0.239
D av	-0.227	***	-0.353
SI av	-0.252	0.437	0.150
thG av	-0.155	-0.334	0.005
SW max	0.457	-0.051	-0.408
	W sh	*D sh*	*G sh*

p-value

L	0.001	≤0.001	0.043
W max	0.076	0.025	0.823
W av	0.001	0.003	0.001
D max	≤0.001	0.096	0.066
D av	0.105	***	0.197
SI av	0.002	≤0.001	0.207
thG av	0.116	0.003	0.962
SW max	0.003	0.797	0.031
	W sh	*D sh*	*G sh*

C. Continental slope

Pearson's correlation coefficient r

L	0.439	0.207	-0.099
W max	0.407	0.145	-0.125
W av	***	***	***
D max	0.442	0.601	-0.023
D av	***	***	***
SI av	0.121	0.231	-0.316
thG av	-0.416	-0.002	0.493
SW max	-0.427	-0.150	0.758
	W sl	*D sl*	*G sl*

p-value

L	0.001	0.014	0.370
W max	0.008	0.179	0.340
W av	***	***	***
D max	0.003	≤0.001	0.868
D av	***	***	***
SI av	0.655	0.076	0.053
thG av	0.020	0.983	≤0.001
SW max	0.060	0.367	≤0.001
	W sl	*D sl*	*G sl*

Spearman's rank correlation coefficient rs

L	0.875	0.371	-0.246
W max	0.700	0.032	-0.141
W av	***	***	***
D max	0.637	0.462	0.112
D av	***	***	***
SI av	-0.234	0.208	-0.383
thG av	-0.504	0.062	0.461
SW max	-0.286	-0.628	0.744
	W sl	*D sl*	*G sl*

p-value

L	≤0.001	≤0.001	0.023
W max	≤0.001	0.772	0.284
W av	***	***	***
D max	≤0.001	≤0.001	0.417
D av	***	***	***
SI av	0.383	0.111	0.018
thG av	0.004	0.597	≤0.001
SW max	0.221	≤0.001	≤0.001
	W sl	*D sl*	*G sl*

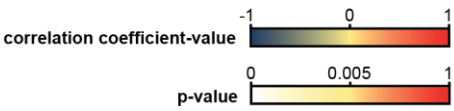

Figure 3.10a-c Heat maps for correlations of canyon morphometrics with parameters of the associated source-to-sink system displaying values of Pearson's correlation coefficient r and Spearman's rank correlation coefficient r_s, and their respective p-values. A. Terrestrial catchment. B. Continental shelf. C. Continental slope. *L* = canyon length; W_{max} = maximum canyon width; W_{av} = average canyon width; D_{max} = maximum canyon depth; D_{av} = average canyon depth; SI_{av} = average canyon sinuosity index; thG_{av} = average canyon thalweg gradient; SW_{max} = maximum canyon sidewall steepness; L_{fls} = fluvial system length; Q_{fls} = average annual fluvial discharge; A_{flsc} = size of the catchment; H_{flsc} = maximum elevation in the catchment area; W_{sh} = shelf width; D_{sh} = shelf-break depth; G_{sh} = average shelf gradient. 4. Slope configuration: W_{sl} = slope width; D_{sl} = slope-break depth; G_{sl} = average slope gradient. *** indicates scarcity of data (N<15).

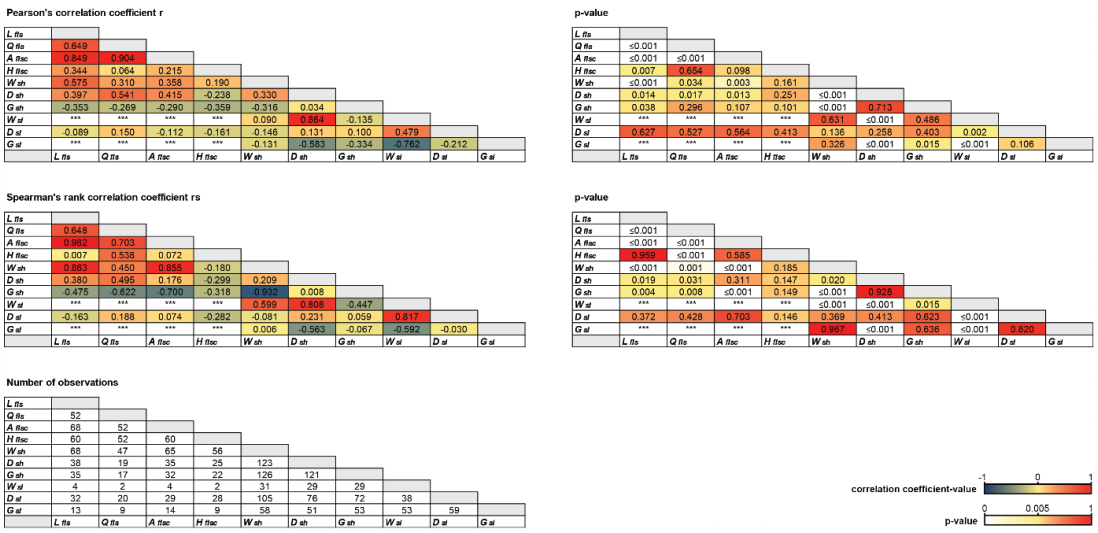

Figure 3.11 Heat maps for correlations of parameters of the source-to-sink system specific to studied submarine canyons displaying values of Pearson's correlation coefficient r and Spearman's rank correlation coefficient r_s, and their respective p-values. L_{fls} = fluvial system length; Q_{fls} = average annual fluvial discharge; A_{flsc} = size of the catchment; H_{flsc} = maximum elevation in the catchment area; W_{sh} = shelf width; D_{sh} = shelf-break depth; G_{sh} = average shelf gradient. 4. Slope configuration: W_{sl} = slope width; D_{sl} = slope-break depth; G_{sl} = average slope gradient. *** indicates scarcity of data (N<15).

3.6.1 Terrestrial catchment (L_{fls}, Q_{fls}, A_{flsc}, H_{flsc})

3.6.1.1 Observations

Fluvial system length displays moderate and statistically significant positive correlation with maximum canyon depth (Fig. 3.12i), and modest but not significant positive correlation with maximum canyon width (Fig. 3.12e).

Similarly, moderate significant positive correlations between catchment size and canyon maximum depth and width are seen (Figs. 3.12g&k).

Average annual fluvial discharge has moderate direct correlations with canyon length (Fig. 3.12b) and average canyon sinuosity (Fig. 3.12n); both relationships are statistically significant.

Moderate statistically significant positive correlations exist between maximum catchment elevation and canyon length (Fig. 3.12d), maximum width (Fig. 3.12h) and average sinuosity (Fig. 3.12p).

3.6.1.2 Interpretations

The observed relationships between canyon length, maximum canyon depth and average canyon sinuosity with attributes of the terrestrial catchment likely reflect how fluvial sediment discharge can promote intra-canyon erosion by down-canyon flows, e.g. the upslope lengthening of canyons at their apices (e.g. Piper and Normark, 2009), their deepening in the region of canyon mouths, and how the streamwise length of more sinuous canyons is inherently longer (see section 3.5.2.2).

The extent to which the morphology of a submarine canyon is affected by fluvial sediment discharge depends on its erosional versus depositional impact on individual canyon morphometrics, which is determined by many factors and their interplay. The bedrock lithology of terrestrial source areas has been invoked as a control on canyon formation in view of how it can influence the runout distance and erosive strength of submarine flows, e.g. by affecting sediment density, composition and transport mechanisms (Smith et al., 2017). In addition, characteristics of the seafloor substrate can impact its erodibility, which also has an effect on the magnitude of intra-canyon erosion by the flows; for example carbonate cementation can

decrease erodibility and stabilise the substrate and canyon walls (e.g. Oiwane et al., 2011), thereby reducing the potential of mass failure on slopes (e.g. Chang et al., 2021) and within canyons. With increasing distance between the river mouth and the submarine canyon head, the sediment transport efficiency decreases as a function of distance and grain size. A global study on sediment delivery to submarine canyons from fluvial systems (Sweet & Blum, 2016) indicates that canyons tend to intercept gravel-sized sediment when their head is within ca. 500 m of a fluvial source, sand-sized sediment when it is within 1 to 5 km via shoreface and delta processes, and silt and clay-sized sediment when it is within ca. 40 km. The segregation of grain sizes in shelf-crossing submarine flows can impact canyon evolution; findings from studies of the Monterey Canyon suggest that the presence of unconsolidated sands within a canyon might be a prerequisite for intra-canyon turbidity current generation (Paull et al., 2018), whereas surficial mud deposits on the canyon floor might promote self-acceleration of these flows (Hereema et al., 2020).

The variability of these factors across S2S systems can explain the weakness with which canyon morphometric parameters are scaled with attributes of the terrestrial catchments. Weakness in correlation may also be due to other controls overprinting the effect of fluvial discharge on canyon geomorphology; these controls may include, for example, intra-canyon sedimentary processes (see section 3.4.2.1), hydrodynamic processes (section 3.4.2.2), structural controls (3.4.2.3) and biogenic processes (3.4.2.4), as well as sediment remobilisation within the shelf and slope.

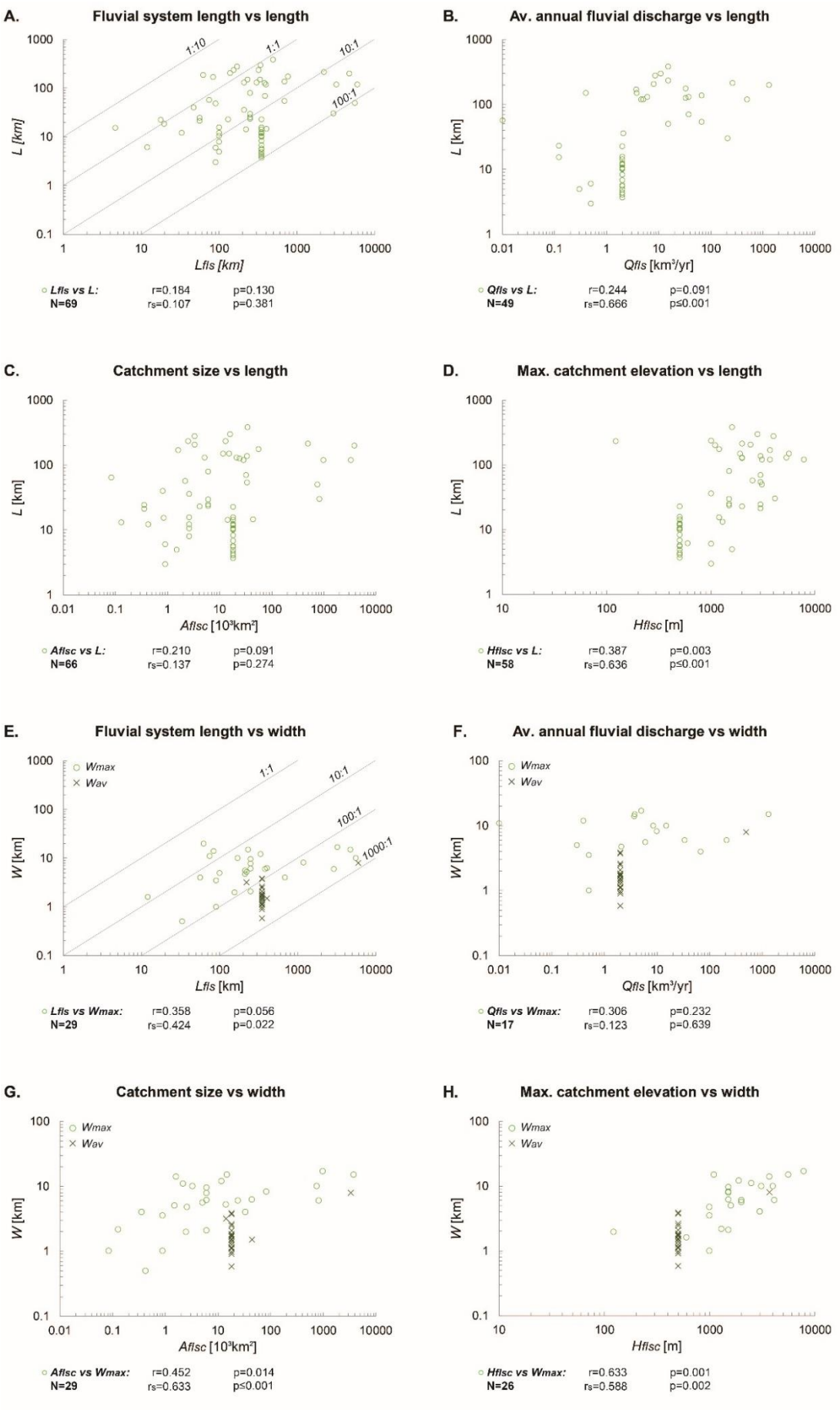
A.
Fluvial system length vs length
1:10
1:1
10:1
100:1
L [km]
Lfls [km]
○ Lfls vs L: r=0.184 p=0.130
N=69 rs=0.107 p=0.381
B.
Av. annual fluvial discharge vs length
L [km]
Qfls [km³/yr]
○ Qfls vs L: r=0.244 p=0.091
N=49 rs=0.666 p≤0.001
C.
Catchment size vs length
L [km]
Aflsc [10³km²]
○ Aflsc vs L: r=0.210 p=0.091
N=66 rs=0.137 p=0.274
D.
Max. catchment elevation vs length
L [km]
Hflsc [m]
○ Hflsc vs L: r=0.387 p=0.003
N=58 rs=0.636 p≤0.001
E.
Fluvial system length vs width
○ Wmax
× Wav
1:1
10:1
100:1
1000:1
W [km]
Lfls [km]
○ Lfls vs Wmax: r=0.358 p=0.056
N=29 rs=0.424 p=0.022
F.
Av. annual fluvial discharge vs width
○ Wmax
× Wav
W [km]
Qfls [km³/yr]
○ Qfls vs Wmax: r=0.306 p=0.232
N=17 rs=0.123 p=0.639
G.
Catchment size vs width
○ Wmax
× Wav
W [km]
Aflsc [10³km²]
○ Aflsc vs Wmax: r=0.452 p=0.014
N=29 rs=0.633 p≤0.001
H.
Max. catchment elevation vs width
○ Wmax
× Wav
W [km]
Hflsc [m]
○ Hflsc vs Wmax: r=0.633 p=0.001
N=26 rs=0.588 p=0.002

I. Fluvial system length vs depth

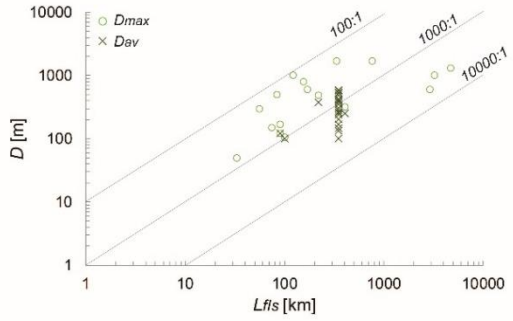

○ **Lfls vs Dmax:**	r=0.414	p=0.098	
N=17	rs=0.736	p=0.001	

J. Av. annual fluvial discharge vs depth

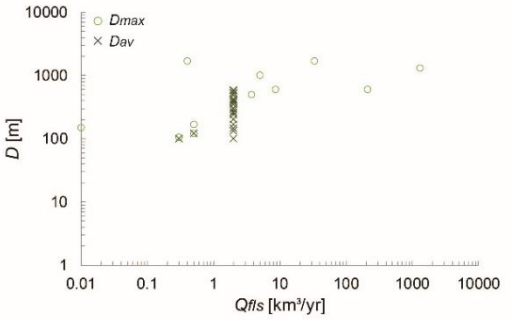

○ **Qfls vs Dmax:**	r=0.316	p=0.343
N=11	rs=0.586	p=0.058

K. Catchment size vs depth

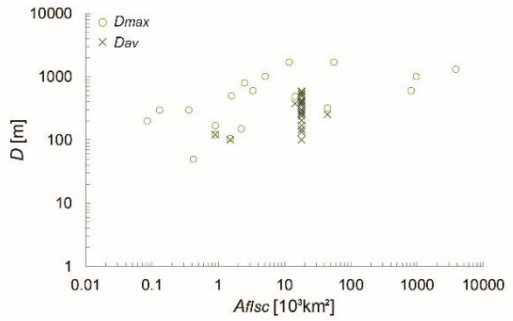

○ **Aflsc vs Dmax:**	r=0.372	p=0.117
N=19	rs=0.737	p≤0.001

L. Max. catchment elevation vs depth

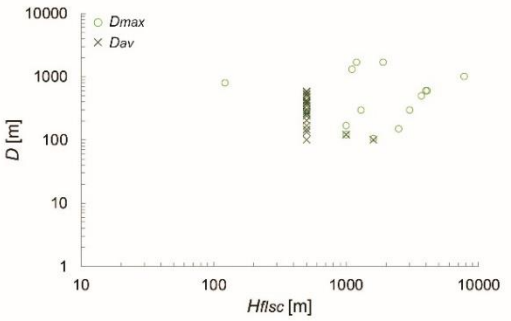

○ **Hflsc vs Dmax:**	r=0.036	p=0.902
N=14	rs=0.126	p=0.669

M. Fluvial system length vs average sinuosity

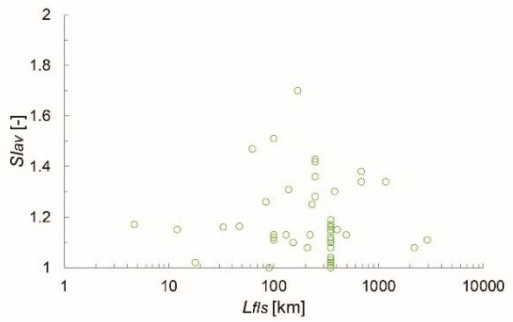

○ **Lfls vs Slav:**	r=-0.075	p=0.601
N=51	rs=-0.165	p=0.248

N. Av. annual fluvial discharge vs average sinuosity

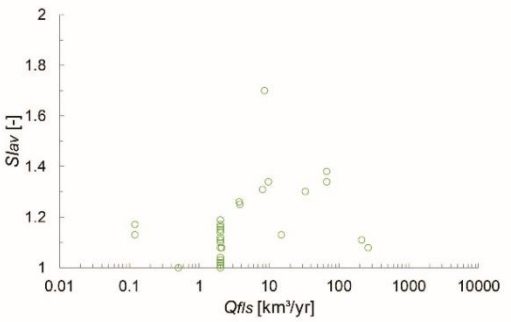

○ **Qfls vs Slav:**	r=0.057	p=0.743
N=35	rs=0.510	p=0.002

O. Catchment size vs average sinuosity

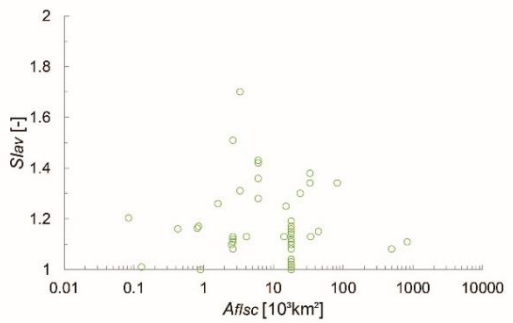

○ **Aflsc vs Slav:**	r=-0.089	p=0.539
N=50	rs=-0.127	p=0.378

P. Max. catchment elevation vs average sinuosity

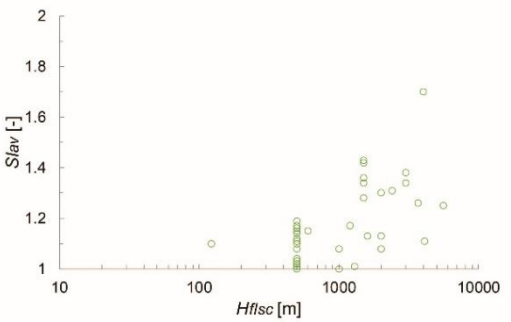

○ **Hflsc vs Slav:**	r=0.586	p≤0.001
N=26	rs=0.602	p≤0.001

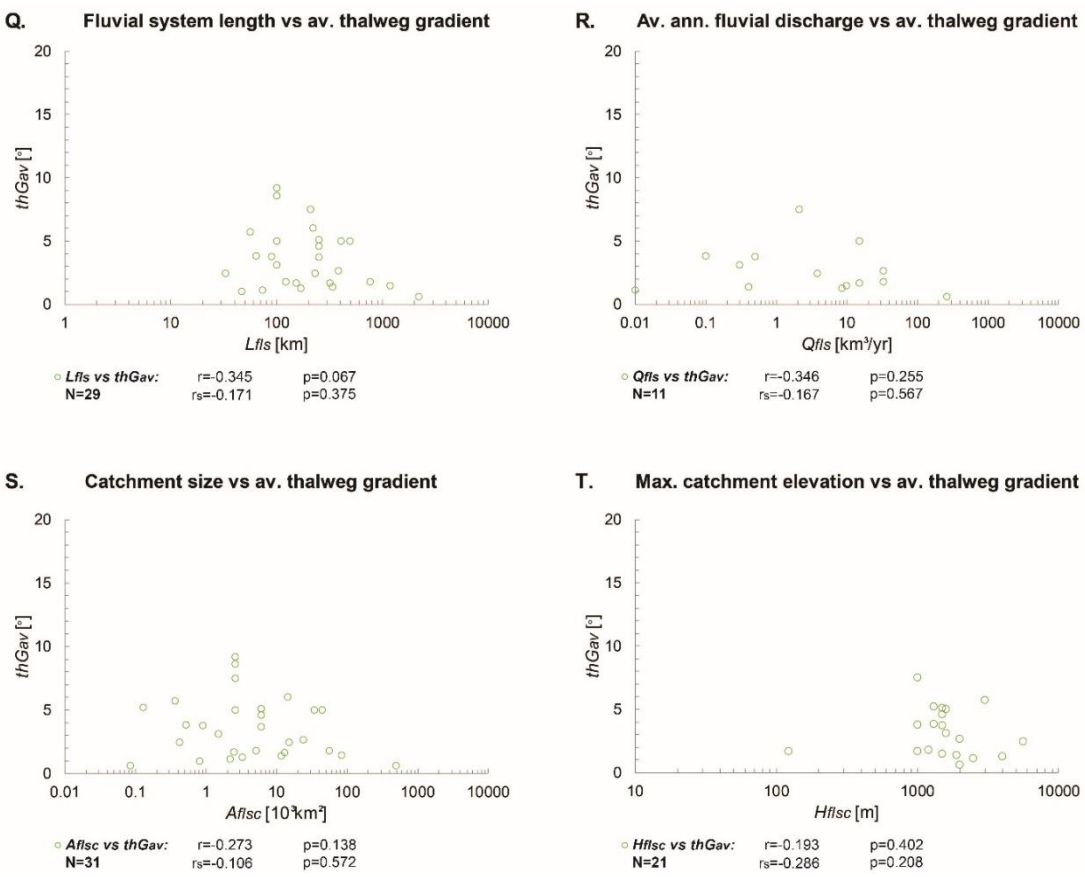

Figure 3.12a-t Scatterplots between attributes of terrestrial catchments and canyon morphometric parameters. N = number of correlations; r = Pearson's correlation coefficient; r_s = Spearman's rank correlation coefficient.

3.6.2 Continental shelf (W_{sh}, G_{sh}, D_{sh})

3.6.2.1 Observations

The shelf width is moderately directly correlated with the maximum canyon sidewall steepness (Fig. 3.13p), and only modestly with average canyon width (Fig. 3.13d) and maximum canyon depth (Fig. 3.13g). The shelf width is directly correlated with the canyon length (Fig. 3.13a) and inversely with the average canyon sinuosity (Fig. 3.13j), but these relationships are weak.

The shelf-break depth correlates significantly with all investigated canyon morphometric parameters except for the maximum canyon sidewall steepness (Fig. 3.13q), exhibiting moderate positive correlation with the canyon length (Fig. 3.13b) and modest correlation with the average canyon sinuosity (Fig. 3.13k); correlations with maximum width (Fig. 3.13e) and

depth (Fig. 3.13h) are weaker. In contrast, the average canyon thalweg gradient shows weak but significant inverse scaling with the shelf-break depth (Fig. 3.13n). Moderate scaling exists between the shelf-break depth and the average canyon width, but the data stem from two geographic regions only: offshore NE Australia and NE Brazil, both associated with shallow (70-85 m) shelves (Fig. 3.13e).

Correlations of canyon morphometric parameters with the average shelf gradient are mostly weak and not significant (Fig. 3.13a-r). Moderate and significant correlation is observed between shelf gradient and average canyon width (Fig. 3.13f), but these results are based on data from two geographic regions only. Modest inverse correlation is seen between shelf gradient and maximum canyon sidewall steepness, which is not statistically significant (Fig. 3.13r).

Submarine canyons with present-day shelf break deeper than 120 m bsl are on average longer and have greater maximum widths and depths, higher average canyon sinuosities and steeper average canyon thalweg gradients than canyons with a shelf-break lower than 120 m bsl. The same trends are seen for groups of canyons distinguished based on a threshold of shelf-break depth of 130 m (Fig. 3.14a-f). Although a greater range in maximum canyon sidewall steepness is seen in canyons associated with shelf breaks deeper than 120 m, average values between both canyon groups are very similar. Data on maximum canyon depth and maximum canyon sidewall steepness that can be employed in this analysis are limited, whereas data on average width and depth are only available for canyons installed on slopes with shelf breaks shallower than 120 m.

3.6.2.2 Interpretations

The width of the shelf plays a role in across-shelf sediment distribution from fluvial outlets to the shelf edge (e.g. Sweet et al., 2020). Narrower shelves are characterised by shorter distances to fluvial outlets that can deliver sediment to canyon heads, and may allow sediment connection of canyons with rivers and littoral cells to be maintained during sea-level highstands (e.g. Covault et al., 2007; Normark et al., 2009; Jipa and Panin, 2020).

Steeper shelf gradients might also inhibit deposition by hyperpycnal flows and promote bedload transport of coarse sediment from rivers across shelves (e.g. Jipa and Panin, 2020).

By contrast, the effect of hydroisostasy on continental levering and the ensuing steepening of continental shelves is thought to be stronger for wider shelves, probably by a factor ≤0.3 since the Last Glacial Maximum (LGM), relative to narrower shelves (Hutton et al., 2013). Nevertheless, despite being more prone to hydroisostatic flexure, wider shelves tend to have gentler gradients than narrower shelves.

Wider shelves also tend to have resulted from greater shelf-edge progradation, which can occur in response to greater rates of sediment supply to the outer shelf and upper slope from terrestrial catchments and from shelf-internal sources (e.g. Mougenot et al., 1983; Carvajal et al., 2009; Blum et al., 2013), as well as from the up-building of slope sediment prisms from drifts (e.g. Fulthorpe and Carter, 1991). However, although a wider shelf indicates a more sustained sediment supply to a shelf margin, sediment transport across wide shelves into submarine canyons is most effective for canyons that have significantly retrograded the shelf and/or are connected with a river, either directly or via shelf channels or shelf-edge deltas. With increasing shelf width, the effectiveness of across-shelf sediment transport from fluvial outlets decreases for coarser grained sediment, leading to variations in grain-size distribution of sediment discharged from rivers across the shelf. Hence, the importance of erosion by submarine flows linked to rivers on canyon morphology becomes likely less significant on shelves wider than 5 km, given the expected paucity of sand grain-size fractions reaching beyond this boundary (section 3.6.1). In addition, the frequency and magnitude of hyperpycnal flows can be affected by factors other than the shelf width, such as salinity of the water body, climate and relative sea-level change (e.g. Mulder et al., 2003; Dadson et al., 2005).

The effectiveness of across-shelf sediment transport is also affected by hydrodynamic processes associated with tidal currents, along-shelf currents and waves (Nittrouer and Wright, 1994; Wang et al., 2010). The ability of

waves to remobilise sediment is greater at shallower depths (Peters and Loss, 2012); this sediment transport mechanism might have a greater areal effect on wide and shallow shelves with lower gradients.

Moreover, the shelf topography can variably affect across-shelf sediment dispersal into submarine canyons: shelf uplift and deformation by tectonic activity (e.g. Johnson et al., 2017) and the presence of reefs (see section 3.4.2.3) can create seafloor topography and modify shelf gradients, which in turn can force sediment transport pathways through shelf valleys and submarine canyons incising the shelf. Currents, waves and flows carrying sediment might also be deflected away from canyons by intra-shelf highs of variable origin.

The subaerial exposure of continental shelves at lowstand can lead to the amalgamation of river catchment areas as confluences are established; this might significantly enhance sediment supply to individual fluvial outlets, and in turn to canyons with sediment connectivity to these systems, especially for large fluvial systems that can arise as wide shelves are exposed (Blum et al., 2013). Additional sediment might be conveyed to canyons from the local erosion of shelf substrate when rivers traverse the exposed shelf (e.g. Sweet et al., 2020).

Some of the scaling relationships between shelf configuration and canyon morphometrics may also be due to covariance with other related parameters. For example, scaling of canyon length with shelf-break depth might in part reflect how deeper shelves are associated with wider slopes, and how shelf-break depths tend to increase for terrestrial catchments associated with larger fluvial systems or multiple fluvial sources, greater average annual discharge and catchment size. However, scaling relationships between shelf-break depth and attributes of the terrestrial catchment are not significant.

During episodes of sea-level lowstand, such as during the LGM, canyons with their heads in vicinity of the shelf-edge could be fed by fluvial systems that had prograded onto the shelves (e.g. Sweet et al., 2020).

In sequence stratigraphic models, routeing of significant volumes of sand-sized sediment across continental slopes to basin floors and the development of submarine fans is perceived to be most effective during relative sea-level lowstands (e.g. Posamentier et al., 1991), which would suggest that canyon evolution by down-canyon sediment gravity flows might also be enhanced during these intervals. Reconstructions and estimates for the eustatic fall during the LGM have been variably placed between ca. 120 m to 135 m bsl (e.g. Clark and Mix, 2002; Simms et al., 2019, and references therein), so that most shelves with shelf breaks shallower than 120 m bsl have likely been subaerially exposed during the LGM. Despite this, the studied canyons hosted on shelves with shelf breaks deeper than 120 m bsl tend to be larger, to be more sinuous, and to have steeper canyon thalweg gradients than those with shelf breaks at 120 m or less. This indicates that sediment connection of canyons to rivers and littoral cells during phases of sea-level lowstands is not as important a control on canyon geomorphology compared to other controls. The findings might also indicate how deeper shelves tend to be associated with larger terrestrial catchments (Fig. 15; Wang et al., 2019).

The complex role of shelf physiography and across-shelf sediment transport, together with covariance in shelf and canyon characteristics in response to common controls on sediment dispersal, explain the limited value of shelf configuration as a predictor of canyon geomorphology.

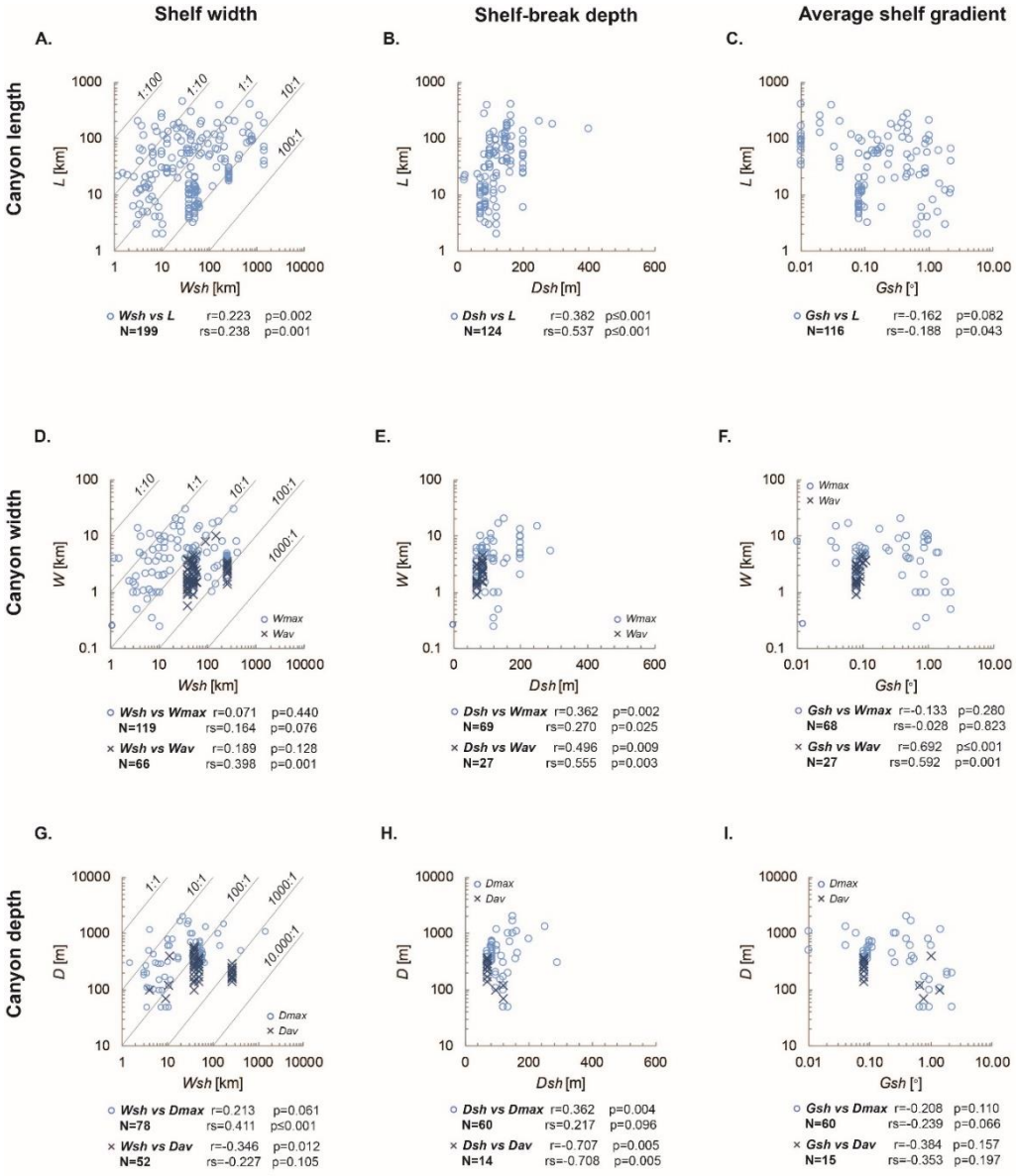
Shelf width
Shelf-break depth
Average shelf gradient
Canyon length
Canyon width
Canyon depth
A.
B.
C.
D.
E.
F.
G.
H.
I.
L [km]
W [km]
D [m]
Wsh [km]
Dsh [m]
Gsh [°]
1:100
1:10
1:1
10:1
100:1
1000:1
10,000:1
Wmax
Wav
Dmax
Dav
Wsh vs L r=0.223 p=0.002
N=199 rs=0.238 p=0.001
Dsh vs L r=0.382 p≤0.001
N=124 rs=0.537 p≤0.001
Gsh vs L r=-0.162 p=0.082
N=116 rs=-0.188 p=0.043
Wsh vs Wmax r=0.071 p=0.440
N=119 rs=0.164 p=0.076
Wsh vs Wav r=0.189 p=0.128
N=66 rs=0.398 p=0.001
Dsh vs Wmax r=0.362 p=0.002
N=69 rs=0.270 p=0.025
Dsh vs Wav r=0.496 p=0.009
N=27 rs=0.555 p=0.003
Gsh vs Wmax r=-0.133 p=0.280
N=68 rs=-0.028 p=0.823
Gsh vs Wav r=0.692 p≤0.001
N=27 rs=0.592 p=0.001
Wsh vs Dmax r=0.213 p=0.061
N=78 rs=0.411 p≤0.001
Wsh vs Dav r=-0.346 p=0.012
N=52 rs=-0.227 p=0.105
Dsh vs Dmax r=0.362 p=0.004
N=60 rs=0.217 p=0.096
Dsh vs Dav r=-0.707 p=0.005
N=14 rs=-0.708 p=0.005
Gsh vs Dmax r=-0.208 p=0.110
N=60 rs=-0.239 p=0.066
Gsh vs Dav r=-0.384 p=0.157
N=15 rs=-0.353 p=0.197

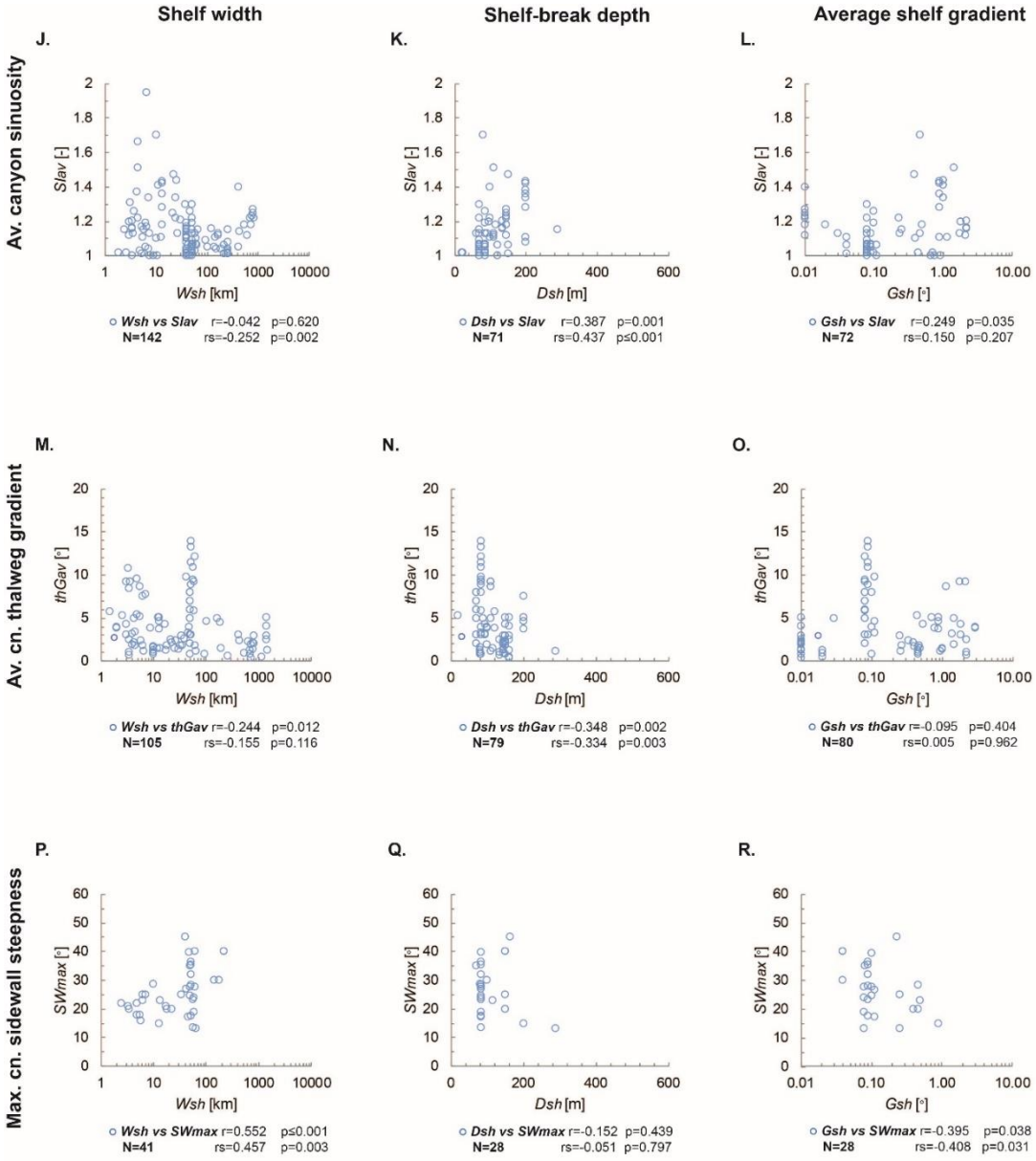

Figure 3.13a-r Scatterplots between attributes of the continental shelf and canyon morphometric parameters. N = number of correlations; r = Pearson's correlation coefficient; r_s = Spearman's rank correlation coefficient.

A. Length

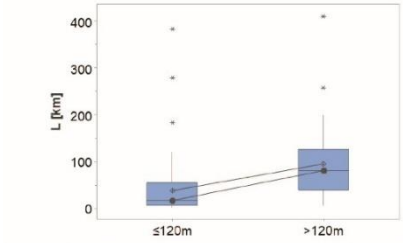

	N	min	mean	StDev	median	max
≤120	**78**	2.00	38.14	58.60	17.02	384.05
>120	**46**	6.00	95.50	74.00	81.30	411.00
T-Value =-7.48 DF = 119 P-Value ≤ 0.001						
≤130	**78**	2.00	37.45	57.15	17.02	384.05
>130	**46**	6.00	96.60	75.00	81.30	411.00
T-Value =-7.55 DF = 119 P-Value ≤ 0.001						

B. Maximum width

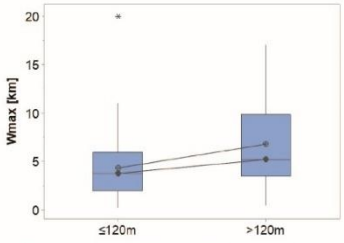

	N	min	mean	StDev	median	max
≤120	**53**	0.25	4.33	3.37	3.78	20.00
>120	**16**	0.50	6.79	4.91	5.20	17.00
T-Value =-1.56 DF = 22 P-Value = 0.134						
≤130	**52**	0.25	4.03	2.58	3.78	11.00
>130	**17**	0.50	7.56	5.73	5.40	20.00
T-Value =-2.46 DF = 18 P-Value = 0.024						

C. Maximum depth

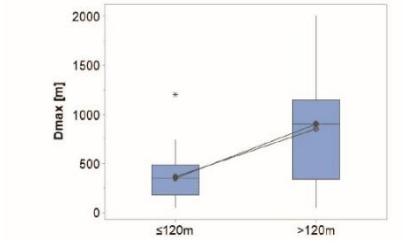

	N	min	mean	StDev	median	max
≤120	**46**	50.00	364.50	225.50	350.00	1200.00
>120	**14**	50.00	854.00	567.00	900.00	2000.00
T-Value =-3.15 DF = 14 P-Value = 0.007						
≤130	**46**	50.00	364.50	225.50	350.00	1200.00
>130	**14**	50.00	854.00	567.00	900.00	2000.00
T-Value =-3.15 DF = 14 P-Value = 0.007						

D. Average canyon sinuosity

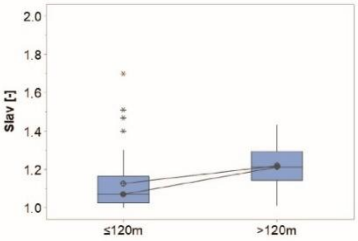

	N	min	mean	StDev	median	max
≤120	**49**	1.00	1.1265	0.14	1.07	1.70
>120	**22**	1.01	1.22	0.12	1.21	1.43
T-Value =-3.15 DF = 48 P-Value = 0.003						
≤130	**48**	1.00	1.12	0.14	1.07	1.70
>130	**23**	1.01	1.23	0.12	1.22	1.47
T-Value =-3.66 DF = 46 P-Value = 0.001						

E. Average canyon thalweg gradient

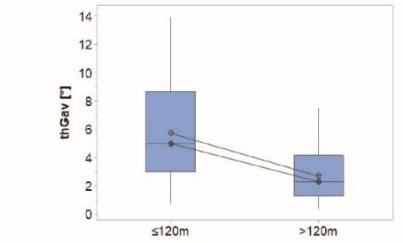

	N	min	mean	StDev	median	max
≤120	**46**	0.78	5.72	3.53	5.00	13.90
>120	**33**	0.40	2.69	1.72	2.30	7.50
T-Value = 5.04 DF = 69 P-Value ≤ 0.001						
≤130	**46**	0.78	5.72	3.53	5.00	13.90
>130	**33**	0.40	2.69	1.72	2.30	7.50
T-Value = 5.04 DF = 69 P-Value ≤ 0.001						

F. Maximum canyon sidewall steepness

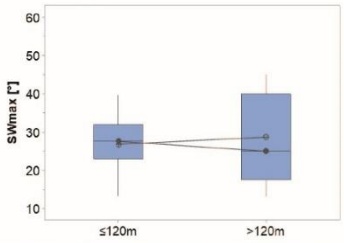

	N	min	mean	StDev	median	max
≤120	**19**	13.40	26.82	7.05	27.60	39.60
>120	**9**	13.30	28.70	12.40	35.00	45.00
T-Value =-0.42 DF = 10 P-Value = 0.681						
≤130	**19**	13.40	26.82	7.05	27.60	39.60
>130	**9**	13.30	28.70	12.40	35.00	45.00
T-Value =-0.42 DF = 10 P-Value = 0.681						

Figure 3.14a-f Boxplots of frequency distributions of canyon morphometric parameters for studied submarine canyons distinguished based on shelf-break depth thresholds of 120 m at the canyon. Tabulated statistics refer to canyons grouped based on shelf-break thresholds of 120 m and 130 mbsl, respectively. N = number of readings; min = minimum value; mean = mean value; StDev = standard deviation; median = median value; max = maximum value.

3.6.3 Continental slope (W_{sl}, G_{sl}, D_{sl})

3.6.3.1 Observations

The slope width exhibits strong and significant correlation with canyon length (Fig. 3.15a), and moderate significant correlations with maximum width (Fig. 3.15d), maximum depth (Fig. 3.15g) and the average canyon thalweg gradient (Fig. 3.15m).

The slope-break depth shows moderate scaling with maximum canyon depth (Fig. 3.15h) and maximum canyon sidewall steepness (Fig. 3.15q), and rather weak but statistically significant correlation with canyon length (Fig. 3.15b).

For the average slope gradient, moderate correlations are demonstrated with maximum canyon sidewall steepness (Fig. 3.15r) and average canyon thalweg gradient (Fig. 3.15o), whereas correlations with other parameters are weak and not significant (Fig. 3.15a-r).

3.6.3.2 Interpretations

The canyon length is the only canyon morphometric parameter that is related to the continental-slope width, as reflected in the strong scaling between these two variables and, to smaller extent, in the relationship between canyon length and slope-break depth.

Positive relationships are seen for slope width with maximum canyon width and depth, and for the latter with slope-break depth; these relationships reflect how intra-canyon erosion is promoted at the canyon mouth (see section 3.5.2.2).

The positive relationship between slope-break depth and maximum canyon depth might also reflect how canyons in open seas tend to be deeper compared to canyons in semi-enclosed and enclosed seas (see section 3.7.4).

The results show that average canyon sinuosity is not correlated to the slope-break depth or to slope steepness. Additional data are needed to evaluate potential correlation between slope width and average canyon sinuosity.

The modest, positive correlation between the overall slope gradient and average canyon thalweg gradient relates to how the average canyon thalweg gradient is constrained by the average gradient of the continental slope; yet important variability is observed. In this study, as in previous ones (e.g. Harris and Whiteway, 2011), the overall canyon thalweg gradient is determined in part by the position of both canyon apex and mouth, which are themselves related to local seafloor relief. The observed moderate negative relationship between slope width and average canyon thalweg gradient reflects how wider slopes tend to display gentler gradients (Fig. 3.11; cf. Sømme et al., 2009).

The moderate, positive scaling seen between maximum canyon sidewall steepness and the average slope gradient may reflect how slopes that are steeper on average may be associated with increased erosion in submarine canyons, in relation to steeper slopes promoting processes of mass failure (e.g. McGregor, 1983; Susanth et al., 2021), and potentially driving retrograde slope failure (Lo Iacono et al., 2014), as well as vertical canyon incision (e.g. Susanth et al., 2021). Following this line of interpretation, the negative correlation of slope width with maximum canyon sidewall steepness might be a record of the covariance between average slope gradient and slope width. An inverse moderate relationship is seen between slope-break depth and maximum canyon sidewall steepness, but the dataset does not include slope-break depths between 4,000 and 6,000 m bsl and dominantly includes canyons associated with continental-slope breaks that are 2,000 to 4,000 m bsl. More data are needed to confirm this relationship.

The lack of correlation between the average slope gradient and maximum canyon dimensions indicate that the average slope gradient has no significant influence on canyon size, in spite of how it might affect the magnitude of retrograde erosion and the erosive strength of down-canyon sediment gravity flows. Also, the average slope gradient does not capture local relief along the slope profiles, which can control sediment bypass (e.g. Soutter et al., 2021); further investigation of the role of slope relief and slope profile types as controls on canyon geomorphology is required.

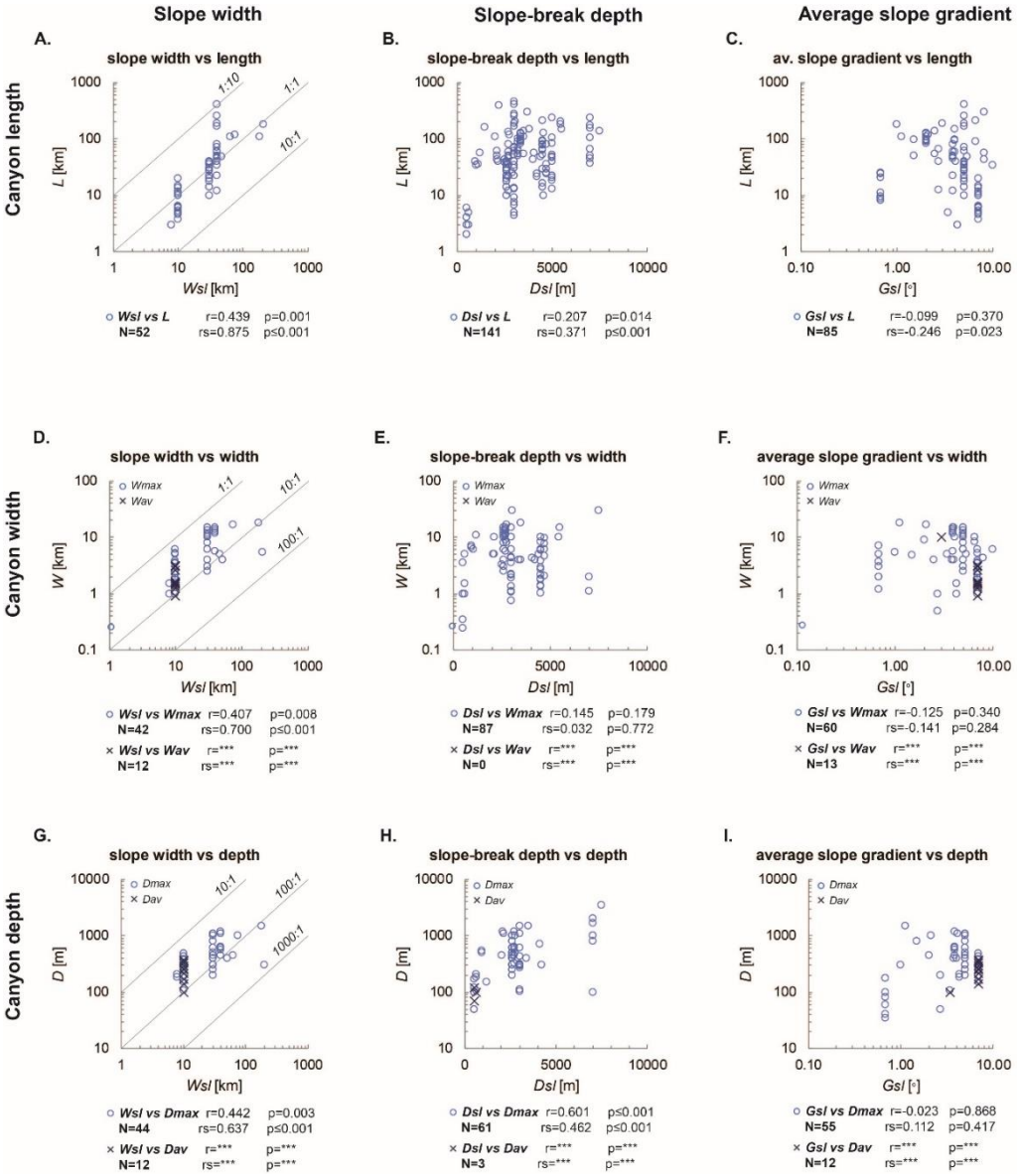
Slope width
Slope-break depth
Average slope gradient
Canyon length
Canyon width
Canyon depth
A.
slope width vs length
1:10
1:1
10:1
L [km]
Wsl [km]
Wsl vs L r=0.439 p=0.001
N=52 rs=0.875 p≤0.001
B.
slope-break depth vs length
Dsl [m]
Dsl vs L r=0.207 p=0.014
N=141 rs=0.371 p≤0.001
C.
av. slope gradient vs length
Gsl [°]
Gsl vs L r=-0.099 p=0.370
N=85 rs=-0.246 p=0.023
D.
slope width vs width
Wmax
Wav
1:1
10:1
100:1
W [km]
Wsl vs Wmax r=0.407 p=0.008
N=42 rs=0.700 p≤0.001
Wsl vs Wav r=*** p=***
N=12 rs=*** p=***
E.
slope-break depth vs width
Dsl vs Wmax r=0.145 p=0.179
N=87 rs=0.032 p=0.772
Dsl vs Wav r=*** p=***
N=0 rs=*** p=***
F.
average slope gradient vs width
Gsl vs Wmax r=-0.125 p=0.340
N=60 rs=-0.141 p=0.284
Gsl vs Wav r=*** p=***
N=13 rs=*** p=***
G.
slope width vs depth
Dmax
Dav
10:1
100:1
1000:1
D [m]
Wsl vs Dmax r=0.442 p=0.003
N=44 rs=0.637 p≤0.001
Wsl vs Dav r=*** p=***
N=12 rs=*** p=***
H.
slope-break depth vs depth
Dsl vs Dmax r=0.601 p≤0.001
N=61 rs=0.462 p≤0.001
Dsl vs Dav r=*** p=***
N=3 rs=*** p=***
I.
average slope gradient vs depth
Gsl vs Dmax r=-0.023 p=0.868
N=55 rs=0.112 p=0.417
Gsl vs Dav r=*** p=***
N=12 rs=*** p=***

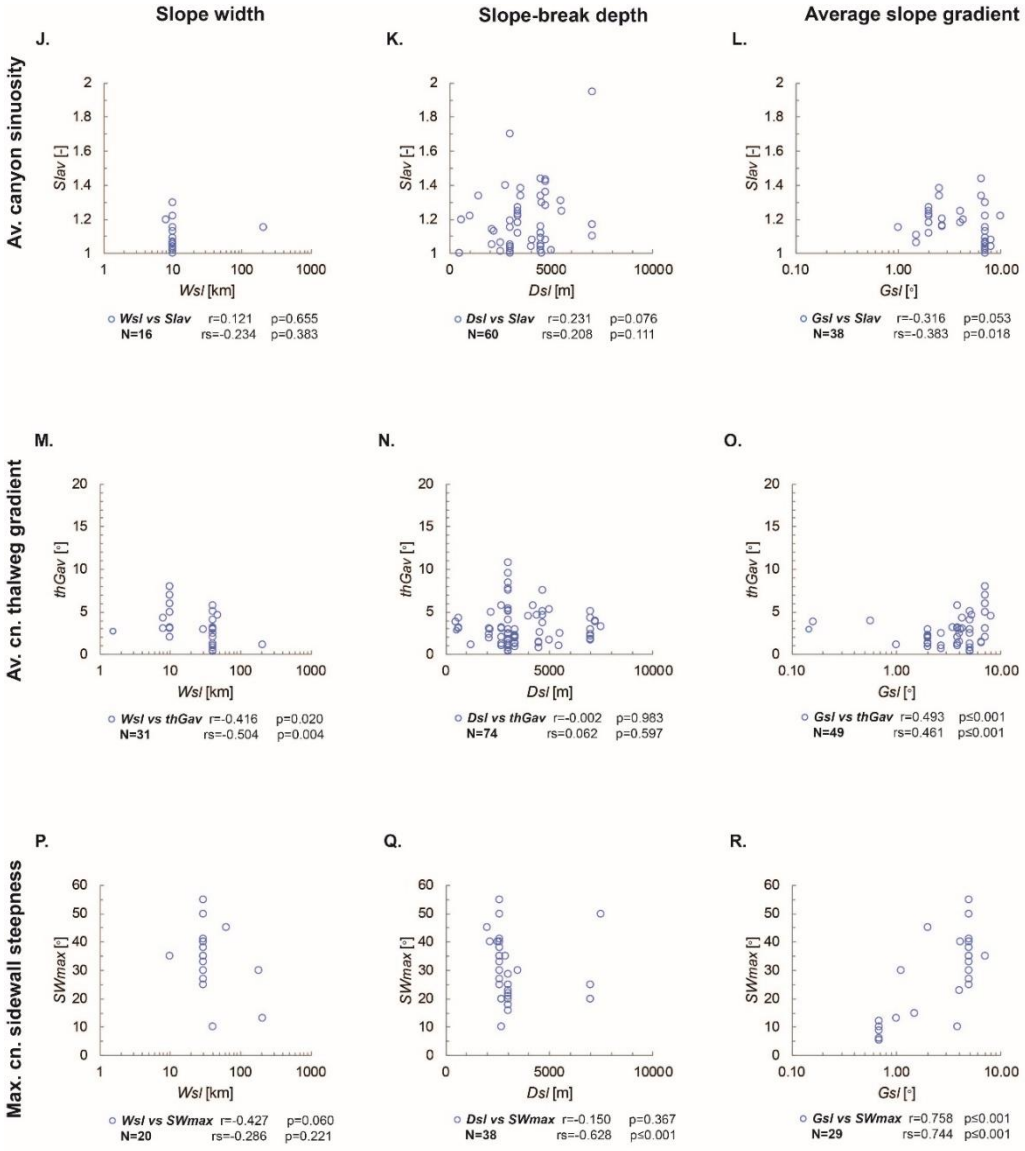

Figure 3.15a-r Scatterplots between attributes of the continental slope and canyon morphometric parameters. N = number of correlations; r = Pearson's correlation coefficient; r_S = Spearman's rank correlation coefficient.

3.7 Variations in canyon morphometric parameters across classes of environments

Descriptive statistics of frequency distributions of canyon morphometric parameters have been evaluated for the entire dataset (Fig. 3.16a-f), as well as for separate groups of canyons reflecting categories of canyon-apex location relative to the shelf-break, continental-margin type, source-to-sink

setting, oceanographic environment, and latitudinal zones (sections 3.7.1 to 3.7.5). This was done to investigate whether and how factors associated with the environmental setting may control canyon geomorphology. Meaningful comparisons of average canyon width and depth as a function of S2S system setting and latitudinal zone, and for average canyon depth relative to canyon-head location, were not possible due to limited data availability.

In addition, ratios of maximum width to maximum depth across the different environmental settings have been assessed (section 3.7.6).

The distributions of each canyon morphometric parameter are graphically presented in form of boxplots and are discussed in sections 3.7.1 to 3.7.6 below.

A. Length

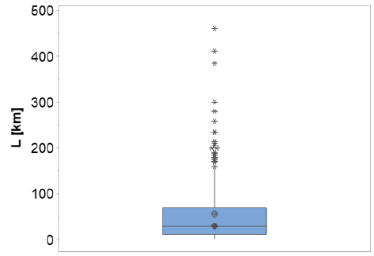

	N	min	mean	StDev	median	max
L	**263**	2.00	56.52	69.15	29.79	460.00

B. Width

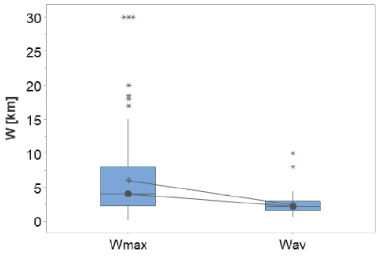

	N	min	mean	StDev	median	max
Wmax	**164**	0.15	5.97	5.43	4.00	30.00
Wav	**66**	0.58	2.41	1.50	2.18	10.00

C. Depth

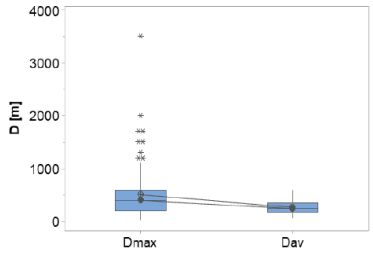

	N	min	mean	StDev	median	max
Dmax	**113**	35.00	508.00	475.10	400.00	3500.00
Dav	**52**	70.00	268.10	126.30	244.00	594.00

D. Average canyon sinuosity

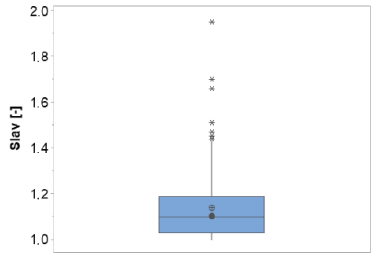

	N	min	mean	StDev	median	max
Slav	**151**	1.00	1.14	0.15	1.1	1.95

E. Average canyon thalweg gradient

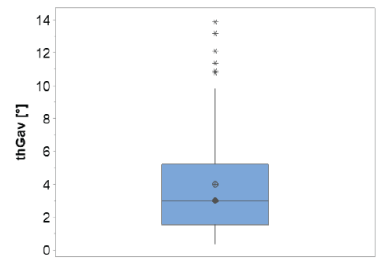

	N	min	mean	StDev	median	max
thGav	**120**	0.40	3.98	3.09	3.00	13.90

F. Maximum canyon sidewall steepness

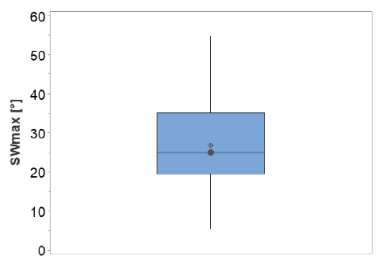

	N	min	mean	StDev	median	max
SWmax	**69**	5.40	26.80	11.48	25.00	55.00

Figure 3.16a-f Boxplots of frequency distributions of the investigated canyon morphometric parameters. *L* = canyon length; W_{max} = maximum canyon width; W_{av} = average canyon width; D_{max} = maximum canyon depth; D_{av} = average canyon depth; SI_{av} = average canyon sinuosity index; thG_{av} = average canyon thalweg gradient; SW_{max} = maximum canyon sidewall steepness; N = number of readings; min = minimum value; mean = mean value; StDev = standard deviation; median = median value; max = maximum value.

3.7.1 Canyon-apex location relative to the shelf break

3.7.1.1 Observations

The studied shelf-incising canyons tend to be longer (Fig. 3.17a), more sinuous (Fig. 3.17f), and with larger average widths (Fig. 3.17c) than slope-confined canyons, on average by factors of 2.25, 1.09 and 1.52, respectively. Across these two groups, these are the morphometric parameters whose mean values differ significantly; differences are also seen in maximum canyon depth that are just above the defined threshold of statistical significance. Although canyons incising the shelf display on average slightly greater maximum and overall widths, slope-confined canyons reach the same values (Figs. 3.17b&c), and the largest value of average width is associated with a slope-confined canyon (Fig. 3.17c). Although greater maximum depths (Fig. 3.17d), and lower overall thalweg gradients (Fig. 3.17g) are seen in canyons incising the shelf, differences in their average values are not statistically significant. The data on average canyon depth are limited, but the results show very similar ranges in values across the two groups (Fig. 17e). On average, the maximum sidewall steepness is similar between groups of canyons classified on the location of the canyon apex relative to the shelf break, but slope-confined canyons display a greater range (Fig. 17h).

For the canyons studied by Harris et al. (2014b), statistical tests reveal significant differences in mean values of length (Fig. 17i) and average depth (Fig. 17j) across the two groups. As in the canyons considered in this study, shelf-incising canyons are on average longer than their slope-confined counterparts, by a factor of 1.47, which is lower than what found in this study (2.25). Harris and Whiteway (2011) also reported mean values of canyon

length; studied shelf-incising canyons with and without a river connection were on average 2.07 and 1.29 times longer, respectively, than canyons with their apex below the shelf break.

3.7.1.2 Interpretations

The greater lengths of shelf-incising canyons may reflect how retrograde incision of the shelf and the promotion of canyon progradation by sediment gravity flows originating on the shelf and in the terrestrial catchment constitute primary controls on the length of submarine canyons. Sediment is supplied to the canyons via coupling with fluvial outlets or littoral cells and locally from within the shelf (sections 3.6.1 & 3.6.2). In addition, canyon heads placed above the storm wave-base can intercept sediment mobilised and transported during storm events (e.g. Sequeiros et al., 2019) (section 3.4.2.2). The finding that shelf-incising canyons are on average longer than their slope-confined counterparts are in agreement with observations by Harris and Whiteway (2011) and Harris et al. (2014b).

Harris et al. (2014b) also show that shelf-incising canyons are on average twice as large in area compared to slope-confined canyons, whereas canyons of the latter group are on average almost twice as deep. However, for the canyons considered in this study, characteristics like the maximum width, maximum depth, average canyon thalweg gradient and maximum canyon sidewall steepness are not related to whether canyons are incised into the shelf. Thus, overall, the relative position of the canyon apex to the shelf break does not tie to these specific geomorphological characteristics. The results may however also reflect how some of the currently slope-confined canyons had a past connection to the shelf, now lost due to backfilling of their proximal parts (e.g. Pratson et al., 2007) and progradation of their heads (e.g., in relation to high sediment supply; cf. Mauffrey et al., 2015).

Slope-confined canyons can be fed by sands overpassing the shelf edge if their heads are in the range of the run-out distance of turbidity currents linked to fluvial discharge or littoral cells (e.g. Cronin et al., 2005; Yin et al., 2019). Canyons in high-latitude settings affected by glaciation can receive

sediment delivered by the progradation of ice sheets onto shelf margins and from floating ice carrying debris (e.g. Gales et al., 2021). Sediment remobilised within the slope can also be distributed to a slope-confined canyon by contour currents if the canyon is coupled with a contourite system (e.g. Wang et al., 2018; Warratz et al., 2019; Serra et al., 2020; Rodrigues et al., 2022 and references therein).

Despite the role of sediment gravity flows in canyon growth and sinuosity increase, mean values of average canyon sinuosity are very similar across the two groups. This indicates that the importance of connections of the canyon to the shelf as a control on its sinuosity might be limited, in contrast with current understanding. Specifically, the process of canyon shelf-breaching, by enabling linkages with shelf and terrestrial sediment sources, has been suggested to lead to distinctively higher sinuosities in shelf-incising canyons compared to slope-confined ones (e.g. Farre et al., 1983; Orange et al., 1994; Wiles et al., 2019). On this basis, the sinuosity of canyons has been utilised to deduct canyon head location relative to the shelf-break on a regional scale in absence of sufficient bathymetric data coverage of proximal parts of canyons (see Wiles et al., 2019). Based on the analyses in this chapter, it appears that the overall canyon sinuosity is not a suitable predictor of the position of the canyon apex relative to the shelf break.

More generally, considering the findings of this work in light of those of earlier studies (Harris and Whiteway, 2011; Harris et al., 2014b; Huang et al. 2014), it is concluded that whether a canyon is incised in the shelf is not a strong predictor of canyon geomorphology overall. Further investigation is necessary to determine the degree to which the volume of a canyon delimited by its 3D surface is related to the relative position of the canyon head on a global scale.

A. Length

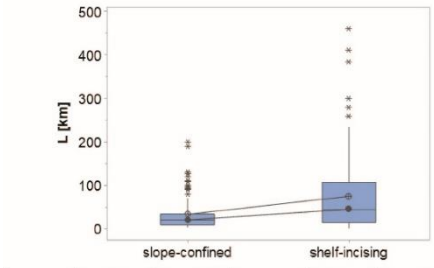

	N	min	mean	StDev	median	max
slope	**98**	3.70	33.37	39.32	21.00	200.00
shelf	**137**	2.00	75.13	84.69	45.00	460.00

T-Value =-4.53 DF = 230 P-Value ≤ 0.001

B. Maximum width

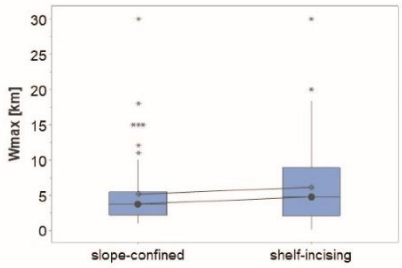

	N	min	mean	StDev	median	max
slope	**64**	1.00	5.12	4.96	3.74	30.00
shelf	**87**	0.15	6.14	5.32	4.79	30.00

T-Value =-0.44 DF = 148 P-Value = 0.658

C. Average width

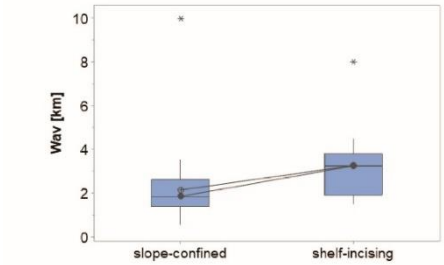

	N	min	mean	StDev	median	max
slope	**45**	0.58	2.15	1.41	1.85	10.00
shelf	**17**	1.51	3.26	1.58	3.25	8.00

T-Value =-3.42 DF = 31 P-Value = 0.002

D. Maximum depth

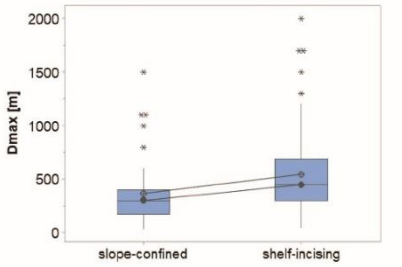

	N	min	mean	StDev	median	max
slope	**39**	35.00	367.30	322.10	300.00	1500.00
shelf	**65**	50.00	545.10	410.10	450.00	2000.00

T-Value =-2.45 DF = 80 P-Value = 0.016

E. Average depth

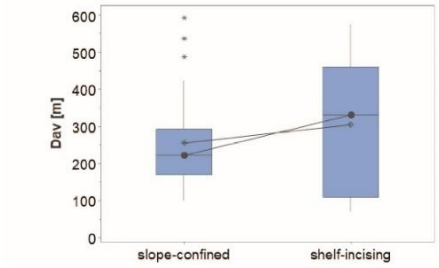

	N	min	mean	StDev	median	max
slope	**39**	100.00	255.30	115.70	222.00	594.00
shelf	**9**	70.00	304.90	183.40	331.00	576.00

T-Value =-0.17 DF = 9 P-Value = 0.868

F. Average canyon sinuosity

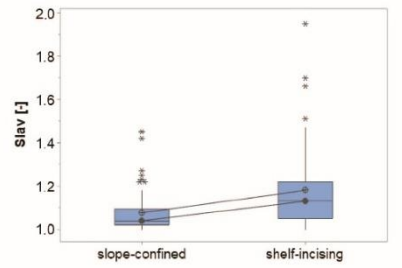

	N	min	mean	StDev	median	max
slope	**61**	1.00	1.08	0.09	1.04	1.45
shelf	**79**	1.00	1.18	0.17	1.13	1.95

T-Value =-4.70 DF = 131 P-Value ≤ 0.001

G. Average canyon thalweg gradient

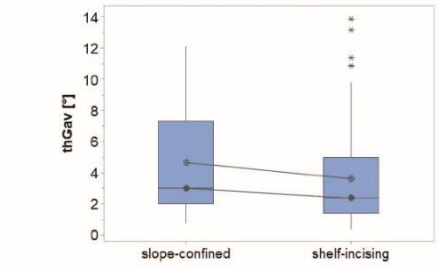

	N	min	mean	StDev	median	max
slope	**29**	0.78	4.65	3.29	3.00	12.10
shelf	**77**	0.40	3.62	3.14	2.37	13.90

T-Value = 1.73 DF = 51 P-Value = 0.090

H. Maximum canyon sidewall steepness

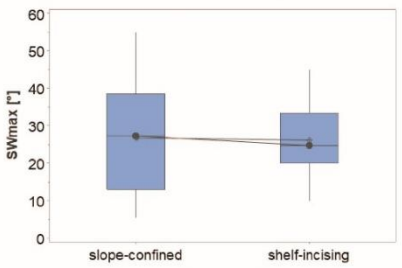

	N	min	mean	StDev	median	max
slope	**30**	5.40	26.82	13.92	27.30	55.00
shelf	**38**	10.00	26.18	8.68	24.80	45.00

T-Value = 0.22 DF = 46 P-Value = 0.825

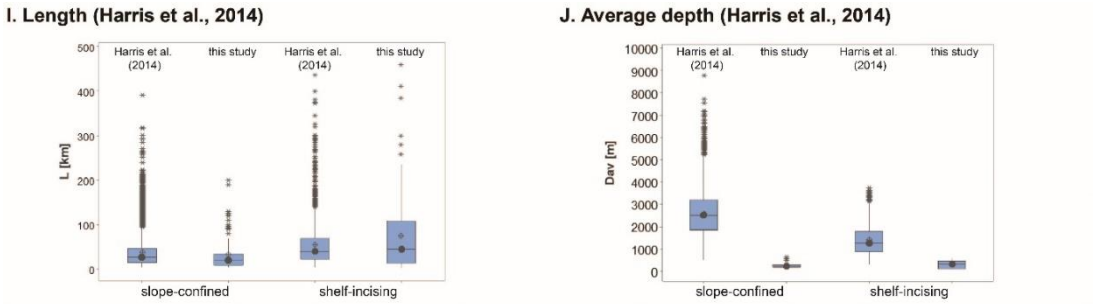

	N	min	mean	StDev	median	max
slope	**7401**	4.10	37.29	33.38	26.92	391.34
shelf	**2076**	3.84	54.82	50.27	39.76	436.33
T-Value =-18.16 DF = 3191 P-Value ≤ 0.001						

	N	min	mean	StDev	median	max
slope	**7401**	507.20	2563.50	978.40	2506.90	8770.30
shelf	**2076**	294.10	1395.00	657.60	1260.10	3746.00
T-Value =55.26 DF = 2972 P-Value ≤ 0.001						

Figure 3.17a-j A.-H. Boxplots of frequency distributions of canyon morphometric parameters for studied canyons classified on the location of the canyon apex relative to the shelf break into slope-confined (N=99) and shelf-incising canyons (N=154). I.&J. Boxplots of canyon length (I) and average depth (J) and results of statistical analyses plotted from the dataset of Harris et al. (2014b) for calibration. *L* = canyon length; W_{max} = maximum canyon width; W_{av} = average canyon width; D_{max} = maximum canyon depth; D_{av} = average canyon depth; SI_{av} = average canyon sinuosity index; thG_{av} = average canyon thalweg gradient; SW_{max} = maximum canyon sidewall steepness; N = number of readings; min = minimum value; mean = mean value; StDev = standard deviation; median = median value; max = maximum value. Results of Two-Sample T-test: DF = degrees of freedom.

3.7.2 Continental-margin type

3.7.2.1 Observations

Submarine canyons located along passive margins tend to be overall deeper (Fig. 3.18e), have steeper thalwegs (Fig. 3.18g) and greater maximum sidewall steepness (Fig. 3.18h), with statistically significant differences in mean values. Groups of canyons associated with active and passive margins exhibit frequency distributions of maximum canyon dimensions (Figs. 3.18a, b&d) and average canyon sinuosity (Fig. 3.18f) that are rather similar. Studied active-margin canyons are on average longer (Fig. 3.18a) and overall wider (Fig. 3.18c). Average values for maximum canyon width (Fig. 3.18b) and depth (Fig. 3.18d) are almost identical across continental-margin types, but canyons from active margins display greater ranges in both morphometric parameters.

On average, continental slopes associated with studied canyons along passive margins tend to be significantly steeper than those along active

margins (~3.22° vs. ~5.16°, respectively; Two-sample t-test: T-Value: -4.13 DF= 70 P-Value ≤0.001; N_{active}= 44; $N_{passive}$= 47).

3.7.2.2 Interpretations

The results suggest that margin type is not a primary predictor of maximum canyon dimensions or canyon sinuosity. Studied canyons along passive margins tend to display larger average depths and steeper canyon thalweg gradients compared to their active-margin counterparts, which tend to have greater average widths. The varied influence of the continental-margin type on different aspects of canyon geomorphology can be explained as follows:

The seafloor relief, which influences sediment transport pathways, hydrodynamic processes and canyon geomorphology, can be sculpted by different processes, which are not limited to one particular continental-margin setting: faulting, although prominent in active-margin environments can also occur along passive margins (e.g. Osmundsen and Redfield, 2011); diapirism can be variably linked to processes acting in both margin types, such as mud and salt movements.

Another aspect to consider is that the physiography of continental margins can vary significantly in both tectonic settings. Although continental shelves along passive margins tend to be wider and with gentler lower-shelf gradients compared to those of active margins (e.g. Inman and Nordstrom, 1971; Blum and Hattier-Womack, 2009; Harris et al., 2014b; Harris and Macmillan-Lawler, 2016; Nyberg et al., 2018b), other shelf morphotypes exist. For example, shelves associated with passive margins can be as narrow as those associated with active margins (e.g. Harris and Macmillan-Lawler, 2016). The continental slopes of active margins are, on average, 1.28 times narrower (36 km) than those of passive margins (46 km); maximum widths are 368 km and 254 km, respectively (Harris et al., 2014b). Given the strong relationship between slope width and canyon length (see section 3.6.3), similarity in the ranges and mean values of canyon length for the two margin types may be partly related to the limited difference in slope width between active and passive margins. By contrast, the steeper average thalweg gradients of passive-margin canyons likely reflect how the average

canyon thalweg gradient is related to the overall slope gradient (cf. section 3.6.3), and that in the dataset overall gradients of continental slopes associated with canyons along passive margins tend to be higher compared to those along active ones. Considering the observed variability in relationships between aspects of catchment, shelf and slope configuration and canyon morphometric parameters (sections 3.6.2 & 3.6.3), contrasting characteristics in margin physiography are not evidently tied to particular geomorphologic characteristics in canyons.

The tendency of canyons from passive margins to have greater maximum sidewall steepness compared to canyons in active-margin settings might be explained by the effect of recurrent seismic activity on the stabilisation of seafloor substrate: although active margins are characterised by recurrent and high-magnitude seismic activity, the occurrence of submarine mass-transport processes can be subdued (e.g. Strozyk et al., 2010). The influence of background seismic activity on slope stability and mass-transport processes is variable and complex: seismic strengthening by recurrent earthquakes has been proposed as an effective mechanism leading to slope stabilization and a decrease in both scale and occurrence of slope-failure processes (e.g. Strozyk et al., 2010; Nelson et al., 2011; Molenaar et al., 2019). Recurrent seismic activity can decrease the potential oversteepening of slopes by inducing a steady remobilization and redistribution of slope deposits (Strozyk et al., 2010). However, at the same time the magnitude of earthquakes controls mass-failure processes, whereby higher-magnitude earthquakes tend to trigger larger-scale slope failures (e.g. Strozyk et al., 2010; Molenaar et al., 2019). Thus, slope failure may play a less important role in controlling canyon morphology on active margins compared to passive margins. Furthermore, earthquakes of small to high magnitudes do occur on passive margins (e.g. Stein et al., 1989; Wolin et al., 2012; Katz and Hamiel, 2018) and might act as a trigger of sediment remobilisation (e.g. Katz and Hamiel, 2018).

The findings herein suggest that submarine-canyon geomorphology does not differ fundamentally between active and passive margins.

A. Length

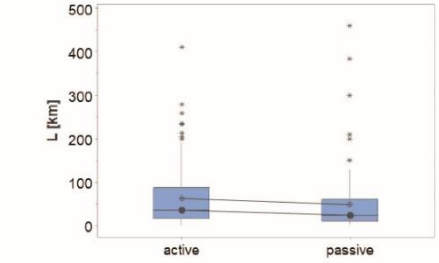

	N	min	mean	StDev	median	max
active	**141**	2.00	62.90	69.85	36.00	411.00
pass.	**122**	3.16	49.15	67.87	24.71	460.00
T-Value = 1.93 DF = 258 P-Value = 0.054						

B. Maximum width

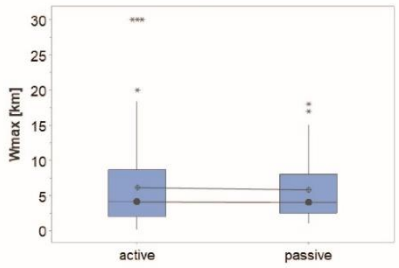

	N	min	mean	StDev	median	max
active	**91**	0.15	6.11	6.19	4.10	30.00
pass.	**73**	1.00	5.79	4.33	4.00	18.00
T-Value =-1.02 DF = 159 P-Value = 0.308						

C. Average width

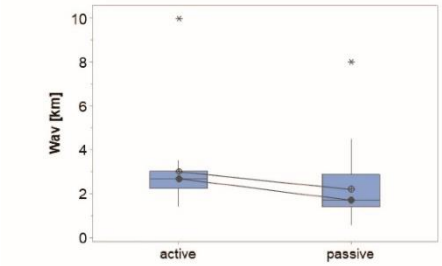

	N	min	mean	StDev	median	max
active	**18**	1.42	3.00	1.83	2.69	10.00
pass.	**48**	0.58	2.19	1.31	1.70	8.00
T-Value = 2.96 DF = 39 P-Value = 0.005						

D. Maximum depth

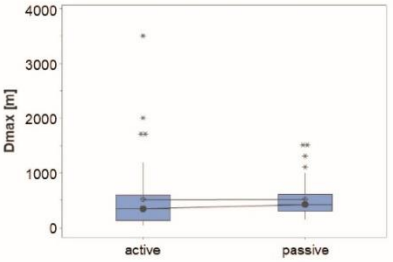

	N	min	mean	StDev	median	max
active	**60**	35.00	505.40	584.40	340.00	3500.00
pass.	**53**	150.00	511.00	314.10	422.60	1500.00
T-Value =-2.38 DF = 90 P-Value = 0.019						

E. Average depth

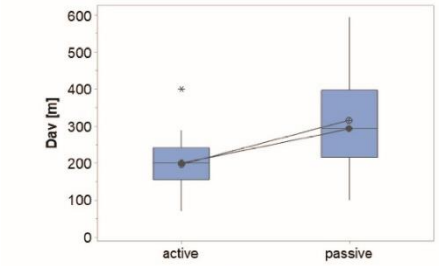

	N	min	mean	StDev	median	max
active	**21**	70.00	196.70	71.10	200.00	400.00
pass.	**31**	100.00	316.40	133.20	293.00	594.00
T-Value =-4.20 DF = 47 P-Value ≤ 0.001						

F. Average canyon sinuosity

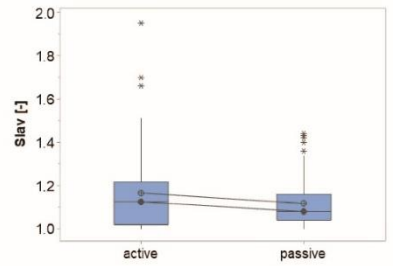

	N	min	mean	StDev	median	max
active	**68**	1.00	1.17	0.19	1.13	1.95
pass.	**83**	1.00	1.12	0.11	1.08	1.44
T-Value = 1.79 DF = 109 P-Value = 0.077						

G. Average canyon thalweg gradient

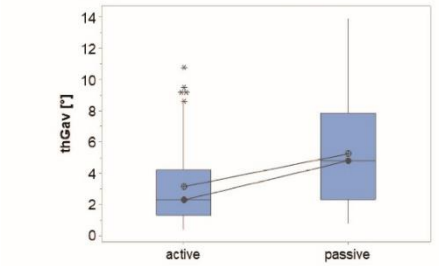

	N	min	mean	StDev	median	max
active	**72**	0.40	3.13	2.47	2.28	10.773
pass.	**48**	0.80	5.24	5.24	4.80	13.90
T-Value =-3.80 DF = 100 P-Value ≤ 0.001						

H. Maximum canyon sidewall steepness

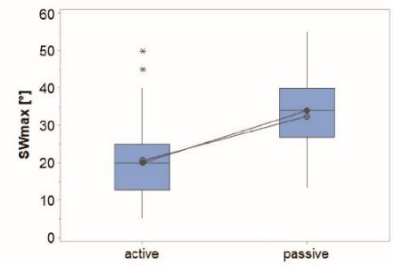

	N	min	mean	StDev	median	max
active	**33**	5.40	20.60	10.80	20.00	50.00
pass.	**36**	13.40	32.50	8.95	34.00	55.00
T-Value =-4.97 DF = 62 P-Value ≤ 0.001						

Figure 3.18a-h Boxplots of frequency distributions of canyon morphometric parameters for studied canyons classified based on the continental-margin type into active-margin (N=153) and passive-margin canyons (N=129) (classification after Harris et al., 2014b). See Figure 3.17 for legend.

3.7.3 Source-to-sink (S2S) system setting

3.7.3.1 Observations

Submarine canyons in continental and insular settings display similar frequency distributions of canyon morphometric parameters. Between the two groups, mean values only differ by a factor 1.08 or lower, except for the average canyon thalweg gradient, which is on average 1.17 times greater in continental-setting canyons. Frequency distributions of average canyon width and depth could not be evaluated due to lack of data for insular canyons (Fig. 3.19a-h).

For studied canyons with a sediment connection to one or several fluvial systems, the size of associated terrestrial catchments tends to be markedly greater in continental settings – on average by a factor of ~100 (341.842 km^2 compared to 3071 km^2; Two-sample t-test: T-Value= 2.10 DF= 30 P-Value=0.044; $N_{continental}$= 31 and $N_{insular}$= 10). Whereas more data is needed to corroborate this finding, the results demonstrate that continental catchments display a great variability in size; studied catchments display a range from 84 km^2 to 3,800,000 km^2. Insular shelves tend to be narrower and steeper than shelves offshore continental landmasses. The shelves of continental settings are on average 4.39 times wider than those of insular settings (108 km compared to 37 km; Two-sample t-test: T-Value=5.29 DF=163 P-Value≤0.001; $N_{continental}$= 167 and $N_{insular}$= 37). Mean overall shelf gradients of insular shelves at the canyon location are 1.8 times greater (0.756° compared to 0.420°; Two-sample t-test: T-Value=-1.88 DF= 24 P-Value= 0.073; $N_{continental}$= 96 and $N_{insular}$= 21).

3.7.3.2 Interpretations

The results indicate that the association of a submarine canyon with a continental landmass or an island is not reflected in important differences in canyon geomorphology, with the caveat that relationships between S2S

system setting and average canyon dimensions remain to be assessed. The similarity in frequency distributions and mean values for individual canyon morphometric parameters across the two groups might reflect how controlling factors are not significantly impacted by the S2S system setting, but also that different controls can generate similar geomorphologic characteristics in canyons across different S2S system settings.

The inherently limited extent of the terrestrial catchment in insular S2S systems compared to continental S2S systems does not appear to be a major factor for submarine-canyon geomorphology. In part, this may be linked to the variability of the scale of islands, with large islands having potentially sizable catchments, and smaller catchments also occurring on continental landmasses.

For canyons associated with volcanic islands (97% of the investigated insular canyons in the study), volcanic activity may be the dominant source of sediment (e.g. Aiello et al., 2020). In such case, uplift and denudation rates are of lesser importance as controlling factors on sediment fluxes to canyons.

In addition, findings from the regional canyon study by Smith et al. (2017) indicate that the prevalence of igneous bedrock lithology in terrestrial source areas might inhibit canyon formation. In volcanic rocks, weathered clay minerals might enhance seafloor cohesion, whereas the lack of mud in plutonic bedrock might inhibit the development of turbidity currents (Smith et al., 2017 and references therein). Hence, the transitioning of hyperpycnal flows (e.g. Zhao et al., 2018), dilute surface river plumes (e.g. Hizzet et al., 2017) and submarine mass failures (e.g. Puig et al., 2014) into turbidity currents might constitute a subordinate evolutionary process in canyons located in front of islands of a volcanic origin. On the other hand, the tendency of volcanic islands to experience slope failures along their flanks (e.g. Le Bas et al., 2007; Chang et al., 2021) and shelf margins (e.g. Quartau et al., 2015) can supply sediment to a canyon by both individual large-scale failures (e.g. Le Bas et al., 2007) and high-frequency smaller failures (e.g. Chang et al., 2021). The importance of volcanic activity as a trigger for submarine slope failures, however, might be subordinate where

other factors prevail, as storm events and onshore failure (Clare et al., 2018). Additionally, sediment transported by oceanic currents can represent a sustained source of sediment to insular canyons, independently of their origin.

Narrow and steep insular shelves promote sediment dispersal to the shelf margin, increased shear stress of sediment gravity flows, and shelfal sediment remobilisation (e.g. Hale et al., 2012; Babonneau et al., 2013). These factors may facilitate canyon activity, countering the effects of the reduced size of terrestrial catchments and limited seafloor erodibility.

A. Length

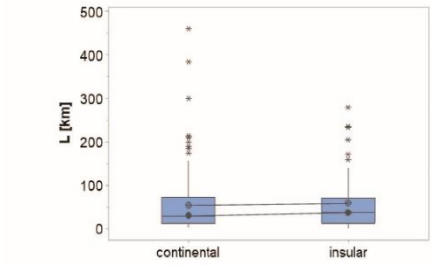

	N	min	mean	StDev	median	max
cont.	177	2.70	54.07	65.22	29.62	460.00
insular	50	2.00	58.36	67.80	37.28	279.67
T-Value = 0.01 DF = 72 P-Value = 0.992						

B. Maximum width

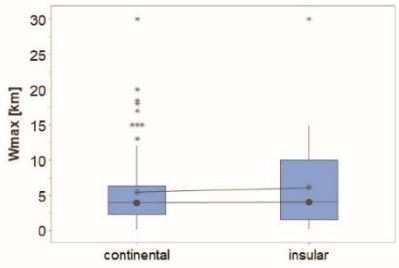

	N	min	mean	StDev	median	max
cont.	101	0.15	5.41	4.89	3.91	30.00
insular	36	0.25	6.06	6.08	4.00	30.00
T-Value = 0.31 DF = 50 P-Value = 0.758						

C. Average width

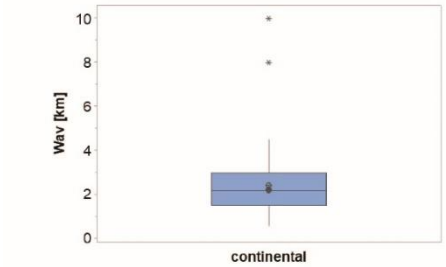

	N	min	mean	StDev	median	max
cont.	66	0.58	2.41	1.50	2.18	10.00
insular	0	***	***	***	***	***
T-Value =*** DF =*** P-Value =***						

D. Maximum depth

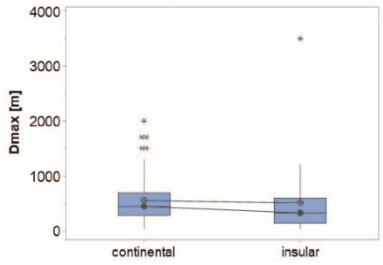

	N	min	mean	StDev	median	max
cont.	60	50.00	553.70	426.40	442.50	2000.00
insular	29	50.00	511.00	648.00	330.00	3500.00
T-Value = 1.39 DF = 43 P-Value = 0.173						

E. Average depth

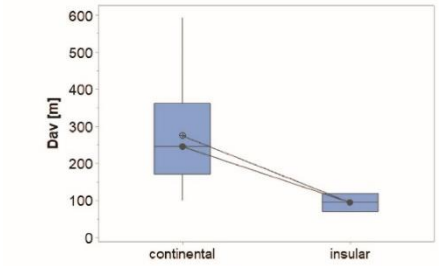

	N	min	mean	StDev	median	max
cont.	50	100.00	275.00	123.70	246.00	594.00
insular	2	70.00	95.00	35.40	95.00	120.00
T-Value =*** DF =*** P-Value =***						

F. Average canyon sinuosity

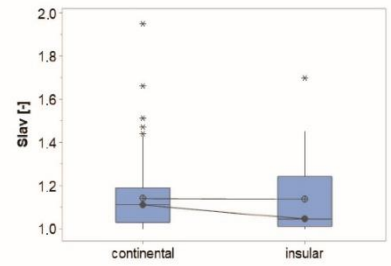

	N	min	mean	StDev	median	max
cont.	129	1.00	1.14	0.15	1.11	1.95
insular	20	1.00	1.14	0.19	1.05	1.70
T-Value = 0.20 DF = 22 P-Value = 0.846						

G. Average canyon thalweg gradient

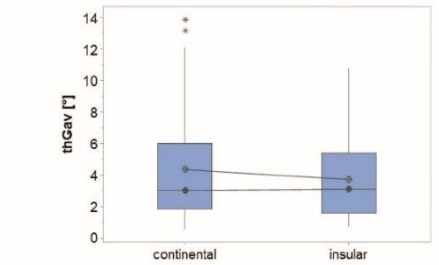

	N	min	mean	StDev	median	max
cont.	77	0.60	4.35	3.31	3.00	13.90
insular	31	0.78	3.71	2.76	3.09	10.77
T-Value = 0.83 DF = 58 P-Value = 0.408						

H. Maximum canyon sidewall steepness

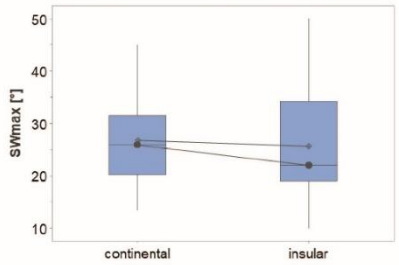

	N	min	mean	StDev	median	max
cont.	28	13.40	26.75	7.96	25.90	45.00
insular	17	10.00	25.67	10.65	22.00	50.00
T-Value = 0.66 DF = 27 P-Value = 0.517						

Figure 3.19a-h Boxplots of frequency distributions of canyon morphometric parameters for studied submarine canyons classified based on the source-to-sink setting into continental-margin (N=189) and insular canyons (N=57). *** denotes data paucity. See Figure 3.17 for legend.

3.7.4 Oceanographic environment

3.7.4.1 Observations

Distributions of canyon length (Fig. 3.20a), maximum width (Fig. 3.20b), average sinuosity (Fig. 3.20f) and average thalweg gradient (Fig. 3.20g) for open-sea canyons and canyons from semi-enclosed or enclosed seas are similar: apart from the thalweg gradient, the mean values of these parameters do not differ to a statistically significant level across the two groups. The average canyon width is greater for canyons located in semi-enclosed and enclosed seas compared to those in open seas, but this observation is based on a small dataset (Fig. 3.20c); conversely, the average depth of open-sea canyons is higher. The differences in mean values of average canyon depth and width across the two groups are only statistically significant for the former. In contrast, marked differences in distributions of maximum canyon depth are seen across the two groups: on average, the maximum canyon depth is 1.91 times higher in open-sea canyons (Fig. 3.20d). Open-sea canyons also tend to have steeper sidewalls than canyons from semi-enclosed and enclosed seas, by a factor of 1.73 on average (Fig. 3.20h). These differences are statistically significant.

Continental slopes located in open-sea settings have on average greater slope-break depths than continental slopes associated with semi-enclosed and enclosed seas (3959 m compared to 3072 m, respectively; T-Value=3.92 DF=98 P-Value≤0.001; $N_{\text{open sea}} = 85$; $N_{\text{se\&e seas}} = 70$).

3.7.4.2 Interpretations

The results suggest that conditions associated with the oceanographic environment may exert an influence on maximum canyon depth, the average canyon gradient and the steepness of canyon margins, but not on canyon length, maximum width and overall sinuosity.

Fundamental differences between the two environments lie in the scale of the water body, in its degree of confinement, and in the presence of thermohaline circulation and major oceanic currents in oceans (e.g. Rahmstorf, 2006; Faugères and Mulder, 2011). In contrast, upwelling and internal waves can affect canyons in both open-oceanic (e.g. Hickey, 1997; Smith et al., 2018) and semi-enclosed seas (e.g. Flexas et al., 2008; Li et al., 2022). The findings of this study might indicate that controlling factors that predominantly affect canyon geomorphology by acting along directions that are transverse to the canyon axis, like slope-parallel currents and lateral slope failures, might have a greater impact on canyon geomorphology in open seas. Oceanic currents might transport greater volumes of sand-sized sediment due to their greater extent and great depth range (e.g. Faugères and Mulder, 2011) compared to those in semi-enclosed and enclosed seas, which can be deposited onto intra-canyon ridges and canyon margins thereby increasing canyon depths and steepening canyon sidewalls by aggradation. Oversteepened margins are in turn more prone to collapse, which can lead to steeper margins over the affected area of the canyon.

The greater sidewall steepness of open-sea canyons might also reflect how the studied high-latitude (sections 3.5.3 & 3.7.5) and passive-margin canyons (section 3.7.2), which tend to have steeper margins, are dominantly located in open-sea settings.

It must be recognised, additionally, that the findings may emerge not because of causal relationships with processes associated with the oceanographic environment, but merely because of positive scaling between canyon depth and sidewall steepness (section 3.4).

A. Length

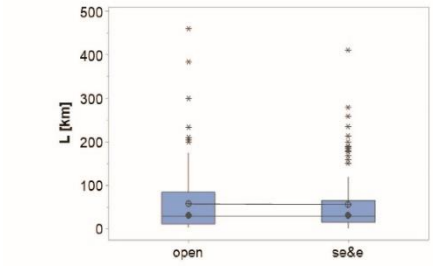

	N	min	mean	StDev	median	max
open	**146**	2.70	57.10	70.36	29.85	460.00
se&e	**117**	2.00	55.80	67.91	29.79	411.00
T-Value =-0.23 DF = 253 P-Value = 0.816						

B. Maximum width

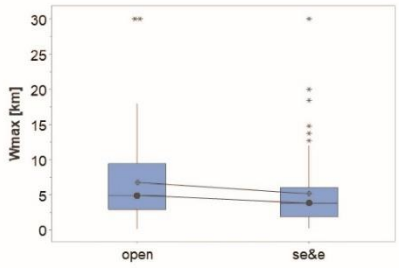

	N	min	mean	StDev	median	max
open	**84**	0.15	6.73	5.72	4.92	30.00
se&e	**80**	0.25	5.16	5.02	3.83	30.00
T-Value = 2.34 DF = 159 P-Value = 0.020						

C. Average width

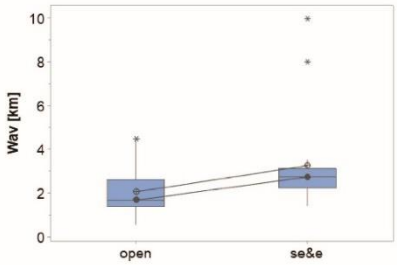

	N	min	mean	StDev	median	max
open	**47**	0.58	2.06	1.00	1.68	4.48
se&e	**19**	1.42	3.26	2.118	2.74	10
T-Value =-3.50 DF = 34 P-Value =0.001						

D. Maximum depth

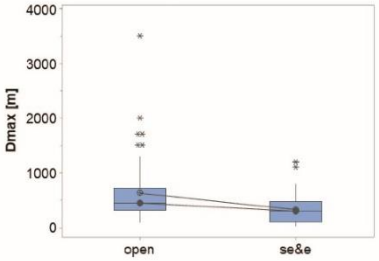

	N	min	mean	StDev	median	max
open	**68**	100.00	627.50	540.70	450.00	3500.00
se&e	**45**	35.00	327.40	271.90	297.00	1200.00
T-Value = 4.74 DF = 74 P-Value ≤ 0.001						

E. Average depth

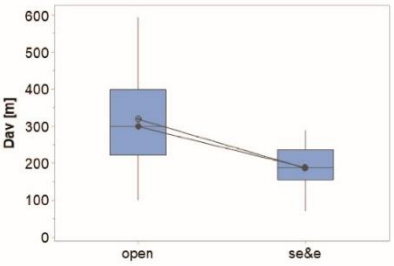

	N	min	mean	StDev	median	max
open	**32**	100.00	319.00	131.90	299.00	594.00
se&e	**20**	70.00	186.50	55.20	188.00	289.00
T-Value = 1.34 DF = 134 P-Value = 0.184						

F. Average canyon sinuosity

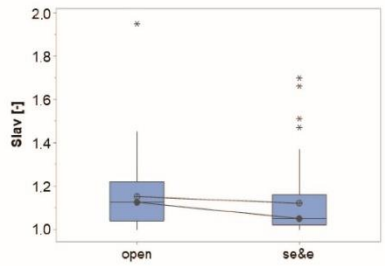

	N	min	mean	StDev	median	max
open	**88**	1.00	1.15	0.15	1.13	1.95
se&e	**63**	1.00	1.12	0.15	1.05	1.70
T-Value = 1.49 DF = 133 P-Value = 0.139						

G. Average canyon thalweg gradient

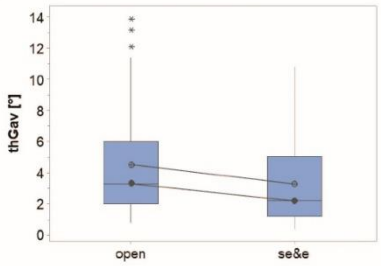

	N	min	mean	StDev	median	max
open	**67**	0.80	4.53	3.22	3.30	13.90
se&e	**53**	0.40	3.28	2.79	2.19	10.77
T-Value = 2.95 DF = 99 P-Value = 0.004						

H. Maximum canyon sidewall steepness

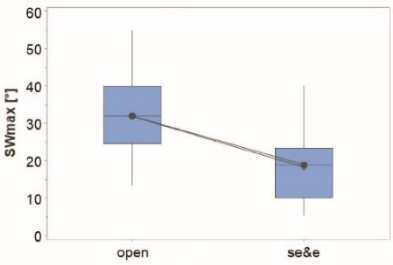

	N	min	mean	StDev	median	max
open	**43**	13.40	31.93	9.59	32.00	55.00
se&e	**26**	5.40	18.32	9.17	19.00	40.00
T-Value = 5.87 DF = 54 P-Value ≤ 0.001						

Figure 3.20a-h Boxplots of frequency distributions of canyon morphometric parameters for studied submarine canyons classified based on the oceanographic environment into submarine canyons associated with open seas (N=162) and semi-enclosed and enclosed seas (N=120). See Figure 3.17 for legend.

3.7.5 Latitudinal zones

Variations in canyon morphometric parameters are evaluated for latitudinal belts assigned to tropical (0-23.5°), temperate (23.5°-66.5°), and polar (>66.5°) zones. The dataset contains fewer data from canyons from polar latitudes compared to canyons in tropical and temperate zones; this reflects the paucity of investigations of high-latitude submarine canyons, despite the large number of canyons in the Arctic and Antarctic regions (Harris and Whiteway, 2011; Harris et al., 2014b). The Arctic canyons in this study are from only two regions: the NW Norwegian margin (N=15) and the Barrow Canyon from the N Alaskan margin. Thus, the representativeness of the data is likely to be limited. Because of this geographic bias, differences in mean values of canyon morphometric parameters from tropical and temperate latitudes have been tested separately.

3.7.5.1 Observations

Results of one-way ANOVA for canyons grouped by latitude range show statistically significant differences in mean values of length (Fig. 3.21a), maximum canyon width (Fig. 3.21b) and maximum canyon sidewall steepness (Fig. 3.21h), but not for maximum canyon depth (Fig. 3.21d).

Based on two-sample t-tests, statistically significant differences are seen for mean values of length (Fig. 3.21a) and average canyon sinuosity (Fig. 3.21f) between canyons of tropical and temperate latitudes. The difference in mean values of average canyon thalweg gradient is just above the threshold of statistical significance (Fig. 3.21g).

3.7.5.2 Interpretations

The observed significant differences in canyon morphometrics may represent a record of latitude-related controls on aspects of canyon geomorphology. Considering the relationship between continental-slope

gradient and average canyon thalweg gradient (section 3.6.3.2), the typically steeper thalwegs of tropical canyons, compared to temperate ones, might be related to the known latitudinal control on carbonate distribution to deep-marine environments (see Figure 3 of O'Mara and Dunne, 2019), in light of how carbonate can act to stabilise the slope substrate by binding and cementation (e.g. Adams and Kenter, 2013 and references therein).

Based on the results of the statistical analyses, submarine canyons do not vary markedly across tropical and temperate latitudinal zones with regards to their maximum width and depth, maximum sidewall steepness, or average sinuosity. Limited latitudinal variations in canyon sinuosity are also documented in the geographic regions examined by Harris and Whiteway (2011).

In contrast, both oversteepening of canyon margins related to high and dispersed sediment supply from glaciated margins (e.g. Martinsen, 2005; Armitage et al., 2010; Gales et al., 2021) and gravitational slope failure from ice loading (Mulder and Moran, 1995) may cause canyon sidewalls to be steeper in high-latitude settings compared to low- and mid-latitude ones. Yet any such inference has to be viewed with caution (see section 3.5.3 for a more detailed discussion).

A. Length

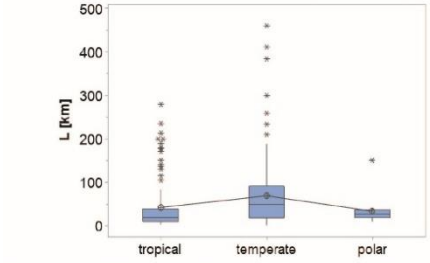

	N	min	mean	StDev	median	max
tropical	108	3.16	42.48	59.48	19.57	279.67
temper.	139	2.00	69.99	76.34	50.93	460.00
polar	16	10.00	34.31	32.30	28.00	150.00
F-Value = 9.62		DF1 = 2 DF2 =53.2955			P-Value ≤ 0.001	
T-Value*=-4.39		DF = 234			P-Value ≤ 0.001	

B. Maximum width

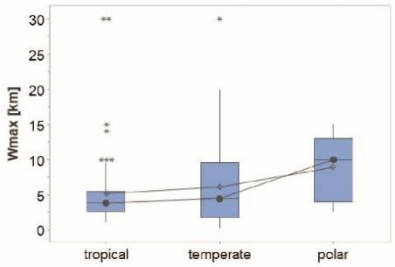

	N	min	mean	StDev	median	max
tropical	70	1.00	5.19	5.12	3.85	30.00
temper.	79	0.15	6.09	5.70	4.49	30.00
polar	15	2.50	8.90	4.61	10.00	15.00
F-Value = 6.86		DF1 = 2 DF2 = 43.3839			P-Value = 0.003	
T-Value*=0.42		DF = 132			P-Value = 0.675	

C. Average width

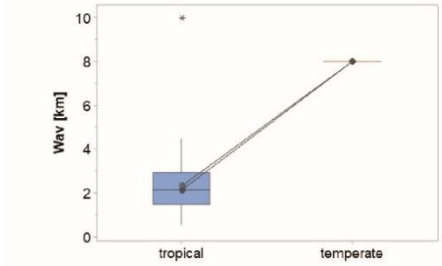

	N	min	mean	StDev	median	max
tropical	65	0.58	2.32	1.339	2.14	10.00
temper.	1	8.00	8.00	***	8.00	8.00
polar	0	***	***	***	***	***
F-Value = ***		DF1 = *** DF2 = ***			P-Value = ***	
T-Value*= ***		DF = ***			P-Value = ***	

D. Maximum depth

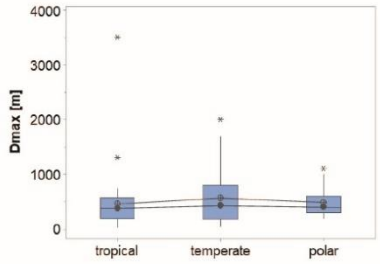

	N	min	mean	StDev	median	max
tropical	49	35.00	458.30	504.20	380.40	3500.00
temper.	49	50.00	564.20	494.60	425.00	2000.00
polar	15	200.00	486.70	274.20	400.00	1100.00
F-Value = 1.14		DF1 = 2 DF2 = 53.2580			P-Value = 0.328	
T-Value*=-0.65		DF = 93			P-Value = 0.518	

E. Average depth

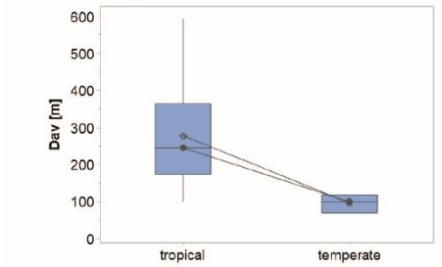

	N	min	mean	StDev	median	max
tropical	49	100.00	278.60	25.20	246.00	594.00
temper.	3	70.00	96.70	25.20	100.00	120.00
polar	0	***	***	***	***	***
F-Value = ***		DF1 = *** DF2 = ***			P-Value = ***	
T-Value*= ***		DF = ***			P-Value = ***	

F. Average canyon sinuosity

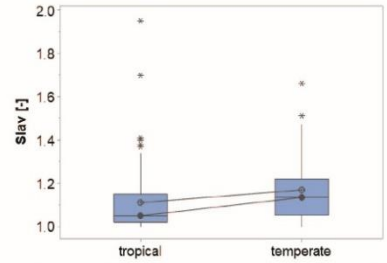

	N	min	mean	StDev	median	max
tropical	79	1.00	1.11	0.16	1.05	1.95
temper.	72	1.00	1.17	0.1395	1.14	1.66
polar	0	***	***	***	***	***
F-Value = ***		DF1 = *** DF2 = ***			P-Value = ***	
T-Value*=-2.77		DF = 148			P-Value = 0.006	

G. Average canyon thalweg gradient

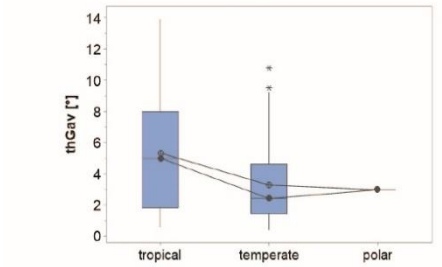

	N	min	mean	StDev	median	max
tropical	41	0.60	5.33	3.78	5.00	13.90
temper.	78	0.40	3.28	2.42	2.42	10.77
polar	1	2.98	2.98	***	2.98	2.98
F-Value = ***		DF1 = *** DF2 = ***			P-Value = ***	
T-Value*= 2.61		DF = 69			P-Value = 0.011	

H. Maximum canyon sidewall steepness

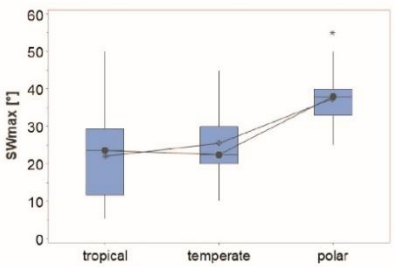

	N	min	mean	StDev	median	max
tropical	26	5.40	22.06	12.02	23.60	50.00
temper.	28	10.00	25.50	8.94	22.50	45.00
polar	15	25.00	37.47	7.82	38.00	55.00
F-Value =19.48		DF1 = 2 DF2 = 42.4993			P-Value ≤ 0.001	
T-Value*=-1.84		DF = 37			P-Value = 0.074	

Figure 3.21a-h Boxplots of frequency distributions of canyon morphometric parameters for studied submarine canyons classified based on latitudinal zones into tropical (N=116), temperate (N=149) and polar canyons (N=16). * indicates that Two-Sample-T-tests have been conducted for submarine canyons in tropical versus temperate latitudinal zones. N = number of readings; min = minimum value; mean = mean value; StDev = standard deviation; median = median value; max = maximum value. Results of Welch's ANOVA test: DF 1 = degrees of freedom numerator; DF 2 = degrees of freedom denominator. Results of Two-Sample T-test: DF = degrees of freedom. *** denotes data paucity.

3.7.6 Width-to-depth ratios

To investigate potential relationships between the ratio between maximum canyon width to maximum canyon depth (wdmax) and environmental factors, 100 submarine canyons of the study for which both maximum width and depth values have been obtained have been considered; aspect ratios have been evaluated for canyons across classes of environments (Fig. 3.22a-f).

3.7.6.1 Observations

Although wdmax ratios for the studied canyons vary over a broad range (2.45 to 73.33), mean and median values of wdmax ratios are in the order of magnitude of 10^1 both for the whole dataset as well as for canyons grouped according to environmental factors. Mean values range between 11 and 20, and only differ significantly from each other for canyons in open seas versus semi-enclosed and enclosed seas (Fig. 3.22e). For canyons grouped into tropical, temperate and polar latitudinal zones, the difference in mean values yields a p-value of 0.011 (Fig. 3.22f).

3.7.6.2 Interpretations

The narrow range in mean and median wdmax ratios and the lack of significant differences in mean values for the majority of canyon environmental classes indicate that maximum width-to-maximum depth ratios in canyons are of limited diagnostic value for inferring the environmental settings. This might reflect that width-to-depth ratios in canyons are not particularly sensitive to environmental controls and that they may inherently scale with processes that control canyon geomorphology

globally. This would imply that width-to-depth ratios in submarine canyons are predominantly controlled by canyon self-organisation and autogenic processes, from the interplay of canyon-floor and margin aggradation and wall failure with intra-canyon sediment gravity flows, as suggested for submarine channels by Shumaker et al. (2018).

The inferred influence of the oceanographic environment on canyon width-to-depth ratios might reflect the way in which both erosional and depositional processes that operate along canyon margins are more strongly affected by the hydrodynamic regime in open seas than semi-enclosed and enclosed ones (see discussion in section 3.7.4).

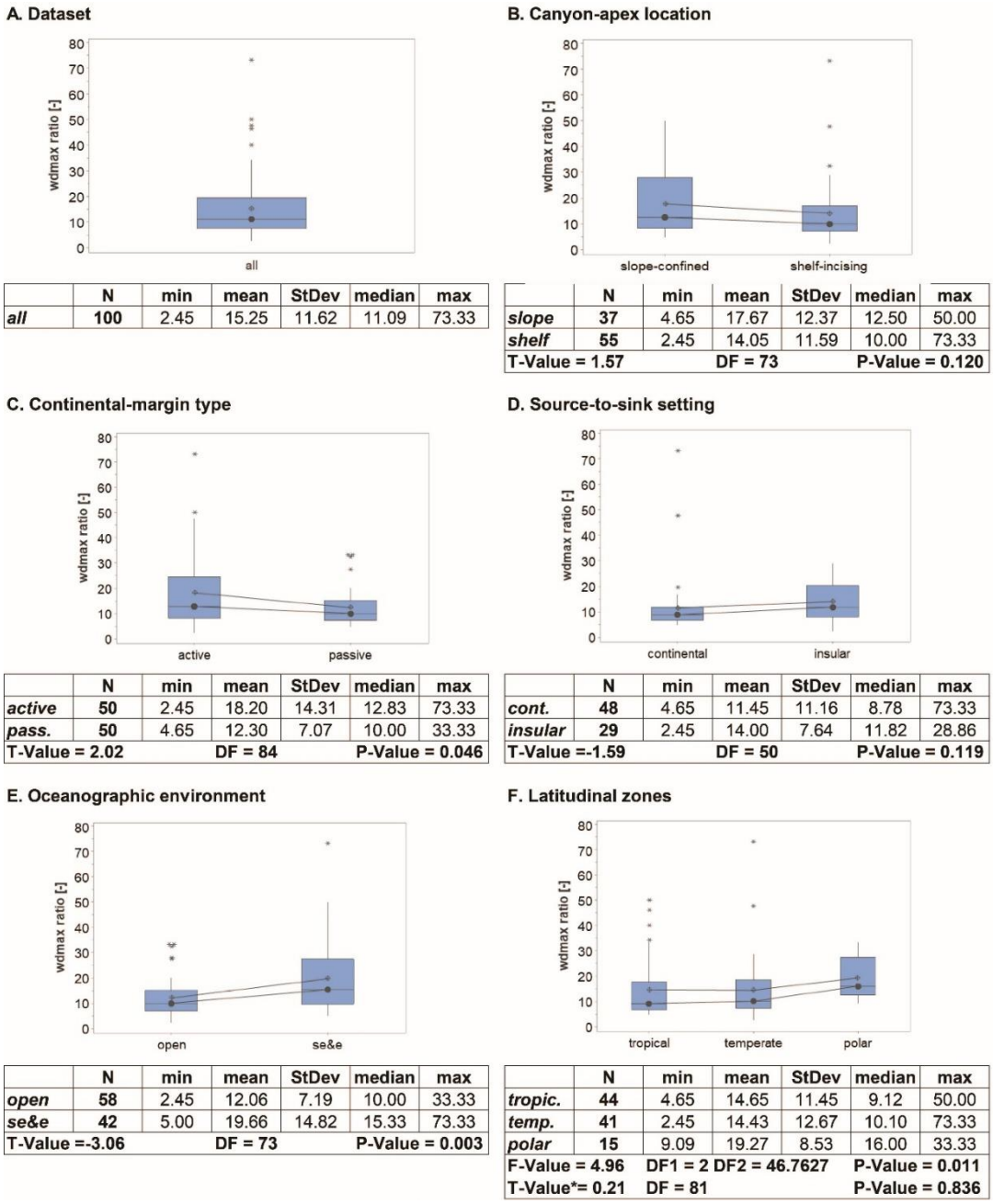

	N	min	mean	StDev	median	max
all	100	2.45	15.25	11.62	11.09	73.33

	N	min	mean	StDev	median	max
slope	37	4.65	17.67	12.37	12.50	50.00
shelf	55	2.45	14.05	11.59	10.00	73.33
T-Value = 1.57			DF = 73			P-Value = 0.120

	N	min	mean	StDev	median	max
active	50	2.45	18.20	14.31	12.83	73.33
pass.	50	4.65	12.30	7.07	10.00	33.33
T-Value = 2.02			DF = 84			P-Value = 0.046

	N	min	mean	StDev	median	max
cont.	48	4.65	11.45	11.16	8.78	73.33
insular	29	2.45	14.00	7.64	11.82	28.86
T-Value =-1.59			DF = 50			P-Value = 0.119

	N	min	mean	StDev	median	max
open	58	2.45	12.06	7.19	10.00	33.33
se&e	42	5.00	19.66	14.82	15.33	73.33
T-Value =-3.06			DF = 73			P-Value = 0.003

	N	min	mean	StDev	median	max
tropic.	44	4.65	14.65	11.45	9.12	50.00
temp.	41	2.45	14.43	12.67	10.10	73.33
polar	15	9.09	19.27	8.53	16.00	33.33
F-Value = 4.96		DF1 = 2 DF2 = 46.7627				P-Value = 0.011
T-Value*= 0.21		DF = 81				P-Value = 0.836

Figure 3.22a-f Boxplots of frequency distributions of maximum-width-to-maximum depth (wdmax) ratios in studied submarine canyons A. for the dataset and B.-F. across classes of environments. * indicates that Two-Sample-T-tests have been conducted for submarine canyons in tropical versus temperate latitudinal zones. See Figure 3.21 for legend.

3.8 Summary and conclusions

To increase understanding of the factors that exert control on canyon geomorphology and their relative importance on a global scale, statistical

analyses were conducted to evaluate relationships between canyon morphometric parameters, and between these and attributes describing the physiographic setting of the canyon, including characteristics of elements of the source-to-sink (S2S) system (catchment, shelf and slope), the bathymetric setting of the canyon and its distance to the shoreline, the canyon-apex location relative to the shelf-break, the continental-margin type, the oceanographic environment, and the latitude of the canyon apex. In addition, selected morphometric parameters describing submarine canyons have been quantitatively characterised, both on a global scale and for different environmental settings (canyon-apex location relative to the shelf-break, continental-margin type, source-to-sink system setting, oceanographic environment and climate zones). Certain forms of scaling in attributes of canyon geomorphology are recognisable on a global scale and across different environmental settings and source-to-sink system configurations (Fig. 3.23a&b and Fig. 3.24a&b).

Key findings of the study are as follows:

(1) Scaling relationships between canyon morphometric attributes tend to be weak, due to the varied influence of environmental allogenic controls and autogenic processes influencing canyon geomorphology. Nevertheless, despite specific regional or local conditions, some scaling relationships between canyon morphometric attributes are more likely recognisable on a global scale than others; these include, for example, scaling between maximum canyon dimensions, or between maximum sidewall steepness and maximum canyon width and depth.

(2) The tendency of canyons to have greater maximum widths and depths with increasing canyon-mouth seafloor depth, the overall weakness in scaling of canyon morphometry with the terrestrial catchment and continental shelf, and the steeper canyon walls seen in canyons associated with open-sea settings compared to canyons in semi-enclosed or enclosed seas, possibly reflect how hydrodynamic processes such as upwelling, longshore drifts and along-slope currents influence canyon geomorphology.

(3) Canyon morphometric parameters may reflect the interplay of different environmental factors. Hence, controls on canyon geomorphology cannot be described by generic models linking geomorphological characteristics to individual environmental parameters. Potential controls on certain canyon morphometric parameters include: the location of the canyon head relative to the shelf break, the continental-margin type, the oceanographic environment, the absolute latitude of the canyon apex, and the depth of the associated shelf break. Data on canyon length, sinuosity, thalweg gradient and maximum sidewall steepness indicate that these morphometric aspects are likely influenced by several environmental controls.

Key findings regarding relationships between the environmental setting and canyon geomorphology include:

(i) Maximum canyon dimensions and overall canyon sinuosity cannot be used to predict the position of the canyon apex relative to the shelf break and vice versa; this challenges concepts linking higher overall sinuosities in canyons to incision of the canyon into the shelf (e.g. Farre et al., 1983; Jobe et al., 2011; Wiles et al., 2019).

(ii) The tendency of passive-margin canyons to develop steeper sidewalls compared to those of active-margin canyons indicates that slope failure might be generally less important for canyons from active margins compared to passive-margin ones, perhaps due to recurrent seismic strengthening of the seafloor substrate, which might act to inhibit mass failures, with the exception of mass failures triggered by high-magnitude earthquakes (e.g. Strozyk et al., 2010; Molenaar et al., 2019).

(iii) Whether a submarine canyon is associated with a continental or insular setting does not exert control on overall canyon geomorphology. Volcanic sediment sources and narrow and steep insular shelves might compensate for the impact of

smaller associated terrestrial catchments on sediment supply to submarine canyons, and for the potential effect igneous bedrock lithology might have on canyon evolution along volcanic islands by affecting seafloor erodibility and the erosive strengths of flows (Smith et al., 2017 and references therein).

(iv) The complex interrelationships between climate-controlled processes are reflected in the weakness of linear and monotonic scaling of latitude with canyon morphometrics and can explain why the latitudinal position of a canyon is not a reliable indicator of overall canyon geomorphology in canyons in tropical and temperate latitudes. The complex role of climate influence on sediment sourcing and dispersal along glaciated continental margins, paired with the effect of ice loading on triggering of mass failures, might explain the observed steeper margins of submarine canyons from higher latitudes. However, in view of geographic bias and the limited sample size, it is possible that the results reflect how the studied higher-latitude canyons are coincidentally associated with passive-margin and open-sea settings, which tend to be associated with distinct distributions in sidewall steepness.

(v) Mean values of maximum width-to-maximum depth ratios in canyons are consistently in the order of magnitude of 10^1 for all investigated canyon classes – regardless of canyon-head location relative to the shelf break, the tectonic-margin type, the S2S setting, the oceanographic environment and the latitudinal zone – albeit with significant global variability in documented values. This might reflect how width-to-depth ratios in submarine canyons are constrained by the interplay of canyon-margin failure and canyon-floor and -margin aggradation by flows.

The quantitative characterisation of how canyon morphometric parameters vary as a function of environmental factors demonstrates that the interplay of

controls on canyon geomorphology is more complex than hitherto considered in canyon classification schemes (e.g. Jobe et al., 2011), numerical (e.g. Wan et al., 2021) and published conceptual models of canyon evolution (e.g. Chiang and Yu, 2006; Micallef et al., 2014), of deep-water systems and of source-to-sink (S2S) systems (e.g. Sømme et al., 2009; Nyberg et al., 2018b). The predictive value of these models can be enhanced by considering the impact of the controlling factors identified in this study – including the hydrodynamic regime of oceans and seas, autogenic canyon processes, characteristics of continental margin physiography and the canyon-physiographic setting.

The findings of this study might also aid in estimation of the original geometry of ancient canyons and channel forms whose infills are now preserved in subsurface and outcrop, and in the interpretation of their formative environments, particularly where information on the environmental setting, margin physiography and bathymetry are limited due to scarcity of data (e.g. Martinsen et al., 2010; Helland-Hansen et al., 2016; Xu et al., 2017).

Results of this work will aid analyses of source-to-sink systems, i.e., spanning fluvial, paralic and deep-water domains (e.g. Sømme et al., 2009; Nyberg et al., 2018b; Wang et al., 2019), by illuminating the response of slope systems to controlling factors on sedimentary processes from terrestrial hinterlands to deep-water environments. Further research is needed to investigate the relative scaling between features of these clastic environments and those of submarine canyons, and of the relative influence of marine hydrodynamic processes on submarine-canyon geomorphology.

A. Relationships between canyon morphometrics

Linear monotonic relationships

	L	Wmax	Wav	Dmax	Dav	Slav	thGav	SWmax
L		0.5	0.8	0.5		0.5	-0.5	
Wmax	0.5		0.8	0.8	0.5	0.4	-0.3	0.4
Wav	0.8	0.8		0.8				
Dmax	0.5	0.8	0.8		1.0			0.4
Dav		0.5		1.0		0.5		***
Slav	0.5	0.4			0.5		-0.3	
thGav	-0.5	-0.3				-0.3		
SWmax		0.4		0.4	***			

Non-linear monotonic relationships

	L	Wmax	Wav	Dmax	Dav	Slav	thGav	SWmax
L		0.6	0.6	0.7		0.5	-0.7	0.3
Wmax	0.6		0.8	0.7		0.4	-0.4	0.4
Wav	0.6	0.8		0.8				
Dmax	0.7	0.7	0.8		1.0			0.4
Dav				1.0		0.5		***
Slav	0.5	0.4			0.5		-0.4	
thGav	-0.7	-0.4				-0.4		
SWmax	0.3	0.4		0.4	***			

B. Relationships between canyon morphometrics and environmental parameters

Linear monotonic relationships & differences between canyon groups

	Lfls	Qfls	Aflsc	Hflsc	Wsh	Dsh	Gsh	Wsl	Dsl	Gsl	Dismin	SDmin	SDmax	Latabs
L				0.4	0.2	0.4		0.4					0.6	
Wmax				0.6		0.4		0.4					0.4	0.2
Wav	***	***	***	***		0.5	0.7							0.5
Dmax		***		***		0.4		0.4	0.6				0.8	
Dav	***	***	***	***		***						-0.4	0.7	-0.4
Slav				0.6		0.4		***					0.6	
thGav		***				-0.3				0.5			-0.3	-0.4
SWmax	***	***	***	***	0.6					0.8	-0.3		0.4	0.5

	cnh. location	margin type	S2S setting	ocean. env.	lat. (ANOVA)	lat. (t-test)	sh. depth 120	sh. depth 130
L	X				X	X	X	X
Wmax					X			
Wav	X	X	***	X	***	***	***	***
Dmax				X				
Dav	***	X	***		***	***	***	***
Slav	X				***	X	X	X
thGav		X		X	***		X	X
SWmax		X		X	X			

Non-linear monotonic relationships & differences between canyon groups

	Lfls	Qfls	Aflsc	Hflsc	Wsh	Dsh	Gsh	Wsl	Dsl	Gsl	Dismin	SDmin	SDmax	Latabs
L		0.7		0.6	0.2	0.5		0.9	0.4				0.7	0.3
Wmax			0.6	0.6				0.7					0.5	0.2
Wav	***	***	***	***	0.4	0.6	0.6				0.4			0.5
Dmax	0.7	***	0.7	***	0.4			0.6	0.5			-0.4	0.8	
Dav	***	***	***	***		***						-0.4	0.7	-0.4
Slav		0.5		0.6	-0.3	0.4		***			-0.3	-0.3	0.5	0.2
thGav		***				-0.3		-0.5		0.5				-0.3
SWmax	***	***	***	***	0.5				-0.6	0.7			0.4	0.4

	cnh. location	margin type	S2S setting	ocean. env.	lat. (ANOVA)	lat. (t-test)	sh. depth 120	sh. depth 130
L	X				X	X	X	X
Wmax					X			
Wav	X	X	***	X	***	***	***	***
Dmax				X				
Dav	***	X	***		***	***	***	***
Slav	X				***	X	X	X
thGav		X		X	***		X	X
SWmax		X		X	X			

correlation coefficient-value -1 0 1

X difference in mean values between canyon groups is statistically significant (p≤0.01)

*** not enough data

Figure 3.23a&b Summary tables displaying relationships of canyon morphometric parameters A. with each other and B. with environmental parameters for results of the correlation analyses and hypothesis testing with a statistical significance ($p \leq 0.1$) and $N \geq 15$ for each parameter and canyon group. *L* = canyon length; W_{max} = maximum canyon width; W_{av} = average canyon width; D_{max} = maximum canyon depth; D_{av} = average canyon depth; SI_{av} = average canyon sinuosity index; thG_{av} = average canyon thalweg gradient; SW_{max} = maximum canyon sidewall steepness; L_{fls} = fluvial system length; Q_{fls} = average annual fluvial discharge; A_{flsc} = size of the catchment; H_{flsc} = maximum elevation in the catchment area; W_{sh} = shelf width; D_{sh} = shelf-break depth; G_{sh} = average shelf gradient. 4. Slope configuration: W_{sl} = slope width; D_{sl} = slope-break depth; G_{sl} = average slope gradient; Dis_{min} = minimum distance between the canyon and shoreline; SD_{min} = minimum seafloor depth at the canyon; SD_{max} = maximum seafloor depth at the canyon; Lat_{abs} = absolute value of the latitude of the canyon apex; *cnh. location* = canyon-apex location relative to the shelf break; *margin type* = continental-margin type; *ocean. env.* = oceanographic environment; *lat.* = latitude at the canyon apex; *sh. depth* = shelf-break depth at the canyon. *** denotes datasets that were deemed too small for statistical analyses.

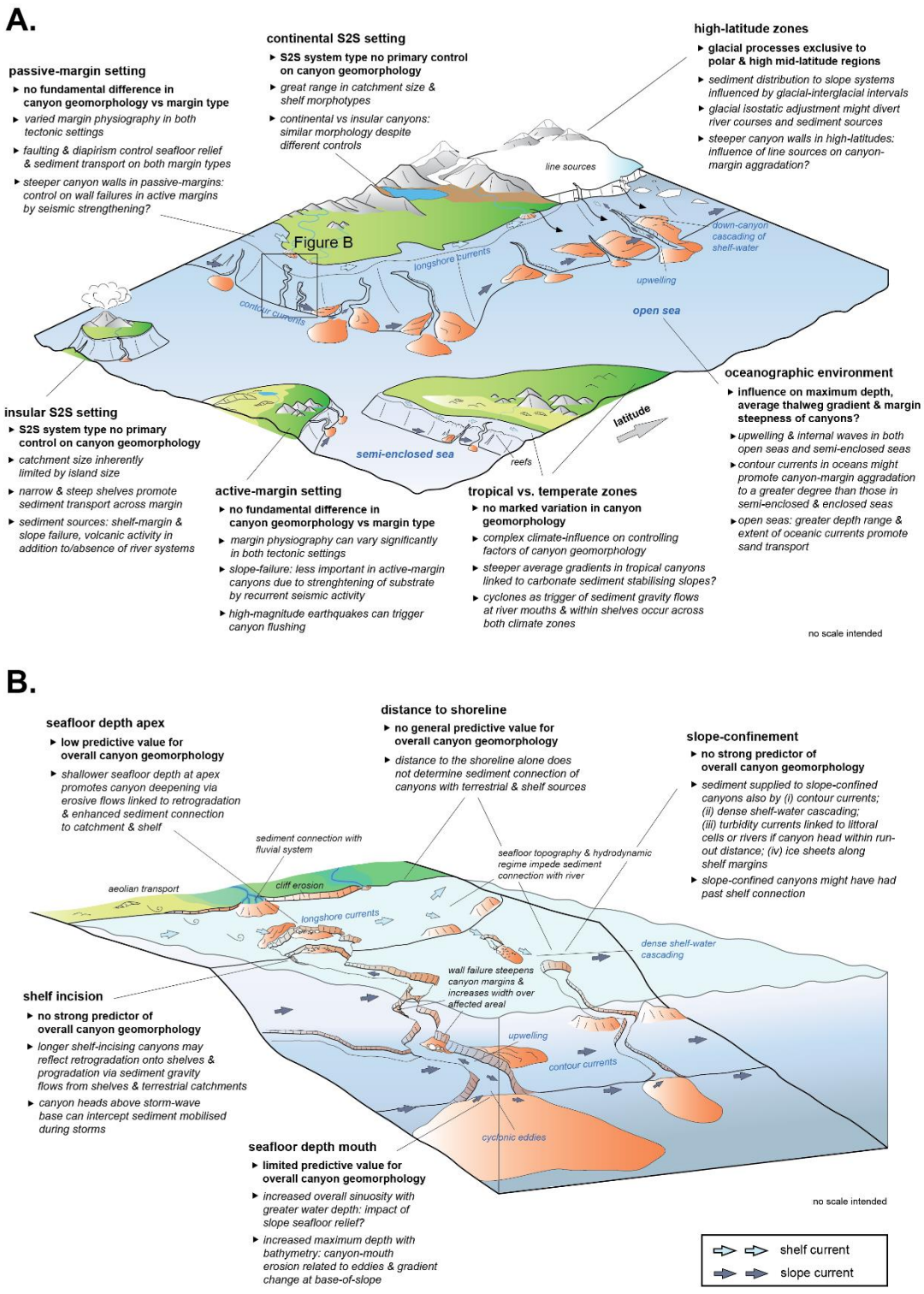

Figure 3.24a&b Schematic diagrams summarising controlling factors of submarine-canyon geomorphology recognised in the literature and whose statistical signature has been evaluated in this study.

4 Tectonic influence on the geomorphology of submarine canyons: implications for deep-water sedimentary systems

4.1 Introduction

As major conduits for the exchange of sediment, organic matter, nutrients, pollutants and water masses across continental margins (e.g. Fildani, 2017; Santora et al., 2018; Maier et al., 2019; Zhong & Peng, 2021), submarine canyons are important components of deep-water environments and of broader source-to-sink (S2S) systems.

Canyon fills and deep-water fans collectively provide a depositional record of the sediment funneled through a connected canyon, and hold valuable information on the long-term evolution of continental margins (e.g. Normark & Carlson, 2003; Hessler & Fildani, 2019). They are more likely preserved when small in size, accommodated on continental crust, and associated with an active-margin setting (e.g. Normark et al., 1993; Normark & Carlson, 2003); this creates bias in the sedimentary record of deep-water systems. As a consequence, insights from ancient systems only provide a selective view on controls on deep-water systems and have limited applicability to modern environments. Moreover, current knowledge of the role of submarine-canyon geomorphology in shaping the configuration of deep-water systems largely relies on insights from a small number of modelling studies based on datasets from passive-margin settings (e.g. Wan et al., 2021) and a small number of comparative global studies with focus on specific aspects of canyon geomorphology (e.g. Normark & Carlson, 2003; Covault et al., 2011a). Furthermore, despite the importance of canyons for the delivery of sediment to deep-water basins, relationships between the geometry of submarine canyons and linked controls have not yet been fully considered in source-to-sink models; previous analyses were limited to the assessment of scaling relationships between canyon morphometric parameters with attributes of terrestrial catchments and continental shelves and slopes, which demonstrate that canyon geomorphology is partially controlled by the configuration of S2S systems (see Chapter 3; e.g. Sømme et al., 2009; Nyberg et al., 2018b; Casalbore et al., 2011).

The quantitative investigation of modern canyons can increase the understanding of the importance of tectonic controls on their

geomorphology, and in turn of the potential role of canyon geomorphology on sediment dispersal to deep-marine sinks. Insights in such relationships may also be useful for the reconstruction and prediction of geometries of deep-water systems and superordinate S2S systems, where these are only partially preserved in outcrop or are partially resolved in surveys of the seafloor and subsurface.

Submarine-canyon geomorphology is governed by multiple environmental factors including their hydrodynamic regime, oceanographic environment, regional climate, and tectonic setting (see Chapter 3; e.g. Harris & Whiteway, 2011; Huang et al., 2014; Puig et al., 2014), which control mechanisms of sediment routeing from terrestrial source areas to marine sinks. In active-margin settings, relatively steep gradients and short transport distances across terrestrial catchments and the adjoining continental shelf promote rapid delivery of solids from the terrestrial hinterland to the deep-marine environment (e.g. Bouma & Scott, 2003; Sømme et al., 2009; Gamberi et al., 2015; Nyberg et al., 2018b; Pierdomenico et al., 2019). In systems with wide shelves along passive margins, sediment routeing to slopes and basin floors is facilitated via shelf channels, shelf-edge deltas and submarine canyons that have cut across the shelf to connect to a river (e.g. Sylvester et al., 2012; Rona et al., 2015).

Some global studies indicate that the overall geomorphology of canyons might not differ fundamentally between tectonically active and passive margins (see Chapter 3; e.g. Harris & Whiteway, 2011). Yet tectonic activity molds the basin topography via its control on the distribution and type of faulting and mass-failures, which have been shown to leave characteristic signatures in the morphology of submarine canyons of active continental margins (e.g. Greene et al., 1991; Chiang & Yu, 2006; Micallef et al., 2014; Corradino et al., 2021; Soutter et al., 2021). Moreover, active margins encompass both convergent and strike-slip tectonic domains, and are characterised by variability in sedimentary basin-morphology and sediment generation, transport and dispersal mechanisms (e.g. Ingersoll, 2012; Ju et al., 2020). Although tectonically active margins host over 50% of submarine canyons globally (Harris & Whiteway, 2011), studies of the genesis and

evolution of submarine canyons associated with active margins are relatively underrepresented in the scientific literature (Micallef et al., 2014).

The aim of this study is to increase understanding of the influence of tectonic setting on the geomorphology of submarine canyons. To achieve this, the geomorphology of 294 modern canyons has been investigated in their S2S context, considering parameters describing their physiographic and tectonic setting. Specific research objectives are as follows: (i) to quantitatively characterise the variability in selected canyon geomorphologic parameters across active (both convergent and strike-slip) and passive continental-margin types; (ii) to evaluate scaling relationships in canyon morphometry and of individual canyon morphometric parameters with attributes describing their environmental setting, discriminating between active and passive margins; (iii) to assess the characteristics of canyon-associated terrestrial catchments, shelves and slopes in active- versus passive-margin settings, and their scaling relationships.

4.2 Dataset and methods

4.2.1 Dataset

For the present study, the database used in Chapter 3 has been extended by defining and characterizing the plate-boundary type for submarine canyons along active margins. To facilitate the analyses, twelve new submarine canyons were added with six canyons from a newly included case study (case study 44, Haida Gwaii canyons, SW Canada; Harris et al., 2014a). In addition, case studies 36 and 39 were extended by four and two canyon elements, respectively, compared to Dataset 1 in Chapter 3. The data presented in this article are made available in the Supplementary Material.

Data on the geomorphology of the canyons have been extracted from high-resolution seabed and subsurface studies from 136 peer-reviewed publications and from open-source worldwide bathymetry (GEBCO 2019 NOAA NCEI Visualization; Google Earth). The dataset is organised as 97 individual case studies, with each case corresponding to one or several

submarine canyons from a geographic location or region, detailed as a self-contained study by the original authors (Fig. 4.1a & Tab. 4.1).

A.

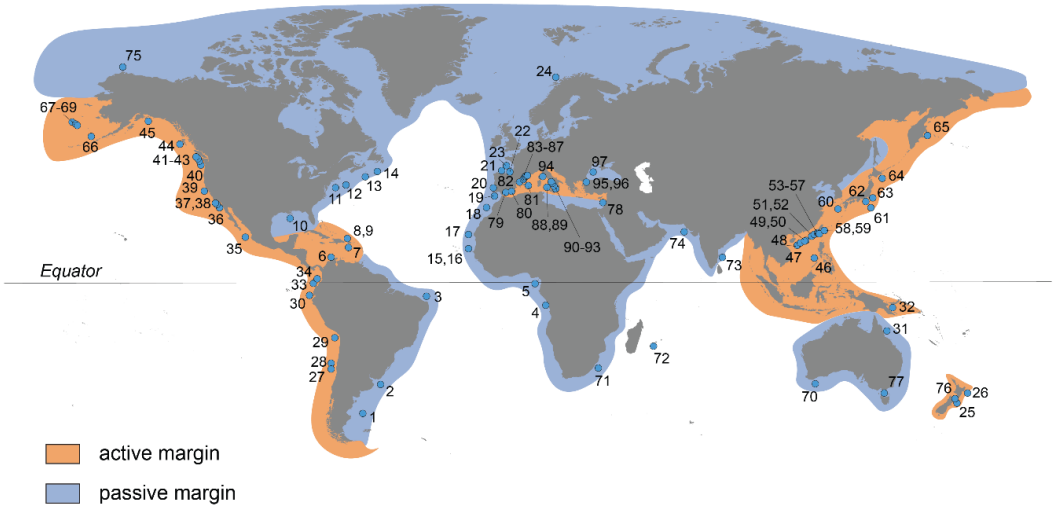

B.

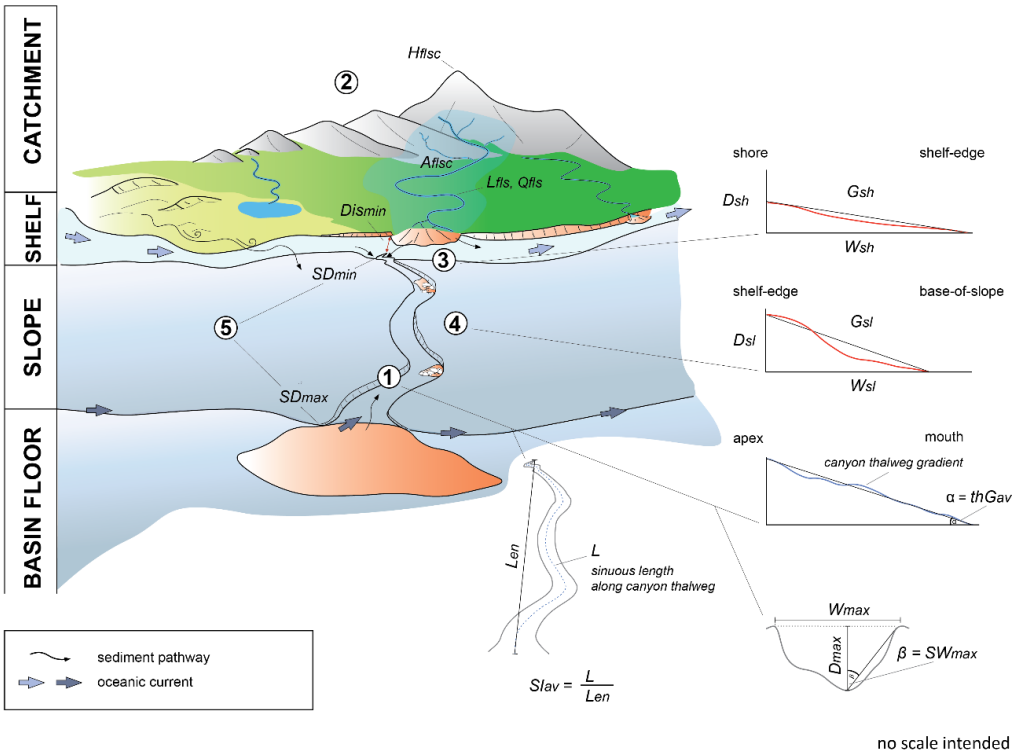

Figure 4.1a&b A. Overview map of the distribution of the 97 case studies and their associated margin-type setting. Continental-margin classification after Harris et al. (2014b) (World map from freevectormaps.com). B. Key parameters investigated in the study: 1. Submarine canyon: L = canyon length along thalweg; L_{en} = canyon length along endpoints; W_{max} = maximum canyon width; D_{max} = maximum canyon depth; SI_{av} = average canyon sinuosity index; thG_{av} = average canyon thalweg gradient; SW_{max} = maximum canyon sidewall steepness. 2. Terrestrial catchment: L_{fls} = fluvial system length; Q_{fls} = average annual fluvial discharge; A_{flsc} = catchment size; H_{flsc} = maximum catchment elevation. 3. Shelf configuration: W_{sh} = shelf width; D_{sh} = shelf-break depth; G_{sh} = average shelf gradient. 4. Slope configuration: W_{sl} = slope width; D_{sl} = slope-break depth; G_{sl} = average slope gradient. 5. Canyon-physiographic setting: SD_{min} = seafloor depth at canyon apex; SD_{max} = seafloor depth at canyon mouth. Dis_{min} = minimum distance of canyon to shoreline.

ID	Case study	No. of canyons	Oceanic region	Reference(s)
1	Patagonia canyons, SE Argentina	8	South Atlantic Ocean	*Lastras et al., 2011a*
2	Mar del Plata Canyon, E Argentina	1	South Atlantic Ocean	*Krastel et al., 2011; Warratz et al., 2019*
3	Potiguar Basin canyons, NE Brazil	14	South Atlantic Ocean	*de Almeida et al., 2015*
4	Congo Canyon, W Democratic Republic of Congo	1	South Atlantic Ocean	*Babonneau et al., 2002; Ferry et al., 2004*
5	Avon & Mahin canyons, SW Nigeria	2	South Atlantic Ocean	*Jimoh et al., 2018*
6	Aguja Canyon, N Colombia	1	North Atlantic Ocean (Caribbean Sea)	*Restrepo-Correa & Ojeda, 2010*
7	Guayanilla canyon system, S Puerto Rico	4	North Atlantic Ocean (Caribbean Sea)	*Trumbull & Garrison, 1973*
8	Arecibo & Quebradillas canyons, NW Puerto Rico	2	North Atlantic Ocean	*Gardner et al., 1980*
9	Mona Canyon, NW Puerto Rico	1	North Atlantic Ocean	*Mondziel et al., 2010*
10	Mississippi Canyon, S USA	1	North Atlantic Ocean (Gulf of Mexico)	*Coleman et al., 1982*
11	Hudson Canyon, NE USA	1	North Atlantic Ocean	*Rona et al., 2015*
12	Lydonia & Oceanographer canyons, NE USA	2	North Atlantic Ocean	*Valentine et al., 1980*

13	Logan Canyon, SE Canada	1	North Atlantic Ocean	*Li et al., 2019*
14	SW Grand Banks Slope canyons, SE Canada	3	North Atlantic Ocean	*Armitage et al., 2010*
15	Dakar Canyon, W Senegal	1	North Atlantic Ocean	*Pierau et al., 2010, 2011*
16	Cayar Canyon, W Senegal	1	North Atlantic Ocean	*Dietz et al., 1968*
17	Timiris Canyon, NW Mauritania	1	North Atlantic Ocean	*Krastel et al., 2004; Antobreh & Krastel, 2006*
18	Agadir Canyon	1	North Atlantic Ocean	*Ercilla et al., 1998; Wynn et al., 2002*
19	Faro & Portimao canyons, SW Portugal	2	North Atlantic Ocean (Gulf of Cadiz)	*Mulder et al., 2006*
20	Nazaré, Cascais & Setubal-Lisbon canyons, W Portugal	4	North Atlantic Ocean	*Arzola et al., 2008; Lastras et al., 2009; Allin et al., 2016*
21	Aviles Canyon system & Navia canyon, N Spain	5	North Atlantic Ocean (Bay of Biscay)	*Goméz-Ballesteros et al., 2014*
22	Capbreton Canyon, SW France	1	North Atlantic Ocean (Bay of Biscay)	*Mazières et al., 2014*
23	Audierne & Blackmud canyons, SW France	2	North Atlantic Ocean (Bay of Biscay)	*Mulder et al., 2012*
24	Lofoten-Vesterålen canyons (incl. Andøya Canyon), NW Norway	15	North Atlantic Ocean	*Rise et al., 2013*
25	Kaikoura Canyon, E New Zealand	1	South Pacific Ocean	*Lewis & Barnes, 1999*
26	Lachlan Canyon, NE New Zealand	1	South Pacific Ocean	*Walsh et al., 2007*
27	Biobío Canyon system, SW Chile	2	South Pacific Ocean	*Bernhardt et al., 2015*
28	San Antonio Canyon, NW Chile	1	South Pacific Ocean	*Hagen et al., 1996; Laursen & Normark, 2002*
29	E Arequipa Basin canyons, NW Chile	3	South Pacific Ocean	*Hagen et al., 1994*
30	Guayaquil & Santa Elena canyons, NW Equador	2	South Pacific Ocean	*Michaud et al., 2015*

31	N Great Barrier Reef canyons, NE Australia	15	South Pacific Ocean (Coral Sea)	*Puga-Bernabéu et al., 2011*
32	Solomon Sea canyons, E & SE Papua New Guinea	8	South Pacific Ocean (Solomon Sea)	*Davies et al., 1987; Galewsky & Silver, 1997*
33	Esmeraldas Canyon, NW Ecuador	1	North Pacific Ocean	*Michaud et al., 2015*
34	Mira & Patia canyons, SW Colombia	2	North Pacific Ocean	*Ratzov et al., 2012*
35	Ipala Canyon, W Mexico	1	North Pacific Ocean (South China Sea)	*Urías Espinosa et al., 2016*
36	La Jolla, Scripps, Sur, Carmel, Noyo & Eel canyons, SW USA	6	North Pacific Ocean	*Le Dantec et al., 2010; Paull et al., 2013*
37	Redondo, Santa Monica & Dume canyons, SW USA	3	North Pacific Ocean	*Gardner et al., 2003; Tubau et al., 2015*
38	Mugu & Hueneme canyons, SW USA	2	North Pacific Ocean	*Piper et al., 1999*
39	Monterey, Soquel, Año Nuevo & Cabrillo canyons, SW USA	4	North Pacific Ocean	*Greene et al., 2002; Xu & Noble, 2009*
40	Astoria Canyon, NW USA	1	North Pacific Ocean	*Hickey, 1997; Bosley et al., 2004*
41	Quinault Canyon, NW USA	1	North Pacific Ocean	*Baker & Hickey, 1986; Carson et al., 1986*
42	Juan de Fuca Canyon, NW USA	1	North Pacific Ocean (heads in the Juan de Fuca Strait)	*Alford & MacCready, 2014*
43	Barkley Canyon, SW Canada	1	North Pacific Ocean	*Allen et al., 2001*
44	Haida Gwaii canyons, SW Canada	6	North Pacific Ocean	*Harris et al., 2014a*
45	Tarr Canyon, NW USA	1	North Pacific Ocean (Gulf of Alaska)	*Carlson et al., 1990*
46	North Palawan Canyon, S China	1	North Pacific Ocean (South China Sea)	*Yin et al., 2018*
47	Modern Central Canyon, S China	1	North Pacific Ocean (South China Sea)	*Su et al., 2015*
48	3 canyons & 4 gullies, S China	3 (4)	North Pacific Ocean (South China Sea)	*Chen et al., 2017*

49	Pearl River Mouth Basin canyons, S China	17	North Pacific Ocean (South China Sea)	*Han et al., 2010; Su et al., 2020*
50	Zhujiang/Pearl River Canyon, S China	1	North Pacific Ocean (South China Sea)	*Han et al., 2010; Ding et al., 2013*
51	Dongsha Canyon, S China	1	North Pacific Ocean (South China Sea)	*Yin et al., 2015*
52	Taiwan Canyon, SW Taiwan	1	North Pacific Ocean (South China Sea)	*Xu et al., 2014*
53	Hongtsai Canyon, SW Taiwan	1	North Pacific Ocean (South China Sea)	*Yu & Chiang, 1995*
54	Fangliao Canyon, SW Taiwan	1	North Pacific Ocean (South China Sea)	*Yu & Lu, 1995; Chiang et al., 2012*
55	Kaoping Canyon, SW Taiwan	1	North Pacific Ocean (South China Sea)	*Chiang & Yu, 2006; Liu et al., 2016*
56	Kaohsiung Canyon, SW Taiwan	1	North Pacific Ocean (South China Sea)	*Yu et al., 1992*
57	Penghu Canyon, SW Taiwan	1	North Pacific Ocean (South China Sea)	*Yu & Chang, 2002; Hsiung & Yu, 2011; Su et al., 2015*
58	Taitung Canyon, SE Taiwan	1	North Pacific Ocean (Philippine Sea)	*Schnürle et al., 1998*
59	Hualien Canyon, SE Taiwan	1	North Pacific Ocean (Philippine Sea)	*Hsiung et al., 2017*
60	Goto Canyon, SW Japan	1	North Pacific Ocean (East China Sea)	*Oiwane et al., 2011*
61	Aoga Shima Canyon, SE Japan	1	North Pacific Ocean (Philippine Sea)	*Klaus & Taylor, 1991*
62	Tenryu Canyon, SE Japan	1	North Pacific Ocean	*Soh & Tokuyama, 2002*
63	Boso Canyon, SE Japan	1	North Pacific Ocean	*Soh et al., 1990*
64	Kushiro Canyon, NE Japan	1	North Pacific Ocean	*Noda et al., 2008; Noda & Tuzino, 2010; Tuzino & Noda, 2010*
65	Submarine canyons of Kamchatka, NE Russia	7	North Pacific Ocean	*Gnibidenko & Svarichevskaya, 1984*
66	Bering Canyon, Bering Sea	1	North Pacific Ocean (Bering Sea)	*Carlson & Karl, 1988; Harris & Whiteway, 2011*

67	Zhemchug, Pervenets & Navarin canyons, Bering Sea	3	North Pacific Ocean (Bering Sea)	*Carlson & Karl, 1988*
68	Middle canyon system, Bering Sea	2	North Pacific Ocean (Bering Sea)	*Carlson & Karl, 1984, 1988*
69	St. Matthew canyon system, Bering Sea	2	North Pacific Ocean (Bering Sea)	*Carlson & Karl, 1984, 1988*
70	Albany canyons, SW Australia	11	Indian Ocean	*Exon et al., 2005*
71	Tugela Canyon, E South Africa	1	Indian Ocean	*Wiles et al., 2013*
72	Saint-Etienne & Pierrefonds canyons, SW La Reunion	2	Indian Ocean	*Babonneau et al., 2013*
73	Palar Basin canyons, E India	20	Indian Ocean	*Susanth et al., 2021*
74	Indus Canyon, SE Pakistan	1	Indian Ocean (Arabian Sea)	*Von Rad & Tahir, 1997; Salmanidou et al., 2019*
75	Barrow Canyon, NW USA	1	Arctic Ocean	*Eittreim et al., 1982; Pisareva et al., 2019*
76	Cook Strait canyons, E New Zealand	9	Cook Strait	*Mountjoy et al., 2009, 2014; Micallef et al., 2014*
77	Bass canyon system, SE Australia	10	Bass Strait	*Mitchell et al., 2007*
78	Akhviz & Sour canyons, NW Israel	2	Mediterranean Sea	*Mart, 1989; Almagor, 1993*
79	Almeria, Western, Eastern & Guadiaro canyons, S Spain	4	Mediterranean Sea	*Alonso & Ercilla, 2003; Palanques et al., 2005*
80	Alías-Almanzora canyon system, SE Spain	4	Mediterranean Sea	*Puig et al., 2017*
81	Menorca Canyon, SW Menorca, Balearic Islands	1	Mediterranean Sea	*Acosta et al., 2002*
82	Orpesa Canyon, NE Spain	1	Mediterranean Sea	*Amblas et al., 2012*
83	Foix Canyon system, NE Spain	3	Mediterranean Sea	*Puig et al., 2000; Tubau et al., 2013*
84	Blanes Canyon, SE France	1	Mediterranean Sea	*Lastras et al., 2011b*

85	Palamós/La Fonera Canyon, NE Spain	1	Mediterranean Sea	*Martin et al., 2006; Palanques et al., 2006b; Lastras et al., 2011b*
86	Cap de Creus Canyon, NE Spain	1	Mediterranean Sea	*Baztan et al., 2005; Lastras et al., 2007, 2011b*
87	Bourcart Canyon, SE France	1	Mediterranean Sea	*Mauffrey et al., 2015*
88	Gulf of Palermo canyons, NW Sicily, Italy	7	Mediterranean Sea	*Lo Iacono et al., 2011, 2014*
89	Gulf of Castellammare canyons, NW Sicily, Italy	2	Mediterranean Sea	*Lo Iacono et al., 2014*
90	Messina Canyon, NE Sicily, Italy	1	Mediterranean Sea	*Ridente et al., 2014*
91	Petrace, Gioia & Mesima canyons, SW Italy	3	Mediterranean Sea	*Pierdomenico et al., 2016, Casalbore et al., 2018*
92	Luna & Infreschi canyons, SW Italy	2	Mediterranean Sea	*Budillon et al., 2011*
93	Dohrn Canyon, SW Italy	1	Mediterranean Sea	*Milia, 2000*
94	Golo system canyons, NE Corsica, France	4 (2)	Mediterranean Sea	*Gervais et al., 2004, 2006*
95	North İmralı Canyon, NW Turkey	1	Sea of Marmara	*Vardar, 2019*
96	Sarköy & Izmit canyons, NW Turkey	2	Sea of Marmara	*Çağatay et al., 2015*
97	Danube/Viteaz Canyon, SE Romania	1	Black Sea	*Popescu et al., 2004*

Table 4.1 Summary of the 97 case studies considered in this study. The numbers of canyons reported in brackets indicate channel forms that were termed as ‘submarine gullies’ by the authors of the original data sources.

4.2.2 Methods

Data on individual canyon morphometric parameters, the physiographic setting of the canyon and characteristics of its associated S2S system have

been coded in the Deep-Marine Architecture Knowledge Store (DMAKS; Cullis et al., 2019), a relational database storing data on characteristics of deep-water sedimentary systems and their environmental settings (see Cullis et al., 2019).

4.2.2.1 Canyon definition

In this study, a submarine canyon is defined as a throughgoing erosional channelform incised into the continental slope; this definition does not therefore consider ancillary criteria that are sometimes used by some authors, such as their origin or minimum size (cf. Harris & Whiteway, 2011). The general definition used herein encompasses smaller channelforms, which are sometimes referred to as ‘submarine gullies’ (e.g. Gervais et al., 2006), ‘submarine gulleys’ (e.g. Normark et al., 2009) or ‘potential submarine canyons’ (e.g. de Almeida et al., 2015), and which might represent forms at the early stage of development of a canyon (e.g. Nelson et al., 2011; Sanchez et al., 2012b; Amblas et al., 2017 and references therein). The terms “canyon” and “gully” (or “gulley”) are not clearly distinguished in terms of size in the wider literature, and both terms are used when referring to smaller channelforms. By also including the presence of overbank deposits/levees and u-shaped channel cross sections in the broad definition of a submarine canyon in this study, the distal parts of some channelforms defined as submarine canyons might relate to ‘submarine channels’ within the region of the lower slope and continental rise as defined by other authors (e.g. Covault et al., 2011a; Hodgson et al., 2022).

4.2.2.2 Study parameters

Canyon morphometrics

Canyon geomorphology has been assessed based on the following morphometric parameters: streamwise canyon length, maximum and average canyon width and depth, canyon sinuosity, average canyon thalweg gradient, and maximum canyon sidewall steepness. Values reported in textual form in the literature sources have only been considered where underpinned by observations on bathymetric surveys with full coverage of the canyon.

Physiographic setting

The physiographic setting of the studied canyons has been characterised by means of attributes describing the bathymetry of the canyon apex and mouth, and the minimum distance of the canyon to the shoreline.

Source-to-sink system (S2S) attributes

For canyons with a present or past sediment connection with a fluvial system, the length and average annual water discharge of the river have been recorded, as well as the size and maximum elevation of its catchment. In cases where canyons are linked with several rivers, the sum of the length of the individual rivers, the sum of their mean annual fluvial discharges and catchment areas, and the maximum elevation of the highest peak in the combined catchments have been recorded; this enables comparison with canyons fed by single fluvial systems. The geometric configuration of the continental margin at the canyon location has been characterised in terms of average gradient of shelf and slope, and depth of shelf break and base of slope below present-day mean sea level.

Tectonic setting

Canyon-hosting continental margins have been classified as active or passive following the classification by Harris et al. (2014b) (see Fig. 4.1a). Active margins have been further differentiated based on the plate-boundary type with which they are associated, as convergent, transform and complex margins. The term ‘complex’ is used here to refer to settings that involve more than one type of plate boundary and sense of motion (e.g. convergent margins with a transform component).

Definitions of the studied parameters are provided in Table 4.2 and illustrated in Figure 4.1b.

Study parameter	**Definition**
Canyon morphometrics	
L [km]**	Streamwise length of the canyon between canyon apex and canyon mouth as measured along the canyon thalweg
W_{max} [km]**	Maximum width of the canyon orthogonal to the canyon length

W_{av} [km]*	Average canyon width over the length of the entire canyon
D_{max} [m]*	Maximum depth of the canyon, i.e. depth of the canyon thalweg relative to the elevation of the canyon margins
D_{av} [m]*	Average canyon thalweg depth over the length of the entire canyon
SI_{av} [-]**	Average canyon sinuosity index, i.e. ratio between the sinuous canyon length measured along its thalweg and the straight distance between canyon apex and canyon mouth
thG_{av} [°]**	Average canyon thalweg gradient, evaluated between canyon apex and canyon mouth
SW_{max} [°]*	Maximum canyon-sidewall steepness, representing the maximum value of gradient between canyon rim and canyon bottom evaluated along the entire length of the canyon
Physiographic setting	
Dis_{min} [km]**	Minimum distance between the canyon and the shoreline
SD_{min} [m]**	Seafloor depth at the top of the canyon
SD_{max} [m]**	Seafloor depth at the mouth of the canyon
Canyon terrestrial catchment	
L_{fls} [km]**	Length of the river with a present-day or previous connection with the canyon, from headwater to river mouth; for canyons connected with several rivers the cumulative length has been considered
Q_{fls} [km^3/yr]*	Mean annual discharge of the fluvial system; for canyons connected with several rivers the cumulative mean annual discharge has been considered
A_{flsc} [km^2]*	Size of the catchment associated with the fluvial system; for canyons connected with several rivers the cumulative catchment area size has been considered
H_{flsc} [m]**	Maximum elevation of the catchment associated with the fluvial system; for canyons connected with several rivers, the elevation of the highest peak in the combined catchments has been considered
Continental shelf	
W_{sh} [km]**	Width of the shelf at the canyon location
G_{sh} [°]**	Average shelf gradient at the canyon location
D_{sh} [m]**	Shelf-break depth at the canyon where the shelf edge is intact and not eroded into by the latter; for

	shelf edges displaying some degree of variability in their bathymetry the maximum depth of the shelf break has been chosen
Continental slope	
W_{sl} [km]**	Width of the slope at the canyon location
G_{sl} [°]**	Average slope gradient between the shelf break and the slope break
D_{sl} [m]**	Slope-break depth at the canyon
Other parameters	
Continental-margin type	For canyons located along continental margins, including canyons associated with islands: (i) active margin, including transform margins; (ii) passive margin (classification after Figure 2 of Harris et al., 2014b)
Active-margin plate-boundary type	Based on the type of plate boundary, active margins are distinguished into (i) convergent, (ii) transform, and (iii) complex margins. The latter category includes settings which involve more than one plate boundary, and margins which display an additional direction of motion, e.g. convergent margins with a transform component

Table 4.2 Overview of the parameters investigated in the study and their definitions.

4.2.3 Statistical analyses

Different types of statistical analyses have been conducted to evaluate scaling relationships within submarine canyons, and between canyon geomorphology and attributes of its environment as a function of the tectonic setting.

Descriptive statistics: Frequency distributions of the studied canyon morphometric parameters have been summarised in terms of minimum, maximum, mean and median values, to reveal differences across margin types and active-margin plate-boundary types.

Hypothesis testing: Hypothesis testing has been used to evaluate the statistical significance of differences in mean values of canyon morphometric parameters across classes of canyons for different tectonic settings and attributes of the source-to-sink system along active and passive margins.

The Welch's two sample t-test (only referred to as 't-test' hereafter) has been used for comparisons between active and passive margins; Welch's ANOVA (only 'ANOVA' hereafter) has been used for comparisons between convergent, transform and complex plate-boundary settings of active margins. The chosen tests allow testing of datasets with non-equal variances. For skewed frequency distributions, a logarithmic variable transformation has been conducted prior to the analyses. In these instances, where differences in mean values are reported in the text, they refer to the transformed variables and not the variables themselves. To enable a pairwise comparison of mean values between the three different active-margin settings, ANOVA has been complemented with Games-Howell post-hoc tests. Test statistics (t-test: T-value; ANOVA: F-value; Games-Howell: T-value), p-values and degrees of freedom (DF) are presented for all tests below each individual figure. To limit the number of false positives, the confidence interval has been set at 99%, with results where p-values are ≤0.01 treated as statistically significant.

Correlation analysis: Correlation analyses have been undertaken to assess pairwise scaling relationships between study parameters. Correlation coefficients quantify the sign and strength of correlation: the Pearson's correlation coefficient (r) describes linear relationships, whereas Spearman's rank correlation coefficient (rs) describes monotonic relationships. The statistical significance of a correlation between two variables is indicated by p-values. A confidence interval of 99% is employed to indicate significant correlations.

4.2.4 Limitations of the study

Data analyses and interpretations are subject to some limitations, including the following:

(1) Metastudies might inherit unidentified data errors from the original literature data sources. This has been minimised by exclusively considering data from peer-reviewed publications and government agency sources.

(2) Although care has been taken to avoid potential bias in the geographic distribution of case studies (see Matos et al., 2018), some geographic bias may exist for canyons from transform margins specifically, which are only considered for two regions (offshore California, Sea of Marmara), both located at temperate latitudes.
(3) Some statistical analyses are based on datasets of limited size. This is the case for data on morphometric parameters of canyons from transform and complex settings, but also for pairs of variables whose correlation is evaluated. Correlation analyses are typically only considered and discussed where the number of observations (N) is equal to or larger than 15, making it explicit when N<15.
(4) Some relationships might represent covariance related to factors that were not assessed in this study, but which may influence canyon geomorphology, such as lithology (e.g. Smith et al., 2017) and rate and direction of relative sea-level changes (e.g. Covault et al., 2011b), among others.

4.3 Results

4.3.1 Scaling between canyon morphometric parameters and the tectonic setting

4.3.1.1 Continental-margin type

Canyon dimensions and aspect ratios

Comparisons of the maximum and average dimensions of submarine canyons along tectonically active and passive margins demonstrate how canyon geometry varies between the two canyon groups.

Canyons in active margins are, on average, longer than those along passive margins – by a factor 1.23 – but the difference in mean is not statistically significant. The longest canyon in the study is associated with a passive margin, but lengths of more than 400 km occur in both groups (Fig. 4.2a). The deepest and widest canyons are seen on active margins. However, these values of depth and width represent individual outliers; ranges in maximum widths and depths are similar for the vast majority of studied

canyons in both margin types, and their mean values are very similar (Figs. 4.2b&d).

Canyons in the two margin types exhibit average widths within the same range. On average, mean canyon width is 1.37 times greater in studied active-margin examples, which show a narrower range in values than their counterparts from passive margins (Fig. 4.2c). However, average-width data relating to canyons from an active-margin setting are associated with two case studies only, both from the South China Sea, whereas average width data for canyons in passive-margin settings are derived from examples from only three geographic regions; therefore, these findings need to be corroborated by additional data in future research. In contrast, the mean average canyon depth is significantly greater for passive margins, by a factor 1.6. The maximum average depth of passive-margin canyons (594 m) is notably higher than that of active-margin ones (400 m) (Fig. 4.2e).

Despite a greater range in aspect ratios of maximum canyon dimensions for examples from active margins, the mean values of streamwise length-to-maximum width (lwmax) (Fig. 4.3a) and maximum width-to-maximum depth (wdmax) (Fig. 4.3b) ratios are similar for the two margin types. In contrast, a statistically significant difference in the mean value of length-to-maximum depth (ldmax) ratio (Fig. 4.3c) is seen; this parameter is on average 2.66 times larger for active-margin canyons.

Average canyon sinuosity, average canyon thalweg gradient and maximum canyon sidewall steepness

The studied active-margin canyons show a greater range in average canyon sinuosity than passive-margin ones, but mean average canyon sinuosity is equally low in both margin types, ~1.1 (Fig. 4.2f).

The range in average canyon thalweg gradient is very similar for the two margin types; thalwegs are, on average, steeper in the studied passive-margin examples to a statistically significant level (Fig. 4.2g).

Canyons situated in passive settings have steeper canyon sidewalls compared to those in tectonically active settings. On average, the maximum

sidewall gradient varies significantly between the two canyon groups, and is larger by a factor 1.56 for passive-margin examples (Fig. 4.2h).

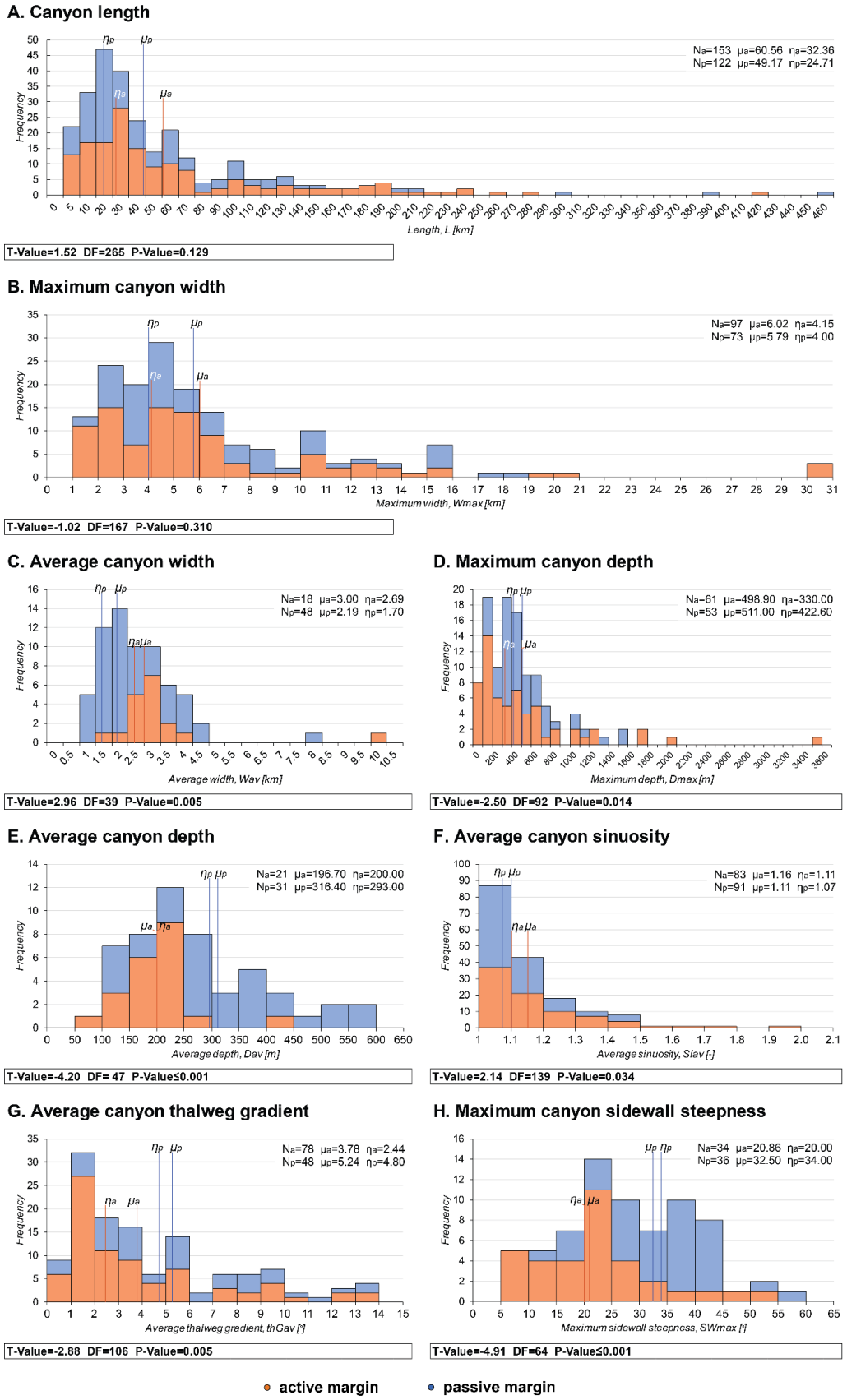

Figure 4.2a-h Stacked histograms of morphometric values in studied submarine canyons in active (a) vs. passive (p) margins. N = number of readings; μ = mean value; η = median value; DF = degrees of freedom.

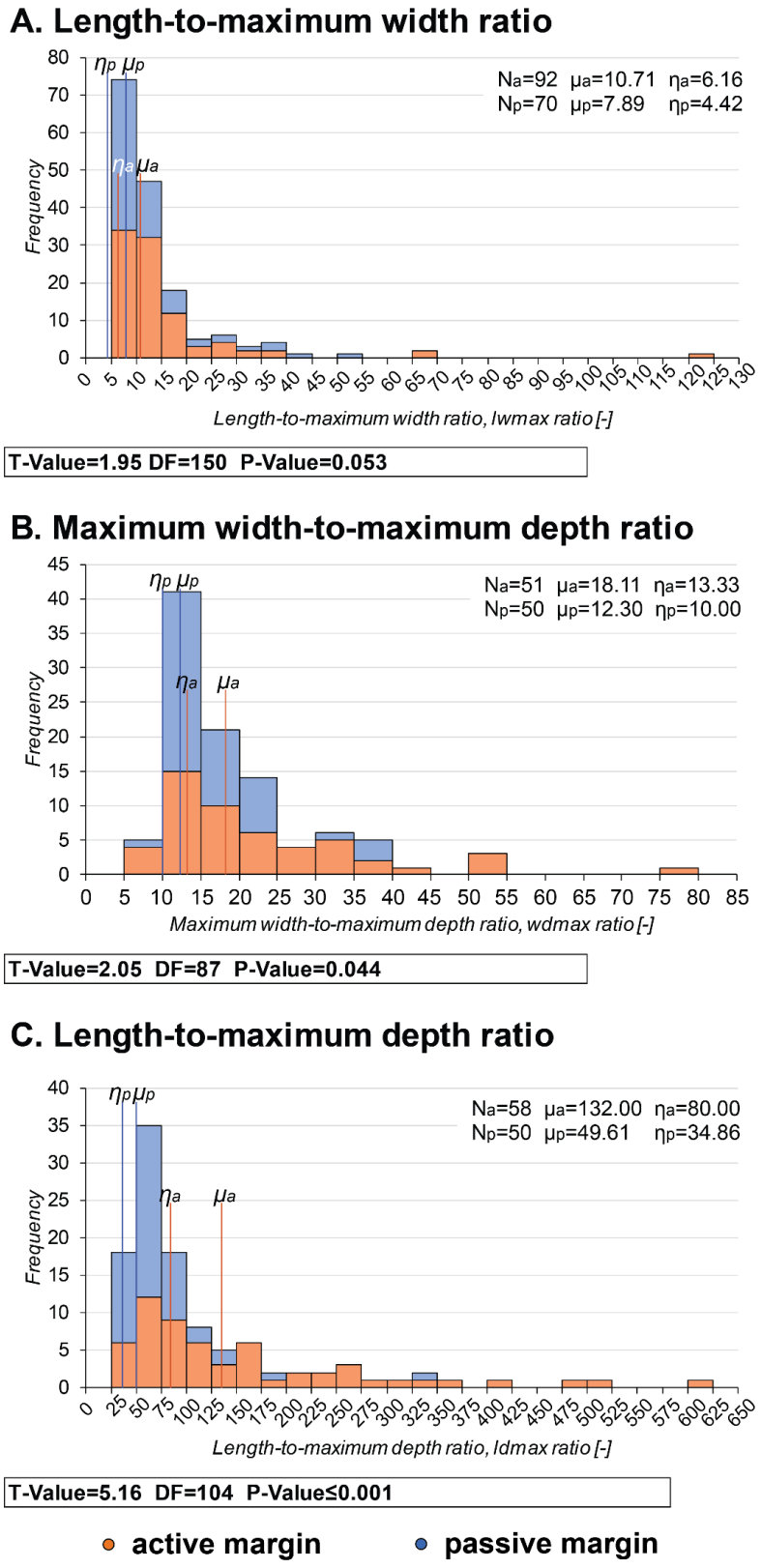

Figure 4.3a-c Stacked histograms of aspect ratios in studied submarine canyons in active (a) vs. passive (p) margins. N = number of readings; μ = mean value; η = median value; DF = degrees of freedom.

4.3.1.2 Active-margin plate-boundary type

Canyon dimensions and aspect ratios

Canyons in convergent settings display the highest maximum values of length, maximum width and depth. Yet, on average, maximum canyon dimensions are greater in canyons located at complex plate boundaries (Figs. 4.4a-c). The maximum width (Fig. 4.4b) and depth (Fig. 4.4c) of canyons from this type of setting are on average significantly higher than that of canyons in convergent settings, by a factor of 1.77 and 1.29, respectively.

The length (Fig. 4.4a) and maximum width (Fig. 4.4b) of canyons along transform plate boundaries are, on average, lower than those of canyons in the other two settings. The mean canyon length does not vary significantly across the three active-margin settings (Fig. 4.4a). Instead, the mean maximum canyon width differs at a statistically significant level between transform and complex settings (Fig. 4.4b), but this variable could only be constrained for twelve transform-setting canyons. Although data on maximum canyon depth for canyons along transform plate boundaries could only be derived for four examples, the data demonstrate that the depth range of canyons in such settings is similar to that of canyons in convergent settings, and larger than that of canyons from complex settings (Fig. 4.4c).

Mean aspect ratios are similar across all three active-margin settings, but relatively few data are available for canyons in transform- and complex-margin settings. Aspect ratios based on maximum canyon dimensions for canyons in convergent settings are highly variable and display the greatest range in values (Fig. 4.4g-i).

Average canyon sinuosity, the average canyon thalweg gradient and maximum canyon sidewall steepness

Frequency distributions of average canyon sinuosity for convergent, transform and complex plate boundaries exhibit similar mean and median values. Based on results of Welch’s ANOVA and Games-Howell post-hoc

tests, no significant differences are seen for average values across the different active-margin plate-boundary types (Fig. 4.4d).

Submarine canyons in complex settings exhibit a greater range in values of the average canyon thalweg gradient than those in convergent margins, but on average, the overall thalweg gradient is only 1.18 times steeper, and not significantly different (Fig. 4.4e).

Canyons in convergent settings display a great range in maximum sidewall steepness, which is on average 20.3°. There exists insufficient data on margin steepness in canyons located in transform and complex settings to conduct meaningful analyses on these, but the data available demonstrate that canyons in these settings can reach gradients of 30.0° and 28.5°, respectively; these values are higher than those recorded in the majority of convergent-margin canyons (Fig. 4.4f).

A. Canyon length

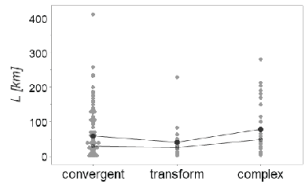

	N	min	mean	StDev	median	max
conv.	108	2.00	59.00	68.47	29.09	411.00
trans.	17	2.50	40.90	52.80	25.10	229.70
comp.	28	3.90	78.50	78.20	48.90	279.70

Welch's ANOVA
F-Value= 1.01 DF Num=2 DF Den=36.7576 P-Value=0.373

Games-Howell

	Dmean	SE	T-Value	adjusted P-Value
conv. vs trans.	-0.100	0.119	-0.84	0.682
conv. vs comp.	0.118	0.119	1.00	0.584
comp. vs trans.	0.218	0.152	1.43	0.335

B. Maximum canyon width

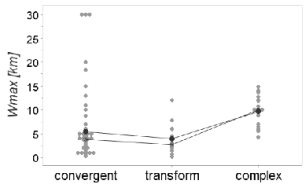

	N	min	mean	StDev	median	max
conv.	67	0.25	5.42	6.60	3.83	30.00
trans.	12	0.15	3.98	3.46	2.73	12.00
comp.	18	4.30	9.62	3.21	10.00	14.80

Welch's ANOVA
F-Value=25.72 DF Num=2 DF Den=27.0868 P-Value≤0.001

Games-Howell

	Dmean	SE	T-Value	adjusted P-Value
conv. vs trans.	-0.124	0.158	-0.78	0.718
conv. vs comp.	0.4356	0.0647	6.73	≤0.001
comp. vs trans.	0.560	0.154	3.64	0.008

C. Maximum canyon depth

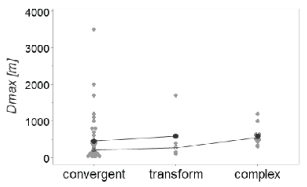

	N	min	mean	StDev	median	max
conv.	43	35.00	459.60	647.90	210.00	3500.00
trans.	4	110.00	588.00	752.00	270.00	1700.00
comp.	15	310.00	594.30	240.50	555.00	1200.00

Welch's ANOVA
F-Value=8.50 DF Num=2 DF Den=7.84612 P-Value=0.011

Games-Howell

	Dmean	SE	T-Value	adjusted P-Value
conv. vs trans.	0.133	0.278	0.48	0.886
conv. vs comp.	0.3686	0.0865	4.26	≤0.001
comp. vs trans.	0.236	0.271	0.87	0.690

D. Average canyon sinuosity

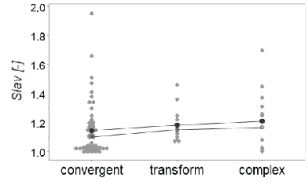

	N	min	mean	StDev	median	max
conv.	58	1.00	1.14	0.18	1.10	1.95
trans.	13	1.07	1.18	0.12	1.15	1.46
comp.	12	1.00	1.21	0.22	1.17	1.70

Welch's ANOVA
F-Value=0.94 DF Num=2 DF Den=22.2231 P-Value=0.405

Games-Howell

	Dmean	SE	T-Value	adjusted P-Value
conv. vs trans.	0.0163	0.0139	1.18	0.477
conv. vs comp.	0.0222	0.0231	0.96	0.613
comp. vs trans.	0.0059	0.0245	0.24	0.969

E. Average canyon thalweg gradient

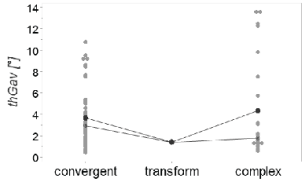

	N	min	mean	StDev	median	max
conv.	52	0.40	3.67	2.63	2.93	10.77
trans.	3	1.30	1.39	0.10	1.38	1.50
comp.	23	0.60	4.34	4.65	1.77	13.60

Welch's ANOVA
F-Value=21.66 DF Num=2 DF Den=37.9576 P-Value≤0.001

Games-Howell

	Dmean	SE	T-Value	adjusted P-Value
conv. vs trans.	-0.3078	0.0498	-6.18	≤0.001
conv. vs comp.	-0.039	0.103	-0.38	0.924
comp. vs trans.	0.2686	0.0943	2.85	0.024

F. Maximum canyon sidewall steepness

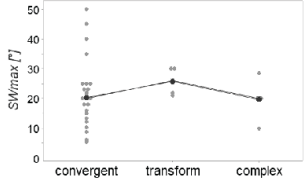

	N	min	mean	StDev	median	max
conv.	26	5.40	20.30	11.75	20.00	50.00
trans.	4	21.00	25.75	4.92	26.00	30.00
comp.	4	10.00	19.63	7.56	20.00	28.50

Welch's ANOVA
F-Value=1.47 DF Num=2 DF Den=7.23013 P-Value=0.291

Games-Howell

	Dmean	SE	T-Value	adjusted P-Value
conv. vs trans.	5.45	3.37	1.62	0.285
conv. vs comp.	-0.68	4.43	-0.15	0.987
comp. vs trans.	-6.12	4.51	-1.36	0.426

G. Length-to-maximum width ratio

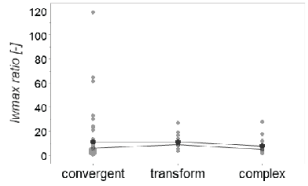

	N	min	mean	StDev	median	max
conv.	64	0.46	11.31	18.06	6.20	118.88
trans.	12	3.88	11.32	6.92	8.94	27.11
comp.	16	1.91	7.85	7.04	5.13	27.97

Welch's ANOVA
F-Value=2.33 DF Num=2 DF Den=28.0361 P-Value=0.116

Games-Howell

	Dmean	SE	T-Value	adjusted P-Value
conv. vs trans.	0.1683	0.0904	1.86	0.172
conv. vs comp.	-0.0525	0.0991	-0.53	0.857
comp. vs trans.	-0.221	0.112	-1.97	0.140

H. Maximum width-to-maximum depth ratio

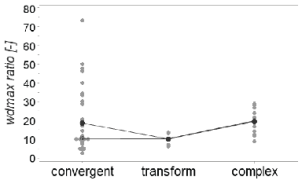

	N	min	mean	StDev	median	max
conv.	34	2.45	18.54	16.71	10.33	73.33
trans.	4	6.15	10.05	3.99	10.20	13.64
comp.	13	8.75	19.48	6.49	19.83	28.86

Welch's ANOVA
F-Value=4.53 DF Num=2 DF Den=9.57062 P-Value=0.041

Games-Howell

	Dmean	SE	T-Value	adjusted P-Value
conv. vs trans.	-0.145	0.110	-1.32	0.434
conv. vs comp.	0.1451	0.0763	1.90	0.150
comp. vs trans.	0.290	0.101	2.87	0.083

I. Length-to-maximum depth ratio

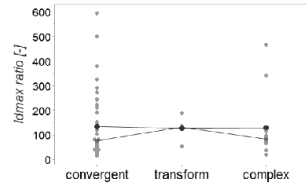

	N	min	mean	StDev	median	max
conv.	42	14.30	133.80	134.4	75.70	593.30
trans.	4	52.60	126.00	56.10	131.20	188.90
comp.	12	18.90	127.70	133.80	82.40	466.10

Welch's ANOVA
F-Value=0.47 DF Num=2 DF Den=9.60212 P-Value=0.641

Games-Howell

	Dmean	SE	T-Value	adjusted P-Value
conv. vs trans.	0.136	0.137	1.00	0.609
conv. vs comp.	0.026	0.126	0.21	0.977
comp. vs trans.	-0.110	0.160	-0.69	0.776

Figure 4.4a-i Dot plots of morphometric values and aspect ratios for the studied submarine canyons from active margins, classified on plate-boundary type. N = number of readings; min = minimum value; mean = mean value; StDev = standard deviation; median = median value; max = maximum value. Results of Welch's ANOVA test: DF Num = degrees of freedom numerator; DF Den = degrees of freedom denominator. Games-Howell post hoc test: Dmean = difference of means; SE = standard error.

4.3.2 Scaling in submarine canyons in active versus passive margins

Results of the correlation analyses of canyon morphometric parameters with each other are presented as heat maps (Fig. 4.5a&b). Additionally, correlations between maximum canyon dimensions and their aspect ratios (Fig. 4.5c-e) and between maximum canyon sidewall steepness and maximum width (Fig. 4.5f) and depth (Fig. 4.5g) are also displayed as scatter plots.

4.3.2.1 Canyon dimensions

Moderate and statistically significant scaling between maximum canyon dimensions is seen for submarine canyons along both active and passive margins (Fig. 4.5a-e).

4.3.2.2 Maximum canyon sidewall steepness versus maximum canyon width and -depth

A moderate linear correlation is seen between maximum sidewall steepness and maximum width in active-margin canyons, whereas the same parameters are weakly correlated in passive-margin canyons (Fig. 4.5f).

Correlations of maximum sidewall steepness with maximum depth (Fig. 4.5g) are weak and not significant for passive-margin examples. In contrast, maximum sidewall steepness displays moderate correlations with maximum depth in canyons along active margins, which are statistically significant.

A. Pearson's correlation coefficient r

Active margin

	L	Wmax	Wav	Dmax	Dav	Slav	thGav	SWmax
L								
Wmax	0.558							
Wav	0.964	0.907						
Dmax	0.540	0.797	***					
Dav	0.824	0.711	0.427	***				
Slav	0.580	0.371	0.248	0.506	0.647			
thGav	-0.528	-0.306	***	-0.193	***	-0.521		
SWmax	0.325	0.507	***	0.568	***	0.051	-0.007	

Passive margin

	L	Wmax	Wav	Dmax	Dav	Slav	thGav	SWmax
L								
Wmax	0.498							
Wav	0.752	0.784						
Dmax	0.712	0.757	0.813					
Dav	0.671	0.506	0.772	0.893				
Slav	0.312	0.181	0.362	0.208	0.394			
thGav	-0.367	-0.351	-0.051	-0.099	0.621	-0.257		
SWmax	0.358	0.355	-0.238	0.121	***	0.106	0.062	

p-value

	L	Wmax	Wav	Dmax	Dav	Slav	thGav	SWmax
L								
Wmax	≤0.001							
Wav	≤0.001	≤0.001						
Dmax	≤0.001	≤0.001	***					
Dav	≤0.001	≤0.001	0.087	***				
Slav	≤0.001	0.004	0.338	0.012	0.002			
thGav	≤0.001	0.049	***	0.245	***	0.001		
SWmax	0.065	0.008	***	0.002	***	0.862	0.975	

p-value

	L	Wmax	Wav	Dmax	Dav	Slav	thGav	SWmax
L								
Wmax	≤0.001							
Wav	≤0.001	≤0.001						
Dmax	≤0.001	≤0.001	≤0.001					
Dav	≤0.001	0.112	≤0.001	≤0.001				
Slav	0.003	0.181	0.012	0.210	0.028			
thGav	0.011	0.036	0.806	0.615	0.041	0.089		
SWmax	0.035	0.040	0.375	0.502	***	0.599	0.812	

B. Spearman's rank correlation coefficient rs

Active margin

	L	Wmax	Wav	Dmax	Dav	Slav	thGav	SWmax
L								
Wmax	0.675							
Wav	0.622	0.842						
Dmax	0.734	0.746	***					
Dav	0.728	0.472	0.421	***				
Slav	0.575	0.336	0.372	0.435	0.300			
thGav	-0.742	-0.327	***	-0.184	***	-0.606		
SWmax	0.196	-0.076	***	0.597	***	0.105	0.261	

Passive margin

	L	Wmax	Wav	Dmax	Dav	Slav	thGav	SWmax
L								
Wmax	0.537							
Wav	0.571	0.773						
Dmax	0.610	0.721	0.821					
Dav	0.667	0.582	0.811	0.893				
Slav	0.534	0.317	0.333	0.291	0.425			
thGav	-0.462	-0.281	0.015	0.030	0.575	-0.181		
SWmax	0.669	0.302	-0.268	0.126	***	-0.007	0.069	

p-value

	L	Wmax	Wav	Dmax	Dav	Slav	thGav	SWmax
L								
Wmax	≤0.001							
Wav	0.006	≤0.001						
Dmax	≤0.001	≤0.001	***					
Dav	≤0.001	0.031	0.093	***				
Slav	≤0.001	0.011	0.142	0.034	0.199			
thGav	≤0.001	0.034	***	0.270	***	≤0.001		
SWmax	0.276	0.713	***	0.001	***	0.720	0.253	

p-value

	L	Wmax	Wav	Dmax	Dav	Slav	thGav	SWmax
L								
Wmax	≤0.001							
Wav	≤0.001	≤0.001						
Dmax	≤0.001	≤0.001	≤0.001					
Dav	≤0.001	0.060	≤0.001	≤0.001				
Slav	≤0.001	0.017	0.022	0.077	0.017			
thGav	0.001	0.097	0.940	0.881	0.064	0.234		
SWmax	≤0.001	0.083	0.316	0.483	***	0.972	0.794	

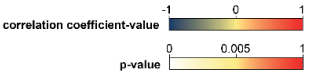

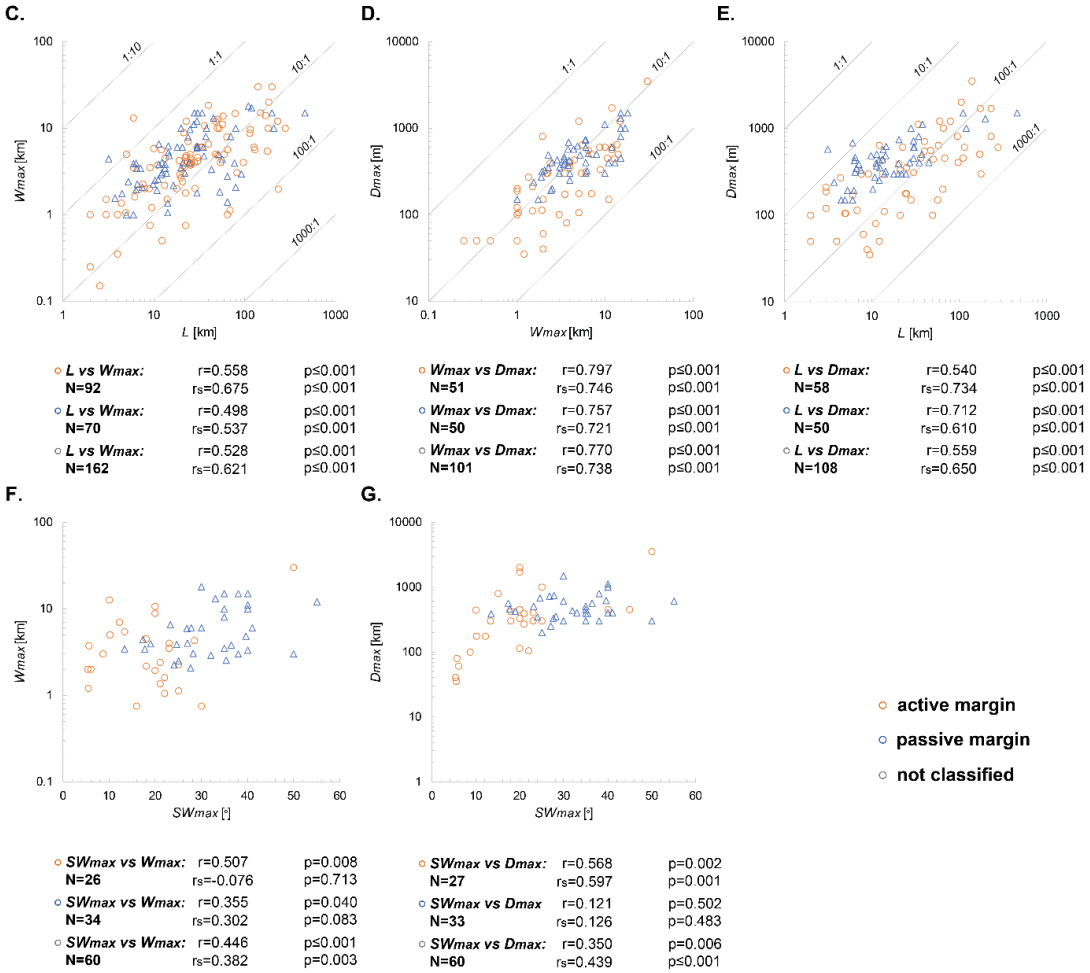

Figure 4.5a-g Results of the correlation analyses of canyon morphometric parameters and aspect ratios with parameters of the physiographic setting at the canyon in active vs. passive margins. A.&B. Overview of results presented as heat maps. C.-G. Scatter plots of results. L = canyon length; W_{max} = maximum canyon width; W_{av} = average canyon width; D_{max} = maximum canyon depth; D_{av} = average canyon depth;SI_{av} = average canyon sinuosity index; thG_{av} = average canyon thalweg gradient; SW_{max} = maximum canyon sidewall steepness; *** = correlations not reported due to small dataset size.

4.3.3 Scaling between canyon morphometric parameters and characteristics of their physiographic setting in active versus passive margins

Results of the correlation analyses of canyon morphometric parameters and aspect ratios with seafloor depth at the canyon apex (section 4.3.3.1) and mouth, and with the distance of the canyon to the nearest shoreline (section 4.3.3.2) are presented as heat maps (Fig. 4.6a&b). In addition, discussed scaling relationships are presented as scatter plots (Fig. 4.7a-h).

4.3.3.1 Seafloor depth at the canyon apex (SD_{min})

In canyons from active and passive margins, the seafloor depth at the canyon apex correlates weakly with canyon length, maximum canyon width and average canyon thalweg gradient (Fig. 4.6a&b). For average canyon width and seafloor depth at the canyon apex, moderate to modest negative correlations are seen in both active and passive margins, which are only significant for the latter (Fig. 4.7a). A negative and significant moderate correlation between seafloor depth and maximum canyon depth is seen for passive-margin canyons; the corresponding relationship is instead weak for canyons along active margins (Fig. 4.7b). Average canyon depth displays negative and modest correlations with the seafloor depth at the canyon apex along passive margins, but these are not significant for the chosen alpha value (Fig. 4.7c).

Moderate inverse relationships between seafloor depth and both average canyon sinuosity (Fig. 4.7d) and maximum canyon sidewall steepness (Fig. 4.47e) exist in active margins, which are statistically significant. For canyons in passive margins, the correlations with apex depth are weak for both morphometric parameters (Figs. 4.7d&e).

For the investigated aspect ratios, significant and moderate positive scaling exists with wdmax ratios of canyons in active settings (Fig. 4.7f). The remaining correlations in both margin types are all weak (Fig. 4.6a&b).

4.3.3.2 Minimum canyon-shoreline distance (Dis_{min})

Correlations between the shortest distance of the canyon to the shoreline with canyon morphometric parameters are weak for all maximum and average canyon dimensions for canyons from both margin types. Relationships with average canyon width in active-margin canyons were not assessed due to insufficient data for the statistical analyses (Fig. 4.6a&b).

Average canyon sinuosity demonstrates modest negative scaling with the minimum distance of the canyon to the shoreline in active margins, whereas weak positive scaling is seen for passive margins; correlations are statistically significant for both margins (Fig. 4.6a&b).

Inverse scaling between the minimum canyon-shoreline distance and the average canyon thalweg gradient is seen in canyons from both margin types. The correlation is weak for examples from active margins, whereas modest, linear negative correlation is seen for passive-margin settings (Fig. 4.6a&b).

With decreasing distance of the canyon to the coastline, the maximum sidewall steepness in active-margin canyons tends to increase, but the strength of this correlation is moderate to modest. Correlation between the two parameters is very weak in examples from passive margins (Fig. 4.7g).

Correlations of aspect ratios with minimum distance to the shoreline are weak for maximum canyon dimensions across both margin types (Fig. 4.6a&b), with the exception of significant moderate and modest scaling displayed for wdmax ratios in active-margin canyons (Fig. 4.7h).

A. Pearson's correlation coefficient r

Active margin

L	-0.043	0.670	0.006
W max	0.184	0.429	-0.195
W av	-0.373	0.909	***
D max	-0.292	0.774	-0.106
D av	0.073	0.834	0.158
SI av	-0.223	0.636	-0.440
thG av	0.197	-0.315	-0.124
SW max	-0.622	0.387	-0.667
lw max	-0.210	0.434	-0.188
wd max	0.628	-0.230	0.552
ld max	0.068	0.229	0.103
	SD min	*SD max*	*Dis min*

Passive margin

L	-0.081	0.570	0.194
W max	0.105	0.376	-0.023
W av	-0.423	0.062	0.323
D max	-0.218	0.615	0.107
D av	-0.457	0.568	0.328
SI av	-0.090	0.450	0.331
thG av	-0.304	-0.477	-0.459
SW max	-0.017	0.339	0.081
lw max	-0.102	0.629	0.244
wd max	0.185	0.114	0.087
ld max	-0.040	0.559	-0.114
	SD min	*SD max*	*Dis min*

p-value

Active margin

L	0.647	≤0.001	0.942
W max	0.116	≤0.001	0.062
W av	0.140	≤0.001	***
D max	0.052	≤0.001	0.426
D av	0.752	≤0.001	0.495
SI av	0.081	≤0.001	≤0.001
thG av	0.135	0.010	0.319
SW max	≤0.001	0.042	≤0.001
lw max	0.076	≤0.001	0.080
wd max	≤0.001	0.171	≤0.001
ld max	0.659	0.135	0.454
	SD min	*SD max*	*Dis min*

Passive margin

L	0.459	≤0.001	0.037
W max	0.471	0.018	0.848
W av	0.003	0.710	0.025
D max	0.183	≤0.001	0.447
D av	0.011	0.004	0.072
SI av	0.439	≤0.001	0.002
thG av	0.042	0.003	0.002
SW max	0.932	0.098	0.641
lw max	0.496	≤0.001	0.048
wd max	0.272	0.557	0.548
ld max	0.812	0.002	0.430
	SD min	*SD max*	*Dis min*

B. Spearman's rank correlation coefficient rs

Active margin

L	-0.097	0.768	0.103
W max	0.028	0.537	0.045
W av	-0.432	0.115	***
D max	-0.242	0.816	-0.088
D av	0.079	0.632	0.286
SI av	-0.500	0.350	-0.464
thG av	-0.087	-0.192	-0.148
SW max	-0.610	0.208	-0.429
lw max	-0.235	0.361	-0.115
wd max	0.520	-0.084	0.424
ld max	-0.023	0.200	0.132
	SD min	*SD max*	*Dis min*

Passive margin

L	-0.198	0.590	0.169
W max	-0.256	0.358	-0.216
W av	-0.553	0.123	0.381
D max	-0.614	0.398	-0.161
D av	-0.412	0.609	0.250
SI av	-0.104	0.402	0.112
thG av	-0.323	-0.501	-0.262
SW max	0.091	0.549	-0.156
lw max	-0.129	0.383	0.147
wd max	0.115	-0.014	-0.001
ld max	0.019	0.098	-0.208
	SD min	*SD max*	*Dis min*

p-value

Active margin

L	0.304	≤0.001	0.234
W max	0.812	≤0.001	0.671
W av	0.083	0.650	***
D max	0.109	≤0.001	0.511
D av	0.734	0.002	0.208
SI av	≤0.001	0.005	≤0.001
thG av	0.513	0.122	0.231
SW max	≤0.001	0.289	0.014
lw max	0.047	0.003	0.284
wd max	0.001	0.620	0.002
ld max	0.880	0.192	0.337
	SD min	*SD max*	*Dis min*

Passive margin

L	0.067	≤0.001	0.070
W max	0.076	0.025	0.075
W av	≤0.001	0.457	0.008
D max	≤0.001	0.029	0.249
D av	0.024	0.002	0.176
SI av	0.372	0.001	0.300
thG av	0.031	0.002	0.086
SW max	0.653	0.004	0.365
lw max	0.386	0.018	0.239
wd max	0.498	0.944	0.997
ld max	0.909	0.612	0.146
	SD min	*SD max*	*Dis min*

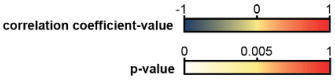

Figure 4.6a&b Results of the correlation analyses of canyon morphometric parameters and aspect ratios with parameters of the physiographic setting at the canyon in active vs. passive margins presented as heat maps. *L* = canyon length along thalweg; L_{en} = canyon length along endpoints; W_{max} = maximum canyon width; D_{max} = maximum canyon depth; SI_{av} = average canyon sinuosity index; thG_{av} = average canyon thalweg gradient; SW_{max} = maximum canyon sidewall steepness; *lwmax* = length-to-maximum width ratio; *wdmax* = maximum width-to-maximum depth ratio; *ldmax* = length-to-maximum depth ratio; SD_{min} = seafloor depth at canyon apex; SD_{max} = seafloor depth at canyon mouth. Dis_{min} = minimum distance of canyon to shoreline; *** = correlations not reported due to small dataset size.

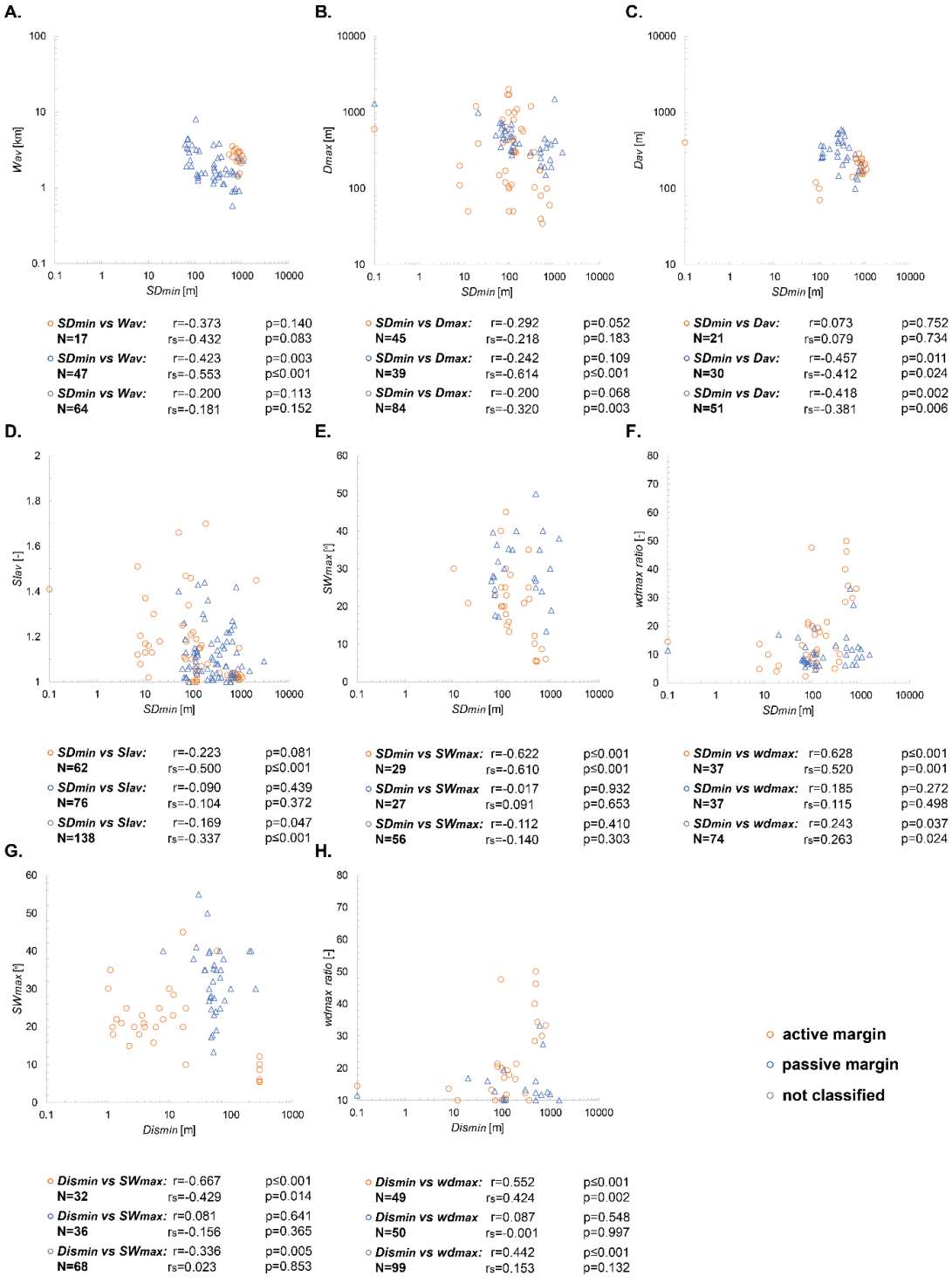

Figure 4.7a-h Scatterplots of attributes of the canyon-physiographic setting with canyon morphometric parameters for submarine canyons of the study in active vs. passive margins. W_{av} = average canyon width; D_{max} = maximum canyon depth; D_{av} = average canyon depth; SI_{av} = average canyon sinuosity index; SW_{max} = maximum canyon sidewall steepness; *wdmax* = maximum width-to-maximum depth ratio; SD_{min} = seafloor depth at canyon apex; Dis_{min} = minimum distance of canyon to shoreline; N = number of readings; r = Pearson's correlation coefficient; rs = Spearman's rank correlation coefficient.

4.3.4 Scaling between canyon morphometry and characteristics of the source-to-sink (S2S) system

Scaling relationships between canyon morphometric parameters and attributes of the terrestrial catchment (Fig. 4.8a-l), shelf (Figs. 4.9a & 4.8m-q) and slope (Fig. 4.9b & 4.8r) have been assessed.

4.3.4.1 Terrestrial catchment (L_{fls}, Q_{fls}, A_{flsc}; H_{flsc})

For the studied canyons with a present and/or past sediment connection with one or several fluvial systems, scaling of canyon length and average canyon sinuosity with attributes of the terrestrial catchment in active and passive margins can be quantified. Statistical analyses on maximum canyon width are limited to active-margin settings in view of data coverage.

Fluvial system length (Lfls)

Correlations of river length with canyon length are weak and not significant for canyons in passive margins. Along active margins, positive and moderate scaling of canyon length with fluvial system length is demonstrated, which is statistically significant (Fig. 4.8a). In contrast, maximum width correlates weakly with river length in canyons along active margins, but relatively strongly for canyons located in passive-margin settings. However, findings for the latter group are based on thirteen observations only (Fig. 4.8e). For average canyon sinuosity, the correlations are weak and not significant for any margin type (Fig. 4.8i).

Average annual fluvial water discharge (Qfls)

The average annual water discharge of the fluvial system displays positive, moderate monotonic correlations with canyon length in canyons of both margin types, as well as overall in the entire dataset; these relationships are statistically significant (Fig. 4.8b). Correlations of average annual fluvial discharge and maximum width are weak in active-margin canyons (Fig. 8f). Positive and monotonic correlations of average canyon sinuosity with this catchment attribute exist for active and passive margins, but these are respectively moderate and weak, and neither is statistically significant (Fig. 4.8j).

Catchment size (Aflsc)

Scaling of canyon length with catchment size is weak for canyons from passive margins (Fig. 4.8c). Moderate, positive monotonic correlations exist for the length (Fig. 4.8c) and maximum width (Fig. 4.8g) in canyons associated with active margins. No correlation is seen between average canyon sinuosity and catchment area for passive-margin canyons; a modest, positive monotonic correlation is seen for active-margin settings, but this is not significant (Fig. 4.8k).

Maximum catchment elevation (Hflsc)

The length of submarine canyons scales positively with the maximum catchment elevation of associated fluvial systems on passive margins. A corresponding relationship is absent for active margins (Fig. 4.8d), whereas maximum canyon width shares positive and moderate correlations with maximum catchment elevation in active-margin canyons (Fig. 4.8h). Moderate, significant correlations are seen between average canyon sinuosity and maximum catchment elevation for both margin types (Fig. 4.8l).

4.3.4.2 Shelf-break depth (D_{sh})

Correlations of shelf-break depth at the canyon location with attributes of canyon geomorphology are weak and not significant for canyons in active-margin settings; in the studied canyons from passive margins, instead, maximum canyon dimensions (Figs. 4.8m-o), average canyon sinuosity (Fig. 4.8p) and maximum canyon sidewall steepness (Fig. 4.8q) correlate moderately or strongly with the shelf-break depth (Fig. 4.9a).

4.3.4.3 Slope width (W_{sl})

Canyon length increases with slope width in active and passive margins; the strength of the relationship is moderate in the former and strong in the latter (Fig. 4.8r). Maximum canyon width and depth do not correlate with the slope width in active margins, but both variables show moderate correlation with the width of passive-margin slopes. However, more data are needed to support the findings for active-margin canyons (Fig. 4.9b).

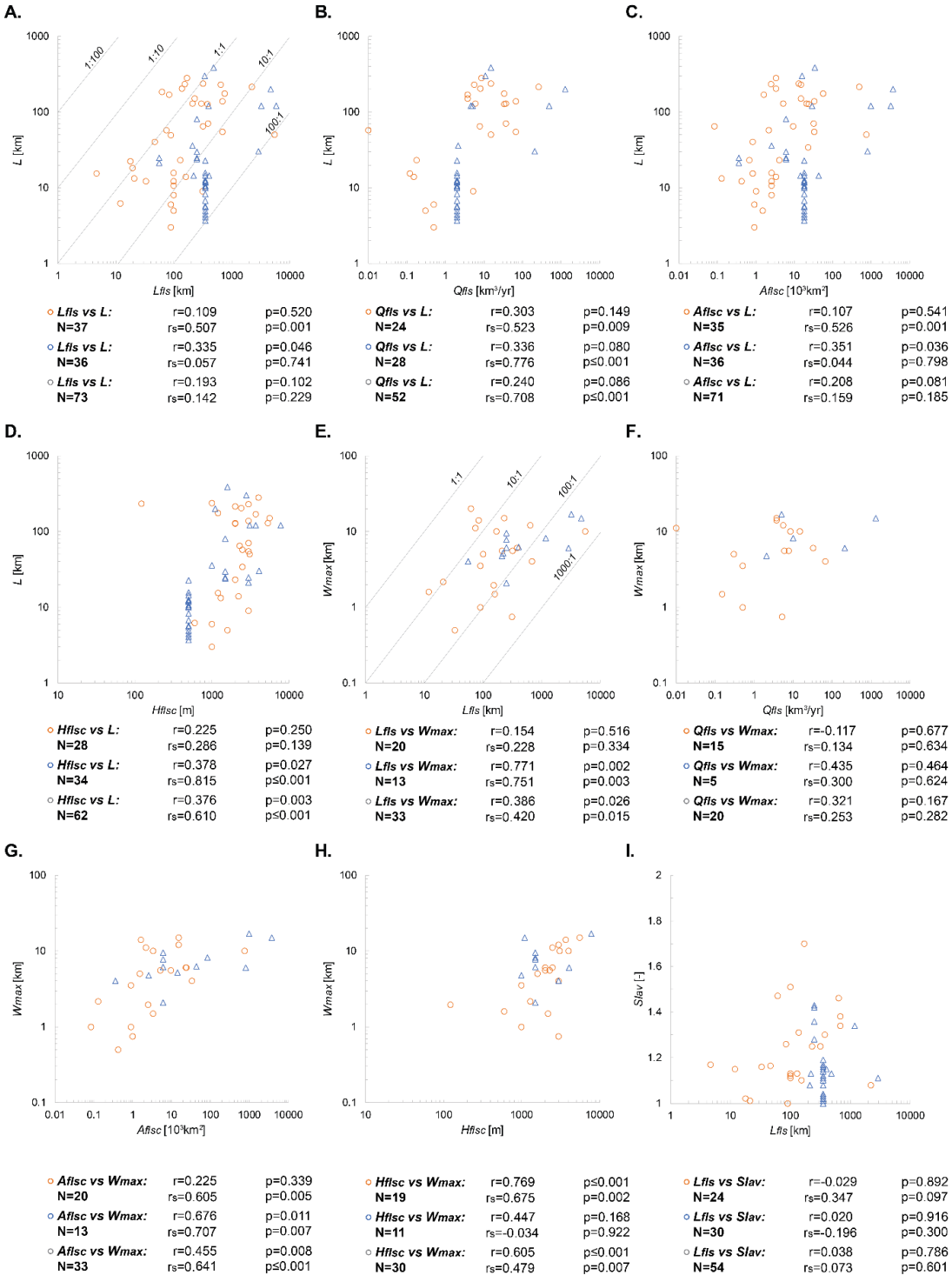

○ ***Lfls vs L:***	r=0.109	p=0.520	○ ***Qfls vs L:***	r=0.303	p=0.149	○ ***Aflsc vs L:***	r=0.107	p=0.541
N=37	rs=0.507	p=0.001	**N=24**	rs=0.523	p=0.009	**N=35**	rs=0.526	p=0.001
○ ***Lfls vs L:***	r=0.335	p=0.046	○ ***Qfls vs L:***	r=0.336	p=0.080	○ ***Aflsc vs L:***	r=0.351	p=0.036
N=36	rs=0.057	p=0.741	**N=28**	rs=0.776	p≤0.001	**N=36**	rs=0.044	p=0.798
○ ***Lfls vs L:***	r=0.193	p=0.102	○ ***Qfls vs L:***	r=0.240	p=0.086	○ ***Aflsc vs L:***	r=0.208	p=0.081
N=73	rs=0.142	p=0.229	**N=52**	rs=0.708	p≤0.001	**N=71**	rs=0.159	p=0.185

○ ***Hflsc vs L:***	r=0.225	p=0.250	○ ***Lfls vs Wmax:***	r=0.154	p=0.516	○ ***Qfls vs Wmax:***	r=-0.117	p=0.677
N=28	rs=0.286	p=0.139	**N=20**	rs=0.228	p=0.334	**N=15**	rs=0.134	p=0.634
○ ***Hflsc vs L:***	r=0.378	p=0.027	○ ***Lfls vs Wmax:***	r=0.771	p=0.002	○ ***Qfls vs Wmax:***	r=0.435	p=0.464
N=34	rs=0.815	p≤0.001	**N=13**	rs=0.751	p=0.003	**N=5**	rs=0.300	p=0.624
○ ***Hflsc vs L:***	r=0.376	p=0.003	○ ***Lfls vs Wmax:***	r=0.386	p=0.026	○ ***Qfls vs Wmax:***	r=0.321	p=0.167
N=62	rs=0.610	p≤0.001	**N=33**	rs=0.420	p=0.015	**N=20**	rs=0.253	p=0.282

○ ***Aflsc vs Wmax:***	r=0.225	p=0.339	○ ***Hflsc vs Wmax:***	r=0.769	p≤0.001	○ ***Lfls vs Slav:***	r=-0.029	p=0.892
N=20	rs=0.605	p=0.005	**N=19**	rs=0.675	p=0.002	**N=24**	rs=0.347	p=0.097
○ ***Aflsc vs Wmax:***	r=0.676	p=0.011	○ ***Hflsc vs Wmax:***	r=0.447	p=0.168	○ ***Lfls vs Slav:***	r=0.020	p=0.916
N=13	rs=0.707	p=0.007	**N=11**	rs=-0.034	p=0.922	**N=30**	rs=-0.196	p=0.300
○ ***Aflsc vs Wmax:***	r=0.455	p=0.008	○ ***Hflsc vs Wmax:***	r=0.605	p≤0.001	○ ***Lfls vs Slav:***	r=0.038	p=0.786
N=33	rs=0.641	p≤0.001	**N=30**	rs=0.479	p=0.007	**N=54**	rs=0.073	p=0.601

J.

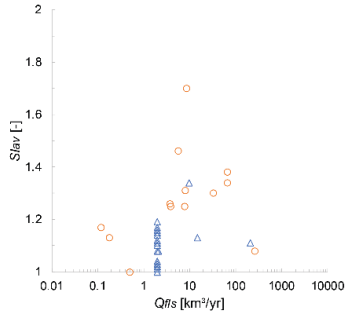

○ ***Qfls vs Slav:***	r=-0.237	p=0.436
N=13	rs=0.433	p=0.140
○ ***Qfls vs Slav:***	r=0.091	p=0.672
N=24	rs=0.324	p=0.122
○ ***Qfls vs Slav:***	r=0.034	p=0.842
N=37	rs=0.554	p≤0.001

K.

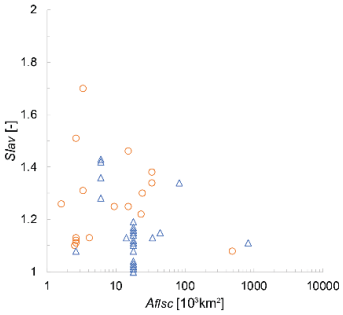

○ ***Aflsc vs Slav:***	r=-0.155	p=0.468
N=24	rs=0.433	p=0.035
○ ***Aflsc vs Slav:***	r=-0.023	p=0.903
N=30	rs=-0.215	p=0.254
○ ***Aflsc vs Slav:***	r=-0.093	p=0.503
N=54	rs=-0.220	p=0.428

L.

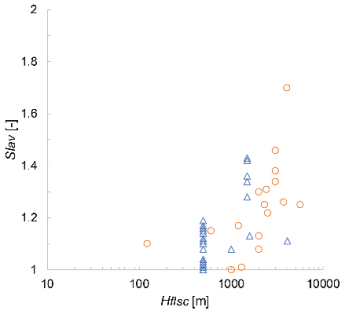

○ ***Hflsc vs Slav:***	r=0.618	p=0.008
N=17	rs=0.757	p≤0.001
○ ***Hflsc vs Slav:***	r=0.417	p=0.027
N=28	rs=0.573	p=0.001
○ ***Hflsc vs Slav:***	r=0.611	p≤0.001
N=45	rs=0.648	p≤0.001

M.

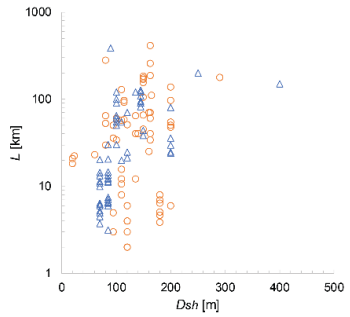

○ ***Dsh vs L:***	r=0.228	p=0.068
N=65	rs=0.192	p=0.126
○ ***Dsh vs L:***	r=0.419	p≤0.001
N=66	rs=0.756	p≤0.001
○ ***Dsh vs L:***	r=0.326	p≤0.001
N=131	rs=0.398	p≤0.001

N.

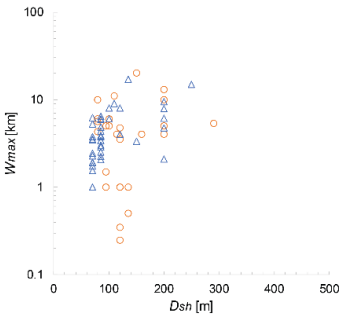

○ ***Dsh vs Wmax:***	r=0.156	p=0.429
N=28	rs=-0.096	p=0.627
○ ***Dsh vs Wmax:***	r=0.554	p≤0.001
N=42	rs=0.598	p≤0.001
○ ***Dsh vs Wmax:***	r=0.359	p=0.002
N=70	rs=0.258	p=0.031

O.

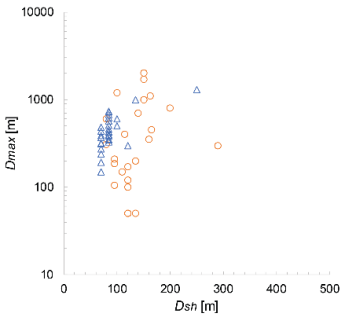

○ ***Dsh vs Dmax:***	r=0.219	p=0.282
N=26	rs=0.378	p=0.057
○ ***Dsh vs Dmax:***	r=0.770	p≤0.001
N=34	rs=0.636	p≤0.001
○ ***Dsh vs Dmax:***	r=0.362	p=0.004
N=60	rs=0.217	p=0.096

P.

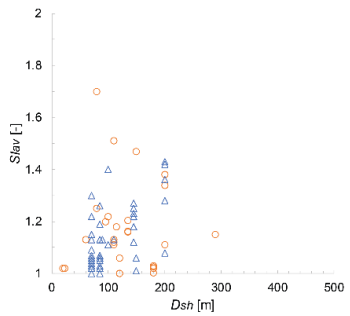

○ ***Dsh vs Slav:***	r=-0.032	p=0.868
N=30	rs=-0.118	p=0.536
○ ***Dsh vs Slav:***	r=0.588	p≤0.001
N=47	rs=0.472	p=0.001
○ ***Dsh vs Slav:***	r=0.263	p=0.021
N=77	rs=0.264	p=0.021

Q.

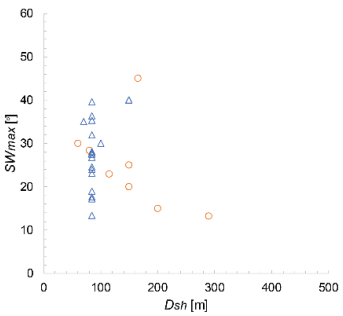

○ ***Dsh vs SWmax:***	r=-0.477	p=0.194
N=9	rs=-0.596	p=0.090
○ ***Dsh vs SWmax***	r=0.545	p=0.013
N=20	rs=0.474	p=0.035
○ ***Dsh vs SWmax:***	r=-0.160	p=0.407
N=29	rs=-0.077	p=0.691

R.

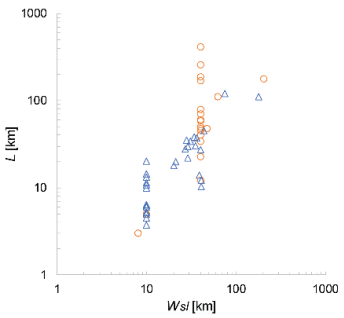

○ ***Wsl vs L:***	r=0.291	p=0.201
N=21	rs=0.573	p=0.007
○ ***Wsl vs L:***	r=0.834	p≤0.001
N=31	rs=0.720	p≤0.001
○ ***Wsl vs L:***	r=0.432	p=0.001
N=52	rs=0.786	p≤0.001

○ **active margin** ○ **passive margin** ○ **not classified**

Figure 4.8a-r Scatterplots of attributes of the terrestrial catchment, shelf and slope with canyon morphometric parameters for submarine canyons of the study in active vs. passive margins. *L* = canyon length; W_{max} = maximum canyon width; SI_{av} = average canyon sinuosity index; thG_{av} = average canyon thalweg gradient; SW_{max} = maximum canyon sidewall steepness; L_{fls} = fluvial system length; Q_{fls} = average annual fluvial discharge; A_{flsc} = catchment size; H_{flsc} = maximum catchment elevation; D_{sh} = shelf-break depth; W_{sl} = slope width; N = number of readings; r = Pearson's correlation coefficient; rs = Spearman's rank correlation coefficient.

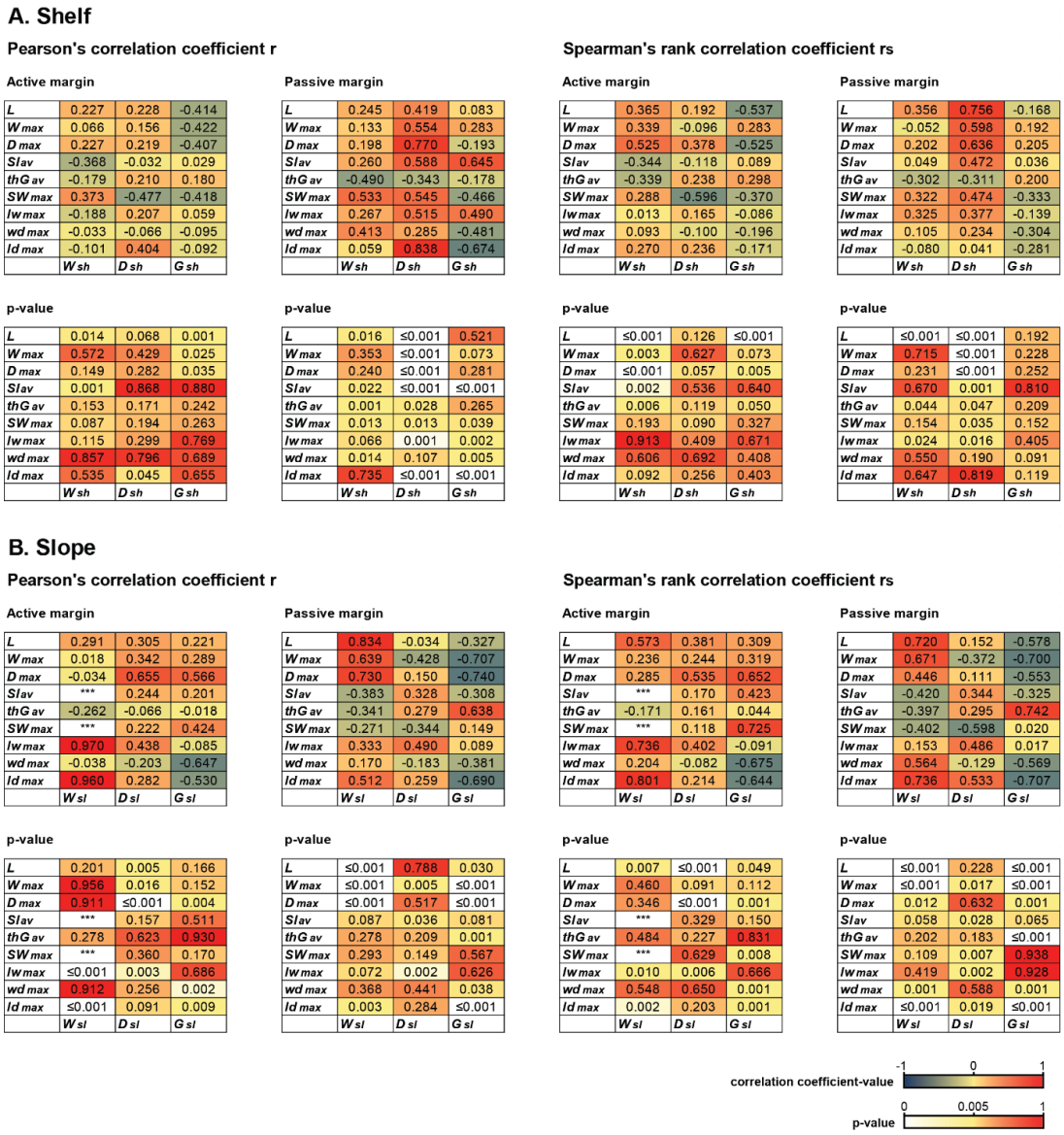

Figure 4.9a&b Results of the correlation analyses of canyon morphometric parameters and aspect ratios with parameters of the A. shelf and B. slope at the canyon in active vs. passive margins presented as heat maps. L = canyon length; W_{max} = maximum canyon width; D_{max} = maximum canyon depth; SI_{av} = average canyon sinuosity index; thG_{av} = average canyon thalweg gradient; SW_{max} = maximum canyon sidewall steepness; lwmax = length-to-maximum width ratio; wdmax = maximum width-to-maximum depth ratio; ldmax = length-to-maximum depth ratio; W_{sh} = shelf width; D_{sh} = shelf-break depth; G_{sh} = average shelf gradient; W_{sl} = slope width; D_{sl} = slope-break depth; G_{sl} = average slope gradient; *** = correlations not reported due to small dataset size.

4.3.5 Characterization of canyon source-to-sink (S2S) system and physiographic setting by tectonic setting

Analyses have been undertaken of (i) attributes of the S2S system and of the physiographic setting, and of how these vary with the margin type (section 4.3.5.1), and of (ii) scaling between attributes of the S2S systems in active and passive margins (section 4.3.5.2). This has been done for the following reasons: (i) to assess commonalities and differences in characteristics of the two margin types, which can be used to refine existing S2S system models; and (ii) to aid recognition of covariance between variables that may be related to the studied canyon morphometric parameters, rendered necessary by data gaps that prevent the application of multivariate techniques.

4.3.5.1 Attributes of the canyon geological contexts and their variations across margin types

Two-sample T-tests undertaken on frequency distributions of the attributes describing canyon terrestrial catchments, continental shelves and slopes (Fig. 4.10a-n) demonstrate that significant differences in mean values of the studied variables are seen for all investigated attributes except for average annual fluvial discharge (Fig. 4.10b), shelf-break depth (Fig. 4.10f), slope-break depth (Fig. 4.10i) and latitude at the canyon apex (Fig. 4.10n).

On average, the length (Fig. 4.10a), average annual water discharge (Fig. 4.10b) and catchment size (Fig. 4.10c) of fluvial systems supplying sediment to the studied canyons are each greater in terrestrial catchments along passive margins. Although the greatest maximum catchment elevation

recorded in the study occurs in a passive-margin drainage basin, terrestrial catchments associated with active margins tend to be higher than along passive margins (Fig. 4.10d).

The widest continental shelves in the study are associated with the submarine canyons of the Bering Sea, but the mean shelf widths of the studied active and passive margins are very similar, albeit slightly greater along the former (Fig. 4.10e). Shelf-breaks tend to be deeper along active margins, but the results do not indicate a significant difference between the two margin types (Fig. 4.10f). The average shelf gradient is on average higher in active-margin systems (Fig. 4.10g).

Canyons of the study along active margins are hosted on wider (Fig. 4.10h) and deeper (Fig. 4.10i) slopes, whereas the average slope gradient tends to be higher in S2S systems associated with the studied passive margins (Fig. 4.10j).

With regard to aspects of the physiographic setting, mean values of seafloor depth at the canyon apex and mouth, of the minimum distance of the canyon to the shoreline, and of the latitude of the canyon apex are similar across the two margin types. Active-margin canyons show a greater bathymetric range, and several of the studied canyons in passive margins are located at higher latitudes (Fig. 4.10k-n).

4.3.5.2 Scaling between attributes of the source-to-sink (S2S) systems of active and passive margins

Correlations between attributes of the terrestrial catchment, shelf and slope in canyon-associated S2S systems grouped into active- and passive-margin settings share similarities, yet exhibit differences regarding their sign, strength and statistical significance. For some attributes, the amount of data prevents meaningful analyses to be undertaken (Fig. 4.11a&b).

Statistically significant scaling relationships are seen across both margin types, but these vary in strength. Strong and positive significant correlations of catchment area with fluvial-system length and average annual fluvial discharge are seen for both margin types. Also, shelf width correlates positively with catchment area and fluvial system length in both margin

types, but the relationship with the latter is stronger in active-margin settings. Strong inverse scaling across both margin types exists between shelf width and the average shelf gradient and between slope width and the average slope gradient in passive margins (Fig. 4.11a&b).

For other pairs of attributes, significant relationships may be seen for a particular margin type only. For example, the maximum elevation of passive-margin catchments shows significant and positive scaling with fluvial system length and average annual fluvial discharge, which is moderate for the former and strong for the latter. For active margins, correlations are weak and modest and not statistically significant. Shelf-break depth and the average shelf gradient display linear, moderate and significant positive correlation with each other in passive margins, but along active margins the same trend is weak, negative and not statistically significant (Fig. 4.11a&b).

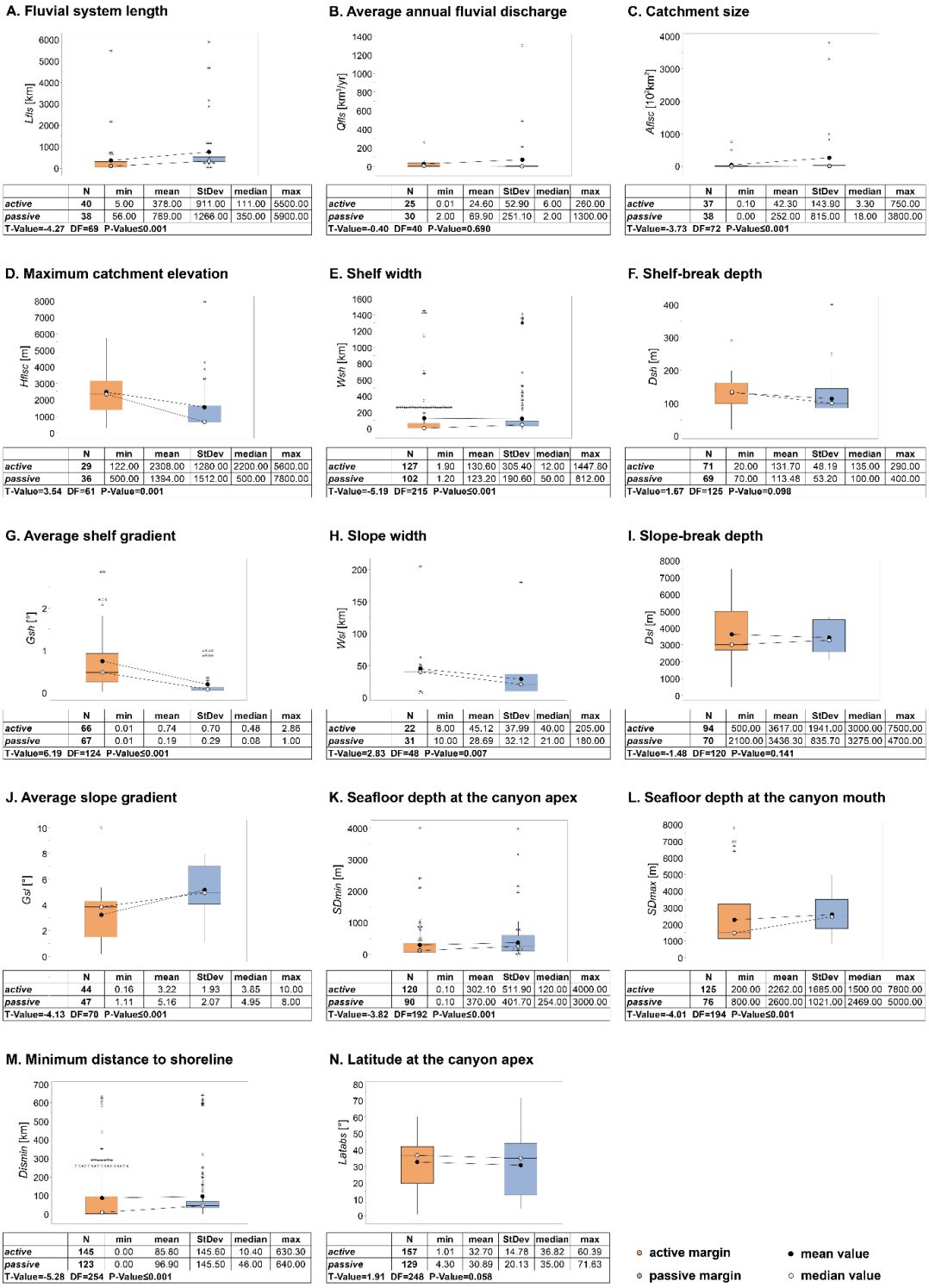

A. Fluvial system length	N	min	mean	StDev	median	max
active	40	5.00	378.00	911.00	111.00	5500.00
passive	38	56.00	769.00	1266.00	350.00	5900.00

T-Value=-4.27 DF=69 P-Value≤0.001

B. Average annual fluvial discharge	N	min	mean	StDev	median	max
active	25	0.01	24.60	52.90	6.00	260.00
passive	30	2.00	69.90	251.10	2.00	1300.00

T-Value=-0.40 DF=40 P-Value=0.690

C. Catchment size	N	min	mean	StDev	median	max
active	37	0.10	42.30	143.90	3.30	750.00
passive	38	0.00	252.00	815.00	18.00	3800.00

T-Value=-3.73 DF=72 P-Value≤0.001

D. Maximum catchment elevation	N	min	mean	StDev	median	max
active	29	122.00	2308.00	1280.00	2200.00	5600.00
passive	36	500.00	1394.00	1512.00	500.00	7800.00

T-Value=3.54 DF=61 P-Value=0.001

E. Shelf width	N	min	mean	StDev	median	max
active	127	1.90	130.60	305.40	12.00	1447.80
passive	102	1.20	123.20	190.60	50.00	812.00

T-Value=-5.19 DF=215 P-Value≤0.001

F. Shelf-break depth	N	min	mean	StDev	median	max
active	71	20.00	131.70	48.19	135.00	290.00
passive	69	70.00	113.48	53.20	100.00	400.00

T-Value=1.67 DF=125 P-Value=0.098

G. Average shelf gradient	N	min	mean	StDev	median	max
active	66	0.01	0.74	0.70	0.48	2.86
passive	67	0.01	0.19	0.29	0.08	1.00

T-Value=6.19 DF=124 P-Value≤0.001

H. Slope width	N	min	mean	StDev	median	max
active	22	8.00	45.12	37.99	40.00	205.00
passive	31	10.00	28.69	32.12	21.00	180.00

T-Value=2.83 DF=48 P-Value=0.007

I. Slope-break depth	N	min	mean	StDev	median	max
active	94	500.00	3617.00	1941.00	3000.00	7500.00
passive	70	2100.00	3436.30	835.70	3275.00	4700.00

T-Value=-1.48 DF=120 P-Value=0.141

J. Average slope gradient	N	min	mean	StDev	median	max
active	44	0.16	3.22	1.93	3.85	10.00
passive	47	1.11	5.16	2.07	4.95	8.00

T-Value=-4.13 DF=70 P-Value≤0.001

K. Seafloor depth at the canyon apex	N	min	mean	StDev	median	max
active	120	0.10	302.10	511.90	120.00	4000.00
passive	90	0.10	370.00	401.70	254.00	3000.00

T-Value=-3.82 DF=192 P-Value≤0.001

L. Seafloor depth at the canyon mouth	N	min	mean	StDev	median	max
active	125	200.00	2262.00	1685.00	1500.00	7800.00
passive	76	800.00	2600.00	1021.00	2469.00	5000.00

T-Value=-4.01 DF=194 P-Value≤0.001

M. Minimum distance to shoreline	N	min	mean	StDev	median	max
active	145	0.00	85.80	145.60	10.40	630.30
passive	123	0.00	96.90	145.50	46.00	640.00

T-Value=-5.28 DF=254 P-Value≤0.001

N. Latitude at the canyon apex	N	min	mean	StDev	median	max
active	157	1.01	32.70	14.78	36.82	60.39
passive	129	4.30	30.89	20.13	35.00	71.63

T-Value=1.91 DF=248 P-Value=0.058

Figure 4.10a-n Boxplots of frequency distributions of attributes of source-to-sink systems and of the canyon-physiographic setting linked to submarine canyons of active and passive margins. N = number of readings; min = minimum value; mean = mean value; StDev = standard deviation; median = median value; max = maximum value; DF = degrees of freedom.

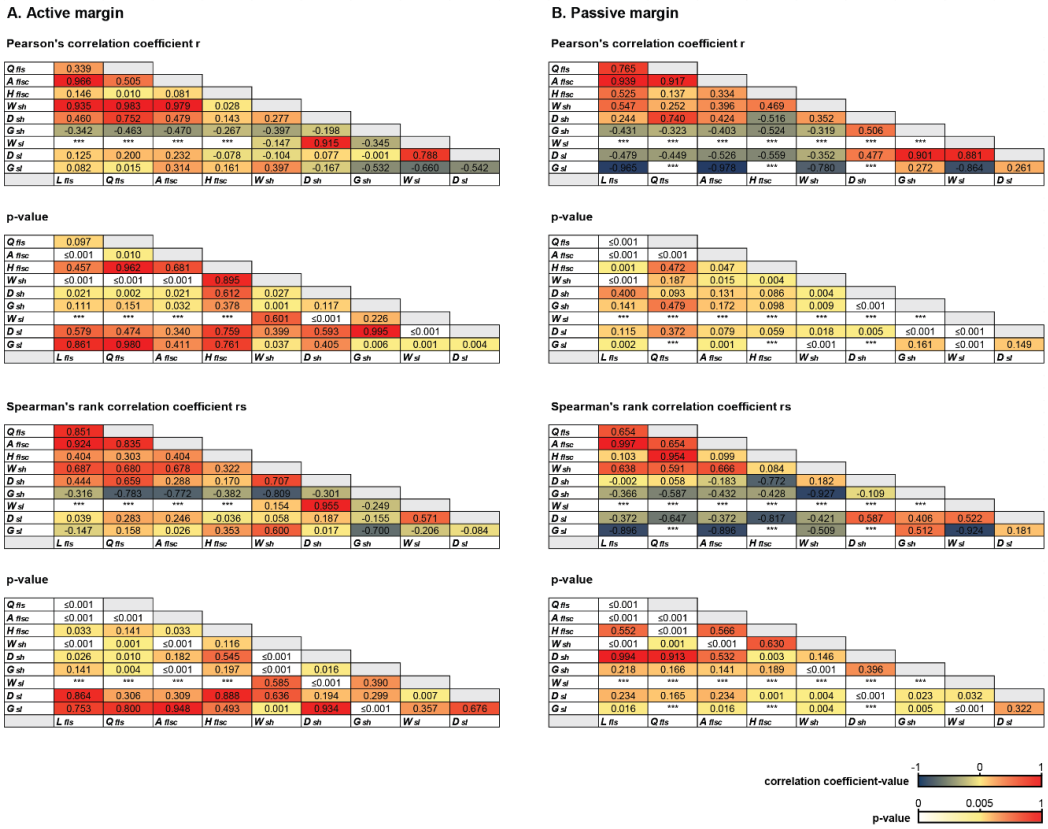

Figure 4.11a&b Results of the correlation analyses of attributes of the source-to-sink system in active vs. passive margins presented as heat maps. L_{fls} = fluvial system length; Q_{fls} = average annual fluvial discharge; A_{flsc} = catchment size; H_{flsc} = maximum catchment elevation; W_{sh} = shelf width; D_{sh} = shelf-break depth; G_{sh} = average shelf gradient; W_{sl} = slope width; D_{sl} = slope-break depth; G_{sl} = average slope gradient; *** = correlations not reported due to small dataset size.

4.4 Discussion

4.4.1 Tectonic influence on controlling factors on submarine-canyon geomorphology

Findings from this study suggest that certain aspects of the morphometry of submarine canyons, and some scaling relationships of canyon morphometric parameters with each other and with attributes of their geological setting, are more strongly expressed in a specific margin type (see Figs. 4.2-4.9), indicating a possible tectonic control. Although commonalities seen in scaling across both margin types indicate that a scaling relationship might not be generally sensitive to factors related to tectonic activity, the possibility

exists that tectonic influences might be overridden by other controlling factors or that different controls in passive and active margins have led to similar geomorphologic expressions in canyons.

In the following sections, the main findings of the study are discussed in the context of a potential tectonic influence on controlling factors on submarine-canyon geomorphology, including intra-canyon sedimentary processes, sediment connection to fluvial and littoral sources, sediment supply to shelf margins and structural controls.

4.4.1.1 Intra-canyon sedimentary processes

The contrast in relative importance of intra-canyon processes along active and passive margins may contribute to certain differences seen in scaling relationships between canyons of the two margin types. For example, intra-canyon-wall failure might be less important as a geomorphic agent in canyons from active margins compared to passive-margin ones (see Chapter 3). This is because slope failures are thought to occur less commonly along active margins compared to passive margins, due to strengthening of the seafloor from recurrent seismic activity (e.g. Strozyk et al., 2010; Nelson et al., 2011; Sawyer & DeVore, 2015; Molenaar et al., 2019); on active margins, large-scale slope failures tend to be linked to high-magnitude earthquakes (e.g. Strozyk et al., 2010; Molenaar et al., 2019). By contrast, active-margin settings with steep terrestrial catchments and narrow and steep shelf configurations promote maintenance of sediment connection of submarine canyons with fluvial outlets and littoral cells even during periods of sea-level highstand, as at present (e.g. Gamberi et al., 2015; Bernhardt & Schwanghart, 2021). Hence, moderate correlations of maximum sidewall steepness with maximum canyon width (Fig. 4.5f) and depth (Fig. 4.5g) in canyons along active margins might reflect the tendency of sediment gravity flows to predominate over intra-canyon slope failure in shaping canyon geomorphology in these settings, via their ability to concurrently increase canyon width, depth and bank steepness by thalweg erosion (e.g. McHargue et al., 2011; Peakall & Sumner, 2015) and canyon margin aggradation from flow overspilling (e.g. Armitage et al., 2010; Soulet et al., 2016). In contrast, the weaker correlations seen for passive-margin canyons

(Figs. 4.5f&g) may be linked to the combined effect of a subordinate influence of sediment gravity flows from the disconnection of canyons to fluvial and intra-shelf sources during periods of sea-level highstand (e.g. Harris & Whiteway, 2011), paired with the variable impact of canyon-wall failure on canyon-wall slopes, canyon width and canyon depth. As a result, relationships between these morphometrics linked to intra-canyon erosion by flows might be overprinted. When deposited near their source, mass failures and their depositional products will lead to lower canyon depths and greater canyon-floor widths over the affected areas, whereas the maximum width between the canyon banks will only increase where the wall collapse extends to the uppermost canyon margin. Intra-canyon slope failures may also have an indirect effect on canyon geomorphology away from the site of failure, particularly when the mass failure transitions into a sediment gravity flow (e.g. Stow, 1986; e.g. Hsu et al., 2008), or when the deposit is remobilised at a later point in time and is transported down canyon (e.g. Khripounoff et al., 2012); as a consequence, mass-failure impact on canyon width, depth and sidewall gradients might vary.

Thus, the co-occurrence of wall failure and sediment gravity flows, which is recognised to act as an autogenic control on the variability in width-to-depth ratios of submarine channels (see Fig. 11 and text in Shumaker et al., 2018), may also be effective in controlling maximum width-to-maximum depth (wdmax) ratios of submarine canyons (see Chapter 3). The smaller mean value and range of wdmax ratio seen for passive-margin canyons compared to active-margin ones (Figs. 4.3b & 4.5d) suggest that width-to-depth aspect ratios in canyons hosted on passive margins tend to be constrained in their magnitude by the way in which wall-collapse may limit canyon-margin aggradation. By contrast, the subordinate role of intra-canyon failure combined with the effect of structural controls on canyon depths and widths (see section 4.4.1.4) can explain the greater range in wdmax ratios seen in active-margin canyons (Figs. 4.3b & 4.5d).

4.4.1.2 Sediment connection to fluvial and littoral sources

Sediment discharge from rivers

Some geomorphic features of submarine canyons are seen to scale, to some degree, with fluvial system length, average annual water discharge, catchment size and maximum catchment elevation. These observations are interpreted to reflect the importance of sediment discharge from rivers as controls on how canyon geomorphology is shaped by erosional and depositional processes (see Chapter 3; cf. Casalbore et al., 2011).

For submarine canyons in active margins, potential causal links between fluvial sediment supply and their length and maximum width are suggested by: (i) moderate scaling of the former with fluvial system length (Fig. 4.8a), average annual water discharge (Fig. 4.8b) and catchment size (Fig. 4.8c), and (ii) moderate scaling of the latter with the area (Fig. 4.8g) and maximum elevation (Fig. 4.8h) of the associated terrestrial catchment. These relationships probably reflect how erosive intra-canyon flows related to fluvial discharge promote lengthening at the canyon head (e.g. Piper & Normark, 2009) and mouth (e.g. Hodgson et al., 2016), as well as canyon widening (e.g. Casalbore et al., 2011).

By contrast, weak correlations of passive-margin canyon length with fluvial system length (Fig. 4.8a) and catchment size (Fig. 4.8c) indicate a lack of control of sediment discharge from rivers on canyon length. This might in part reflect how retrogressive slope failure tends to be a more prominent process along passive margins compared to active ones, and how sediment connection of canyons with fluvial sources in passive-margin settings tend to diminish through time at times of marine transgression (see section 4.4.1.1). For example, incised valleys along passive margins are thought to be more prone to infill during transgressive and highstand intervals due to their commonly shallower depths compared to those along active margins, promoting the disconnection of canyon heads from fluvial sediment sources in passive-margin settings (Harris & Whiteway, 2011). Also, flooding events are less likely to trigger hyperpycnal flows at the mouth of rivers along passive margins, due to the increased sand-grade sediment segregation in their larger coastal and alluvial floodplains (e.g. Milliman & Syvitski, 1992;

Sømme et al., 2009). In addition, larger terrestrial catchments are less affected by extreme weather events, in proportion to their size, compared to smaller ones (e.g. Sømme et al., 2009; Reid & Frostick, 2011).

Despite this, comparably strong scaling of canyon length with average annual fluvial discharge for passive-margin canyons (Fig. 4.8b) might reflect that long-lived sediment-laden turbulent flows (*sensu* Zavala, 2020) linked to discharge from rivers are efficient in traversing wide shelves and entire canyons even during periods of sea-level highstand. and are effective in increasing canyon lengths by erosion at the canyon head and at its mouth. Such hyperpycnal flows are thought to be common at the mouths of medium to large rivers associated with low-gradient terrestrial catchments, and to be able to cover distances of up to several hundred kilometers (Zavala, 2020). The relationship might also reflect how fluvially discharged sediments build up on the shelf in front of river mouths and are remobilised at a later point in time in form of high-volume sediment gravity flows, for example by spring tides (e.g. Talling et al., 2022).

Seafloor depth at the canyon apex

Inverse relationships of average canyon width (Fig. 4.7a) and maximum (Fig. 4.7b) and average canyon depth (Fig. 4.7c) with seafloor depth at the canyon apex seen for canyons from passive margins might reflect how canyons with apices located at greater water depths are more likely to be disconnected from terrestrial and intra-shelf sources, at present and during past sea-level lowstands. Unless such canyons are coupled with a contouritic system (e.g. Warratz et al., 2019), intra-canyon erosion would be limited to mass-wasting events on the slope proximal to and within the canyon, and to wave erosion.

Active-margin canyons tend to have steeper sidewalls if their canyon apex is closer to the shoreline (Fig. 4.7g) and/or at shallower seafloor depth (Fig. 4.7e), whereas in passive margins the maximum canyon sidewall steepness does not correlate with both physiographic parameters (Figs. 4.7e&g). This finding supports the hypothesis that erosive flows originating from within the shelf and terrestrial catchment may be more important in carving steep

canyon walls in active settings compared to passive ones (section 4.4.1.1). This study also finds that average canyon sinuosity and wdmax ratios of canyons in active settings show moderate scaling with canyon bathymetry at the apex, inverse for the former (Fig. 4.7d) and positive for the latter (Fig. 4.7f), which can also be ascribed to the influence of such erosive flows.

4.4.1.3 Sediment supply to shelf margins

The moderate scaling of shelf-break depth with canyon length (Fig. 4.8m), maximum width (Fig. 4.8n) and depth (Fig. 4.8o), and average canyon sinuosity (Fig. 4.8p) for passive-margin canyons might reflect to some degree how higher rates of sediment supply from terrestrial source areas promote subsidence along continental margins and act to push the slope break into deeper waters (cf. Sweet & Blum, 2016; Wang et al., 2019). In contrast, relationships between the shelf-break depth and maximum canyon dimensions and overall canyon sinuosity are weak for active-margin canyons (Figs. 4.8m-p), even though terrestrial catchments in active margins can be characterised by high rates of sediment supply (see also sections 4.4.1.2 & 4.4.1.4), which can be associated with narrow shelves promoting sediment routeing to canyons (e.g. Blum & Hattier-Womack, 2009). This observation may reflect, in part, the relative importance of structural controls on geomorphologic evolution in active settings (see section 4.4.1.4), including the structural control of shelf-break migration (e.g. Han et al., 2016).

4.4.1.4 Structural controls

Faulting and diapirism and their effects related to both gravitational failure and tectonic activity (e.g. Rowan et al., 2004; Hudec & Jackson, 2007; Yang et al., 2020) constitute structural controls that might affect canyon geomorphology in different ways through their influence on sediment-transport and canyon pathways (e.g. Chiang et al., 2012; Doo et al., 2015; Urías Espinosa et al., 2016); they can also do so by reshaping canyon walls (e.g. Yu & Chang, 2002; Bernhardt et al., 2015).

The greater impact of faulting and diapirism linked to tectonic activity on margin configuration, seafloor topography and sedimentary processes in active-margin settings compared to passive-margin ones (e.g. Yang et al.,

2020) may explain some of the differences in scaling and canyon-morphometric characteristics seen between canyons across different tectonic settings.

The value of slope width for predicting canyon length (Sømme et al., 2009; see Chapter 3) is lower in active margins than in passive ones (Fig. 4.8r), which is possibly related to a greater and more prolonged impact of tectonic convergence on slope physiography in active margins compared to passive margins (e.g. Pratson et al., 2007; Yang et al., 2020), and its variable influence on canyon length. Canyon pathways can be deflected by positive topography created by faults and diapirs (e.g. Li et al., 2021), or develop along intra-slope depressions as transform faults (e.g. Greene et al., 1991), or axes of intra-slope basins (e.g. Bourget et al., 2010), thereby increasing canyon length relative to the width of the slope. On the other hand, emerging seafloor topography can lead to canyon abandonment by redirecting sediment pathways (e.g. Chiang et al., 2012), whereas the presence of intra-slope basins (e.g. Harris et al., 2014a) and highs (e.g. Hsiung et al., 2014) can inhibit further extension of the canyon across the slope.

Given the general importance of structural controls on canyon length and average canyon sinuosity in active margins, it is unsurprising that the results indicate that both canyon morphometric parameters are not generally different between the different categories of active margins (convergent, transform and complex settings; Figs. 4a&d).

In contrast, the fact that the maximum width of canyons from complex settings is on average larger compared to that of canyons from convergent and transform ones (Fig. 4.4b) suggests that such settings may be inherently more favourable to the development of wide canyons. In tectonically complex settings with strike-slip tectonics, such as the Cook Strait sector, New Zealand, and offshore Taiwan in the East China Sea, a local widening of canyons might be promoted by the concurrence of transform faulting coupled with recurrent sediment gravity flows, where canyons intersect with strike-slip faults (e.g. Schnürle et al., 1998; Micallef et al., 2014).

In case of the SW Taiwan margin canyons, instead, the development of very wide canyons might be explained by the high frequency of hyperpycnal flows at river mouths (e.g. Milliman & Kao, 2005; Liu et al., 2013). The formation of hyperpycnal flows in the region is favored by enhanced erosion rates in terrestrial catchments from earthquake-related landslides (e.g. Dadson et al., 2005), extended periods of precipitation during the monsoonal wet season (e.g. Zhang et al., 2022a) and associated with typhoons (e.g. Dadson et al., 2005; Milliman & Kao, 2005; Zhang et al., 2018), as well as from decreased levels of salinity of the ambient oceanic water due to high freshwater discharge along the margin (e.g. Dadson et al., 2005).

Despite the fact that both mean canyon length (Fig. 4.2a) and mean maximum canyon depth (Fig. 4.2d) are not significantly different in active and passive margins, length-to-maximum depth (ldmax) ratios are on average significantly higher in active margins (Fig. 4.3c). The findings might reflect how enhanced seafloor relief linked to tectonics tends to increase canyon length, while simultaneously inhibiting canyon deepening. A downcanyon decrease in the erosive power of canyon-traversing flows may be caused by the capture of coarser sediment fractions by intra-slope depressions (e.g. Soutter et al., 2021) and by flow deceleration upstream of slope topography leading to deposition of coarser sediment (e.g. Soutter et al., 2020). Although the data on the average depth of canyons from active and passive margins show that active-margin canyons tend to be significantly shallower (Fig. 4.2e), further investigation is needed to corroborate the findings in view of the limited geographic coverage of the dataset.

4.4.2 Canyon geomorphology and associated characters of deep-water systems

Despite the importance of sediment connection of submarine canyons to sediment sources in terrestrial catchments, shelves and slopes, and the lithological characteristics of source areas for the evolution of deep-water systems (e.g. Normark & Carlson, 2003; Smith et al., 2017; Hessler & Fildani, 2019; Bernhardt & Schwanghart, 2021), the character of a deep-

water system is ultimately controlled by the efficiency of sediment transport through canyons to deep-marine sinks (Hessler & Fildani, 2019).

Stratigraphic forward modelling experiments by Wan et al. (2021) for delta-canyon-fan systems in a passive-margin setting suggest that sediment routeing to basin floor sinks is promoted for shallow and low-sinuosity canyons.

Results by Wan et al. (2021) suggest that intra-canyon basinward transport of coarser grain-size fractions is more efficient in shallower canyons. Canyons along active margins tend to be shallower than passive-margin canyons (Fig. 4.2e), but they also tend to exhibit increased intra-canyon relief, which can inhibit the down-canyon erosive strength of flows via mass extraction (see section 4.4.1.4). This suggests that the relationship identified by Wan et al. (2021) might not be applicable for canyons in active-margin settings. Similarly, the impact of canyon depth on grain-size segregation within canyons might be subdued in canyons associated with passive-margin settings where slope relief is increased by gravitational loading.

The rate of thalweg lateral migration, which determines the canyon sinuosity, controls the caliber of sediment transported down-canyon; in more sinuous canyons, a relatively larger proportion of coarse sediment is deposited along the inner bends and the proximal part of the canyon, whereas in canyons with lower sinuosity the coarser sediment can be more effectively transported down-slope (Wan et al., 2021). Given that the average sinuosity of canyons is neither generally different between active and passive margins (Fig. 4.2f this study; Harris & Whiteway, 2011; see also Chapter 3), nor seemingly different across the considered active-margin settings (Fig. 4.4d), the control of canyon sinuosity on sediment transport dynamics and grain-size segregation is probably not fundamentally different between active- and passive-margin settings and across active margins with different types of plate boundaries.

However, the influence of canyon geomorphology on sediment connection across deep-water environments might be absent or less prominent for active margins where canyons experience “flushing” initiated by large-

magnitude earthquakes (e.g. Atwater et al., 2014; Goldfinger et al., 2012), due to the remobilization of large volumes of sediment, including coarser grain size fractions, and related substrate erosion within the canyon (e.g. Mountjoy et al., 2018).

These aspects highlight the need for modelling studies and conceptual models of S2S and deep-water systems to better consider the wide range of boundary conditions associated with characteristics of continental margins.

4.4.3 Implications of the findings and future work

The comparisons of frequency distributions of canyon morphometric parameters for different tectonic settings (Figs. 4.2a-h and 4.4a-i) corroborate results of earlier quantitative global studies, showing that canyon morphometrics are variably sensitive to factors related to the tectonic-margin type (see Chapter 3; e.g. Harris & Whiteway, 2011). These insights suggest that overall canyon geomorphology cannot be predicted from the tectonic setting alone. The findings that canyons along active margins display a greater variability in aspect ratios of maximum canyon dimensions (Figs. 4.3a-c) indicate that the size of canyon fills in the stratigraphic record might be less reliably estimated from outcrop and subsurface data in active-margin settings compared to passive margins. Moreover, aspects of canyon morphometry in canyons associated with convergent settings are not fundamentally different compared to those in complex settings (Figs. 4.4a-i), suggesting that canyon geomorphology is not primarily controlled by the complexity of the tectonic regime in active-margin settings. Despite this, complex tectonics may be preferentially associated with canyons with larger maximum widths and depths (Figs. 4b&c, see also section 4.4.1.4).

The analysis also shows that scaling relationships of canyon morphometric parameters with attributes of the physiographic setting (Figs. 4.6a&b and 4.7a-h) and source-to-sink (S2S) system (Figs. 4.8a-r and 4.9a&b) might vary between active and passive margins. The same applies for scaling relationships between the different canyon morphometric parameters (Fig. 4.5a-g), and for scaling between attributes of S2S systems (Fig. 4.11a&b). These findings are important because they demonstrate that the

relationships between continental-margin types and the configuration of deep-water systems is more complex than hitherto recognised in conceptual, experimental and numerical models.

The variable and complex influence of the tectonic setting on sediment routeing along S2S systems, on canyon geomorphology, and on the degree of confinement of deep-water fans in settings such as intra-slope basins (e.g. Budillon et al., 2011; Hsiung et al., 2014), lower slopes with complex seafloor topography (e.g. Hsiung et al., 2018), and trenches (e.g. Thornburg et al., 1990; McArthur & Tek, 2021) raises the question whether scaling relationships between submarine canyons and deep-water fans can be predicted. This needs to be investigated in future work.

4.5 Conclusions

A global metastudy of geomorphic characteristics of submarine canyons as a function of the tectonic setting has been conducted. The key findings of the study are that:

(1) Overall canyon geomorphology is not generally different between active and passive margins and across different plate-boundary environments in tectonically active settings.
(2) The role of slope failure as a mechanism governing the morphology of canyons may be subordinate for canyons associated with active margins, compared to passive-margin examples, possibly due to seismic strengthening of seafloors in the former. This indicates that width-to-depth ratios might be inherently limited in their magnitude in canyons in passive-margin settings due to the interplay of intra-canyon sediment flows and canyon-wall failure, with the latter counteracting canyon-margin accretion while promoting canyon widening and aggradation of canyon floors.
(3) Scaling relationships of individual canyon morphometric parameters and aspect ratios of maximum canyon dimensions with attributes of the S2S system and the physiographic setting have been demonstrated for (i) active margins, (ii) passive margins, and (iii) across both margin types. The scaling relationships vary broadly in

magnitude of correlation, but are seldom strong; this reflects how canyon geomorphology is shaped by the complex interplay of different controls, which are only in part influenced by the tectonic setting.

(4) The findings suggest that canyon geomorphology can be to some degree predicted in S2S systems in active and passive margins, but that the predictive value of attributes of the environmental setting might vary across different tectonic settings.

(5) Insights from this study suggest possible genetic links between aspects of canyon geomorphology and characteristics of the physiographic environment related to the tectonic setting. This finding can be applied to improve and help constrain conceptual, experimental and numerical models of submarine canyons and canyon-associated sedimentary systems at source-to-sink scale by (i) demonstrating how the relative importance of controlling factors on canyon morphometry might vary across different tectonic settings; (ii) providing a quantitative characterization of canyon morphometric attributes and associated parameters of the physiographic and environmental setting that can be applied to constrain models in a realistic manner; and (iii) illustrating how insights from the analyses can augment existing semi-quantitative models of source-to-sink systems for different tectonic settings, which have not yet expressly considered submarine-canyon morphometry (e.g. Sømme et al., 2009; Nyberg et al., 2018b).

5 Controls on the geometry of shelf-edge deltas

5.1 Introduction

Shelf-edge deltas (e.g. Steel et al., 2003) – also termed shelf-margin deltas (e.g. Suter & Berryhill, 1985; Porębski & Steel, 2003; Tian et al., 2019), lowstand wedge deltas (e.g. DiBona & von der Borch, 1993) or lowstand wedges (e.g. Algan et al., 2002) – are important components of source-to-sink (S2S) systems due to their role as primary facilitators of sediment transport from continental and paralic realms to deep-water environments (e.g. Steel et al., 2003; Covault et al., 2009; Sylvester et al., 2012; Moscardelli et al., 2019; Gong et al., 2021). Shelf-edge deltas can form related to sea-level regression when rivers extend across the exposed shelf ('forced regression', e.g. Steel et al., 2003; Porębski & Steel, 2006) but also during phases of sea-level highstand provided a sufficiently high sediment supply from the river and narrow shelf width ('normal regression', e.g. Porębski & Steel, 2006; Uroza & Steel, 2008).

Shelf-edge deltas can directly distribute sediment onto continental slopes and basin floors in the following ways: (i) by gravity flows at the mouth of their distributary channel networks (e.g. Posamentier 2003; Almeida Junior et al., 2020); (ii) from the collapse of delta fronts, commonly in response to oversteepening of deposits (e.g. Peng et al., 2017) and triggered by slippage on co-genetic growth faults (e.g. Gillis et al., 2020); (iii) from their progradation across basin slopes (e.g. Porębski & Steel, 2003; Wang et al., 2022a); (iv) and via a direct or indirect linkage to submarine canyons (e.g. Carvajal & Steel, 2009; Sylvester et al., 2012; Liu et al., 2018). A causal link between the genesis and evolution of erosional channel forms on the slope and the presence of shelf-edge deltas is inferred for some S2S systems (e.g. Posamentier, 2003; Perov & Bhattacharya, 2011; Sanchez et al., 2012b; Wang et al., 2022a). As such, it is known that shelf-edge deltas likely exert control on the configuration of their superordinate S2S systems, and especially on down-system deeper-water systems (e.g. Porębski & Steel, 2003; Sylvester et al., 2012).

Moreover, shelf-edge deltas themselves act as large-scale sediment sinks along shelf margins (e.g. Steel et al., 2003; Dixon et al., 2012). Their

stratigraphies constitute recorders of palaeoenvironmental conditions in the linked terrestrial catchments and receiving body of water, with prior studies commonly focussing on the latter (e.g. Cummings et al., 2006; Carvajal & Steel, 2009; Bowman & Johnson, 2014). In addition, shelf-edge delta successions are important targets as reservoirs for petroleum exploration due to their high sand volumes and association with submarine fans (e.g. Suter & Berryhill, 1985; Liu et al., 2018; Wang et al., 2022a). Because of their significant size and reservoir properties, shelf-edge delta successions also have potential value as geological sites for subsurface carbon sequestration and hydrogen storage, and can constitute geothermal reservoirs (e.g. Bachu & McEwen, 2011; Callas et al., 2022; Muhammed et al., 2022).

Furthermore, recognition of the presence of deposits of shelf-edge deltas aids the identification of the location of the shelf margin in ancient S2S sedimentary successions (e.g. Porębski & Steel, 2003), and allows for reconstruction of the effects of repeated sea-level changes at shelf margins (e.g. Gong et al., 2015).

Despite their crucial role in sediment dispersal to shallow- and deep-marine environments, and their influence on slope and basin-floor systems, shelf-edge deltas are commonly overlooked, else are not considered in detail. Their lack in existing models that describe S2S systems is perhaps due to the paucity of 3D high resolution studies of shelf-edge deltaic deposits until the early 2010s (Sylvester et al., 2012) and the fact that there exist relatively few reported examples that developed during the present-day highstand conditions (e.g. Daniell et al., 2020). In subsurface and outcrop their recognition can be difficult where information to constrain the physiographic environment is limited, for example the spatial position of a delta relative to the shelf margin (e.g. Porębski & Steel, 2003), or where the lack of micropalaeontological and organic geochemical analyses prevents an unequivocal identification of the formative palaeo-bathymetry of sedimentary deposits (e.g. Dziadzio et al., 2016). These two factors may contribute to the relatively limited number of ancient shelf-edge deltaic successions identified

and described in the literature compared to the large number of coastal deltas recognised globally during present day (e.g. Nienhuis et al., 2020).

Quantitative studies of the sedimentary record of incised-valley fills (Wang et al., 2019; 2020) and Gilbert-type deltas (Budai et al., 2021) have generated new insights into genetic relationships between morphometric characteristics of fluvial systems along continental margins and their controls. Findings of these studies demonstrate a great variability in geometries of both sedimentary systems. However, they suggest that, although river geomorphology is shaped in complex ways by the influence of environmental factors on river-forming processes, some scaling relationships in parts of fluvial systems can be recognised globally and for specific environmental classes.

The aim of this chapter is to demonstrate and explain the effects of controlling factors on geometric aspects of shelf-edge deltas, thereby expanding existing S2S models and providing tools for the estimation and prediction of expected deltaic sedimentary architectures in outcrop and subsurface settings. The specific objectives of this research are as follows.

(i) To quantitatively investigate shelf-edge deltaic deposits with respect to their depositional architecture (lobe vs. lobe complexes) and in terms of their geometry from their lengths, widths, thicknesses and areas on a global scale and in relation to a range of environmental variables.

(ii) To evaluate geometric scaling relationships within deltaic elements (1) in general; and (2) classified based on their hierarchical level (i.e. lobe vs. lobe complex), with particular consideration of the following:
- present-day characteristics of the associated terrestrial catchment and modern shelf width of the superordinate S2S system; by this, this study explores whether this approach reveals scaling relationships between shelf-edge delta geometry and aforementioned S2S system attributes, which might enable first-order predictions of palaeogeographic environments to be made in geographic regions with limited data availability;

- the palaeolatitudinal position of the shelf-edge delta during its evolution.

5.2 Dataset and methods

5.2.1 Dataset

A global, literature-derived dataset of 112 Permian to late Quaternary examples of shelf-edge deltaic elements has been collated to investigate controlling factors that influence shelf-edge delta geometry. The dataset is based on outcrop, seafloor and subsurface data originally presented in 50 peer-reviewed publications. Corresponding to the study of one or several shelf-edge deltas by a particular group of researchers, the data are organised in 39 case studies (Fig. 5.1 & Tab. 5.1); these are coded according to the standard of the Shallow-Marine Architecture Knowledge Store (SMAKS), a relational database that enables the storage of data of clastic sedimentary systems, including environmental parameters and metadata (Colombera et al., 2016). In addition, bespoke attributes such as the fluvial feeder-system type and source-to-sink system setting have been created to achieve the set objectives.

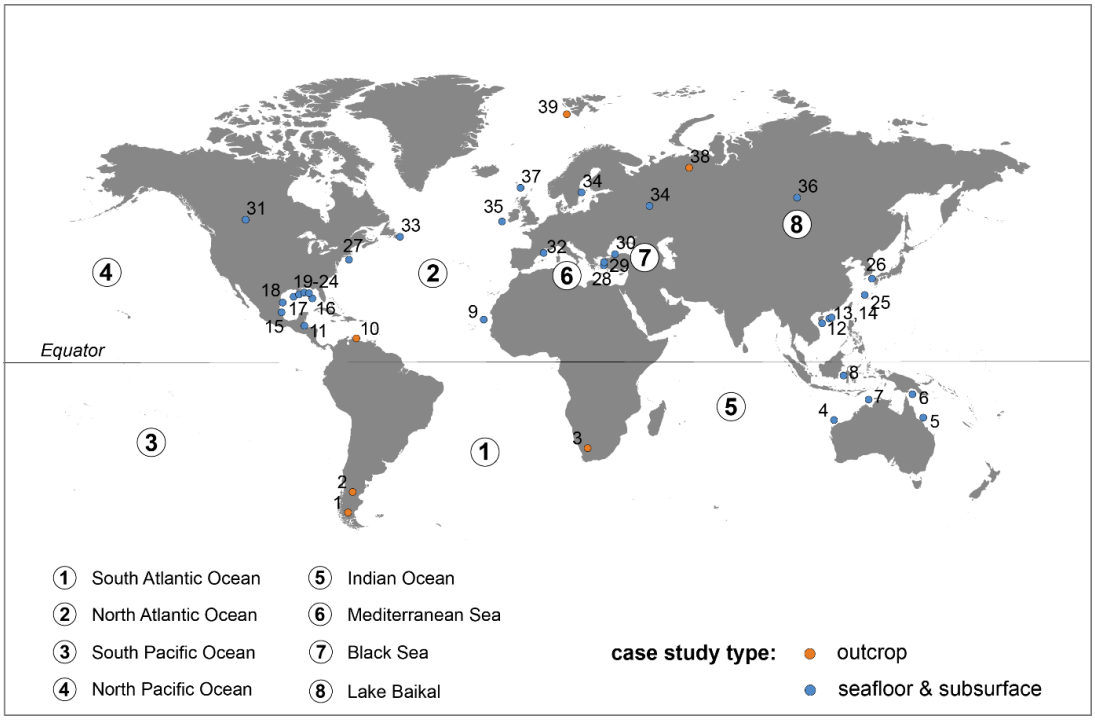

Figure 5.1 Overview map of distribution of the 39 case studies and survey type (World map from freevectormaps.com).

ID	Case study	No. of elements (c/l/u)	Geographic region	Age	Reference(s)
1	Dorotea Fm., Magellan Basin, S Chile	-/-/1	South America	Upper Cretaceous	*Schwartz & Graham, 2015*
2	Lajas & Los Molles fms., S Neuquen Basin, Argentina	1/3/-	South America	Lower-Middle Jurassic	*Almeida Junior et al., 2020*
3	Lower Kookfontein Fm., Tanqua Karoo Basin, S Africa	-/-/1	Africa	Permian-Triassic	*Dixon et al., 2013*
4	Shelf-edge deltas, N Carnavon Basin, NW Australia	-/3/-	Australia	Miocene	*Sanchez et al., 2012a; 2012b*
5	Shelf-edge deltas, Great Barrier Reef, NE Australia	-/3/-	Australia	Mid-Pleistocene	*Daniell et al., 2020*
6	Shelf-edge delta, N Ashmore Trough, Gulf of Papua	1/4/-	Australia	Late Pleistocene	*Tcherepanov et al., 2008; Droxler & Jorry, 2013*
7	Bonaparte Delta, NW Australia	1/3/-	Australia	Late Quaternary	*Bourget et al., 2014*
8	Mahakam Delta, E Borneo, Indonesia	1/-/-	Asia	Late Pleistocene	*Roberts & Sydow, 1996; Roberts et al., 2000*
9	Shelf-edge deltas, offshore W Africa	-//3	Africa	Pleistocene	*McMaster et al., 1970a; 1970b; 1971*
10	Mayaro Fm., Palaeo-Orinoco Delta	-/-/1	South America	Pliocene	*Bowman & Johnson, 2014*
11	Shelf-edge delta, offshore Belize	1/-/-	Central America	Late Pleistocene	*Droxler & Jorry, 2013*
12	Shelf-edge deltas, offshore S Hainan Island	-/-/2	Asia	Late Miocene and Pliocene	*Liu et al., 2018*
13	Zhujiang Fm., Baiyun Sag, Pearl River Mouth Basin, N South China Sea	1/-/-	Asia	Early Miocene	*Yu et al., 2021*
14	Zuhai Fm., Baiyun Sag, Pearl River	-/-/4	Asia	Late Oligocene	*Wang et al., 2022a*

	Mouth Basin, N South China Sea				
15	Shelf-edge deltas, NW Gulf of Mexico, USA	2/7/-	North America	Late Pleistocene	*Suter & Berryhill, 1985; Banfield & Anderson, 2004; Anderson, 2005; Anderson et al., 2015*
16	Shelf-edge deltas, NE Gulf of Mexico, USA	1/-/4	North America	Pleistocene	*Gardner et al., 2005*
17	Shelf-edge deltas N Gulf of Mexico, USA	-/1/6	North America	Pleistocene	*Abdulah et al., 2004; Anderson et al., 2004*
18	Upper Wilcox Group, Rosita Delta System, Gulf Coast Basin, S Texas, USA	3/2/-	North America	Palaeogene	*Edwards, 1980; 1981*
19	Shelf-edge delta, offshore Louisiana, N Gulf of Mexico, USA	1/-/-	North America	Mid-Pleistocene	*Perov & Bhattacharya, 2011*
20	Mississippi Canyon, Block 109, N Gulf of Mexico, USA	-/-/2	North America	Mid-Pliocene	*Mayall et al., 1992*
21	Fuji-Einstein shelf-edge delta, NE Gulf of Mexico, USA	1/5/-	North America	Mid- to Upper Pleistocene	*Sylvester et al, 2012*
22	Western shelf-edge delta	-/-/1	North America	Late Quaternary	*Sager et al., 1999*
23	Shelf-edge deltas, NE Gulf of Mexico, USA	4/11/-	North America	Upper Pleistocene	*Sager et al., 1999; Gardner et al., 2007*
24	Lagniappe shelf-edge delta, N Gulf of Mexico, USA	1/-/-	North America	Late Pleistocene	*Roberts et al., 2000; 2004; Roberts & Fillon, 2014*
25	Shelf-edge delta, N Okinawa Trough, offshore SW Japan	-/-/1	Asia	Late Pleistocene	*Li et al., 2020a*
26	Shelf-edge deltas, Korea Strait	1/-/2	Asia	Late Pleistocene	*Yoo et al., 2017*
27	Shelf-edge deltas, Baltimore Canyon Trough, NE USA	1/2/2	North America	Early Cretaceous	*Poag et al., 1990*
28	Bakircay shelf-edge delta, Turkey	-/1/-	Asia	Late Pleistocene	*Aksu et al., 1987*
29	Gediz shelf-edge delta, Turkey	1/-/-	Asia	Late Pleistocene	*Aksu & Piper, 1983; Aksu et al., 1987*

30	Sakarya shelf-edge delta, Turkey, S Black Sea	1/-/-	Asia	Late Quaternary	*Algan et al., 2002*
31	Shelf-edge deltas Clinothem 9 & 10	-/-/2	North America	Late Cretaceous (Maastrichtian)	*Carvajal & Steel, 2009*
32	Shelf-edge delta, Rhône shelf, S France	/-/1	Europe	Late Pleistocene	*Tesson et al., 1990*
33	Missiauga Fm., Nova Scotia, Canada	-/-/1	North America	Early Cretaceous	*Cummings & Arnott, 2005; Cummings et al., 2006*
34	Shelf-edge delta, Poland	-/-/1	Europe	Lower Oligocene	*Dziadzio et al., 2016*
35	Shelf-edge deltas, Porcupine Basin, offshore W Ireland	1/1/2	Europe	Palaeogene (Palaeocene-Early Eocene)	*Ryan et al., 2009*
36	Selenga River Delta, Lake Baikal, Siberia, Russia	-/-/1	Asia	Late Quaternary	*Dong et al., 2016*
37	Munkagrunner Ridge shelf-edge delta, Faroe-Shetland Basin	-/-/1	Europe	Mid-Eocene	*Olavsdottir et al., 2010*
38	Shelf-edge delta, W Siberia, Russia	-/-/1	Asia	Lower Cretaceous	*Pinous et al., 1999*
39	Eocene Battfjellet Fm., Spitsbergen	-/-/2	Europe	Eocene	*Uroza & Steel, 2008*

Table 5.1 Overview of the 39 case studies of the study (for their geographic location see also Figure 5.1). No. of elements = numbers of deltaic elements investigated; c = delta complex; l = delta lobe; u = unclassified hierarchical level of the deltaic element; Fm. = formation.

5.2.2 Studied variables

Shelf-edge delta geometry has been investigated in terms of (i) variability of geometric parameters of deltaic architectural elements, and (ii) relationships between delta geometry and attributes of the environmental setting. The following sections provide an overview of the studied variables and their definitions (see also Figures 5.2, 5.3 & Tab. 5.2).

Shelf-edge delta definition

Two types of definitions of shelf-edge deltas exist in the literature. Some authors apply the term *sensu lato*, i.e., by also including deltas that terminate

in the vicinity of the shelf margin (e.g. Sanchez et al., 2012b). According to other authors, shelf-edge deltas are defined *sensu stricto* as deltas that prograded onto the shelf edge (e.g. Almeida Junior et al., 2020). In this study, shelf-edge deltas were considered that were interpreted by the original authors with a high confidence to have physically reached the shelf margin during the time of delta activity.

5.2.2.1 Deltaic elements

Shelf-edge deltas are composite, terminal depositional environments of rivers consisting of different architectural element types and subenvironments (e.g. Edwards, 1981; Schwartz & Graham, 2015; see Fig. 5.2a&b this study). The evolutionary history of a shelf-edge delta is recorded in part in its internal hierarchical organisation; shelf-edge deltas can display simple or complex configurations depending, for example, on the number of developed lobes, which correspond to the drainage history of the associated fluvial system(s) (e.g. Roberts et al., 2000).

In this study, a *delta lobe* is defined as a sedimentary body consisting of cogenetic delta top, delta-front, and prodelta deposits associated with a specific drainage configuration of a fluvial system. A *delta-lobe complex* – 'lobe complex' hereafter – represents a unit of an immediately higher hierarchical order recognised by the original authors, which encompasses a group of delta lobes (Figure 5.3). For some shelf-edge deltas of the study, the internal hierarchical organisation of their stratigraphy is not described in the literature; thus, hierarchical levels could not be assigned. Where this is the case, the hierarchy of the deltaic architectural elements is recorded as "unclassified". It may also be the case that a third level of hierarchical order exists, where a group of delta-lobe complexes forms a set of delta complexes; however, such potential cases are not formally categorised in this study.

Geometries of delta lobes, lobe complexes and unclassified delta elements have been characterised in terms of the following geometric parameters: (i) dip length, (ii) width along strike, (iii) thickness and (iv) plan-view area. Based on the type of observation, measurements have been categorised into

maximum, true, partial and unlimited values (cf. Colombera et al., 2016), which are defined as follows.

- *Maximum values* of length, width, thickness and area represent the true maximum extent of the sedimentary unit.
- *True values* are measurements which have been recorded along the main axes of a delta element and include observations of the element boundaries, but which may not represent the maximum value.
- *Partial values* comprise measurements along or parallel to the main axes of a delta element but for which one of the element boundaries is not observed or eroded.
- *Unlimited values* include observations of architectural elements whose boundaries are not seen and/or have been eroded.

The latter three types of observations are explicitly considered due to the large-scale nature of shelf-edge deltas and the fact that full observation of the entire system in seafloor, subsurface and outcrop settings is dependent on both the area and depth range covered by a survey, versus the size of the shelf-edge delta. Moreover, individual deltaic element boundaries tend to be obscured in plan-view in shelf-edge deltas with a multi-lobate architecture, and with increasing number of delta lobes (see also section 5.2.4).

Where true, partial and unlimited values were obtained from published datasets, the largest measured value was recorded. A schematic overview of the different types of dimensional values is provided in Figure 5.3.

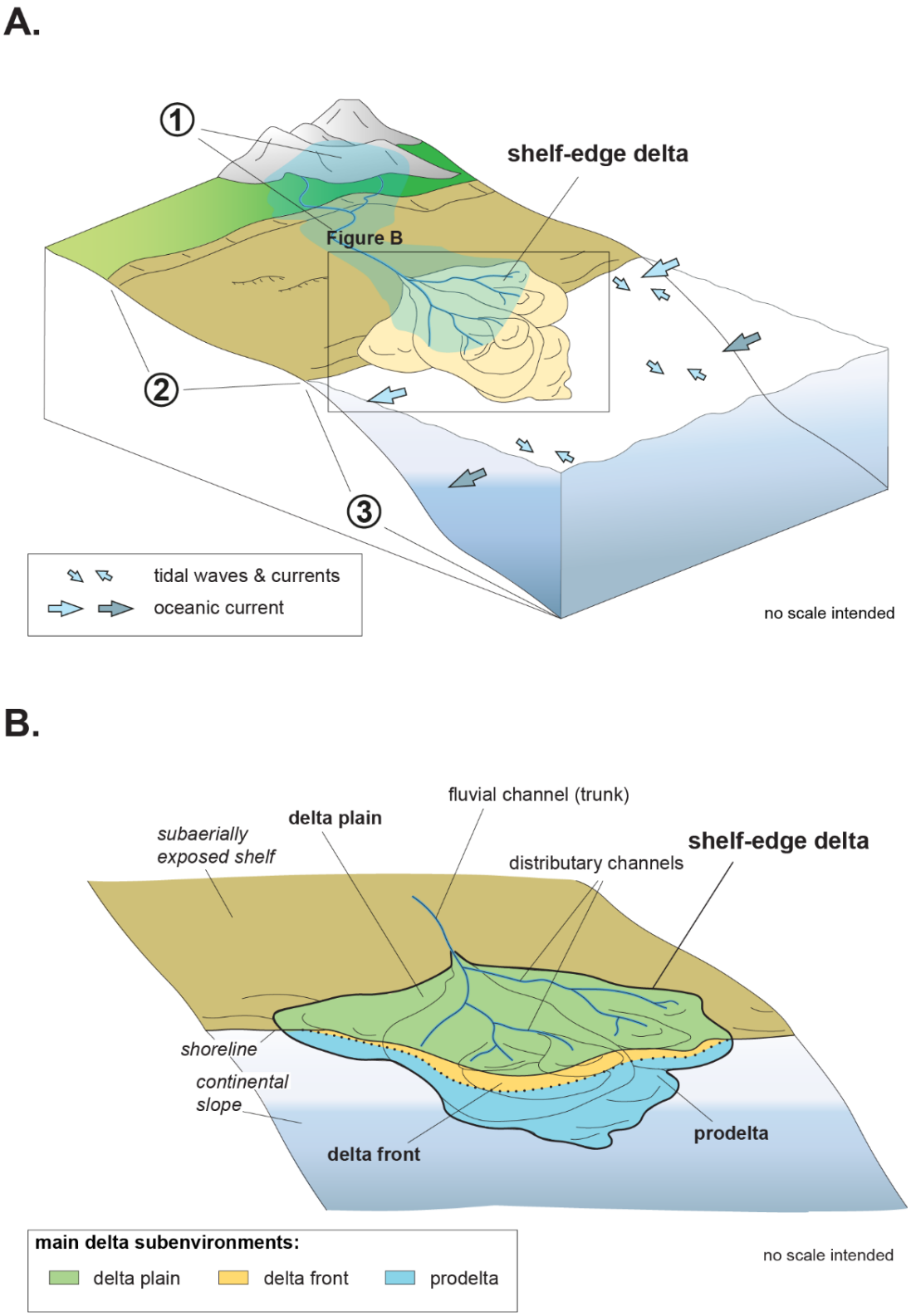

Figure 5.2a&b A. Conceptual model of a shelf-edge delta in context of the main segments of a source-to-sink system. 1 = Terrestrial catchment; 2 = Continental shelf (emerged); 3 = Continental slope. B. Main depositional subenvironments within a shelf-edge delta. Depicted shelf-edge delta evolution during lowstand conditions.

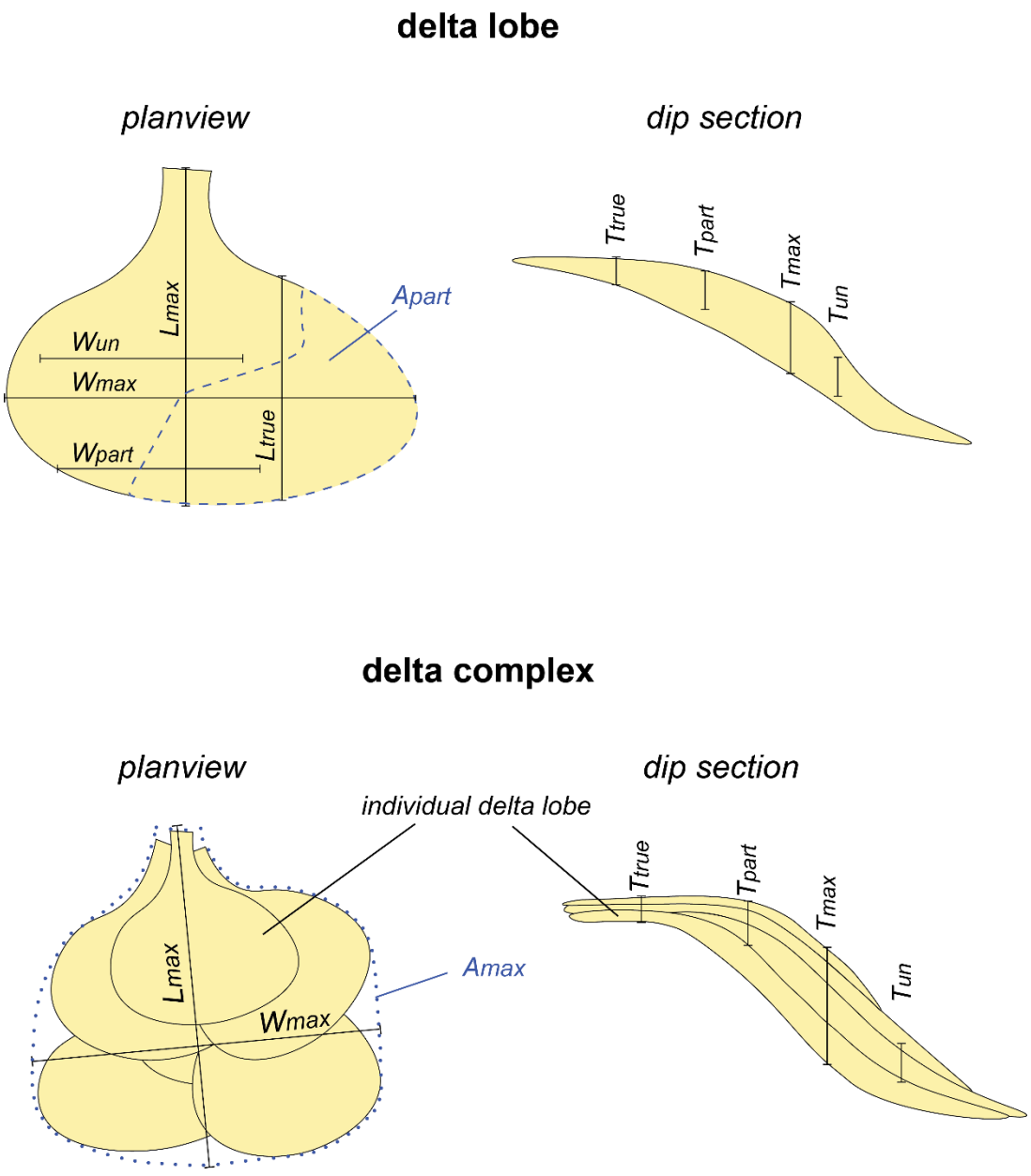

Value type	Code	Definition
Maximum	*max*	the true maximum dimension along the axis of an architectural element
True	*true*	a true value along the axis of an architectural element but not the maximum value
Partial	*part*	one boundary is known whereas the other is not observed or eroded
Unlimited	*un*	value measured for an architectural element whose boundaries are not seen

Figure 5.3 Schematic illustration of hierarchical relationships between deltaic elements and of value types of measurements and their definitions in this study. *L* = length; *W* = width; *T* = thickness; *A* = area.

5.2.2.2 Source-to-sink (S2S) system attributes

Data on aspects of the physiographic setting and source-to-sink system during the time of delta activity that can be drawn from the literature, where

available, include the position of the palaeo-shoreline, catchment characteristics of the palaeo-river, and palaeo-bathymetry. However, meaningful correlation analyses of relationships between geometric parameters of deltaic elements and characteristics of their terrestrial catchments and the local configuration of the margin are not possible because of the relatively small numbers of observations in the overall dataset. Also, due to the paucity of modern examples of shelf-edge deltas that are active during current highstand conditions in the case studies (see Tab. 5.1), such relationships cannot be evaluated within the framework of modern S2S systems, for which a better spatial control exists. Instead, for shelf-edge deltas of Late Pleistocene age, characteristics from the present-day environment were extrapolated. The following proxy variables were obtained.

- *Terrestrial catchment:* The length, average annual fluvial discharge, catchment area and maximum elevation of the modern fluvial system at the location of the delta; for deltas fed by multiple rivers, their cumulative length, annual discharge, and catchment areas as well as the maximum elevation of the highest peak in the combined catchment have been considered. Values were obtained, where reported, from the publication(s) associated with the case study, from the fluvial database of Milliman & Farnsworth (2011), and Google Earth.
- *Shelf width:* The modern shelf width at the delta location relative to the present-day shoreline has been recorded from maps in the publications used in the case studies and from open-source worldwide bathymetry datasets (https://www.ncei.noaa.gov/maps/bathymetry/, n.d., GEBCO 2019 NOAA NCEI Visualization; Google Earth). The shelf edge is defined by an abrupt change in gradient between the outer continental shelf and upper continental slope (e.g. Dietz & Menard, 1951; Harris & Macmillan-Lawler, 2016), which is reflected in the narrowing of spacing between bathymetric contour lines over a short distance in this region.

This approach is subject to various types of uncertainty, and the degree to which present-day observations are applicable varies across the studied variables. For example, discharge rates of a river and the size of the associated drainage basin might display significant variability over a glacial-interglacial cycle due to fluctuations in climate, which in turn affect precipitation and erosion rates. Similarly, sea-level change related to glaciation and deglaciation exerts control on the width of shelves and on the size of the continents that rivers may traverse. Also, differences in the maximum elevation of catchments between the Late Pleistocene and the present day are expected to exist in relation to postglacial isostatic responses.

5.2.2.3 Environmental attributes

Hydrodynamic-process regime

Based on the interpretation by the original authors of the case studies, the hydrodynamic-process regime under which a shelf-edge delta was deposited has been classified as (i) fluvial-dominated or (ii) mixed-process. A mixed-process regime is assigned where hydrodynamic processes of the marine or lacustrine water body are identified as the predominant control, or of equal importance as the delta-associated fluvial system(s) on characteristics of its depositional record. In marine settings, wave- and current activity have been inferred to exert a major control on the depositional record of shelf-edge deltas from the erosion and redistribution of delta deposits related to tides (e.g. Uroza & Steel, 2008; Yoo et al., 2017) and unidirectional oceanic currents (e.g. Yoo et al., 2017), whereas storm influence can act in both marine and lacustrine settings (e.g. Dziadzio et al., 2016). In some cases, a mixed-process regime category is applied to systems in which the process regime changes over time (e.g. Roberts et al., 2000) or varies laterally within a shelf-edge delta (e.g. Carvajal & Steel, 2009; Schwartz & Graham, 2015; Laugier & Plink-Björklund, 2016).

Fluvial feeder-system type

The fluvial feeder-system type has been assigned as “single source” or “multiple source”, depending on whether the depositional evolution of a

shelf-edge delta is associated with a single river or two or more fluvial systems, respectively.

Source-to-sink (S2S) system setting

To assess the role of the S2S system configuration of continental landmasses versus islands on shelf-edge delta geometry, shelf-edge deltaic elements have been classified as being associated with either a (i) continental, or an (ii) insular S2S system setting, depending on whether the terrestrial catchment, shelf and slope of the delta-building fluvial system(s) are associated with a continental landmass (continental setting) or an island (insular setting).

Oceanographic environment

The studied shelf-edge deltas are classified based on their oceanographic environment as being associated with either (i) open seas, or (ii) semi-enclosed and enclosed seas. The first class constitutes oceanic environments that may be characterised by oceanic gyres and that share hydrodynamic interactions with adjacent seas. The second class comprises seas, gulfs and straits, which display limited hydrodynamic connection to bordering oceans and seas and where oceanic gyres are absent. Shelf-edge deltas active in lakes were not considered.

Palaeolatitude

Relationships between processes related to the latitudinal position of a shelf-edge delta and its geometric characteristics have been assessed by referring to the absolute latitude of a shelf-edge delta during its period of activity, in both northern and southern hemispheres. Palaeolatitude data were commonly lacking in the case studies. To obtain palaeolatitudes for the studied shelf-edge deltas, the ‘palaeolatitude calculator’ (model version 2.1) has been used; this is an open-source online tool that enables determination of palaeolatitudes for a specified age or age range and a palaeomagnetic reference frame (van Hinsbergen et al., 2015). Modern latitudes of the studied systems were measured from figures in the literature and from open-source bathymetry and satellite imagery as follows.

(i) For delta lobes and lobe complexes, the latitude at their respective downdip delta toe has been measured where data coverage of the distal part of the element is given.

(ii) In case studies with limited spatial coverage, as in some of the outcrop or subsurface studies based on borehole data, the centre point of the study area has been chosen.

(iii) From the age range determined by authors, palaeolatitude was obtained for the mean age between lower and upper age boundary.

Based on the palaeolatitudinal location, the influence of climate related to major latitudinal belts has been investigated for shelf-edge deltaic deposits in tropical zones (latitudes between 0° and 23.5°) and temperate zones (between 23.5° and 66.5°). Only two shelf-edge deltas of the study are located in polar zones at latitudes ≥ 66.5°.Some of the shelf-margin successions considered herein are located at mid- and high-temperate latitudes, in regions that might have been glaciated in the past.

For case studies 8, 25, 28, 29, 30, 31 and 34 (see Table 5.1), where the site of the case study is located on an unconstrained plate, the palaeolatitude could not be obtained with the ‘palaeolatitude calculator’ tool (van Hinsbergen et al., 2015). For Late Quaternary shelf-edge deltas (Late Pleistocene or Holocene) the modern latitude has been used. This also includes case studies 8, 25, 28, 29 and 30.

Study parameter	**Definition**
Geometric attributes of deltaic elements	
L [m]**	Length of the delta element measured along the axis between updip delta tip and downdip delta toe, or parallel to it
W [m]**	Width of the delta element measured orthogonal to the length axis
T [m]**	Recorded thickness of the delta element
A [km^2]**	Area of the delta element
Terrestrial catchment [1]	

L_{fls} [km]**	Length of the fluvial system associated with the shelf-edge deltaic deposits from headwater to river mouth; for multiple-sourced shelf-edge deltaic elements the cumulative length has been recorded
Q_{flsc} [km^3/yr]**	Mean annual discharge of the fluvial system; for multiple-sourced shelf-edge deltaic elements the cumulative length has been recorded
A_{flsc} [km^2]*	Size of the drainage area associated with the fluvial system; for multiple-sourced shelf-edge deltaic elements the cumulative length has been recorded
H_{flsc} [m]**	Maximum elevation of the catchment of the fluvial system; for shelf-edge deltaic elements sourced by several rivers the elevation of the highest peak in the combined catchments has been considered
Continental shelf [1]	
W_{sh} [km]**	Width of the modern shelf at the location of the delta
Environmental setting	
Fluvial-feeder system type*	Based on the association with an individual or several fluvial systems: (i) single-source vs. (ii) multiple-source
Hydrodynamic-process regime*	The predominant process regime during deposition of the shelf-edge delta as interpreted by authors of the case studies, and classified as (i) fluvial-dominated vs. (ii) mixed-process; the latter category comprises process regimes characterised by different hydrodynamic processes acting concurrently or alternating over time
Source-to-sink system setting**	Association of the shelf-edge delta with a (i) continental or (ii) insular margin
Oceanographic environment**	(i) Open seas: large-scale oceanic environments with unrestricted hydrodynamic connection to adjacent oceans and seas & characterised by oceanic gyres; (ii) Semi-enclosed and enclosed seas: smaller-scale seas, gulfs and straits with limited

	hydrodynamic exchange with connected seas, largely land-bound & no oceanic gyres
Lat_{abs} [°]**	Absolute palaeolatitude at the shelf-edge delta location (see section 5.2.2.3 for details on the calculation)
[1] only investigated for shelf-edge deltaic elements of a Late Pleistocene or younger age	

Table 5.2 Study parameters considered in this study. A single asterisk (*) denotes values that have been retrieved from the literature as stated by the authors. Two asterisks (**) denote values that have been obtained either from the literature, as reported by the original authors, from open-source bathymetry, or have been calculated, or a combination thereof.

5.2.3 Statistical analyses

All statistical analyses were carried out in Minitab 19. The following statistical methods have been applied.

- *Descriptive statistics*: Descriptive statistics have been evaluated for frequency distributions of geometric parameters of deltaic elements in general and for delta lobes and delta complexes. In addition, descriptive statistics have been assessed for deltaic elements classified based on (i) fluvial feeder-system type, (ii) hydrodynamic-process regime, (iii) source-to-sink system setting, (iv) oceanographic environment, and (v) absolute palaeolatitudinal position of the shelf-edge delta; within a class.
- *Correlation analysis*: Relationships between geometric parameters of deltaic elements – in general and for delta lobes and delta complexes – and between delta element geometries and environmental attributes have been investigated to explore the strength and sign of correlation between pairs of studied variables.

Because the full observation of shelf-edge deltaic elements in outcrop and in subsurface is often hindered due to their size and obscurement or erosion of element boundaries (see section 5.2.4), true, partial and unlimited values often correspond to the largest possible morphometric measurements obtainable from a published dataset. Therefore, statistical analyses have been conducted based on inclusion of observations of these types. In cases where

the sample size of maximum values of morphometric parameters of deltaic elements was sufficiently high, additional statistical analyses were undertaken separately.

5.2.4 Limitations of the study

The following limitations are likely to affect the results and interpretations presented in this study:

(i) In metastudies, unidentified data errors in the original datasets might be inherited by the collated dataset. This has been minimised in the present study by only considering peer-reviewed publications.

(ii) Geographic bias is likely introduced from the geographic distribution of published studies. For example, many case studies are centred on the Gulf of Mexico (see Fig. 5.1), due to the special economic interest in this geographic region, most commonly for hydrocarbon exploration (e.g. Lore et al., 1999). In contrast, shelf-edge deltas recognised in some regions are relatively understudied, such as those of the West African (e.g. McMaster, 1970a, b; 1971) and Belize (e.g. Ferro et al., 1999; Droxler & Jorry, 2013) continental margins.

(iii) The size of the dataset is affected by the paucity of modern shelf-edge deltas and by challenges in the identification of their ancient counterparts in outcrop and in subsurface data. As a consequence, some of the statistical analyses are based on few observations (see Figs. 5.4 to 5.13) or on observations from modern S2S systems (see sections 5.3.2.1 & 5.3.2.2). Statistical analyses based on different types of observations have limited value because they include underestimates of values. For example, partial thickness values of deltaic elements will return a lower average thickness and will skew the frequency distribution to smaller values.

(iv) Shelf-edge deltas might not be entirely covered by seafloor and subsurface surveys (e.g. Liu et al., 2018), and are unlikely to be fully displayed in outcrop (e.g. Schwartz & Graham, 2015; Almeida Junior et al., 2020). Hence, due to the large scale of shelf-edge deltas, maximum element dimensions are likely underrepresented

in datasets of case studies covering a smaller area than the actual shelf-edge delta. Moreover, geometric values of delta elements obtained from seafloor maps and seismic datasets are likely smaller than the true values. This is because boundaries between the distal, fine-grained parts of delta lobes and the adjacent seafloor are difficult to determine at this level of data resolution. Furthermore, in multilobate shelf-edge deltas, element boundaries and areas of older delta lobes might be partially or entirely obscured by younger ones in plan-view (e.g. Figure 6 of Sylvester et al., 2012). As a consequence, partial and unlimited observations are more likely in systems with a more complex architecture. Also, with increasing depth, shelf-edge deltaic deposits in the subsurface tend to be less clearly imaged on seismic reflection datasets and therefore characterised in less detail.

(v) In addition, 3D datasets are less common than 2D and 1D datasets, meaning that the entire shelf-edge delta is not usually surveyed, and morphometric measurements are unlikely to represent maximum values.

(vi) The type of survey and its data resolution can affect inferences of the process regime. The interpretation of the hydrodynamic regime is often founded on the shape of the shelf-edge delta and its lobes, as outlined by mappable palaeoshorelines, in absence of high-resolution sedimentological analyses (e.g. Abdulah et al., 2004; Sanchez et al., 2012a). However, it has been argued that tidal signatures in shelf-edge deltas can only be reliably assessed from the latter, giving rise to the possibility that this class of shelf-edge delta is more common than has been acknowledged hitherto (see Cummings, 2006).

(vii) Commonly, thickness values corrected for compaction, which varies with depth of burial, were not reported by the original authors.

(viii) Some environmental factors and processes are thought to influence the development and preservation potential of shelf-edge deltas in the depositional record. This might lead to certain delta

subenvironments being relatively underrepresented in the dataset and also affects the type of observation for delta-element geometries. For example, where delta tops and delta fronts have been eroded by rivers (e.g. Steel et al., 2003), waves (e.g. transgressive ravinement, Yoo et al., 2017; Santra et al., 2013), mass failures (e.g. Dixon et al., 2012; 2013), or retrogradation of submarine canyon heads (e.g. Dasgupta & Buatois, 2015), geometric values represent partial or unlimited observations.

(ix) Some relationships between shelf-edge delta geometry and attributes of the environmental setting might be the expression of covariance between said variables and factors that were not evaluated in this study.

(x) Although the definitions of both a delta lobe and a delta complex – as applied in the literature and adopted in this project – establish a direct hierarchical relationship between the two types of deltaic elements, their definitions are not bound to a specific hierarchical level within a shelf-edge delta. Thus, each of these hierarchies can be applied to describe deltaic units of variable size and temporal significance.

5.3 Results

In the following sections, the results of the statistical analyses are presented. Descriptive statistics of frequency distributions of geometric parameters of deltaic elements were investigated for the entire dataset (section 5.3.1.1) and for shelf-edge delta elements classified based on the following environmental attributes: (i) hydrodynamic-process regime (section 5.3.3.1), fluvial feeder-system type (section 5.3.3.2), source-to-sink system setting (section 5.3.3.3), oceanographic environment (section 5.3.3.4), and palaeolatitudinal zone (section 5.3.3.5). All frequency distributions are graphically displayed as boxplots, with the results of the statistical analyses reported below the corresponding figures.

Scaling relationships within shelf-edge deltaic elements were assessed by correlation analyses, with the data shown as scatterplots (section 5.3.1.2).

Additional correlation analyses were conducted to explore scaling relationships between delta-element geometric parameters and variables of the terrestrial catchment (section 5.3.2.1), shelf width (section 5.3.2.2) and palaeolatitude (section 5.3.2.3).

5.3.1 Shelf-edge delta geometry

Of the 112 deltaic elements in the study, 46 could be classified as delta lobes, and 23 as delta complexes. Although the majority of values for each geometric parameter were obtained from partial observations (see Fig. 5.4a-d), assessment of their frequency distributions help to constrain minimum values of shelf-edge delta dimensions, in general and for different hierarchical levels, and to identify variation in value distributions in the dataset.

5.3.1.1 Frequency distributions of shelf-edge deltaic elements

Deltaic elements

Deltaic elements of shelf-edge deltas display a wide range in dimensions and areal extent. The studied shelf-edge deltaic elements are at least 1.01 km long, 2.73 km wide, 9.4 m thick and have a minimum area of 4 km^2. For all types of observations, median values of lengths, widths, thicknesses and areas are 16.46 km, 18.80 km, 80 m, and 1,265 km^2, respectively. The greatest length (121 km), width (200 km) and area (15,276 km^2) are seen in delta elements of the Bissagos Delta (offshore W Africa; McMaster et al., 1970b) that could not be classified in terms of their hierarchical level and only constitute a true maximum value in case of shelf-edge delta width. Five of the studied shelf-edge deltas display delta-element thicknesses of 900 metres, the Zapata and Duval delta complexes (Upper Wilcox Group, Rosita Delta System, Gulf Coast Basin, S Texas, USA; Edwards, 1980; 1981), and Cape Charles Delta, Ocean City Delta and Long Branch Delta (Baltimore Canyon Trough, NE USA; Poag et al., 1990). These values represent partial observations (Fig. 5.4a-d).

Delta lobes versus delta complexes

For delta lobes, a minimum partial length of 1.01 km and a maximum length of 87.34 km are seen, the latter of which is a true maximum value. Delta

complexes are at least 2.50 km long; the greatest length value of 88.92 km for this higher-order element represents a partial observation (Fig. 5.4a).

Minimum partial width observations in both delta lobes and lobe complexes of the study are almost identical at 2.73 km and 2.80 km, respectively; these observations are from the same shelf-edge delta. The maximum width of 177.30 km seen in a delta complex corresponds to its full width. In contrast, the 80.77 km maximum width observed in a delta lobe is a partial value (Fig. 5.4b).

The studied delta lobes and complexes are at least 9.40 m and 25 m thick, respectively. At 900 m, the greatest maximum thickness of all examined delta elements of the study is seen in a lobe complex. The maximum thickness observed for a delta lobe with 663 m represents a true value (Fig. 5.4c).

A partial area of 6,975 km^2 was recorded for the largest area of a delta complex in the study, which is 1.79 times larger than the full area of 3,902 km^2 seen for an entire delta lobe (Fig. 5.4d).

A. Length

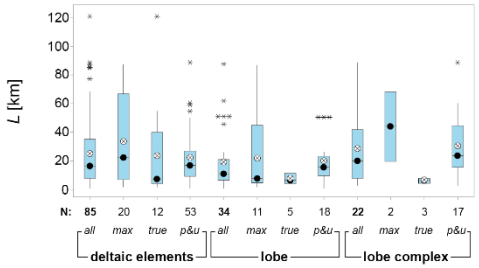

	N	min	mean	StDev	median	max
L all	**85**	1.01	25.20	24.88	16.46	121.00
L lobe	**34**	1.01	19.02	19.99	11.42	87.34
L comp	**22**	2.50	28.58	23.22	20.08	88.92

B. Width

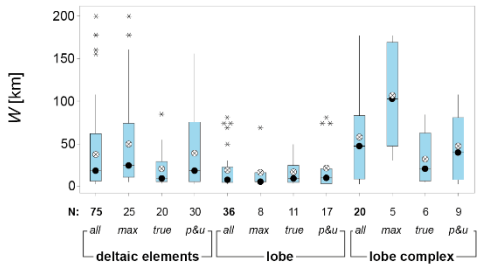

	N	min	mean	StDev	median	max
W all	**75**	2.73	37.49	43.70	18.80	200.00
W lobe	**36**	2.73	18.72	22.24	8.25	80.77
W comp	**20**	2.80	57.70	50.70	47.50	177.30

C. Thickness

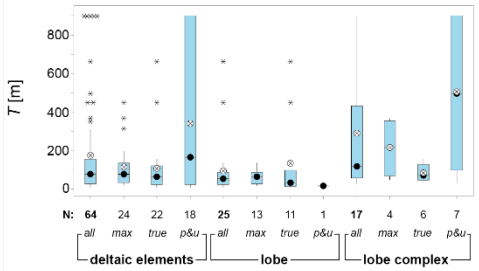

	N	min	mean	StDev	median	max
T all	**64**	9.40	176.90	249.80	80.00	900.00
T lobe	**25**	9.40	94.10	146.90	55.00	663.00
T comp	**17**	25.00	289.40	318.60	120.00	900.00

D. Area

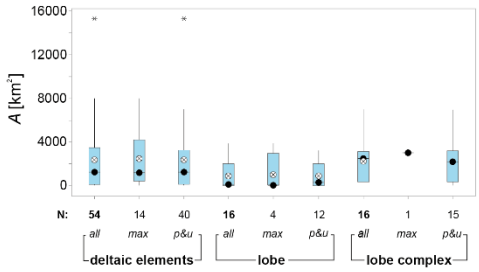

	N	min	mean	StDev	median	max
A all	**54**	4.00	2356.00	2812.00	1265.00	15276.0
A lobe	**16**	4.00	878.00	1339.00	109.00	3902.00
A comp	**16**	9.00	2222.00	2032.00	2480.00	6975.00

● **mean value** ⊗ **median value**

Figure 5.4a-d Boxplots of frequency distributions of geometries observed in studied shelf-edge deltas for deltaic elements (N=112), overall and separately for delta lobes (N=46) and lobe complexes (N=23). *L* = length; *W* = width; *T* = thickness; *A* = area; max = maximum value; true = true value; p&u = partial or unlimited value; N = number of readings; min = minimum value; mean = mean value; StDev = standard deviation; median = median value; max = maximum value.

5.3.1.2 Scaling relationships of geometric parameters in shelf-edge deltas

Independently of hierarchical level and type of observation, the morphometric parameters of shelf-edge deltas display moderate to strong, positive and statistically significant correlations (Fig. 5.5a-f). Strong scaling is seen between length and width (Fig. 5.5a), whereas correlations between other variables are moderate in strength (Fig. 5.5b-f).

Correlations of maximum values are based on few observations (Fig. 5.5a-f), but the results show strong and statistically significant scaling of maximum length with maximum width (Fig. 5.5a, N=12) and area (Fig. 5.5d, N=8), and of the latter with maximum width (Fig. 5.5e, N=6).

A.

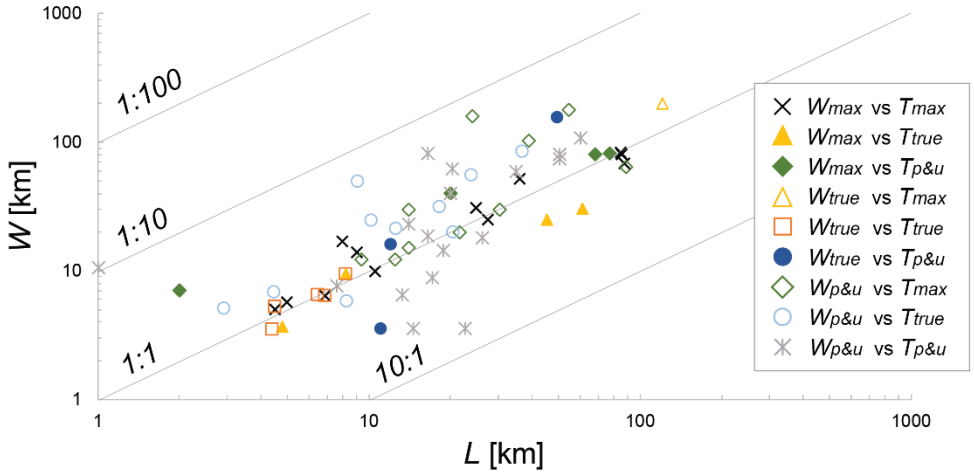

all max	r=0.971 p≤0.001 rs=0.937 p≤0.001 N=12
all	r=0.733 p≤0.001 rs=0.822 p≤0.001 N=69

B.

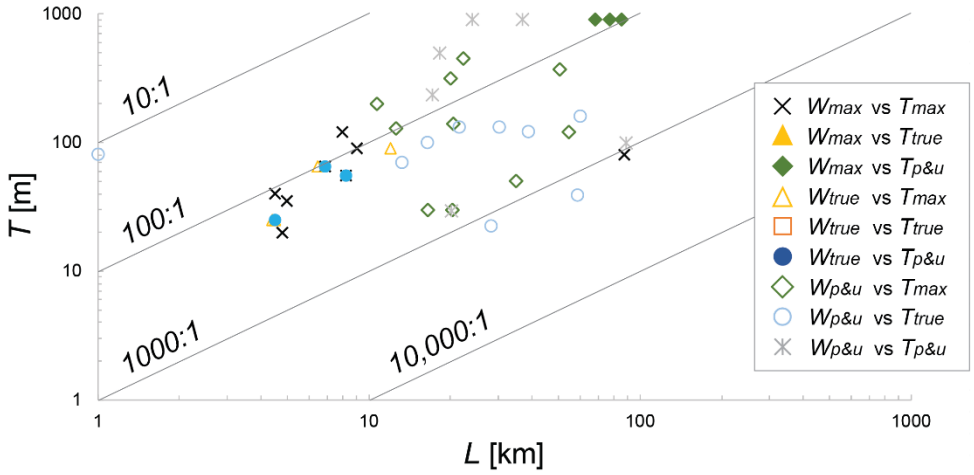

all max	r=0.254 p=0.543 rs=0.714 p=0.047 N=8
all	r=0.471 p=0.001 rs=0.546 p≤0.001 N=43

C.

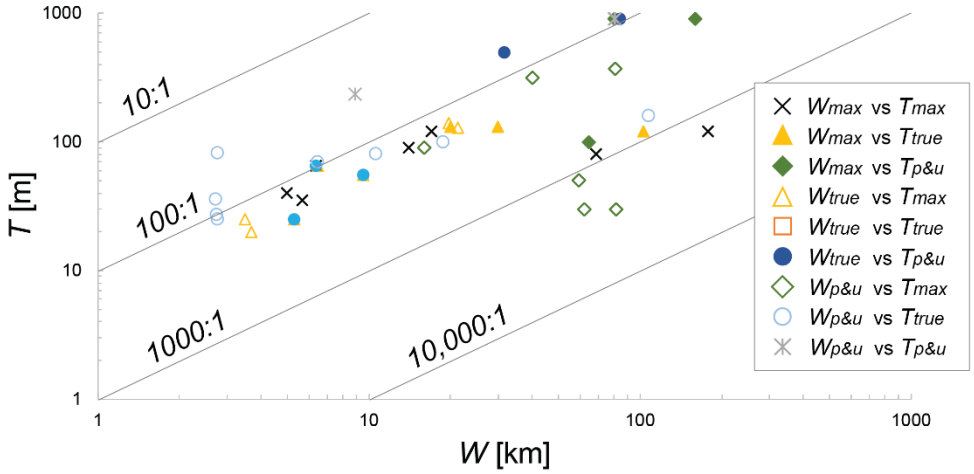

all max	r=0.590 p=0.163 rs=0.829 p=0.021 N=7
all	r=0.539 p≤0.001 rs=0.698 p≤0.001 N=42

D.

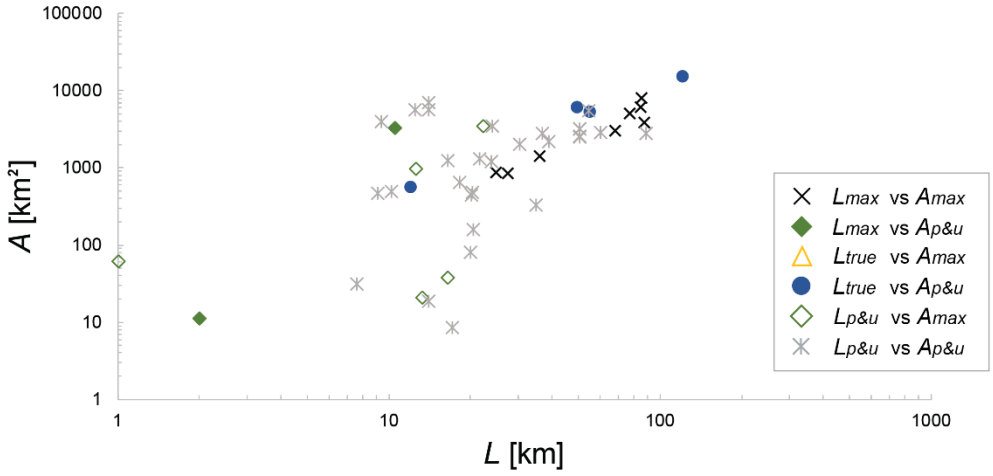

all max	r=0.877 p=0.004 rs=0.833 p=0.010 N=8
all	r=0.682 p≤0.001 rs=0.553 p≤0.001 N=48

E.

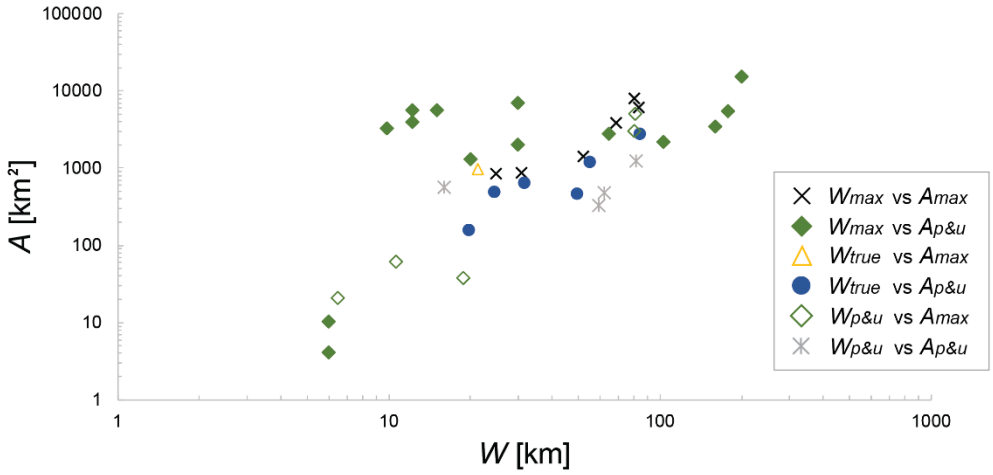

all max	r=0.907 p=0.013 rs=0.943 p=0.005 N=6
all	r=0.640 p≤0.001 rs=0.617 p≤0.001 N=47

F.

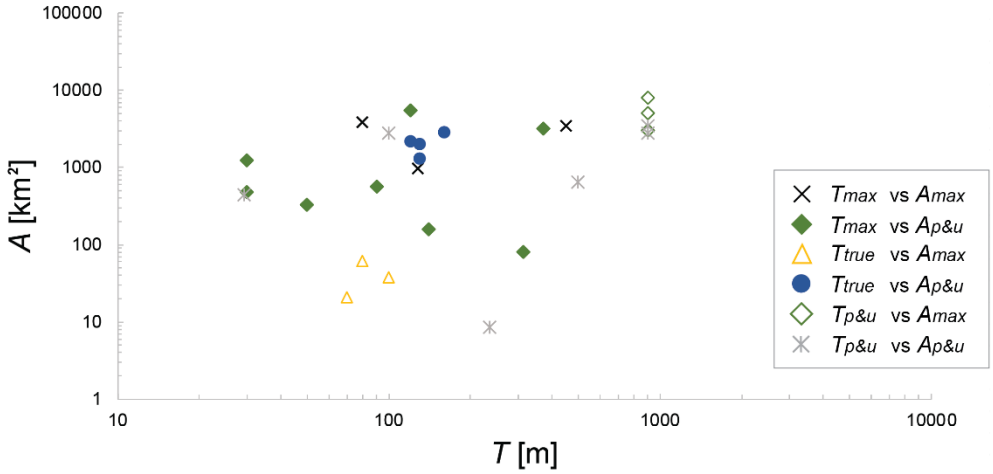

all max	r=* p=* rs=* p=* N=3
all	r=0.585 p=0.001 rs=0.479 p=0.011 N=27

Figure 5.5a-f Scatterplots of deltaic element geometric parameters with each other. *L* = length; *W* = width; *T* = thickness; *A* = area; max = only maximum values; all = maximum, true, partial and unlimited values; W_{sh} = modern shelf width at the delta location; r = Pearson's correlation coefficient; rs = Spearman's rank correlation coefficient; N = number of observations; * = not enough data for statistical analyses.

5.3.2 Scaling relationships of delta geometric parameters with environmental variables

Relationships between geometric parameters of shelf-edge deltaic elements and characteristics of the terrestrial catchment (section 5.3.2.1), shelf width (section 5.3.2.2) and palaeolatitude (section 5.3.2.3) were investigated. Correlation analyses including attributes of the two S2S system segments were focussed on deltaic elements from Late Quaternary shelf-edge deltas; some results in section 5.3.2.1 are additionally compared with correlation analyses performed on shelf-edge deltas of any age.

5.3.2.1 Terrestrial catchment (L_{fls}, Q_{fls}, A_{flsc}, H_{flsc})

With only four, six and three observations each, the samples are too small to investigate correlations of maximum length, thickness and area of deltaic elements with attributes of the terrestrial catchment in shelf-edge deltas of Late Pleistocene and younger age. Maximum width values are available for eleven deltaic elements, which return the following results:

Maximum width displays strong, positive and monotonic correlations with both the catchment area (Fig. 5.6a) and the maximum elevation (Fig. 5.6b) of the modern fluvial system(s) supplying the shelf-edge delta during its evolution. For both fluvial system length (Fig. 5.6c) and average annual fluvial discharge (Fig. 5.6d), correlations with maximum width are positive, weak and moderate in strength. None of the correlations are statistically significant.

Additional statistical analyses were conducted to establish whether strong correlations between maximum width and the size and maximum elevation of the catchment are also seen for shelf-edge deltas of any age.

The catchment area shows weak and moderate, positive correlations with maximum width, which are not statistically significant (N=14) (Fig. 5.6e).

Correlations of maximum width and maximum catchment elevation (N=15) reveal a positive, monotonic correlation, which is moderate in strength and not statistically significant. The Bissagos Delta (offshore W Africa) is an outlier in the results, in that it displays the greatest width value in the study (200 km) but is associated with a very low value of maximum catchment elevation (55 m) (Fig. 5.6f). After its removal from the analysis, the monotonic correlation is both strong and statistically significant (r=0.506 p=0.065; rs=0.881 p≤0.001 N=14).

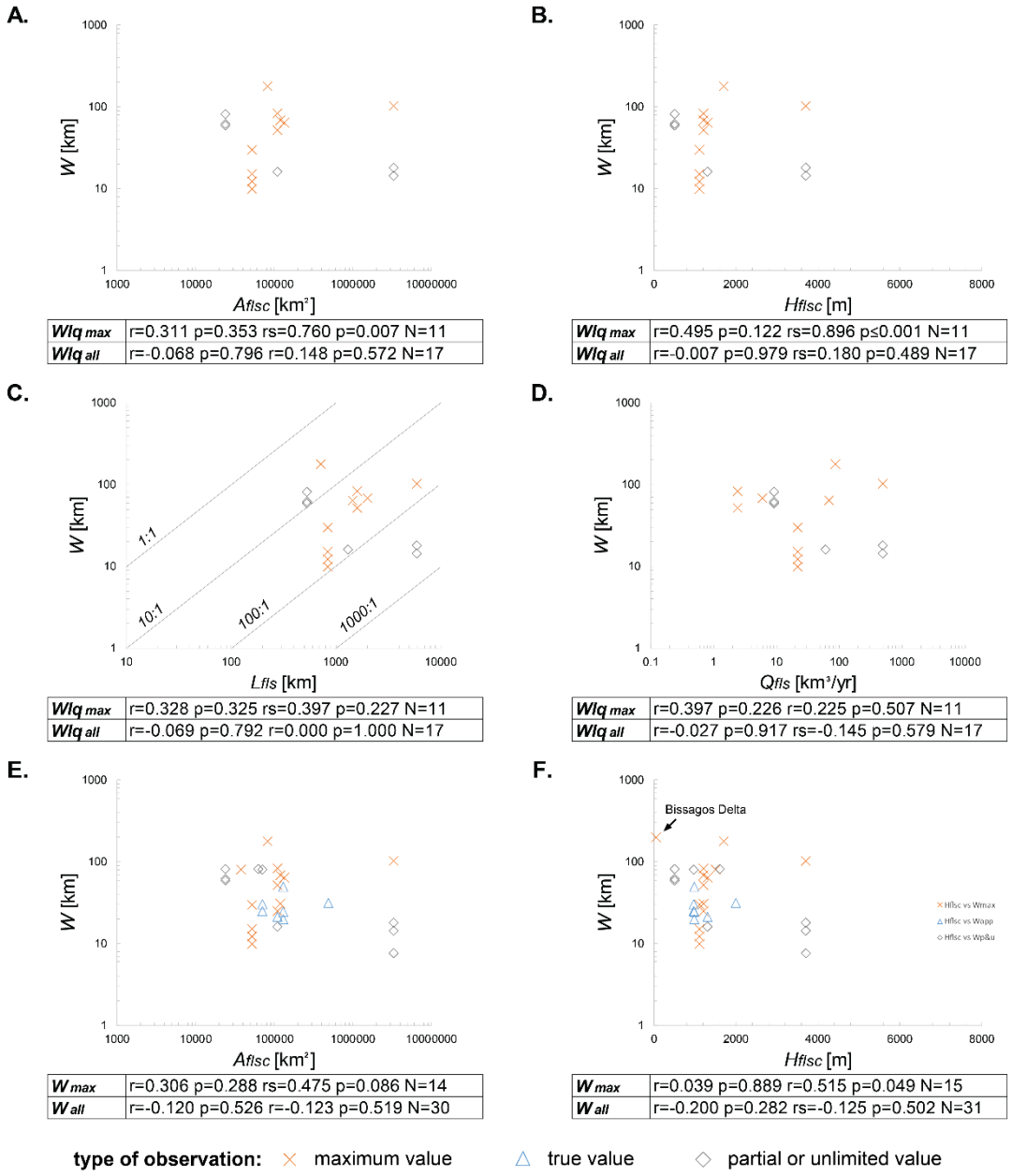

Wlq max	r=0.311 p=0.353 rs=0.760 p=0.007 N=11
Wlq all	r=-0.068 p=0.796 r=0.148 p=0.572 N=17

Wlq max	r=0.495 p=0.122 rs=0.896 p≤0.001 N=11
Wlq all	r=-0.007 p=0.979 rs=0.180 p=0.489 N=17

Wlq max	r=0.328 p=0.325 rs=0.397 p=0.227 N=11
Wlq all	r=-0.069 p=0.792 r=0.000 p=1.000 N=17

Wlq max	r=0.397 p=0.226 r=0.225 p=0.507 N=11
Wlq all	r=-0.027 p=0.917 rs=-0.145 p=0.579 N=17

W max	r=0.306 p=0.288 rs=0.475 p=0.086 N=14
W all	r=-0.120 p=0.526 r=-0.123 p=0.519 N=30

W max	r=0.039 p=0.889 r=0.515 p=0.049 N=15
W all	r=-0.200 p=0.282 rs=-0.125 p=0.502 N=31

Figure 5.6a-f Scatterplots of data on terrestrial catchment attributes and the width of deltaic elements A.-D. Late Quaternary examples of shelf-edge deltas in the study. E&F. All shelf-edge deltas independent of their age. All catchment values were obtained from the modern counterpart of the fluvial system or -systems the shelf-edge delta was associated with during its evolution. *W* = width; max = only maximum values; all = maximum, true, partial and unlimited values; *lq* = Late Quaternary examples; A_{flsc} = catchment size; H_{flsc} = maximum catchment elevation; L_{fls} = fluvial system length; Q_{fls} = average annual fluvial discharge; r = Pearson's correlation coefficient; rs = Spearman's rank correlation coefficient; N = number of observations.

5.3.2.2 Shelf width (W_{sh})

Strong and positive, statistically significant correlations are seen for modern shelf width with maximum length (Fig. 5.7a) and thickness (Fig. 5.7c) of deltaic elements in Late Quaternary shelf-edge deltas of Pleistocene or younger age. In contrast, weak and modest correlations exist with maximum width (Fig. 5.7b). With only three observations, the sample size is too small to assess relationships between maximum area and shelf width (Fig. 5.7d). Independently of the type of observation, moderate and positive correlations are displayed for length, (Fig. 5.7a) and thickness (Fig. 5.7c) values of deltaic elements with shelf width, and a modest and positive correlation for width (Fig. 5.7b), which are statistically significant. For the delta-element area, correlations are weak (Fig. 5.7d).

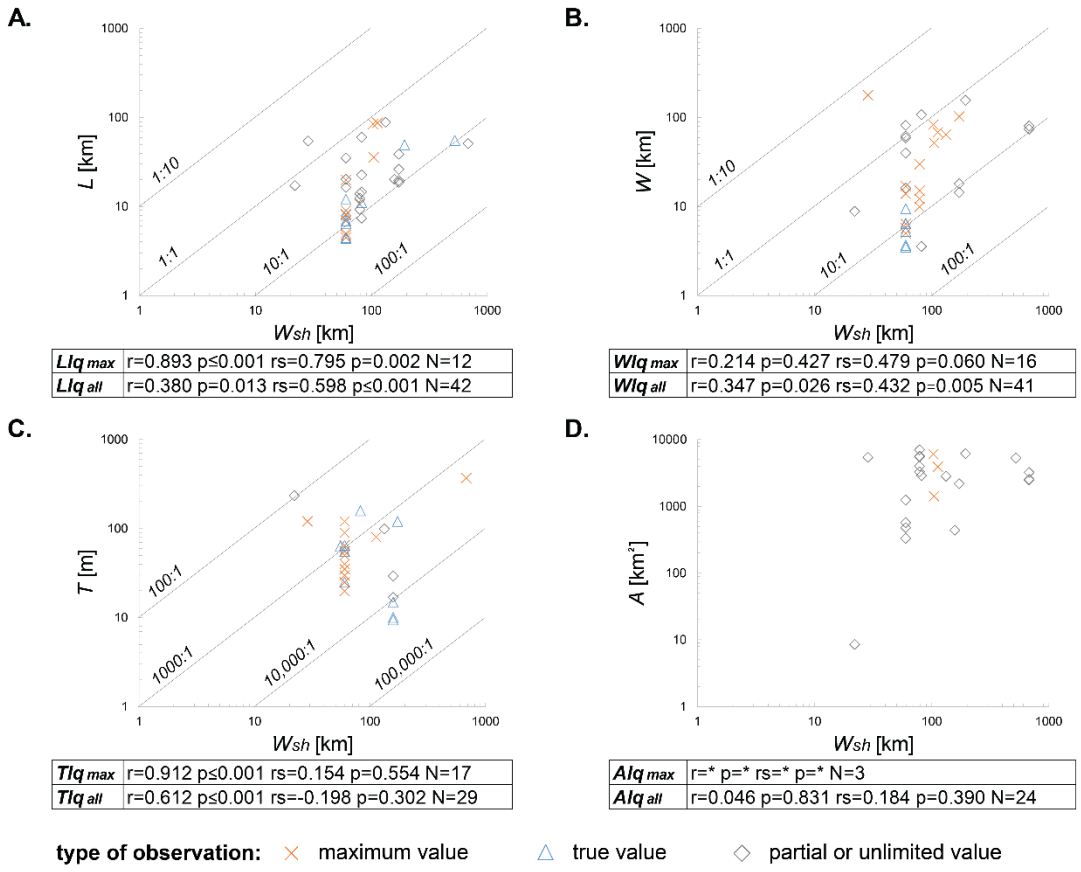

Llq max	r=0.893 p≤0.001 rs=0.795 p=0.002 N=12
Llq all	r=0.380 p=0.013 rs=0.598 p≤0.001 N=42

Wlq max	r=0.214 p=0.427 rs=0.479 p=0.060 N=16
Wlq all	r=0.347 p=0.026 rs=0.432 p=0.005 N=41

Tlq max	r=0.912 p≤0.001 rs=0.154 p=0.554 N=17
Tlq all	r=0.612 p≤0.001 rs=-0.198 p=0.302 N=29

Alq max	r=* p=* rs=* p=* N=3
Alq all	r=0.046 p=0.831 rs=0.184 p=0.390 N=24

Figure 5.7a-d Scatterplots of data on modern shelf widths and deltaic element geometric parameters for the studied Late Quaternary shelf-edge deltas. *L* = length; *W* = width; *T* = thickness; *A* = area; max = only maximum values; all = maximum, true, partial and unlimited values; W_{sh} = modern shelf width at the delta location; r = Pearson's correlation coefficient; rs = Spearman's rank correlation coefficient; N = number of observations; * = not enough data for statistical analyses.

5.3.2.3 Palaeolatitude (Lat_{abs})

The palaeolatitude of the shelf-edge delta shows no correlation with maximum length (Fig. 5.8a), and only weak negative correlation with maximum width (Fig. 5.8b). Moderate and negative, monotonic correlation is seen for maximum thickness (Fig. 5.8c) and a moderate, positive correlation for maximum area (Fig. 5.8d), but the latter is based on fourteen observations only. None of the correlations are statistically significant but the p value for the correlation of palaeolatitude with maximum delta-element thickness is only slightly above the threshold of significance (p=0.018, Fig. 5.8c).

For deltaic elements of any type, correlations of geometric parameters with the palaeolatitude of the shelf-edge delta are weak and negative, except for a very weak positive and monotonic correlation seen for the planform area (Fig. 5.8a-d).

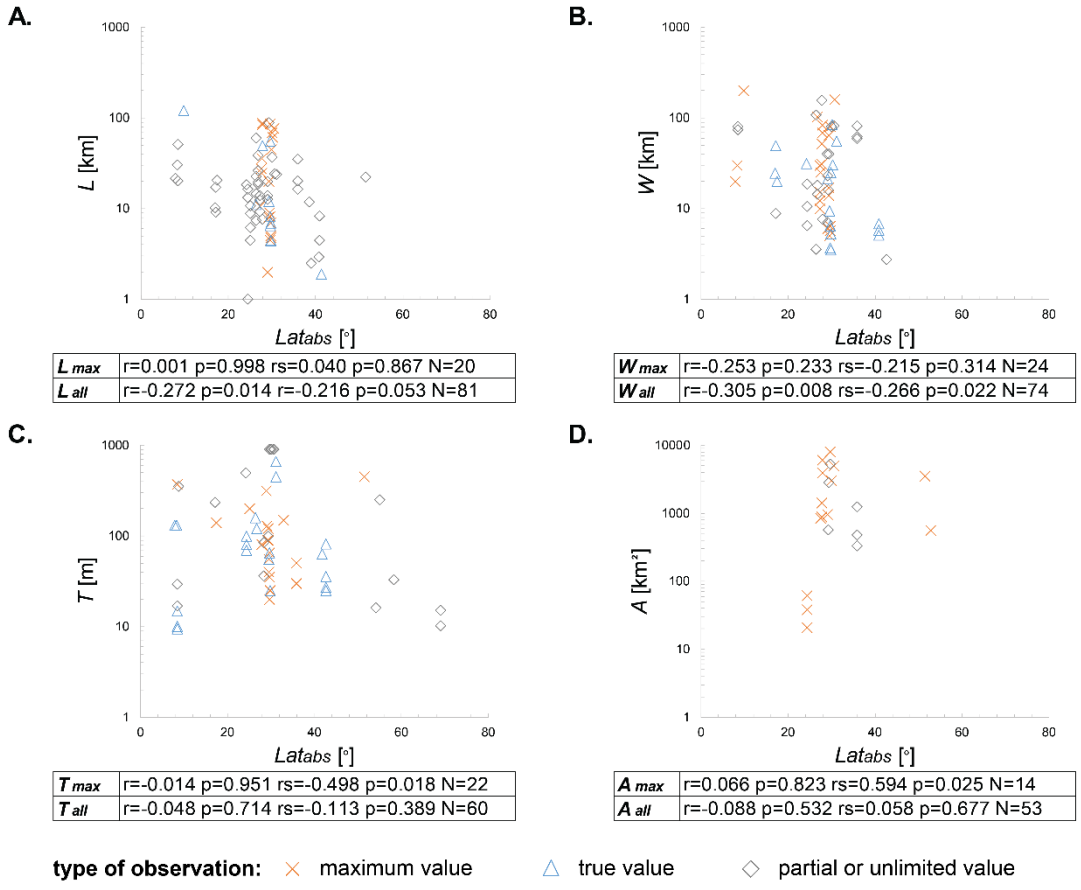

Figure 5.8a-d Scatterplots of data on the absolute palaeolatitude of shelf-edge deltas and deltaic element geometric parameters. *L* = length; *W* = width; *T* = thickness; *A* = area; *max* = only maximum values; *all* = maximum, true, partial and unlimited values; Lat_{abs} = absolute latitudinal position of the shelf-edge delta; r = Pearson's correlation coefficient; rs = Spearman's rank correlation coefficient; N = number of observations.

5.3.3 Delta geometries versus environmental controls

5.3.3.1 Hydrodynamic-process regime

Groups of deltas classified according to their process regime as being fluvial- and mixed-dominated exhibit different frequency distributions of length (Fig. 5.9a), width (Fig. 5.9b) and thickness (Fig. 5.9c), but similar distributions of planform area (Fig. 5.9d). On average, deltaic elements

deposited under the influence of a mixed-process regime have lengths, widths, thicknesses, and areas greater than deltaic elements where the hydrodynamic regime of the river is dominant, by a factor of 1.79, 1.99, 1.78 and 1.09, respectively (Fig. 5.9a-d). Despite this, the greatest length and area were recorded for the class of fluvial-dominated elements, with 87.34 km and 6,064 km^2, respectively, compared to 59.10 km and 5,481 km^2 for deltaic elements associated with a mixed-process regime (Figs. 5.9a&d).

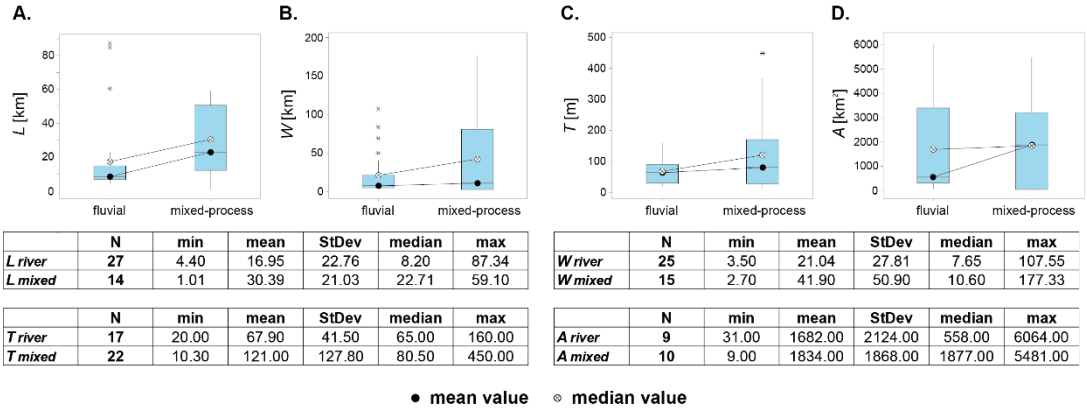

	N	min	mean	StDev	median	max
L river	27	4.40	16.95	22.76	8.20	87.34
L mixed	14	1.01	30.39	21.03	22.71	59.10

	N	min	mean	StDev	median	max
W river	25	3.50	21.04	27.81	7.65	107.55
W mixed	15	2.70	41.90	50.90	10.60	177.33

	N	min	mean	StDev	median	max
T river	17	20.00	67.90	41.50	65.00	160.00
T mixed	22	10.30	121.00	127.80	80.50	450.00

	N	min	mean	StDev	median	max
A river	9	31.00	1682.00	2124.00	558.00	6064.00
A mixed	10	9.00	1834.00	1868.00	1877.00	5481.00

Figure 5.9a-d Boxplots of frequency distributions of geometries seen in deltaic elements of shelf-edge deltas associated with fluvial-dominated (N=28) and mixed-process regimes (N=27) as interpreted in the literature. *L* = length; *W* = width; *T* = thickness; *A* = area; N = number of readings; min = minimum value; mean = mean value; StDev = standard deviation; median = median value; max = maximum value.

5.3.3.2 Fluvial feeder-system type

Only six shelf-edge deltaic elements associated with more than one fluvial system were included in the study; the mean recorded length and width of these elements are higher than the median of the 42 and 32 investigated deltaic elements fed by a single river, by a factor of 4.37 and 3.05, respectively (Fig. 5.10a&b). The highest values for length (Fig. 5.10a), width (Fig. 5.10b) and area (Fig. 5.10d) are seen in multiple-sourced shelf-edge deltas. The greatest observed thickness values in both deltaic elements linked to single fluvial sources and multiple sources are 900 m (Fig. 10c). Notably, shelf-edge deltaic elements fed by several rivers exhibit areas that are on average almost twice as high as those of single-sourced deltas, by a factor of 1.90; the greatest recorded area of 15,276 km^2 is 1.91 times higher

than the 8,000 km^2 seen for shelf-edge deltaic elements fed by a single river system (Fig. 5.10d).

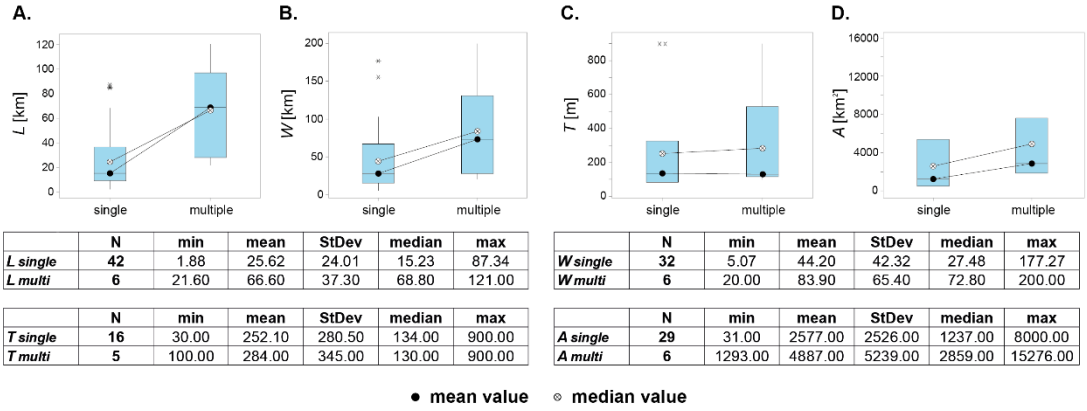

	N	min	mean	StDev	median	max
L single	42	1.88	25.62	24.01	15.23	87.34
L multi	6	21.60	66.60	37.30	68.80	121.00

	N	min	mean	StDev	median	max
W single	32	5.07	44.20	42.32	27.48	177.27
W multi	6	20.00	83.90	65.40	72.80	200.00

	N	min	mean	StDev	median	max
T single	16	30.00	252.10	280.50	134.00	900.00
T multi	5	100.00	284.00	345.00	130.00	900.00

	N	min	mean	StDev	median	max
A single	29	31.00	2577.00	2526.00	1237.00	8000.00
A multi	6	1293.00	4887.00	5239.00	2859.00	15276.00

● mean value ⊗ median value

Figure 5.10a-d Boxplots of frequency distributions of geometries seen in deltaic elements of shelf-edge deltas associated with single rivers (N=48) and multiple fluvial systems (N=6). *L* = length; *W* = width; *T* = thickness; *A* = area; N = number of readings; min = minimum value; mean = mean value; StDev = standard deviation; median = median value; max = maximum value.

5.3.3.3 Source-to-sink (S2S) system setting

Data on shelf-edge deltas associated with an insular source-to-sink system are limited, as the dataset only comprises four deltaic elements. The two values of length for insular deltaic elements are greater than the median of the 60 deltaic elements located in continental settings (Fig. 5.11a). Similarly, the only value of insular delta-element width (177.27 km) is higher than all but one of the 52 width values of investigated deltaic elements situated in a continental environment (Fig. 5.11b). The greatest thickness of a deltaic element in an insular setting (120 m) exceeds the average value of 109.80 m for the 28 sampled deltaic elements along continental margins, but the maximum thickness of 370 m recorded for an outlier in the latter class is more than three times higher (Fig. 5.11c). Similarly, the maximum area of a deltaic element along a continental margin is almost three times higher than for a deltaic element associated with an island, with 15,276 km^2 compared to 5,481 km^2 (Fig. 5.11d).

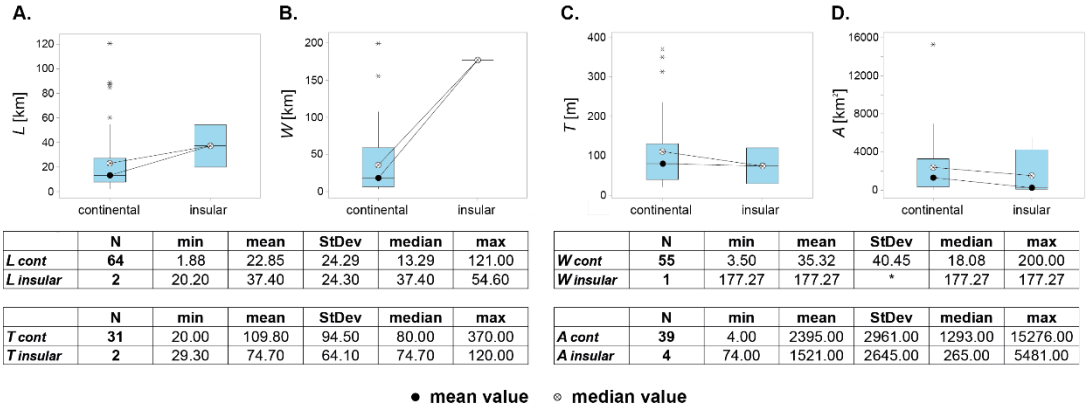

	N	min	mean	StDev	median	max
L cont	64	1.88	22.85	24.29	13.29	121.00
L insular	2	20.20	37.40	24.30	37.40	54.60

	N	min	mean	StDev	median	max
W cont	55	3.50	35.32	40.45	18.08	200.00
W insular	1	177.27	177.27	*	177.27	177.27

	N	min	mean	StDev	median	max
T cont	31	20.00	109.80	94.50	80.00	370.00
T insular	2	29.30	74.70	64.10	74.70	120.00

	N	min	mean	StDev	median	max
A cont	39	4.00	2395.00	2961.00	1293.00	15276.00
A insular	4	74.00	1521.00	2645.00	265.00	5481.00

Figure 5.11a-d Boxplots of frequency distributions of geometries seen in deltaic elements of shelf-edge deltas associated with continental (N=70) and insular (N=4) source-to-sink settings. *L* = length; *W* = width; *T* = thickness; *A* = area; N = number of readings; min = minimum value; mean = mean value; StDev = standard deviation; median = median value; max = maximum value.

5.3.3.4 Oceanographic environment

Few deltaic elements were characterised for shelf-edge deltas in open-sea settings (N=9). In this class of systems, all four investigated geometric parameters are on average higher than those of deltaic elements in semi-enclosed and enclosed seas, and the greatest length, width, and area values are seen in shelf-edge deltas building onto oceanic shelves (Fig. 5.12a-d). In contrast, the largest observed value of thickness belongs to a deltaic element associated with a semi-enclosed or enclosed sea, which is 2.57 times thicker than the maximum value from open-sea examples (Fig. 5.12c). The greatest maximum area recorded in a deltaic element associated with an open sea is 2.19 times higher than in a semi-enclosed or enclosed sea (Fig. 5.12d).

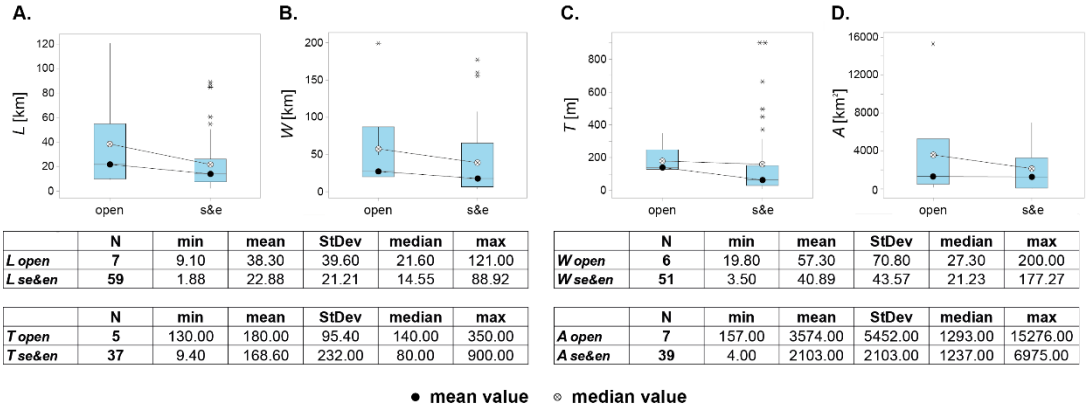

	N	min	mean	StDev	median	max
L open	7	9.10	38.30	39.60	21.60	121.00
L se&en	59	1.88	22.88	21.21	14.55	88.92

	N	min	mean	StDev	median	max
W open	6	19.80	57.30	70.80	27.30	200.00
W se&en	51	3.50	40.89	43.57	21.23	177.27

	N	min	mean	StDev	median	max
T open	5	130.00	180.00	95.40	140.00	350.00
T se&en	37	9.40	168.60	232.00	80.00	900.00

	N	min	mean	StDev	median	max
A open	7	157.00	3574.00	5452.00	1293.00	15276.00
A se&en	39	4.00	2103.00	2103.00	1237.00	6975.00

Figure 5.12a-d Boxplots of frequency distributions of geometries seen in deltaic elements of shelf-edge deltas associated with open seas (N=9) and semi-enclosed seas (N=77). *L* = length; *W* = width; *T* = thickness; *A* = area; N = number of readings; min = minimum value; mean = mean value; StDev = standard deviation; median = median value; max = maximum value.

5.3.3.5 Palaeolatitudinal zone

The sample size of shelf-edge deltas that developed at temperate palaeolatitudes (23.5° to 66.5° degrees, N=87) is about four times greater than that of deltas located at tropical palaeolatitudes (0° to 23.5° degrees, N=20). Nevertheless, the mean and maximum values of length, width and planform area of deltaic elements in deltas from tropical latitudes are greater than those of deltaic elements from temperate latitudes. Instead, the average and maximum element thickness are higher in systems from temperate zones, by a factor of 1.57 and 2.43, respectively (Fig. 5.13a-d). Frequency distributions of length, width and thickness for deltaic elements of the two latitudinal zones differ notably (Fig. 5.13a-c). Distributions of areas and their mean values are rather similar, apart from the maximum area recorded for a deltaic element in tropical latitudes, which constitutes an outlier at 15,276 km^2 and is almost twice as high as the highest value exhibited for a deltaic element within the temperate zone (Fig. 5.13d).

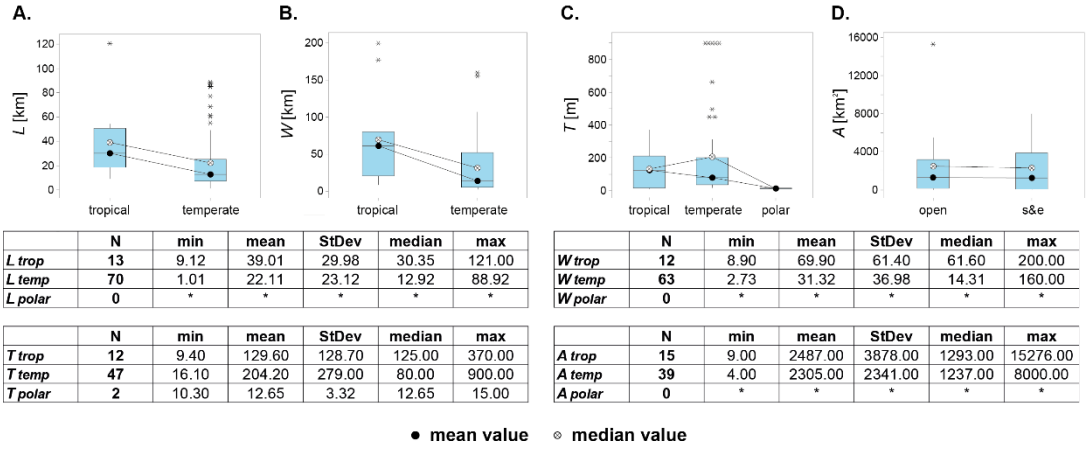

	N	min	mean	StDev	median	max
L trop	13	9.12	39.01	29.98	30.35	121.00
L temp	70	1.01	22.11	23.12	12.92	88.92
L polar	0	*	*	*	*	*

	N	min	mean	StDev	median	max
W trop	12	8.90	69.90	61.40	61.60	200.00
W temp	63	2.73	31.32	36.98	14.31	160.00
W polar	0	*	*	*	*	*

	N	min	mean	StDev	median	max
T trop	12	9.40	129.60	128.70	125.00	370.00
T temp	47	16.10	204.20	279.00	80.00	900.00
T polar	2	10.30	12.65	3.32	12.65	15.00

	N	min	mean	StDev	median	max
A trop	15	9.00	2487.00	3878.00	1293.00	15276.00
A temp	39	4.00	2305.00	2341.00	1237.00	8000.00
A polar	0	*	*	*	*	*

Figure 5.13a-d Boxplots of frequency distributions of geometries seen in deltaic elements of shelf-edge deltas associated with tropical (0° to 23.5° degrees; N=20), temperate (23.5° to 66.5° degrees; N=87) and polar (> 66.5° degrees; N=2) latitudinal zones. *L* = length; *W* = width; *T* = thickness; *A* = area; N = number of readings; min = minimum value; mean = mean value; StDev = standard deviation; median = median value; max = maximum value.

5.4 Discussion

5.4.1 Variability in geometric characteristics of shelf-edge deltas

Frequency distributions of true maximum values of length, width, thickness and area demonstrate a great variability in the geometric characteristics of shelf-edge deltaic elements, of any type, as well as in hierarchical categories of delta lobes and lobe complexes (Fig. 5.4a-d). These findings have important implications for the interpretation of the physiographic context of a deltaic succession seen in subsurface and outcrop, for which limited control exists on the position and bathymetry of the coastline, shelf-break or slope. In particular, the results highlight that some overlap exists between the orders of magnitude of delta-element dimensions in small shelf-edge deltaic bodies and the scale of dimensions recognised in other delta types, for example Gilbert-type deltas (e.g. Budai et al., 2021). This suggests that the dimensions of a delta and its components are not reliable criteria for the distinction between shelf-edge deltas and other delta types classified based on their relative position within the shelf. This consideration applies in particular to smaller-scale deltaic bodies.

5.4.2 Controlling factors on shelf-edge delta geometry

Despite the limited number of observations on the full extent of shelf-edge deltaic bodies obtainable from the literature for consideration in this study, the results indicate the existence of several scaling relationships (i) within shelf-edge deltaic elements (Fig. 5.5a-f), and (ii) between shelf-edge delta geometry and environmental variables (Figs. 5.6 to 5.13), which can be observed on a global scale. In plan-view, shelf-edge deltas are characterised by lobate to strike-elongated shapes (e.g. Suter & Berryhill, 1985; Porębski & Steel, 2003; Yoo et al., 2017), which are inferred to be influenced by factors such as seafloor topography, channel-avulsion patterns, and the hydrodynamic regime. In the following sections, potential causative mechanisms for some scaling relationships between delta geometry and environmental variables are discussed.

5.4.2.1 Hydrodynamic-process regime

The plan-view geometry of shelf-edge deltas is likely controlled by the hydrodynamic regime at the shelf edge, which in comparison to shorelines and inner-shelf environments along wide shelves is characterised by a higher-energetic hydrodynamic-process regime through the unmitigated impact of oceanic swells and increased wave influence (e.g. Porębski & Steel, 2006 and references therein). Lobate-shaped shelf-edge deltas are thought to develop where the influence of the fluvial system is predominant and sediment discharge at the mouths of distributaries leads to the development of lobate bodies (e.g. Anderson, 2005). In contrast, shelf-edge deltas elongated parallel to the shoreline are thought to develop due to the strong influence of unidirectional oceanic currents (e.g. Yoo et al., 2017) and waves (e.g. Suter & Berryhill, 1985; Anderson, 2005), causing the erosion and redeposition of deltaic sediments along delta fronts and decreasing basinward sediment transport.

The results presented herein indicate that the area of deltaic elements does not differ significantly between river-dominated and mixed-process regimes (Fig. 5.9d), which suggests that the total areal extent of shelf-edge deltas is not primarily controlled by the dispersal and redistribution of sediment by hydrodynamic processes. Yet, the findings suggest that shelf-edge deltas

tend to be wider when associated with a mixed-process regime (Fig. 5.9b) from the wave reworking of sediment along the coastline via longshore drift, corroborating the view of a causal link between delta plan-view shape and hydrodynamic regime. The, on average, greater thickness of studied deltaic elements in environments characterised by a mixed-process regime compared to river-dominated shelf-edge deltas – by a factor of 1.78 (Fig. 5.9c) – could reflect how the process of delta accretion might be inhibited where bypass of sediment beyond the shelf edge is facilitated by hyperpycnal flows driven by fluvial activity (e.g. Bouma & Scott, 2003).

Future studies from a larger dataset are desirable to assess the importance of individual marine hydrodynamic processes as controls on delta geometry, for example in shelf-edge deltas that are interpreted as predominantly wave-, tide- or storm-dominated.

5.4.2.2 Terrestrial catchment

Although based on a limited dataset, positive correlations are seen between the maximum width of Late Quaternary deltaic elements and the size (Fig. 5.6a) and maximum elevation (Fig. 5.6b) of corresponding modern terrestrial catchments. These relationships are likely a reflection of positive relationships demonstrated globally for annual sediment load with maximum catchment elevation and catchment area (see Figs. 2.13 & 2.14 in Milliman & Farnsworth, 2011); larger volumes of sediment tend to be transported to shelf-edge deltas from terrestrial catchments with larger drainage areas and higher elevations.

The relationship of maximum width with maximum catchment elevation might also be valid for ancient shelf-edge delta systems (Fig. 5.6f, see section 5.3.2.1), but this needs assessment from a larger dataset on drainage systems of ancient shelf-edge deltas.

The tendency towards greater widths (Fig. 5.10b) and areas (Fig. 5.10d) displayed in shelf-edge deltas sourced by multiple fluvial feeder systems can be explained by how multiple point sources are effective in constructing a widespread distributary network, and that cumulatively, sediment discharge of several rivers might tend to exceed that of single rivers. The observed

greater lengths of deltaic elements associated with multiple fluvial feeders (Fig. 5.10a) might reflect the way in which sediment-supply rates drive the rate of progradation of shelf margins, by lengthening the deltas developed there. As discussed in section 5.4.2.7, extensive distributary networks and multiple point sources can favour the development of lobe complexes, which are inherently larger than individual delta lobes.

5.4.2.3 Margin configuration

A larger width-to-length ratio of deltaic elements does not necessarily relate to the remobilization of delta deposits by currents and waves alone (see section 5.4.2.1). The displayed tendency of shelf-edge deltaic elements to have, on average, greater widths compared to their lengths, by a factor of 1.49, and very similar maximum length values for both delta lobes and lobe complexes (Fig. 5.4a&b), is likely related to how delta length – as opposed to delta width – is to a greater degree controlled by characteristics of the margin configuration. The fact that the length of a delta top updip of the shelf break is controlled by the width of the shelf is reflected in the strong scaling relationship seen for the maximum length of deltaic elements with modern shelf width (Fig. 5.7a). In addition, the gradient of the upper slope exerts control on delta length by promoting substrate instability, which can trigger the cannibalisation of delta-front deposits and limit delta progradation (e.g. Tesson et al., 1990; Roberts & Sydow, 1996).

In contrast, neither the slope gradient nor the shelf width constitutes a primary control on the width of a delta, because shelf-edge deltas can develop extensive delta plains within the shelf. Although the shelf width does not limit the lateral or vertical growth of shelf-edge deltas in a direct manner, the results indicate that shelf-edge deltaic elements tend to have greater widths (Fig. 5.7b) and thicknesses (Fig. 5.7c) with increasing shelf width. This probably reflects how larger fluvial systems are effective in constructing wider shelves and larger deltas due to their high sediment discharge volumes (e.g. Blum & Hattier-Womack, 2009; Blum et al., 2013).

5.4.2.4 Source-to-sink (S2S) setting

Based on a small dataset relating to four shelf-edge deltaic elements only, it is observed that the association of a shelf-edge delta with an insular setting does not inherently limit the development of lengths, widths, thicknesses and areas comparable to those seen in shelf-edge deltas in continental settings (Fig. 5.11a-d). However, these findings might, in part, reflect how all four shelf-edge deltas from insular S2S settings were located within semi-enclosed and enclosed seas and occurred at tropical latitudes. Low-latitudinal settings are associated with greater lengths (Fig. 5.13a & section 5.3.3.5), and some deltaic elements in semi-enclosed and enclosed seas constitute outliers with very large thickness values (Fig. 5.12b & section 5.3.3.4).

5.4.2.5 Oceanographic environment

The evaluation of frequency distributions of lengths and widths of shelf-edge deltaic elements suggests that deltaic elements in open-sea settings tend to be longer, wider, and areally more extensive than their counterparts in semi-enclosed and enclosed seas (Fig. 5.12a-d). The findings might indicate that the hydrodynamic regime in open seas promotes greater shelf-edge delta size, perhaps related to a wider radius of sediment dispersal from both (i) fluvial discharge, and (ii) erosion and redeposition of deltaic deposits due to stronger oceanic currents and waves in oceans compared to semi-enclosed and enclosed seas. Additionally, delta size might be promoted in open seas by the action of more extensive littoral cells that are able to carry higher volumes of sediment (e.g. Boyd et al., 2008), and from larger-scale sediment accretion onto shelf-edge deltas by oceanic currents. The findings need future investigation.

5.4.2.6 Palaeolatitude

With increasing latitude, mean annual precipitation rates, which exert control on fluvial water and sediment discharge, tend to decrease (Milliman & Farnsworth, 2011). Yet, this trend is not reflected in relationships between the geometric parameters of deltaic elements and the absolute latitudes of the shelf-edge deltas during their formation (Fig. 5.8a-d).

The findings show that the obtained maximum length values of deltaic elements display a wide distribution – extending over two orders of magnitude – within the very narrow latitudinal range of 27° to 31° degrees and are exceeded in several cases by true and partial length values at both lower and higher latitudes (Fig, 5.8a). When combined, these attributes indicate that no monotonic relationship exists between delta-element length and the absolute latitude of the shelf-edge delta. The lack of correlation between the absolute palaeolatitude of the shelf-edge delta and the maximum length of deltaic elements probably relates to the fact that delta-element length is primarily controlled by aspects of the margin configuration (see section 5.4.2.3).

The tendency of deltaic elements from tropical shelf-edge deltas to be longer compared to temperate ones (Fig. 5.13a) might be promoted by the stabilising effect of carbonate on slope substrate by processes of binding and cementation (e.g. Adams & Kenter, 2013, and references therein), which in turn might decrease the magnitude and frequency of delta-front collapse related to slope failure. The intermixing of fluvially derived siliciclastic sediment with carbonate biogenic material might also have a strengthening effect on subaqueous delta front deposits and might reduce delta cannibalisation. Another factor that might contribute to the stabilization of delta fronts in low-latitudinal shelf-edge deltas is the presence of reef systems along shorelines, which might lead to the redirection of longshore currents away from the shore and by this decrease their impact on remobilization of delta sediments. The presence of atoll islands along continental margins can have a complex influence on marine hydrodynamic processes. Where atoll islands exist basinward of shelf-edge deltas, as in the case of the Late Quaternary Belize margin (e.g. Ferro et al., 1999; Droxler & Jorry, 2013), their topography can create a narrow strait-like corridor, which might lead to the focussing of longshore currents and waves, which in turn might amplify their erosive effects. In such settings, delta width might be promoted by the redistribution of delta sediments in a downstream direction (e.g. Ferro et al., 1999). By contrast, where waves and currents approach the coastline orthogonal to the margin, the atoll reef functions as a

barrier, which may deflect and disperse wave- and current energies related to tides, winds and storm events.

The findings might also reflect how many of the studied shelf-edge deltas from tropical latitudes are located in an open-sea setting, which appears to be associated with the development of greater lengths in shelf-edge deltas compared to semi-enclosed and enclosed seas (see section 5.4.2.5).

Weak negative correlation between palaeolatitude and maximum width is seen (Fig. 5.8b), which possibly reflects how the width of delta lobes and delta complexes is not primarily controlled by the volume of sediment delivered by terrestrial catchments, but rather by the hydrodynamics of marine processes (see also section 5.4.2.1).

The results presented herein indicate that processes linked to latitude have a moderate influence on the thickness of deltaic elements. Moderate negative correlation between the maximum thickness of deltaic elements and palaeolatitude is observed in examples located between 8° and 51° degrees (Fig. 5.9c); this could be related to the effect of overall decrease in average annual precipitation with increasing latitude (e.g. Milliman & Farnsworth, 2011) on sediment erosion rates in terrestrial catchments.

5.4.2.7 Shelf-edge delta architecture

The progradational, aggradational and lateral stacking of delta lobes constitutes one mechanism to drive shelf-edge delta growth. Delta-lobe complexes can develop in response to both allogenic controls, such as sea-level changes (e.g. Suter & Berryhill, 1985; Kolla et al., 2000), changes in seafloor topography related to sediment load at distributary mouths (e.g. Roberts & Sydow, 1996), tectonic activity and salt diapirism, and the autogenic process of topographic compensation by lobe switching (e.g. Suter & Berryhill, 1985; Kolla et al., 2000; Hiscott, 2003). This control on shelf-edge delta size is reflected in the finding that lobe complexes of the study tend to exhibit greater lengths, widths, thicknesses and areas than single delta lobes (Fig. 5.4a-d).

Moreover, the formation of a delta complex may be associated with the coalescence of lobes fed by different fluvial sources, which collectively might

distribute larger volumes of sediment to a shelf-margin and build more extensive distributary networks, compared to a single fluvial system (see also section 5.4.2.2).

Despite this, the results also demonstrate that single delta lobes can exhibit dimensions and areal extents which exceed the maximum dimensions and areas of some delta complexes in the study (Fig. 5.4a-d). Hence, the results suggest that the internal hierarchical organisation of shelf-edge deltas cannot be reliably estimated based on their geometry and vice versa.

5.5 Conclusions

The geometry of shelf-edge deltaic bodies and of deltaic elements classified based on their hierarchical level into lobes and lobe complexes has been quantitatively investigated from a global dataset of 112 deltaic elements of Permian to Late Quaternary age to characterise variability in the geometry of deltaic elements, and to identify possible controlling factors on shelf-edge delta geometry.

The global database compiled for this study constitutes the first one that has systematically quantified geometric attributes of shelf-edge deltaic elements and characteristics of the S2S systems and environmental settings associated with a shelf-edge delta.

Some of the key findings from this study are summarised in Figure 14 and are as follows:

(1) Shelf-edge deltaic bodies display a great variability in their geometry including smaller-scale forms, which suggests that the relative position of a delta within the shelf cannot be reliably inferred based on its dimensions and areal extent.
(2) Moderate to strong scaling is seen for lengths, widths, thicknesses and areas of deltaic elements.
(3) The internal hierarchical organization of shelf-edge deltas (single lobe vs. multiple lobes) cannot be reliably estimated based on their geometry and vice versa.

(4) Hydrodynamic conditions and margin configuration in open sea areas associated with the development of shelf-edge deltas with greater lengths and widths compared to their counterparts in semi-enclosed and enclosed seas.
(5) Size and maximum elevation of terrestrial catchments might exert influence on the width of shelf-edge deltaic elements due to higher annual sediment load.
(6) Deltas sourced by multiple rivers tend to be longer, wider and areally more extensive than deltas supplied by a single fluvial system, which may reflect the widespread distributary networks and high sediment supply of margins fed by multiple sediment sources.
(7) Palaeolatitude is not an effective predictor of shelf-edge delta geometry.

The findings of this study indicate that shelf-edge delta geometry can be predicted to some degree and linked to variables of the environment and S2S system; some scaling relationships are recognisable on a global scale. These insights can aid in the spatial reconstruction of shelf-edge deltas and their associated environments in outcrop and subsurface studies. Moreover, the results of this study might be used as a framework for testing of scaling relationships of shelf-edge deltas and their superordinate S2S systems in numerical and experimental studies. For example, the oceanographic environment has thus far received little attention in modelling studies of shelf- and slope systems, but possibly also exerts control on the geomorphology of submarine canyons (see Chapter 3).

Given the limited availability of observations on the full extent of shelf-edge deltas in the literature several of the findings listed above must be considered preliminary; further work is needed to see if they can be established more securely.

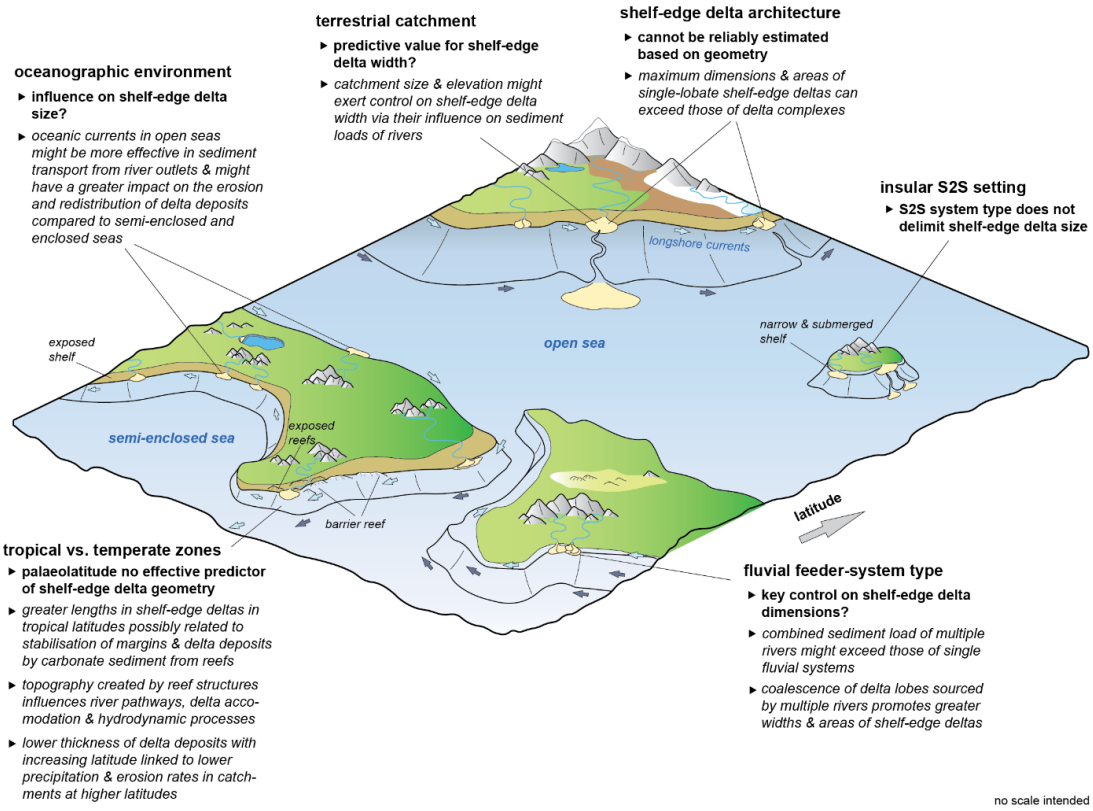

Figure 5.14 Schematic diagram summarising controlling factors of shelf-edge delta geometry recognised in the literature and whose global significance is indicated from the results in this study.

6 Discussion

6.1 Controlling factors of morphometric characteristics of submarine canyons and shelf-edge deltas: implications for conceptual and semi-quantitative models

For some geographic regions, the geomorphologies of late Quaternary submarine canyons along modern margins (e.g. NE Brazil, de Almeida et al., 2015; SW U.S.A., Tubau et al., 2015; SE India, Susanth et al., 2021) and plan-view geometries of Late Quaternary shelf-edge deltaic deposits (e.g. Gulf of Mexico, U.S.A., Olariu & Ambrose, 2016) display distinct differences over short distances of only kilometres to tens of kilometres, suggesting that local conditions prevail over regional-scale controls in determining their overall geomorphologies. This observation, in turn, raises the question as to what extent the geomorphologies of these systems can be reliably predicted in models and reconstructed based on knowledge of their environmental parameters, which has driven the research conducted in this project and is addressed in Research Objectives I and II (Chapter 1). This question is also important with regard to the general applicability of conceptual models of their evolution (submarine canyons, e.g. Micallef et al., 2014) and classification schemes (submarine canyons, e.g. Jobe et al., 2011) developed based on the study of these systems in a regional context to other geographic regions.

The finding of this project that morphometric attributes of both submarine canyons and shelf-edge deltas show variable and rarely strong scaling with characteristics of their superordinate S2S system on a global scale aligns with findings from quantitative analyses of morphometric characteristics of submarine fans (see Nyberg et al., 2018b) and incised-valley fills (see Wang et al., 2019) studied in context of their superordinate S2S systems. The dominant effect of local controls over regional-scale ones likely contributes to the observed general lack of strong scaling relationships seen for these different types of sedimentary systems; together, they corroborate the view that each S2S system is characterised by a unique set of controlling factors (Sømme et al., 2009). Therefore, knowledge of the factors which influence characteristics of sedimentary environments in S2S systems, and their impact strength, is crucial for the reconstruction of a S2S system and its

subenvironments, because the interplay of various controls can enhance, decrease or even eliminate scaling relationships within a S2S system (e.g. Nyberg et al., 2018b). For this, the moderate and strong scaling relationships demonstrated in this work are particularly useful, because their correlation strength suggests that these scaling relationships are more widely recognisable across S2S systems.

Research Objective III of this work (Chapter 1) seeks to revise and extend conceptual models of submarine canyons and shelf-edge deltas (see section 1.2). Based on the results of the three individual studies, conceptual and semi-quantitative holistic models of shelf-edge delta- and submarine-canyon geomorphology are devised as a function of environmental variables that were identified in this research as their controls. These models represent end-members of pairs of variables along a spectrum of different possible morphometric characteristics of canyons, shelf-edge deltas and segments of their associated S2S systems, and groups within environmental classes. For the models, only correlation coefficients with absolute values of 0.5 or greater – representing a moderate or strong scaling relationship – were considered (for a discussion of the full breadth of results from each study see Chapters 3, 4 and 5, respectively).

Because the amount of available data from the literature did not enable the conduction of multivariate analyses (e.g. principal component analysis, Sharma et al., 2015; cluster analysis, Eltahan et al., 2021) to allow for the identification of the relative importance of individual controlling factors and assessment of their co-influence on aspects of submarine-canyon and shelf-edge delta geomorphology, the end-member models proposed in this chapter only consider scaling relationships between pairs of study variables. As such, they do not take into account the co-influence of multiple environmental variables on a morphometric attribute; this will need investigation in future research. For example, delta-element thickness shows positive scaling with shelf width (section 6.1.1) and tends to be greater for mixed-process regimes (section 6.1.3), which in turn suggests that shelf-edge delta thickness might be particularly promoted along continental margins associated with wide shelves and where marine hydrodynamic

processes are either equal to or dominant over fluvial processes. Thus, the combined influence of controls on morphometric characteristics of shelf-edge deltas and submarine canyons needs further investigation.

For simplicity, the conceptual models presented in the following sections (Figs. 6.1 to 6.7) depict shelf-edge deltas during lowstand conditions where continental shelves where subaerially exposed due to the vast majority of examples being interpreted – where reported – by the original authors as formed during phases of normal or forced shoreline regression. By contrast, submarine canyons are displayed during highstand conditions associated with submerged shelves, as seen during the present day.

6.1.1 Continental-margin configuration

6.1.1.1 Accommodation and bypass of sediment

On a most fundamental level, the geomorphology of every sedimentary system is determined by (i) the morphometric characteristics of the accommodation, and (ii) sediment transport dynamics, over time. The inherent, physical control of slope width on the accommodation of submarine canyons, and their successful traversing of continental slopes over time by retrogressive erosion at the canyon apex and down-slope progradation at the canyon mouth (e.g. Pratson et al., 2007) is reflected in the positive, monotonic correlation seen between canyon length and slope width (Fig. 6.1a). Of the correlations of canyon morphometrics with variables of the S2S system, the canyon-physiographic setting, and the latitudinal position of the canyon apex in Chapter 3, this constitutes the only strong scaling relationship identified in the dataset, with an absolute correlation coefficient value greater than 0.8. Correspondingly, the inherent control of the width of continental shelves on accommodation of shelf-edge deltas is seen in the tendency of shelf-edge deltaic elements to become longer with increasing shelf width (Fig. 6.1c); the scaling relationship is strong for the twelve observations of full deltaic element length and moderate for the 39 partial values obtained for the dataset of the shelf-edge delta study.

In addition to the width of the continental slope, its overall gradient delimits the steepness of the average canyon thalweg gradient (Fig. 6.1a) – defined

here as the gradient measured between canyon apex and -mouth – its physical control being demonstrated by the positive and moderate scaling seen between the two variables. Moreover, the average canyon thalweg gradient is ultimately controlled by the extent of a canyon along the shelf-slope profile, and the local elevation at the position of its apex and -mouth.

In contrast to the continental slope, the continental shelf configuration, as a direct control on canyon morphology, is only relevant for canyons which have cut across it, which in part accounts for the general scarcity of moderate correlations and absence of any strong correlation seen for studied canyons in Chapter 3 with shelf width, shelf-break depth and the average shelf gradient.

6.1.1.2 Shelf- and slope gradients as drivers of autogenic and allogenic sedimentary processes in submarine canyons and shelf-edge deltas

Both seafloor topography and gradients govern sediment transport dynamics across continental margins to submarine canyons and shelf-edge deltas. Pre-existing seafloor topography and evolving relief linked to reef built-up (e.g. Ferro et al., 1999; Puga-Bernabéu et al., 2011), salt diapirism (e.g. Cumberpatch et al., 2021 and references therein) or tectonic activity (e.g. Chiang et al., 2012) control sediment pathways and might disconnect canyons and shelf-edge deltas from fluvial and intra-shelf sediment sources over time. Also, seafloor gradients exert influence on the transport distance of sediment gravity flows (e.g. Tournadour et al., 2017) and the gravitational remobilisation of sediment deposits (e.g. Piper et al., 2012). The globally displayed positive correlation of maximum sidewall steepness in studied canyons with the average slope gradient in Chapter 3 (Fig. 6.1a) possibly represents such a causal link, where canyon excavation and the steepening of canyon margins is promoted along steeper continental slopes due to more frequent occurrences of mass failures within submarine canyons and along adjacent and proximal slope areas.

Although not evaluated here due to lack of data, steep shelf- and slope gradients are expected to counteract and delimit the growth of shelf-edge deltas by destabilising delta deposits and triggering mass-failures within the

delta from their control on the surface gradients of delta lobes (e.g. Roberts & Sydow, 1996). This autogenic process probably inhibits the lengthening and thickening of deltaic elements in shelf-edge deltas associated with narrow and steep shelves (Fig. 6.1c).

6.1.1.3 Co-relationships of continental-margin configuration with morphometric attributes of submarine canyons and shelf-edge deltas

Other moderate correlations of morphometrics in submarine canyons and shelf-edge deltas with attributes of their associated continental margins are interpreted here as co-relationships arising from scaling relationships between morphometric attributes of shelves and slopes, respectively. The tendency of canyons to become longer with increasing shelf-break depth (Fig. 6.1d) is probably related to the strong positive scaling of shelf-break depth with slope width, and the latter being a primary control of canyon length, whereas the average canyon thalweg gradient tends to decrease along wider slopes due to the inverse relationship of slope width with the average slope gradient (Fig. 6.1a).

The observed increase of maximum width and depth in submarine canyons with increasing width of the continental slope might reflect that along wider slopes canyons are more likely to intercept and incorporate pre-existing negative topographic relief as intra-slope basins and faults (Fig. 6.1b). Considering that submarine mass failure can occur on low-gradient slopes (≤2°) provided specific sets of conditions – including pore pressure and the percentage of organic matter in sediment – which are still not fully understood (e.g. Urlaub et al., 2015 and references therein), and that with increasing shelf width sediment connection of a canyon with fluvial and littoral systems becomes less likely (e.g. Bernhardt & Schwanghart, 2021), the positive correlation of maximum canyon sidewall steepness with shelf width is possibly random, else constitutes an unidentified co-relationship (Fig. 6.1e).

In addition to the inherent control of shelf width on deltaic-element length (section 6.1.1.1), the increase in size of shelf-edge deltas with increasing shelf width probably reflects how the progradation of shelves and shelf-edge

deltas is concurrently driven by high sediment supply from terrestrial hinterlands to the shelf margin (e.g. Carvajal et al., 2009). Moreover, during sea-level lowstands the merging of rivers is promoted within wider shelves (e.g. Sømme et al., 2009; Covault et al., 2011b), which increases the sediment volume distributed to a shelf-edge delta, and in turn delta size (see section 6.1.2). Another contributing factor might be that the volume of sediment, that is locally sourced to a shelf-edge delta from incision of the shelf substrate by the associated river, tends to increase with increasing shelf width. The inverse relationship between delta-element thickness and shelf width corroborates in part findings from a recent study by Soutter et al. (2023) of continental shelves along the margins of the Americas. The results by Soutter et al. (2023) suggest that narrow shelves tend to be associated with thinner sediment thickness and increased seismicity in terrestrial catchments, reflecting how tectonic activity constitutes a control on shelf width by delimiting shelf accommodation and promoting sediment routeing to deep-water environments (see Soutter et al., 2023 and references therein), factors which both have an inhibiting influence on the size of a shelf-edge delta. In addition, narrower shelves might accommodate thinner shelf-edge deltaic elements related to steeper overall shelf gradients promoting both non-deposition and remobilisation of sediments in shelf-edge deltas (Fig. 6.1c).

Conceptual models

Based on the identified moderate and strong scaling relationships with attributes of the continental-margin configuration, the following five pairs of end-member models of slope- and shelf configuration versus morphometric characteristics of submarine canyons and shelf-edge deltas are identified:

(1) Narrow and steep continental slopes promote short canyons with steep margins, whereas wide and low-gradient continental slopes promote long canyons with gentle margins (Fig. 6.1a).
(2) Submarine canyons tend to have low maximum-width and -depth values when associated with a narrow slope, whereas along a wide slope, canyons display the greatest maximum widths and -depths (Fig. 6.1b).

(3) Short, narrow and thin shelf-edge deltaic elements tend to develop along narrow and steep shelves; by contrast, long, wide and thick shelf-edge deltaic elements preferably form along wide and low-gradient shelves (Fig. 6.1c).

(4) Submarine canyons accommodated on deep shelves tend to be longer than submarine canyons on shallow shelves (Fig. 6.1d).

(5) Submarine canyons associated with narrow shelves tend to have more gentle margins compared to those associated with wide shelves (Fig. 6.1e).

A.

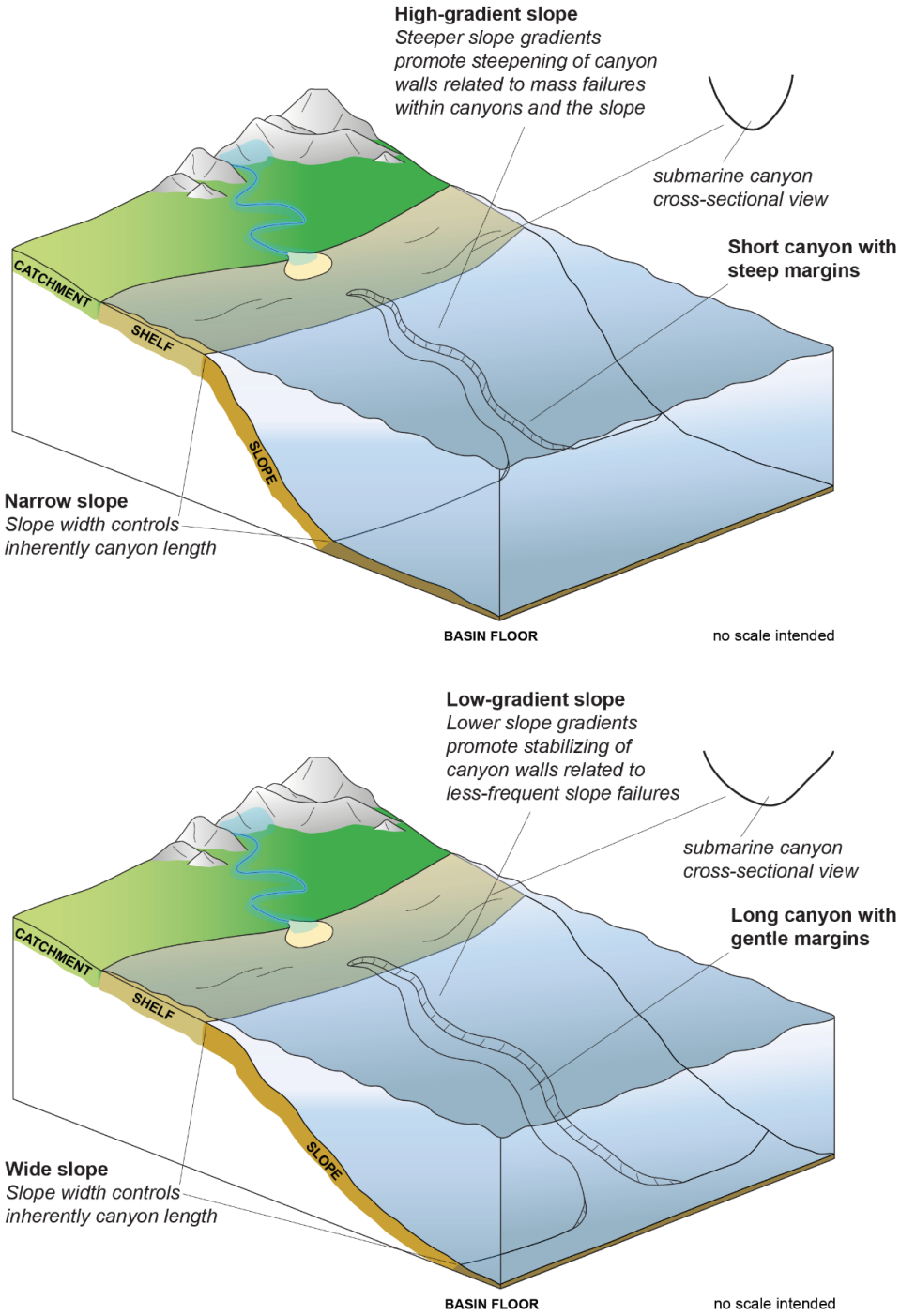
High-gradient slope
Steeper slope gradients promote steepening of canyon walls related to mass failures within canyons and the slope
submarine canyon cross-sectional view
Short canyon with steep margins
CATCHMENT
SHELF
SLOPE
Narrow slope
Slope width controls inherently canyon length
BASIN FLOOR
no scale intended
Low-gradient slope
Lower slope gradients promote stabilizing of canyon walls related to less-frequent slope failures
submarine canyon cross-sectional view
Long canyon with gentle margins
CATCHMENT
SHELF
SLOPE
Wide slope
Slope width controls inherently canyon length
BASIN FLOOR
no scale intended

B.

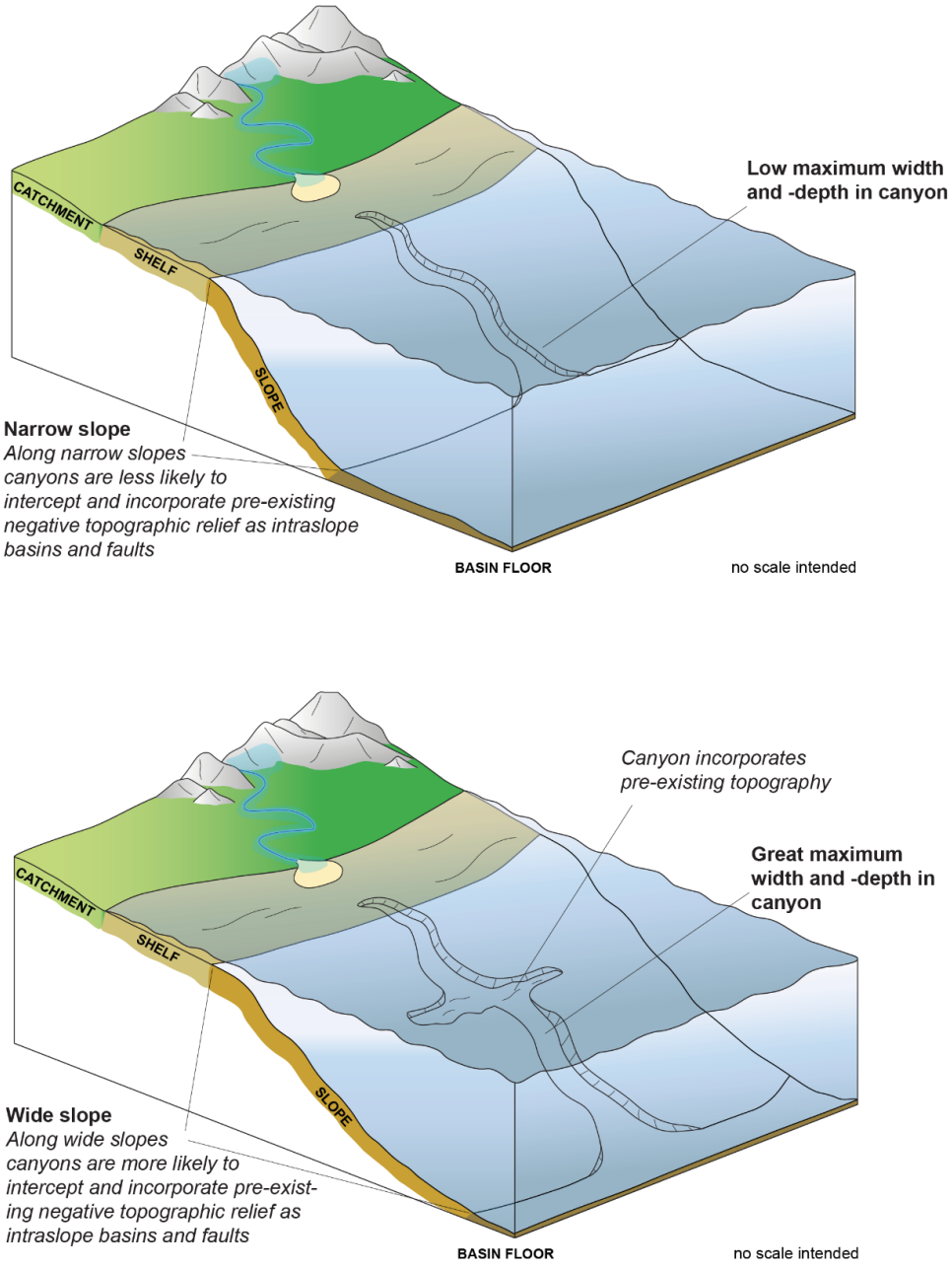

Figure 6.1a-e (continued).

C.

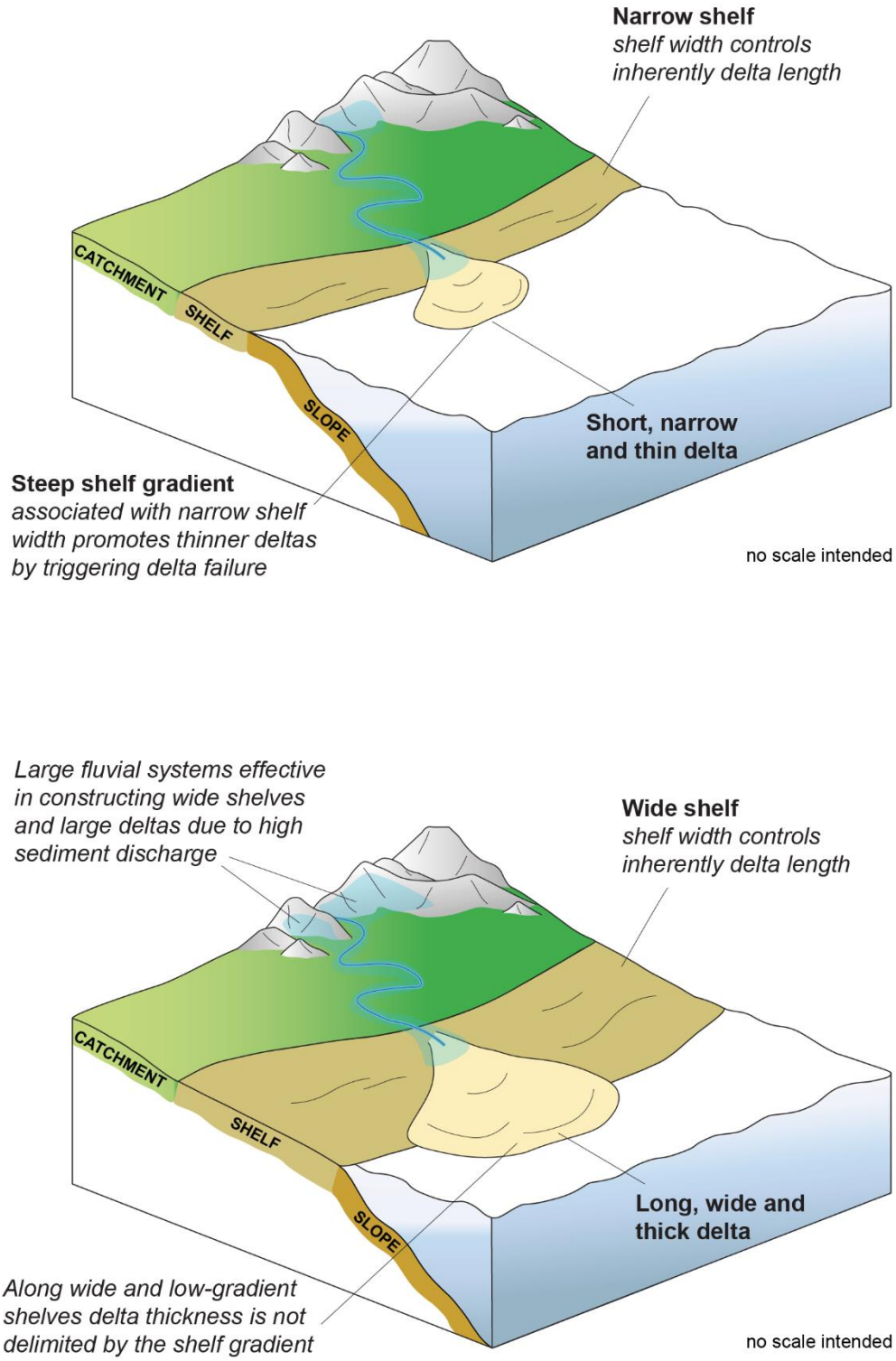

Figure 6.1a-e (continued).

D.

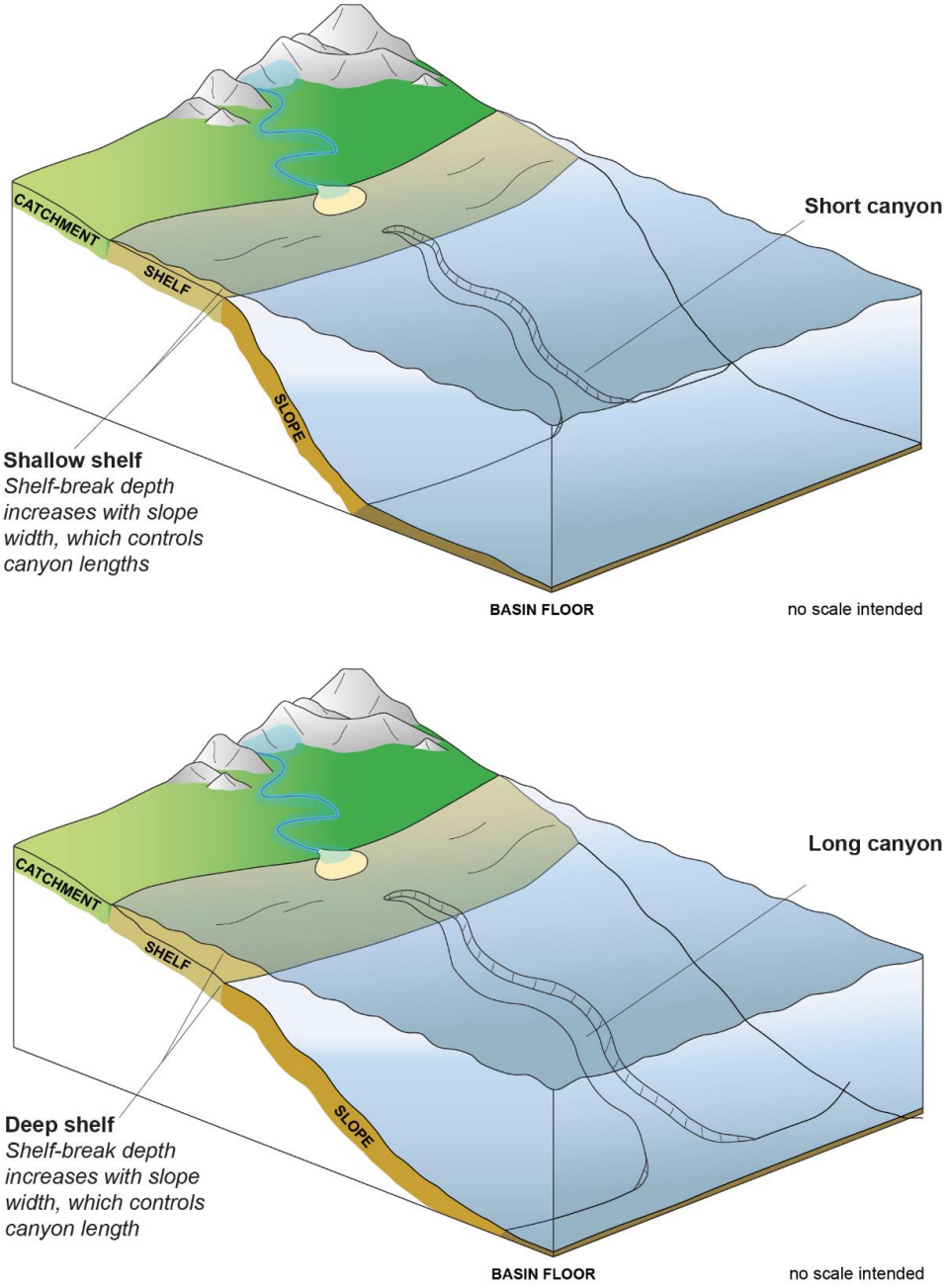

Figure 6.1a-e (continued).

E.

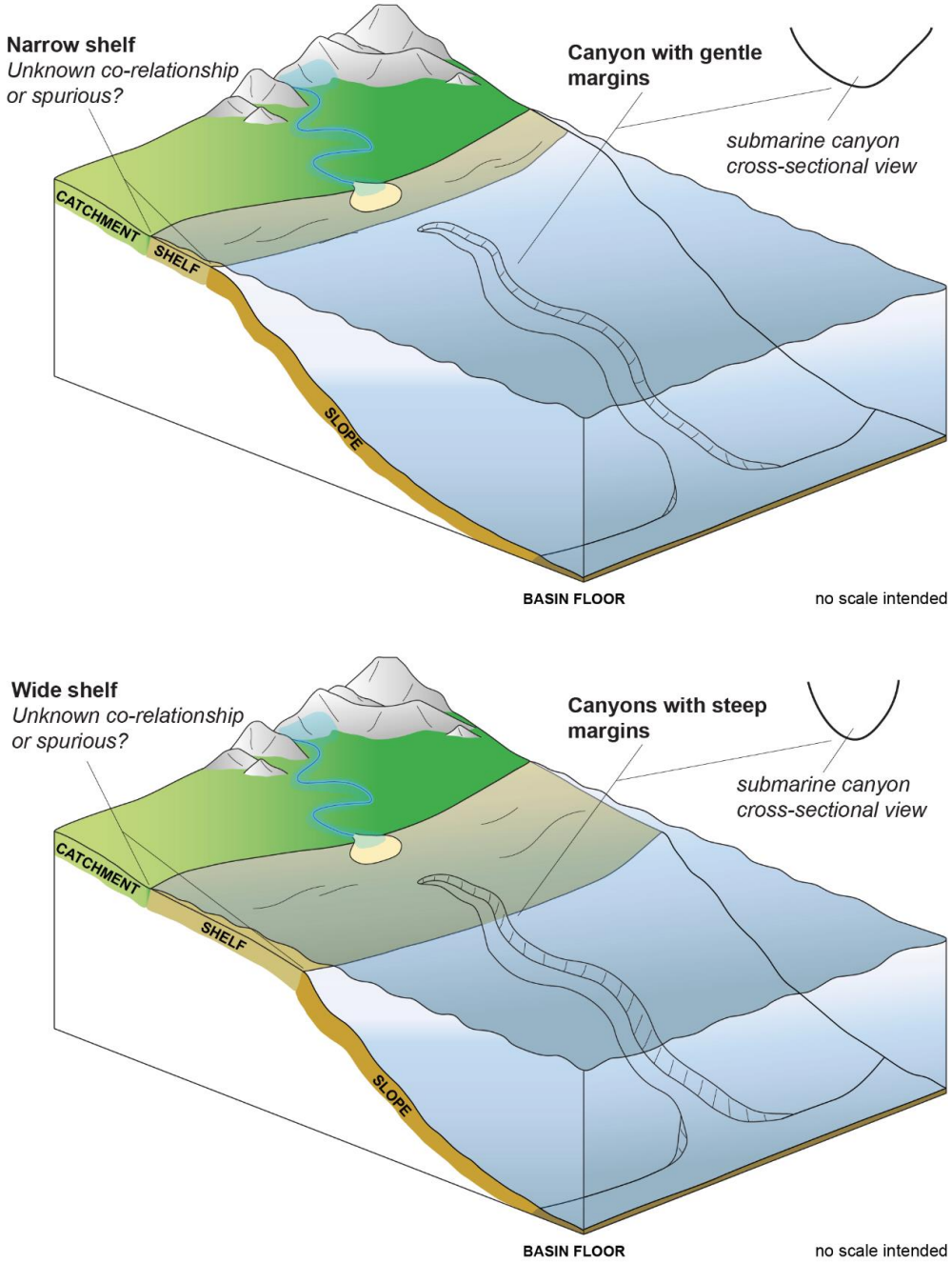

Figure 6.1a-e Conceptual models of morphometric attributes in submarine canyons and shelf-edge deltas and their scaling with end-members of shelf- and slope configuration in a source-to-sink system. A. length, average canyon thalweg gradient and maximum sidewall steepness in a submarine canyon vs. slope configuration. B. Maximum width and -depth in a submarine canyon vs. slope width. C. Length, maximum width and -thickness in a shelf-edge delta element vs. shelf configuration. D. Length in a submarine canyon vs. shelf-break depth. E. Maximum sidewall steepness in a submarine canyon vs. shelf width.

6.1.2 Terrestrial catchment characteristics

The important but relative role of sediment supply from terrestrial catchments in shaping the geomorphology of sedimentary systems along the longitudinal S2S system profile downstream of rivers has been demonstrated by previous quantitative studies of submarine fans (e.g. Sømme et al., 2009; Nyberg et al., 2018b) and incised valley-fills (Wang et al., 2019). Findings of this work show that this also applies to shelf-edge deltas and submarine canyons:

Using data from modern fluvial systems at the shelf-edge delta location as proxies due to the paucity of data on palaeo-drainage characteristics, studied examples of shelf-edge deltas of Late Pleistocene age suggest that larger drainage basins and higher terrestrial source areas produce wider shelf-edge deltaic elements (Fig. 6.2a; see also Chapter 5). The recognition of these observations in younger S2S systems on a global scale likely reflects how sediment supply to rivers increases with drainage basin size (e.g. Sømme et al., 2009; Milliman & Farnsworth) and the effective transport of terrestrial sediment to shelf-edge deltas and deposition in shelf-edge deltaic sinks over relatively short time scales. At the hierarchical level of a delta complex, element width is controlled by the width of the individual delta lobes and the extent of their lateral stacking related to lobe switching; the positive relationship might in part reflect how shoreline progradation rates increase with catchment size and avulsion frequency scales positively with the former (see Colombera & Mountney, 2022). The results in Chapter 5 also indicate that the scaling relationship seen between delta-element width and maximum elevation of modern drainage basins is recognisable in older S2S systems, unless the source area is characterised by very low elevations. This is for example the case in terrestrial catchments where orogens have significantly diminished due to long-term erosion.

Preliminary findings for studied shelf-edge deltas indicate that despite constituting terminal depositional systems of rivers, deltaic elements lack strong scaling with characteristics of the terrestrial catchment. This probably reflects in part how the fluvial sediment load does not reach the shelf edge but is deposited in more proximal terrestrial sinks as coastal plains (e.g.

Goodbred Jr. & Kuehl, 1998; Phillips & Slattery, 2006), the bypassing of fluvial sediment across shelf-edge deltas to deep-water environments (e.g. Mellere et al., 2003; Kim et al., 2013; Straub, 2019), the remobilisation of delta deposits and their down-slope transport (e.g. Porębski & Steel, 2003; Dixon et al., 2012), and erosion of delta deposits by marine currents and waves (e.g. Berné et al., 1998; Ferro et al., 1999). The occurrence and magnitude of above processes, and their relevance as drivers of shelf-edge delta evolution and resulting delta geomorphology, are influenced by external factors such as tectonics and sea level. For example, during phases of sea-level lowstand basinward transport/delta bypass of sediment might be enhanced due to the extension of rivers across the shelf edge (e.g. Mellere et al., 2003; Porębski & Steel, 2006). By contrast, the efficiency of delta-front erosion by waves might be enhanced during phases of sea-level transgression (e.g. Porębski & Steel, 2006). Moreover, the signature of fluvial sediment supply might be overprinted by additional sediment accreted onto a shelf-edge delta by littoral cells, and from locally sourced shelf sediments excavated during the progradation of the fluvial system to the shelf margin (e.g. Blum & Törnqvist, 2000; Blum & Hattier-Womack, 2009; Blum et al., 2013). The contribution of the latter to the sediment budget of the shelf-edge delta is probably highly variable, depending on factors as the incision depth of the incised valley – which in turn is controlled by factors as the shelf gradient and lithology of the shelf substrate (see Wang et al., 2019, and references therein) – the shelf width, and the proportion of volume from the intra-shelf source relative to the catchment source. As discussed in section 6.1.1, fluvial sediment deposition in shelf-edge deltas is also inherently controlled by the shelf width, and by the shelf and slope gradient from their influence on delta surface gradients and the triggering of mass failures and sediment gravity flows within sufficiently steep deltas.

The results of the shelf-edge delta study in Chapter 5 complement those by Wang et al. (2019), whose global investigation of 151 incised-valley fills showed only modest strengths of positive correlations of width, thickness and cross-sectional area of incised-valley fills with the catchment area for incised-valleys in general, which the authors ascribed to the complex

interplay of variables of the terrestrial catchment and shelf segments on the enlargement of incised valleys.

Results from the global investigation of shelf-edge deltas in this project also indicate that the confluence of rivers exerts control on shelf-edge delta geometry with lengths, widths, thicknesses and areas of sampled deltaic elements tending to be greater in shelf-edge deltas associated with multiple rivers over systems fed by a single fluvial system. This likely reflects that cumulative sediment budgets of several rivers tend to be higher than those of individual ones, although this may not always apply, e.g. in case of large rivers draining multiple catchments, as the modern Amazon River (e.g. Milliman & Farnsworth, 2011). In terms of the configuration of the terrestrial drainage-and-shelf-edge delta system, shelf-edge deltas fed by different rivers might be associated with a multiple point source instead of a single point source where individual shelf-edge deltas along the same continental margin have merged over time (Fig. 6.2b).

The results of the correlation analyses in Chapter 3 of submarine canyons with a sediment connection to one or several rivers show that the canyons become longer and more sinuous with increasing average annual fluvial discharge (Fig. 6.2c) and maximum catchment elevation (Fig. 6.2d). Submarine canyons of the study have also greater maximum canyon depths when associated with longer fluvial systems (Fig. 6.2e) and larger drainage basins (Fig. 6.2f). In addition, maximum canyon width shows positive scaling with the maximum elevation (Fig. 6.2d) and size (Fig. 6.2f) of terrestrial catchments. These moderate scaling relationships between canyon morphometrics and characteristics of the terrestrial catchment were not unexpected, considering that scaling relationships of terrestrial catchment attributes with aspects of submarine-fan geomorphology have been demonstrated for submarine fans on a global scale (e.g. Sømme et al., 2009; Nyberg et al., 2018b), documenting the successful routeing of large volumes of sediment from hinterlands to deep-sea basins.

As discussed for shelf-edge deltas, the findings can be linked to the increase in fluvial sediment supply with increasing size and elevation of the associated terrestrial catchment. Greater sediment discharge volumes at the

mouth of rivers in turn promote the height and runout distances of sediment gravity flows in submarine canyons, which promotes intra-canyon erosion (e.g. Talling et al., 2022) and, where flow heights exceed canyon depth, aggradation of canyon margins. The findings from the global canyon study highlight the efficiency of fluvial sediment discharge in modifying aspects of canyon geomorphology and align with those by Harris & Whiteway (2011), who found for their dataset that modern shelf-incising submarine canyons with a fluvial connection were on average longer than both canyons that had retrograded into the shelf but were not connected with a river and slope-confined canyons, by factors of 1.61 and 2.07, respectively.

Conceptual models

From the moderate scaling relationships of shelf-edge delta and canyon morphometrics with attributes of the terrestrial catchment, six different end-member models of terrestrial catchment characteristics versus morphometric characteristics of submarine canyons and shelf-edge deltas emerge:

(1) Small and low terrestrial catchments generate narrow shelf-edge delta elements, due to low sediment supply to shelf margins. In contrast, large and high terrestrial catchments promote the formation of wide deltaic elements in shelf-edge deltas (Fig. 6.2a).
(2) The control of terrestrial sediment supply on the size of a shelf-edge delta is also reflected in the tendency of delta-element dimensions and area in shelf-edge deltas fed by multiple rivers to exceed those of shelf-edge deltas supplied by single fluvial systems (Fig. 6.2b).
(3) Short and straight canyons develop in front of fluvial systems with low average annual fluvial discharge. By contrast, long and sinuous canyons evolve where the canyon shares a sediment connection with a fluvial system with high average annual discharge (Fig. 6.2c).
(4) In S2S system with low elevation of the terrestrial catchment, submarine canyons are short, have low average sinuosity and narrow maximum widths, whereas in S2S systems associated with high orogens, the canyons are characterised by great lengths, high average sinuosities, and great maximum widths (Fig. 6.2d).

(5) The maximum depth of a canyon scales positively with river length; hence, shallow canyons are expected to develop where short rivers discharge onto continental margins, and deep canyons distally of long rivers (Fig. 6.2e).

(6) The lowest maximum widths and depths are found in submarine canyons that are supplied by small terrestrial catchments; wide and deep canyons form where the drainage basin size is large (Fig. 6.2f).

A.

Small and low terrestrial catchment

low volumes of sediment discharge from low and small terrestrial catchments

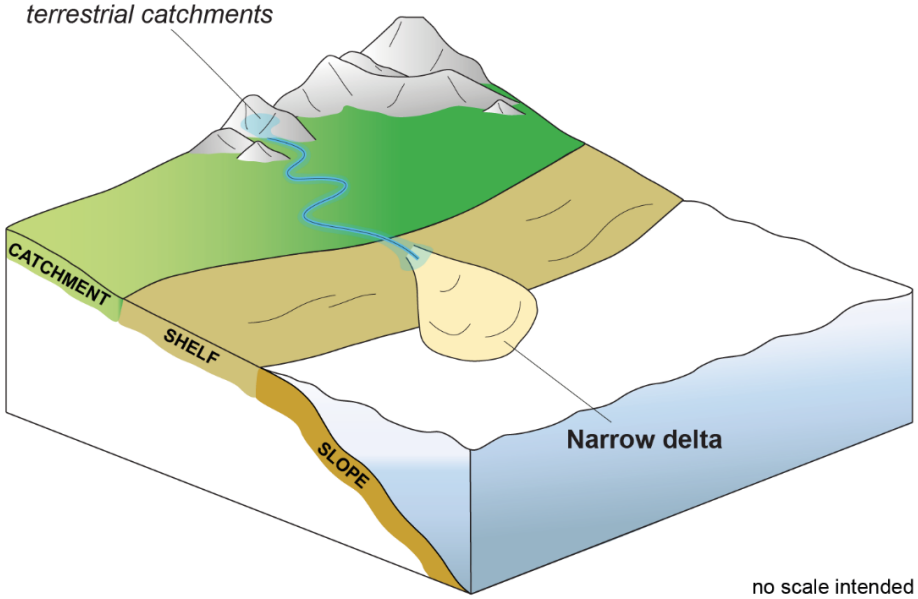

no scale intended

Large and high terrestrial catchment

high volumes of sediment discharge from large and high terrestrial catchments

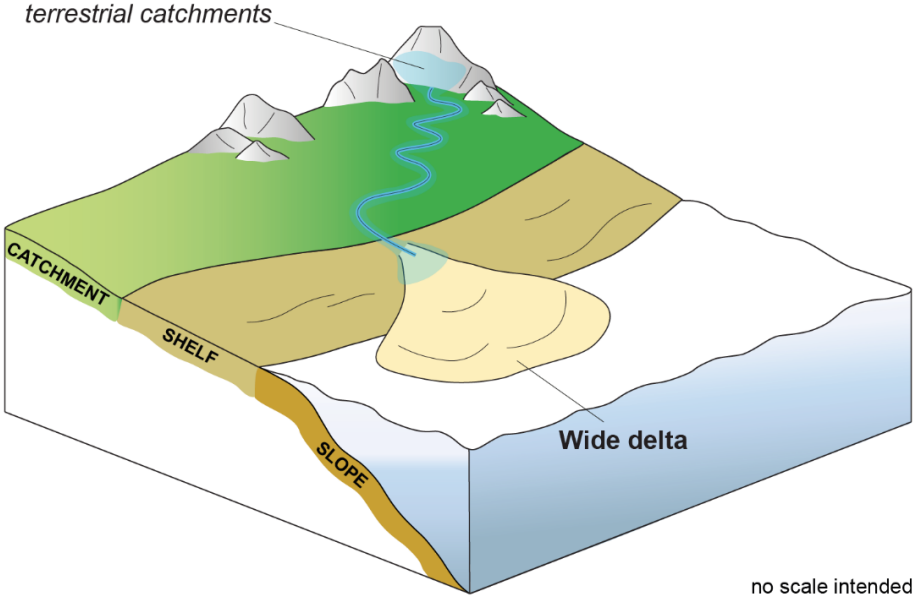

no scale intended

B.

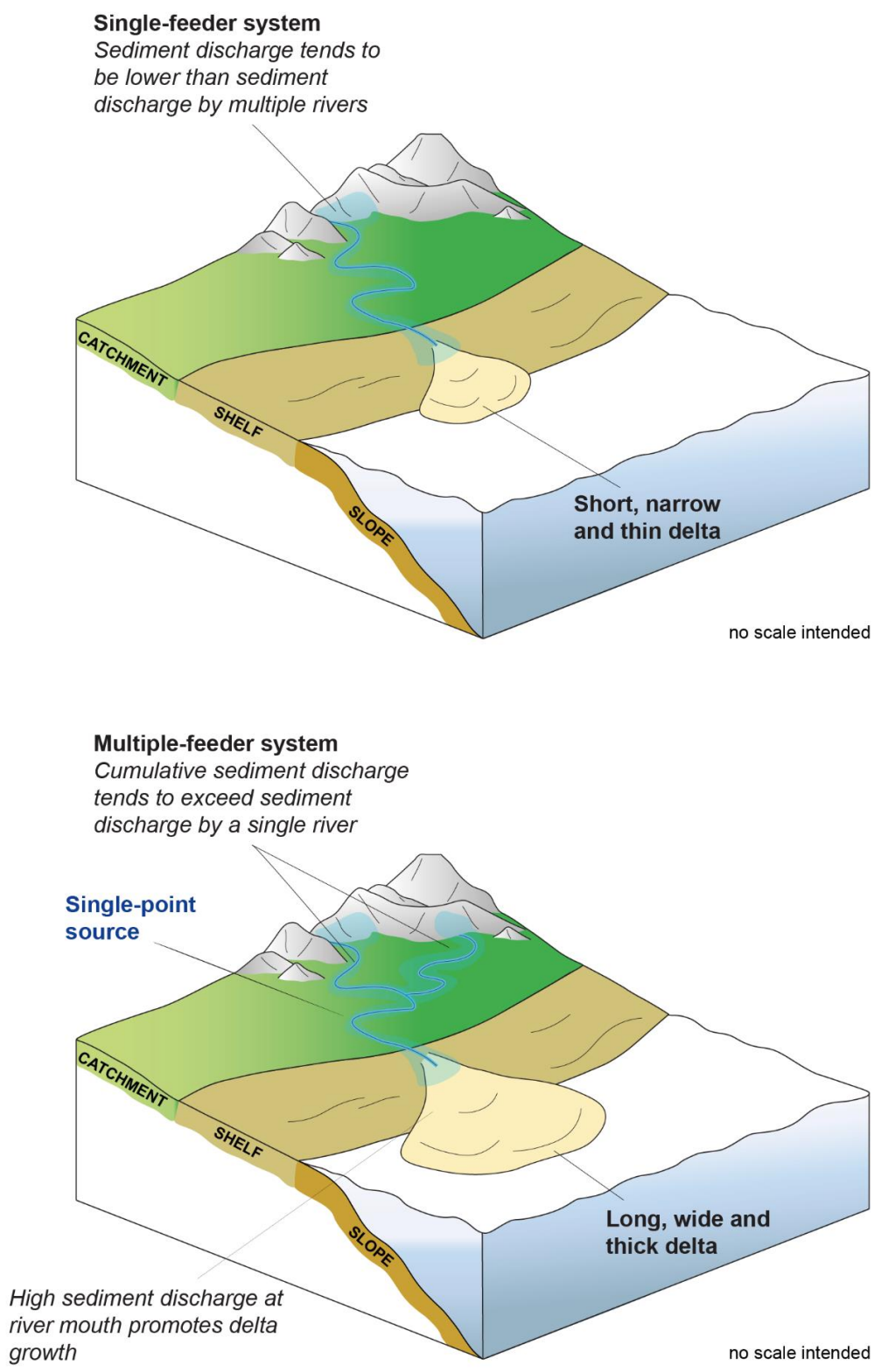

Figure 6.2a-f (continued).

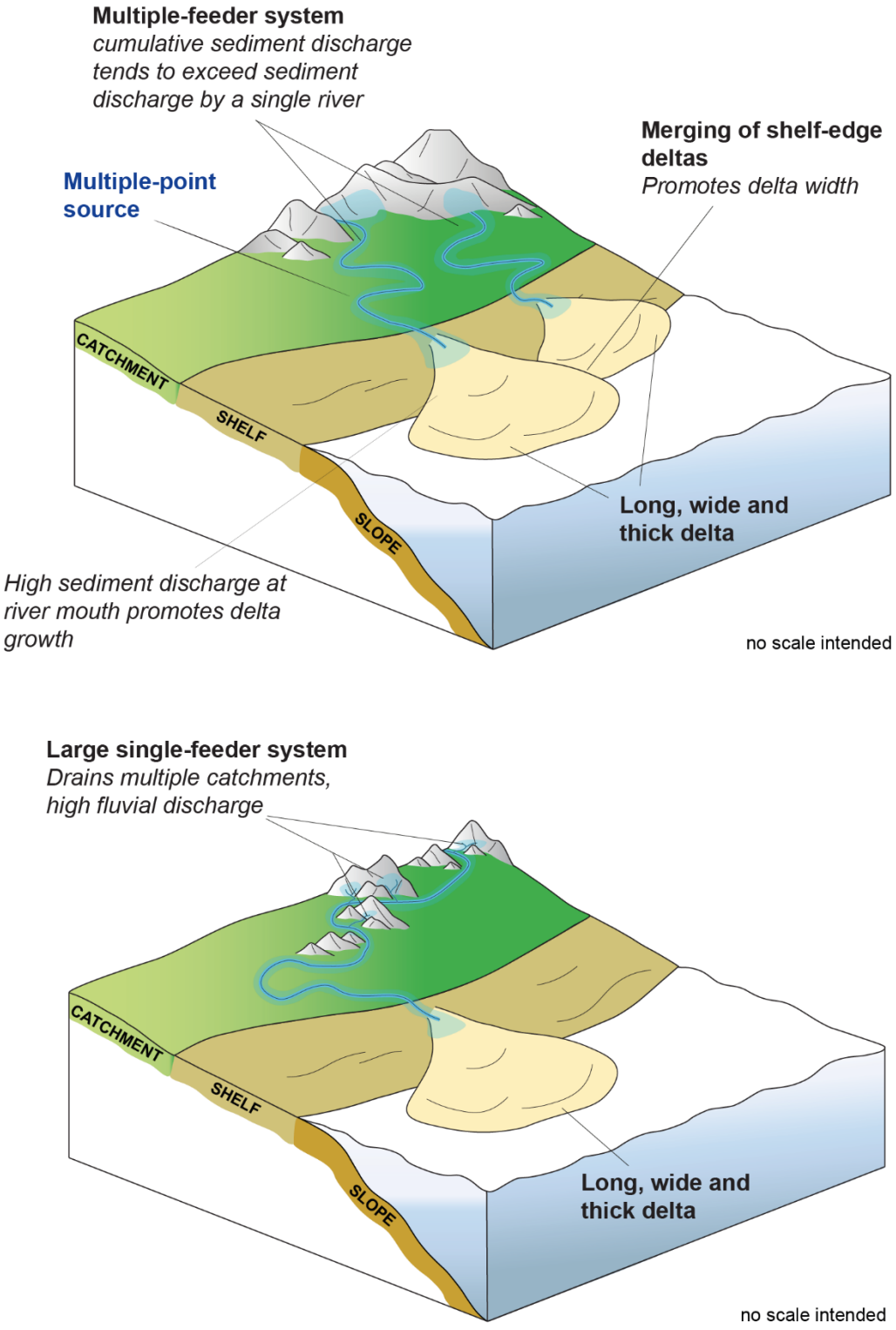

Figure 6.2a-f (continued).

C.

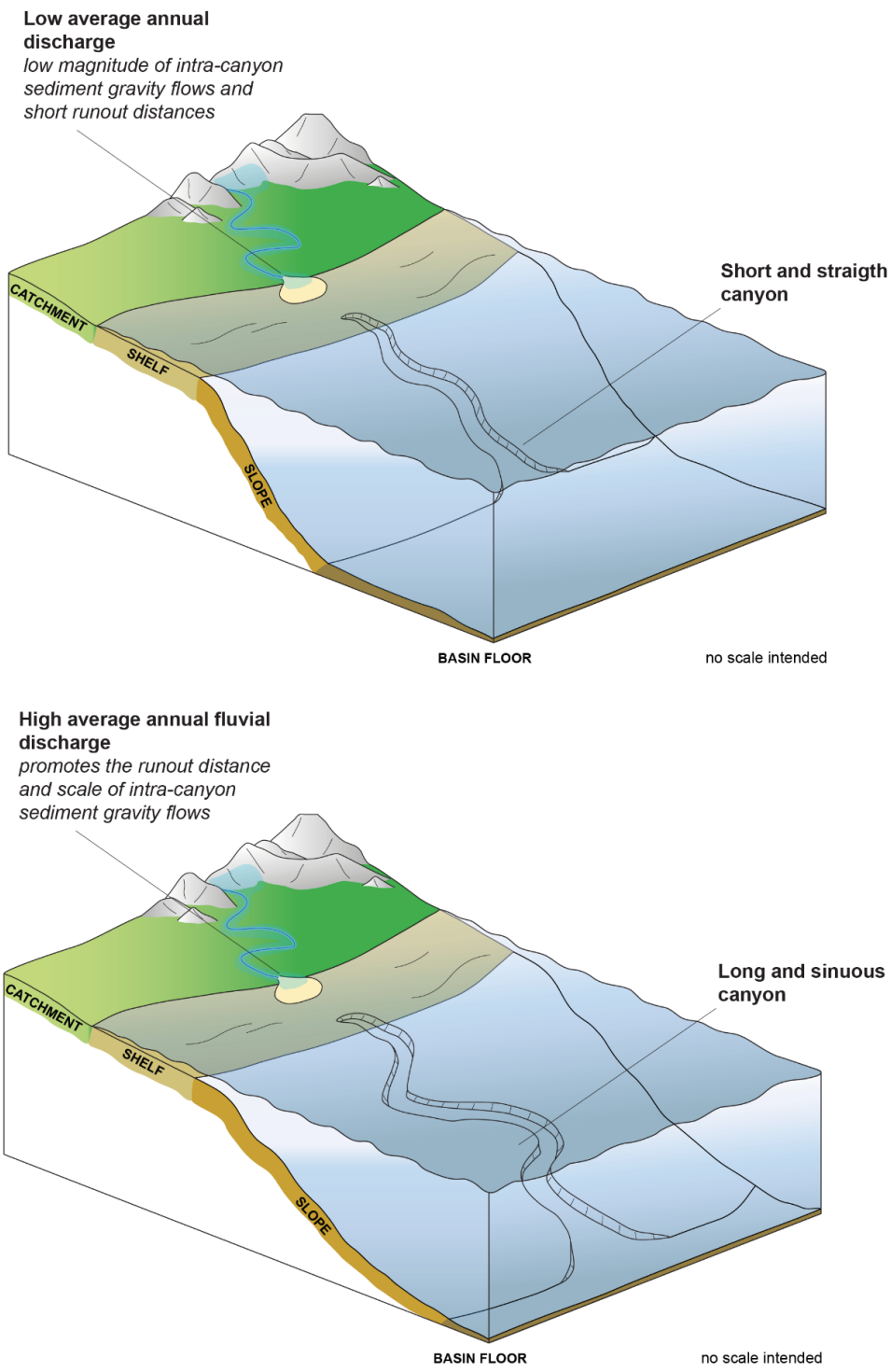

Figure 6.2a-f (continued).

D.

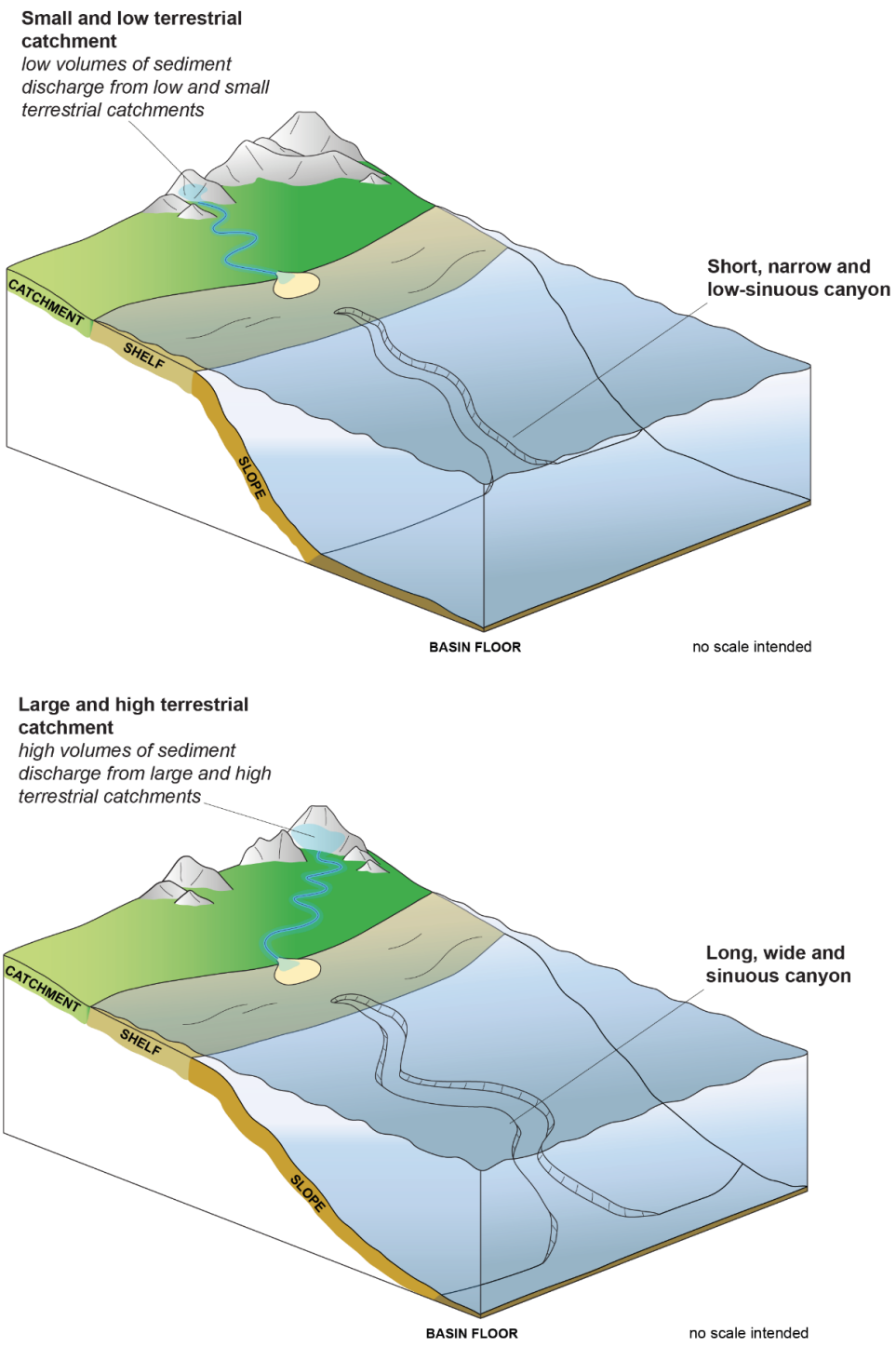

Figure 6.2a-f (continued).

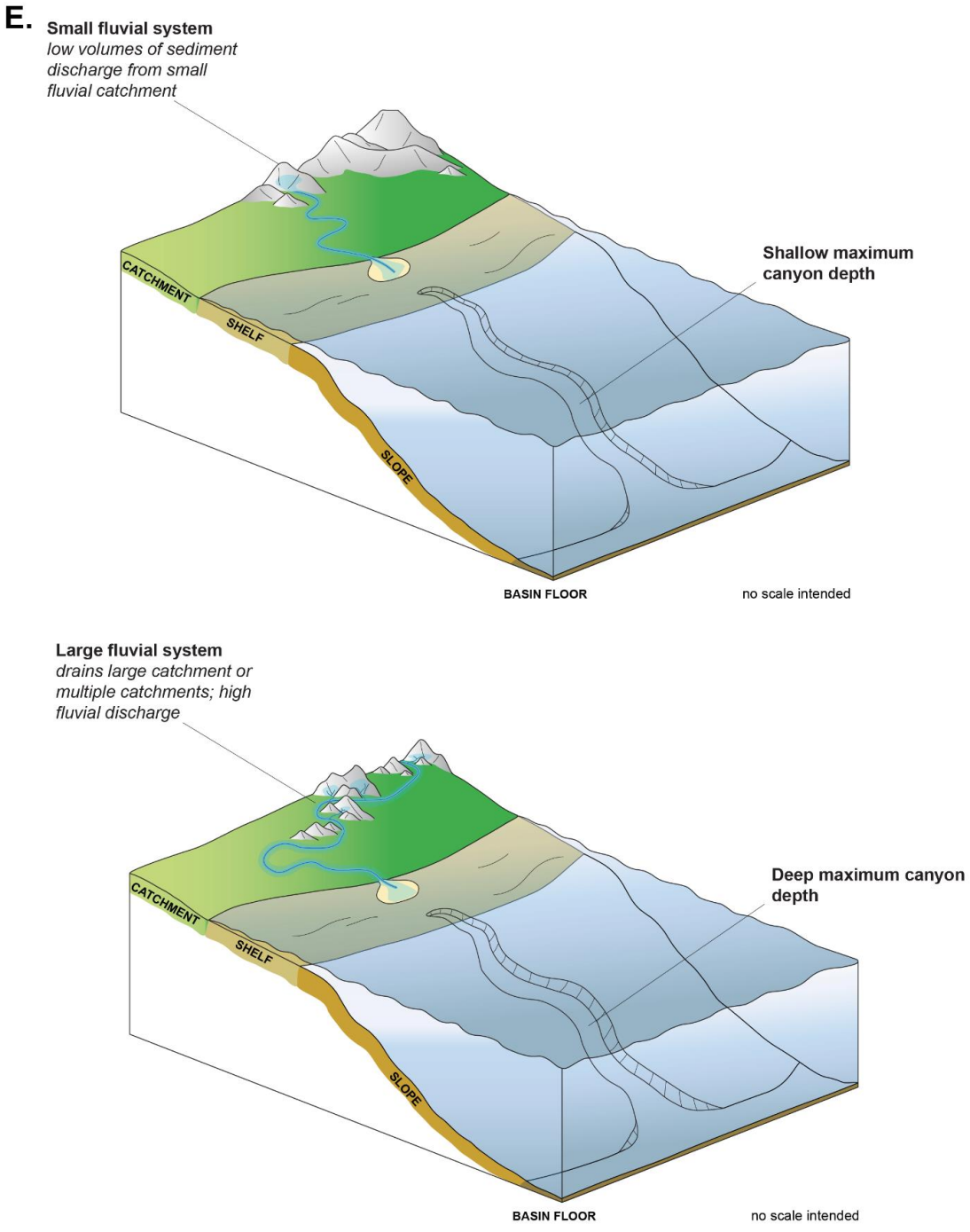

Figure 6.2a-f (continued).

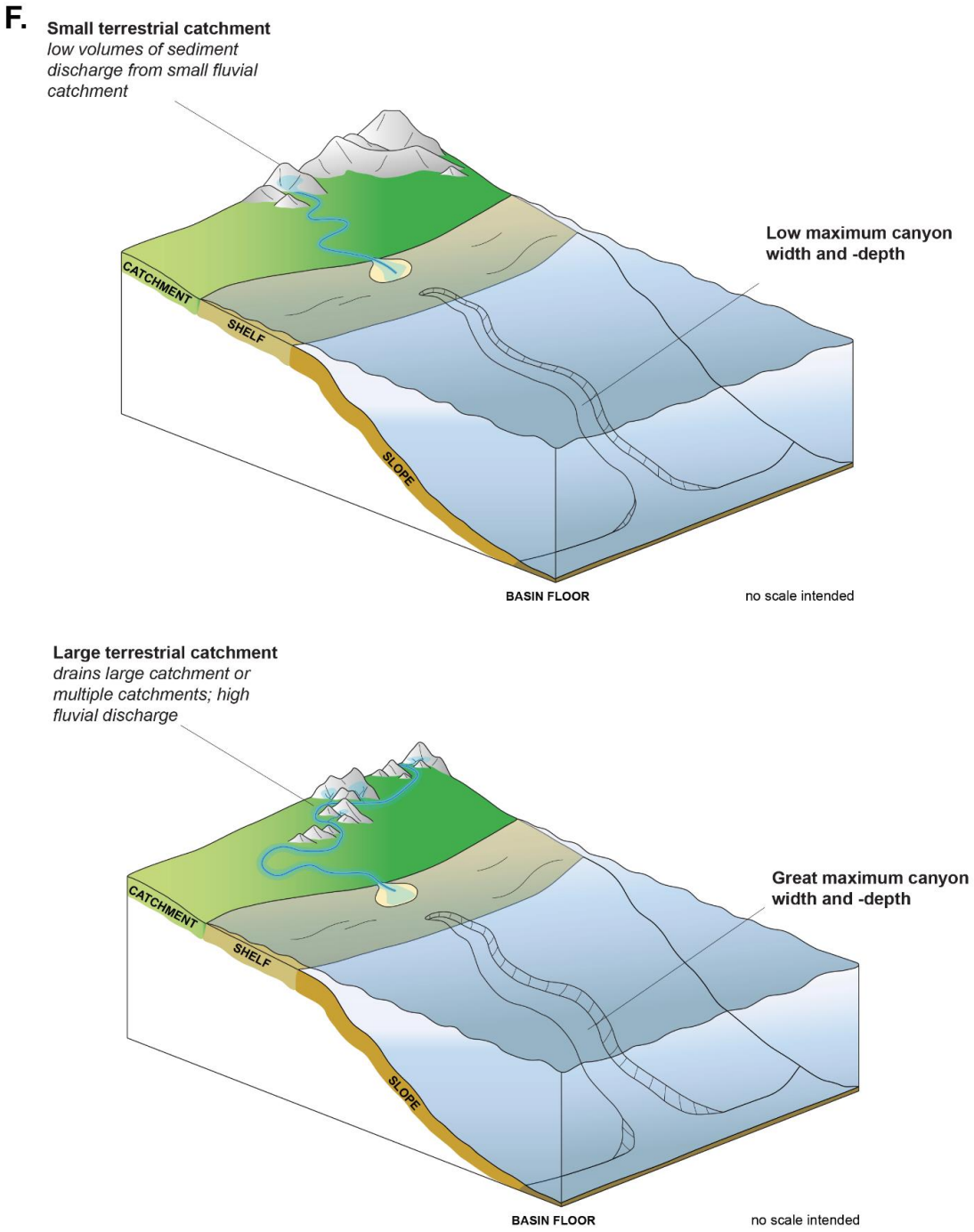

Figure 6.2a-f Conceptual models of morphometric attributes in shelf-edge deltas and submarine canyons and their scaling with end-members of terrestrial catchment characteristics in a source-to-sink system. A. Shelf-edge delta element width vs. size and maximum elevation of the terrestrial catchment. B. Shelf-edge delta element dimensions and area vs. fluvial feeder-system type. C. Length and average sinuosity in a submarine canyon vs. average annual fluvial discharge. D. Length, maximum width and average sinuosity in a submarine canyon vs. maximum catchment elevation. E. Maximum depth in a submarine canyon vs. fluvial system length. F. Maximum width and depth in a submarine canyon vs. terrestrial catchment size.

6.1.3 Marine hydrodynamic processes: oceanographic environment and hydrodynamic-process regime

The importance of marine hydrodynamic processes for canyon-fed S2S systems is demonstrated in modern submarine canyons which are supplied by sediment-carrying currents within the shelf and slope (e.g. Warratz et al., 2019; Serra et al., 2022; Rodrigues et al., 2022). Moreover, the classification of deltas according to their hydrodynamic-process regime is commonly applied (Dixon et al., 2012 and references therein; Gong et al., 2016 and references therein). Furthermore, longshore currents have been considered to some degree in S2S system models as means of sediment transport (e.g. Sømme et al., 2009; Covault et al., 2011b; Bhattacharya et al., 2016). Despite these aspects, neither the oceanographic environment nor the hydrodynamic-process regime has until now been applied as a criterion for the classification of S2S systems or deep-water systems.

However, differences seen in global frequency distributions of morphometric parameters of studied submarine canyons (Chapter 3) and shelf-edge deltas (Chapter 5) for S2S systems located within an ocean versus a semi-enclosed or enclosed sea – the latter group also including straits and gulfs in the definition applied in this work – indicate that the oceanographic environment exerts control on the geomorphology of both types of sedimentary systems. The demonstrated tendencies of submarine canyons to develop greater maximum depths and maximum sidewall steepness, and of shelf-edge deltas to have greater lengths, widths and areas when associated with an open-sea setting, might be explained by a greater magnitude of currents and waves in oceans compared to semi-enclosed and enclosed seas, and their impact on erosional and depositional processes within both types of sedimentary systems (Fig. 6.3a&b). This interpretation is partially supported by findings from Wang et al. (2020), who demonstrated for modern environments at the location of 49 late Quaternary incised-valley fills on average statistically significantly greater mean wave heights in open-sea settings compared to semi-enclosed and enclosed seas, by a factor of ~1.5 (see their Figure 11a). The relationships might also in part reflect how terrestrial catchments associated with continental margins facing oceans

tend to have larger drainage basins and higher sediment discharge to the marine environment compared to margins associated with semi-enclosed seas (e.g. Peucker-Ehrenbrink, 2009). Another factor might be that marine basins in oceans tend to have greater depths compared to those located in semi-enclosed seas (e.g. Dierssen & Theberge, 2014). However, some semi-enclosed seas reach water depths comparable to those in open seas (e.g. South China Sea; see Figure 4 of Dierssen & Theberge, 2014).

Marine currents and waves have been invoked to be able to influence the geometry of a shelf-edge delta from their redistribution of sediment within delta fronts, promoting widening of shelf-edge deltas (e.g. Berné et al., 1998; Yoo et al., 2017). The results of Chapter 5 corroborate this inferred relationship by demonstrating that deltaic elements tend to be wider and thicker in shelf-edge deltas characterised by a mixed-process regime compared to fluvially dominated shelf-edge deltas. In addition to the redistribution of delta sediments, currents and waves probably also promote delta growth by dispersing sediment from discharge at river mouths, and by supplying sediment from intra-shelf environments to the delta. Also, where slope currents transport sediment at relatively shallow water depths, these might function as a sediment source to a shelf-edge delta (Fig. 6.4).

Although scaling relationships between submarine-fan geomorphology and both the oceanographic environment and the hydrodynamic-process regime of a delta have not yet been quantitatively assessed, the influence of contour currents on submarine-fan deposits is documented in modern S2S systems around the world (e.g. Rodrigues et al., 2022). Moreover, fluctuations in sediment budgets transferred from terrestrial hinterlands to deep-water basins related to sediment addition and removal by slope-parallel contourite systems (e.g. Rodrigues et al., 2022) probably contribute to the weakening of scaling between attributes of the terrestrial catchment and submarine-fan geomorphology, with those scaling relationships being only moderate in strength (e.g. Nyberg et al., 2018b).

Together, these findings suggest that marine hydrodynamic processes constitute a general control on the geomorphology of sedimentary systems in marine environments from their influence on the accretion, non-deposition

and removal of sediment. As such, the oceanographic environment and the hydrodynamic-process regime should be included as criteria in classification schemes of S2S systems that comprise submarine canyons, shelf-edge deltas, or both, in their configuration.

Conceptual models

The following three end-member models of moderate scaling relationships of shelf-edge delta and canyon morphometrics with environmental characteristics of marine hydrodynamic processes are proposed here:

(1) Submarine canyons associated with an open-sea setting have greater maximum depths and steeper margins than canyons in semi-enclosed and enclosed seas (Fig. 6.3a).
(2) Deltaic elements in shelf-edge deltas are longer, wider and larger in open oceans compared to semi-enclosed and enclosed seas (Fig. 6.3b).
(3) Deltaic deposits tend to be wider and thicker in shelf-edge deltas that are associated with a mixed-process regime than their counterparts characterised by a fluvially dominated process regime (Fig. 6.4).

A.

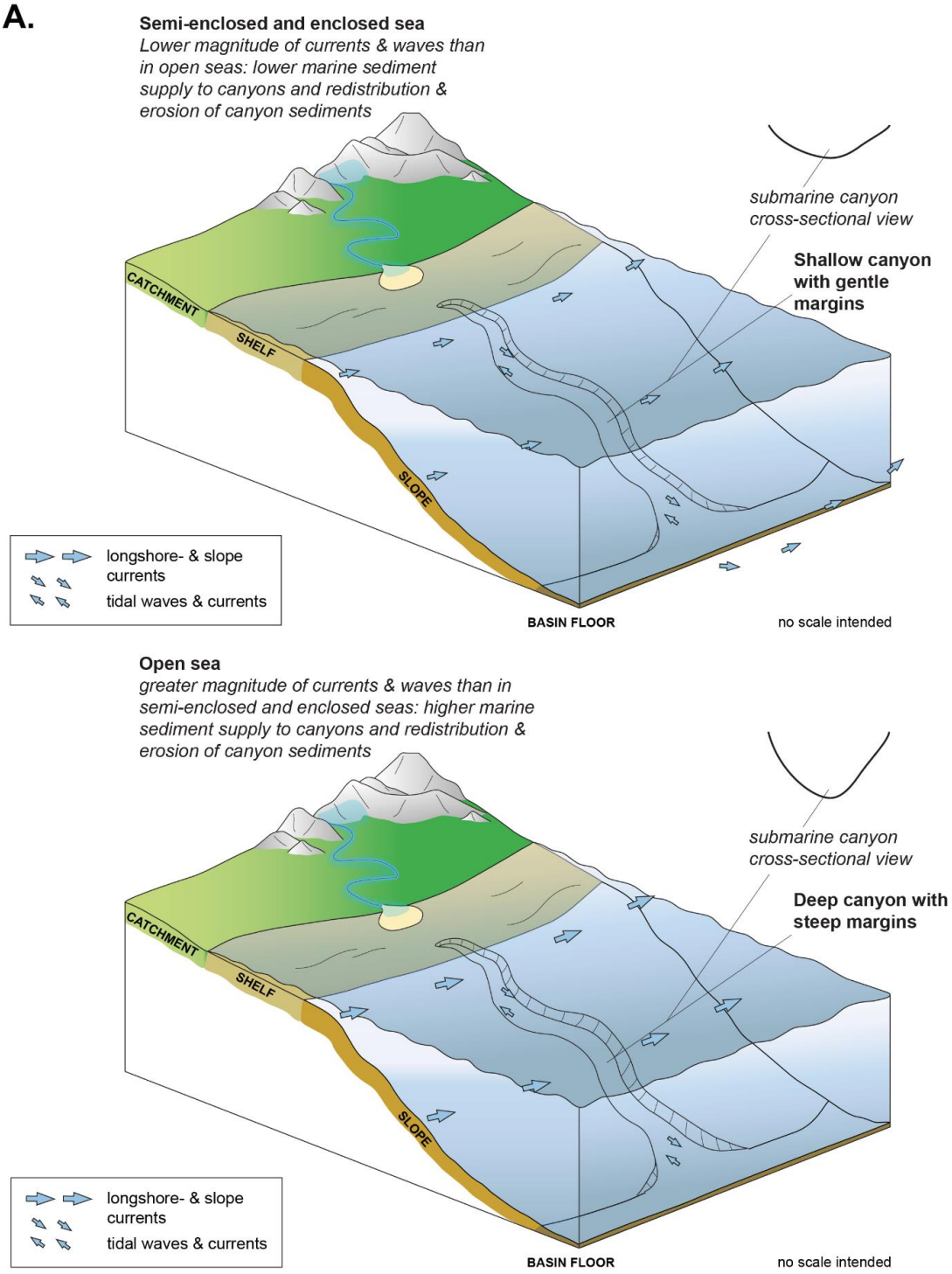
Semi-enclosed and enclosed sea
Lower magnitude of currents & waves than in open seas: lower marine sediment supply to canyons and redistribution & erosion of canyon sediments
submarine canyon cross-sectional view
Shallow canyon with gentle margins
CATCHMENT
SHELF
SLOPE
longshore- & slope currents
tidal waves & currents
BASIN FLOOR
no scale intended
Open sea
greater magnitude of currents & waves than in semi-enclosed and enclosed seas: higher marine sediment supply to canyons and redistribution & erosion of canyon sediments
submarine canyon cross-sectional view
Deep canyon with steep margins
CATCHMENT
SHELF
SLOPE
longshore- & slope currents
tidal waves & currents
BASIN FLOOR
no scale intended

B.

Semi-enclosed and enclosed sea

Lower magnitude of currents & waves than in open seas: lower marine sediment supply, redistribution & reworking of delta sediments

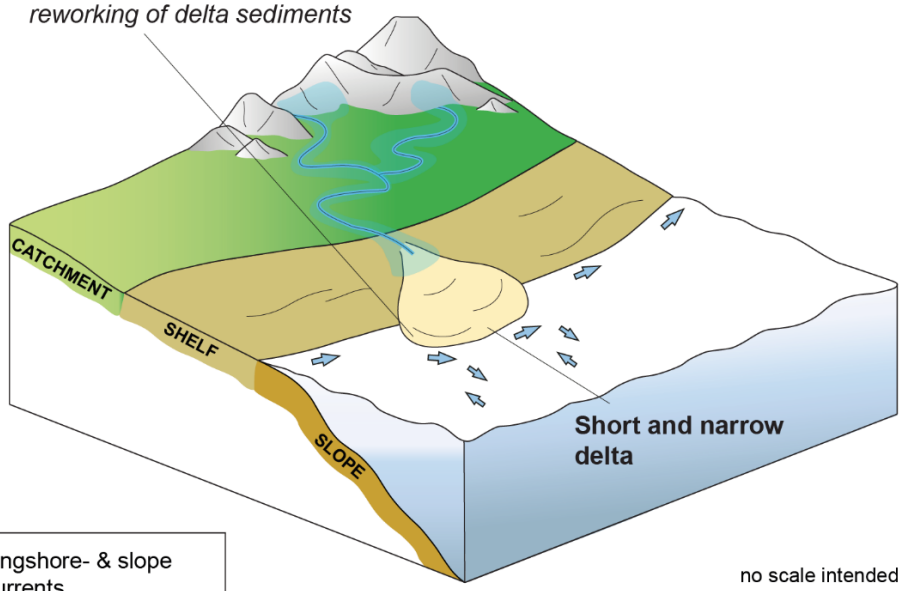

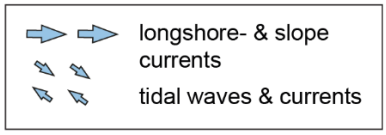

no scale intended

Open sea

greater magnitude of currents & waves than in semi-enclosed and enclosed seas: higher sediment supply, redistribution & reworking of delta sediments

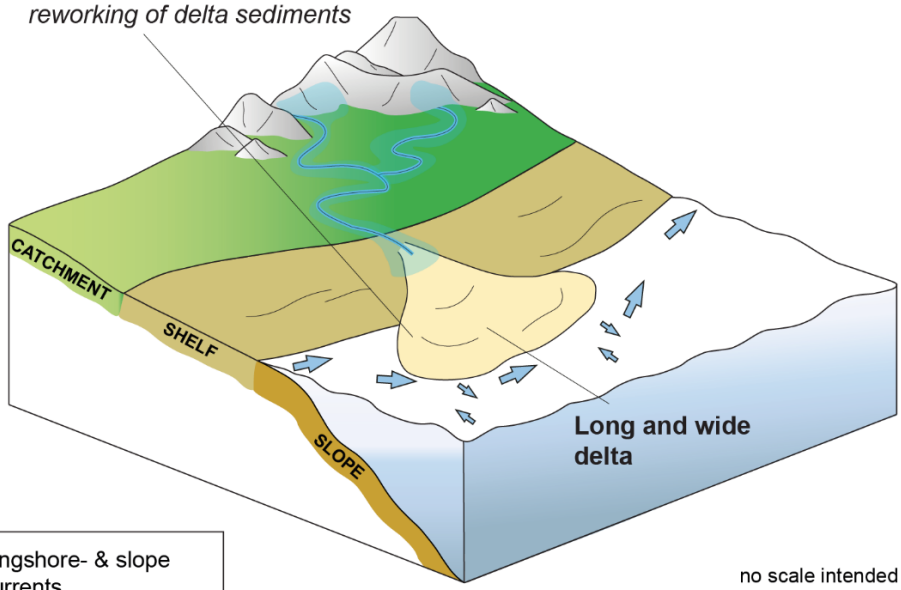

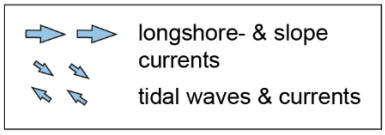

no scale intended

Figure 6.3a&b Conceptual models of morphometric attributes in submarine canyons and shelf-edge deltas and their scaling with end-members of the oceanographic environment of a source-to-sink system. A. Maximum depth and sidewall steepness in a submarine canyon vs. the oceanographic environment. B. Length, width and area in shelf-edge deltaic elements vs. the oceanographic environment.

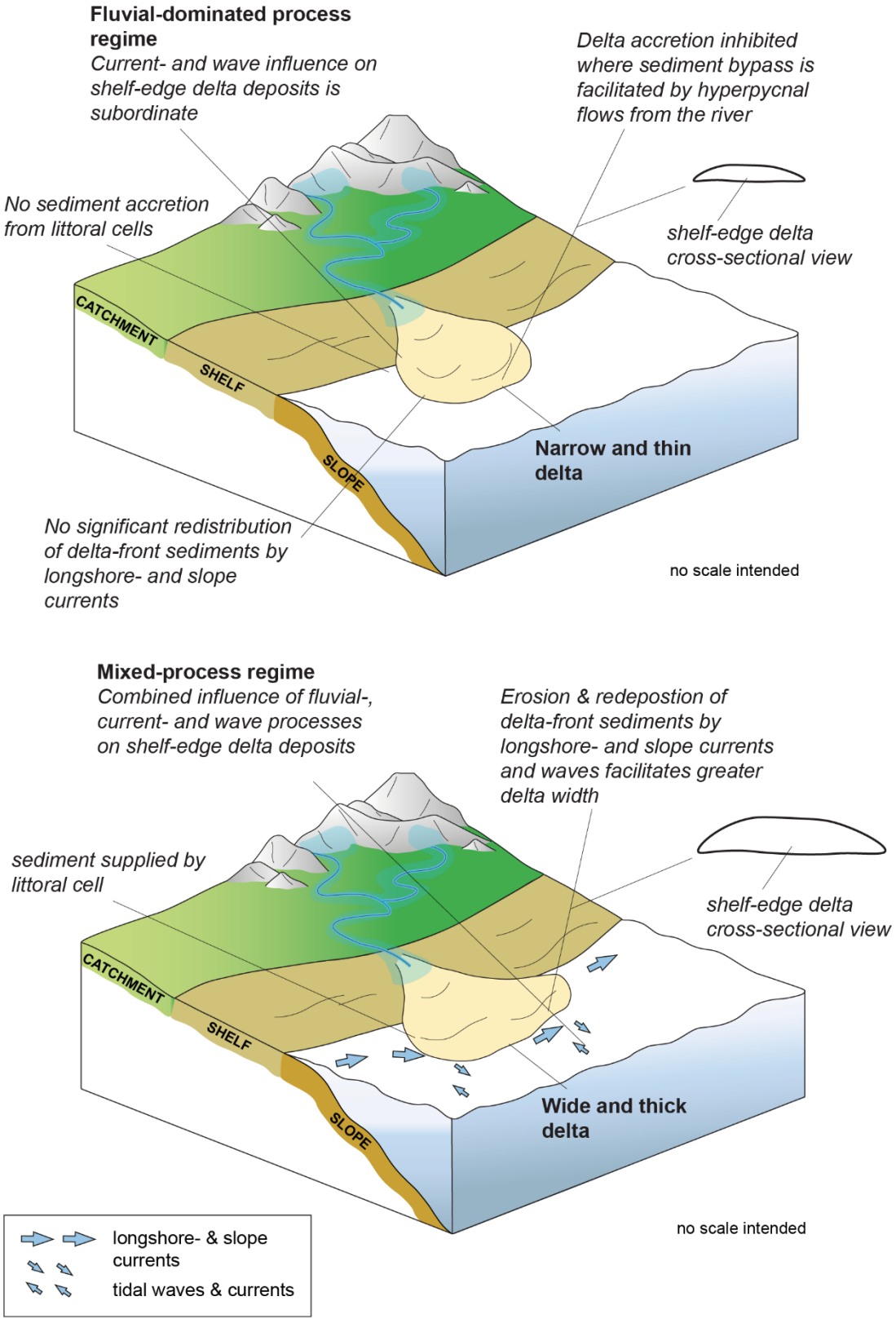

Figure 6.4 Conceptual models of morphometric attributes in shelf-edge deltas and their scaling with end-members of the hydrodynamic-process regime in a source-to-sink system at the terrestrial to marine transition. Width and thickness in a shelf-edge deltaic element vs. the hydrodynamic-process regime.

6.1.4 Tectonic setting

The influence of the tectonic setting on a S2S system is complex because it can affect the S2S system in its entirety from its most proximal source to its most distal sink. Tectonic activity might impact a S2S system across its various segments in multitudinous ways from its effect on (i) topographic relief, which exerts control on sediment transport pathways and accommodation of sediment sinks (e.g. Nyberg et al., 2018b and references therein; Baudouy et al, 2021; Cronin et al., 2023), (ii) the promotion of sediment erosion and remobilisation induced by faulting (e.g. Harders et al., 2011) and seismic activity (e.g. Vanmaercke et al., 2014; Mountjoy et al., 2018), and (iii) syn- or post-depositional deformation (e.g. Baudouy et al., 2021).

Variability in frequency distributions of morphometric characteristics of submarine canyons grouped into active and passive margins – the former also including transform margins – was assessed in the global metastudy in Chapter 3, which revealed the absence of a general difference in overall canyon geomorphology as a function of the margin type. This finding likely reflects how processes which are not exclusively linked to tectonic activity can generate similar morphologies in canyons to those caused by it. For example, seafloor topography can be shaped independently of the margin type by carbonate reef growth (e.g. Puga-Bernabéu et al., 2011) and salt diapirism (e.g. Cumberpatch et al., 2021). Moreover, submarine mass failures can be triggered unrelated to faulting or seismic activity by gravitational instability related to high depositional rates (e.g. Piper et al., 2012; Stoecklin et al., 2017), extrusion of gas hydrates (e.g. Wan et al., 2021b), and leaching of salt by offshore freshened groundwater contained in marine sediments (e.g. Saadatkhah et al., 2023), to name a few. The finding that canyons accommodated on passive margins tend to display on average steeper margins compared to canyons along active ones, however, indicates a control that might be more prevalent in one setting over the other. A possible explanation could be fewer occurrences and lower magnitudes of slope failures within active-margin canyons, caused by seismic strengthening of the substrate from recurrent low-magnitude seismic activity

(e.g. Strozyk et al., 2010; Nelson et al., 2011; Sawyer and DeVore, 2015; Greene et al., 2018; Molenaar et al., 2019). Consolidation of canyon walls and margins from seismic strengthening possibly also enables canyons along active margins to develop greater maximum width-to-maximum depth (wd_{max}) ratios from the maintained aggradation of margin deposits. By contrast, passive-margin canyons are more likely to be constrained in their wd_{max} ratios by canyon-wall failure. This autogenic control on channel ratios has been suggested for submarine channels (see Figure 11 and text in Shumaker et al., 2018). Nonetheless, the control of seismic strengthening on canyon morphology might be overprinted in geographic regions where large-scale mass failures are induced by high-magnitude earthquakes (e.g. Mountjoy et al., 2018), though (Fig. 6.5a).

Subsequently, the role of tectonic influence on the geomorphology of submarine canyons has been more deeply explored in Chapter 4 with focus on (i) scaling relationships within canyons in active- versus passive-margin settings and with their S2S system, and (ii) frequency distributions of canyon morphometrics grouped based on the plate-boundary type. As for the margin type, the findings indicate that the plate-boundary type exerts no fundamental control on morphometric attributes in submarine canyons, which strongly suggests that the value of knowledge of the tectonic setting as a predictor of canyon geomorphology is limited. Despite this, displayed differences in strength and statistical significance for some of the scaling relationships between canyon morphometrics and attributes of their superordinate S2S system across active and passive margins in Chapter 4 emphasize the relevance of the tectonic setting for the applicability of scaling relationships for palaeogeographic reconstructions. Nevertheless, due to the comparably low sample size of canyons associated with transform margins, the informative value of the results for this type of tectonic setting is limited and will need further investigation.

The tendency of canyons along complex plate boundaries to have greater maximum widths than canyons in convergent settings might reflect how the combined influence of axial intra-canyon sediment transport and transform faulting are effective in increasing canyon widths (e.g. Micallef et al., 2014)

(Fig. 6.5b), but this can also be achieved in regions where canyons share a sediment connection with fluvial systems with high and regular fluvial sediment discharge (e.g. SW Taiwan; see Milliman & Kao, 2005; Liu et al., 2013).

For shelf-edge deltas, the influence of the continental-margin type on their geometries could not be evaluated due to insufficient data. However, incised-valley fills of the study by Wang et al. (2019) showed to be on average significantly thicker on active margins and to have greater cross-sectional areas than on passive margins, albeit catchment areas of the studied S2S systems were on average 3.57 times larger along passive margins compared to active ones. The authors linked their findings to the wide-range influence of convergent tectonic activity on aspects of catchment and shelf physiography, climate, sediment yield and transport processes, and hydrodynamic processes in rivers, which in combination promote the deepening and widening of incised valleys (see Wang et al., 2019, and references therein).

In contrast to incised valleys, shelf-edge delta elements might display less pronounced differences in their geometry between active- and passive-margin environments due to the co-influence of shelf width and fluvial sediment discharge on delta dimensions:

Results from Chapter 5 indicate that delta-element width scales positively with shelf width (see section 6.1.1) and delta-element dimensions tend to be larger in S2S systems fed by multiple rivers unless being sourced by a large single river, in both instances related to high sediment discharge (see section 6.1.2). For S2S systems along passive margins with large catchments and wide and shallow shelves, this suggests the development of an overall large shelf-edge delta. In contrast, for passive-margin S2S systems with small drainage areas and wide and low-gradient shelves the length of the shelf-edge delta might be proportionally greater compared to its width and thickness. Due to the low gradient of the shelf, mass failure as an important mechanism for redistribution of sediments within the delta plain is unlikely.

In S2S systems situated on a convergent margin characterised by a small but high relief terrestrial catchment and a narrow and steep shelf, large volumes of the high sediment discharge from the terrestrial catchment might not be permanently deposited in the shelf-edge delta because a steep shelf gradient promotes fluvial incision of the shelf-edge delta and by this bypassing of sediment to slope- and basin-floor environments. Moreover, the narrow shelf width inherently delimits maximum delta length, and along narrow shelves individual catchments are less likely to converge during phases of sea-level lowstand (e.g. Sømme et al., 2009; Covault et al., 2011b), a mechanism which probably promotes delta width due to the increase in fluvial sediment discharge and merging of delta deposits (see section 6.1.2).

The potential effect of seismic strengthening as a control on the steepness of margins and width-to-depth ratios in submarine canyons has been discussed in Chapter 4. Although modern continental slopes along active and passive margins have on average very similar widths and display the same maximum widths (see Table 3 of Harris et al., 2014b), delta-front failure might be more prevalent along passive margins due to seismic strengthening of delta deposits related to recurrent seismic activity along active margins. Large shelf-edge deltas might also be more prone to the generation of hyperpycnal flows (see section 6.2.2), which suggests that shelf-edge deltas associated with large catchments and wide shelves might not display significantly greater lengths and thicknesses compared to those along narrow shelves. Assuming a variable influence of the tectonic setting on allogenic and autogenic processes in shelf-edge deltas and on individual delta dimensions, differences in the geometry of shelf-edge deltaic elements between active and passive margins might be more nuanced than for incised-valley fills (Fig. 6.6a&b).

Conceptual models

Although the results of the statistical analyses from Chapter 3 and 4 suggest that overall geomorphic signatures in submarine canyons classified based on the tectonic setting are not distinctively different for both the tectonic-

margin type and the plate-boundary type, these two end-member models are suggested based on the findings:

(1) Submarine canyons along passive margins tend to have steeper margins than canyons along active ones, which can be explained by the stabilising effect of seismic strengthening in active tectonic settings on continental slopes and canyon margins. However, where canyons experience flushing related to high-magnitude earthquakes, the imprint of seismic strengthening on canyon-margin steepness might be overprinted (Fig. 6.5a).

(2) Submarine canyons associated with complex plate boundary configurations tend to display greater maximum widths compared to their counterparts in convergent settings (Fig. 6.5b).

A.

Active margin
Seismic strenghtening of the seafloor reduces slope failure and stabilises canyon margins

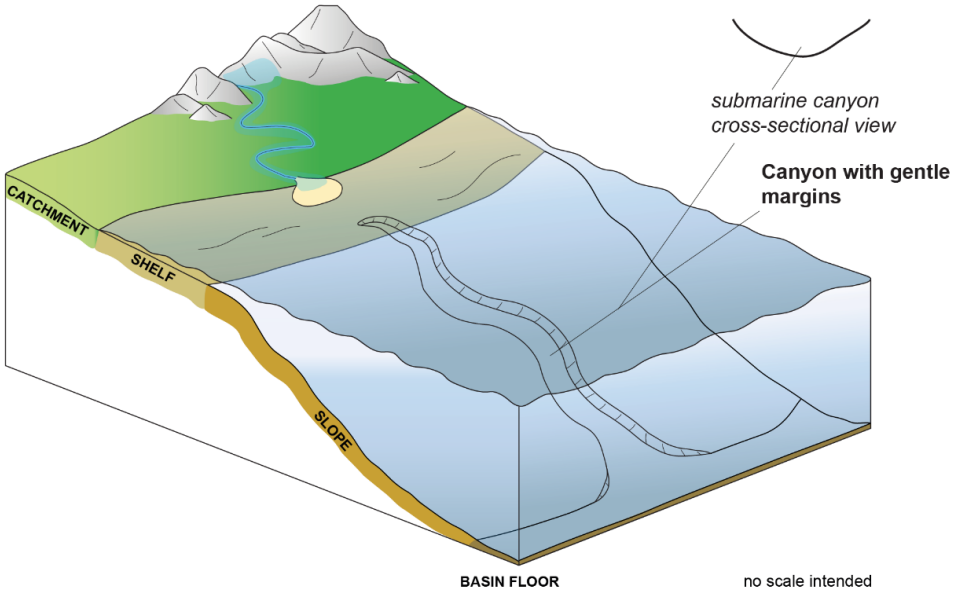

Passive margin
Absence of seismic strenghtening of the seafloor increases occurrences of slope failure and collapse of canyon margins

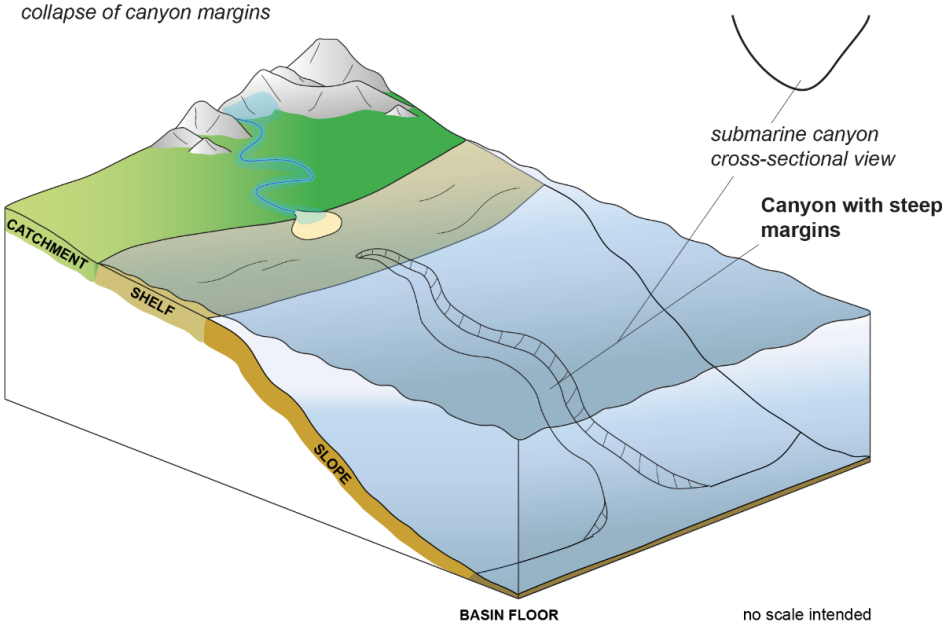

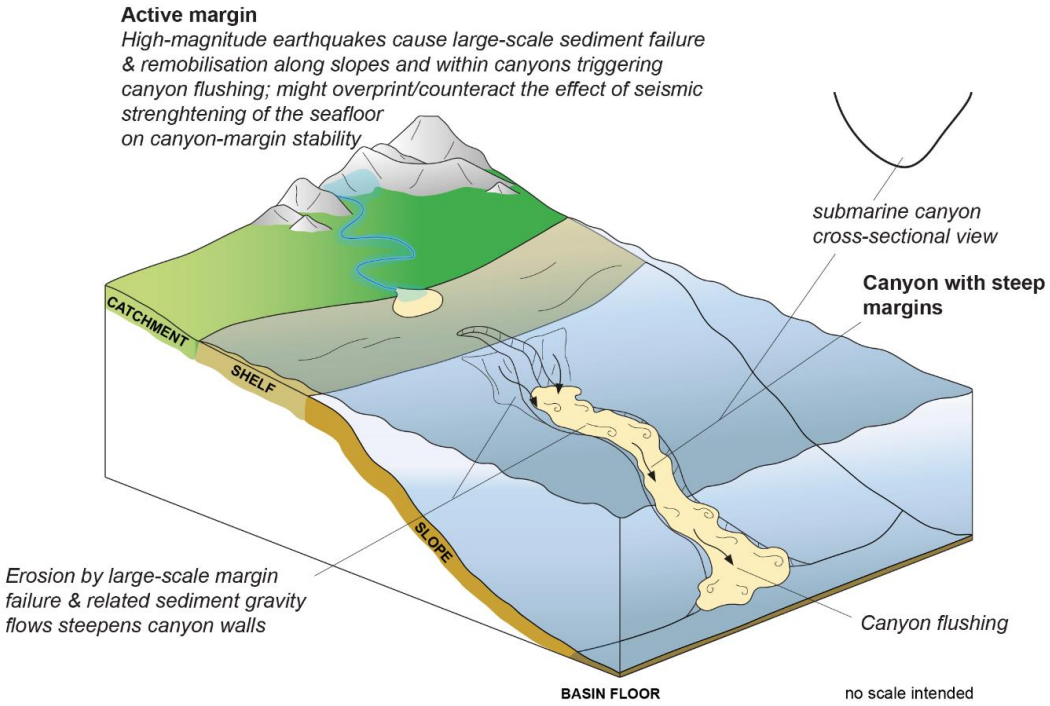

B.

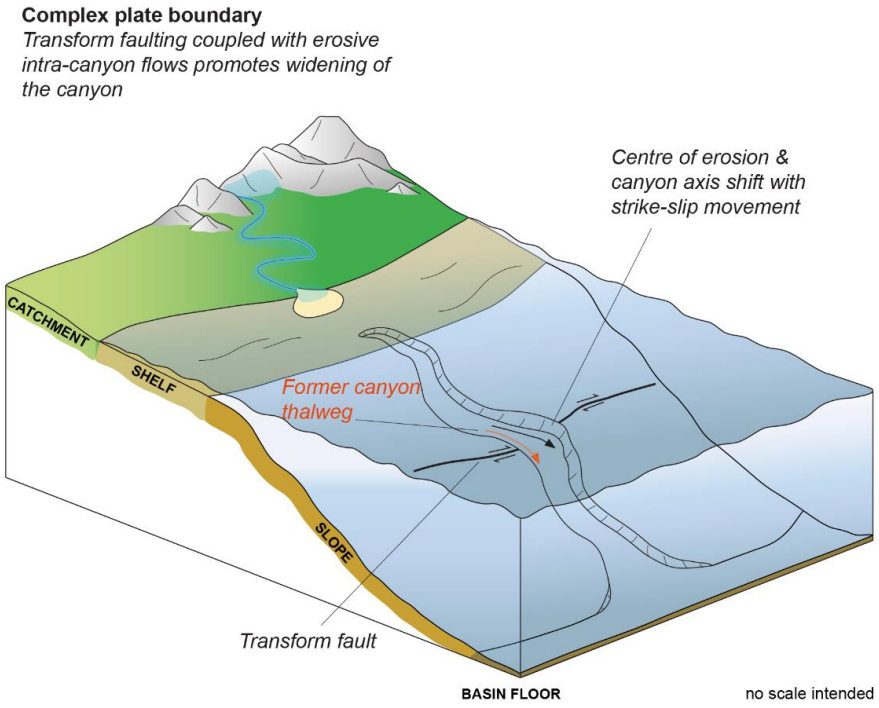

Figure 6.5a&b Conceptual models of morphometric attributes in submarine canyons and their scaling with end-members of the tectonic setting. A. Maximum canyon sidewall steepness vs. the margin type. B. Maximum canyon width vs. the plate-boundary type.

A. Partial S2S system model of Wang et al. (2019)

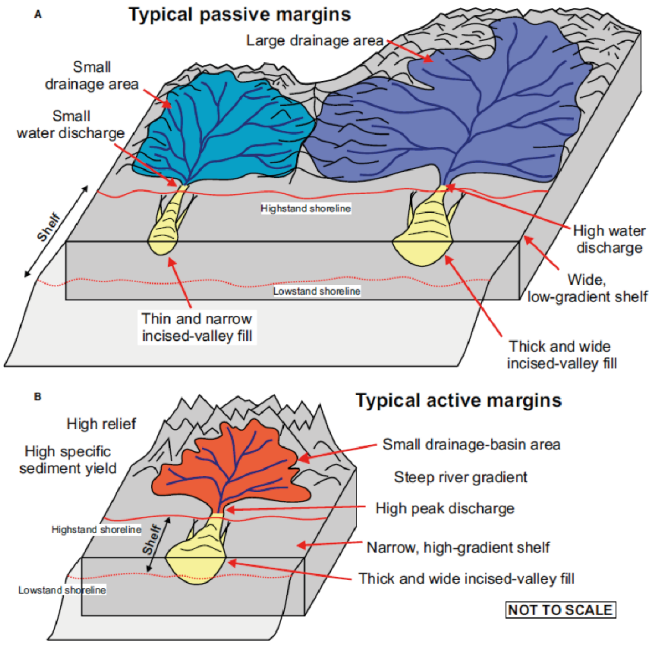

B. Extended partial S2S system model of Wang et al. (2019)

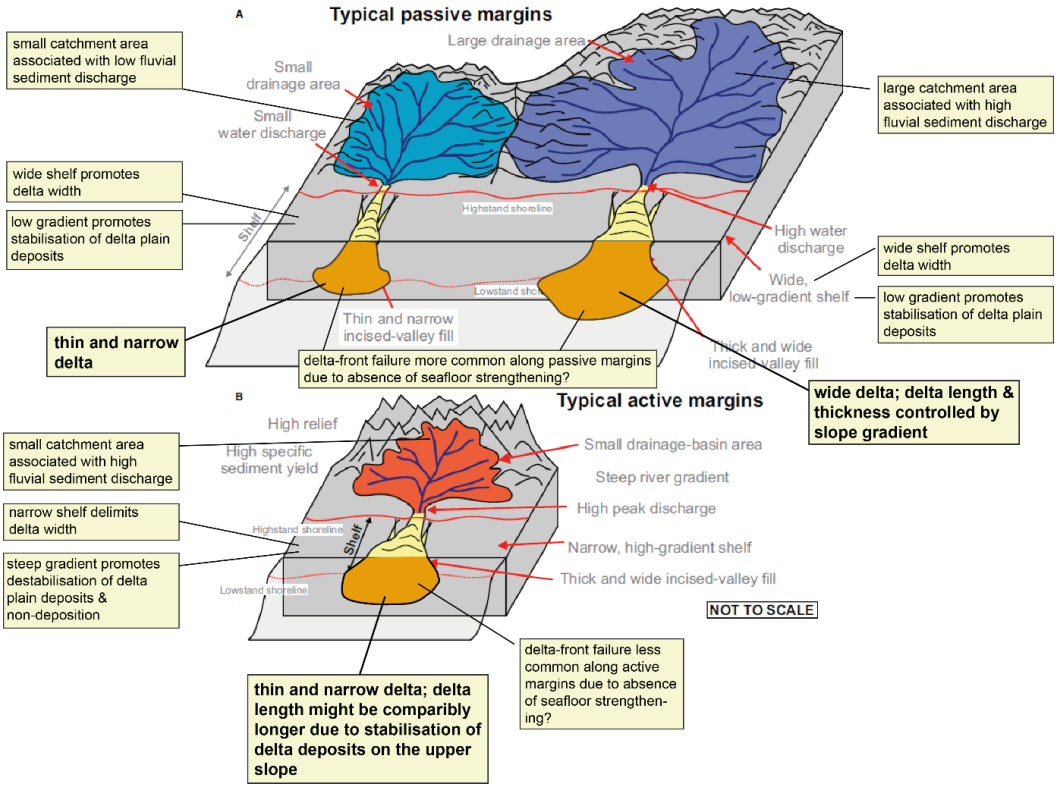

Figure 6.6a&b A. Conceptual, semi-quantitative model of incised-valley fill geometries along passive and active margins in Wang et al. (2019; their Figure 16). In contrast to this research, which comprised transform margins with convergent margins under the class of active margins, Wang et al. (2019) grouped transform margins and passive margins together. B. Extended S2S system model from Wang et al. (2019) with integrated findings from this project for shelf-edge delta geometry. Modifications of the original figure by Wang et al. (2019) comprise added text in yellow boxes and shelf-edge delta elements in orange colour.

6.1.5 Latitude

The evaluation of scaling relationships between aspects of sedimentary systems and their latitudinal position in quantitative studies is challenging due to the general paucity of studies of sedimentary systems in high-latitudinal settings compared to those in tropical and temperate zones (this study, Figures 3.1, 4.1 and 5.1; e.g. Figure 3, Sømme et al., 2009; Figure 4, Nyberg et al., 2018b: Figure 1, Wang et al., 2019). Although the datasets compiled by Harris & Whiteway (2011, see their Table 1) and Harris et al. (2014b, see their Table 9) comprise a large number of submarine canyons, correlation analyses between latitude and canyon morphology were only evaluated for average canyon sinuosity in shelf-incising canyons in Harris & Whiteway (2011), which showed no scaling (see their Figure 9). Results for the global study of submarine canyons in Chapter 3 suggest that this relationship is generally absent in canyons, independent of the location of the canyon apex relative to the shelf break.

Overall, correlation analyses of morphometric attributes of submarine canyons (Chapter 3) with the absolute latitudinal position of the sedimentary system returned weak correlations. The only correlations of moderate strength seen in the global study of submarine canyons in Chapter 3 is a positive correlation of average canyon width with latitude, but the sampled canyons stem only from six geographic regions and cover a latitudinal range between ~4° and ~29° degrees. Hence, the finding needs future corroboration from a larger dataset and under consideration of lateral variability along basin margins in terms of processes and their depositional products (e.g. Steventon et al., 2020).

The displayed tendency of deltaic elements in shelf-edge deltas to become thinner with increasing values of absolute latitude might reflect how the average annual precipitation which tends to decrease with increasing latitude (e.g. Milliman & Farnsworth, 2011) influences erosion rates in drainage basins and fluvial discharge rates. However, with p=0.018 the p-value is marginally above the ≤0.001 threshold of significance defined in this study and the correlation coefficient is slightly below 0.5 (rs=-0.498). To confirm the existence of this scaling relationship, more data are needed.

The results of this project suggested generally weak scaling of absolute latitude with morphologic attributes of submarine canyons and deltaic elements in shelf-edge deltas can be related to how the complex co-influence and interplay of climate-sensitive variables which exert control on sediment transport dynamics within a S2S system, as subaerial erosion rates, precipitation, and vegetation cover probably masks any existing monotonic or linear variability with latitude, as the decrease of annual precipitation rates with increasing latitude (see section 3.5.3). Moreover, the prevalence of weak to modest strengths in scaling probably also reflects that the influence of latitude on morphometric attributes of submarine canyons and shelf-edge delta elements tends to be generally subordinate compared to other factors controlling their geomorphologies, as those identified in this project.

Despite the paucity of linear and monotonic scaling relationships with latitude, differences in frequency distribution of morphometric attributes in submarine canyons and shelf-edge deltaic elements for tropical (0 to 23.5°) and temperate (23.5° to 66.5°) zones suggest that one or several factors which are prevalent or limited to a particular latitudinal range might constitute a dominant control on aspects of their geomorphologies. Such a factor might pose the high density of reef systems in tropical latitudes compared to temperate ones, although reefs associated with cold-water corals also occur in temperate environments (e.g. Roberts et al., 2006; https://data.unep-wcmc.org/datasets/1) and the strengthening of substrate by carbonate cementation related to carbonate shedding (e.g. Oiwane et al., 2011; Chang et al., 2021). The strengthening of substrate by carbonate cementation can

explain both the observed tendencies of submarine canyons in tropical latitudes to have steeper thalweg gradients (Fig. 6.7a) and of studied shelf-edge deltas in tropical latitudes to have greater lengths and widths than their counterparts in temperate ones (Fig. 6.7b).

Moreover, the presence of atolls offshore continental margins might favour the development of wider shelf-edge deltaic elements due to the focussing of margin-parallel currents and dispersing effect on current- and wave energies (Fig. 6.7b).

Conceptual models

Under the caveat that establishing causal linkages between individual climate-influenced controls and morphometric characteristics of shelf-edge deltas and submarine canyons is difficult, the following two end-member models are proposed here to explain differences in the morphology of the two sedimentary system types between tropical (0 to 23.5°) and temperate (23.5° to 66.5°) latitudes:

(1) Submarine canyons in tropical latitudes are characterised by steeper average thalweg gradients compared to canyons in temperate latitudinal settings, which might be explained by the strengthening of continental slopes by carbonate cementation (Fig. 6.7a).
(2) Shelf-edge deltas of the study associated with low-latitudinal, tropical settings are longer and wider than those associated with temperate latitudes. The stabilising effect of carbonate cements on continental slopes might lower the occurrence of delta-front failures and promote the outbuild of shelf-edge deltas. Moreover, the presence of atoll islands might shelter deltas from oceanic currents and waves while amplifying the effect of longshore currents, which in turn promote delta widening by sediment redistribution (Fig. 6.7b).

A.

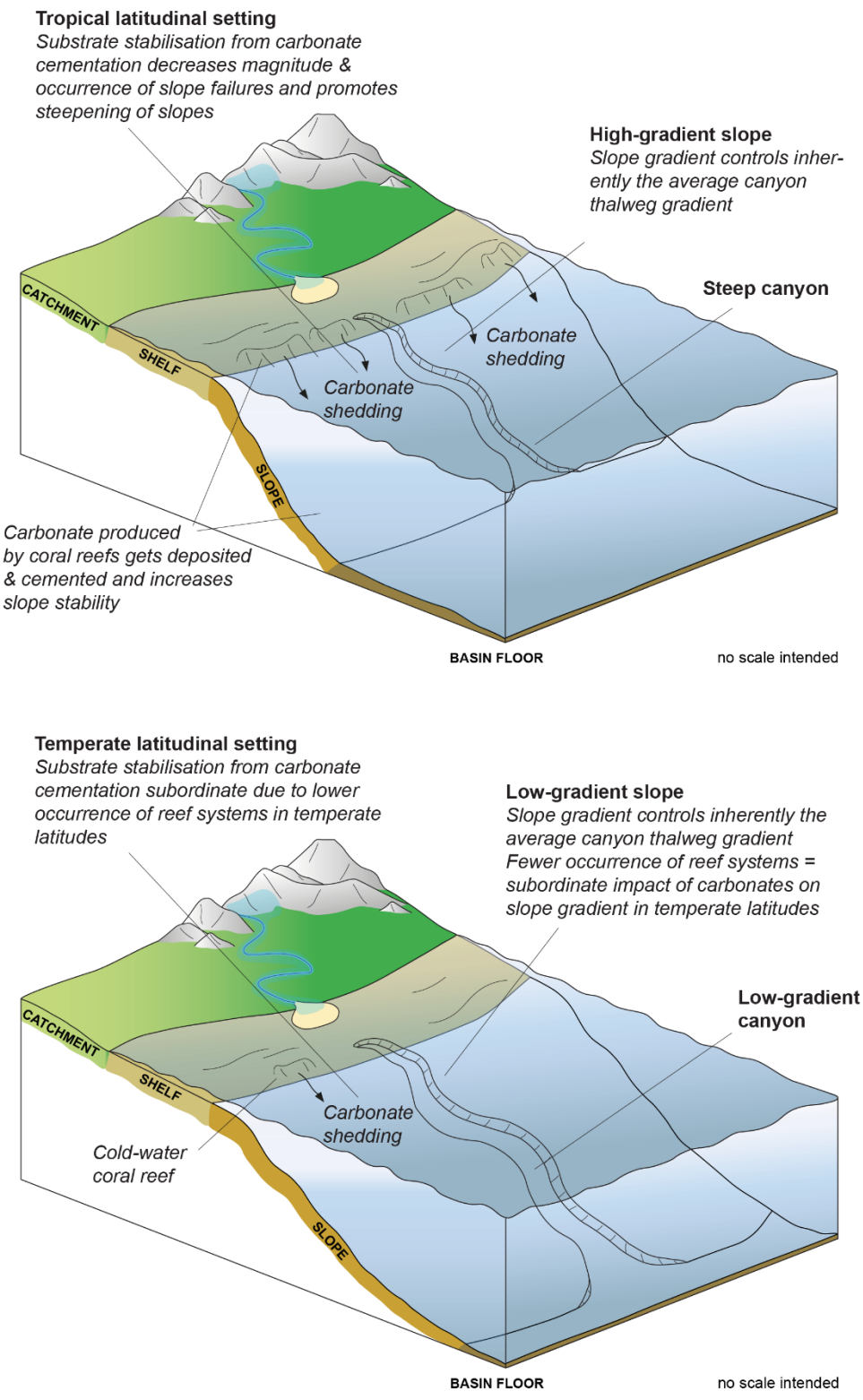
Tropical latitudinal setting
Substrate stabilisation from carbonate cementation decreases magnitude & occurrence of slope failures and promotes steepening of slopes
High-gradient slope
Slope gradient controls inherently the average canyon thalweg gradient
Steep canyon
CATCHMENT
SHELF
SLOPE
Carbonate shedding
Carbonate shedding
Carbonate produced by coral reefs gets deposited & cemented and increases slope stability
BASIN FLOOR
no scale intended
Temperate latitudinal setting
Substrate stabilisation from carbonate cementation subordinate due to lower occurrence of reef systems in temperate latitudes
Low-gradient slope
Slope gradient controls inherently the average canyon thalweg gradient
Fewer occurrence of reef systems = subordinate impact of carbonates on slope gradient in temperate latitudes
Low-gradient canyon
CATCHMENT
SHELF
SLOPE
Carbonate shedding
Cold-water coral reef
BASIN FLOOR
no scale intended

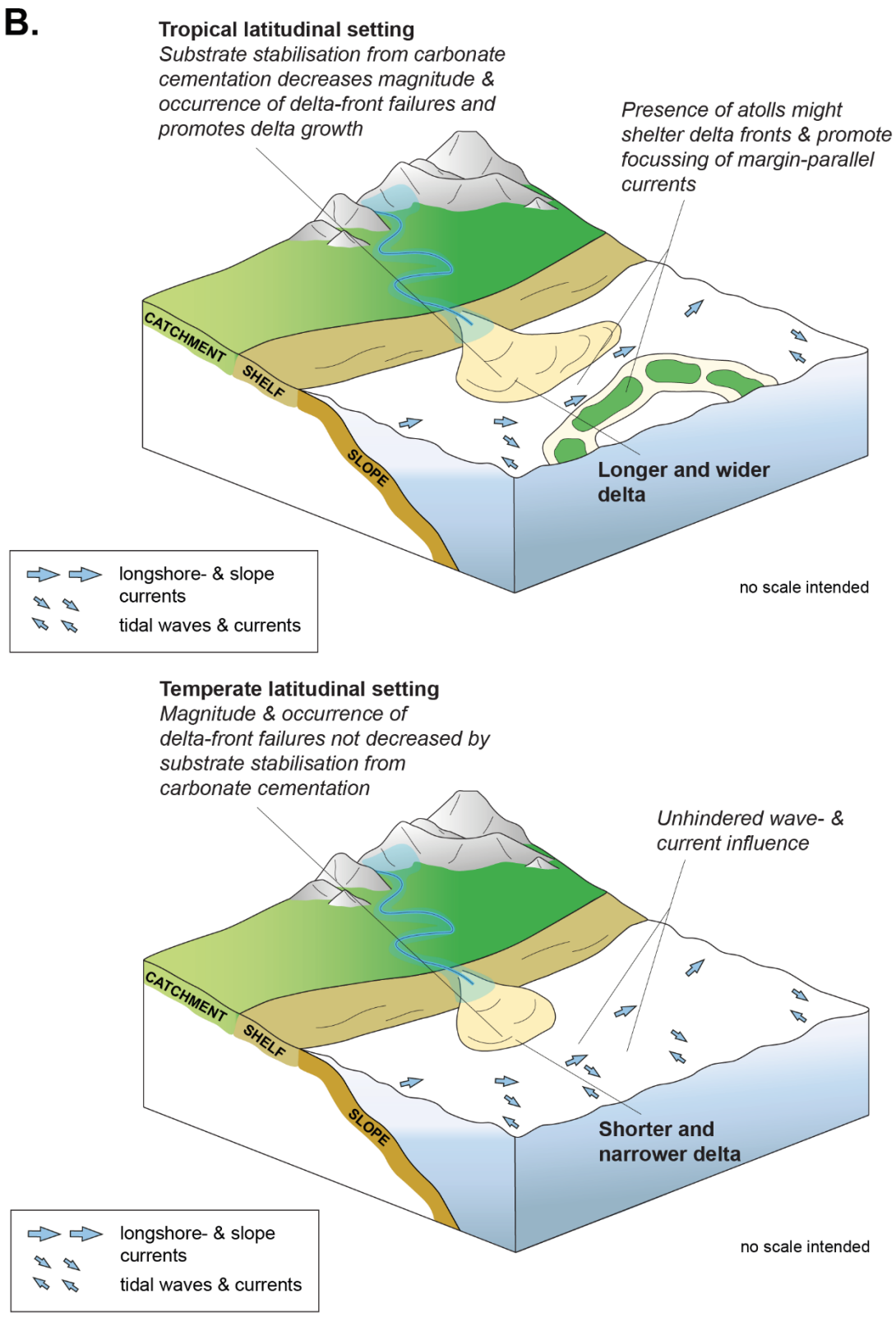

Figure 6.7a&b Conceptual models of morphometric attributes in submarine canyons and shelf-edge deltas and their scaling with the latitudinal setting of a source-to-sink system. A. Average canyon thalweg gradient vs. the latitudinal zone. B. Length and maximum width in a shelf-edge delta vs. the latitudinal zone.

6.2 Influence of morphometric characteristics of shelf-edge deltas and submarine canyons on sediment delivery across shallow and deep-water environments

Given the important role of submarine canyons and shelf-edge deltas as facilitators of sediment routeing from source areas within the terrestrial catchment and continental shelf to slope- and basin-floor environments, Research Objective IV was set to identify potential environmental settings which promote sediment dispersal by these systems across continental margins from their influence on aspects on submarine-canyon and shelf-edge delta morphologies.

6.2.1 Submarine-canyon geomorphology

Due to the paucity of experimental and numerical modelling studies of deep-water systems and entire source-to-sink system that consider aspects of canyon geomorphology (e.g. Wan et al., 2021), and relatively few documented ancient examples of S2S systems where large canyon fills are preserved in outcrop (Anderson et al., 2006), little is known about the role of submarine-canyon geomorphology in controlling sediment delivery to deep-marine environments. Results from a recent stratigraphic forward modelling study by Wan et al. (2021) for S2S systems with a delta-canyon-fan configuration associated with a passive-margin setting showed that a shallow canyon depth and low canyon-sinuosity promote sediment routeing of coarser grain sizes to basin-floor systems.

Albeit based on a dataset of modest size, results of the hypothesis testing in Chapters 3 and 4 indicate that overall lower canyon depths are promoted along tectonically active margins and within semi-enclosed and enclosed seas, which suggests that these environmental settings might promote sediment dispersal via canyons to deep-water systems compared to canyons along passive margins and located within open seas (Figs. 6.8a&b). The sample sizes of average depth values in Dataset 1 were not sufficient to assess differences in mean values of average canyon depth for studied canyons classified based on the canyon apex location relative to the shelf break, the S2S system setting, and the latitudinal zone. Despite this,

hypothesis testing conducted in this work for the comparably larger global dataset compiled by Harris et al. (2014b) showed that slope-confined canyons have on average greater depths than shelf-incising ones, by the factor 1.84. This suggests that irrespective of a sediment connection of a canyon to a river, the physical connection with the shelf poses another factor that enhances sediment dispersal to deep-water environments within canyons.

Results from the experiments by Wan et al. (2021) also showed that with increasing canyon sinuosity the efficiency of down-canyon sediment transport decreased, likely due to the deposition of coarser sediment at inner canyon bends (Wan et al., 2021). Nevertheless, this control on sediment dispersal across deep-water systems is likely not important in many S2S systems given that although submarine canyons show a wide range in average canyon sinuosity they tend to have very low overall sinuosities: The sampled canyons of this study (Chapters 3 & 4) show the same trend as seen in the large global dataset compiled by Harris & Whiteway (2011); canyons in both datasets have on average a very low overall sinuosity of ~1.1. Considering that the results in Chapter 3 and 4 suggest that average canyon sinuosity is not generally different for canyons classified based on the canyon-apex location, tectonic-margin type and plate-boundary type along active margins, the S2S system setting, the oceanographic environment, and the latitudinal setting, the efficiency of sediment routeing through canyons to basin-floor systems as a function of canyon sinuosity is likely not significantly influenced by these environmental variables. By contrast, the moderate positive scaling of average canyon sinuosity with maximum catchment elevation seen in Chapter 3 and Chapter 4 indicates that in S2S systems with a fluvial system-canyon configuration sediment transfer within the slope segment becomes less efficient with increasing elevation of the drainage basin (Figs. 6.8c&d).

However, as already discussed in Chapter 4, the efficiency of down-slope transport in shallow and/or low-sinuosity canyons might be counteracted in S2S systems with high relief of the continental slope, where the inherited topography forces grain-size segregation in down-canyon sediment gravity

flows (Fig. 6.8e). This is likely the case along continental margins shaped by convergent tectonic activity and/or by salt diapiric intrusions, which can occur along both active and passive margins. For this reason the average slope gradient and the average canyon thalweg gradient – the latter defined as the gradient between canyon apex and canyon mouth in this work – are not reliable predictors of sediment transport efficiency because they do not capture intra-canyon relief.

Because longer canyons tend to have higher overall sinuosities (Chapter 3), and sediment gravity flows have to travel greater distances to reach the basin floor, canyon length constitutes another morphometric parameter that affects the efficiency of across-slope sediment transport. Nonetheless, in S2S systems along continental margins where littoral cells and contourite systems exist, longer canyons might favour sediment dispersal to deep-water systems because they are more likely to intercept these sediment sources. Hence, the control of canyon length on sediment delivery to deep-water environments is ambiguous.

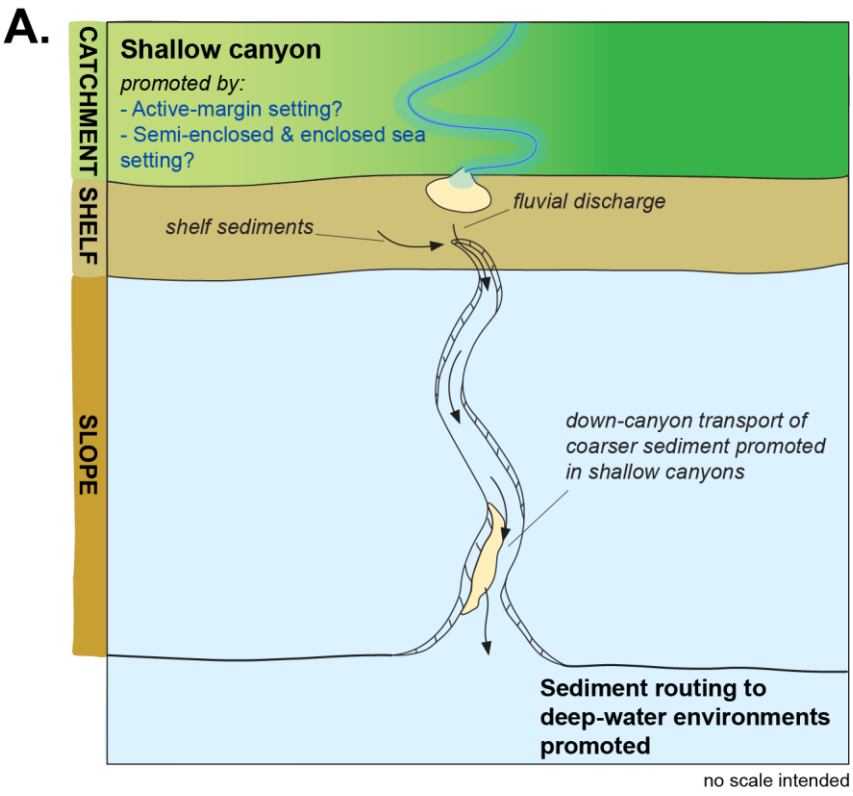

B.

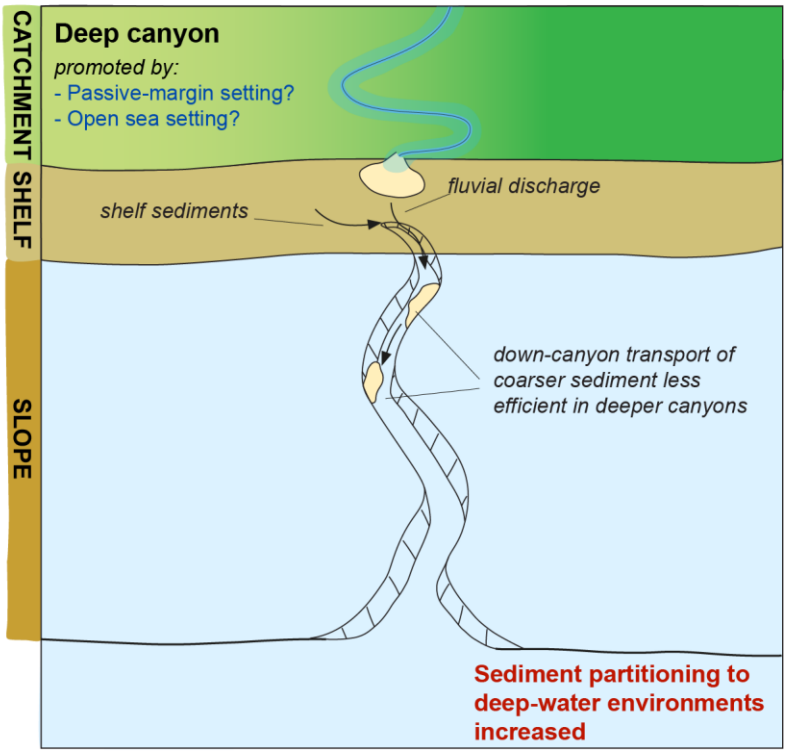

no scale intended

C.

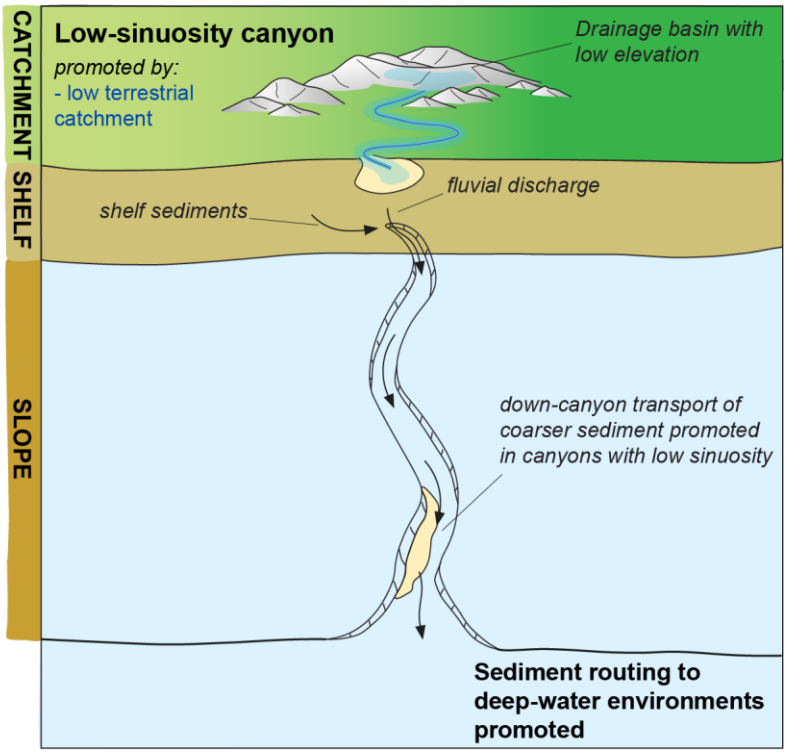

no scale intended

D.

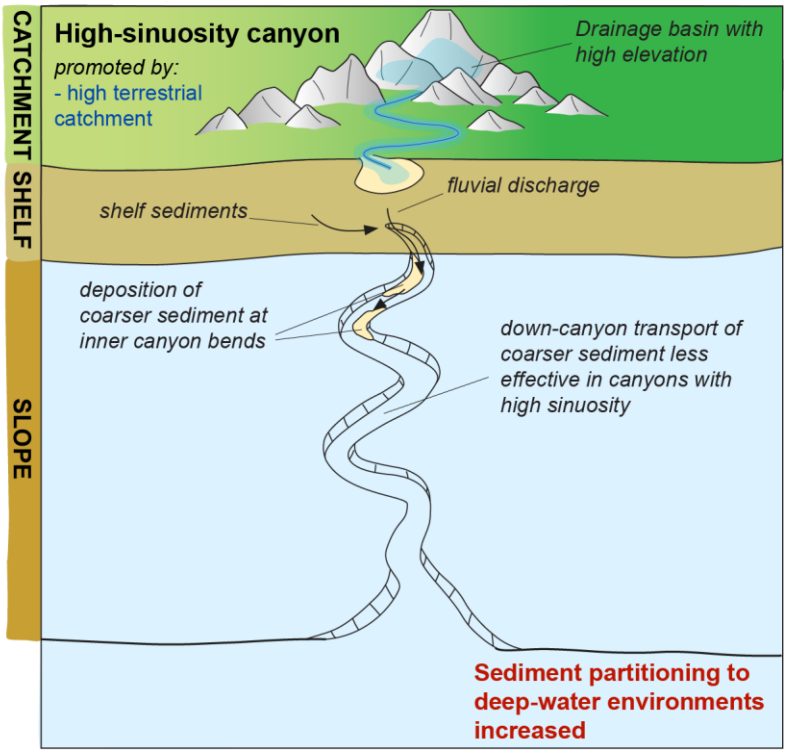

no scale intended

E.

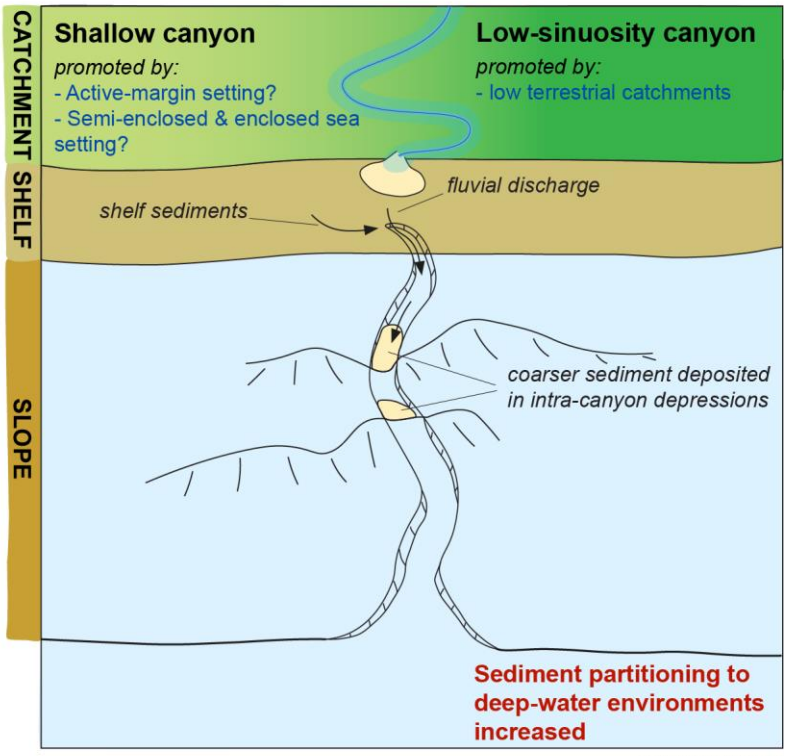

no scale intended

Figure 6.8a-e Conceptual models of relationships between aspects of submarine-canyon geomorphology and sediment routeing to deep-water environments as a function of environmental variables. A. Shallow submarine canyons. B. Deep submarine canyon. C. Low-sinuosity submarine canyon. D. High-sinuosity submarine canyon. E. Along continental margins characterised by high intra-slope relief variability, sediment transport across slope might be inhibited in shallow and high-sinuosity submarine canyons.

6.2.2 Shelf-edge delta geometry

With shelf-edge deltas being considered important drivers for the delivery of fluvial sediment to deep-water environments (e.g. Steel et al., 2003; Covault et al., 2009; Sylvester et al., 2012; Gong et al., 2021), quantitative (e.g. Dixon et al., 2012; Gong et al., 2016), and experimental studies (e.g. Straub, 2019) of these systems have focused on identifying environmental factors which promote sediment routeing to slope- and basin-floor systems.

Genetic relationships between the dominant process-regime of shelf-edge deltas and associated deep-water environments were suggested by Dixon et al. (2012), who proposed based on their study of 29 margin successions in nine different geographic regions that river-dominated shelf-edge deltas facilitate the development of slope channels and basin-floor fans, whereas the latter are rarely generated distally of wave-dominated shelf-edge deltas (see Table 1 of Dixon et al., 2012). Their findings were augmented by findings from the larger dataset collated in the review of 42 shelf-edge deltas and their associated deep-water systems by Gong et al. (2016). Albeit small in size, the authors showed that sand-rich slope- and basin-floor fans can develop distally of wave-dominated shelf-edge deltas. Another finding by Gong et al. (2016) was that sand-rich submarine fans formed in S2S systems associated with both low and high supply of sand, suggesting that the magnitude of fluvial sediment discharge does not fundamentally control sediment routeing to deep-marine environments. Instead, the transport efficiency of sediment from shallow-marine to deep-water environments is controlled by the rheology of sediment gravity flows and the proportion of coarse- and fine-grained fractions (e.g. Amy et al., 2006; Baker & Baas, 2022).

Few physical experimental studies have focused on sediment routeing from shelf-edge deltas to deep-water environments, which is probably linked to challenges in efficiently generating sediment transport across delta fronts (e.g. Straub, 2019). Outcomes of flume-tank (e.g. Straub, 2019) and numerical modelling experiments (e.g. Harris et al., 2016) suggest that long-term sediment routeing of fluvial sediment via shelf-edge deltas to deep-water systems is not controlled by the magnitude or period of sea level cycles. However, shelf-edge delta size might play a role for the timing of sediment routeing to continental slopes and basin floors within a sea-level cycle due to the inferred increase in scale of autogenic processes in a shelf-edge delta with increasing delta size (see Straub, 2019 and references therein).

Although underexplored as a control, shelf-edge delta size might constitute an important but overlooked factor for the efficiency of sediment delivery to slope- and basin-floor environments from its influence on the delta-surface gradient. Sylvester et al. (2012, p.55) proposed that “if mouth-bar sediment failure is considered an important source of sediment for channelised gravity flows”, a shelf-edge delta must reach a critical size so that its surface gradient is sufficiently high for the generation of turbidity currents with long runout distances and capacity to transport sand-sized sediment. Moreover, the interaction of longshore currents with tidal processes, combined with changes in margin orientation, has been demonstrated to facilitate sand delivery across the shelf-break in absence of a fluvial outlet (see Boyd et al., 2008). Hence, it can be assumed that the length of a shelf-edge delta through its influence on shoreline morphology (e.g. Bart & Anderson, 2004) constitutes a factor for the efficiency of routeing of sediment transported by littoral cells to deep-marine environments.

These two aspects suggest that larger and longer shelf-edge deltas are more efficient in sediment supply to deep-water environments compared to smaller and shorter ones and promote the distribution of larger volumes of sediment and coarser grain-size fractions to slope- and basin-floor systems. Therefore, from the shown tendency of studied shelf-edge deltas to display greater lengths, widths and areas when associated with multiple fluvial

feeder systems, a mixed-process regime, and/or an open-sea setting (see sections 6.1.2 & 6.1.3, respectively), it can be inferred that sediment dispersal to deep-water parts of S2S systems with a shelf-edge delta configuration is favoured in longer and larger deltas along margins characterised by one or several of these environmental variables (Fig. 6.9a&b). Nevertheless, the results in Chapter 5 also show that individual shelf-edge deltas of the study associated with a single-feeder system, fluvial-dominated process regime or semi-enclosed and enclosed sea setting display lengths, widths and thicknesses higher than some of the shelf-edge deltas fed by multiple rivers, associated with a mixed-process regime or open-sea setting. Hence, the feeder-system type, process regime and oceanographic setting are not generally indicative of shelf-edge delta size and deep-water sediment transport at the location of the shelf-edge delta. Also, other variables which likely affect sediment sourcing from shelf-edge deltas to deep-water environments are the steepness of the continental shelf and upper slope via their control on delta gradients, with steeper deltas probably promoting delta-front failure (e.g. Roberts & Sydow, 1996).

However, despite the presence of environmental controls that favour shelf-edge delta growth and sediment routeing across shelf-edge deltas, these factors can be counteracted along continental margins where the energy of a longshore current is sufficiently high to dampen or inhibit sediment transfer across-slope and/or where storm waves act as a hydrodynamic fence to prevent sediment dispersal to deep-water environments (e.g. Gong et al., 2016, and references therein) (Fig. 6.9c).

Therefore, efficiency in sediment routeing to deep-water environments related to delta geometry cannot be exclusively linked to individual environmental factors, but knowledge of several of the environmental factors discussed above might aid in predicting the probability and magnitude of sediment transfer to continental slopes and basin floors.

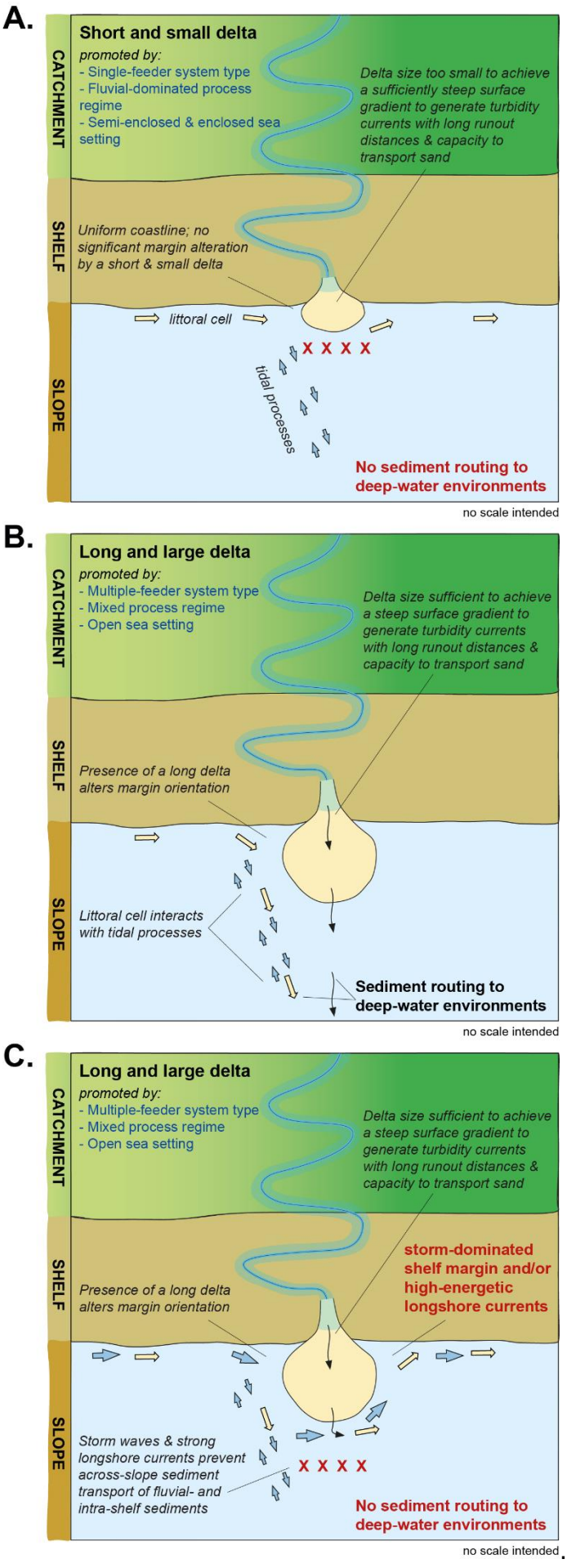
A.
CATCHMENT
SHELF
SLOPE
Short and small delta
promoted by:
- Single-feeder system type
- Fluvial-dominated process regime
- Semi-enclosed & enclosed sea setting
Delta size too small to achieve a sufficiently steep surface gradient to generate turbidity currents with long runout distances & capacity to transport sand
Uniform coastline; no significant margin alteration by a short & small delta
littoral cell
X X X X
tidal processes
No sediment routing to deep-water environments
no scale intended
B.
CATCHMENT
SHELF
SLOPE
Long and large delta
promoted by:
- Multiple-feeder system type
- Mixed process regime
- Open sea setting
Delta size sufficient to achieve a steep surface gradient to generate turbidity currents with long runout distances & capacity to transport sand
Presence of a long delta alters margin orientation
Littoral cell interacts with tidal processes
Sediment routing to deep-water environments
no scale intended
C.
CATCHMENT
SHELF
SLOPE
Long and large delta
promoted by:
- Multiple-feeder system type
- Mixed process regime
- Open sea setting
Delta size sufficient to achieve a steep surface gradient to generate turbidity currents with long runout distances & capacity to transport sand
storm-dominated shelf margin and/or high-energetic longshore currents
Presence of a long delta alters margin orientation
Storm waves & strong longshore currents prevent across-slope sediment transport of fluvial- and intra-shelf sediments
X X X X
No sediment routing to deep-water environments
no scale intended

Figure 6.9a-c Conceptual models of relationships between shelf-edge delta size and sediment routeing to deep-water environments as a function of environmental variables. A. Short and small shelf-edge delta. B. Long and large shelf-edge delta. C. Along continental margins characterised by high-energetic longshore currents and/or storm waves, sediment transport across slope might be inhibited in long and large deltas.

6.3 Scaling relationships of shelf-edge delta- and submarine canyon geomorphologies: applications and limitations

6.3.1 Reconstruction of characteristics of submarine canyons, shelf-edge deltas, and their associated source-to-sink (S2S) systems in outcrop and subsurface

The scaling relationships identified in Chapters 3, 4 and 5 for submarine canyons and shelf-edge deltas, and the holistic semi-quantitative end-member models presented in section 6.1 of this chapter can be used for spatial reconstructions of S2S systems with shelf-edge delta and/or submarine canyon configuration in outcrop and subsurface studies with limited spatial data coverage or where palaeoenvironments are only partially preserved. In turn, knowledge of characteristics of the S2S system and environmental or physiographic variables identified in this project as controlling factors of morphometric attributes of shelf-edge deltas and submarine canyons might be used to predict geomorphologic aspects of these systems. This approach has already been shown to be reliable for other sedimentary systems and their superordinate S2S systems, e.g. for the reconstruction of palaeo-catchments from channel-belt thicknesses and bankfull depths based on well log data (Xu et al., 2017). In addition to the application to S2S systems on Earth, findings from the three studies might aid in the reconstruction of S2S systems and their subenvironments on other extraterrestrial planetary bodies, such as Mars (e.g. McLennan et al., 2019). However, due to the novelty of most of the findings in this project, these will need testing and validation by field, experimental- and modelling studies.

6.3.1.1 Applications

Although certain environmental variables might be more challenging to identify in outcrop and subsurface studies of ancient S2S systems – as for

example the oceanographic environment and hydrodynamic regime – others like fluvial, shelf and slope environments might be more readily recognisable in seismic datasets, cores, and outcrop, so that the size of terrestrial catchments and width of shelf and slope segments can be partially or entirely determined, depending on the degree of preservation and areal coverage of the S2S system by a survey. Where only partial values of sedimentary environments are obtained these values are still useful because they can be used as first-order estimates for minimum dimensions of shelf-edge deltas and submarine canyons based on the scatterplots in the three metastudies. Moreover, the strong scaling relationship identified in this research for delta-element width with both catchment area and maximum catchment elevation in present-day environments suggests that modern catchment data can be used as a proxy for palaeo-catchments of S2S systems.

Despite the great variability displayed in morphometric attributes of both submarine canyons and shelf-edge deltas on a global scale (Chapters 3 to 5), findings of this PhD project also suggest that various moderate or strong scaling relationships between individual morphometrics can be recognised generally in both shelf-edge deltas and submarine canyons – irrespective of the specific set of environmental variables at the location of a S2S system. Thus, first-order estimates of the geomorphology of the two sedimentary systems in outcrop, seafloor and subsurface data can be made even with limited knowledge of the environmental setting. This is particularly useful in ancient S2S systems where it is likely that not all environmental variables can be identified, and in large S2S systems that are only partially surveyed, preserved or only partially crop out.

Furthermore, the identified scaling relationships in modern canyons of their maximum widths, and maximum and average depths with the seafloor depth at the canyon mouth might be particularly useful to estimate the scale and bathymetric depth range of the continental slope in outcrop and subsurface surveys with limited bathymetric and palaeoenvironmental information and in geographic regions where the original palaeogeography has been reorganised by tectonic activity.

Findings in Chapter 5 show that the geometry of a shelf-edge delta cannot be inferred based on its internal hierarchical organization into a single lobe versus multiple lobes. Conversely, the size of a shelf-edge delta is not a reliable criterion to indicate whether the delta is composed of a single lobe or multiple hierarchically nested units. Nevertheless, for the demonstrated moderate correlations of (i) deltaic-element width with size and maximum elevation of the modern drainage basin, and (ii) length and thickness with shelf width, the results indicate that these scaling relationships are recognisable across different hierarchical scales of observations in shelf-edge deltas and are not scale-specific. Consequently, palaeoenvironmental reconstructions might still be undertaken from outcrop, seismic, core and well data, where the entirety of the shelf-edge delta is not covered by the data, but rather where only individual lobes are recorded by the data.

6.3.1.2 Limitations

The results of this research have identified two major limitations regarding the reconstruction of shelf-edge deltas, submarine canyons, and their superordinate S2S systems in outcrop and subsurface studies based on scaling relationships. First, many scaling relationships are weak, modest or moderate, which delimits the preciseness of predictions. Second, findings from this research demonstrate that morphometric parameters of both shelf-edge deltas and submarine canyons can display the same tendencies in scaling across different environments, in which cases environmental variables cannot be unequivocally inferred from geomorphological characteristics.

In addition, the strength of scaling relationships can vary across different S2S systems due to various factors, which include – but are not limited to – the following:

With increasing degree of deformation and fragmentation of the S2S system and its sedimentary subenvironments the accuracy of predictions for scaling relationships decreases; in ancient S2S system with increasing age due to long-term compaction and sustained or recurrent tectonic processes over time, but also in younger and modern S2S systems along continental

margins, where high sediment erosion rates in terrestrial catchments result in high burial rates within their marine segments, and where S2S systems are located along active plate boundaries. For example, reconstructions based on maximum catchment elevation become less reliable in S2S systems where high erosion- or uplift rates have significantly changed the height of mountain ranges over time.

Scaling relationships of submarine canyons and shelf-edge deltas with the terrestrial catchment of the S2S system can also be weakened due to the influence of marine hydrodynamic processes. This might be the case where large quantities of fluvial sediment discharge do not reach the canyon apex, e.g. due to interception by longshore currents, and where delta deposits are eroded by marine currents and waves (e.g. Berné et al., 1998) or the subsequent incision by distributary channels (e.g. Steel et al., 2003). Similarly, a sufficient strength of slope currents might prevent the deposition of fluvial sediment along canyon margins and within the canyon, thus inhibiting sediment transport down-canyon. These processes are likely particularly efficient in S2S systems where the current crosses a canyon at a location with low relief. Furthermore, the bathymetric depth of shelf and slope currents along a margin relative to the bathymetric depth range occupied by the canyon determines the degree to which sediment transport across a continental margin might be disrupted and can thus be highly variable across different S2S systems.

The applicability of findings from the two global studies of modern submarine canyons and their superordinate S2S systems to ancient margin successions might also be decreased for S2S systems which developed under different environmental conditions. For example, although the age of many of the studied canyons are not well-constrained, their evolution is linked to the same pattern of sea-level variations during the Late Quaternary. Considering how sea-level changes can affect sediment connectivity of submarine canyons to rivers and intra-shelf sediment sources (e.g. Covault et al., 2011b; Mauffrey et al., 2017), sediment remobilisation within the shelf and erosion from sea cliffs along palaeoshorelines (e.g. Henrich et al., 2010; Pierau et al., 2010; Covault et al., 2011b), different sea-level curves during

other geological periods and diverging patterns across different regions likely have a variable impact on processes shaping canyon morphology. Moreover, it cannot be ruled out that some correlations of the terrestrial catchment with morphometrics of submarine canyons and shelf-edge deltas produced weak results due to the short window of observation in Late Quaternary S2S systems and sediment being stored in intermediate sinks between terrestrial hinterlands and deep-water environments as in coastal plains (e.g. Phillips & Slattery, 2006) and submarine-canyon heads (e.g. Mauffrey et al., 2015).

Furthermore, some scaling relationships in submarine canyons might have been overprinted by the influence of anthropogenic activity on sediment dispersal across the S2S system over the last century. This is probably the case in some of the S2S systems where canyons are sourced by fluvial sediment discharge. Along continental margins where deforestation in terrestrial catchments increases run-off rates of precipitation and enhances surface erosion, sediment discharge rates to shallow- and deep-marine environments can be significantly elevated (e.g. Carter et al., 2016). By contrast, the retention of fluvial sediment load and its non-delivery further down-system, for example due to the artificial regulation of fluvial discharge through the construction of reservoirs and hydroelectric dams (e.g. Li et al., 2020b), and the artificial rerouteing of rivers (e.g. Higgins et al., 2018), affects not only hydrodynamic processes in fluvial systems, but also sediment transfer across terrestrial catchments to shelf-, slope- and basin-floor segments. Also, it still remains unclear to what degree macro-pollutants like microplastics in rivers might alter dynamic properties of subaqueous sediment transport (e.g. Scherer et al., 2020; Petersen & Hubbart, 2021), which in turn might affect sediment transport distances and the generation of hyperpycnal flows at the mouths of rivers. In addition to the potential anthropogenic interference with sediment budgets and transport pathways within terrestrial catchments, other anthropogenic actions might influence the redistribution of sediment in marine environments and within submarine canyons and overprint pre-industrial signals across S2S systems. For example, sustained trawling activity on a decadal scale from fishing vessels

has been shown to significantly increase sediment supply rates to submarine canyons and prevent sediment accumulation along canyon flanks (e.g. Paradis et al., 2017; 2022 and references therein).
The above-discussed caveats suggest that the predictive strength of scaling relationships in S2S systems associated with shelf-edge deltas and submarine canyons can be highly variable depending on the suite of external and environmental factors exerting influence on sediment erosion, transport, and deposition along and across a continental margin. This has to be considered when applying scaling relationships to the reconstruction of sedimentary environments and challenges the universal applicability of semi-quantitative models of S2S systems.

6.3.2 Implications for industrial applications

Findings from this study might be of interest for various sectors of industry: large-scale, sand-rich shelf-edge deltas (e.g. Sneider, 2003; Yu et al., 2021) and submarine canyons (e.g. Anderson et al., 2006) are, due to their size and the favourable porosity characteristics of their sand-prone deposits, of long-standing economic interest as reservoirs for the exploration of hydrocarbons. Due to their reservoir qualities they might also constitute potential storage sites for CO_2 sequestration (e.g. Bachu & McEwen, 2011; Callas et al., 2022) and hydrogen (e.g. Muhammed et al., 2022). Similarly, sand deposits within submarine canyons can function as reservoirs if they are of sufficiently large volume.

The (i) identified scaling relationships for aspects of shelf-edge delta geometry and submarine-canyon geomorphology with attributes of the S2S system, in particular those of moderate strength or higher, and of environmental variables which seem to promote their size (section 6.1), and (ii) morphometric characteristics which promote sediment routeing to deep-water basins (section 6.2), might aid identification of S2S systems and continental margins where S2S segment characteristics and environmental conditions are favourable for the development of shelf-edge deltas and submarine canyons whose accumulated deposits are likely sufficiently large to function as major reservoirs.

6.3.3 Planning and conducting of field surveys, experimental- and modelling studies

The results from the three projects undertaken as the main body of this research can also aid the planning and conduction of field surveys, experimental- and modelling studies involving submarine canyons and shelf-edge deltas, by informing cost- and time-benefit decisions. Depending on the research focus and knowledge of the presence or absence of a scaling relationship and its strength, studies can specifically include or discard study variables that may or not may aid the purpose of research. For example, due to their often-large-scale dimensions it might be cost-intensive to fully survey the entirety of a S2S system, individual S2S segments, shelf-edge deltas and/or submarine canyons on the seafloor, in subsurface or outcrop. Along continental margins where remnants of terrestrial catchments are preserved that supplied deep-water basins offshore (e.g. Martinsen et al., 2010), scaling relationships between catchment characteristics and morphometric aspects of shelf-edge deltas and submarine canyons may be used to make first-order estimates of morphologic characteristics within distal parts of associated S2S systems.

7 Conclusions

7.1 Overarching conclusions of this project

This research was conducted to increase understanding of the controls on the geomorphologies of submarine canyons and shelf-edge deltas. The aim of this project was realised from the global study of examples of the two sedimentary system types in context of their physiographic and environmental settings, utilising published datasets, open-source bathymetry data, and statistical analyses.

The following key findings have emerged from this project:

(i) Morphometric attributes of shelf-edge deltas and submarine canyons – both in general and as a function of individual environmental variables – display a great range in values, which highlights both the complexity and variability in geomorphologies of the two sedimentary system types.

(ii) Despite this, the results arising from this study demonstrate that individual aspects of shelf-edge delta- and submarine-canyon geomorphologies tend to differ between environmental settings, indicating that certain environmental variables impact their geomorphologic evolution and, considering the multitude of controls of both system types, have a predominant influence relative to others. This is true for both sedimentary system types for the environmental classes of oceanographic environment and latitudinal setting. The separate evaluation of the role of the fluvial feeder system type for shelf-edge deltas, and the tectonic-margin and plate-boundary types for submarine canyons, also indicates an influence of these environmental parameters on their geomorphologies. By contrast, the S2S system setting, i.e., whether the S2S system is associated with a continental or insular margin, does not constitute a primary control on the geomorphologies of either submarine canyons or shelf-edge deltas. However, more data is needed to corroborate the findings for the latter.

(iii) Scaling relationships of morphometric attributes in submarine canyons and shelf-edge deltas, and of their morphometric attributes with variables of their associated S2S system and physiographic setting are mostly weak, modest and moderate, but strong in some cases. This reflects the complex interplay of allogenic and autogenic processes influencing their geomorphologies and how several controls might amplify, weaken or overprint a scaling relationship.

(iv) The complex influence of controlling factors on the geomorphology of shelf-edge deltas and submarine canyons is reflected by the outcomes of the statistical analyses. In particular, this can be inferred from (1) high variability in values of morphometric attributes in submarine canyons and shelf-edge deltas, (2) the prevalence of weak to moderate scaling relationships, and (3) some environmental settings displaying the same relationships with geomorphologic aspects of the two sedimentary system types. This highlights that some degree of uncertainty exists regarding the predictability of morphologies in submarine canyons and shelf-edge deltas. This has not been commonly accounted for in previous conceptual models at sedimentary system- to continental-margin scale and needs to be considered in future models. The findings also demonstrate that conceptual models of canyons and shelf-edge deltas, and of their superordinate S2S systems, which are based on local- and regional-scale studies, are not generally applicable to other geographic regions. However, where scaling relationships display moderate or high correlation, the results suggests that these scaling relationships can be more widely recognised across S2S systems.

(v) It is not possible to reliably predict the original geomorphologies of submarine canyons and shelf-edge deltas from partial knowledge of their morphometric attributes and individual controls from outcrop and subsurface data. Instead, the degree of predictability depends on the co-occurrence of multiple controls acting along a

margin, the characteristics of the S2S system, and the physiographic setting of the submarine canyon and shelf-edge delta. This key finding suggests that classification schemes and conceptual models of these sedimentary system types, and of S2S systems including submarine canyons and shelf-edge deltas in their configuration, which are based on a single factor or few criteria, are not representative of the complex ways in which these two types of sedimentary system at the shelf-to-slope transition are controlled in their evolution.

(vi) The finding of this project that various scaling relationships of submarine canyons and shelf-edge deltas with variables of the associated S2S system, physiographic and environmental setting exist, clearly shows that the accuracy of prediction increases with the amount of information available on the physiography and environment but also depends on the variability of individual morphometric attributes. The data basis provided by this research can be applied to evaluate sets of controls along a specific margin and associated with a particular S2S system. This, in turn aids in assessing the combined impact of factors on the geomorphologic aspects of submarine canyons and shelf-edge deltas, and also in appraising the predictive use of environmental variables to predict canyon- and delta morphometric attributes, and vice versa. With such knowledge, first-order estimates of original geometries of submarine canyons and shelf-edge deltas and their associated S2S systems can be made.

(vii) Although it is not always clear whether a scaling relationship constitutes a true genetic link or has arisen from covariance, the results of the global-scale assessment of scaling relationships between morphometric attributes within submarine canyons and shelf-edge deltas, and with variables of their environment and physiographic setting, indicate the existence of boundary conditions for the development of certain morphotypes of these sedimentary systems. This is particularly the case where

morphometric attributes appear to be mainly influenced by one factor, as canyon length by slope width, but also where several variables probably promote the development of a morphometric characteristic. For example, delta-element width tends to be greater in shelf-edge deltas associated with multiple rivers, larger and higher terrestrial catchments and open seas, which suggests that S2S systems comprising these characteristics are more likely to facilitate the development of delta morphotypes with great widths. However, the predictability also in part depends on whether one or some of the other environmental characteristics of the S2S system and margin might somehow limit or restrict the along-strike growth of shelf-edge deltas.

The new findings from this thesis bring into focus controls on the evolution of both shelf-edge deltas and submarine canyons, which have only marginally been considered in previous conceptual models of the two types of sedimentary systems and their superordinate S2S systems, as the oceanographic environment and certain marine hydrodynamic processes including margin-parallel shelf- and slope currents, littoral drift and internal waves in submarine canyons. Based on the results from the three individual studies new holistic semi-quantitative S2S models have been devised, which consider genetic links of aspects of shelf-edge delta- and submarine-canyon geomorphology with variables of their environmental setting.

Both the outcomes of the statistical analyses and the applicability of the proposed conceptual models as a framework for the reconstruction of ancient examples of shelf-edge deltas and submarine canyons and their palaeoenvironments in the depositional record will need testing and validation from future field-, experimental- and numerical studies. The latter two are particularly suited to test hydrodynamic influences on delta- and canyon morphologies. The potential variety of sediment pathways, sediment sources and -sinks within each segment, and the complex influences of their controlling factors highlight both the need for further refinement of S2S system models, but also the challenges to link characteristics of sedimentary environments to individual controlling factors.

Some of the key findings of this project are summarised in Figure 7.1.

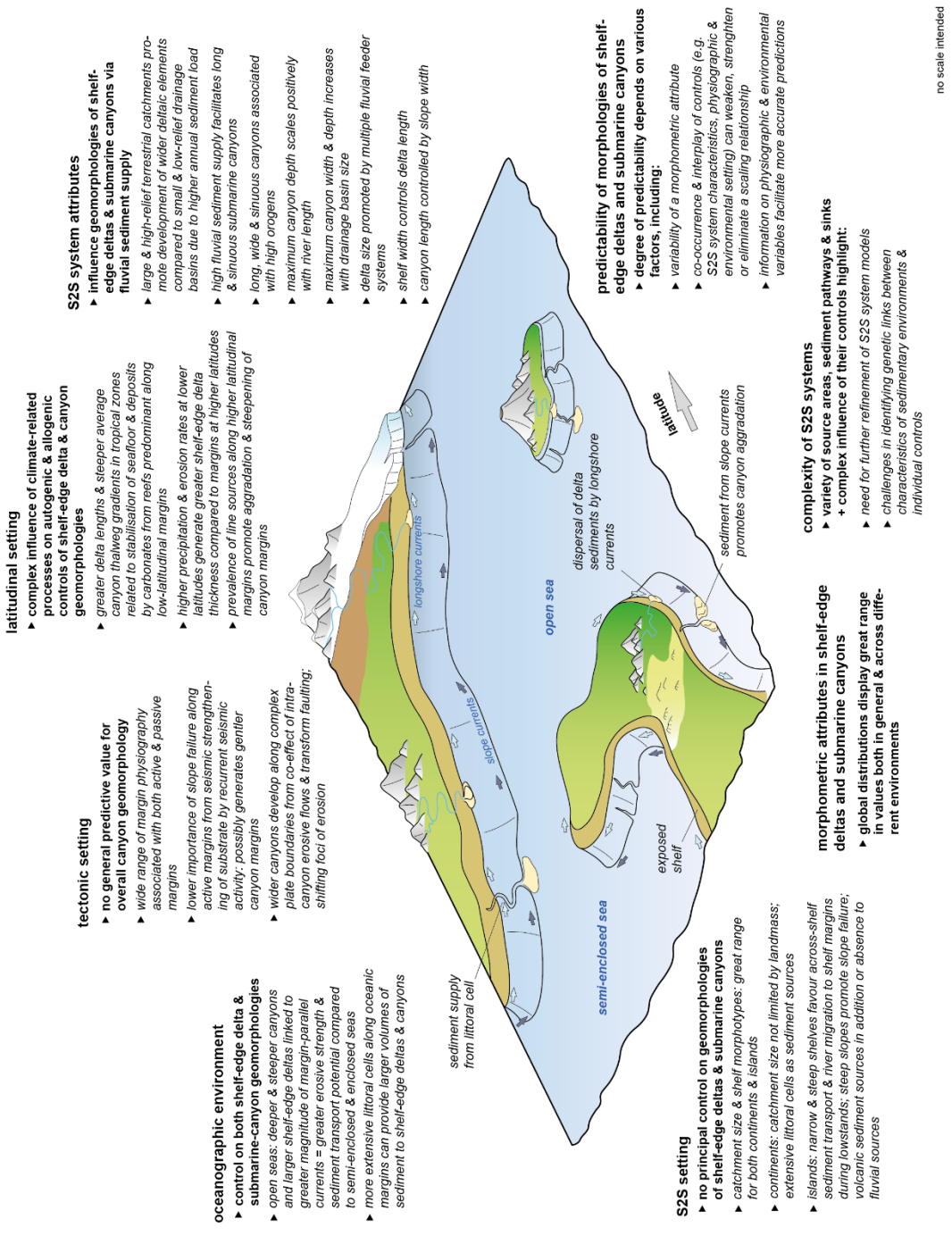

Figure 7.1 Schematic diagram summarising some of the key findings of this project regarding controlling factors of the geomorphologies of submarine canyons and shelf-edge deltas recognised in the literature and indicated from the results in this study.

7.2 Future research

Findings from this project show prospective areas for future research of source-to-sink systems with a submarine-canyon and/or shelf-edge delta

configuration, which include the (i) testing of study variables that were not considered in this project (section 7.3.1), (ii) exploration of genetic links and scaling of submarine canyons and shelf-edge deltas with other sedimentary systems (section 7.3.2), (iii) re-evaluation of some of the findings from a larger dataset (section 7.3.3), (iv) utilisation of other statistical techniques based on larger sample sizes (section 7.3.4), (v) evaluation of the successions of submarine canyons and shelf-edge deltas as repositories for storage of carbon dioxide (section 7.3.5), and (vi) application of findings for S2S systems on Earth to extraterrestrial planetary bodies (e.g. Mars) (section 7.3.6).

7.2.1 Prospective study variables for future quantitative analyses of submarine canyons and shelf-edge deltas

The following sections highlight potential variables as focus for future quantitative studies of submarine canyons and shelf-edge deltas.

7.2.1.1 Morphometric attributes of submarine canyons and shelf-edge deltas

Despite the vast number of study variables tested in all three meta-analyses, some morphometric attributes of submarine canyons and shelf-edge deltas were not considered due to lack of data available in the literature, including canyon volume, and the surface gradient and volume of shelf-edge deltaic elements.

7.2.1.2 Architectural elements of submarine canyons and shelf-edge deltas

Scaling relationships of submarine canyons and shelf-edge deltas with characteristics of their environment might vary in strength depending on the hierarchical level of observation, as seen in submarine fans; Pettinga et al. (2018) demonstrated for channels and lobate bodies in submarine fans a lack of scaling with the terrestrial catchment, which contrasts with well-established scaling relationships on level of the superordinate fan (e.g. Sømme et al., 2009; Nyberg et al., 2018b). These findings raise the question whether architectural elements of shelf-edge deltas and submarine-canyon

fills might be similarly affected to different degrees by certain controlling factors.

The quantitative study of lower-hierarchical architectural elements in submarine-canyon fills (channel elements and levees; e.g. Dykstra & Kneller, 2007; Shang et al., 2015) and shelf-edge deltas (distributary channels and mouth bars; e.g. Dixon et al., 2013; Almeida Junior et al., 2020), and of deltaic subenvironments (delta plain, delta front and prodelta; e.g. Carvajal & Steel, 2009; Ambrose & Hentz, 2012; Schwartz & Graham, 2015) from published subsurface and outcrop datasets as a function of their superordinate S2S system and environmental setting would aid to increase understanding of spatial and hierarchical variability of process-response relationships within the two sedimentary system types. Such knowledge would be particularly useful for the reconstruction of palaeoenvironments based on limited available data where canyons and shelf-edge delta are only partially surveyed or preserved.

Similarly, it is unknown whether scaling relationships identified in individual canyons also translate to the level of a canyon system. This could be explored by investigating variables as the dimensions of canyon systems, the number of tributaries and distributaries and catchment characteristics of tributaries.

7.2.1.3 Environmental factors and processes

Environmental factors which might have an influence on the morphology of submarine canyons that were not assessed but have arisen from the analyses as potential important controls are sediment supply rates from longshore currents and contourite systems to canyons, and the hydrodynamic-process regime at the location of the canyon. Although a classification scheme of the latter does not presently exist, this could be devised by adapting a classification scheme similar to the one introduced by Galloway (1975) for deltas – which is also widely used for shelf-edge deltas (e.g. Dixon et al., 2012 and references therein; Gong et al., 2016 and references therein; see also Chapter 5) – by grouping canyons based on the relative influence of fluvial- and marine hydrodynamic processes.

In addition, bedrock lithology in terrestrial catchments has been suggested as a factor controlling canyon formation (see Smith et al., 2017) and might therefore impact the geomorphology of submarine canyons by influencing the scale of erosion within canyons related to sediment gravity flows from fluvial discharge. Moreover, within the marine part of a S2S system, substrate lithology within the shelf and slope segments affects the degree of canyon downcutting (e.g. De Pippo et al., 1999; Oiwane et al., 2011).

Another parameter that can be quantified is the subaqueous drainage network of tributaries associated with a submarine canyon (e.g. Pratson & Ryan, 1996; Bernhardt et al., 2015), which might affect canyon morphology depending on its size and discharge rates in a way that can be globally recognised, similar to those of terrestrial drainage basins and their associated rivers (e.g. Sømme et al., 2009; Nyberg et al., 2018b).

A further significant shortcoming for the development of semi-quantitative S2S system models extending across shelf and slope environments lies in the current limited understanding of genetic links between geomorphologic characteristics of submarine canyons and shelf-edge deltas with certain sediment transport processes, including marine currents, hemipelagic fallout, aeolian- and glacial transport, which might occur over great distances and span across various S2S system segments.

7.2.2 Genetic links of submarine canyons and shelf-edge deltas with other sedimentary systems within the source-to-sink (S2S) system

Along continental margins where submarine canyons are located on the continental slope below shelf-edge deltas, their geomorphologies might be impacted by their co-genetic evolution. Sediment dispersal from shelf-edge deltas by sediment gravity flows to the continental slope has been suggested to promote the enlargement of pre-existing slope channels (e.g. Sanchez et al., 2012b). By contrast, both the progradation of deltas to the shelf margin and the growth of shelf-edge deltas might be inhibited where submarine canyons have retrograded in front of river mouths due to the non-deposition and bypassing of fluvial sediment into canyon heads (e.g. Fisher et al., 2021). Moreover, shelf-edge deltaic deposits might be cannibalised where

submarine canyons tap into them (e.g. Dasgupta & Buatois, 2015). However, it is also important to note that the evolution of both sedimentary systems also occurs independently of each other, e.g. where canyons retrograde onto the shelf related to tectonic and submarine erosional processes (e.g. Algan et al., 2002). Despite this limitation, the evaluation of scaling relationships between morphometric characteristics of shelf-edge deltas and associated submarine canyons in general and as a function of environmental controls would shed light on genetic links between the geomorphologic evolution of both sedimentary system types.

7.2.3 Re-evaluation of scaling relationships seen in submarine canyons and shelf-edge deltas from larger datasets in the future

The reassessment of scaling relationships of sedimentary environments investigated in the initial study by Sømme et al. (2009) from a larger dataset compiled by Nyberg et al. (2018b) has highlighted how scaling relationships might change in their strength with increasing dataset size. With more data available from new studies of submarine canyons and shelf-edge deltas it may be possible in the future to reconduct statistical analyses to reassess relationships between pairs of variables that were based on few observations and/or on few geographic regions.

In particular, the paucity of high-resolution studies of sedimentary environments in high-latitudinal environments, which is not only demonstrated for submarine canyons and shelf-edge deltas in the collated datasets of this work but also in metastudies of S2S systems (e.g. Sømme et al., 2009; Nyberg et al., 2018b), submarine-channel-lobe systems (e.g. Pettinga et al., 2018), incised-valley fills (e.g. Wang et al., 2019), and Gilbert-type deltas (e.g. Budai et al., 2021), limits the informative value of analyses related to the latitudinal setting. Therefore, there currently exists uncertainty on how applicable findings from quantitative studies of S2S systems and their subenvironments in low- and temperate latitudinal regions may be to high-latitudinal systems, and whether processes and S2S system configurations related to high latitudinal settings lead to different morphologic signatures in submarine canyons and shelf-edge deltas.

Considering the relatively small amount of data currently available on morphometric attributes of shelf-edge deltaic elements in published datasets, a reanalysis of controlling factors of shelf-edge delta geometry in the future from a larger dataset is desirable. Moreover, testing of the indicated causal links between shelf-edge delta geometries and environmental variables by numerical and experimental modelling will provide more data to validate or refute the existence of such relationships.

7.2.4 Application of other statistical techniques

One key finding of the project is that neither shelf-edge deltas nor submarine canyons are uniformly influenced in their geomorphology by individual controls (see section 7.2). However, the concurrence of different sets of controls might lead to specific geomorphologies, which would increase the predictive power of S2S system models, if known. Given a sufficiently robust dataset, multivariate statistical techniques, such as principal component analysis (e.g. Sharma et al., 2015) and cluster analysis (e.g. Eltahan et al., 2021), might aid in the quantitative assessment of the relative importance of individual factors on the morphologic attributes of shelf-edge deltas and submarine canyons and facilitate the further refinement of the semi-quantitative conceptual models proposed in Chapter 6.

7.2.5 Submarine canyons and shelf-edge deltas as repositories for the storage of carbon dioxide

The gained new insights on controls on the geomorphologies of submarine canyons and shelf-edge deltas and relationships between their morphometric characteristics and environmental variables can also aid in the assessment of submarine canyons and shelf-edge deltas in the depositional record as suitable repositories for the storage of carbon dioxide (e.g. Bachu & McEwen, 2011; Teng & Zhang, 2018; Callas et al., 2022).

7.2.6 Application of findings to extraterrestrial planetary source-to-sink (S2S) systems

Lastly, the results of this project might at some point be applied to facilitate comparisons between scaling relationships seen in terrestrial versus extraterrestrial planetary S2S systems (e.g. Grotzinger et al., 2013) such as

Mars (e.g. Grotzinger et al., 2011; 2013; McLennan et al., 2019) and Titan (e.g. Grotzinger et al., 2013; Lapôtre et al., 2022). For example, with new data emerging from the ongoing mapping of sedimentary systems on Mars (https://trek.nasa.gov/mars), such assessment would provide valuable insights into the applicability of process-response relationships seen in sedimentary systems and across sedimentary environments on Earth to Martian ones, and might aid in the reconstruction of palaeoenvironments and palaeoenvironmental conditions on Mars.

List of References

Abdulah, K.C., Anderson, J.B., Snow, J.N., Holdford-Clark, L. 2004. The late Quaternary Brazos and Colorado deltas, offshore Texas, U.S.A. – Their evolution and the factors that controlled their deposition. In: Anderson, J.B., Fillon, R.H. (eds) Late Quaternary Stratigraphic Evolution of the Northern Gulf of Mexico Margin. SEPM Spec. Publ. 79, 237-269.

Acosta, J., Canals, M., López-Martínez, Muñoz, A., Herranz, P., Urgeles, R., Palomo, C., Casamor, J.L. 2002. The Balearic promontory geomorphology (western Mediterranean): morphostructure and active processes. Geomorphology. 49, 177-204.

Adams, E.W., Kenter, J.A.M. 2013. So different, yet so similar: comparing and contrasting siliciclastic and carbonate slopes. In: K. Verwer, T.E. Playton, P.M. Harris (eds) Deposits, Architecture, and Controls of Carbonate Margin, Slope and Basinal Settings. SEPM Spec. Publ. 115, 14-25.

Aiello, G., Iorio, M., Molisso, F., Sacchi, M. 2020 Integrated morpho-bathymetric, seismic-stratigraphic, and sedimentological data on the Dohrn Canyon (Naples Bay, Southern Tyrrhenian Sea): Relationships with volcanism and tectonics. Geosciences. 10:319, 38 pp.

Aksu, A.E., Piper, D.J.W. 1983. Progradation of the late Quaternary Gediz Delta, Turkey. Mar. Geol. 54, 1-25.

Aksu, A.E., Piper, D.J.W., Konuk, T. 1987. Late Quaternary tectonic and sedimentary history of outer Izmir and Candarli Bays, Western Turkey. Mar. Geol. 76, 89-104.

Alford, M. H., MacCready, P. 2014. Flow and mixing in Juan de Fuca Canyon, Washington. Geophys. Res. Lett. 41, 1608-1615.

Algan, O., Gökaşsan, E., Gazioğlu, C., Yücel, Z.Y., Alpar, B. Güneysu, C., Kirci, E., Demirel, S., Sari, E., Ongan, D. 2002. A high-resolution seismic study in Sakarya Delta and Submarine Canyon, southern Black Sea shelf. Cont. Shelf Res. 22 (10), 1511-1527.

Allen, C., Peakall, J., Hodgson, D.M., Bradbury, W., Booth, A.D. 2022. Latitudinal changes in submarine channel-levee system evolution, architecture and flow processes. Front. Earth Sci. 10:976852, 26 pp.

Allen, P.A. 2008. From landscapes into geological history. Nature. 451, 274-276.

Allen, P.A. 2017. Sediment Routing Systems. Cambridge University Press, Cambridge U.K. 407 pp.

Allen, S.E., Durrieu de Madron, X. 2009. A review of the role of submarine canyons in deep-ocean exchange with the shelf. Ocean Sci. 5, 607-620.

Allen, S.E., Vindeirinho, C., Thomson, R.E., Foreman, M.G.G., Mackas, D.L. 2001. Physical and biological processes over a submarine canyon during an upwelling event. Can. J. Fish. Aquat. Sci. 58, 671-684.

Allin, J.R., Hunt, J.E., Talling, P.J., Clare, M.A., Pope, E., Masson, D.G. 2016. Different frequencies and triggers of canyon filling and flushing events in Nazaré Canyon, offshore Portugal. Mar. Geol. 371, 89-105.

Almagor, G. 1993. Continental slope processes off northern Israel and southernmost Lebanon and their relation to onshore tectonics. Mar. Geol. 112, 151-169.

Almeida Junior, F.N., Steel, R.J., Olariu, C., Gan, Y., Gomes Paim, P.S. 2020. River-dominated and tide-influenced shelf-edge delta systems: Coarse-grained deltas straddling the Early-Middle Jurassic shelf-slope break and transforming downslope, Lajas-Los Molles formations, Neuquén Basin, Argentina. Sedimentology. 67, 2883-2916.

Alonso, B., Ercilla, G. 2003. Small turbidite systems in a complex tectonic setting (SW Mediterranean Sea): morphology and growth patterns. Mar. Pet. Geol. 19, 1225-1240.

Alvarez-Solas, J., Robinson, A., Montoya, M., Ritz, C. 2013. Iceberg discharges of the last glacial period driven by oceanic circulation changes. PNAS. 110 (41), 16350-16354.

Amblas, D., Ceramicola, S., Gerber, T.P., Canals, M., Chiocci, F.L., Dowdeswell, J.A., Harris, P.T., Huvenne, V.A.I., Lai, S.Y.J., Lastras, G., Lo Iacono, C., Micallef, A., Mountjoy, J.J., Paull, C.K., Puig, P., Sanchez-Vidal, A. 2017. Submarine canyons and gullies. In: Micallef, A., Krastel, S., Savini, A. (eds) Submarine Geomorphology, Springer, Cham, Switzerland. pp. 251-272.

Amblas, D., Gerber, T.P., De Mol, B., Urgeles, R., Garcia-Castellanos, Canals, M., Pratson, L.F., Robb, N., Canning, J. 2012. Survival of a submarine canyon during long-term outbuilding of a continental margin. Geology. 40 (6), 543-546.

Amy, L.A., Talling, P.J., Edmonds, V.O., Sumner, E.J., Lesueur, A. 2006. An experimental investigation of sand-mud suspension settling behaviour: implications for bimodal mud contents of submarine flow deposits. Sedimentology. 53, 1411-1434.

Anderson, J.B., Rodriguez, A., Abdulah, K.C., Fillon, R., Banfield, L., McKeown, H.A., Wellner, J.S. 2004. Late Quaternary stratigraphic evolution of the Northern Gulf of Mexico margin: A synthesis. In: Anderson, J.B., Fillon, R.H. (eds) Late Quaternary Stratigraphic Evolution of the Northern Gulf of Mexico Margin. SEPM Spec. Publ. 79, 1-23.

Anderson, J.B. 2005. Diachronous development of late Quaternary shelf-margin deltas in the northwestern Gulf of Mexico: Implications for sequence stratigraphy and deep-water reservoir occurrence. In: Giosan, L., Bhattacharya, J.P. (eds) River Deltas – Concepts, Models, and Examples. SEPM Spec. Publ. 83, 257-276.

Anderson, J.B., Wallace, D.J., Simms, A.R., Rodriguez, A.B., Weight, R.W.R., Taha, Z.P. 2015. Recycling sediments between source and sink during a eustatic cycle: Systems of late Quaternary northwestern Gulf of Mexico Basin. Earth-Sci. Rev. 153, 111-138.

Anderson, K.S., Graham, S.A., Hubbard, S.M. 2006. Facies, architecture, and origin of a reservoir-scale sand-rich succession within submarine canyon fill: Insights from Wagon Caves Rock (Paleocene), Santa Lucia Range, California, U.S.A. J. Sediment. Res. 76, 819-838.

Anka, Z., Séranne, M., Lopez, M., Scheck-Wenderoth, M., Savoye, B. 2009. The long-term evolution of the Congo deep-sea fan: A basin-wide view of the interaction between a giant submarine fan and a mature passive margin (ZaiANgo project). Tectonophysics. 470, 42-56.

Antobreh, A.A., Krastel, S. 2006. Morphology, seismic characteristics and development of Cap Timiris Canyon, offshore Mauritania: a newly discovered canyon preserved-off a major arid climatic region. Mar. Pet. Geol. 23, 37-59.

Aranguiz, R., Shibayama, T. 2013. Effect of submarine canyons on tsunami propagation; a case study of the Biobio Canyon, Chile. Coast. Eng. J. 55 (4), 1350016-1-1350016-23.

Armitage, D.A., Piper, D.J.W., McGee, D.T., Morris, W.R. 2010. Turbidite deposition on the glacially influenced, canyon-dominated Southwest Grand Banks Slope, Canada. Sedimentology. 57, 1387-1408.

Arzola, R.G., Wynn, R.B., Lastras, G., Masson, D.G., Weaver, P.P.E. 2008. Sedimentary features and processes in the Nazaré and Setúbal submarine canyons, west Iberian margin. Mar. Geol. 250, 64-88.

Atwater, B.F., Carson, B., Griggs, G.B., Johnson, H.P., Salmi, M.S. 2014. Rethinking turbidite paleoseismology along the Cascadia subduction zone. Geology. 4289), 827-830.

Azaroff, A., Miossec, C., Lanceleur, L., Guyoneaud, R., Monperrus, M. 2020. Priority and emerging micropollutants distribution from coastal to continental slope sediments: a case study of Capbreton Submarine Canyon (North Atlantic Ocean). Sci. Total Environ. 703, 135057.

Babonneau, N., Savoye, B., Cremer, M., Klein, B. 2002. Morphology and architecture of the present canyon and channel system of the Zaire deep-sea fan. Mar. Pet. Geo. 19, 445-467.

Babonneau, N., Delacourt, C., Cancouët, R., Sisavath, E., Bachèlery, P., Mazuel, A., Jorry, S.J., Deschamps, A., Ammann, J., Villeneuve. 2013. Direct sediment transfer form land to deep-sea: insights into shallow multibeam bathymetry at La Réunion Island. Mar. Geol. 346, 47-57.

Bachu, S., McEwen, T. 2011. Geological media and factors for the long-term emplacement and isolation of carbon dioxide and radioactive waste. In: Toth, F.L. (ed) Geological Disposal of Carbon Dioxide and Radioactive Waste: A Comparative Assessment. Adv. Global Change Res. 44, 23-79.

Bailey, L.P., Clare, M.A., Rosenberger, K.J., Cartigny, M.J.B., Talling, P.J., Paull, C.K., Gwiazda, R., Parsons. D.R., Simmons, S.M., Xu, J., Haigh, I.D., Maier, K.L., McGann, M., Lundstren, E. 2021. Preconditioning by sediment accumulation can produce powerful turbidity currents without major external triggers. Earth Planet. Sci. Lett. 562:116845.

Baker, E.T., Hickey, B.M. 1986. Contemporary sedimentation processes in and around an active West Coast submarine canyon. Mar. Geol. 71, 15-34.

Baker, M.L., Baas, J.H. 2022. Does sand promote or hinder the mobility of cohesive sediment gravity flows? Sedimentology. 70, 1110-1130.

Baker, M.L., Baas, J.H., Malarkey, J., Silva Jacinto, R., Craig, M.J., Kane, I.A., Barker, S. 2017. The effect of clay type on the properties of cohesive sediment gravity flows and their deposits. J. Sediment. Res. 87, 1176-1195.

Banfield; L.A., Anderson, J.B. 2004. Late Quaternary evolution of the Rio Grande Delta: Complex response to eustasy and climate change. In: Anderson, J.B., Fillon, R.H. (eds) Late Quaternary Stratigraphic Evolution of the Northern Gulf of Mexico Margin. SEPM Spec. Publ. 79, 289-306.

Bart, P.J., Anderson, J.B. 2004. Late Quaternary stratigraphic evolution of the Alabama and West Florida outer continental shelf. In: Anderson, J.B., Fillon, R.H. (eds) Late Quaternary stratigraphic evolution of the Northern Gulf of Mexico margin. SEPM Spec. Publ. 79, 43-53.

Baudouy, L., Haughton, P.D.W., Walsh, J.J. 2021. Evolution of a fault-controlled, deep-water sub-basin, Tabernas, SE Spain. Front. Earth Sci. 9:767286, 24 pp.

Baztan, J., Berné, S., Olivet, J.-L., Rabineau, M., Aslanian, D., Gaudin, M., Réhault, J.-P., Canals, m. 2005. Axial incision: The key to understand submarine canyon evolution (in the western Gulf of Lion). Mar. Pet. Geol. 22 (6-7), 805-826.

Benjamin, U., Huuse, M., Hodgetts, D. 2015. Canyon-confirmed pockmarks on the western Niger Delta slope. J. Afr. Earth Sci. 107, 15-27.

Berné, S., Lericolais, G., Marseet, T., Bourillet, J.F., de Batist, M. 1998. Erosional offshore sand ridges and lowstand shorefaces: Examples from tide- and wave-dominated environments of France. J. Sediment. Res. 68 (4), 540-555.

Bernhardt, A., Melnick, D., Jara-Muñoz, J., Argandoña, B., González, J., Strecker, M.R. 2015. Controls on submarine canyon activity during sea-level highstands. The Bíobío canyon system offshore Chile. Geosphere. 11 (4), 1226-1255.

Bernhardt, A., Schwanghart, W. 2021. Where and why do submarine canyons remain connected to the shore during sea-level rise? Insights from global topographic analysis and Bayesian regression. Geophys. Res. Lett. 48:e2020GL092234, 15 pp.

Bhattacharya, J.P., Copeland, P., Lawton, T.F., Holbrook, J. 2016. Estimation of source area, river paleo-discharge, paleoslope, and sediment

budgets of linked deep-time depositional systems and implications for hydrocarbon potential. Earth-Sci. Rev. 153, 77-110.

Blum, M.D., Hattier-Womack, J. 2009. Climate change, sea-level change, and fluvial sediment supply to deepwater depositional systems. In: Kneller, B., Martinsen, O.J., McCaffrey, B. (eds) External Controls on Deep Water Depositional Systems: Climate, Sea-Level, and Sediment Flux. SEPM Spec. Publ. (CD version) 92, 15-39.

Blum, M., Martin, J., Milliken, K., Garvin, M. 2013. Paleovalley systems: insights from Quaternary analogs and experiments. Earth-Sci. Rev. 116, 128-169.

Blum, M. Rogers, K., Gleason, J., Najman, Y., Cruz, J., Fox, L. 2018. Allogenic and autogenic signals in the stratigraphic record of the deep-sea Bengal Fan. Sci. Rep. 8:7973, 13 pp.

Blum, M.D., Törnqvist, T.E. 2000. Fluvial responses to climate and sea-level change: a review and look forward. Sedimentology. 47 (1), 2-48.

Bosley, K.L., Lavelle, J.W., Brodeur, R.D., Wakefield, W.W., Emmet, R.L., Baker, E.T., Rehmke, K.M. 2004. Biological and physical processes in and around Astoria submarine Canyon, Oregon, USA. J. Mar. Syst. 50, 21-37.

Bouma, A.H., Scott, E.D. 2003. Source-to-sink: the importance of the updip coastal area in defining deep-water sand characteristics. In: Roberts, H.H., Rosen, N.C., Fillon, R.H., Anderson, J.B. (eds) Shelf Margin Deltas and Linked Down Slope Petroleum Systems – Global Significance and Future Exploration Potential. SEPM Spec. Publ. 23, 597-617.

Bourget, J., Zaragosi, S., Ellouz-Zimmermann, N., Mouchot, N., Garlan, T., Schneider, J.-L., Lanfumey, V., Lallemant, S. 2010. Turbidite system architecture and sedimentary processes along topographically complex slopes: the Makran convergent margin. Sedimentology. 58 (2), 376-406.

Bourget, J., Ainsworth, R.B., Thompson, S. 2014. Seismic stratigraphy and geomorphology of a tide or wave dominated shelf-edge delta (NW Australia): Process-based classification from 3D seismic attributes and implications for the prediction of deep-water sands. Mar. Pet. Geol. 57, 359-384.

Bowman, A.P., Johnson, H.D. 2014. Storm-dominated shelf-edge delta successions in a high accommodation setting: The palaeo-Orinoco Delta (Mayaro Formation), Columbus Basin, South-East Trinidad. Sedimentology. 61, 792-835.

Boyd, R., Ruming, K., Goodwin, I., Sandstrom, M., Schröder-Adams, C. 2008. Highstand transport of coastal sand to the deep ocean: A case study from Fraser Island, southeast Australia. Geology. 36 (1), 15-18.

Brun, L., Pairaud, I., Silva Jacinto, R., Garreau, P., Dennielou, B. 2023. Strong hydrodynamic processes observed in the Mediterranean Cassidaigne submarine canyon. Front. Mar. Sci. 10:1078831, 17 pp.

Brunt, R. L., Hodgson, D. M., Flint, S. S., Pringle, J. K., Di Celma, C. N., Prelat, A., Grecula, M. 2013. Confined to unconfined: Anatomy of a base of slope succession, Karoo Basin, South Africa. Mar. Pet. Geol. 41, 206-221.

Budai, S., Colombera, L., Mountney, N.P. 2021. Quantitative characterization of the sedimentary architecture of Gilbert-type deltas. Sediment. Geol. 426:106022, 18 pp.

Budillon, F., Conforti, A., Tonielli, R., De Falco, G., Di Martino, G., Innangi, S., Marsella, E. 2011. The Bulgheria canyon-fan: a small-scale proximal system in the eastern Tyrrhenian Sea (Italy). Mar. Geophys. Res. 32, 83-97.

Çağatay, M.N., Uçarkus, G., Eriş, K.K., Henry, P., Gasperini, L., Polonia, A. 2015. Submarine canyons of the Sea of Marmara. In: Briand, F. (ed) Submarine canyon dynamics in the Mediterranean and tributary seas – an integrated geological, oceanographic and biological perspective. CIESM Workshop Monographs 47, 123-135.

Callas, C., Saltzer, S.D., Davis, J.S., Hashemi, S.S., Kovscek, A.R., Okoroafor, E.R., Wen, G., Zoback, M.D., Benson, S.M. 2022. Criteria and workflow for selecting depleted hydrocarbon reservoirs for carbon storage. Appl. Energy. 324:119668, 15 pp.

Canals, M., Puig, P., Durrieu de Madron, X., Heussner, S., Palanques, A., Fabres, J. 2006. Flushing submarine canyons. Nature. 444, 354-357.

Carlson, P.R., Bruns, T.R., Fisher, M.A. 1990. Development of slope valleys in the glacimarine environment of a complex subduction zone, Northern Gulf of Alaska. In: Dowdeswell, J.A., Scourse, J.D. (eds) Glacimarine Environments; Processes and Sediments. Geol. Soc. London Spec. Publ. 53, 139-153.

Carlson, P.R., Karl, H.A. 1984. Discovery of two new large submarine canyons in the Bering Sea. Mar. Geol. 56, 159-179.

Carlson, P.R., Karl, H.A. 1988. Development of large submarine canyons in the Bering Sea, indicated by morphologic, seismic, and sedimentologic characteristics. Geol. Soc. Am. Bull. 100, 1594-1615.

Carson, B., Baker, E.T., Hickey, B.M., Nittrouer, C.A., DeMaster, D.J., Thorbjarnarson, K.W., Snyder, G.W. 1986. Modern sediment dispersal and accumulation in Quinault Submarine Canyon – A summary. Mar. Geol. 71, 1-13.

Carter, L., Gavey, R., Talling, P.J., Liu, J.T. 2014. Insights into submarine geohazards from breaks in subsea telecommunication cables. Oceanography. 27 (2), 58-67.

Carter, L., Orpin, A.R., Kuehl, S.A. 2016. From mountain source to ocean sink – the passage of sediment across an active margin, Waipaoa Sedimentary System, New Zealand. Mar. Geol. 270, 1-10.

Carvajal, C., Steel, R. 2009. Shelf-edge architecture and bypass of sand to deep water: Influence of shelf-edge processes, sea level, and sediment supply. J. Sediment. Res. 79, 652-672.

Carvajal, C., Steel, R., Petter, A. 2009. Sediment supply: the main driver of shelf-margin growth. Earth-Sci. Rev. 96, 221-248.

Casalbore, D., Chiocci, F.L., Scarascia Mugnozza, G., Tommasi, P., Sposato, A. 2011. Flash-flood hyperpycnal flows generating shallow-water landslides at Fiumara mouths in Western Messina Strait (Italy). Mar. Geophys. Res. 32, 257-271.

Casalbore, D., Falcini, F., Martorelli, E., Morelli, E., Bosman, A., Calarco, M., Chiocci, F.L. 2018. Characterization of overbanking features on the lower reach of the Gioia-Mesima canyon-channel system (southern Tyrrhenian Sea) through integration of morpho-stratigraphic data and physical modelling. Prog. Oceanogr. 169, 66-78.

Chang, Y.-C., Mitchell, N. C., Quartau, R. 2021. Landslides in the upper submarine slopes of volcanic islands: The central Azores. Geochem., Geophys., Geosyst. 22:e2021GC009833, 21 pp.

Chen, H., Zhan, W., Li, L., Wen, M.-M. 2017. Occurrence of submarine canyons, sediment waves and mass movements along the northern continental slope of the South China Sea. J. Earth Syst. Sci. 126:73, 28 pp.

Chen, H., Wood, L.J., Gawthorpe, R.L. 2020. Sediment dispersal and redistributive processes in axial and transverse deep-time source-to-sink

systems of marine rift basins: Dampier Sub-basin, Northwest Shelf. Australia. Basin Research. 33 (1), 227-249.

Chiang, C.-S., Yu, H.-S. 2006. Morphotectonics and incision of the Kaoping submarine canyon, SW Taiwan orogenic wedge. Geomorphology. 80, 199-213.

Chiang, C.-S., Yu, H.-S., Noda, A., TuZino, T., Su, C.-C. 2012. Avulsion of the Fangliao submarine canyon off southwestern Taiwan as revealed by morphological analysis and numerical simulation. Geomorphology. 177-178, 26-37.

Clare, M.A., Le Bas, T., Price, D.M.,Hunt, J.E., Sear, D., Cartigny, M.J.B.,Vellinga, A., Symons, W., Firth, C., Cronin, S. 2018. Complex and cascading triggering of submarine landslides and turbidity currents at volcanic islands revealed from integration of high-resolution onshore and offshore surveys. Front. Earth Sci. 6:223, 24 pp.

Clark, P.U., Mix, A.C. 2002. Ice sheets and sea level of the Last Glacial Maximum. Quat. Sci. Rev. 21, 1-7.

Clift, P.D. 2020. Asian monsoon dynamics and sediment transport in SE Asia. J. Asian Earth Sci. 195:104352, 11 pp.

Clift, P.D., Giosan, L. 2013. Sediment fluxes and buffering in the post-glacial Indus Basin. Basin Res. 25, 1-18.

Coleman, J.M., Prior, D.B., Lindsay, J.F. 1982. Formation of the Mississippi Canyon. Trans. GCAGS 32, 519-519.

Colombera, L., Mountney, N.P., Hodgson, D.M., McCaffrey, W.D. 2016. The Shallow-Marine Architecture Knowledge Store: A database for the characterization of shallow-marine and paralic depositional systems. Mar. Pet. Geol. 75, 83-99.

Colombera, L., Mountney, N.P. 2022. Scale dependency in quantifications of the avulsion frequency of coastal rivers. Earth-Sci. Rev. 230:104043, 23 pp.

Connolly, T.P., Hickey, B.M. 2014. Regional impact of submarine canyons during seasonal upwelling. J. Geophys. Res. Oceans. 119, 953-975.

Corradino, M., Pepe, F., Burrato, P., Kanari, M., Parrino, N., Bertotti, G., Bosman, A., Casalbore, D., Ferranti, L., Martorelli, E., Monaco, C., Sacchi, M., Tibor, G. 2021. An integrated multiscale method for the characterization

of active faults in offshore areas. The case of Sant'Eufemia Gulf (offshore Calabria, Italy). Front. Earth Sci. 9:670557, 18 pp.

Cosgrove, G.I.E., Colombera, L., Mountney, N.P. 2021. Quantitative analysis of the sedimentary architecture of eolian successions developed under icehouse and greenhouse climatic conditions. Geol. Soc. Am. Bull. 133 (11/12), 2625-2644.

Covault, J.A., Graham, S.A. 2010. Submarine fans at all sea-level stands: tectono-morphologic and climatic controls on terrigenous sediment delivery to the deep sea. Geology. 38 (10), 939-942.

Covault, J.A., Normark, W.R., Romans, B.W., Graham, S.A. 2007. Highstand fans in the California borderland: The overlooked deep-water depositional systems. Geology. 35 (9), 783-786.

Covault, J.A., Romans, B.W., Graham, S.A. 2009. Outcrop expression of a continental-margin-scale shelf-edge delta from the Cretaceous Magallanes Basin, Chile. J. Sediment. Res. 79, 523-539.

Covault, J.A., Fildani, A., Romans, B.W., McHargue, T. 2011a. The natural range of submarine canyon-and-channel longitudinal profiles. Geosphere. 7 (2), 313-332.

Covault, J.A., Romans, B.W., Graham, S.A., Fildani, A., Hilley, G.E. 2011b. Terrestrial source to deep-sea sink sediment budgets at high and low sea levels: insights from tectonically active southern California. Geology. 39 (7), 619-622.

Cronin, B.T., Akhmetzhanov, A.M., Mazzini, A., Akhmanov, G., Ivanov, M., Kenyon, N.H., TTR-10 Shipboard Scientists. 2005. Morphology, evolution and fill: implications for sand and mud distribution in filling deep-water canyons and slope channel complexes. Sediment. Geol. 179, 71-97.

Cronin, B.T., Nemčok, M., Doran, H. 2023. Transform margin source-to-sink clastic deposystems. In: Nemčok, M., Doran, H., Doré, A.G., Ledvényiová, L., Rybár, S. (eds) Tectonic Development, Thermal History and Hydrocarbon Habitat Models of Transform Margins: their Differences from Rifted Margins. Geol. Soc. London, Spec. Publ. 524, 387-419.

Crutchley, G.J., Kroeger, K.F., Pecher, I.A., Mountjoy, J.J., Gorman, A.R. 2017. Gas hydrate formation amid submarine canyon incision: Investigations from New Zealand's Hikurangi Subduction Margin. Geochem., Geophys., Geosyst. 18, 4299-4316.

Cullis, S., Patacci, M., Colombera, L., Bührig, L., McCaffrey, W.D. 2019. A database solution for the quantitative characterisation and comparison of deep-marine siliciclastic depositional systems. Mar. Pet. Geol. 102, 321-339.

Cumberpatch, Z.A., Soutter, E.L., Kane, I.A., Casson, M., Vincent, S.J. 2020. Evolution of a mixed siliciclastic-carbonate deep-marine system on an unstable margin: The Cretaceous of the Eastern Greater Caucasus, Azerbaijan. Basin Res. 33 (1), 612-647.

Cummings, D.I., Arnott, R.W.C. 2005. Growth-faulted shelf-margin deltas: a new (but old) play type, offshore Nova Scotia. Bulletin Can. Pet. Geol. 53 (3), 211-236.

Cummings, D.I., Arnott, R.W.C., Hart, B.S. 2006. Tidal signatures in a shelf-margin delta. Geology. 34 (4), 249-252.

Dadson, S., Hovius, N., Pegg, S., Dade, W.B., Horng, M.J., Chen, H. 2005. Hyperpycnal river flows from an active mountain belt. J. Geophys. Res. 110:F04016, 13 pp.

Daniell, J., Manoy, T., Beaman, R.J., Webster, J.M., Puga-Bernabéu, Á. 2020. Shelf-edge delta and reef development on a mixed siliciclastic-carbonate margin, Central Great Barrier Reef. J. Sediment. Res. 90, 1286-1304.

Dasgupta, S., Buatois, L.A. 2015. High-frequency stacking pattern and stages of canyon/gully evolution across a forced regressive shelf-edge delta-front. Mar. Pet. Geol. 68, 40-53.

Davies, A., Simmons, M.D. 2021. Demand for ‘advantaged’ hydrocarbons during the 21st century energy transition. Energy Rep. 7, 4483-4497.

Davies, H.L., Keene, J.B., Hashimoto, K., Joshima, M., Stuart, J.E., Tiffin, D.L. 1987. Bathymetry and canyons of the Western Solomon Sea. Geo-Mar. Lett. 6, 181-191.

Davies, R.J., Thatcher, K.E., Mathias, S.A., Yang, J. 2012. Deepwater canyons: an escape route for methane sealed by methane hydrate. Earth Planet. Sci. Lett. 323-324, 72-78.

de Almeida, N.M., Vital, H., Gomes, M. P. 2015. Morphology of submarine canyons along the continental margin of the Potiguar Basin, NE Brazil. Mar. Pet. Geol. 68, 307-324.

De Pippo, T., Ilardi, M., Pennetta, M. 1999. Main observations on genesis and morphological evolution of submarine valleys. Z. Geomorphology. 43 (1), 91-111.

DiBona, P.A., von der Borch, C.C. 1993. Sedimentary geology and evolution of an outcropping shelf-margin delta, late Proterozoic Wonoka Formation, South Australia. Am. Assoc. Pet. Geol. Bull. 77 (6), 963-979.

Dierssen, H.M., Theberge, A.E. Jr. 2014. Bathymetry: features and hypsography. In: Wang, Y. (ed) Encyclopedia of Natural Resources – Water and Air – Volume II. Taylor & Francis, 1-7.

Diesing, M. 2020. Deep-sea sediments of the global ocean. Earth Syst. Sci. Data. 12 (4), 3367-3381.

Dietz, R.S., Knebel, H.J., Somers, L.H. 1968. Cayar Submarine Canyon. Geol. Soc. Am. Bull. 79, 1821-1828.

Dietz, R.S., Menard, H.W. 1951. Origin of abrupt change in slope at continental shelf margin. Am. Assoc. Pet. Geol. Bull. 35 (9), 1994-2016.

Ding, W., Li, J., Li, J., Fang, Y., Tang, Y. 2013. Morphotectonics and evolutionary controls on the Pearl River Canyon system, South China Sea. Mar. Geophys. Res. 34, 221-238.

Dixon, J.F., Steel, R.J., Olariu, C. 2012. Shelf-edge delta regime as predictor of deep-water deposition. J. Sediment. Res. 82, 681-687.

Dixon, J.F., Steel, R.J., Olariu, C. 2013. A model for cutting and healing of deltaic mouth bars at the shelf edge: mechanism for basin-margin accretion. J. Sediment. Res. 83, 284-299.

Dong, T.Y., Nittrouer, J.A., Il`cheva, E., Pavlov, M., McElroy, B., Czapiga, M.J., Ma, H., Parker, G. 2016. Controls on gravel termination in seven distributary channels of the Selenga River Delta, Baikal Rift basin, Russia. Geol. Soc. Am. Bull. 128 (7/8), 1297-1312.

Doo, W.-B., Hsu, S.-K., Lo, C.-L., Chen, S.-C., Tsai, C.-H., Lin, J.-Y., Huang, Y.-P., Huang, Y.-S., Chiu, S.-D., Ma, Y.-F. (2015). Gravity anomalies of the active mud diapirs off southwest Taiwan. Geophys. J. Int. 203, 2089-2098.

Dowdeswell, E.K., Todd, B.J., Dowdeswell, J.A. 2016. Canyons and slides on the continental slope seaward of shallow banks, Labrador margin, eastern Canada. In: Dowdeswell, J.A., Canals, M., Jakobsson, M., Todd,

B.J. (eds) Atlas of Submarine Glacial Landforms: Modern, Quaternary and Ancient. Geol. Soc. London Memoirs 46, 405-406.

Dowdeswell, J.A., Ó Cofaigh, C., Pudsey, C.J. 2004. Continental slope morphology and sedimentary processes at the mouth of an Antarctic palaeo-ice stream. Mar. Geol. 204, 203-214.

Droxler, A.W., Jorry, S.J. 2013. Deglacial origin of barrier reefs along low-latitude mixed siliciclastic and carbonate continental shelf edges. Annu. Rev. Mar. Sci. 2013. 5, 165-90.

Dziadzio, P.S., Matyasik, I., Garecka, M., Szydlo. 2016. Lower Oligocene Menilite Beds, Polish Outer Carpathians: supposed deep-sea flysch locally reinterpreted as shelfal, based on new sedimentological, micropalaeontological and organic-geochemical data. Prace naukowe Instytutu nafty i Gazu 213, Krakow, Poland. 120 pp.

Edwards, M.B. 1980. The Live Oak Delta Complex: An unstable shelf / edge delta in the deep Wilcox trend of South Texas. Trans. GCAGS 30, 71-79.

Edwards, M.B. 1981. Upper Wilcox Rosita Delta System of South Texas: Growth-faulted shelf-edge deltas. Am. Assoc. Pet. Geol. Bull. 65 (1), 54-73.

Eittreim, S., Grantz, A., Greenberg, J. 1982. Active geologic processes in Barrow Canyon, Northeast Chukchi Sea. Mar. Geol., 50, 61-76.

Eltahan, A.M.H., Abd Elhamid, A.M.I., Abdelaziz, S.M. 2021. Multivariate statistical analysis of geomorphological parameters for Sinai Peninsula. Alex. Eng. J. 60, 1389-1402.

Ercilla, G., Alonso, B., Perez-Belzuz, F., Estrada, F., Baraza, J., Farran, M., Canals, M., Masson, D. 1998. Origin, sedimentary processes and depositional evolution of the Agadir turbidite system, central eastern Atlantic. J. Geol. Soc. London. 155 (6), 929-939.

Exon, N.F., Hill, P.J., Mitchell, C., Post, A. 2005. Nature and origin of the submarine Albany canyons off southwest Australia. Aust. J. Earth Sci. 52 (1), 101-115.

Fanelli, E., Bianchelli, S., Danovaro, R. 2018. Deep-sea mobile megafauna of Mediterranean submarine canyons and open slopes: Analysis of spatial and bathymetric gradients. Prog. Oceanogr. 168, 23-34.

Farre, J.A., McGregor, B.A., Ryan, W.B.F., Robb, J.M. 1983. Breaching the shelfbreak: passage from youthful to mature phase in submarine canyon

evolution. In: Stanley, D.J., Moore, G.T. (eds) The Shelfbreak: Critical Interface on Continental Margins. SEPM Spec. Publ. 33, 25-39.

Faugères, J.-C., Mulder, T. 2011. Chapter 3 – Contour currents and contourite drifts. In: Hüneke, H., Mulder, T. (eds) Deep-Sea Sediments. Dev. in Sedimentology. 63, 149-214.

Fernandez-Arcaya, U., Ramirez-Llodra, E., Aguzzi, J., Allcock, A.L., Davies, J.S., Dissanayake, A., Harris, P., Howell, K., Huvenne, V.A.I., Macmillan-Lawler, M., Martín, J., Menot, L., Nizinski, M., Puig, P., Rowden, A.A., Sanchez, F., Van den Beld, I.M.J. 2017. Ecological role of submarine canyons and need for canyon conservation: a review. Front. Mar. Sci. 4:5, 26 pp.

Fernane, L., Matougui, R., Amarni, N., Belkessa, R. 2022. Variation in canyon morphology and their relationship with tectonic: the example of the western Algerian margin. Arab. J. Geosci. 15:254, 19 pp.

Ferro, C.E., Droxler, A.W., Anderson, J.B., Mucciarone, D. 1999. Late Quaternary shift of mixed siliciclastic-carbonate environments induced by glacial eustatic sea-level fluctuations in Belize. In: Harris, P.M., Simo, J.A. (eds) Advances in Carbonate Sequence Stratigraphy: Application to Reservoirs, Outcrops and Models. SEPM Spec. Publ. 63, 385-411.

Ferry, J.-N., Babonneau, N., Mulder, T., Parize, O., Raillard, S. 2004. Morphogenesis of Congo submarine canyon and valley: implications about the theories of the canyons formation. Geodin. Acta. 17, 241-251.

Fiduk, J.C. 1995. Influence of submarine canyon erosion and sedimentation on allochthonous salt body geometry: the pathway of Bryant canyon in garden banks. GCSSEPM Foundation 16th Annual Research Conference Salt, Sediment and Hydrocarbons. December 3-6, 1995. pp. 41-51.

Fildani, A. 2017. Submarine canyons: a brief review looking forward. Geology, 45 (4), 383-384.

Fisher, W.L., Galloway, W.E., Steel, R.J., Olariu, C., Kerans, C., Mohrig, D. 2021. Deep-water depositional systems supplied by shelf-incising submarine canyons: Recognition and significance in the geologic record. Earth-Sci. Rev. 214:103531, 62 pp.

Flexas, M.M., Boyer, D.L., Espino, M. Puigdefàbregas, J., Rubio, A., Company, J.B. 2008. Circulation over a submarine canyon in the NW Mediterranean. J. Geophys. Res. 113:C12002, 18 pp.

Fournier, F. 1949. Les facteur climatiques de l’érosion du sol. Bull. Assoc. Geogr. Fr. 203, 97-103.

Fulthorpe, C.S., Carter, R.M. 1991. Continental-shelf progradation by sediment-drift accretion. Geol. Soc. Am. Bull. 103, 300-309.

Gales, J.A., Forwick, M., Laberg, J.S., Vorren, T.O., Larter, R.D., Graham, A.G.C., beaten, N.J., Amundsen, H.B. 2013. Arctic and Antarctic submarine gullies – A comparison of high latitude continental margins. Geomorphology. 201, 449-461.

Gales, J., Rebesco, M., De Santis, L., Bergamasco, A., Colleoni, F., Kim, S., Accettella, D., Kovacevic, V., Liu, Y., Olivo, E., Colizza, E., Florindo-Lopez, C., Zgur, F., McKay, R. 2021. Role of dense shelf water in the development of Antarctic submarine canyon morphology. Geomorphology. 372:107453, 15 pp.

Galewsky, J., Silver, E.A. 1997. Tectonic controls on facies transitions in an oblique collision: The western Solomon Sea, Papua New Guinea. Geol. Soc. Am. Bull. 109 (10), 1266-1278.

Galloway, W.E. 1975. Process framework for describing the morphologic and stratigaphic evolution of deltaic depositional systems. In: Broussard, M.L. (ed) Deltas: Models for Exploration. Houston, Texas, U.S.A. pp. 87-98.

Gamberi, F., Rovere, M., Marani, M.P., Dykstra, M. 2015. Modern submarine canyon feeder-system and deep-sea fan growth in a tectonically active margin (northern Sicily). Geosphere. 11 (2), 307-319.

Gardner, J.V., Dartnell, P., Mayer, L.A., Hughes Clarke, J.E. 2003. Mar. Environ. Res. 56, 15-46.

Gardner, J.V., Dartnell, P., Mayer, L.A., Hughes Clarke, J.E., Calder, B.R., Duffy, G. 2005. Shelf-edge deltas and drowned barrier-island complexes on the northwest Florida outer continental shelf. Geomorphology. 64, 133-166.

Gardner, J.V., Calder, B.R., Hughes Clarke, J.E., Mayer, L.A., Elston, G., Rzhanov, Y. 2007. Drowned shelf-edge deltas, barrier islands and related features along the outer continental shelf north of the head of De Soto Canyon, NE Gulf of Mexico. Geomorphology. 89, 370-390.

Gardner, W.D., Glover, L.K., Hollister, C.D. 1980. Canyons off Northwest Puerto Rico: studies of their origin and maintenance with the nuclear research submarine NR-1. Mar. Geol. 37, 41-70.

Gaudin, M., Berné, S., Jouanneau, J.-M., Palanques, A., Puig, P., Mulder, T., Cirac, P., Rabineau, M., Imbert, P. 2006. Massive sand beds attributed to deposition by dense water cascades in the Bourcart canyon head, Gulf of Lions (northwestern Mediterranean Sea). Mar. Geol. 234, 111-128.

Gervais, A., Mulder, T., Savoye, B., Gonthier, E. 2006. Sediment distribution and evolution of sedimentary processes in a small sandy turbidite system (Golo system, Mediterranean Sea): implications for various geometries based on core framework. Geo-Mar. Lett. 26, 373-395.

Gervais, A., Savoye, B., Piper, D.J.W., Mulder, T., Cremer, M., Pichevin, L. 2004. Present morphology and depositional architecture of a sandy confined submarine system: the Golo turbidite system (eastern margin of Corsica). In: Lomas, S.A., Joseph, P. (eds) Confined Turbidite Systems. Geol. Soc. London Spec. Publ. 222, 59-89.

Gillis, E., Wright, R., Mitchell, V., Montevecchi, N. 2020. Definition of the Churchill River Delta and its petroleum potential, offshore Labrador, Canada. Interpretation. 8 (2), 14 pp.

Gnibidenko, H.S., Svarichevskaya, L.V. 1984. The submarine canyons of Kamchatka. Mar. Geol. 54, 277-307.

Goldfinger, C., Nelson, C.H., Morey, A.E., Johnson, J.R., Patton, J., Karabanov, E., Gutiérrez-Pastor, J., Eriksson, A.T., Gracia, E., Dunhill, G., Enkin, R.J., Dallimore, A. Vallier, T. 2012. Turbidite event history – Methods and implications for Holocene paleoseismicity of the Cascadia subduction zone. U.S. Geol. Surv. Prof. Paper 1661-F, 170 pp.

Gómez-Ballesteros, M., Druet, M., Muñoz, A., Arrese, B., Rivera, J., Sánchez, F., Cristobo, J., Parra, S., García-Alegre, A., González-Pola, C., Gallastegui, J., Acosta, J. 2014. Geomorphology of the Avilés Canyon System, Cantabrian Sea (Bay of Biscay). Deep Sea Res. Part II Top. Stud. Oceanogr. 106, 99-117.

Gomis-Cartesio, L.E., Potayos-Moré, M., Flint, S.S., Hodgson, D.M., Brunt, R.L., DeV. Wickens, H. 2017. In: Hampson, G.J., Reynolds, A.D., Kostic, B., Wells, M.R. (eds) Geol. Soc. London Spec. Publ. 444 (1), 393-418.

Gong, C., Steel, R.J., Wang, Y., Lin, C., Olariu, C. 2016. Grain size and transport regime at shelf edge as fundamental controls on delivery of shelf-edge sands to deepwater. Earth-Sci. Rev. 157, 32-60.

Gong, C., Li, D., Steel, R.J., Peng, Y., Xu, S., Wang, Y. 2021. Delta-to-fan source-to-sink coupling as a fundamental control on the delivery of coarse clastics to deepwater: Insights from stratigraphic forward modelling. Basin Research. 33 (6), 2960-2983.

Gong, C., Wang, Y., Pyles, D.R., Steel, R.J., Xu, S., Xu, Q., Li, D. 2015. Shelf-edge trajectories and stratal stacking patterns: Their sequence-stratigraphic significance and relation to styles of deep-water sedimentation and amount of deep-water sandstone. Am. Ass. Pet. Geol. Bull. 99 (7), 1211-1243.

Goni, G., DeMaria, M., Knaff, J., Sampson, C., Ginis, I., Bringas, F., Mavume, A., Lauer, C., Lin, I.-I., Ali, M.M., Sandery, P., Ramos-Buarque, S., Kang, K., Mehra, A., Chassignet, E., Halliwell, G. 2009. Applications of satellite-derived ocean measurements to tropical cyclone intensity forecasting. Oceanography. 22 (3),190-197.

Goodbred Jr., S.L., Kuehl, S.A. 1998. Floodplain processes in the Bengal Basin and the storage of Ganges-Brahmaputra river sediment: an accretion study using ^{137}Cs and ^{210}Pb geochronology. Sediment. Geol. 121, 239-258.

Green, A. 2011. Submarine canyons associated with alternating sediment starvation and shelf-edge wedge development. Northern KwaZulu-Natal continental margin, South Africa. Mar. Geol. 284, 114-126.

Greene, H.G., Clarke Jr., S.H., Kennedy, M.P. 1991. Tectonic evolution of submarine canyons along the California continental margin. In: Osborne, R.H. (ed) From Shoreline to Abyss: Contributions in Marine Geology in Honor of Francis Parker Shepard. SEPM Spec. Publ. 46, 231-248.

Greene, H.G., Maher, N.M., Paull, C.K. 2002. Physiography of the Monterey Bay National Marine Sanctuary and implications about continental margin development. Mar. Geol. 181, 55-82.

Greene, H.G., Vaughn Barrie, J., Brothers, D.S., Conrad, J.E., Conway, K., East. A.E., Enkin, R., Maier, K.L., Nishenko, S.P., Walton, M.A.L., Rohr, K.M.M. 2018. Slope failure and mass transport processes along the Queen Charlotte Fault Zone, western British Columbia. In: Lintern, D. G., Mosher, D. C., Moscardelli, L. G., Bobrowsky, P. T., Campbell, C., Chaytor, J. D., Clague, J. J.; Georgiopoulou, A., Lajeunesse, P., Normandeau, A., Piper, D. J. W., Scherwath, M., Stacey, C., Turmel, D. (eds) Subaqueous Mass Movements. Geol. Soc. London Spec. Publ. 477, 22 pp.

Grotzinger, J.P., Hayes, A.G., Lamb, M.P., McLennan, S.M. 2013. Sedimentary processes on Earth, Mars, Titan and Venus. In: Mackwell, S.J., Simon-Miller, A.A., Harder, J.W., Bullock, M.A. (eds) Comparative Climatology of Terrestrial Planets. Tuscon, Arizona, U.S.A. pp. 439-472.

Grotzinger, J., Beaty, D., Dromart, G., Gupta, S., Harris, M., Hurowitz, J., Kocurek, G., McLennan, S., Miliken, R., Ori, G.G., Sumner, D. 2011. Mars sedimentary geology: Key concepts and outstanding questions. Astrobiology. 11 (1), 77-87.

Ha, S., Colizza, E., Torricella, F., Langone, L., Giglio, F., Kuhn, G., Macrì, P., Khim, B.-K. 2022. Glaciomarine sediment deposition on the continental slope and rise of the central Ross Sea since the Last Glacial Maximum. Mar. Geol. 445:106752, 15 pp.

Hagen, R.A., Bergersen, D.D., Moberly, R., Coulbourn, W.T. 1994. Morphology of a large meandering submarine canyon system on the Peru-Chile forearc. Mar. Geol. 119, 7-38.

Hagen, R.A., Vergara, H., Naar, D.F. 1996. Morphology of San Antonio submarine canyon on the central Chile forearc. Mar. Geol. 129, 197-205.

Hale, R.P., Nittrouer, C.A., Liu, J.T., Keil, R.G., Ogston, A.S. 2012. Effects of a major typhoon on sediment accumulation in Fangliao Submarine Cayon, SW Taiwan. Mar. Geol. 326-328, 116-130.

Han, J., Xu, G., Li, Y., Zhuo, H. 2016. Evolutionary history and controlling factors of the shelf breaks in the Pearl River Mouth Basin, northern South China Sea. Mar. Pet. Geol. 77, 179-189.

Han, X., Li, J., Chu, F., Li, J., Yang, F. 2010. Geomorphology and tectonic interpretation of Zhujiang Submarine Canyon, in the northern South China Sea. OCEANS'10 IEEE SYDNEY, Conference. May 24-27, 2010. 4 pp.

Harders, R., Ranero, C.R., Weinrebe, W., Behrmann, J.H. 2011. Submarine slope failures along the convergent continental margin of the Middle America Trench. Geochem. Geophys. Geosys. 12 (6):Q05S32, 26 pp.

Harris, P.T., Barrie, J.V., Conway, K.W., Greene, H.G. 2014a. Hanging canyons of Haida Gwaii, British Columbia, Canada: fault-control on submarine canyon geomorphology along active continental margins. Deep Sea Res. Part II Top. Stud. Oceanogr. 104, 83-92.

Harris, P.T., Macmillan-Lawler, M. 2016. Global overview of continental shelf geomorphology based on the SRTM30_PLUS 30-Arc Second Database. In:

Finkl, C., Makowski, C. (eds) Seafloor Mapping along Continental Shelves: Research and Techniques for Visualizing Benthic Environments. Coast. Res. Library 13, 169-190.

Harris, P.T., Macmillan-Lawler, M., Rupp, J., Baker, E.K., 2014b. Geomorphology of the oceans. Mar. Geol. 352, 4-24.

Harris, P., Whiteway, T. 2011. Global distribution of large submarine canyons: Geomorphic differences between active and passive continental margins. Mar. Geol. 285, 69-86.

Hayden, A.T., Lamb, M.P., McElroy, B.J. 2021. Constraining the timespan of fluvial activity from the intermittency of sediment transport on Earth and Mars. Geophys. Res. Lett. 48, e2021GL092598, 13 pp.

Heijnen, M.S., Mienis, F., Gates, A.R., Bett, B.J., Hall, R.A., Hunt, J., Kane, I.A., Pebody, C., Huvenne, V.A.I., Soutter, E.L., Clare, M.A. 2022. Challenging the highstand-dormant paradigm for land-detached submarine canyons. Nature Communications. 13:3448, 11 pp.

Helland-Hansen, W., Sømme, T.O., Martinsen, O.J., Lunt, I. 2016. Deciphering Earth's natural hourglasses: perspectives on source-to-sink analysis. J. Sediment. Res. 86, 1008-1033.

Hemming, S.R. 2004. Heinrich events: massive late Pleistocene detritus layers of the North Atlantic and their global climate imprint. Rev. Geophys. 42 (1):RG1005, 43 pp.

Henrich, R., Cherubini, Y., Meggers, H. 2010. Climate and sea level induced turbidite activity in a canyon system offshore the hyperarid Western Sahara (Mauritania): the Timiris Canyon. Mar. Geol. 275, 178-198.

Heezen, B.C., Ewing, M. 1952. Turbidity currents and submarine slumps, and the 1929 Grand Banks earthquake. Am. J. Sci. 250, 849-873.

Hereema, C.J., Talling, P.J., Cartigny, M.J., Paull, C.K., Bailey, L., Simmons, S.M., Parsons, D.R., Clare, M.A., Gwiazda, R., Lundsten, E., Anderson, K., Maier, K.L., Xu, J.P., Sumner, E.J., Rosenberger, K., Gales, J., McGann, M., Carter, l., Pope, E., Monterey Coordinated Can-yon Experiment (CCE) Team. 2020. What determines the downstream evolution of turbidity currents? Earth Planet. Sci. Lett. 532, 116023.

Hernández-Molina, F.J., Sierro, F.J., Llave, E., Roque, C., Stow, D.A.V., Williams, T., Lofi, J., Van der Schee, M., Arnáiz, A., Ledesma, S., Rosales, C., Rodríguez-Tovar, F.J. 2016. Evolution of the gulf of Cadiz margin and

southwest Portugal contourite depositional system: Tectonic, sedimentary and paleoceanographic implications from IODP expedition 339. Mar. Geol. 377, 7-39.

Hessler, A.M., Fildani, A. 2019. Deep-sea fans: tapping into Earth's changing landscapes. J. Sediment. Res. 89 (11), 1171-1179.

Hickey, B.M. 1997. The response of a steep-sided, narrow canyon to time-variable wind forcing. J. Phys. Oceanogr. 27 (5), 697-726.

Higgins, S.A., Overeem, I., Rogers, K.G., Kalina, E.A. 2018. River linking in India: Downstream impacts on water discharge and suspended sediment transport to deltas. Elem. Sci. Anth. 6 (20), 24 pp.

Hiscott, R.N. 2003. Latest Quaternary Baram Prodelta, Northwestern Borneo. In: Sidi, F.H., Nummedal, D., Imbert, P., Darman, H., Posamentier, H.W. (eds) Tropical Deltas of Southeast Asia – Sedimentology, Stratigraphy, and Petroleum Geology. SEPM Spec. Publ. 76, 89-107.

Hizzet, J.L., Hughes Clarke, J. E., Sumner, E. J., Cartigny, M. J. B., Talling, P. J., Clare, M.A. 2018. Which triggers produce the most erosive, frequent, and longest runout turbidity currents on deltas? Geophys. Res. Lett. 45, 855-863.

Hodgson, D.M., Kane, I.A., Flint, S.S., Brunt, R.L., Ortiz-Karpf, A. 2016. Time-transgressive confinement on the slope and the progradation of basin-floor fans: implications for the sequence stratigraphy of deep-water deposits. J. Sediment. Res. 86, 73-86.

Hodgson, D.M., Peakall, J., Maier, K.L. 2022. Submarine channel mouth settings: processes, geomorphology, and deposits. Front. Earth Sci. 10:790320, 20 pp.

Hotchkiss, F.S., Wunsch, C. 1982. Internal waves in Hudson Canyon with possible geological implications. Deep-Sea Res. 29 (4a), 415-442.

Hsiung, K.-H., Kanamatsu, T., Ikehara, K., Shiraishi, K., Horng, C.-S., Usami, K. 2017. Morpho-sedimentary features and sediment dispersal systems of the southwest end of the Ryukyu Trench: a source-to-sink approach. Geo-Mar. Lett. 37, 561-577.

Hsiung, K.-H., Yu, H.-S. 2011. Morpho-sedimentary evidence for a canyon-channel-trench interconnection along the Taiwan-Luzon plate margin, South China Sea. Geo-Mar. Lett. 31, 215-226.

Hsiung, K.-H., Yu, H.-S., Chiang, C.-S. 2014. Seismic characteristics, morphology and formation of the ponded Fangliao Fan off southwestern Taiwan, northern South China Sea. Geo-Mar. Lett. 34, 59-74.

Hsiung, K.-H., Yu, H.-S., Chiang, C.-S. 2018. The modern Kaoping transient fan offshore SW Taiwan: morphotectonics and development. Geomorphology. 300, 151-163.

Hsu, S.-K., Kuo, J., Lo, C.-L., Tsai, C.-H., Doo, W.-B., Ku, C.-Y., Sibuet, J.-C. 2008. Turbidity currents, submarine landslides and the 2006 Pingtung earthquake off SW Taiwan. Terr. Atmos. Ocean. Sci. 19 (6), 767-772.

Huang, Z., Nichol, S.L., Harris, P.T., Caley, M.J. 2014. Classification of submarine canyons of the Australian continental margin. Mar. Geol. 357, 362-383.

Hudec, M.R., Jackson, M.P.A. 2007. Terra infirma: understanding salt tectonics. Earth-Sci. Rev. 82, 1-28.

Huhn, K., Paul, A., Seyferth, M. 2007. Modeling sediment transport patterns during an upwelling event. J. Geophys. Res. 112:C10003, 14 pp.

Hutton, E.W.H., Syvitski, J.P.M., Watts, A.B. 2013. Isostatic flexure of a finite slope due to sea-level rise and fall. Comput. Geosci. 53, 58-68.

Iglesias, O., Lastras, G., Souto, C., Costa, S., Canals, M. 2014. Effects of coastal submarine canyons on tsunami propagation and impact. Mar. Geol. 350, 39-51.

Ingersoll, R.V. 2012. Chapter 1: Tectonics of sedimentary basins, with revised nomenclature. In: Busby, C., Azor, A. (eds) Tectonics of Sedimentary Basin: Recent Advances. Blackwell Publishing, Oxford, U.K. pp. 3-43.

Inman, D., Nordstrom, C. 1971. On the tectonic and morphologic classification of coasts. J. Geol. 79 (1),1-21.

Itoh, M., Pickart, R.S., Kikuchi, T., Fukamachi, Y., Oshima, K.I., Simizu, D., Arrigo, K.R., Vagle, S., He, J., Ashjian, C., Mathis, J.T., Nishino, S., Nobre, C. Water properties, heat and volume fluxes of Pacific water in Barrow Canyon during summer 2010. Deep Sea Res. Part I Oceanogr. Res. Pap. 102, 43-54.

Jimoh, R.O., Tang, Y., Li, J., Awosika, L.F., Li, H., Akinnigbage, E.A., Adeleye, A.O. 2018. The architecture of the lower parts of submarine

canyons on the western Nigerian continental margin. Acta Oceanol. Sin. 37 (7), 28-40.

Jipa, D.C., Panin, N. 2020. Narrow shelf canyons vs. wide shelf canyons: Two distinct types of Black Sea submarine canyons. Quat. Int. 540, 120-136.

Jobe, Z.R., Lowe, D.R., Uchytil, S.J. 2011. Two fundamentally different types of submarine canyons along the continental margin of Equatorial Guinea. Mar. Pet. Geol. 28, 843-860.

Johnson, S.Y., Hartwell, S.R., Sorlien, C.C., Dartnell, P., Ritchie, A.C. 2017. Shelf evolution along a transpressive transform margin, Santa Barbara Channel, California. Geosphere. 13 (6), 2041-2077.

Jordi, A., Klinck, J.M., Basterretxea, Orfila, A., Tintoré, J. 2008. Estimation of shelf-slope exchanges induced by frontal instability near submarine canyons. J. Geophys. Res. 113:C05016, 10 pp.

Ju, Y., Wang, G., Li, S., Sun, Y., Suo, Y., Somerville, I., Li, W., He, B., Zheng, M., Yu, K. 2022. Geodynamic mechanism and classification of basins in the Earth system. Gondwana Res. 102, 200-228.

Kagami, H., Kuramochi, H., Shima, Y. 1991. Submarine canyons in the Bellinghausen and Riiser-Larsen Seas around Antarctica. Proc. NIPR Symp. Antarct. Geosc. 5, 84-98.

Katz, O., Hamiel, Y. The nature of small to medium earthquakes along the Eastern Mediterranean passive continental margins, and their possible relationships to landslides and submarine salt-tectonic-related shallow faults. 2018. In: Lintern, D.G., Mosher, D.C., Moscardelli, L.G., Bobrowsky, P.T., Campbell, C., Chaytor, J.D., Clague, J.J., Georgiopoulou, A., Lajeunesse, P., Normandeau, A., Piper, D.J.W., Scherwath, M., Stacey, C., Turmel, D. (eds) Subaqueous Mass Movements. Geol. Soc. London Spec. Publ. 477, 8 pp.

Khripounoff, A., Crassous, P., Bue, N.L., Dennielou, B., Jacinto, R.S. (2012). Different types of sediment gravity flows detected in the Var submarine canyon (northwestern Mediterranean Sea). Progr. Oceanogr. 106, 138-153.

Kim, Y., Kim, W., Cheong, D., Muto, T., Pyles, D.R. 2013. Piping coarse-grained sediment to a deep water fan through a shelf-edge delta bypass channel: Tank experiments. J. Geophys. Res. Earth Surf. 118, 2279-2291.

King, E.V., Conley, D.C., Masselink, G., Leonardi, N., McCarroll, Scott, T. 2019. The impact of waves and tides on residual sand transport on a

sediment-poor, energetic, and macrotidal continental shelf. J. Geophys. Res: Oceans. 124, 4974-5002.

Klaus, A., Taylor, B. 1991. Submarine canyon development in the Izu-Bonin Forearc: a SeaMARC II and seismic survey of Aoga Shima Canyon. Mar. Geophys. Res. 13, 131-152.

Kober, F., Zeilinger, G., Hippe, K., Marc, O., Lendzioch, T., Grischott, R., Christl, M., Kubik, P.W., Zola, R. 2015. Tectonic and lithological controls on denudation rates in the central Bolivian Andes. Tectonophysics. 657, 230-244.

Kolla, V., Biondi, P., Long, B., Fillon, R. 2000. Sequence stratigraphy and architecture od the late Pleistocene Lagniappe delta complex, northeast Gulf of Mexico. In: Hunt, D., Gawthorpe, R.L. (eds) Sedimentary Responses to Forced Regressions. Geol. Soc. London Spec. Publ. 172, 291-327.

Krastel, S., Hanebuth, T.J.J., Antobreh, A.A., Henrich, R., Holz, C., Kölling, M., Schulz, H.D., Wien, K. Eos Trans. Am. Geophys. Union. 85(42), 417-432.

Krastel, S., Wefer, G., Hanebuth, T.J.J., Antobreh, A.A., Freudenthal, T., Preu, B., Schwenk, T., Strasser, M., Violante, R., Winkelmann, D., M78/3 shipboard scientific party. 2011. Sediment dynamics and geohazards off Uruguay and the de la Plata River region (northern Argentina and Uruguay). Geo-Mar. Lett. 31, 271-283.

Kuehl, S.A., Alexander, C.R., Blair, N.E., Harris, C.K., Marsaglia, K.M., Ogston, A.S., Orpin, A.R., Roering, J.J., Bever, A.J., Bilderback, E.L., Carter, L., Cerovski-Darriau, C., Childress, L.B., Corbett, D.R., Hale, R.P., Leithold, E.L., Litchfield, N., Moriarty, J.M., Page, M.J., Pierce, L.E.R., Upton, P., Walsh, J.P. 2016. A source-to-sink perspective of the Waipaoa River margin. Earth-Sci. Rev. 153, 301-334.

Lai, S.Y.J., Gerber, T.P., Amblas, D. 2016. An experimental approach to submarine canyon evolution. Geophys. Res. Lett. 43, 2741-2747.

Langbein, W.B., Schumm, S.A. 1958. Yield of sediment in relation to mean annual precipitation. Trans.-Am. Geophys. Union. 39 (6), 1076-1084.

Lapôtre, M.G.A., Malaska, M.J., Cable, M.L. 2022. The role of seasonal sediment transport and sintering in shaping Titan’s landscapes: A hypothesis. Geophys. Res. Lett. 49, e2021GL097605. 10 pp.

Lastras, G., Acosta, J., Muñoz, A., canals, M. 2011a. Submarine canyon formation and evolution in the Argentine Continental Margin between 44°30'S and 48°S. Geomorphology. 128, 116-136.

Lastras, G., Canals, M., Amblas, D., Lavoie, C., Church, I., De mol, B., Duran, R., Calafat, A.M., Hughes-Clarke, J.E., Smith, C.J., Heussner, S., "Euroléon" cruise shipboard party. 2011b. Understanding sediment dynamics of two large submarine valleys from seafloor data: Blanes and La Fonera canyons, northwestern Mediterranean Sea. Mar. Geol. 280, 20-39.

Lastras, G., Arzola, R.G., Masson, D.G., Wynn, R.B., Huvenne, V.A.I., Hühnerbach, V., Canals, M. 2009. Geomorphology and sedimentary features in the Central Portuguese submarine canyons, Western Iberian margin. Geomorphology. 103, 310-329.

Lastras, G., Canals, M., Urgeles, R., Amblas, D., Ivanov, M., Droz, L., Dennielou, B., Fabrés, J., Schoolmeester, T., Akhmetzhanov, A., Orange, D., García-García. 2007. A walk down the Cap de Creus canyon, Northwestern Mediterranean Sea: Recent processes inferred from morphology and sediment bedforms. Mar. Geol. 246, 176-192.

Laugier, F.J., Plink-Björklund, P. 2016. Defining the shelf edge and the three-dimensional shelf edge to slope facies variability in shelf-edge deltas. Sedimentology. 63, 1280-1320.

Laursen, J., Normark, W.R. 2002. Late Quaternary evolution of the San Antonio Submarine Canyon in the central Chile forearc (~33°S). 2002. Mar. Geol. 188, 365-390.

Le Bas, T.P., Masson, R., D.G., Holtom, R.T., Grevemeyer, I. 2007. Slope failures of the flanks of the Southern Cape Verde Islands. In: Lykousis V., Sakellariou D., Locat J. (eds) Submarine Mass Movements and Their Consequences. Advances in Natural and Technological Hazards Research, 27, 337-345.

Le Dantec, N., Hogarth, L.J., Driscoll, N.W., Babcock, J.M., Barnhardt, W.A., Schwab, W.C. 2010. Tectonic controls on nearshore sediment accumulation and submarine canyon morphology offshore La Jolla, Southern California. Mar. Geol. 268, 115-128.

Lee, G.H., Watkins, J.S., Bryant, W.R. 1996. Bryant Canyon Fan System: An unconfined, large river-sourced system in the Northwestern Gulf of Mexico. Am. Ass. Pet. Geol. Bull. 80 (3), 340-357.

Lee, I.H., Liu, J.T., Chuang, W.-S., Xu, J. 2009. Internal tidal currents in the Gaoping (Kaoping) Submarine Canyon. J. Mar. Sys. 76, 397-404.

Lewis, K.B., Barnes, P.M. 1999. Kaikoura Canyon, New Zealand: active conduit from near-shore sediment zones to trench-axis channel. Mar. Geol. 162, 39-69.

Li, A., Cai, F., Wu, N., Li, Q., Yan, G., Sun, Y., Dong, G., Luo, D. 2020a. Late Pleistocene shelf-edge delta clinoforms along the rift margin of the northern Okinawa Trough. Geol. J. 55 (9), 6450-6461.

Li, M.Z., Prescott, R.H., Robertson, A.G. 2019. Observation of internal tides and sediment transport processes at the head of Logan Canyon on central Scotian Slope, eastern Canada. J. Mar. Syst. 193, 103-125.

Li, S., Alves, T.M., Li, W., Wang, X., Rebesco, M., Li, J., Zhao, F., Yu, K., Wu, S. 2022. Morphology and evolution of submarine canyons on the northwest South China Sea margin. Mar. Geol. 443:106695, 12 pp.

Li, T., Wang, S., Liu, Y., Fu, B., Gao, D. 2020b. Reversal of the sediment load increase in the Amazon basin influenced by divergent trends of sediment transport from the Solimões and Madeira Rivers. Catena. 195:104804, 9 pp.

Li, W., Li, S., Alves, T.M., Rebesco, M., Feng, Y. 2021. The role of sediment gravity flows on the morphological development of a large submarine canyon (Taiwan Canyon), north-east South China Sea. Sedimentology. 68, 1091-1108.

Liu, B.Q., Shao, L.-Y., Wang, X.-T., Li, Y.-N., Xu, J. 2019. Application of channel-belt scaling relationship to Middle Jurassic source-to-sink system in the Saishiteng area of the northern Qaidam Basin, NW China. J. Palaeogeogr. 8:16, 17 pp.

Liu, H., Meng, J., Zhang, Y., Yang, L. 2018. Pliocene seismic stratigraphy and deep-water sedimentation in the Qiongdongnan Basin, South China Sea: Source-to-sink systems and hydrocarbon accumulation significance. 2018. Geol. J. 54, 392-408.

Liu, J.T., Hsu, R.T., Hung, J.-J., Chang, Y.-P., Wang, Y.-H., Rendle-Bühring, R.H., Lee, C.-L., Huh, C.-A., Yang, R.J. 2016. From the highest to the deepest: The Gaoping River-Gaoping Submarine Canyon dispersal system Earth-Sci. Rev. 153, 274-300.

Liu, J.T., Kao, S.-J., Huh, C.-A., Hung, C.-C. 2013. Gravity flows associated with flood events and carbon burial: Taiwan as instructional source area. Annu. Rev. Mar. Sci. 5, 47-68.

Liu, J.T., Yin, H.-L. 2004. Sediment dynamics in a submarine canyon: a case of river-sea interaction. Mar. Geol. 207, 55-81.

Lo Iacono, C., Sulli, A., Agate, M. 2014. Submarine canyons of north-western Sicily (Southern Tyrrhenian Sea): variability in morphology, sedimentary processes and evolution on a tectonically active margin. Deep Sea Res. Part II Top. Stud. Oceanogr. 104, 93-105.

Lo Iacono, C., Sulli, A., Agate, M., Lo Presti, V., Pepe, F., Catalano, R. 2011. Submarine canyon morphologies in the Gulf of Palermo (Southern Tyrrhenian Sea) and possible implications for geo-hazard. Mar. Geophys. Res. 32, 127-138.

Lopez-Fernandez, P., Calafat, A., Sanchez-Vidal, A., Canals, M., Flexas, M.M., Cateura, J., Company, J.B. 2013. Multiple drivers of particle fluxes in the Blanes submarine canyon and southern open slope: results of a year round experiment. Prog. Oceanogr. 118, 95-107.

Lore, G.L., Ross, K.M., Bascle, B.J., Nixon, L.D., Klazynski, R.J. 1999. Assessment of conventionally recoverable hydrocarbon resources of the Gulf of Mexico and Atlantic outer continental shelf. OCS Report MMS 99-0034. New Orleans, U.S.A. 186 pp.

Maier, K.L., Johnson, S.Y., Hart, P. 2018. Controls on submarine canyon head evolution: Monterey Canyon, offshore central California. Mar. Geol. 404, 24-40.

Maier, K.L., Rosenberger, K.J., Paull, C.K., Gwiazda, R., Gales, J., Lorenson, T., Barry, J.P., Talling, P.J., McGann, M., Xu, Jingping, X., Lundsten, E., Anderson, K., Litvin, S.Y., Parsons, D.R., Clare, M.A., Simmons, S.M., Sumner, E.J., Cartigny, M.J.B. 2019. Sediment and organic carbon transport and deposition driven by internal tides along Monterey Canyon, offshore California. Deep Sea Res. Part I Oceanogr. Res. Pap. 153:103108, 21 pp.

Marchès, E., Mulder, T., Cremer, M., Bonnel, C., Hanquiez, V., Gonthier, E., Lecroart, P. 2007. Contourite drift construction influenced by capture of Mediterranean Outflow Water deep-sea current by the Portimão submarine canyon (Gulf of Cadiz, South Portugal). Mar. Geol. 242, 247-260.

Mart, Y. 1989. Sediment distribution in Akhziv Canyon off Northern Israel. Geo-Mar. Lett. 9, 77-83.

Martín, J., Palanques, A., Puig, P. 2006. Composition and variability of downward particulate matter fluxes in the Palamós submarine canyon (NW Mediterranean). J. Mar. Syst. 60, 75-97.

Martinsen, O.J. 2005. Deep-water sedimentary systems of Arctic and North Atlantic margins: An introduction. Nor. J. Geol. 85, 261-266.

Martinsen, O.J., Sømme, T.O., Thurmond, J.B., Helland-Hansen, W., Lunt, I. 2010. Source-to-sink systems on passive margins: theory and practice with an example from the Norwegian continental margin. In: Vining, B.A., Pickering, S.C. (eds) Petroleum Geology: From Mature Basins to New Frontiers – Proceedings of the 7th Petroleum Geology Conference 7, 913-920.

Matos, F.L., Ross, S.W., Huvenne, V.A.I., Davies, J.S., Cunha, M.R. 2018. Canyons pride and prejudice: Exploring the submarine canyon research landscape, a history of geographic and thematic bias. Prog. Oceanogr. 169, 6-19.

Mauffrey, M.A., Berné, S., Jouet, G., Giresse, P., Gaudin, M. 2015. Sea-level control on the connection between shelf-edge deltas and the Bourcart canyon head (western Mediterranean) during the last glacial/interglacial cycle. Mar. Geol. 370, 1-19.

Mauffrey, M.-A., Urgeles, R., Berné, S., Canning, J. 2017. Development of submarine canyons after the Mid-Pleistocene transition on the Ebro margin, NW Mediterranean: The role of fluvial connections. Quat. Sci. Rev. 158, 77-93.

May, J.A., Warme, J.E., Slater, R.A. 1983. Role of submarine canyons on shelfbreak erosion and sedimentation: Modern and ancient examples. In: Stanley, D.J., Moore, G.T. The Shelfbreak: Critical Interface on Continental Margins. SEPM Spec. Publ. 33, 315-332.

Mayall, M.J., Yeilding, C.A., Oldroyd, J.D., Pulham, A.J. 6 Sakurai, S. 1992. Facies in a shelf-edge delta – An example from the subsurface of the Gulf of Mexico, Middle Pliocene, Mississippi Canyon, Block 109. Am. Assoc. Pet. Geol. Bull. 76 (4), 435-448.

Mazières, A., Gillet, H., Castelle, B., Mulder, T., Guyot, C., Garlan, T., Mallet, C. 2014. High-resolution morphobathymetric analysis and evolution of

Capbreton submarine canyon head (Southeast Bay of Biscay—French Atlantic Coast) over the last decade using descriptive and numerical modelling. Mar. Geol. 351, 1-12.

McArthur, A.D., Tek, D.E. 2021. Controls on the origin and evolution of deep-ocean trench-axial channels. Geology. 49 (8), 883-888.

McCarroll, R.J., Masselink, G., Wiggins, M., Scott, T., Billson, O., Conley, D.C., Valiente, N.G. 2019. High-efficiency gravel longshore sediment transport and headland bypassing over an extreme wave event. Earth Surf. Process. Landforms. 44, 2720-2727.

McGregor, B.A. 1983. Submarine canyon and slope processes on the U.S. Atlantic continental margin. Open-File Report 83-735. U.S. Geological Survey. 34 pp.

McHargue, T., Pyrcz, M.J., Sullivan, M.D., Clark, J.D., Fildani, A., Romans, B.W., Covault, J.A., Levy, M., Posamentier, H.W., Drinkwater, N.J. 2011. Architecture of turbidite channel systems on the continental slope: patterns and predictions. Mar. Pet. Geol. 28, 728-743.

McLennan, S.M., Grotzinger, J.P., Hurowitz, J.A., Tosca, N.J. 2019. The sedimentary cycle on Early Mars. Annu. Rev. Earth Planet. Sci. 47, 91-118.

McMaster, R.L., De Boer, J., Ashraf, A. 1970a. Magnetic and seismic reflection studies on continental shelf off Portuguese Guinea, Guinea, and Sierra Leone, West Africa. Am. Assoc. Pet. Geol. Bull. 54 (1), 158-167.

McMaster, R.L., Lachance, T.P., Ashraf, A. 1970b. Continental shelf geomorphic features off Portuguese Guinea, Guinea, and Sierra Leone (West Africa). Mar. Geol. 9, 203-213.

McMaster, R.L., Milliman, J.D., Ashraf, A. 1971. Continental shelf and upper slope sediments off Portuguese Guinea, Guinea, and Sierra Leone, West Africa. J. Sed. Pet. 41 (1), 150-158.

Meade, R.H., 1972. Transport and deposition of sediments in estuaries. In: Nelson, B.C. (ed) Environmental Framework of Coastal Plain Estuaries: Geological Society of America, Memoir 133, 91-120.

Meade, R.H. 1982. Sources, sinks, and storage of river sediment in the Atlantic drainage of the United States: J. Geol. 90, 235-252.

Mellere, D., Breda, A., Steel, R. 2003. Fluvially incised shelf-edge deltas and linkages to upper slope channels (Central Tertiary Basin). In: Roberts, H.H.,

Rosen, N.C., Fillon, R.H., Anderson, J.B. Shelf Margin Deltas and Linked Down Slope Petroleum Systems – Global Significance and Future Exploration Potential. SEPM Spec. Publ. 23, 231-266.

Mencaroni, D., Urgeles, R., Camerlenghi, A., Llopart, J., Ford, J., Sanchez Serra, C., Meservy, W., Gràcia, E., Rebesco, M., Zitellini, N. 2021. A mixed turbidite-contourite system related to a major submarine canyon: The Marquês de Pombal Drift (south-west Iberian margin). Sedimentology. 68 (5), 2069-2096.

Micallef, A., Mountjoy, J.J., Barnes, P.M., Canals, M., Lastras, G. 2014. Geomorphic response of submarine canyons to tectonic activity: insights from the Cook Strait canyon system, New Zealand. Geosphere. 10 (5), 905-929.

Michaud, F., Proust, J.N., Collot, J.Y., Lebrun, J.F., Witt, C., Ratzov, G., Pouderoux, H., Martillo, C., Hernández, M.J., loayza, G., Penafiel, L., Schenini, L., Dano, A., Gonzalez, M., Barba, D., De Min, L., Ponce, G., Urresta, A., Calderon, M. 2015. Quaternary sedimentation and active faulting along the Ecuadorian shelf: preliminary results of the ATACAMES Cruise (2012). Mar. Geophys. Res. 36, 81-98.

Milia, A. 2000. The Dohrn Canyon: a response to the eustatic fall and tectonic uplift of the outer shelf along the eastern Tyrrhenian Sea margin, Italy. Geo-Mar. Lett. 20, 101-108.

Milliman, J., Farnsworth, K. 2011. River Discharge to the Coastal Ocean: A Global Synthesis. Cambridge University Press, Cambridge, U.K. 384 pp.

Milliman, J.D., Kao, S.-J. 2005. Hyperpycnal discharge of fluvial sediment to the ocean: impact of super-typhoon Herb (1996) on Taiwanese rivers. J. Geol. 113, 503-516.

Milliman, J.D., Syvitski, P.M. 1992. Geomorphic/tectonic control of sediment discharge to the ocean: the importance of small mountainous rivers. J. Geol. 100, 525-544.

Mitchell, J.K., Holdgate, G.R., Wallace, M.W., Gallagher, S.J. 2007. Marine geology of the Quaternary Bass Canyon system, southeast Australia: a cool-water carbonate system. Mar. Geol. 237, 71-96.

Moeck, I. 2014. Catalog of geothermal play types based on geologic controls. Renew. Sustain. Energ. Rev. 37, 867-882.

Molenaar, A., Moernaut, J., Wiemer, G., Dubois, N., Strasser, M. 2019. Earthquake impact on active margins: tracing surficial remobilization and seismic strengthening in a slope sedimentary sequence. Geophys. Res. Lett. 46, 6015-6023.

Mondziel, S., Grindlay, N., Mann, P., Escalona, A., Abrams, L. 2010. Morphology, structure, and tectonic evolution of the Mona canyon (northern Mona passage) from multibeam bathymetry, side-scan sonar, and seismic reflection profiles. Tectonics. 29:TC2003, 23 pp.

Moore, G.T. 1969. Interaction of rivers and oceans – Pleistocene petroleum potential. Am. Assoc. Pet. Geol. Bull. 53 (12), 2421-2430.

Morrison, A.K., Hogg, A. McC., England, M.H., Spence, P., 2020. Warm circumpolar deep water transport toward Antarctica driven by local dense water exports in canyons. Sci. Adv. 6:eaav2516, 9 pp.

Morton, R.A., Suter, J.R. 1996. Sequence stratigraphy and composition of late Quaternary shelf-margin deltas, Northern Gulf of Mexico. Geol. Soc. Am. Bull. 80 (4), 505-530.

Moscardelli, L., Ochoa, J., Lunt, I., Zahm, L. 2019. Mixed siliciclastic-carbonate systems and their impact for the development of deep-water turbidites in continental margins: A case study from the Late Jurassic to Early Cretaceous Shelburne subbasin in offshore Nova Scotia. Am. Assoc. Pet. Geol. Bull. 103 (10), 2487-2520.

Mougenot, D., Boillot, G., Rehault, J.-P. 1983. Prograding shelfbreak types on passive continental margins: some European examples. In: Stanley, D.J., Moore, G.T. (eds) The Shelfbreak: Critical Interface on Continental Margins. SEPM Spec. Publ. 33, 25-39.

Mountjoy, J.J., Barnes, P.M., Pettinga, J.R. 2009. Morphostructure and evolution of submarine canyons across an active margin: Cook Strait sector of the Hikurangi Margin, New Zealand. Mar. Geol. 260, 45-68.

Mountjoy, J.J., Micallef, A., Stevens, C.L., Stirling, M.W. 2014. Holocene sedimentary activity in a non-terrestrially coupled submarine canyon: Cook Strait Canyon system, New Zealand. Deep Sea Res. Part II Top. Stud. Oceanogr. 104, 120-133.

Mountjoy, J.J., Howarth, J.D., Orpin, A.R., Barnes, P.M., Bowden, D.A., Rowden, A.A., Schimel, A.C.G., Holden, C., Horgan, H.J., Nodder, S.D., Patton, J.R., Lamarche, G., Gerstenberger, M., Micallef, A., Pallentin, A.,

Kane, T. 2018. Earthquakes drive large-scale submarine canyon development and sediment supply to deep-ocean basins. Sci. Adv. 4 (3):eaar3748, 8 pp.

Muhammed, N.S., Haq, B., Al Shehri, D., Al-Ahmed, A., Rahman, M.M., Zaman, E. 2022. A review on underground hydrogen storage: Insight into geological sites, influencing factors and future outlook. Energ. Rep. 8, 461-499.

Mulder, T., Ducassou, E., Gillet, H., Hanquiez, V., Tournadour, E., Combes, J., Eberli, G.P., Kindler, P., Gonthier, E., Conesa, G., Robin, C., Sianipar, R., Reijmer, J.J.G., François, A. 2012. Canyon morphology on a modern carbonate slope of the Bahamas: evidence of regional tectonic tilting. Geology. 40 (9), 771-774.

Mulder, T., Lecroart, P., Hanquiez, V., Marches, E., Gonthier, E., Guedes, J.-C., Thiébot, E., Jaaidi, B., Kenyon, N., Voisset, M., Perez, C., Sayago, M., Fuchey, Y., Bujan, S. 2006. Geo-Mar. Lett. 26 (1), 31-41.

Mulder, T., Moran, K. 1995. Relationship among submarine instabilities, sea level variations, and the presence of an ice sheet on the continental shelf: an example from the Verrill Canyon Area, Scotian Shelf. Paleoceanography. 1995. 10 (1), 137-154.

Mulder, T., Syvitski, J.P.M. 1995. Turbidity currents generated at river mouths during exceptional discharges to the World oceans. J. Geol. 103, 285-299.

Mulder, T., Syvitski, J.P.M., Migeon, S., Faugères, J.-C., Savoye, B. 2003. Marine hyperpycnal flows: initiation, behavior and related deposits. A review. Mar. Pet. Geol. 20, 861-882.

Mulder, T., Zaragosi, S., Garlan, T., Mavel, J., Cremer, M., Sottolichio, A., Sénéchal, N., Schmidt, S. 2012. Present deep-submarine canyons activity in the Bay of Biscay (NE Atlantic). Mar. Geol. 295-298, 113-127.

Nelson, C.H., Carlson, P.R., Byrne, J.V., Alpha, T.R. 1970. Development of the Astoria Canyon-Fan physiography and comparison with similar systems. Mar. Geol. 8, 259-291.

Nelson, C.H., Escutia, C., Damuth, J.E., Twichell Jr., D.C. 2011. Interplay of mass-transport and turbidite-system deposits in different active tectonic and passive continental margin settings: external and local controlling factors. In:

Shipp, R.C., Weimer, P., Posamentier, H.W. (eds) Mass-Transport Deposits in Deepwater Settings. SEPM Spec. Publ. 96, 39-66.

Nienhuis, J.H., Ashton, A.D., Edmonds, D.A., Hoitink, A.J.F., Kettner, A.J., Rowland, J.C., Törnqvist, T.E. 2020. Global-scale human impact on delta morphology has led to net land area gain. Nature. 577, 514-518.

Nittrouer, C.A., Wright, L.D. 1994. Transport of particles across continental shelves. Rev. Geophys. 32 (1), 85-113.

Noda, A., TuZino, T., Furukawa, R., Joshima, M., Uchida, J. 2008. Physiographical and sedimentological characteristics of submarine canyons developed upon an active forearc slope: the Kushiro Submarine Canyon, northern Japan. Geol. Soc. Am. Bull. 120 (5/6), 750-767.

Noda, A., TuZino, T. 2010. Shelf-slope sedimentation during the late Quaternary on the southwestern Kuril forearc margin, northern Japan. Sediment. Geol. 232, 35-51.

Normark, W.R., Barnes, N.E., Coumes, F. 1983. Rhône Deep-Sea Fan: A review. Geo. Mar. Lett. 3, 155-160.

Normark, W.R., Carlson, P.R. 2003. Giant submarine canyons: Is size any clue to their importance in the rock record? In: Chan, M.A., Archer, A.W. (eds) Extreme depositional environments: Mega end members in geologic time. 370, 175-190.

Normark, W.R., Piper, D.J.W., Romans, B.W., Covault, J.A., Dartnell, P., Sliter, R.W. 2009. Submarine canyon and fan systems of the California Continental Borderland. In: Lee, H.J., Normark, W.R. (eds) Earth Science in the Urban Ocean: The Southern California Continental Borderland. Spec. Paper Geol. Soc. Am. 454, 141-168.

Normark, W.R., Posamentier, H., Mutti, E. 1993. Turbidite systems: State of the art and future directions. Rev. Geophys. 31 (2), 91-116.

Nyberg, B., Gawthorpe, R.L., Helland-Hansen, W. 2018a. The distribution of rivers to terrestrial sinks: Implications for sediment routing systems. Geomorphology. 316, 1-23.

Nyberg, B., Helland-Hansen, W., Gawthorpe, R.L., Sandbakken, P., Eide, C.H., Sømme, T., Hadler-Jacobsen, F., Leiknes, S. 2018b. Revisiting morphological relationships of modern source-to-sink segments as a first-order approach to scale ancient sedimentary systems. Sediment. Geol. 373, 111-133.

Oiwane, H., Tonai, S., Kiyokawa, S., Nakamura, Y., Suganuma, Y., Tokuyama, H. 2011. Geomorphological development of the Goto Submarine Canyon, northeastern East China Sea. Mar. Geol. 288, 49-60.

Olariu, M.I., Ambrose, W.A. 2016. Process regime variability across growth faults in the Paleogene Lower Wilcox Guadalupe Delta, South Texas Gulf Coast. Sed. Geol. 341, 27-49.

Olavsdottir, J., Bodlreel, L.O., Andersen, M.S. 2010. Development of a shelf margin delta due to uplift of Munkagrunnur Ridge at the margin of Faroe-Shetland Basin: a seismic sequence stratigraphy study. Pet. Geosci. 16, 91-103.

Orange, D.L., Anderson, R.S., Breen, N.A. 1994. Regular canyon spacing in the submarine environment: the link between hydrology and geomorphology. GSA Today. 4 (2), 35-39.

Osmundsen, P.T., Redfield, T.F. 2011. Crustal taper and topography at passive continental margins. Terra Nova. 23 (6), 349-361.

Palanques, A., El Khatab, M., Puig, P., Masqué, P., Sánchez-Cabeza, J.A., Isla, E. 2005. Downward particle fluxes in the Guadiaro submarine canyon depositional system (north-western Alboran Sea), a river flood dominated system. Mar. Geol. 220, 23-40.

Palanques, A., Durrieu de Madron, X., Puig, P., Fabres, J. Guillén, J., Calafat, A., Canals, M., Heussner, S., Bonnin, J. 2006a. Suspended sediment fluxes and transport processes in the Gulf of Lions submarine canyons. The role of storms and dense water cascading. Mar. Geol. 234, 43-61.

Palanques, A., Martín, J., Puig, P., Guillén, J., Company, J.B., Sardá, F. 2006b. Evidence of sediment gravity flows induced by trawling in the Palamós (Fonera) submarine canyon (northwestern Mediterranean). Deep Sea Res. Part I Oceanogr. Res. Paper 53, 201-214.

Paldor, A., Katz, O., Aharonov, E., Weinstein, Y., Roditi-Elasar, M., Lazar, A., Lazar, B. 2020. Deep submarine groundwater discharge—Evidence from Achziv Submarine Canyon at the exposure of the Judea Group confined aquifer, eastern Mediterranean. J. Geophys. Res. Oceans. 125:e2019JC015435, 16 pp.

Paradis, S., Arjona-Camas, M., Goñi, M., Palanques, A., Masqué, P., Puig, P. 2022. Contrasting particle fluxes and composition in a submarine canyon

affected by natural sediment transport events and bottom trawling. Front. Mar. Sci. 9:1017052, 20 pp.

Paradis, S., Puig, P., Masqué, P., Juan-Díaz, X., Martín, J., Palanques, A. 2017. Bottom-trawling along submarine canyons impacts deep sedimentary regimes. Sci. Rep. 7:43332, 12 p.

Parra, J.G., Marsaglia, K.M., Rivera, K.S., Dawson, S.T., Walsh, J.P. 2012. Provenance of sand on the Poverty Bay shelf, the link between source and sink sectors of the Waipaoa River sedimentary system. Sediment. Geol. 280, 208-233.

Patruno, S., Hampson, G.J., Jackson, C. A.-L. 2015. Quantitative characterisation of deltaic and subaqueous clinoforms. Earth-Sci. Rev. 142, 79-119.

Patruno, S., Helland-Hansen, W. 2018. Clinoforms and clinoform systems: Review and dynamic classification scheme for shorelines, subaqueous deltas, shelf edges and continental margins. Earth-Sci. Rev. 185, 202-233.

Patsch, K., Griggs, G. 2006. Littoral cells, sand budgets, and beaches: Understanding California's shoreline. Institute of Marine Sciences, University of California, Santa Cruz. 40 pp.

Paull, C.K., Caress, D.W., Lundsten, E., Gwiazda, R., Anderson, K., McGann, M., Conrad, J., Edwards, B., Sumner, E.J. 2013. Anatomy of the La Jolla Submarine Canyon system; offshore southern California. Mar. Geol. 335, 16-34.

Paull, C.K., Talling, P.J., Maier, K.L., Parsons, D., Xu, J., Caress, D.W., Gwiazda, R., Lundsten, E.M., Anderson, K., Barry, J.P., Chaffey, M., O'Reilly, T., Rosenberger, K.J., Gales, J.A., Kieft, B., McGann, M., Simmons, S.M., McCann, M., Sumner, E.J., Clare, M.A., Cartigny, M.J. 2018. Powerful turbidity currents driven by dense basal layers. Nat. Commun. 9:4114, 9 pp.

Peakall, J., Kane, I.A., Masson, D.G., Keevil, G., McCaffrey, W., Corney, R. 2012. Global (latitudinal) variation in submarine channel sinuosity. Geology. 40 (1), 11-14.

Peakall, J., Sumner, E.J. 2015. Submarine channel flow processes and deposits: a process-product perspective. Geomorphology. 244, 95-120.

Pechlivanidou, S., Cowie, P.A., Hannisdal, B., Whittaker, A.C., Gawthorpe, R.L., Pennos, C., Riiser, O.S. 2018. Source-to-sink analysis in an active

extensional setting: Holocene erosion and deposition in the Sperchios rift, central Greece. Basin Res. 30, 522-543.

Peng, Y., Steel, R.J., Olariu, C. 2017. Transition from storm wave-dominated outer shelf to gullied upper slope: The mid-Pliocene Orinoco shelf margin, South Trinidad. Sedimentology. 64, 1511-1539.

Perov, G., Bhattacharya, J.P. 2011. Pleistocene shelf-margin delta: Intradeltaic deformation and sediment bypass, northern Gulf of Mexico. Am. Assoc. Pet. Geol. Bull. 95 (9), 1617-1641.

Peters, S.E., Loss, D.P. 2012. Storm and fair-weather wave base: a relevant distinction? Geology. 40 (6), 511-514.

Petersen, F., Hubbart, J. 2021. The occurrence and transport of microplastics: The state of the science. Sci. Total Env. 758:143936, 12 pp.

Pettinga, L., Jobe, Z., Shumaker, L., Howes, N. 2018. Morphometric scaling relationships in submarine channel-lobe systems. Geology. 46 (9), 819-822.

Peucker-Ehrenbrink, B. 2009. Land2Sea database of river drainage basin sizes, annual water discharges, and suspended sediment fluxes. Geochem. Geophys. Geosyst. 10 (6):Q06014, 10 pp.

Phillips, J.D., Slattery, M.C. 2006. Sediment storage, sea level, and sediment delivery to the ocean by coastal plain rivers. Prog. Phys. Geogr. 30 (4), 513-530.

Pico, T., Mitrovica, J.X., Braun, J., Ferrier, K.L. 2018. Glacial isostatic adjustment deflects the path of the ancestral Hudson River. Geology. 46 (7), 591-594.

Pinous, O.V., Karogodin, Y.N., Ershov, S.V., Sahagian, D.L. 1999. Sequence stratigraphy, facies, and sea level change of the Hauterivian productive complex, Priobskoe Oil Field (West Siberia). Am. Assoc. Pet. Geol. Bull. 83 (6), 972-999.

Pierau, R., Hanebuth, T.J.J., Krastel, S., Henrich, R. 2010. Late Quaternary climatic events and sea-level changes recorded by turbidite activity, Dakar Canyon, NW Africa. Quat. Res. 73, 385-392.

Pierau, R., Henrich, R., Preiß-Daimler, I., Krastel, S., Geersen, J. 2011. Sediment transport and turbidite architecture in the submarine Dakar Canyon off Senegal, NW-Africa. J. African Earth Sci. 60, 196-208.

Pierdomenico, M., Martorelli, E., Dominguez-Carrío, C., Gili, J.M., Chiocci, F.L. 2016. Seafloor characterization and benthic megafaunal distribution of an active submarine canyon and surrounding sectors: The case of Gioia Canyon (Southern Tyrrhenian Sea). J. Mar. Syst. 157, 101-117.

Pierdomenico, M., Casalbore, D., Latino Chiocci, F. 2019. Massive benthic litter funnelled to deep sea by flash-flood generated hyperpycnal flows. Sci. Rep. 9:5330, 10 pp.

Piper, D.J.W., Hiscott, R.N., Normark, W.R. 1999. Outcrop-scale acoustic facies analysis and latest Quaternary development of Hueneme and Dume submarine fans, offshore California. Sedimentology. 46, 47-78.

Piper, D.J.W., Mosher, D.C., Campbell, D.C. 2012. 9 - Controls on the distribution of major types of submarine landslides. In: Clague, J.J., Stead, D. (eds) Landslides. Types, Mechanisms and Modeling. Cambridge University Press, Cambridge, U.K. pp. 95-107.

Piper, D.J.W., Normark, W.R. 2009. Processes that initiate turbidity currents and their influence on turbidites: A marine geology perspective. J. Sediment. Res. 79, 347-362.

Pisareva, M.N., Pickart, R.S., Lin, P., Fratantoni, P.S., Weingartner, T.J. 2019. On the nature of wind-forced upwelling in Barrow Canyon. Deep Sea Res. Part II Top. Stud. Oceanogr. 162, 63-78.

Poag, C.W., Swift, B.A., Schlee, J.S., Ball, M.M., Sheetz, L.L. 1990. Early Cretaceous shelf-edge deltas of the Baltimore Canyon Trough: Principal sources for sediment gravity deposits of the northern Hatteras Basin. Geology. 18, 149-152.

Popescu, I., Lericolais, G., Panin, N., Normand, A., Dinu, C., Le Drezen, E. 2004. The Danube submarine canyon (Black Sea): morphology and sedimentary processes. Mar. Geol. 206, 249-265.

Porcile, G., Pittaluga, M.B., Frascati, A., Sequeiros, O.E. 2020. Typhoon-induced megarips as triggers of turbidity currents offshore tropical river deltas. Commun. Earth & Environ. 1 (2), 13 pp.

Porębski, S.J., Steel, R.J. 2003. Shelf-margin deltas: their stratigraphic significance and relation to deepwater sands. Earth-Sci. Rev. 62, 283-326.

Porębski, S.J., Steel, R.J. 2006. Deltas and sea-level change. J. Sediment. Res. 76, 390-403.

Posamentier, H. W., Erskine, R. D., Mitchum, R. M., Jr. 1991. Models for submarine-fan deposition within a sequence-stratigraphic framework, in: Weimer, P., Link, M. H. (eds) Seismic facies and sedimentary processes of submarine fans and turbidite systems. Frontiers in Sedimentary Geology. Springer, New York. pp. 127-136.

Posamentier, H.W. 2003. A linked shelf-edge delta and slope-channel turbidite system: 3D seismic case study from the Eastern Gulf of Mexico. In: Roberts, H.H., Rosen, N.C., Fillon, R.H., Anderson, J.B. Shelf Margin Deltas and Linked Down Slope Petroleum Systems – Global Significance and Future Exploration Potential. SEPM Spec. Publ. 23, 115-134.

Post, A.L., Przeslawski, R., Nanson, R., Siwabessy, J., Smith, D., Kirkendale, L.A., Wilson, N.G. 2022. Modern dynamics, morphology and habitats of slope-confined canyons on the northwest Australian margin. Mar. Geol. 444:106694, 18 pp.

Power, W., Mountjoy, J., Lane, E., Popinet, S., Wang, X. 2016. Assessing landslide-tsunami hazard in submarine canyons, using the Cook Strait Canyon System as an example. J. Tsunami Soc. Int. 35 (3), 145-166.

Pratson, L.F., Coakley, B.J. 1996. A model for the headward erosion of submarine canyons induced by downslope-eroding sediment flows. Geol. Soc. Am. Bull. 108 (2), 225-234.

Pratson, L.F., Nittrouer, C.A., Wiberg, P.L., Steckler, M.S., Swenson, J.B., Cacchione, D.A., Karson, J.A., Murray, A.B., Wolinsky, M.A., Gerber, T.P., Mullenbach, B.L., Spinelli, G.A., Fult-horpe, C.S., O'Grady, D.B., Parker, G. Driscoll, N.W., Burger, R.L., Paola, C., Orange, D.L., Field, M.E., Friedrichs, C.T., Fedele, J.J. 2007. Seascape evolution on clastic continental shelves and slopes. In: Nittrouer, C.A., Austin, J.A., Field, M.E., Kravitz, J.H., Syvitski, J.P.M., Wiberg, P.L. (eds) Continental Margin Sedimentation: From Sediment Transport to Sequence Stratigraphy. Blackwell Publishing, Oxford. pp. 339-380.

Pratson, L.F., Ryan, W.B.F., Mountain, G.S., Twichell, D.C. 1994. Submarine canyon initiation by downslope-eroding sediment flows: evidence in late Cenozoic strata on the New Jersey continental slope. Geol. Soc. Am. Bull. 106, 395-412.

Puga-Bernabéu, A., Webster, J.M., Beaman, R.J., Guilbaud, V. 2011. Morphology and controls on the evolution of a mixed carbonate–siliciclastic

submarine canyon system, Great Barrier Reef margin, north-eastern Australia. Mar. Geol. 289, 100-116.

Puig, P., Durán, R., Muñoz, A., Elvira, E., Guillén, J. 2017. Submarine canyon-head morphologies and inferred sediment transport processes in the Alías-Almanzora canyon system (SW Mediterranean): on the role of the sediment supply. Mar. Geol. 393, 21-34.

Puig, P., Ogston, A.S., Mullenbach, B.L., Nittrouer, C.A., Parsons, J.D., Sternberg, R.W. 2004. Storm-induced sediment gravity flows at the head of the Eel submarine canyon, northern California margin. J. Geophys. Res. 109:c03019, 10 pp.

Puig, P., Palanques, A., Guillén, J., García-Ladona. 2000. Deep slope currents and suspended particle fluxes in and around the Foix submarine canyon (NW Mediterranean). 47, 343-366. Deep Sea Res. Part I Oceanogr. Res. Paper 47, 343-366.

Puig, P., Palanques, A., Martín, J. 2014. Contemporary sediment-transport processes in submarine canyons. Annu. Rev. Mar. Sci. 6, 53-77.

Quartau, R., Madeira, J., Mitchell, N.C., Tempera, F., Silva, P.F., Brandão, F. 2015. The insular shelves of the Faial-Pico Ridge (Azores archipelago): A morphological record of its evolution. Geochem., Geophys., Geosyst. 16, 1401-1420.

Rahmstorf, S. 2006. Thermohaline Ocean Circulation. In: Elias, S.A. (ed) Encyclopedia of Quaternary Sciences. Elsevier, Amsterdam. pp. 739-750.

Ramsay, P.J., Smith, A.M., Mason, T.R. 1996. Geostrophic sand ridge, dune fields and associated bedforms from the Northern KwaZulu-Natal shelf, south-east Africa. Sedimentology. 43, 407-419.

Rasmussen, E.S. 1994. The relationship between submarine canyon fill and sea-level change: an example from Middle Miocene offshore Gabon, West Africa. Sediment. Geol. 90, 61-75.

Ratzov, G., Sosson, M., Collot, J.-Y., Migeon, S. 2012. Late Quaternary geomorphologic evolution of submarine canyons as a marker of active deformation on convergent margins: The example of the South Colombian margin. Mar. Geol. 315-318, 77-97.

Reading, H.G., Collinson, J.D. 1996. Clastic Coasts. In: Reading, H.G. (ed) Sedimentary Environments: Processes, Facies and Stratigraphy. Blackwell Science, Oxford. pp. 154-231.

Reid, I., Frostick, L.E. 2011. Chapter 13: Channel form, flows and sediments of endogenous ephemeral rivers in deserts. In: Thomas, D.S.G. (ed) Arid Zone Geomorphology: Process, Form and Change in Drylands, 301-332.

Restrepo-Correa, I.C., Ojeda, G.Y. 2010. Geologic controls on the morphology of La Aguja submarine canyon. J. South. Am. Earth. Sci. 29, 861-870.

Ridente, D., Martorelli, E., Bosman, A., Chiocci, F.L. 2014. High-resolution morpho-bathymetric imaging of the Messina Strait (Southern Italy). New insights on the 1908 earthquake and tsunami. Geomorphology. 208, 149-159.

Rise, L., Bøe, R., Riis, F., Bellec, V.K., Laberg, J.S., Eidvin, T., Elvenes, S., Thorsnes, T. 2013. The Lofoten-Vesterålen continental margin, North Norway: Canyons and mass-movement activity. Mar. Pet. Geol. 45, 134-149. Mar. Pet. Geol. 45, 134-149.

Roberts, H.H., Sydow, J. 1996. The offshore Mahakam Delta: Stratigraphic response of late Pleistocene-to-modern sea level cycle. 25th Annual Convention Proceedings (Volume 1), 147-161.

Roberts, H.H., Sydow, J., Robalin, J., Fillon, R. 2000. A comparison of two late Pleistocene shelf-edge deltas (Indonesia and Gulf of Mexico) – Stratigraphic architecture, system tracts, bounding surfaces, and reservoir potential. Trans. GCAGS 50, 361-367.

Roberts, H.H., Fillon, R.H. 2014. The role of turbidites in gas-charging of shelf-edge delta sand bodies: Lagniappe Delta, Gulf of Mexico. Trans. GCAGS 64, 339-347.

Roberts, H.H., Fillon, R.H., Kohl, B., Robalin, J.M., Sydow, J.C. 2004. Depositional architecture of the Lagniappe Delta: Sediment characteristics, timing of depositional events, and temporal relationship with adjacent shelf-edge deltas. In: Anderson, J.B., Fillon, R.H. (eds) Late Quaternary Stratigraphic Evolution of the Northern Gulf of Mexico Margin. SEPM Spec. Publ. 79, 143-188.

Roberts, J.M., Wheeler, A.J., Freiwald, A. 2006. Reefs of the deep: The biology and geology of cold-water coral ecosystems. Science. 312, 543-547.

Rodrigues, S., Hernández-Molina, F.J., Fonnesu, M., Miramontes, E., Rebesco, M., Campell, D.C. 2022. A new classification system for mixed (turbidite-contourite) depositional systems: Examples, conceptual models

and diagnostic criteria for modern and ancient records. Earth. Sci. Rev. 230:104030, 31 pp.

Romans, B.W., Normark, W.R., McGann, M.M., Covault, J.A., Graham, S.A. 2009. Coarse-grained sediment delivery and distribution in the Holocene Santa Monica Basin, California: implications for evaluating source-to-sink flux at millennial time scales. Geol. Soc. Am. Bull. 121 (9/10), 1394-1408.

Romans, B.W., Castelltort, S., Covault, J.A., Fildani, A., Walsh, J.P. 2016. Environmental signal propagation in sedimentary systems. Earth-Sci. Rev. 153, 7-29.

Rona, P.A. 1970. Submarine Canyon Origin on Upper Continental Slope off Cape Hatteras. J. Geol. 78 (2), 141-152.

Rona, P., Guida, V., Scranton, M., Gong, D., Macelloni, L., Pierdomenico, M., Diercks, A.-R., Asper, V., Haag, S. 2015. Hudson submarine canyon head offshore New York and New Jer-sey: a physical and geochemical investigation. Deep Sea Res. Part II Top. Stud. Oceanogr. 121, 213-232.

Rowan, M.G., Peel, F.J., Vendeville, B.C. 2004. Gravity-driven fold belts on passive margins. In: McClay, K.R. (ed) Thrust Tectonics and Hydrocarbon Systems. Am. Ass. Pet. Geol. Memoir 82, 157-182.

Ruiz-Angulo, A., Zavala-Hidalgo, J. 2016. Internal wave observations in the Petacalco Canyon, México. In: Klapp, J., Sigalotti, L., Medina, A., López, A., Ruiz-Chavarría, G. (eds) Recent Advances in Fluid Dynamics with Environmental Applications. Environmental Science and Engineering. Springer, Cham. pp. 203-213.

Ryan, M.C., Helland-Hansen, W., Johannessen, E.P., Steel, R.J. 2009. Erosional vs. accretionary shelf margins: the influence of margin type on deepwater sedimentation: an example from the Porcupine Basin, offshore western Ireland. Basin Res. 21, 676-703.

Saadatkhah, N., Kassim, A., Siat, Q.A., Micallef, A. 2023. Salt leaching by freshwater and its impact on seafloor stability: An experimental investigation. Mar. Geol. 455:106959, 10 pp.

Sager, W.W., Schroeder, W.W., Davies, K.S., Rezak, R. 1999. A tale of two deltas: seismic mapping of near surface sediments on the Mississippi – Alabama outer shelf and implications for recent sea level fluctuations. Mar. Geol. 160, 119-136.

Saldías, G.S., Allen, S.E. 2020. The influence of a submarine canyon on the circulation and cross-shore exchanges around an upwelling front. J. Phy. Oceanogr. 50, 1677-1698.

Salmanidou, D.M., Heidarzadeh, M., Guillas, S. 2019. Probabilistic landslide-generated tsuna-mis in the Indus Canyon, NW Indian Ocean, using statistical emulation. Pure Appl. Geophys. 176, 3099-3114.

Sanchez, C.M., Fulthorpe, C.S., Steel, R.J. 2012a. Middle Miocene-Pliocene siliciclastic influx across a carbonate shelf and influence of deltaic sedimentation on shelf construction, Northern Carnarvon Basin, Northwest Shelf of Australia. Basin Res. 24, 664-682.

Sanchez, C.M., Fulthorpe, C.S., Steel, R.J. 2012b. Miocene shelf-edge deltas and their impact on deepwater slope progradation and morphology, Northwest Shelf of Australia. Basin Res. 24, 683-698.

Santora, J.A., Zeno, R., Dorman, J.G., Sydeman, W.J. 2018. Submarine canyons represent an essential habitat network for krill hotspots in a large marine ecosystem. Sci. Rep. 8, 7579.

Santra, M., Goff, J.A., Steel, R.J., Austin Jr., J.A. 2013. Forced regressive and lowstand Hudson paleo-Delta system: Latest Pliocene growth of the outer New Jersey shelf. Mar. Geol. 339, 57-70.

Sawyer, D.E., DeVore, J.R. 2015. Elevated shear strength of sediments on active margins: evidence for seismic strengthening. Geophys. Res. Lett. 42, 10216-10221.

Schattner, U., Lazar, M. 2016. Hierarchy of source-to-sink systems – Example from the Nile distribution across the eastern Mediterranean. Sediment. Geol. 343, 119-131.

Scherer, C., Weber, A., Stock, F., Vurusic, S., Egerci, H., Kochleus, C., Arendt, N., Foeldi, C., Dierkes, G., Wagner, M., Brennholt, N., Reifferscheid, G. 2020. Comparative assessment of microplastics in water and sediment of a large European river. Sci. Total Env. 738:139866, 11 pp.

Schwartz, T.M., Graham, S.A. 2015. Stratigraphic architecture of a tide-influenced shelf-edge delta, Upper Cretaceous Dorotea Formation, Magallanes-Austral Basin, Patagonia. Sedimentology. 62, 1039-1077.

Schnürle, P., Liu, C.-S., Lallemand, S.E., Reed, D. 1998. Structural controls of the Taitung Canyon in the Huatung Basin East of Taiwan. TAO. 9 (3), 453-472.

Schultz, D.M., Bosart, L.F., Colle, B.A., Davies, H.C., Dearden, C., Keyser, D., Martius, O., Roebber, P.J., Steenburgh, W.J., Volkert, H., Winters, A.C. Extratropical cyclones: a century of research on meteorology's centerpiece. Meteorol. Monogr. 59, 16.1-16.56.

Sequeiros, O.E., Pittaluga, M.B., Frascati, A., Pirmez, C., Masson, D.G., Weaver, P., Crosby, A.R., Lazzaro, G., Botter, G., Rimmer, J.G. 2019. How typhoons trigger turbidity currents in submarine canyons. Sci. Rep. 9:9220, 15 pp.

Serra, C.S., Martínez-Loriente, S., Gràcia, E., Urgeles, R., Vizcaino, A., Perea, H., Bartolome, R., Pallàs, R., Lo Iacono, C., Diez, S., Dañobeitia, Terrinha, P., Zitellini, N. 2020. Tectonic evolution, geomorphology and influence of bottom currents along a large submarine canyon system: The São Vicente Canyon (SW Iberian margin). Mar. Geol. 426:106219, 16 pp.

Sharma, S.K., Gajbhiye, S., Tignath, S. 2015. Application of principal component analysis in grouping geomorphic parameters of a watershed for hydrological modelling. Appl. Water Sci. 5, 89-96.

Sheng, H., Gao, J.H., Kettner, A.J., Shi, Y., Wang, Y.P., Chen, Y. 2019. Variations in fluvial discharge of rivers over the last millennium along the eastern coast of the Liaodong Peninsula, China. J Asian Earth Sci. 184:103993, 18 pp.

Shepard, F.P. 1936. The underlying causes of submarine canyons. Proc. Natl. Acad. Sci. U.S.A. 22 (8), 496-502.

Shepard, F.P. 1972. Submarine canyons. Earth-Sci. Rev. 8, 1-12.

Shepard, F.P., Marshall, N.F., McLoughlin, P.A. 1974. "Internal waves" advancing along submarine canyons. Science. 183 (4121), 195-198.

Shepard, F.P. 1976. Tidal components of currents in submarine canyons. J. Geol. 84 (3), 343-350.

Shepard, F.P., McLoughlin, P.A., Marshall, N.F., Sullivan, G.G. 1977. Current-meter recordings of low-speed turbidity currents. Geology. 5 (5), 297-301.

Shepard, F.P. 1981. Submarine canyons: multiple causes and long-time persistence. Am. Assoc. Pet. Geol. Bull. 65 (6), 1062-1077.

Shumaker, L.E., Jobe, Z.R., Johnstone, S.A., Pettinga, L.A., Cai, D.X., Moody, J.D. 2018. Controls on submarine channel-modifying processes

identified through morphometric scaling relationships. Geosphere. 14 (5), 2171-2187.

Shyu, J.B.H., Sieh, K., Chen, Y.-G. 2005. Tandem suturing and disarticulation of the Taiwan orogen revealed by its neotectonics elements. Earth Planet. Sci. Lett. 233, 167-177.

Simmons, S. M., Azpiroz-Zabala, M., Cartigny, M. J. B., Clare, M. A., Cooper, C., Parsons, D. R., Pope, E. L., Sumner, E. J. and Talling, P. J. 2020. Novel Acoustic Method Provides First Detailed Measurements of Sediment Concentration Structure Within Submarine Turbidity Currents. J. Geophys. Res.: Oceans. 125 (5):e2019JC015904, 24 pp.

Simms, A.R., Lisiecki, L., Gebbie, G. Whitehouse, P.L. 2019. Balancing the last glacial maximum (LGM) sea-level budget. Quat. Sci. Rev. 205, 143-153.

Smith, D.P., Ruiz, G., Kvitek, R., Iampietro, P.J. 2005. Semiannual patterns of erosion and deposition in upper Monterey Canyon from serial multibeam bathymetry. Geol. Soc. Am. Bull. 117 (9/10), 1123-1133.

Smith, M. E., Finnegan, N. J., Mueller, E. R., Best, R. J. 2017. Durable terrestrial bedrock predicts submarine canyon formation. Geophys. Res. Lett. 44:10332-10340, 9 pp.

Smith, M.E., Werner, S.H., Buscombe, D., Finnegan, N.J., Sumner, E.J., Mueller, E.R. 2018. Seeking the shore: evidence for active submarine canyon head incision due to coarse sediment supply and focusing of wave energy. Geophys. Res. Lett. 45:12403-12413, 11 pp.

Snedden, J.W., Galloway, W.E., Milliken, K.T., Xu, J., Whiteaker, T., Blum, M.D. 2018. Validation of empirical source-to-sink scaling relationships in a continental-scale system: The Gulf of Mexico basin Cenozoic record. Geosphere. 14 (2), 768-784.

Sneider, J.S. 2003. Shelf margin deltas and associated deep-water deposits: Implications on reservoir distribution and hydrocarbon entrapment, Block VI-1, Ulleung Basin, East Sea, South Korea. In: Roberts, H.H., Rosen, N.C., Fillon, R.H., Anderson, J.B. (eds) Shelf margin deltas and linked down slope petroleum systems – Global significance and future exploration potential. SEPM Spec. Publ. 23, 115-134.

Soh, W., Tokuyama, H. 2002. Rejuvenation of submarine canyon associated with ridge subduction, Tenryu Canyon, off Tokai, central Japan. Mar. Geol. 187, 203-220.

Soh, W., Tokuyama, H., Fujioka, K., Kato, S., Taira, A. 1990. Morphology and development of a deep-sea meandering canyon (Boso Canyon) on an active plate margin, Sagami Trough, Japan. Mar. Geol. 91, 227-241.

Soulet, W., Migeon, S., Gorini, C., Rubino, J.-L., Raisson, F., Bourges, P. 2016. Erosional versus aggradational canyons along a tectonically-active margin: the northeastern Ligurian margin (western Mediterranean Sea). Mar. Geol. 382, 17-36.

Sømme, T.O., Helland-Hansen, W., Martinsen, O.J., Thurmond, J.B. 2009. Relationships between morphological and sedimentological parameters in source-to-sink systems: a basis for predicting semi-quantitative characteristics in subsurface systems. Basin Res. 21, 361-387.

Son, J.-H., Heo, K.-Y., Choi, J.-W., Kwon, J.-I. 2022. Long-lasting upper ocean temperature responses induced by intense typhoons in mid-latitude. Sci. Rep. 12:5752, 8 pp.

Soutter, E.L., Bell, D., Cumberpatch, Z.A., Ferguson, R.A., Spychala, Y.T., Kane, I.A., Eggenhuisen, J.T. 2020. The influence of confining topography orientation on experimental turbidity currents and geological implications. Earth Sci. 8:540633, 25 pp.

Soutter, E.L., Kane, I.A., Hodgson, D.M., Flint, S. 2021. The concavity of submarine canyon longitudinal profiles. J. Geophys. Res. Earth. Surf. 126:e2021JF006185, 16 pp.

Soutter, E.L., Kane, I.A., Hodgson, D.M., Flint, S.S. 2023. Controls on continental shelf width: A machine learning approach. Geomorphology. 436:108729, 8 pp.

Starke, J., Ehlers, T.A., Schaller, M. 2020. Latitudinal effect of vegetation on erosion rates identified along western South America. Science. 367, 1358-1361.

Steel, R., Porębski, S.J., Plink-Bjorklund, P., Mellere, D., Schellpeper, M. 2003. Shelf-edge delta types and their sequence-stratigraphic relationships. In: Roberts, H.H., Rosen, N.C., Fillon, R.H., Anderson, J.B. Shelf Margin Deltas and Linked Down Slope Petroleum Systems – Global Significance and Future Exploration Potential. SEPM Spec. Publ. 23, 205-230.

Stein, S., Cloetingh, S., Sleep, N.H., Wortel, R. 1989. Passive margin earthquakes, stresses and rheology. In: Gregerssen, S., Basham, P.W.

(eds) Earthquakes at North-Atlantic Passive Margins: Neotectonics and Postglacial Rebound, 266, 231-259.

Steventon, M.J., Jackson, C. A.-L., Hodgson, D.M., Johnson, H.D. 2020. Lateral variability of shelf-edge and basin-floor deposits, Santos Basin, offshore Brazil. J. Sed. Res. 90 (9), 1198-1221.

Stoecklin, A., Friedli, B., Puzrin, A.M. 2017. Sedimentation as a control for large submarine landslides: Mechanical modelling and analysis of the Santa Barbara Basin. J. Geophys. Res: Solid Earth. 122, 8645-8663.

Stow, D. (1986). Deep Clastic Seas In: Reading, H.G. (ed) Sedimentary Environments and Facies, 399-443.

Straub, K.M. 2019. Morphodynamics and stratigraphic architecture of shelf-edge deltas subject to constant vs. dynamic environmental forcings: A laboratory study. Front. Earth Sci. 7:121, 16 pp.

Straub, K.M., Mohrig, D. 2009. Constructional canyons built by sheet-like turbidity currents: observations from offshore Brunei Darussalam. J. Sediment. Res. 79, 24-39.

Strozyk, F., Strasser, M., Förster, A., Kopf, A., Huhn, K. 2010. Slope failure repetition in active margin environments: constraints from submarine landslides in the Hellenic fore arc, eastern Mediterranean. J. Geophys. Res. Earth. 115:B08103, 13 pp.

Sweet, M.L., Blum, M.D. 2016. Connections between fluvial to shallow marine environments and submarine canyons: implications for sediment transfer to deep water. J. Sediment. Res. 86, 1147-1162.

Sweet, M.L., Gaillot, G.T., Jouet, G., Rittenour, T.M., Toucanne, S., Marsset, T., Blum, M.D. 2020. Sediment routing from shelf to basin floor in the Quaternary Golo System of Eastern Corsica, France, western Mediterranean Sea. Geol. Soc. Am. Bull. 132 (5/6), 1217-1234.

Su, M., Hsiung, K.-H., Zhang, C., Xie, X., Yu, H.-S., Wang, Z. 2015. The linkage between longitudinal sediment routing systems and basin types in the northern South China Sea in perspective of source-to-sink. J. Asian Earth Sci. 111, 1-13.

Su, M., Lin, Z., Wang, C., Kuang, Z., Liang, J., Chen, H., Liu, S., Zhang, B., Luo, K., Huang, S., Wu, Q. 2020. Geomorphologic and infilling characteristics of the slope-confined submarine canyons in the Pearl River Mouth Basin, northern South China Sea. Mar. Geol. 424:106166, 17 pp.

Susanth, S., Kurian, P.J., Bijesh, C.M., Twinkle, D., Tyagi, A., Rajan, S. 2021. Controls on the evolution of submarine canyons in steep continental slopes: geomorphological insights from Palar Basin, southeastern margin of India. Geo-Mar. Lett. 41:14, 27 pp.

Suter, J.R., Berryhill Jr., H.L. 1985. Late Quaternary shelf-margin deltas, Northwest Gulf of Mexico. Geol. Soc. Am. Bull. 69 (1), 77-91.

Sweet, M.L., Blum, M.D. 2016. Connections between fluvial to shallow marine environments and submarine canyons: implications for sediment transfer to deep water. J. Sediment. Res. 86, 1147-1162.

Sylvester, Z., Deptuck, M., Prather, B.E., Pirmez, C., O'Byrne, C. 2012. Seismic stratigraphy of a shelf-edge delta and linked submarine channels in the northeastern Gulf of Mexico. In: Prather, B.E., Deptuck, M.E., Mohrig, D., Van Hoorn, B., Wynn, R.B. (eds) Application of the Principles of Seismic Geomorphology to Continental Slope and Base-of-Slope Systems: Case Studies from Seafloor and Near-Seafloor Analogues. SEPM Spec. Publ. 99, 31-59.

Sylvester, Z., Pirmez, C. 2017. Latitudinal changes in the morphology of submarine channels: reevaluating the evidence for the influence of the Coriolis force. In: Fraticelli ,C.M., Markwick, P.J., Martinius, A.W., Suter, J.W (eds) Latitudinal Controls on Stratigraphic Models and Sedimentary Concepts. SEPM Spec. Publ. 108, 11 pp.

Syvitski, J.P.M., Kettner, A.J., Overeem, I., Hutton, E.W.H., Hannon, M.T., Brakenridge, G.R., Day, J., Vörösmarty, C., Saito, Y., Giosan, L., Nicholls, R.J. 2009. Sinking deltas due to human activities. Nat. Geosci. 2, 681-686.

Talling, P.J., Baker, M.L., Pope, E., Ruffell, S.C., Silva Jacinto, R., Heijnen, M.S., Hage, S., Simmons, S.M., Hasenhündl, M., Heerema, C.J., McGhee, C., Apprioual, R., Ferrant, A., Cartigny, M.J.B., Parsons, D.R., Clare, M.A., Tshimanga, R.M., Trigg, M.A., Cula, C.A., Faria, R., Gaillot, A., Bola, G., Wallance, D., Griffiths, A., Nunny, R., Urlaub, M., Peirce, C., Burnett, R., Neasham, J., Hilton, R.J. 2022. Longest sediment flows yet measured show how major rivers connect efficiently to deep sea. Nature Comm. 13: 4193, 15 pp.

Tcherepanov, E.N., Droxler, A.W., Lapointe, P., Dickens, G.R., Bentley, S.J., Beaufort, L., Peterson, L., Daniell, J., Opdyke, B.N. 2008. Neogene evolution of the mixed carbonate-siliciclastic system in the Gulf of Papua, Papua New Guinea. J. Geophys. Res. 113: F01S21, 15 pp.

Teng, Y., Zhang, D. 2018. Long-term viability of carbon sequestration in deep-sea sediments. Sci. Adv. 4:eaao6588, 9 pp.

Teixeira, B.M.N., Astini, R.A., Gomez, F.J., Morales, N., Pimentel, M.M. 2018. Source-to-sink analysis of continental rift sedimentation: Triassic Cuyo basin, Precordillera Argentina. Sediment. Geol. 376, 164-184.

Tesson, M., Gensous, B., Allen, G.P., Ravenne, C. 1990. Late Quaternary deltaic lowstand wedges on the Rhône continental shelf, France. Mar. Geol. 91, 325-332.

Thornburg, T.M., Kulm, L.D., Hussong, D.M. 1990. Submarine-fan development in the southern Chile Trench: A dynamic interplay of tectonics and sedimentation. Am. Geol. Soc. Bull. 102, 1658-1680.

Tian, D., Jiang, T., Liu, B., Liu, J., Zhang, Z., Xu, H., Cheng, C. 2019. Early Miocene sedimentary processes and their hydrocarbon implications in the Baiyun Sag of Pearl River Mouth Basin, northern south China sea. Mar. Pet. Geol. 101, 132-147.

Tofelde, S., Bernhardt, A., Guerit, L., Romans, B.W. 2021. Times associated with source-to-sink progradation of environmental signals during landscape transience. Front. Earth Sci. 9:628315, 26 pp.

Torres Acosta, V., Schildgen, T.F., Clarke, B.A., Scherler, D., Bookhagen, B., Wittmann, H., von Blanckenburg, F., Strecker, M.R. 2015. Lithosphere. 7 (4), 408-420.

Tournadour, E., Mulder, T., Borgomano, J., Gillet, H., Chabaud, L., Ducassou, E., Hanquiez, V., Etienne, S. 2017. Submarine canyon morphologies and evolution in modern carbonate settings: The northern slope of Little Bahama Bank, Bahamas. Mar. Geol. 391, 76-97.

Trumbull, J.V.A., Garrison, L.E. 1973. Geology of a system of submarine canyons South of Puerto Rico. J. Res. U.S. Geol. Survey. 1 (3), 293-299.

Tubau, X., Lastras, G., Canals, M., Micallef, A., Amblas, D. 2013. Significance of the fine drainage pattern for submarine canyon evolution: the Foix Canyon System, Northwestern Mediterranean Sea. Geomorphology. 184, 20-37.

Tubau, X., Paull, C.K., Lastras, G., Caress, D.W., Canals, M., Lundsten, E., Anderson, K., Gwiazda, R., Amblas, D. 2015. Submarine canyons of Santa Monica Bay, Southern California: variability in morphology and sedimentary processes. Mar. Geol. 365, 61-79.

TuZino, T., Noda, A. 2010. Architecture and evolution of the Kushiro submarine canyon in the Kurile Trench forearc slope, North-western Pacific. Sedimentology. 57, 611-641.

Twichell, D.C., Nelson, H., Damuth, J.E. 2000. Late-stage development of the Bryant Canyon turbidite pathway on the Louisiana continental slope. In: Weimer, P. (ed) Deep-Water Reservoirs of the World. SEPM Spec. Publ. 20, 1032-1045.

Urías Espinosa, J., Bandy, W.L., Mortera Gutiérrez, C.A., Núñez Cornú, F. J., Mitchell, N.C. 2016. Multibeam bathymetric survey of the Ipala Submarine Canyon, Jalisco, Mexico (20°N): The southern boundary of the Banderas Forearc Block? Tectonophysics. 671, 249-263.

Urlaub, M., Talling, P.J., Zervos, A., Masson, D. 2015. What causes large submarine landslides on low gradient (≤2°) continental slopes with slow (~0.15 m/kyr) sediment accumulation? J. Geophys. Res. Solid Earth. 120, 6722-6739.

Uroza, C.A., Steel, R.J. 2008. A highstand shelf-margin delta system from the Eocene of West Spitsbergen, Norway. Sediment. Geol. 203, 229-245.

Valentine, P.C., Uzmann, J.R., Cooper, R.A. 1980. Geology and biology of Oceanographer Submarine Canyon. Mar. Geol. 38, 283-312.

Vanmaercke, M., Kettner, A.J., van den Eeckhaut, M., Poesen, J., Mamaliga, A., Verstraeten, G., Rãdoane, M. Obreja, F., Upton, P., Syvitski, J.P.M., Govers, G. 2014. Moderate seismic activity affects contemporary sediment yields. Prog. Phys. Geogr. 38 (2), 145-172.

van Hinsbergen, D.J.J., de Groot, L.V., van Schaik, S.J., Spakman, W., Bijl, P.K., Sluijs, A., Langereis, C.G., Brinkhuis, H. 2015. A paleolatitude calculator for paleoclimate studies. PLoS One. 10 (6):e0126946, 21 pp.

Vardar, D. 2019. Morphological definition of the North İmralı Canyon in the Sea of Marmara. Arab. J. Geosci. 12:76, 10 pp.

Voigt, I., Henrich, R., Preu, B.M., Piola, A.R., Hanebuth, T.J.J., Schwenk, T., Chiessi, C.M. 2013. A submarine canyon as a climate archive – Interaction of the Antarctic Intermediate Water with the Mar del Plata Canyon (Southwest Atlantic). Mar. Geol. 341, 46-57.

von Rad, U., Tahir, M. 1997. Late Quaternary sedimentation on the outer Indus shelf and slope (Pakistan): evidence from high-resolution seismic data and coring. Mar. Geol. 138, 193-236.

Walsh, J.P., Alexander, C.R., Gerber, T., Orpin, A.R., Sumners, B.W. 2007. Demise of a submarine canyon? Evidence for highstand infilling on the Waipaoa River continental margin, New Zealand. Geophys. Res. Lett. 34:L20606, 5 pp.

Wan, L., Bianchi, V., Hurter, S., Salles, T., Zhang, Z., Yuan, X. 2021. Morphological controls on delta-canyon-fan systems: Insights from stratigraphic forward models. Sedimentology. 69 (2), 864-890.

Wang, H., Bi, N., Wang, Y., Saito, Y., Yang, Z. 2010. Tide-modulated hyperpycnal flows off the Huanghe (Yellow River) mouth, China. Earth Surf. Process. Landf. 35, 1315-1329.

Wang, R., Colombera, L., Mountney, N.P. 2019. Geological controls on the geometry of incised-valley fills: insights from a global dataset of late-Quaternary examples. Sedimentology. 66 (6), 2134-2168.

Wang, R., Colombera, L., Mountney, N.P. 2020. Quantitative analysis of the stratigraphic architecture of incised-valley fills: A global comparison of Quaternary systems. Earth Sci. Rev. 200:102988, 25 pp.

Wang, S., Lin, C., Li, H., Zhang, H. Zhang, Z., Zhang, B. 2022a. Sequence stratigraphy and sedimentary characteristics of the shelf-edge delta and slope fan systems in the Late Oligocene, Baiyun Sag, Pearl River Mouth Basin, China. Mar. Pet. Geol. 136:105441, 15 pp.

Wang, X., Cai, F., Sun, Z., Li, Q., Li, A., Sun, Y., Wang, H., Sun, Q. 2022b. Tectonic and oceanographic controls on the slope-confined dendritic canyon system in the Dongsha Slope, South China Sea. Geomorphology. 410:108285, 15 pp.

Wang, X., Zhuo, H., Wang, Y., Mao, P., He, M., Chen, W., Zhou, J., Gao, S., Wang, M. 2018. Controls of contour currents on intra-canyon mixed sedimentary processes: Insights from the Pearl River Canyon, northern South China Sea. Mar. Geol. 406, 193-213.

Warratz, G., Schwenk, T., Voigt, I., Bozzano, G., Henrich, R., Violante, R., Lantzsch, H. 2019. Interaction of a deep-sea current with a blind submarine canyon (Mar del Plata Canyon, Argentina). Mar. Geol. 417:106002, 15 pp.

Waterhouse, A.F., Allen, S.E., Bowie, A.W. 2009. Upwelling flow dynamics in long canyons at low Rossby number. J. Geophys. Res. 114:C05004, 18 pp.

Waterhouse, A.F., Mackinnon, J.A., Musgrave, R.C., Kelly, S.M., Pickering, A., Nash, J. 2017. Internal tide convergence and mixing in a submarine canyon. J. Phys. Oceanograph. 47 (2), 303-322.

Wetzel, A. 1993. The transfer of river load to deep-sea fans: A quantitative approach. Am. Assoc. Pet. Geol. Bull. 77 (10), 1679-1692.

Whiteway, T., 2009. Australian bathymetry and topography grid, June 2009. Geoscience Australia, Department of Industry, Tourism and Resources, 2009.

Wiles, E., Green, A., Watkeys, M., Botes, R., Jokat, W. 2019. Submarine canyons of NW Madagascar: a first geomorphological insight. Deep Sea Res. Part II Top. Stud. Oceanogr. 161, 5-15.

Wiles, E., Green, A., Watkeys, M., Jokat, W., Krocker, R. 2013. The evolution of the Tugela canyon and submarine fan: a complex interaction between margin erosion and bottom current sweeping, southwest Indian Ocean, South Africa. Mar. Pet. Geol. 44, 60-70.

Wilson, L. 1973. Variations in mean annual sediment yield as a function of mean annual precipitation. Am. J. Sci. 273, 335-349.

Wolin, E., Stein, S., Pazzaglia, F., Meltzer, A., Kafka, A., Berti, C. 2012. Mineral, Virginia, earthquake illustrates seismicity of a passive-aggressive margin. Geophys. Res. Lett. 39:L02305, 7 pp.

Wynn, R.B., Weaver, P.P.E., Masson, D.G., Stow, D.A.V. 2002. Turbidite depositional architecture across three interconnected deep-water basins on the north-west African margin. Sedimentology. 49, 669-695.

Xu, J., Snedden, J.W., Galloway, W.E., Milliken, K.T., Blum, M.D. 2017. Channel-belt scaling relationship and application to early Miocene source-to-sink systems in the Gulf of Mexico basin. Geosphere. 13 (1), 179-200.

Xu, J.P. 2011. Measuring currents in submarine canyons: technological and scientific progress in the past 30 years. Geosphere. 7 (4), 868-876.

Xu, J.P., Noble, M.A. 2009. Currents in Monterey Submarine Canyon. J. Geophys. Res. 114:C03004, 20 pp.

Xu, S., Wang, Y., Peng, X., Zou, H., Qiu, Y., Gong, C., Zhuo, H. 2014. Origin of Taiwan Canyon and its effects on deepwater sediment. Sci. China Earth Sci. 57 (11), 2769-2780.

Yang, X., Peel, F.J., McNeill, L.C., Sanderson, D.J. 2020. Comparison of fold-thrust belts driven by plate convergence and gravitational failure. Earth-Sci. Rev. 203:103136, 21 pp.

Yin, S., Li, J., Ding, W., Gao, J., Ding, W., Wang, Y. 2018. Migration of the lower North Palawan submarine canyon: characteristics and controls. Int. Geol. Rev. 62 (7-8), 988-1005.

Yin, S., Lin, L., Pope, E.L., Li, J., Ding, W., Wu, Z., Ding, W., Gao, J., Zhao, D. 2019. Continental slope-confined canyons in the Pearl River Mouth Basin in the South China Sea dominated by erosion, 2004-2018. Geomorphology. 344, 60-74.

Yin, S., Wang, L., Guo, Y, Zhong, G. 2015. Morphology, sedimentary characteristics, and origin of the Dongsha submarine canyon in the northeastern continental slope of the South China Sea. Sci. China Earth Sci. 58, 971-985.

Yoo, D.-G., Kim, K.-J., Lee, G.-S., Kim, G.-Y., Bae, S.-H. 2017. Seismic stratigraphic reconstruction of late Pleistocene lowstand wedges on the shelf margin and trough region of the Korea Strait: a review. Geosci. J. 21 (6), 933-949.

Yu, H.-S., Chiang, C.-S. 1995. Morphology and origin of the Hongtsai Submarine Canyon West of the Hengchun Peninsula, Taiwan. J. Geol. Soc. China. 38 (1), 81-93.

Yu, H.-S., Chang, J.-F. 2002. The Penghu Submarine Canyon off Southwestern Taiwan: morphology and origin. TAO. 13 (4), 547-562.

Yu, H.-S., Liu, C.S., Lee, J.-T. 1992. The Kaohsiung Submarine Canyon: a modern aborted canyon and its morphology and echo character. Acta Oceangr. Taiwan. 28, 19-30.

Yu, H.-S., Lu, J.C. 1995. Development of the shale diapir-controlled Fangliao Canyon on the continental slope off southwestern Taiwan. J. Asian Earth Sci. 11 (4), 265-276.

Yu, Y., Cai, L., Zhang, C., Wang, L., Zhu, R., Huang, Y., Cao, T. 2021. Sedimentary sequence, evolution model and petroleum geological significance of forced regression: A case study of the Miocene Zhujiang Formation of the Pearl River Mouth Basin in the Northern South China Sea. J. Mar. Sci. Eng. 9:1298, 20 pp.

Zavala, C. 2020. Hyperpycnal (over density) flows and deposits. J. Palaeogeogr. 9:17, 21 pp.

Zecchin, M., Catuneanu, O., Caffau, M. 2019. Wave-ravinement surfaces: Classification and key characteristics. Earth-Sci. Rev. 188, 210-239.

Zhang, Y., Liu, Z., Zhao, Y., Colin, C., Zhang, X., Wang, M., Zhao, S., Kneller, B. 2018. Long-term in situ observations on typhoon-triggered turbidity currents in the deep sea. Geology. 46 (8), 675-678.

Zhang, F., Hu, Y., Fan, X., Yu, W., Liu, X., Jin, Z. 2022a. Controls on seasonal erosion behavior and potential increase in sediment evacuation in the warming Tibetan Plateau. Catena. 209:105797, 12 pp.

Zhang, F., Zeng, C., Wang, G., Wang, L., Shi, X. 2022b. Runoff and sediment yield in relation to precipitation, temperature and glaciers on the Tibetan Plateau. Int. Soil Water Conserv. Res. 10, 197-207.

Zhao, L., Ouillon, R., Vowinckel, B., Meiburg, E., Kneller, B., He, Z. 2018. Transition of a hyperpycnal flow into a saline turbidity current due to differential diffusivities. Geophys. Res. Lett. 45, 11875-11884.

Zhong, G., Peng, X. 2021. Transport and accumulation of plastic litter in submarine canyons – The role of gravity flows. Geology. 49, 581-586.

Websites

https://data.unep-wcmc.org/datasets/1

https://earth.google.com/web/

https://freevectormaps.com

https://www.ncei.noaa.gov/maps/bathymetry/

https://trek.nasa.gov/mars

List of Abbreviations

1D:	1-dimensional
2D:	2-dimensional
3D:	3-dimensional
ANOVA:	Analysis of Variance
DMAKS:	Deep-Marine Architecture Knowledge Store
e.g.:	exempli gratia; “for example”
Fm.:	Formation
GEBCO:	General Bathymetric Chart of the Oceans
i.e.:	id est; “that is”
LGM:	Last Glacial Maximum
mbsl:	meters below sea level
NCEI:	National Centres for Environmental Information
NOAA:	National Oceanic and Atmospheric Administration
S2S:	Source-to-sink
SMAKS:	Shallow-Marine Architecture Knowledge Store
vs.:	versus

Appendix A
List of study variables and their definitions

The following table contains a list of study variables applied in the three individual studies of chapters 3, 4 and 5 – abbreviated in the table as “3”, “4” and “5”, respectively – and their definitions.

Study variable	Definition
Morphometric attributes (3, 4 & 5)	
Canyon morphometric attributes (3 & 4)	
L [km]**	Streamwise length of the canyon between canyon apex and canyon mouth as measured along the canyon thalweg
W_{max} [km]**	Maximum width of the canyon orthogonal to the canyon length
W_{av} [km]*	Average canyon width over the length of the entire canyon
D_{max} [m]*	Maximum depth of the canyon, i.e. depth of the canyon thalweg relative to the elevation of the canyon margins
D_{av} [m]*	Average canyon thalweg depth over the length of the entire canyon
SI_{av} [-]**	Average canyon sinuosity index, i.e. ratio between the sinuous canyon length measured along its thalweg and the straight distance between canyon apex and canyon mouth
thG_{av} [°]**	Average canyon thalweg gradient, evaluated between canyon apex and canyon mouth
SW_{max} [°]*	Maximum canyon-sidewall steepness, representing the maximum value of gradient between canyon rim and canyon bottom, evaluated along the entire length of the canyon
Shelf-edge deltaic morphometric attributes (5)	
L [m]**	Length of the delta element measured along the axis between updip delta tip and downdip delta toe, or parallel to it
W [m]**	Width of the delta element measured orthogonal to the length axis
T [m]**	Recorded thickness of the delta element
A [km^2]**	Area of the delta element
Physiographic setting (3 & 4)	

Canyon apex location	The location of the canyon apex relative to the shelf break, classified as ‘shelf-incising’ or ’slope-confined’
Dis_{min} [m]**	Minimum distance between the canyon and the shoreline
SD_{min} [m]**	Seafloor depth at the top of the canyon; for canyons with several tributaries at their head the shallowest seafloor depth has been recorded
SD_{max} [m]**	Seafloor depth at the mouth of the canyon
Source-to-sink (S2S) system (3, 4 & 5)	
Terrestrial catchment [1] (3, 4 & 5)	
L_{fls} [km]**	Length of the fluvial system from headwater to river mouth (i) with a present-day or previous connection with the canyon; (ii) associated with the shelf-edge deltaic deposits; for multiple-sourced shelf-edge deltaic elements the cumulative length has been recorded
Q_{fls} [km^3/yr]*	Mean annual discharge of the fluvial system; for canyons and shelf-edge deltas connected with several rivers the cumulative mean annual discharge has been considered
A_{flsc} [km^2]*	Size of the catchment associated with the fluvial system; for canyons and shelf-edge deltas connected with several rivers the maximum area of the combined catchment has been considered
H_{flsc} [m]**	Maximum elevation of the catchment area relative to sea level; for canyons and shelf-edge deltas connected with several rivers the elevation of the highest peak in the combined catchment has been considered
Continental shelf (3, 4 & 5)	
W_{sh} [km]** (3, 4 & 5)	Width of the shelf at the canyon and shelf-edge delta location
G_{sh} [°]** (3 & 4)	Average shelf gradient at the canyon location
D_{sh} [m]** (3 & 4)	Shelf-break depth at the canyon; for shelf edges with variable bathymetry, the deepest point is considered
Continental slope (3 & 4)	
W_{sl} [km]**	Width of the slope at the canyon location
G_{sl} [°]**	Average slope gradient between the shelf break and the slope break
D_{sl} [m]**	Slope-break depth at the canyon

Environmental setting (3, 4 & 5)	
Lat_{abs} [°]** (3 & 5)	Absolute value of the latitude at the (i) canyon apex; (ii) downdip delta toe; where data coverage of the distal part of the delta element is given this is measured, else the centre point of the study are has been used; from the age range determined by authors, palaeolatitude was obtained for the mean age between lower and upper age boundary
Source-to-sink setting (3 & 5)	Physiography of the source-to-sink system a canyon or shelf-edge delta are associated with, classified as: (i) continental setting; (ii) insular setting; canyons situated in trenches between islands and continents have not been included
Continental-margin type (3 & 4)	For canyons located along continental margins, including canyons associated with islands: (i) active margin (including both convergent and transform settings); (ii) passive margin
Active-margin plate-boundary type (4)	Based on the type of plate boundary, active margins are distinguished into (i) convergent, (ii) transform, and (iii) complex margins. The latter category includes settings which involve more than one plate boundary, and margins which display an additional direction of motion, e.g. convergent margins with a transform component
Oceanographic environment (3 & 5)	(i) Open seas: large-scale oceanic environments with unrestricted hydrodynamic connection to adjacent oceans and seas & characterised by oceanic gyres; (ii) Semi-enclosed and enclosed seas: smaller-scale seas, gulfs and straits with limited hydrodynamic exchange with connected seas, largely land-bound & no oceanic gyres
[1] Only investigated for shelf-edge deltaic elements of a Late Pleistocene or younger age	

Table A Overview and definition of the study variables that have been considered in this project. Three asterisks (***) denote values that have been calculated. Two asterisks (**) denote values that have been obtained either from the literature, as reported by the original authors, from open-source bathymetry, or have been calculated, or a combination thereof. A single asterisk (*) denotes values that have been retrieved from the literature, as stated by the original authors.

Appendix B
Datasets 1, 2 and 3

Appendix B comprises data sheets with the raw Datasets 1, 2 and 3 used in the three studies presented in Chapters 3, 4 and 5, respectively.

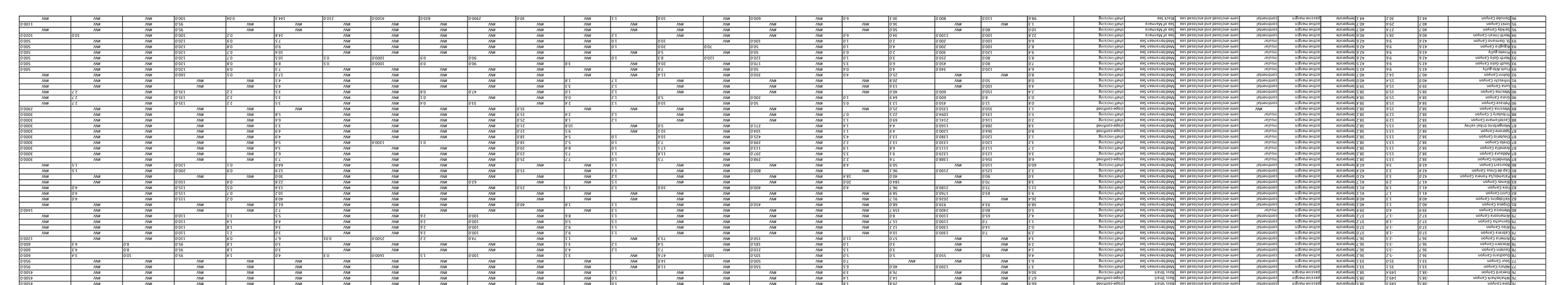
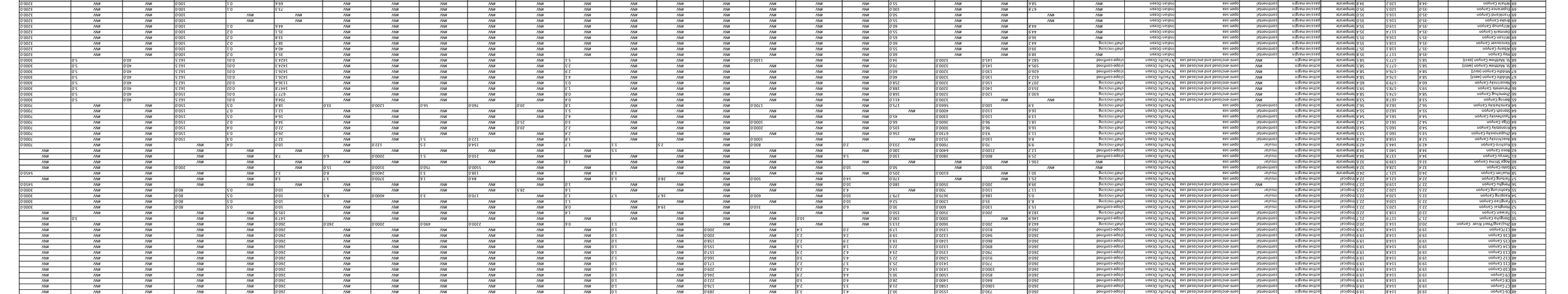

case_study_ID	original_name	latitude	longitude	tal_alt_pT1	climate_zone	morph_type	plate_boundary_type	lith_setting	oceanographic_setting	oceanographic_region	os_type	SOmin_alt [m]	Dsmax_alt [m]	L_alt [km]	Wmax_alt [km]
1	Canyon A5	-45.5	55.1	43.8	temperate	passive margin	any	continental	open sea	S Atlantic Ocean	slope-confined	5310	3500	126.1	any
1	Canyon A6	-45.5	55.1	43.8	temperate	passive margin	any	continental	open sea	S Atlantic Ocean	slope-confined	5310	3500	126.1	any
1	Canyon A4	-45.5	55.1	43.8	temperate	passive margin	any	continental	open sea	S Atlantic Ocean	slope-confined	5310	3500	126.1	any
1	Canyon A7	-45.5	55.1	43.8	temperate	passive margin	any	continental	open sea	S Atlantic Ocean	slope-confined	5310	3500	126.1	any
1	Canyon A8	-45.5	55.1	43.8	temperate	passive margin	any	continental	open sea	S Atlantic Ocean	slope-confined	5310	3500	126.1	any
1	Canyon A3	-45.5	55.1	43.8	temperate	passive margin	any	continental	open sea	S Atlantic Ocean	slope-confined	5310	3500	126.1	any
2	Ski Canyon	-45.5	55.1	43.8	temperate	passive margin	any	continental	open sea	S Atlantic Ocean	slope-confined	5310	3500	126.1	any
2	Pike Bravo Canyon	-45.5	55.1	43.8	temperate	passive margin	any	continental	open sea	S Atlantic Ocean	slope-confined	5310	3500	126.1	any
3	Orinoco Canyon	-4.1	36.5	4.3	tropical	passive margin	any	continental	open sea	S Atlantic Ocean	shelf-incising	4110	3500	70.9	any
3	Amazon Canyon	-4.1	36.5	4.3	tropical	passive margin	any	continental	open sea	S Atlantic Ocean	shelf-incising	4110	3500	70.9	any
3	Xingu Canyon	-4.1	36.5	4.3	tropical	passive margin	any	continental	open sea	S Atlantic Ocean	shelf-incising	4110	3500	70.9	any
3	Para do Mel Canyon	-4.1	36.5	4.3	tropical	passive margin	any	continental	open sea	S Atlantic Ocean	shelf-incising	4110	3500	70.9	any
3	Maranhao Channel-Canyon	-4.1	36.5	4.3	tropical	passive margin	any	continental	open sea	S Atlantic Ocean	shelf-incising	4110	3500	70.9	any
3	Maraca Canyon	-4.1	36.5	4.3	tropical	passive margin	any	continental	open sea	S Atlantic Ocean	shelf-incising	4110	3500	70.9	any
3	Jaci Canyon	-4.1	36.5	4.3	tropical	passive margin	any	continental	open sea	S Atlantic Ocean	shelf-incising	4110	3500	70.9	any
3	Icatu Canyon	-4.1	36.5	4.3	tropical	passive margin	any	continental	open sea	S Atlantic Ocean	shelf-incising	4110	3500	70.9	any
3	Jabo	-4.1	36.5	4.3	tropical	passive margin	any	continental	open sea	S Atlantic Ocean	shelf-incising	4110	3500	70.9	any
3	Moa Canyon	-4.1	36.5	4.3	tropical	passive margin	any	continental	open sea	S Atlantic Ocean	shelf-incising	4110	3500	70.9	any
3	Apodi-Mossoro Canyon	-4.1	36.5	4.3	tropical	passive margin	any	continental	open sea	S Atlantic Ocean	shelf-incising	4110	3500	70.9	any
3	Piranhas-Acu Canyon	-4.1	36.5	4.3	tropical	passive margin	any	continental	open sea	S Atlantic Ocean	shelf-incising	4110	3500	70.9	any
3	Ponta do Mel Canyon	-4.1	36.5	4.3	tropical	passive margin	any	continental	open sea	S Atlantic Ocean	shelf-incising	4110	3500	70.9	any
3	Jaguaribe-Acu Canyon	-4.1	36.5	4.3	tropical	passive margin	any	continental	open sea	S Atlantic Ocean	shelf-incising	4110	3500	70.9	any
3	Mararia Canyon	-4.1	36.5	4.3	tropical	passive margin	any	continental	open sea	S Atlantic Ocean	shelf-incising	4110	3500	70.9	any
3	Jaguaribe Canyon	-4.1	36.5	4.3	tropical	passive margin	any	continental	open sea	S Atlantic Ocean	shelf-incising	4110	3500	70.9	any
3	Sao Caetano Canyon	-4.1	36.5	4.3	tropical	passive margin	any	continental	open sea	S Atlantic Ocean	shelf-incising	4110	3500	70.9	any
3	Piranhas Canyon	-4.1	36.5	4.3	tropical	passive margin	any	continental	open sea	S Atlantic Ocean	shelf-incising	4110	3500	70.9	any
3	Curimata Canyon	-4.1	36.5	4.3	tropical	passive margin	any	continental	open sea	S Atlantic Ocean	shelf-incising	4110	3500	70.9	any
3	Cruz Canyon	-4.1	36.5	4.3	tropical	passive margin	any	continental	open sea	S Atlantic Ocean	shelf-incising	4110	3500	70.9	any
3	Tibau Canyon	-4.1	36.5	4.3	tropical	passive margin	any	continental	open sea	S Atlantic Ocean	shelf-incising	4110	3500	70.9	any
3	Agua Canyon	-4.1	36.5	4.3	tropical	passive margin	any	continental	open sea	S Atlantic Ocean	shelf-incising	4110	3500	70.9	any
3	Jaguaribe Canyon	-4.1	36.5	4.3	tropical	passive margin	any	continental	open sea	S Atlantic Ocean	shelf-incising	4110	3500	70.9	any
3	Jaua Canyon	-4.1	36.5	4.3	tropical	passive margin	any	continental	open sea	S Atlantic Ocean	shelf-incising	4110	3500	70.9	any
3	Apodi Canyon	-4.1	36.5	4.3	tropical	passive margin	any	continental	open sea	S Atlantic Ocean	shelf-incising	4110	3500	70.9	any
3	Mundau Canyon	-4.1	36.5	4.3	tropical	passive margin	any	continental	open sea	S Atlantic Ocean	shelf-incising	4110	3500	70.9	any
3	Mundau-Paraiba

case_study_ID	original_name	element_type	age	latitude [°]	longitude [°]	palaeolatitude_abs [°]	palaeo_climate_zone	hydrodynamic_process_regime	fluvial_feeder_system_type	S2S_system_setting	oceanographic_environment	L_all [km]	length_type	W_all [km]	width_type	T_all [m]	thickness_type	A_all [km2]	area_type	Lfls_modern [km]	Aflsc_modern [km2]	Hflsc_modern [m]	Qfls_modern [km3/yr]	Wsh_modern [km]
1	Dorotea delta	delta (unclassified)	Upper Cretaceous	-50.8	-72.8	55.0	temperate	mixed-process	single point source	#NV	#NV	#NV	#NV	#NV	#NV	250.0	unlimited observed	#NV	#NV	#NV	#NV	#NV	#NV	#NV
2	shelf-edge delta complex	delta complex	Lower-Middle Jurassic	-39.7	-71.0	42.6	temperate	mixed-process	#NV	#NV	#NV	#NV	#NV	2.8	Unlimited observed	81.4	True	#NV	#NV	#NV	#NV	#NV	#NV	#NV
2	delta lobe 1	delta lobe	Lower-Middle Jurassic	-39.7	-71.0	42.6	temperate	mixed-process	#NV	#NV	#NV	#NV	#NV	2.7	Unlimited observed	35.5	True	#NV	#NV	#NV	#NV	#NV	#NV	#NV
2	delta lobe 2	delta lobe	Lower-Middle Jurassic	-39.7	-71.0	42.6	temperate	mixed-process	#NV	#NV	#NV	#NV	#NV	2.8	Unlimited observed	26.9	True	#NV	#NV	#NV	#NV	#NV	#NV	#NV
2	delta lobe 3	delta lobe	Lower-Middle Jurassic	-39.7	-71.0	42.6	temperate	mixed-process	#NV	#NV	#NV	#NV	#NV	2.8	Unlimited observed	25.1	True	#NV	#NV	#NV	#NV	#NV	#NV	#NV
3	Pienaarsfontein shelf-edge delta	delta (unclassified)	Permian-Triassic	-32.8	20.0	58.3	temperate	#NV	#NV	#NV	#NV	#NV	#NV	#NV	#NV	33.0	unlimited observed	#NV	#NV	#NV	#NV	#NV	#NV	#NV
4	delta lobe 11	delta lobe	Miocene	-19.2	116.0	24.4	temperate	mixed-process	#NV	#NV	#NV	13.3	Partial observed	6.5	Unlimited observed	70.0	True	21.0	Maximum	#NV	#NV	#NV	#NV	#NV
4	delta lobe 12	delta lobe	Miocene	-19.2	116.0	24.4	temperate	mixed-process	#NV	#NV	#NV	1.0	Partial observed	10.6	Unlimited observed	80.0	True	61.0	Maximum	#NV	#NV	#NV	#NV	#NV
4	delta lobe 15	delta lobe	Miocene	-19.2	116.0	24.4	temperate	mixed-process	#NV	#NV	#NV	16.5	Partial observed	18.8	Unlimited observed	100.0	True	38.0	Maximum	#NV	#NV	#NV	#NV	#NV
5	shelf-edge delta (Unit 3)	delta lobe	Mid-Pleistocene	-18.7	148.0	17.4	tropical	river-dominated	single point source	continental	open sea	20.5	Unlimited observed	19.8	True	140.0	Maximum	157.0	Partial observed	710.0	130000.0	980.0	10.0	100.5
5	Myrmidon Reef delta	delta lobe	Mid-Pleistocene	-18.4	147.4	17.1	tropical	river-dominated	single point source	continental	open sea	10.2	Partial observed	24.5	True	#NV	#NV	494.0	Partial observed	710.0	130000.0	980.0	10.0	130.5
5	Bowl Reef delta	delta lobe	Mid-Pleistocene	-18.5	147.7	17.1	tropical	river-dominated	single point source	continental	open sea	9.1	Partial observed	49.5	True	#NV	#NV	462.0	Partial observed	710.0	130000.0	980.0	10.0	124.0
6	Shelf-edge delta Gulf of Papua (Ashmore Trough)	delta complex	Late Pleistocene	-9.7	144.7	8.4	tropical	#NV	#NV	insular	semi-enclosed and enclosed sea	20.2	Unlimited observed	#NV	#NV	29.3	unlimited observed	#NV	#NV	#NV	4000.0	#NV	#NV	158.0
6	lobe 1	delta lobe	Late Pleistocene	-9.7	144.7	8.4	tropical	#NV	#NV	#NV	semi-enclosed and enclosed sea	#NV	#NV	#NV	#NV	10.1	True	#NV	#NV	#NV	4000.0	#NV	#NV	158.0
6	lobe 2	delta lobe	Late Pleistocene	-9.7	144.7	8.4	tropical	#NV	#NV	#NV	semi-enclosed and enclosed sea	#NV	#NV	#NV	#NV	14.9	True	#NV	#NV	#NV	4000.0	#NV	#NV	158.0
6	lobe 3	delta lobe	Late Pleistocene	-9.7	144.7	8.4	tropical	#NV	#NV	#NV	semi-enclosed and enclosed sea	#NV	#NV	#NV	#NV	9.4	True	#NV	#NV	#NV	4000.0	#NV	#NV	158.0
6	lobe 4	delta lobe	Late Pleistocene	-9.7	144.7	8.4	tropical	#NV	#NV	#NV	semi-enclosed and enclosed sea	#NV	#NV	#NV	#NV	16.8	Partial observed	#NV	#NV	#NV	4000.0	#NV	#NV	158.0
7	Late Quaternary Bonaparte Delta	delta complex	Late Quaternary	-9.5	128.4	8.4	tropical	mixed-process	#NV	continental	semi-enclosed and enclosed sea	50.6	Unlimited observed	80.8	Unlimited observed	370.0	Maximum	3205.9	Partial observed	#NV	#NV	#NV	#NV	681.8
7	lobe 1 (Depocentre A)	delta lobe	Late Quaternary	-9.5	128.4	8.4	tropical	mixed-process	#NV	continental	semi-enclosed and enclosed sea	50.6	Unlimited observed	73.7	Unlimited observed	#NV	#NV	2517.6	Partial observed	#NV	#NV	#NV	#NV	681.8
7	lobe 2 (Depocentre B)	delta lobe	Late Quaternary	-9.5	128.4	8.4	tropical	mixed-process	#NV	continental	semi-enclosed and enclosed sea	50.6	Unlimited observed	80.8	Unlimited observed	#NV	#NV	3205.9	Partial observed	#NV	#NV	#NV	#NV	681.8
7	lobe 3 (Depocentre C)	delta lobe	Late Quaternary	-9.5	128.4	8.4	tropical	mixed-process	#NV	continental	semi-enclosed and enclosed sea	50.6	Unlimited observed	73.7	Unlimited observed	#NV	#NV	2567.5	Partial observed	#NV	#NV	#NV	#NV	681.8
8	Mahakam Delta (during the Late Pleistocene)	delta complex	Late Pleistocene	-0.8	117.8	0.8	tropical	mixed-process	single point source	insular	semi-enclosed and enclosed sea	54.6	Partial observed	177.3	Maximum	120.0	Maximum	5481.0	Partial observed	720.0	82000.0	1700.0	87.0	28.6
9	Bissagos Delta	delta (unclassified)	Pleistocene (Middle or Late)	11.2	-16.8	9.8	tropical	#NV	multiple point source	continental	open sea	121.0	Partial observed	200.0	Maximum	#NV	#NV	15276.0	Partial observed	530.0	#NV	40.0	#NV	140.0
9	Orango Delta	delta (unclassified)	Pleistocene (Middle or Late)	9.9	-16.5	8.3	tropical	#NV	multiple point source	continental	open sea	30.4	Partial observed	30.0	Maximum	130.0	True	2036.0	Partial observed	#NV	#NV	#NV	#NV	175.0
9	Nunez Delta	delta (unclassified)	Pleistocene (Middle or Late)	9.4	-15.6	7.9	tropical	#NV	multiple point source	continental	open sea	21.6	Partial observed	20.0	Maximum	130.0	True	1293.0	Partial observed	250.0	#NV	#NV	#NV	179.0
10	palaeo-Orinoco Delta (Pliocene Mayaro Fm.)	delta (unclassified)	Pliocene	10.2	-61.0	8.7	tropical	mixed-process	single point source	continental	#NV	#NV	#NV	#NV	#NV	350.0	unlimited observed	#NV	#NV	2800.0	1100000.0	6000.0	1100.0	114.0
11	Shelf-edge delta offshore Belize	delta complex	Late Pleistocene	17.4	-88.0	17.1	tropical	mixed-process	#NV	continental	semi-enclosed and enclosed sea	17.1	Partial observed	8.9	Unlimited observed	235.0	Partial observed	8.6	Partial observed	#NV	#NV	#NV	#NV	22.0
12	Western shelf-edge delta (Seismic facies F1)	delta (unclassified)	Pliocene	17.6	110.2	18.9	tropical	#NV	single point source	insular	semi-enclosed and enclosed sea	#NV	#NV	#NV	#NV	#NV	#NV	90.0	Partial observed	#NV	#NV	#NV	#NV	#NV
12	Eastern shelf-edge delta (Seismic facies F2)	delta (unclassified)	Late Miocene-Middle Pliocene (?)	18.2	110.9	19.9	tropical	#NV	single point source	insular	semi-enclosed and enclosed sea	#NV	#NV	#NV	#NV	#NV	#NV	74.0	Partial observed	163.0	3693.0	#NV	#NV	#NV
13	Zhujiang Fm. Shelf-edge delta	delta complex	Early Miocene	19.9	113.0	24.3	temperate	#NV	single point source	#NV	semi-enclosed and enclosed sea	18.3	Partial observed	31.6	True	495.9	unlimited observed	653.5	Partial observed	2200.0	490000.0	2000.0	260.0	#NV
14	Shelf-edge delta system (CS3-3)	delta (unclassified)	Late Oligocene	19.9	115.1	25.1	temperate	#NV	single point source	continental	semi-enclosed and enclosed sea	10.7	Unlimited observed	#NV	#NV	200.0	Maximum	#NV	#NV	2200.0	490000.0	2000.0	260.0	232.0
14	shelf-edge delta (CS3-3 stage 1)	delta (unclassified)	Late Oligocene	19.9	115.1	25.1	temperate	#NV	single point source	continental	semi-enclosed and enclosed sea	8.9	Partial observed	#NV	#NV	#NV	#NV	2200.0	490000.0	2000.0	260.0	232.0
14	shelf-edge delta (CS3-3 stage 2)	delta (unclassified)	Late Oligocene	19.9	115.1	25.1	temperate	#NV	single point source	continental	semi-enclosed and enclosed sea	6.2	Unlimited observed	#NV	#NV	#NV	#NV	2200.0	490000.0	2000.0	260.0	232.0
14	shelf-edge delta (CS3-3 stage 3)	delta (unclassified)	Late Oligocene	19.9	115.1	25.1	temperate	#NV	single point source	continental	semi-enclosed and enclosed sea	4.5	Unlimited observed	#NV	#NV	#NV	#NV	2200.0	490000.0	2000.0	260.0	232.0
15	Rio Grande Delta	delta complex	Late Pleistocene	26.4	-96.2	26.4	temperate	river-dominated	multiple point source	continental	semi-enclosed and enclosed sea	60.4	Partial observed	107.5	Unlimited observed	160.0	True	2905.0	Partial observed	#NV	#NV	#NV	#NV	82.0
15	lobe 1	delta lobe	Late Pleistocene	26.4	-96.2	26.4	temperate	river-dominated	#NV	continental	semi-enclosed and enclosed sea	7.4	Unlimited observed	#NV	#NV	#NV	#NV	#NV	#NV	#NV	#NV	#NV	#NV	82.0
15	lobe 2	delta lobe	Late Pleistocene	26.4	-96.2	26.4	temperate	river-dominated	#NV	continental	semi-enclosed and enclosed sea	22.6	Unlimited observed	3.5	Unlimited observed	#NV	#NV	#NV	#NV	#NV	#NV	#NV	#NV	82.0
15	lobe 3	delta lobe	Late Pleistocene	26.4	-96.2	26.4	temperate	river-dominated	#NV	continental	semi-enclosed and enclosed sea	11.1	True	3.5	Unlimited observed	#NV	#NV	#NV	#NV	#NV	#NV	#NV	#NV	82.0
15	lobe 4	delta lobe	Late Pleistocene	26.4	-96.2	26.4	temperate	river-dominated	#NV	continental	semi-enclosed and enclosed sea	14.6	Unlimited observed	3.5	Unlimited observed	#NV	#NV	#NV	#NV	#NV	#NV	#NV	#NV	82.0
15	Mississippi River Delta (during the Wisconsinan)	delta complex	Late Pleistocene	26.9	-92.7	26.8	temperate	#NV	single point source	continental	semi-enclosed and enclosed sea	38.9	Unlimited observed	102.7	Maximum	120.0	True	2176.0	Partial observed	5900.0	3300000.0	3700.0	490.0	172.0
15	lobe 1	delta lobe	Late Pleistocene	26.9	-92.7	26.8	temperate	#NV	single point source	continental	semi-enclosed and enclosed sea	19.6	Partial observed	#NV	#NV	#NV	#NV	5900.0	3300000.0	3700.0	490.0	172.0
15	lobe 2	delta lobe	Late Pleistocene	26.9	-92.7	26.8	temperate	#NV	single point source	continental	semi-enclosed and enclosed sea	26.2	Partial observed	18.1	Partial observed	#NV	#NV	5900.0	3300000.0	3700.0	490.0	172.0
15	lobe 3	delta lobe	Late Pleistocene	26.9	-92.7	26.8	temperate	#NV	single point source	continental	semi-enclosed and enclosed sea	18.8	Partial observed	14.3	Partial observed	#NV	#NV	5900.0	3300000.0	3700.0	490.0	172.0
16	Destin delta	delta (unclassified)	Late Pleistocene	27.6	-85.0	27.3	temperate	#NV	single point source	continental	semi-enclosed and enclosed sea	10.5	Maximum	9.9	Maximum	#NV	#NV	3287.0	Partial observed	840.0	52000.0	1100.0	22.0	79.0
16	29-40 delta	delta (unclassified)	Late Pleistocene	27.6	-85.0	27.3	temperate	#NV	single point source	continental	semi-enclosed and enclosed sea	14.0	Unlimited observed	15.0	Maximum	#NV	#NV	5584.0	Partial observed	840.0	52000.0	1100.0	22.0	79.0
16	29-20 delta	delta complex	Late Pleistocene	27.6	-85.0	27.3	temperate	#NV	single point source	continental	semi-enclosed and enclosed sea	14.0	Unlimited observed	30.0	Maximum	#NV	#NV	6975.0	Partial observed	840.0	52000.0	1100.0	22.0	79.0
16	Madison Swanson delta	delta (unclassified)	Late Pleistocene	27.6	-85.0	27.3	temperate	#NV	single point source	continental	semi-enclosed and enclosed sea	12.5	Unlimited observed	12.2	Maximum	#NV	#NV	5623.0	Partial observed	840.0	52000.0	1100.0	22.0	79.0
16	Twin Ridges delta	delta (unclassified)	Late Pleistocene	27.6	-85.0	27.3	temperate	#NV	single point source	continental	semi-enclosed and enclosed sea	9.4	Unlimited observed	12.3	Maximum	#NV	#NV	3977.0	Partial observed	840.0	52000.0	1100.0	22.0	79.0
17	Stage 3 Colorado Delta (older)/La Vaca River delta	delta (unclassified)	Upper Pleistocene	27.8	-96.2	27.8	temperate	#NV	single point source	continental	semi-enclosed and enclosed sea	35.9	Maximum	52.2	Maximum	#NV	#NV	1422.8	Maximum	1600.0	110000.0	1200.0	2.4	104.3
17	Stage 3 Colorado Delta (younger)	delta (unclassified)	Upper Pleistocene	27.9	-95.3	27.9	temperate	river-dominated	single point source	continental	semi-enclosed and enclosed sea	84.9	Maximum	83.7	Maximum	#NV	#NV	6064.4	Maximum	1600.0	110000.0	1200.0	2.4	103.1
17	Stage 3 Brazos Delta/delta lobe (Mound 4 in SFU 1)	delta lobe	Upper Pleistocene	27.9	-95.5	27.9	temperate	river-dominated	single point source	continental	semi-enclosed and enclosed sea	87.3	Maximum	68.7	Maximum	80.0	Maximum	3901.8	Maximum	2000.0	120000.0	1200.0	6.0	112.9
17	Stage 6 Colorado Delta	delta (unclassified)	Late Mid-Pleistocene	27.6	-95.9	27.5	temperate	#NV	single point source	continental	semi-enclosed and enclosed sea	27.5	Maximum	24.9	Maximum	#NV	#NV	850.3	Maximum	1600.0	110000.0	1200.0	2.4	98.7
17	Stage 6 Brazos Delta	delta (unclassified)	Late Mid-Pleistocene	27.8	-94.8	27.8	temperate	#NV	single point source	continental	semi-enclosed and enclosed sea	24.8	Maximum	30.9	Maximum	#NV	#NV	878.7	Maximum	2000.0	120000.0	1200.0	6.0	117.4
17	fluvial-dominated shelf margin delta (SFU 9)	delta (unclassified)	#NV	27.0	-95.0	#NV	temperate	river-dominated	#NV	continental	semi-enclosed and enclosed sea	8.7	Unlimited observed	#NV	#NV	#NV	#NV	#NV	#NV	#NV	#NV	#NV	#NV	100.0
17	Western Louisiana Delta	delta (unclassified)	Late Pleistocene	27.9	-93.7	27.8	temperate	#NV	single point source	continental	semi-enclosed and enclosed sea	49.4	True	155.7	Partial observed	#NV	#NV	6123.2	Partial observed	#NV	#NV	#NV	#NV	193.0
18	Live Oak delta complex	delta complex	Palaeogene	27.9	-98.0	31.1	temperate	#NV	#NV	#NV	semi-enclosed and enclosed sea	23.9	Partial observed	54.9	True	#NV	#NV	1218.0	Partial observed	#NV	#NV	#NV	#NV	#NV
18	Luling Delta	delta lobe	Palaeogene	27.9	-98.0	31.1	temperate	#NV	#NV	#NV	semi-enclosed and enclosed sea	#NV	#NV	#NV	#NV	663.0	True	#NV	#NV	#NV	#NV	#NV	#NV	#NV
18	Slick Delta	delta lobe	Palaeogene	27.9	-98.0	31.1	temperate	mixed-process	#NV	#NV	semi-enclosed and enclosed sea	#NV	#NV	#NV	#NV	450.0	True	#NV	#NV	#NV	#NV	#NV	#NV	#NV
18	Zapata delta complex	delta complex	Palaeogene	26.5	-98.8	30.1	temperate	#NV	#NV	#NV	semi-enclosed and enclosed sea	36.7	Partial observed	84.3	True	900.0	unlimited observed	2784.0	Partial observed	#NV	#NV	#NV	#NV	#NV
18	Duval delta complex	delta complex	Palaeogene	27.3	-98.4	30.7	temperate	#NV	#NV	#NV	semi-enclosed and enclosed sea	24.0	Partial observed	160.0	Maximum	900.0	unlimited observed	3445.0	Partial observed	#NV	#NV	#NV	#NV	#NV
19	Shelf-margin delta (SF1 & SF2) offshore Louisiana	delta (unclassified)	Mid-Pleistocene	28.0	-91.8	27.9	temperate	river-dominated	single point source	continental	semi-enclosed and enclosed sea	7.6	Unlimited observed	7.7	Unlimited observed	#NV	#NV	31.0	Partial observed	5900.0	3300000.0	3700.0	490.0	170.0
20	Upper delta	delta (unclassified)	Mid-Pliocene	28.9	-89.0	28.3	temperate	mixed-process	#NV	#NV	semi-enclosed and enclosed sea	#NV	#NV	#NV	#NV	83.8	unlimited observed	#NV	#NV	#NV	#NV	#NV	#NV	#NV
20	Lower delta	delta (unclassified)	Mid-Pliocene	28.9	-89.0	28.3	temperate	mixed-process	#NV	#NV	semi-enclosed and enclosed sea	#NV	#NV	#NV	#NV	36.6	unlimited observed	#NV	#NV	#NV	#NV	#NV	#NV	#NV
21	Fuji-Einstein delta	delta complex	Quaternary (Mid- to Upper Pleistocene)	29.2	-88.0	29.0	temperate	#NV	#NV	continental	semi-enclosed and enclosed sea	20.0	Unlimited observed	40.0	Unlimited observed	313.0	Maximum	80.8	partial observed	#NV	#NV	#NV	#NV	120.3
21	delta lobe 1	delta lobe	Quaternary (Mid- to Upper Pleistocene)	29.2	-88.0	29.0	temperate	#NV	#NV	continental	semi-enclosed and enclosed sea	2.0	Maximum	7.0	Partial observed	#NV	#NV	11.3	partial observed	#NV	#NV	#NV	#NV	120.3
21	delta lobe 2	delta lobe	Quaternary (Mid- to Upper Pleistocene)	29.2	-88.0	29.0	temperate	#NV	#NV	continental	semi-enclosed and enclosed sea	14.0	Partial observed	23.0	Partial observed	#NV	#NV	18.7	partial observed	#NV	#NV	#NV	#NV	120.3
21	delta lobe 3	delta lobe	Quaternary (Mid- to Upper Pleistocene)	29.2	-88.0	29.0	temperate	#NV	#NV	continental	semi-enclosed and enclosed sea	#NV	#NV	#NV	#NV	#NV	#NV	14.8	partial observed	#NV	#NV	#NV	#NV	120.3
21	delta lobe 4	delta lobe	Quaternary (Mid- to Upper Pleistocene)	29.2	-88.0	29.0	temperate	#NV	#NV	continental	semi-enclosed and enclosed sea	#NV	#NV	6.0	Maximum	#NV	#NV	10.3	partial observed	#NV	#NV	#NV	#NV	120.3
21	delta lobe 5	delta lobe	Quaternary (Mid- to Upper Pleistocene)	29.2	-88.0	29.0	temperate	#NV	#NV	continental	semi-enclosed and enclosed sea	#NV	#NV	6.0	Maximum	#NV	#NV	4.1	partial observed	#NV	#NV	#NV	#NV	120.3
22	Western shelf-edge delta	delta (unclassified)	Late Quaternary	29.4	-87.8	29.0	temperate	#NV	single point source	continental	semi-enclosed and enclosed sea	12.6	Partial observed	21.2	True	128.0	Maximum	961.0	Maximum	1300.0	110000.0	1300.0	60.0	114.7
23	Delta complex a	delta complex	Quaternary (Upper Pleistocene)	29.6	-87.3	29.3	temperate	river-dominated	#NV	continental	semi-enclosed and enclosed sea	20.0	Maximum	40.0	Partial observed	#NV	#NV	#NV	#NV	#NV	#NV	#NV	#NV	60.0
23	Delta a1	delta lobe	Quaternary (Upper Pleistocene)	29.5	-87.4	29.3	temperate	river-dominated	single point source	continental	semi-enclosed and enclosed sea	12.0	True	16.0	Partial observed	90.0	Maximum	567.0	Partial observed	1300.0	110000.0	1300.0	60.0	60.0
23	Delta a2	delta lobe	Quaternary (Upper Pleistocene)	29.6	-87.3	29.4	temperate	river-dominated	#NV	continental	semi-enclosed and enclosed sea	8.0	Maximum	17.0	Maximum	120.0	Maximum	#NV	#NV	#NV	#NV	#NV	#NV	60.0
23	Delta a3	delta lobe	Quaternary (Upper Pleistocene)	29.7	-87.3	29.4	temperate	river-dominated	#NV	continental	semi-enclosed and enclosed sea	9.0	Maximum	14.0	Maximum	90.0	Maximum	#NV	#NV	#NV	#NV	#NV	#NV	60.0
23	Delta complex b	delta complex	Quaternary (Upper Pleistocene)	29.8	-87.2	29.6	temperate	river-dominated	#NV	continental	semi-enclosed and enclosed sea	8.2	True	9.5	True	55.0	True	#NV	#NV	#NV	#NV	#NV	#NV	60.0
23	Delta b1	delta lobe	Quaternary (Upper Pleistocene)	29.8	-87.2	29.6	temperate	river-dominated	#NV	continental	semi-enclosed and enclosed sea	4.5	Maximum	5.0	Maximum	40.0	Maximum	#NV	#NV	#NV	#NV	#NV	#NV	60.0
23	Delta b2	delta lobe	Quaternary (Upper Pleistocene)	29.8	-87.2	29.6	temperate	river-dominated	#NV	continental	semi-enclosed and enclosed sea	8.2	Maximum	9.5	True	55.0	Maximum	#NV	#NV	#NV	#NV	#NV	#NV	60.0
23	Delta c	delta lobe	Quaternary (Upper Pleistocene)	29.9	-87.1	29.7	temperate	river-dominated	#NV	continental	semi-enclosed and enclosed sea	6.5	True	6.5	True	65.0	Maximum	#NV	#NV	#NV	#NV	#NV	#NV	60.0
23	Delta complex d	delta complex	Quaternary (Upper Pleistocene)	30.0	-87.0	29.7	temperate	river-dominated	#NV	continental	semi-enclosed and enclosed sea	6.9	True	6.4	True	65.0	True	#NV	#NV	#NV	#NV	#NV	#NV	60.0
23	Delta d1	delta lobe	Quaternary (Upper Pleistocene)	30.0	-87.0	29.7	temperate	river-dominated	#NV	continental	semi-enclosed and enclosed sea	5.0	Maximum	5.7	Maximum	35.0	Maximum	#NV	#NV	#NV	#NV	#NV	#NV	60.0
23	Delta d2	delta lobe	Quaternary (Upper Pleistocene)	30.0	-87.0	29.7	temperate	river-dominated	#NV	continental	semi-enclosed and enclosed sea	6.9	Maximum	6.4	Maximum	65.0	Maximum	#NV	#NV	#NV	#NV	#NV	#NV	60.0
23	Delta complex e	delta complex	Quaternary (Upper Pleistocene)	30.0	-86.7	29.8	temperate	river-dominated	#NV	continental	semi-enclosed and enclosed sea	4.5	True	5.3	True	25.0	True	#NV	#NV	#NV	#NV	#NV	#NV	60.0
23	Delta e1	delta lobe	Quaternary (Upper Pleistocene)	30.1	-86.7	29.8	temperate	river-dominated	#NV	continental	semi-enclosed and enclosed sea	4.5	True	5.3	True	25.0	Maximum	#NV	#NV	#NV	#NV	#NV	#NV	60.0
23	Delta e2	delta lobe	Quaternary (Upper Pleistocene)	30.0	-86.7	29.8	temperate	river-dominated	#NV	continental	semi-enclosed and enclosed sea	4.4	True	3.5	True	25.0	Maximum	#NV	#NV	#NV	#NV	#NV	#NV	60.0
23	Delta f	delta lobe	Quaternary (Upper Pleistocene)	30.0	-86.6	29.7	temperate	river-dominated	#NV	continental	semi-enclosed and enclosed sea	4.8	Maximum	3.7	True	20.0	Maximum	#NV	#NV	#NV	#NV	#NV	#NV	60.0
24	Lagniappe Delta (during the Late Pleistocene)	delta complex	Late Pleistocene	29.6	-88.0	29.3	temperate	#NV	multiple point source	continental	semi-enclosed and enclosed sea	88.9	Partial observed	64.5	Maximum	100.0	Partial observed	2812.0	Partial observed	1440.0	135000.0	1300.0	68.5	132.2
25	Late Pleistocene shelf-edge delta N Okinawa Trough	delta (unclassified)	Late Pleistocene	29.7	127.6	29.7	temperate	#NV	single point source	continental	open sea	55.1	True	#NV	#NV	#NV	#NV	5300.6	Partial observed	6300.0	1800000.0	3200.0	900.0	521.7
26	Unit A Shelf-edge delta	delta (unclassified)	Late Pleistocene	34.9	129.2	35.9	temperate	#NV	single point source	continental	semi-enclosed and enclosed sea	34.9	Partial observed	59.3	Unlimited observed	50.0	Maximum	333.2	Partial observed	530.0	24000.0	500.0	9.2	60.0
26	Unit B Shelf-edge delta	delta (unclassified)	Late Pleistocene	34.9	129.2	35.9	temperate	#NV	single point source	continental	semi-enclosed and enclosed sea	20.3	Partial observed	62.1	Unlimited observed	30.0	Maximum	480.6	Partial observed	530.0	24000.0	500.0	9.2	60.0
26	Unit C Shelf-edge delta	delta (unclassified)	Late Pleistocene	34.9	129.2	35.9	temperate	mixed-process	single point source	continental	semi-enclosed and enclosed sea	16.5	Partial observed	81.4	Unlimited observed	30.0	Maximum	1237.2	Partial observed	530.0	24000.0	500.0	9.2	60.0
27	Cape Charles Delta	delta (unclassified)	Early Cretaceous	37.3	-74.8	29.6	temperate	#NV	single point source	#NV	#NV	85.5	Maximum	80.0	Maximum	900.0	unlimited observed	8000.0	Maximum	660.0	38000.0	1500.0	10.0	#NV
27	Ocean City Delta	delta complex	Early Cretaceous	38.0	-73.8	30.0	temperate	#NV	single point source	#NV	#NV	68.4	Maximum	80.2	Partial observed	900.0	unlimited observed	3000.0	Maximum	710.0	71000.0	960.0	32.0	#NV
27	S delta lobe	delta lobe	Early Cretaceous	37.8	-74.0	29.8	temperate	#NV	single point source	#NV	#NV	45.2	Maximum	25.0	True	#NV	#NV	#NV	#NV	710.0	71000.0	960.0	32.0	#NV
27	N delta lobe	delta lobe	Early Cretaceous	38.3	-73.8	30.2	temperate	#NV	single point source	#NV	#NV	61.5	Maximum	30.5	True	#NV	#NV	#NV	#NV	710.0	71000.0	960.0	32.0	#NV
27	Long Branch Delta	delta (unclassified)	Early Cretaceous	39.0	-72.5	30.5	temperate	#NV	multiple point source	#NV	#NV	77.2	Maximum	81.2	Partial observed	900.0	unlimited observed	5000.0	Maximum	1190.0	63000.0	1600.0	25.0	#NV
28	Bakircay shelf-edge delta (depositional sequence 2)	delta lobe	Late Pleistocene	38.5	26.5	38.5	temperate	#NV	single point source	continental	semi-enclosed and enclosed sea	11.8	Partial observed	#NV	#NV	#NV	#NV	#NV	#NV	100.0	3400.0	1400.0	0.7	#NV
29	Late Pleistocene Gediz Delta (Unit 2/depositional sequence 2)	delta complex	Late Pleistocene	39.0	27.2	39.0	temperate	#NV	single point source	continental	semi-enclosed and enclosed sea	2.5	Unlimited observed	#NV	#NV	#NV	#NV	#NV	#NV	350.0	18000.0	1500.0	2.3	#NV
30	Sakarya shelf-edge delta (Unit 2)	delta (unclassified)	Late Quaternary	41.3	30.6	41.3	temperate	#NV	single point source	continental	semi-enclosed and enclosed sea	1.9	True	#NV	#NV	#NV	#NV	#NV	#NV	820.0	57000.0	1000.0	5.6	#NV
31	Clinothem 9 shelf-edge delta	delta (unclassified)	Late Cretaceous (Maastrichtian)	41.5	-108.5	#NV	#NV	mixed-process	#NV	#NV	#NV	59.1	Unlimited observed	#NV	#NV	38.8	True	#NV	#NV	#NV	#NV	#NV	#NV	#NV
31	Clinothem 10 shelf-edge delta	delta (unclassified)	Late Cretaceous (Maastrichtian)	41.7	-107.5	#NV	#NV	mixed-process	#NV	#NV	#NV	28.3	Unlimited observed	#NV	#NV	22.4	True	#NV	#NV	#NV	#NV	#NV	#NV	#NV
32	progradational lowstand deltaic wedge (Unit C)	delta (unclassified)	Late Pleistocene	43.2	4.8	41.7	temperate	#NV	#NV	continental	semi-enclosed and enclosed sea	#NV	#NV	#NV	#NV	63.4	True	#NV	#NV	#NV	#NV	#NV	#NV	55.0
33	Missisauga Delta	delta (unclassified)	Early Cretaceous	43.5	-60.3	33.0	temperate	mixed-process	single point source	#NV	open sea	#NV	#NV	#NV	#NV	150.0	Maximum	#NV	#NV	4000.0	1200000.0	1900.0	340.0	#NV
34	Shelf-edge delta section B	delta (unclassified)	Lower Oligocene	49.6	21.2	#NV	temperate	#NV	#NV	#NV	#NV	#NV	#NV	#NV	#NV	81.0	Maximum	#NV	#NV	#NV	#NV	#NV	#NV	#NV
35	shelf-edge delta or their lobe 1	delta (unclassified)	Palaeogene (Palaeocene-Early Eocene)	52.4	-13.2	40.8	temperate	#NV	single point source	#NV	#NV	2.9	Partial observed	5.1	True	#NV	#NV	#NV	#NV	#NV	#NV	#NV	#NV	#NV
35	shelf-edge delta or their lobe 2	delta (unclassified)	Palaeogene (Palaeocene-Early Eocene)	52.4	-13.1	40.9	temperate	#NV	single point source	#NV	#NV	4.5	Partial observed	6.8	True	#NV	#NV	#NV	#NV	#NV	#NV	#NV	#NV	#NV
35	shelf-edge delta	delta complex	Palaeogene (Palaeocene-Early Eocene)	52.5	-13.0	40.9	temper

Appendix C
Published versions of chapters 3 and 4

Chapters 3 and 4 have been published as follows:

- **Chapter 3:** Bührig, L.H., Colombera, L., Patacci, M., Mountney, N.P., & McCaffrey, W.D. 2022a. A global analysis of controls on submarine-canyon geomorphology. *Earth-Science Reviews*. 233, 104150. doi:10.1016/j.earscirev.2022.104150
- **Chapter 4:** Bührig, L.H., Colombera, L., Patacci, M., Mountney, N.P., & McCaffrey, W.D. 2022b. Tectonic influence on the geomorphology of submarine canyons: implications for deep-water sedimentary systems. *Frontiers in Earth Science*. 10:836823. doi:10.3389/feart.2022.836823

The two articles are included in the following pages.

Earth-Science Reviews 233 (2022) 104150

Contents lists available at ScienceDirect

Earth-Science Reviews

journal homepage: www.elsevier.com/locate/earscirev

A global analysis of controls on submarine-canyon geomorphology

Laura H. Bührig *, Luca Colombera, Marco Patacci, Nigel P. Mountney, William D. McCaffrey

School of Earth and Environment, University of Leeds, LS2 9JT, United Kingdom

ARTICLE INFO

Keywords:
Quantitative analysis
Scaling relationships
Geometry
Source-to-sink
Deep marine
Continental slope

ABSTRACT

The role of possible controlling factors in influencing the geomorphology of submarine canyons has been investigated using a database of 282 globally distributed modern examples collated from the literature and open-source worldwide bathymetry. Canyon geomorphology has been characterised quantitatively in terms of maximum and average canyon dimensions, canyon sinuosity, average canyon thalweg gradient, and maximum canyon sidewall steepness. An assessment is made of how geomorphological characteristics vary with respect to the position of the canyon apex relative to the shelf break, continental-margin type, terrestrial source-to-sink system setting, oceanographic environment, and latitude. Scaling relationships between canyon morphometric parameters, and correlations between these and attributes of the canyon physiographic settings, terrestrial catchments, and continental shelves and slopes, have been quantified.

Key findings are as follows: (i) a number of scaling relationships describing canyon morphometry (e.g. scaling between maximum canyon dimensions, relationships of maximum canyon sidewall steepness with maximum canyon width and depth) can be recognised globally, suggesting their general predictive value; (ii) possible causal links are identified between hydrodynamic processes (e.g. upwelling, longshore- and along-slope currents) and canyon morphology; (iii) potential predictors of aspects of canyon geomorphology include whether a canyon is incised into the shelf or confined to the slope, the continental-margin type, the oceanographic environment, latitude, and shelf-break depth; (iv) similarity in the distributions of maximum width-to-maximum depth ratios across all settings suggests that the relative magnitudes of canyon-margin erosion and intra-canyon deposition do not vary greatly depending on setting or canyon size.

The relationships between canyon geomorphology and environmental variables identified in this study may be incorporated into conceptual models describing canyon geomorphology and its relationship both to other elements of deep-water systems, and to its broader source-to-sink context. The results provide a framework for future experimental and numerical studies of canyon geomorphology.

1. Introduction

Submarine canyons constitute important conduits for the transfer of water masses, sediment, nutrients, organic matter and pollutants between shallow- and deep-marine environments, across continental slopes (Harris and Whiteway, 2011; Fildani, 2017). They control the sorting and segregation of sediments that are ultimately deposited in deep-marine environments, via their morphology (e.g. Soutter et al., 2021; Wan et al., 2021) and distance from fluvial outlets and littoral cells (e.g. Sweet and Blum, 2016; Sweet et al., 2020). Their ability to intercept and influence oceanic currents along shelves (e.g. Jordi et al., 2008) and slopes (e.g. Marchès et al., 2007; Voigt et al., 2013), can set hydrodynamic conditions in vicinity of their location (e.g. Allen et al., 2001; Connolly and Hickey, 2014; Saldías and Allen, 2020). Submarine canyons can impact the formation and evolution of slope systems by reducing local gradients (Orange et al., 1994), capturing and redirecting sediment pathways from adjacent canyons (e.g. Bernhardt et al., 2015), and functioning as tributaries to other canyons (e.g. Mountjoy et al., 2009). Buried canyons that are partially infilled can influence the pathways of younger ones by forming negative seafloor topography that can confine sediment transport (e.g. Pratson et al., 1994). Thus, they represent a crucial link for sediment routing from terrestrial hinterlands, across and along shelves and slopes, to intra-slope and basin-floor sinks.

The presence of submarine canyons can also influence the formation of gas hydrates (Crutchley et al., 2017) and the associated processes of trapping and release of hydrocarbons (e.g. Davies et al., 2012; Benjamin et al., 2015). Canyons can promote salt migration within the subsurface and impact the geometry of salt bodies (Fiduk, 1995), can increase the

* Corresponding author.
E-mail address: lhbuehrig@gmail.com (L.H. Bührig).

https://doi.org/10.1016/j.earscirev.2022.104150
Received 16 December 2021; Received in revised form 25 June 2022; Accepted 5 August 2022
Available online 14 August 2022
0012-8252/© 2022 The Authors. Published by Elsevier B.V. This is an open access article under the CC BY license (http://creativecommons.org/licenses/by/4.0/).

salinity of shelf waters via upwelling of deeper slope waters (e.g. Connolly and Hickey, 2014), and can tap into groundwater aquifers (e.g. Paldor et al., 2020). The association of submarine canyons with hydrocarbon-bearing deposits can promote vertical hydrocarbon migration and expulsion, which in turn can generate trains of pockmarks in younger canyons (e.g. Benjamin et al., 2015). Pockmarks can also form atop of canyon fills as a result of sediment compaction (e.g. Jobe et al., 2011); given that these structures can reach diameters of several hundred metres and depths of tens of metres (e.g. Jobe et al., 2011; Benjamin et al., 2015), their presence might affect canyon internal flows and flow pathways on the seafloor.

Submarine canyons are also important for faunal communities, for which they provide significant habitats. Aspects of their physiography have been suggested to exert control on the biodiversity and abundance of faunal assemblages; these aspects include canyon spacing, gradient, dendricity and sinuosity (Fanelli et al., 2018), canyon size and magnitude of incision of the shelf (Santora et al., 2018). The effect of submarine-canyon geomorphology on hydrodynamic processes also impacts the spatial distribution of faunal communities like zooplankton (Allen et al., 2001).

Submarine canyons are linked to potential geohazards, due to the ability of intra-canyon slope failures to trigger tsunamis (e.g. Orange et al., 1994; Power et al., 2016), and to the influence of canyon geomorphology on tsunami propagation (e.g. Aranguiz and Shibayama, 2013; Iglesias et al., 2014). Moreover, canyon-crossing seafloor telecommunication cables are at risk of breakage from canyon-margin failure and canyon-traversing sediment gravity flows (e.g. Heezen and Ewing, 1952; Hsu et al., 2008; Carter et al., 2014). Such flows are also considered responsible for the displacement of marine pipelines (e.g. Porcile et al., 2020), hence posing a hydrocarbon leakage hazard, for example. Moreover, it has been suggested that the upslope transport of warm water currents through submarine canyons along Antarctica contributes to the acceleration of ice sheet loss, which in turn influences global sea-level rise (e.g. Morrison et al., 2020; Gales et al., 2021, and references therein).

The sedimentary fills of submarine canyons, and their linkage to down-system submarine fans (e.g. Covault et al., 2011b; Jobe et al., 2011) and contourite-drift systems (e.g. Wang et al., 2018; Warratz et al., 2019; Serra et al., 2020; Rodrigues et al., 2022, and references therein), make them important references and targets for hydrocarbon exploration. Canyons can represent significant sinks for both macro- (e.g. Pierdomenico et al., 2019; Zhong and Peng, 2021) and micro-pollutants (e.g. Azaroff et al., 2020).

Hence, the study of submarine canyons represents a key area of interest for research linked to a broad range of scientific disciplines (Matos et al., 2018).

Source-to-sink (S2S) research investigates sediment budget dynamics and process-response relationships in both ancient and modern sedimentary systems. Scaling relationships between sedimentary systems and attributes of segments of the S2S profile are commonly established. However, the focus of such studies has been chiefly on fluvial systems and submarine fans, whereas the submarine canyons that link them remain relatively understudied (e.g. Sømme et al., 2009; Nyberg et al., 2018).

Quantitative studies provide a means for the systematic investigation of scaling relationships across and within sedimentary environments, with consideration of environmental controls such as climate, hydrodynamic processes, or tectonic setting, which dictate sediment source areas, transport pathways and sinks (e.g. Wang et al., 2019, 2020; Budai et al., 2021; Cosgrove et al., 2021). Such studies enable an assessment of the relative importance of autogenic versus allogenic controls on aspects of the geomorphology, architecture and facies characteristics of subenvironments, and of scaling-relationships they may exhibit. Such insights can be applied to infer the geometrical characteristics of formative subenvironments based on preserved architectures seen in outcrop and subsurface studies (e.g. Martinsen et al., 2010; Xu et al., 2017), and to inform laboratory and modelling studies (Nyberg et al., 2018). The applied usefulness of scaling relationships for the reconstruction and modelling of sedimentary systems at different scales of observations has been highlighted by various authors (e.g. Sømme et al., 2009; Martinsen et al., 2010; Helland-Hansen et al., 2016; Bhattacharya et al., 2016; Xu et al., 2017; Nyberg et al., 2018).

Scaling relationships between aspects of canyon geomorphology and controlling factors have been identified in quantitative studies of submarine canyons at regional, continental, and global scales (see section 2.2). However, relationships between canyon morphometric parameters have only been partially investigated using global datasets, and the general applicability of such relationships across environmental settings is largely unconstrained. This study addresses these knowledge gaps.

The aim of this study is to improve our understanding of controlling factors on submarine-canyon geomorphology, and of the extent to which scaling relationships of canyon morphometric parameters – both mutually and with attributes of their physiographic and environmental setting – can be recognised in modern canyons. To achieve this, a global database has been built utilising datasets from published case studies of submarine canyons combined with data obtained from open-source bathymetry to support the following research objectives:

(i) to characterize morphometric parameters of submarine canyons, both generally and with consideration of the role of environmental factors (canyon-apex location relative to the shelf-break, continental-margin type, source-to-sink system setting, oceanographic environment and climate zones);
(ii) to identify and assess scaling relationships between canyon morphometric parameters;
(iii) to evaluate relationships between canyon morphometric parameters and other variables, including canyon bathymetry, distance between the canyon apex and the shoreline, attributes of the catchment, shelf and slope, and latitude of the canyon;
(iv) to identify and discuss possible causal links between observed scaling relationships and autogenic and allogenic controls, the configuration of the associated source-to-sink system, and the environmental setting.

2. Background

2.1. Controls on submarine canyon evolution

Submarine canyons are highly complex sedimentary systems whose evolution is influenced by a wide range of processes and environmental factors (e.g. Shepard, 1936, 1981; Pratson and Coakley, 1996; Pratson et al., 2007), as demonstrated in the recent comprehensive literature reviews by Puig et al. (2014) and Amblas et al. (2017). Despite being well studied, the genesis and long-term evolution of submarine canyons remain topics of ongoing debate, and require further understanding (e.g. Pratson et al., 2007, and references therein; Baztan et al., 2005; Puig et al., 2014; Smith et al., 2017, 2018). The relative importance of controls on canyon geomorphology is still not well understood (Li et al., 2022).

Various physiographic and environmental factors are known to influence canyon evolution by exerting controls on connectivity to sediment sources, on mechanisms of sediment distribution, and on types of canyon evolutionary processes. Physiographic factors that have been invoked include the distance of the canyon to fluvial outlets and littoral cells (e.g. Sweet and Blum, 2016; Sweet et al., 2020), shelf width and gradient in the vicinity of the canyon (e.g. Covault and Graham, 2010; Gamberi et al., 2015; Jipa and Panin, 2020; Bernhardt and Schwanghart, 2021), and continental-slope gradients (e.g. McGregor, 1983; Orange et al., 1994; Lo Iacono et al., 2014). Environmental factors comprise local- and regional-scale tectonics (e.g. Ratzov et al., 2012; Micallef et al., 2014; de Almeida et al., 2015; Soutter et al., 2021), sea-level fluctuations (e.g. Rasmussen, 1994; Mitchell et al., 2007; Maier et al.,

2018), and climate (e.g. Henrich et al., 2010), including glaciations (e.g. Harris et al., 2014; Gales et al., 2021).

The oceanographic regime is also thought to influence gully formation and failures along canyon walls (e.g. Wang et al., 2022), and is a possible cause for particular geomorphic characteristics of Arctic and Antarctic gullies (Gales et al., 2013). Also, a global study of late Quaternary incised-valley fills by Wang et al. (2020) demonstrated that the facies architecture of valley fills varies across open oceans and semi-enclosed and enclosed seas, which exhibit contrasting hydrodynamics. Considering the role of marine hydrodynamic processes in the delivery of sediment to canyons, and in intra-canyon sediment transport and erosion (see section 4.2.2), and given the genetic linkage between cross-shelf lowstand fluvial systems and submarine canyons (e.g. Harris and Whiteway, 2011; Maier et al., 2018), more research is needed to establish whether and how canyon geomorphology varies as a function of the oceanographic setting.

Anthropogenic influences can also affect the evolution of modern submarine canyons, in several ways. Sediment gravity flows can be triggered by trawling (e.g. Palanques et al., 2006; Lopez-Fernandez et al., 2013), whereas farming and deforestation (e.g. Milliman and Farnsworth, 2011), and the artificial diversion (e.g. Higgins et al., 2018) or damming of rivers (e.g. Sheng et al., 2019) may impact catchment processes and fluvial discharge rates, which in turn can impact sediment delivery to submarine canyons (e.g. Mazières et al., 2014; Puig et al., 2017).

2.2. Submarine canyon studies

Submarine canyons have been the subject of many prior studies: Matos et al. (2018) conducted a review of the scientific literature on submarine canyons published between 1929 and 2016, considering 1,968 publications. These authors identified a geographical bias in prior canyon research: less than 10% of the canyons mapped globally by Harris et al. (2014) are covered by the literature, and almost half of the 1,968 publications concentrate exclusively on 11 intensively studied submarine canyons. Consequently, research efforts have largely been directed towards the particular environmental conditions and set of controls associated with a limited subset of canyons, depending on the thematic focus of the case study (see Matos et al., 2018). However, the rate at which studies on submarine canyons are published has further accelerated in recent years (Matos et al., 2018), due in part to technological advances in data acquisition and processing (e.g. Xu, 2011; Urías Espinosa et al., 2016; Simmons et al., 2020; Bailey et al., 2021). Here we summarise examples of regional, continental, and global-scale quantitative studies of submarine-canyon geomorphology that consider the canyon physiographic and environmental setting, focussing on aspects of these studies that are relevant to the research presented in this paper.

Canyon classification schemes based on case studies from specific regions have been proposed to be universally applicable, for example where specific sets of controls are associated with a canyon (canyon-head location relative to the shelf break, type of intracanyon sedimentary processes, sediment sources and sediment characteristics; cf. Jobe et al., 2011), and models for canyon evolution have been considered relevant to canyons that developed under similar external controls, as for canyons associated with active margins (e.g. Micallef et al., 2014). However, a study of 713 submarine canyons located offshore Australia by Huang et al. (2014) revealed great variability and complexity in aspects of canyon geomorphology at the continental scale, which challenges the applicability of insights generated by regional studies at a larger scale. The authors established a hierarchical classification of shelf-incising and slope-confined canyons based on the following canyon metrics: percentage of canyon area characterised by slope gradients exceeding 15°, average canyon thalweg gradient, volume subtended by the canyon channelform, canyon-head incision depth, and distance to the nearest neighbouring canyon. Their findings demonstrate a higher number of canyon classes for slope-confined canyons compared to shelf-incising ones (see Figures 6 & 7 of Huang et al., 2014).

Relationships between canyon geomorphology and the position of the canyon head relative to the shelf-break were also recognised in other regional-scale studies. In a study of 80 canyons offshore California (Santora et al., 2018), differences in frequency distributions of canyon dimensions were documented across shelf-incising versus slope-confined canyons, whereby shelf-incising canyons tend to have greater areas, lengths, widths and mean depths. Additionally, the authors found that canyon area scaled positively with canyon length and width, independently of the canyon-head location relative to the shelf-margin. Li et al. (2022) documented pronounced differences in 48 shelf-incised submarine canyons from the northwest South China Sea.

Furthermore, relationships between characteristics of S2S systems and canyon geomorphology are demonstrated in a number of regional-scale studies. For example, Jipa and Panin (2020) noted that the few submarine canyons in the N and NW region of the Black Sea were associated with continental shelves up to 200 km wide, large fluvial systems of several thousand kilometres length and low-relief catchments of up to several hundred metres elevation. Such canyons were characterised by a single main stem and had large submarine fans as distal segments. By contrast, submarine canyons along the E and NE Black Sea margins, characterised by (i) high-elevation catchments, (ii) short feeder rivers (up to several hundred kilometres length), and (ii) shelves that are rarely wider than 15 km, tend to form dendritic drainage networks and are more closely spaced; also, their submarine fans tend to form a continuous apron-like zone. Their findings were in part corroborated by those of Fernane et al. (2022), who demonstrated that submarine canyons along the western Algerian margin display a greater degree of dendricity and incision into the shelf where they are associated with a narrow shelf configuration compared to canyons associated with wide shelf margins.

For the interpretation of autogenic and allogenic controls on canyon geomorphology, an improved understanding of the sensitivity of canyon morphometric parameters to seafloor processes and environmental factors is required. In contrast to regional studies, global-scale studies have the potential to constrain the variability in potential controls more fully in a broad range of environmental settings. Previous global-scale studies that have investigated aspects of submarine canyon geomorphology (e.g. Nelson et al., 1970; De Pippo et al., 1999; Sømme et al., 2009; Covault et al., 2011a; Harris and Whiteway, 2011; Harris et al., 2014; Soutter et al., 2021) and assessed the relative importance of factors promoting sediment-connection of canyons to shorelines (Bernhardt and Schwanghart, 2021) constitute important contributions to a fuller understanding of submarine canyon evolution. Nevertheless, such global investigations of the geomorphology of modern submarine canyons have been limited to individual canyon morphometric parameters and to consideration of specific environmental controls, with the datasets being limited in terms of their geographic coverage prior to the advent of a global inventory of modern submarine canyons – comprising 5,849 canyons – compiled by Harris and Whiteway (2011).

In their global study, De Pippo et al. (1999) compiled a database of selected aspects of the geomorphology of 50 submarine canyons, including canyon length, average gradient, and cross-sectional profile, together with variables describing their environmental setting (see Figure 1 of De Pippo et al., 1999). For example, the authors applied their database to tease out possible relationships between canyon geomorphology and potential controls posed by the morphological and tectonic characteristics of the associated continental margin; they additionally assessed relationships between canyon morphometric parameters, e.g. for canyon length and average canyon thalweg gradient (see Figure 5 of De Pippo et al., 1999).

Leveraging advancements in bathymetric mapping of seafloors, the study by Harris and Whiteway (2011) provided a summary of aspects of canyon geomorphology and their physiographic setting for 5,849 submarine canyons classified on geographic region, continental-margin type, location of the canyon-head relative to the shelf-break and

connection to a fluvial system. The following variables were considered: canyon length, average thalweg gradient, average sinuosity, bathymetric range, spacing, and dendricity; descriptive statistics were presented for canyons classified on margin type, canyon-head location relative to the shelf break, connection to a fluvial system, and geographic region (Table 1 of Harris and Whiteway, 2011). Statistical analyses revealed that active-margin canyons are on average steeper and shorter than their counterparts along passive margins, whereas overall canyon sinuosity tends to be similar (Figure 8 of Harris and Whiteway, 2011). In addition, the authors documented relationships between mean values of canyon parameters obtained for groups of canyons classified by geographic regions and distinguished into active- and passive-margin settings. Canyons associated with an insular-margin setting were excluded from the correlation analyses. Moreover, the authors demonstrated the lack of a relationship between latitude and average canyon sinuosity for shelf-incising canyons (Figure 9 of Harris and Whiteway, 2011). The importance of fluvial sediment connection on canyon length was inferred from the observation that canyons associated with fluvial systems and incising the shelf tend to be longer than shelf-incising canyons without a river connection and slope-confined canyons, by factors 1.60 and 2.07, respectively. In non-polar regions, Harris and Whiteway (2011) showed a positive linear relationship between the percentage of shelf-incising canyons in a geographic region and sediment discharge from rivers (Figure 10 of Harris and Whiteway, 2011).

In the first published digital geomorphic seafloor map by Harris et al. (2014), the authors identified 9,477 submarine canyons. The significant number of newly recognised canyons reflect in part the higher resolution of seafloor data, but also the fact that canyons associated with plateaux adjoined to continental margins were also incorporated, unlike in Harris and Whiteway (2011; see Harris et al., 2014). Harris et al. (2014) calculated mean values of canyon area and length both for the global dataset and separately for major geographic regions. The results were further distinguished based on the location of the canyon head relative to the shelf break. In addition, the mean incision depth was reported for shelf-incising canyons in all regions (see their Table 9) and for slope-confined ones in general (Harris et al., 2014). On average, canyons in the latter group display greater average depth, shorter lengths and about half the area, compared to canyons that incise the shelf. Harris et al. (2014) also showed that submarine canyons in polar regions are, on average, about twice as large in area relative to the global average; in addition to characteristics of the slope and basin-floor environments in these settings, Harris et al. (2014) linked these attributes to a control by sediment supply to deep-marine environments during glacial intervals of the Cenozoic. Arctic and Antarctic canyons tend to be the longest of all differentiated geographic regions, but only by a modest margin; compared to submarine canyons in the South Atlantic, for example, their average lengths are only 1.20 and 1.21 times larger. Shelf-incising canyons of the Arctic and Antarctica also tend to have the largest values of mean incision depth across all investigated regions, but on average they are only 1.035 and 1.006 times deeper than canyons in the North Atlantic. These findings, together with the low variability in mean values of average canyon sinuosity for polar and non-polar regions documented by Harris and Whiteway (2011), suggest that factors related to latitudinal setting variably control aspects of submarine-canyon geomorphology, and that the strength in scaling might show pronounced regional variabilities.

Two global studies that have focused on the longitudinal profiles of submarine canyons are the studies by Covault et al. (2011a) and Soutter et al. (2021), who investigated the longitudinal profiles of a combination of 20 canyon and channels and of 377 submarine canyons, respectively. Covault et al. (2011a) established links between the longitudinal-profile shape – classified as convex, slightly concave or very concave – and both the margin type and the depositional architecture of deep-water environments (see their Fig. 9). Soutter et al. (2021) instead investigated and discussed relationships between the Normalised Concavity Index of canyon profiles and controlling factors including attributes of the terrestrial catchment, climate and tectonic setting, as well as canyon-head location relative to the shelf break. The authors inferred a dominant tectonic control on canyon concavity, that the connection to a river is a secondary control, and that the climate of the hinterland is a relatively subordinate factor.

Collectively, these examples document the variability in canyon morphometrics but in a way that suggests that there is no individual factor or single set of overriding controls emerging from their analyses.

The quantitative global assessment of canyon geomorphology undertaken in this study with consideration of aspects of the S2S system and of the environmental and physiographic setting aims to augment the findings of these earlier studies, and the current empirical knowledge of canyon geomorphology and of its links to potential controls.

3. Dataset and methodology

A database was collated that stores data describing the geomorphology of submarine canyons, their environmental context and geological controlling factors. Data have been sourced from 282 globally distributed modern submarine canyons and have been grouped into 96 separate case studies, with each case study corresponding to the study of one or several submarine canyons by a particular group of researchers (Fig. 1. and Table 1). The database comprises literature-derived, high-resolution bathymetric surveys of the seabed and high-resolution seismic datasets of the shallow subsurface, derived from 135 publications (Table 1) and open-source worldwide bathymetry data sets (https://www.ncei.noaa.gov/maps/bathymetry/, n.d, GEBCO 2019 NOAA NCEI Visualization; Google Earth).

3.1. Submarine canyon definition

In this study, a submarine canyon is defined as a single dominantly erosional channel form incised into a continental slope. The chosen definition of submarine canyon does not consider criteria relating to bathymetric setting, minimum canyon dimensions (cf. Harris and Whiteway, 2011), genetic origin, or canyon cross-sectional shape, and is therefore inclusive of what other authors commonly refer to as 'gullies' (e.g. Field et al., 1999; Gales et al., 2013; Chen et al., 2017), 'gulleys' (e.g. Gulliksen, 1978) or 'potential submarine canyons' (e.g. de Almeida et al., 2015). A general definition was adopted for the following reasons: (i) submarine gullies have been considered to constitute forms at the early stage of canyon formation (e.g. Amblas et al., 2017); (ii) canyon geomorphologic attributes such as canyon size can be inherently limited by their physiographic setting; and (iii) both terms are variably used for smaller-scale erosional channel-forms on the slope.

The canyon apex is defined as the point of the shallowest bathymetry and canyon mouth as the most distal point, along a canyon axis. The term "canyon apex" has been used herein in preference to "canyon head", the latter being a common but loosely defined term in the literature referring to the proximal part of a submarine canyon. Therefore "canyon apex" is used *sensu stricto* and "canyon head" *sensu lato*. In networks of connected channel forms, each channel-form is treated as an individual submarine canyon, whereas the network itself is termed a 'canyon system' (e.g. Mitchell et al., 2007; Mountjoy et al., 2009).

3.2. Study variables

Data on submarine canyons, environmental setting and external controlling factors have been coded in the form of attributes recorded in the Deep-Marine Architecture Knowledge Store (DMAKS; Cullis et al., 2019). DMAKS is a relational database that allows the systematic and standardised collation of data on deep-water sedimentary systems, as originally obtained using different methods (e.g. outcrop, core, seismic, bathymetric, sonar imaging). DMAKS stores data on the architectural, geomorphological and facies characteristics of deep-water depositional systems, as well as on their external controls and depositional context

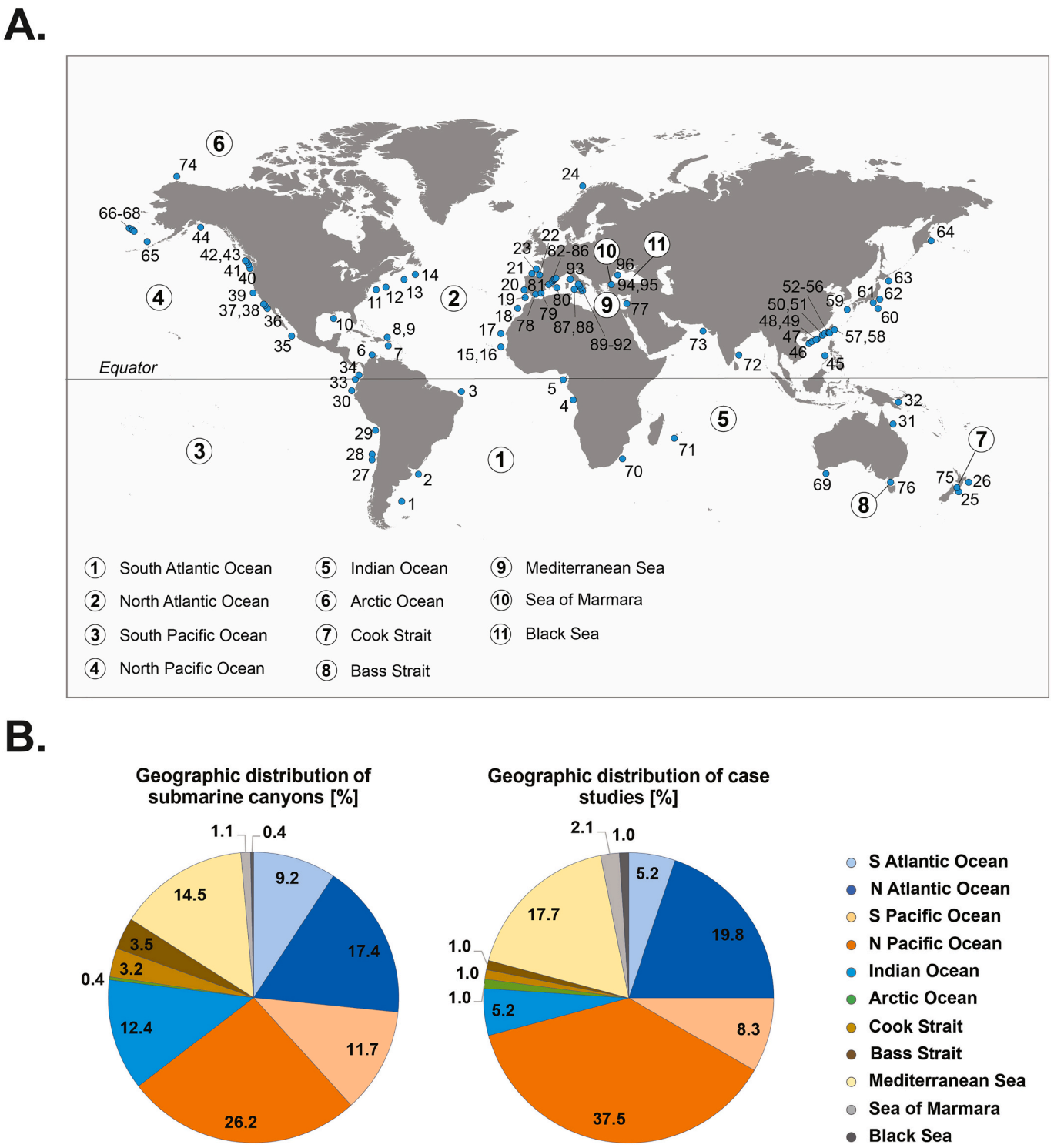

Fig. 1. A. Overview map of distribution of the 96 case studies. B. Geographic distribution of the 96 case studies and 282 studied submarine canyons (World map from freevectormaps.com).

(Cullis et al., 2019). Several additional bespoke attributes have been added to DMAKS to enable the present study.

The dataset for this study has been obtained from multiple sources, including the peer-reviewed literature and government agency sources. Values were extracted from the texts or manually measured or calculated by us. Inherent to this approach are various sources of error, including the heterogeneity of the dataset and undetected errors in the primary datasets; these limitations are discussed in section 3.3.

The full set of variables employed in the analyses undertaken in this study is summarised in Table 2.

3.2.1. *Canyon morphometric parameters*

Canyon geomorphology has been characterised by the following six morphometric parameters: (i) canyon length, (ii) canyon width (maximum and streamwise average), (iii) canyon bankfull depth (maximum and streamwise average), (iv) overall canyon sinuosity, (v) average canyon thalweg gradient, and (vi) maximum canyon sidewall steepness (Fig. 2a). Definitions of these variables are reported in Table 2.

Table 1
Overview of the 96 case studies and associated 135 literature data sources of the present study. Numbers in brackets refer to channel forms termed as submarine 'gullies' by the authors. See Fig. 1 for locations.

ID	Case study	No. of canyons	Oceanic region	Reference(s)
1	Patagonia canyons, SE Argentina	8	South Atlantic Ocean	Lastras et al., *2011a*
2	Mar del Plata Canyon, E Argentina	1	South Atlantic Ocean	Krastel et al., *2011*; Warratz et al., *2019*
3	Potiguar Basin canyons, NE Brazil	14	South Atlantic Ocean	de Almeida et al., *2015*
4	Congo Canyon, W Democratic Republic of Congo	1	South Atlantic Ocean	Babonneau et al., *2002*;Ferry et al., *2004*
5	Avon and Mahin canyons, SW Nigeria	2	South Atlantic Ocean	Jimoh et al., *2018*
6	Aguja Canyon, N Colombia	1	North Atlantic Ocean (Caribbean Sea)	Restrepo-Correa and Ojeda, *2010*
7	Guayanilla canyon system, S Puerto Rico	4	North Atlantic Ocean (Caribbean Sea)	Trumbull and Garrison, *1973*
8	Arecibo and Quebradillas canyons, NW Puerto Rico	2	North Atlantic Ocean	Gardner et al., *1980*
9	Mona Canyon, NW Puerto Rico	1	North Atlantic Ocean	Mondziel et al., *2010*
10	Mississippi Canyon, S USA	1	North Atlantic Ocean (Gulf of Mexico)	Coleman et al., *1982*
11	Hudson Canyon, NE USA	1	North Atlantic Ocean	Rona et al., *2015*
12	Lydonia and Oceanographer canyons, NE USA	2	North Atlantic Ocean	Valentine et al., *1980*
13	Logan Canyon, SE Canada	1	North Atlantic Ocean	Li et al., *2019*
14	SW Grand Banks Slope canyons, SE Canada	3	North Atlantic Ocean	Armitage et al., *2010*
15	Dakar Canyon, W Senegal	1	North Atlantic Ocean	Pierau et al., *2010, 2011*
16	Cayar Canyon, W Senegal	1	North Atlantic Ocean	Dietz et al., *1968*
17	Timiris Canyon, NW Mauritania	1	North Atlantic Ocean	Krastel et al., 2004; Antobreh and Krastel, *2006*
18	Agadir Canyon, SW Morocco	1	North Atlantic Ocean	Ercilla et al., *1998*; Wynn et al., *2002*
19	Faro and Portimao canyons, SW Portugal	2	North Atlantic Ocean (Gulf of Cadiz)	Mulder et al., *2006*
20	Nazaré, Cascais and Setubal-Lisbon canyons, W Portugal	4	North Atlantic Ocean	Arzola et al., *2008*; Lastras et al., *2009*; Allin et al., *2016*
21	Aviles Canyon system and Navia canyon, N Spain	5	North Atlantic Ocean (Bay of Biscay)	Gómez-Ballesteros et al., *2014*
22	Capbreton Canyon, SW France	1	North Atlantic Ocean (Bay of Biscay)	Mazières et al., *2014*
23	Audierne and Blackmud canyons, SW France	2	North Atlantic Ocean (Bay of Biscay)	Mulder et al., 2012a, 2012b
24	Lofoten-Vesterålen canyons (incl. Andøya Canyon), NW Norway	15	North Atlantic Ocean	Rise et al., *2013*
25	Kaikoura Canyon, E New Zealand	1	South Pacific Ocean	Lewis and Barnes, *1999*
26	Lachlan Canyon, NE New Zealand	1	South Pacific Ocean	Walsh et al., *2007*
27	Biobío Canyon system, SW Chile	2	South Pacific Ocean	Bernhardt et al., *2015*
28	San Antonio Canyon, NW Chile	1	South Pacific Ocean	Hagen et al., *1996*; Laursen and Normark, *2002*
29	E Arequipa Basin canyons, NW Chile	3	South Pacific Ocean	Hagen et al., *1994*
30	Guayaquil and Santa Elena canyons, NW Equador	2	South Pacific Ocean	Michaud et al., *2015*
31	N Great Barrier Reef canyons, NE Australia	15	South Pacific Ocean (Coral Sea)	Puga-Bernabéu et al., *2011*
32	Solomon Sea canyons, E and SE Papua New Guinea	8	South Pacific Ocean (Solomon Sea)	Davies et al., 1987; Galewsky and Silver, 1997
33	Esmeraldas Canyon, NW Ecuador	1	North Pacific Ocean	Michaud et al., *2015*
34	Mira and Patia canyons, SW Colombia	2	North Pacific Ocean	Ratzov et al., *2012*
35	Ipala Canyon, W Mexico	1	North Pacific Ocean	Urías Espinosa et al., *2016*
36	La Jolla and Scripps canyons, SW USA	2	North Pacific Ocean	Le Dantec et al., *2010*;Paull et al., *2013*
37	Redondo, Santa Monica and Dume canyons, SW USA	3	North Pacific Ocean	Gardner et al., *2003*; Tubau et al., *2015*
38	Mugu and Hueneme canyons, SW USA	2	North Pacific Ocean	Piper et al., *1999*;
39	Monterey and Soquel canyons, SW USA	2	North Pacific Ocean	Greene et al., *2002*; Xu and Noble, *2009*
40	Astoria Canyon, NW USA	1	North Pacific Ocean	Hickey, *1997*; Bosley et al., *2004*
41	Quinault Canyon, NW USA	1	North Pacific Ocean	Baker and Hickey, *1986*;Carson et al., *1986*
42	Juan de Fuca Canyon, NW USA	1	North Pacific Ocean (heads in the Juan de Fuca Strait)	Alford and MacCready, *2014*
43	Barkley Canyon, SW Canada	1	North Pacific Ocean	Allen et al., *2001*
44	Tarr Canyon, NW USA	1	North Pacific Ocean (Gulf of Alaska)	Carlson et al., *1990*
45	North Palawan Canyon, S China	1	North Pacific Ocean (South China Sea)	Yin et al., *2018*
46	Modern Central Canyon, S China	1	North Pacific Ocean (South China Sea)	Su et al., *2015*
47	3 canyons and 4 gullies, S China	3 (4)	North Pacific Ocean (South China Sea)	Chen et al., *2017*
48	Pearl River Mouth Basin canyons, S China	17	North Pacific Ocean (South China Sea)	Han et al., *2010*;Su et al., *2020*
49	Zhujiang/Pearl River Canyon, S China	1	North Pacific Ocean (South China Sea)	Han et al., *2010*; Ding et al., *2013*
50	Dongsha Canyon, S China	1	North Pacific Ocean (South China Sea)	Yin et al., *2015*
51	Taiwan Canyon, SW Taiwan	1	North Pacific Ocean (South China Sea)	Xu et al., *2014*
52	Hongtsai Canyon, SW Taiwan	1	North Pacific Ocean (South China Sea)	Yu and Chiang, *1995*

(*continued on next page*)

Table 1 (*continued*)

ID	Case study	No. of canyons	Oceanic region	Reference(s)
53	Fangliao Canyon, SW Taiwan	1	North Pacific Ocean (South China Sea)	Yu and Lu, *1995*; Chiang et al., *2012*
54	Gaoping/Kaoping Canyon, SW Taiwan	1	North Pacific Ocean (South China Sea)	Chiang and Yu, *2006*;Liu et al., *2016*
55	Kaohsiung Canyon, SW Taiwan	1	North Pacific Ocean (South China Sea)	Yu et al., *1992*
56	Penghu Canyon, SW Taiwan	1	North Pacific Ocean (South China Sea)	Yu and Chang, *2002*;Hsiung and Yu, *2011*;Su et al., *2015*
57	Taitung Canyon, SE Taiwan	1	North Pacific Ocean (Philippine Sea)	Schnürle et al., *1998*
58	Hualien Canyon, SE Taiwan	1	North Pacific Ocean (Philippine Sea)	Hsiung et al., *2017*
59	Goto Canyon, SW Japan	1	North Pacific Ocean (East China Sea)	Oiwane et al., *2011*
60	Aoga Shima Canyon, SE Japan	1	North Pacific Ocean (Philippine Sea)	Klaus and Taylor, *1991*
61	Tenryu Canyon, SE Japan	1	North Pacific Ocean	Soh and Tokuyama, *2002*
62	Boso Canyon, SE Japan	1	North Pacific Ocean	Soh et al., *1990*
63	Kushiro Canyon, NE Japan	1	North Pacific Ocean	Noda et al., *2008*; Noda and TuZino, *2010*;TuZino and Noda, *2010*
64	Submarine canyons of Kamchatka, NE Russia	7	North Pacific Ocean	Gnibidenko and Svarichevskaya, *1984*
65	Bering Canyon, Bering Sea	1	North Pacific Ocean (Bering Sea)	Carlson and Karl, *1988*;Harris and Whiteway, *2011*
66	Zhemchug, Pervenets and Navarin canyons, Bering Sea	3	North Pacific Ocean (Bering Sea)	Carlson and Karl, *1988*
67	Middle canyon system, Bering Sea	2	North Pacific Ocean (Bering Sea)	Carlson and Karl, *1984, 1988*
68	St. Matthew canyon system, Bering Sea	2	North Pacific Ocean (Bering Sea)	Carlson and Karl, *1984, 1988*
69	Albany canyons, SW Australia	11	Indian Ocean	Exon et al., *2005*
70	Tugela Canyon, E South Africa	1	Indian Ocean	Wiles et al., *2013*
71	Saint-Etienne and Pierrefonds canyons, SW La Reunion	2	Indian Ocean	Babonneau et al., *2013*
72	Palar Basin canyons, E India	20	Indian Ocean	Susanth et al., *2021*
73	Indus Canyon, SE Pakistan	1	Indian Ocean (Arabian Sea)	von Rad and Tahir, *1997*;Salmanidou et al., *2019*
74	Barrow Canyon, NW USA	1	Arctic Ocean	Eittreim et al., *1982*; Pisareva et al., *2019*
75	Cook Strait canyons, E New Zealand	9	Cook Strait	Mountjoy et al., *2009, 2014*;Micallef et al., *2014*
76	Bass canyon system, SE Australia	10	Bass Strait	Mitchell et al., *2007*
77	Akhviz and Sour canyons, NW Israel	2	Mediterranean Sea	Mart, *1989*; Almagor, *1993*
78	Almeria, Western, Eastern and Guadiaro canyons, S Spain	4	Mediterranean Sea	Alonso and Ercilla, *2003*;Palanques et al., *2005*
79	Alías-Almanzora canyon system, SE Spain	4	Mediterranean Sea	Puig et al., *2017*
80	Menorca Canyon, SW Menorca, Balearic Islands	1	Mediterranean Sea	Acosta et al., *2002*
81	Orpesa Canyon, NE Spain	1	Mediterranean Sea	Amblas et al., *2012*
82	Foix Canyon system, NE Spain	3	Mediterranean Sea	Puig et al., *2000*; Tubau et al., *2013*
83	Blanes Canyon, SE France	1	Mediterranean Sea	Lastras et al., *2011b*
84	Palamós/La Fonera Canyon, NE Spain	1	Mediterranean Sea	Martín et al., *2006*; Palanques et al., *2006*;Lastras et al., *2011b*
85	Cap de Creus Canyon, NE Spain	1	Mediterranean Sea	Baztan et al., *2005*; Lastras et al., *2007, 2011b*
86	Bourcart Canyon, SE France	1	Mediterranean Sea	Mauffrey et al., *2015*
87	Gulf of Palermo canyons, NW Sicily, Italy	7	Mediterranean Sea	Lo Iacono et al., *2011, 2014*
88	Gulf of Castellammare canyons, NW Sicily, Italy	2	Mediterranean Sea	Lo Iacono et al., *2014*
89	Messina Canyon, NE Sicily, Italy	1	Mediterranean Sea	Ridente et al., *2014*
90	Petrace, Gioia and Mesima canyons, SW Italy	3	Mediterranean Sea	Pierdomenico et al., *2016*,Casalbore et al., *2018*
91	Luna and Infreschi canyons, SW Italy	2	Mediterranean Sea	Budillon et al., *2011*
92	Dohrn Canyon, SW Italy	1	Mediterranean Sea	Milia, *2000*
93	Golo system canyons, NE Corsica, France	4 (2)	Mediterranean Sea	Gervais et al., *2004, 2006*
94	North İmralı Canyon, NW Turkey	1	Sea of Marmara	Vardar, *2019*
95	Sarköy and Izmit canyons, NW Turkey	2	Sea of Marmara	Çağatay et al., *2015*
96	Danube/Viteaz Canyon, SE Romania	1	Black Sea	Popescu et al., *2004*

Values reported by authors have only been included for studies based on surveys that include bathymetric coverage of the entire canyon area. Average width and depth values were obtained from the literature for canyons surveyed by high-resolution bathymetry and where bathymetric data were derived from 3D seismic surveys.

3.2.2. *Environmental attributes and external controls*

For the investigation of relationships between submarine canyon geomorphology and the environmental context of the submarine canyons, attributes have been defined to record (i) canyon physiographic setting, (ii) the configuration of the canyon terrestrial catchment, continental shelf and slope, and (iii) external controls operating at the location of the canyon (Table 2 & Fig. 2).

3.2.2.1. Physiographic setting. The bathymetry of the canyon is characterised by the seafloor depth at its apex and mouth (Tab. 2). For canyons with several tributaries at their head, the shallowest seafloor depth has been recorded. The canyons are also classified in relation to the position of their apices relative to the shelf-break as either (i) shelf-incising,

Table 2
Overview and definition of the variables that have been considered in this work. Three asterisks (***) denote values that have been calculated. Two asterisks (**) denote values that have been obtained either from the literature, as reported by the original authors, measured or calculated. A single asterisk (*) denotes values that have been retrieved from the literature, as stated by the original authors.

Code	Definition
Canyon morphometrics	
L [km]**	streamwise length of the canyon between canyon apex and canyon mouth as measured along the canyon thalweg
W_{max} [km]**	maximum width of the canyon orthogonal to the canyon length
W_{av} [km]*	average canyon width over the length of the entire canyon
D_{max} [m]*	maximum depth of the canyon, i.e. depth of the canyon thalweg relative to the elevation of the canyon margins
D_{av} [m]*	average canyon thalweg depth over the length of the entire canyon
SI_{av} [-]**	average canyon sinuosity index, i.e. ratio between the sinuous canyon length measured along its thalweg and the straight distance between canyon apex and canyon mouth
thG_{av} [°]**	average canyon thalweg gradient, evaluated between canyon apex and canyon mouth
SW_{max} [°]*	maximum canyon-sidewall steepness, representing the maximum value of gradient between canyon rim and canyon bottom, evaluated along the entire length of the canyon
Physiographic setting	
canyon apex location	the location of the canyon apex relative to the shelf break, classified as 'shelf-incising' or 'slope-confined'
Dis_{min} [km]**	minimum distance between the canyon and the shoreline
SD_{min} [m]**	seafloor depth at the top of the canyon; for canyons with several tributaries at their head the shallowest seafloor depth has been recorded
SD_{max} [m]**	seafloor depth at the mouth of the canyon
Canyon terrestrial catchment	
L_{fls} [km]**	length of the river with a present-day or previous connection with the canyon, from headwater to river mouth; for canyons connected with several rivers the cumulative length has been considered
Q_{fls} [km^3/yr]*	mean annual discharge of the fluvial system; for canyons connected with several rivers the cumulative mean annual discharge has been considered
A_{flsc} [km^2]*	size of the catchment associated with the fluvial system; for canyons connected with several rivers the maximum elevation of the combined catchment has been considered
H_{flsc} [m]**	maximum elevation of the catchment area relative to sea level; for canyons connected with several rivers the elevation of the highest peak in the combined catchment has been considered
Continental shelf	
W_{sh} [km]**	width of the shelf at the canyon location
G_{sh} [°]**	average shelf gradient at the canyon location
D_{sh} [m]**	shelf-break depth at the canyon; for shelf edges with variable bathymetry, the deepest point is considered
Continental slope	
W_{sl} [km]**	width of the slope at the canyon location
G_{sl} [°]**	average slope gradient between the shelf break and the slope break
D_{sl} [m]**	slope-break depth at the canyon
Other parameters	
Lat_{abs} [°]**	absolute value of the latitude of the canyon apex
source-to-sink setting	physiography of the source-to-sink system the canyon is associated with, classified as: (i) continental setting; (ii) insular setting; canyons situated in trenches between islands and continents have not been included
continental-margin type	for canyons located along continental margins, including canyons associated with islands: (i) active margin (including both convergent and transform settings); (ii) passive margin
oceanographic environment	(i) open sea: canyons located in an oceanic environment with open hydrodynamic interaction with adjacent seas; exposed to oceanic gyres; (ii) semi-enclosed and enclosed sea: canyons located in a sea which is largely bounded by landmasses and therefore has no or limited hydrodynamic interaction and connection with oceans; the definition includes seas, gulfs and straits

where the canyon extends into the continental shelf, or (ii) slope-confined, where the apex of the canyon is situated below the shelf break (cf. Jobe et al., 2011; Huang et al., 2014).

3.2.2.2. Source-to-sink-system attributes. Relationships between the geomorphology of submarine canyons and attributes of their terrestrial catchment have been investigated for canyons with sediment connectivity to a fluvial system at present or in the past. For these canyons, descriptors of fluvial system length, mean annual fluvial discharge, catchment area and maximum catchment area elevation (Tab. 2), have been recorded. Sediment connectivity of a submarine canyon with a fluvial source is defined based on the following three criteria:

(i) *The submarine canyon displays a present connection with a fluvial system.* This includes canyons fronting a river mouth, canyons for which across-shelf sediment transport from a fluvial outlet has been inferred by authors, e.g. from sedimentary structures on the seafloor as sediment waves (e.g. Puig et al., 2017), and canyons connected to up-dip subenvironments, such as shelf channels and tributary canyons, which are physically connected with a fluvial system.
(ii) *The submarine canyon was connected to a river in the past.* This includes canyons that might not currently be connected to a fluvial system, e.g. due to present-day sea-level highstand conditions or to river-mouth shift of natural or anthropogenic cause, but that are known to have been connected in the past to a river (e.g. Sweet et al., 2020).
(iii) *The canyon apex is located within 5 km of a fluvial outlet.* This criterion has been considered in view of the typical length-scale over which sand tends to be distributed to submarine canyons by rivers that lack a bathymetric connection to the canyons (see Sweet and Blum, 2016).

For canyons linked with several rivers, their cumulative length, mean annual fluvial discharge and catchment area have been recorded, to enable comparison with canyons fed by single fluvial systems. For investigation of relationships between canyon geomorphology and maximum elevation of the terrestrial catchment, the elevation above mean sea level of the highest point in the combined catchment has been recorded.

The continental shelf and slope hosting the canyons have been described in terms of width, average gradient and depth.

3.2.2.3. Continental-margin type. The source-to-sink system has been classified as being associated with either a passive or a tectonically active continental margin, the latter comprising canyons along both convergent and transform plate boundaries, following the continental-margin classification of Harris et al. (2014; see their Fig. 2).

3.2.2.4. Source-to-sink setting. The source-to-sink setting associated with the studied canyons has been classified on whether the terrestrial catchment, shelf and slope are associated with continental landmasses (continental setting) or an island (insular setting). Canyons which could not be unambiguously assigned to a setting have not been included.

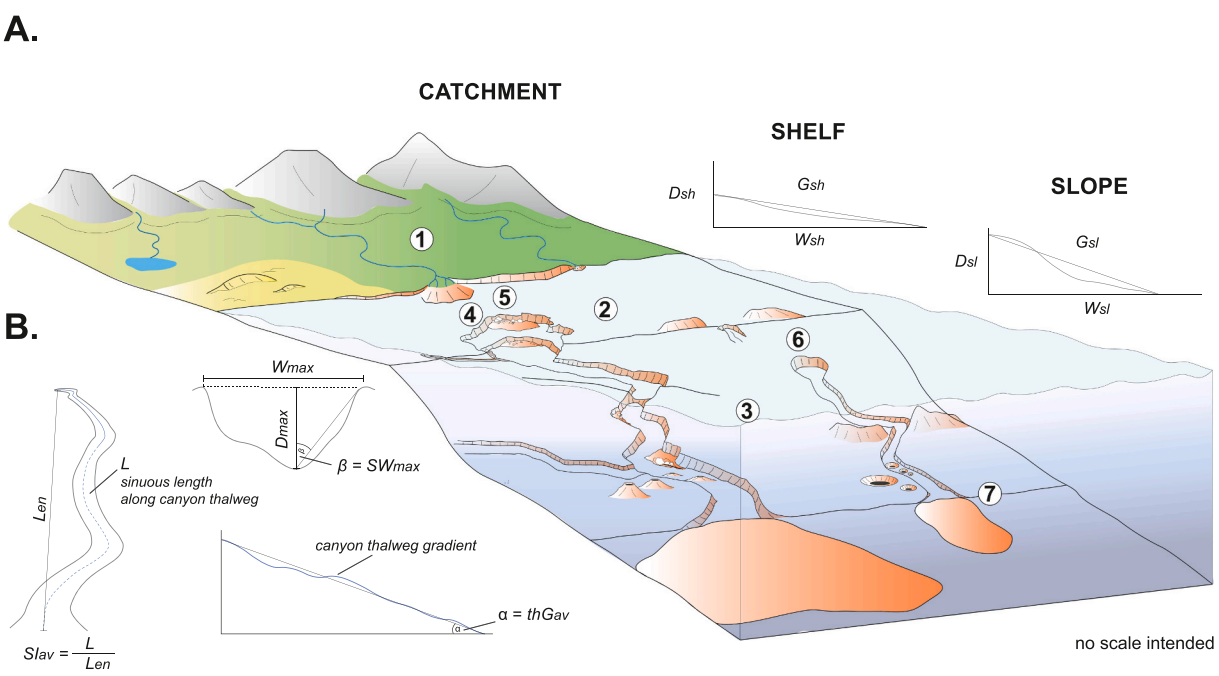

Fig. 2. A. Attributes of the source-to-sink system and physiographic setting investigated in the study: 1. Terrestrial catchment: fluvial system length, average annual fluvial discharge, catchment size, maximum elevation. 2. Shelf configuration: width, depth, average gradient. 3. Slope configuration: width, depth, average gradient. 4. Canyon-apex location relative to the shelf-break. 5. Minimum distance to shoreline. 6. Seafloor depth at the top of the canyon. 7. Seafloor depth at the canyon mouth. B. Key canyon morphometric parameters considered in the study: L= canyon length along thalweg L_{en} = canyon length along endpoints; W_{max} = maximum canyon width; D_{max} = maximum canyon depth; SI_{av} = average canyon sinuosity index; thG_{av} = average canyon thalweg gradient; SW_{max} = maximum canyon sidewall steepness.

3.2.2.5. Oceanographic environment. To investigate the possible controls exerted by hydrodynamic processes that vary with scale and marine water-mass confinement, and potential relationships between canyon morphometric parameters and the scale and degree of confinement of the seas where they occur, canyons are classified with respect to their oceanographic environment. To this end, two groups have been distinguished: (i) open seas, which comprise the World's oceans and experience hydrodynamic interactions with adjacent seas; they may be characterised by the occurrence of oceanic gyres; (ii) semi-enclosed and enclosed seas, which are largely bounded by landmasses and are therefore characterised by a limited hydrodynamic interaction with the oceans or seas with which they are connected; this second class includes seas, gulfs and straits.

3.2.2.6. Latitude. The latitudinal positions of canyon heads are recorded as absolute values for both hemispheres. For the investigation of latitude-related climatic influences on processes affecting canyon geomorphology, latitude values have been assigned to categories that relate to major climate belts, i.e., into tropical (corresponding to latitudes between 0° and 23.5°), temperate (between 23.5° and 66.5°), and polar zones (corresponding to latitudes higher than 66.5°). This simplified approach has been implemented for the following reasons: (i) existing climate classification schemes are commonly based on parameters of the terrestrial catchment and would therefore have limited applicability to canyons that do not receive significant fluvial discharge or none at all; moreover, climatic conditions in the marine environment are commonly not considered in these schemes; (ii) climate histories, including temperature and precipitation, would have to be reconstructed for both the present and the past to permit a consistent analysis of their impact on canyon evolution; this becomes particularly challenging for submarine canyons associated with large source-to-sink systems; (iii) the age of inception of the majority of the canyons in the present study is poorly constrained, so that climate histories cannot be matched closely to canyon age.

3.3. Statistical analysis

Relationships between canyon morphometric parameters and descriptors of physiographic setting and external controlling factors have been investigated by statistical analyses.

(i) Descriptive statistics of frequency distributions of canyon morphometric parameters are evaluated for classes of: canyon-apex location relative to the shelf-break, continental-margin type, source-to-sink setting, oceanographic environment, and latitudinal position of the canyon apex or head. Comparisons between distributions of values in canyon groups are undertaken.

(ii) Statistical testing has been used to evaluate whether differences in mean values of canyon morphometrics between groups of canyons are statistically significant. For assessment across two groups, two-sample t-tests have been conducted, whereas differences in mean values between more than two canyon groups have been assessed by means of one-way analysis of variance (ANOVA). To test datasets with heteroscedastic distributions, Welch's t-test and Welch's ANOVA have been used throughout. Test statistics, degrees of freedom (DF) and P-values are presented for all tests. Results with p-values $\leq$0.01 are reported as statistically significant. Prior to the analyses, a logarithmic variable transformation is applied to skewed frequency distributions.

(iii) Correlation analysis has been applied to investigate pairwise relationships between the studied parameters from the individual values obtained for each studied canyon. The strength and sign of correlation between two parameters is quantified by Pearson's correlation coefficient (r), to reveal linear relationships, and by Spearman's rank correlation coefficient (r_s), to reveal monotonic relationships. A correlation is considered statistically significant for p-values $\leq$0.01.

Although statistical analyses have been performed for any number of

readings (N), the results are commonly presented and discussed when N≥15; it is explicitly stated when N<15.

All statistical analyses have been undertaken in Minitab 19.

3.4. Limitations of the study

Some of the key limitations of this study can be summarised as follows.

(i) In studies of submarine canyons there exists some geographic and thematic bias, as recognised by Matos et al. (2018), and some of that bias may have been inherited by this work. For example, logistic, financial and environmental challenges to investigating submarine canyons in polar regions might explain the relative scarcity of local- and regional-scale case studies of submarine canyons in the Arctic and Antarctica. Also, research efforts might be more focused on specific classes of canyons: for example, larger submarine canyons might be of particular interest for studies of marine habitats or as modern analogues for ancient systems in hydrocarbon exploration. Despite this, an effort has been made to compile a globally representative dataset of case studies of submarine canyons associated with different types of environmental settings (see Fig. 1 & Table 1). The study also incorporates 12 canyon studies published after 2016, which were not considered by Matos et al. (2018) in their analysis.

(ii) The scale of slope channel forms recognised in the case studies depends on data resolution, which sets the limit of the smallest mappable geomorphic features, and affects the precision of measurements. Due to heterogeneity in data types, some variability in resolution is expected.

(iii) As in any metastudy, erroneous data reported in the primary data sources may have been inadvertently included in the database. However, all reasonable measures have been taken to ensure data accuracy.

(iv) Although this study considers many environmental factors that may act as controls on canyon geomorphology, some relationships might arise from covariance of such factors with one or several parameters that have not been included in our analyses.

(v) Shelf-margin and base-of-slope depths of continental margins lacking distinct morphological breaks at the shelf-slope transition and/or in the base-of-slope region are difficult to determine precisely. As such, these attributes may have not been reported in the literature, and have not been included in the current dataset.

(vi) Despite the ability afforded by studies of modern canyons to constrain physiographic setting, external factors and process-response relationships, measurements of the physical characteristics of canyons and their settings only represent snapshots of the temporal evolution of the studied forms.

(vii) The continental-margin type, source-to-sink setting, and oceanographic environment constitute factors that apply to the entire extent of the studied canyons, and thus allow consistent grouping. In contrast, along their length, some submarine canyons might stretch across two latitudinal zones. The position of the canyon apex relative to the shelf break can be variable over time, but incision of the shelf by the canyon does not per se represent a more mature evolutionary stage of the canyon. Some canyons that are presently slope-confined might have had a physical connection to the shelf in the past: their canyon heads and proximal parts may have been backfilled (Pratson et al., 2007) or may have prograded basinwards (Mauffrey et al., 2015). This must be considered in analyses of frequency distributions of canyon morphometrics across slope-confined and shelf-incising forms.

4. Scaling relationships between canyon morphometrics

4.1. Observations

Correlation strengths between canyon morphometric parameters are highly variable, with only some correlations being strong and statistically significant (Figs. 3 & 4 a-o).

Maximum dimensions of the studied canyons are moderately correlated with each other (Fig. 4a-c). Strong relationships that are statistically significant exist for average canyon width with maximum width (Fig. 3), length (Fig. 4a) and maximum depth (Fig. 4c), and for the latter with average depth (Fig. 3). In addition, modest significant scaling is demonstrated for maximum width and average depth (Fig. 4c). In contrast, correlations of average canyon depth with canyon length (Fig. 4b) and average canyon width (Fig. 4c) are weak and not significant. Strong correlations between length and canyon width, and no correlation between canyon length and average depth, are also observed in the dataset by Harris et al. (2014) (Fig. 4p&q).

Average canyon sinuosity shows significant, respectively modest and moderate, positive correlations with canyon length (Fig. 4d) and average canyon depth (Fig. 4f), and modest correlations with maximum canyon width (Fig. 4e). The negative correlation between sinuosity and average canyon thalweg gradient is significant but rather weak (Fig. 4m), whereas no correlation is seen between sinuosity and maximum canyon sidewall steepness (Fig. 4n).

The average canyon thalweg gradient demonstrates moderate negative correlation with canyon length (Fig. 4g) and weak negative correlation with maximum canyon width (Fig. 4h), both of which are statistically significant. The positive moderate correlation between thalweg gradient and average canyon depth is not statistically significant (N = 12; Fig. 4i). No correlation exists between thalweg gradient and either average width (Fig. 4h) and maximum sidewall steepness (Fig. 4o).

Positive, modest and statistically significant relationships are seen between maximum canyon sidewall steepness and both maximum canyon width (Fig. 4k) and depth (Fig. 4l), whereas the maximum canyon sidewall steepness is weakly correlated with canyon length (Fig. 4j).

4.2. Interpretations

Correlations between pairs of canyon morphometric parameters suggest that both considered canyon characteristics may be affected by the same process or controlling factors.

In some cases, correlations may arise – either in part or fully – due to covariance with other parameters, and this may be inherent in the definition of the parameters themselves. For example, more sinuous canyons tend to have longer streamwise canyon length for a given slope extent, whereas deeper channel forms are expected to have steeper margins.

In addition, some canyon morphometrics appear to be more strongly related to certain environmental controls; this is discussed in sections 5, 6 and 7.

4.2.1. Sedimentary processes

Because the effects of sedimentary processes on canyon evolution depend primarily on the sediment volumes they mobilise, their erosive strength and their areal extent, sedimentary processes can affect canyon morphometrics in different ways, at different locations along a canyon and even during the same event (e.g. Su et al., 2020). The ability of sediment gravity flows and slope failures to trigger one another (e.g. Pratson and Coakley, 1996; Bernhardt et al., 2015) and the common transition of the latter into the former (e.g. Puig et al., 2014) makes it difficult to differentiate between the relative importance of these processes in shaping canyon geomorphology. As a consequence, it may not be possible to establish causal links between intra-canyon-scaling

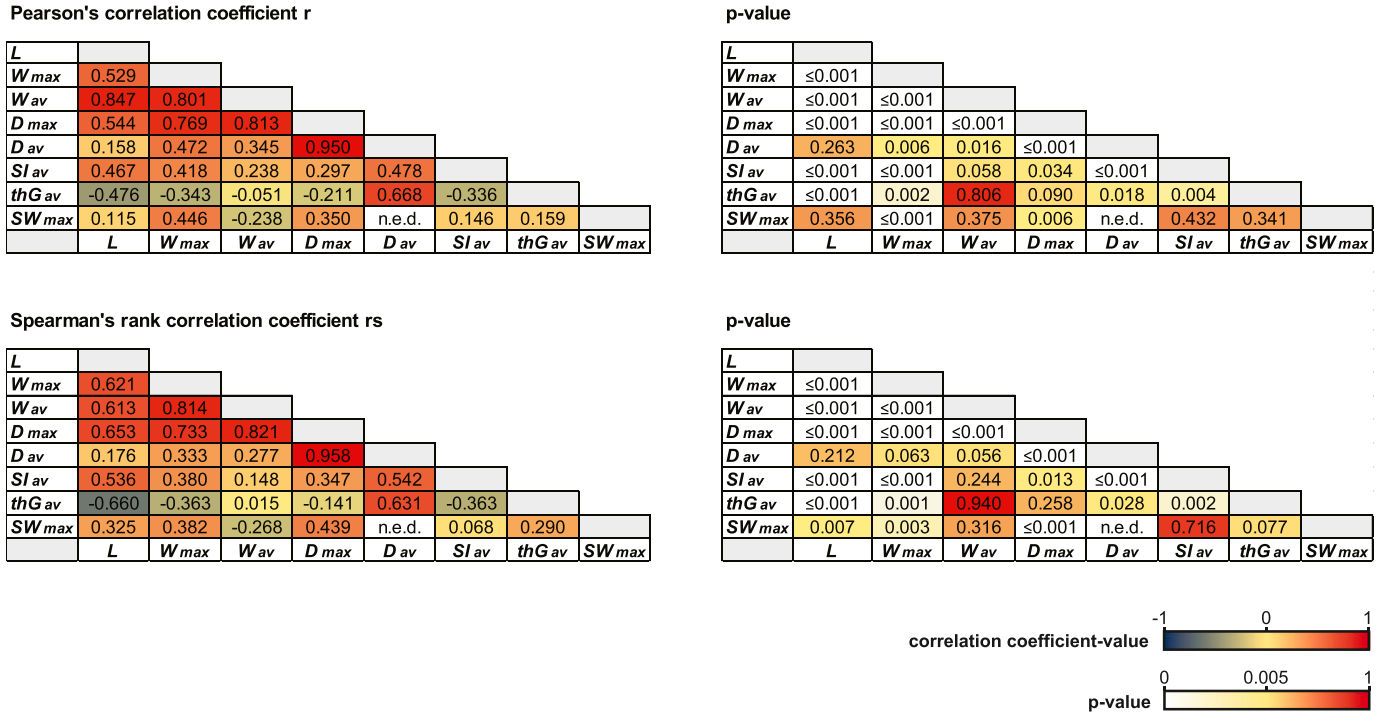

Fig. 3. Heat maps of correlations of canyon morphometric parameters for canyons of the study displaying values of Pearson's correlation coefficient r and Spearman's rank correlation coefficient rs, and their respective p-values. L = canyon length; W_{max} = maximum canyon width; W_{av} = average canyon width; D_{max} = maximum canyon depth; D_{av} = average canyon depth; SI_{av} = average canyon sinuosity index; thG_{av} = average canyon thalweg gradient; SW_{max} = maximum canyon sidewall steepness. n.e.d. = not enough data to facilitate statistical analyses.

relationships and sediment-transport mechanisms. Nevertheless, observed scaling between some canyon morphometric parameters suggests that the influence of one or several controlling factors tends to be prevalent, giving rise to canyon geomorphologic characteristics that are recognizable on a global scale despite specific regional or local conditions.

Canyon enlargement can be driven by active erosive processes, such as primary erosion by sediment gravity flows passing through the canyon (e.g. Li et al., 2021) or by slope failure within the canyon and on the adjacent slope (e.g. Post et al., 2022), but also by accretion of the adjacent slope or of ridges between canyons, which may be caused by along-slope currents (e.g. Rona, 1970), by background sedimentation or spillover of sediment gravity flows passing through canyons (e.g. Straub and Mohrig, 2009; Armitage et al., 2010), or due to primary carbonate production (e.g. Shepard, 1972; Tournadour et al., 2017). By contrast, intra-canyon aggradation, e.g. by backfilling (Cronin et al., 2005), sediment accumulation in canyon heads (e.g. Walsh et al., 2007) and hemipelagic sedimentation (e.g. Jobe et al., 2011) weaken the effect of erosive processes on positive scaling relationships in canyon morphometry, for example by shortening canyons and decreasing their depths.

The fact that these processes can variably modify individual canyon morphometric parameters is likely reflected in the observed scaling between maximum and average canyon dimensions. The rather strong scaling of canyon length with average canyon width may be linked to the ability of down-canyon flows to maintain their erosive behaviour beyond the canyon mouth. The moderate scaling of canyon length with maximum width might be related to the fact that lateral slope failures lead to local widening of the canyon over the excavated area, but may only increase canyon length where the mobilised sediment volume – which might also comprise intra-canyon sediment sources – is sufficient to extend the canyon beyond its present mouth. This may arise, for example, by breaching of intra-slope structural highs or by facilitating the progradation of the continental rise. Retrograde slope failures act as a primary cause of canyon lengthening (e.g. Orange et al., 1994; Pratson and Coakley, 1996; Pratson et al., 2007) and might cause the local widening of canyons in their proximal parts in correspondence of slump scars, where these are intercepted (e.g. Mulder et al., 2012a, 2012b). Relatively strong scaling of maximum depth with maximum and average width in the sampled canyons may in part reflect simultaneous canyon-margin aggradation and intra-canyon erosion. The positive scaling between maximum width and maximum canyon sidewall steepness can in part be explained by lateral canyon-slope failures causing a local increase in canyon width and canyon sidewall steepness, and by thalweg erosion.

4.2.2. *Hydrodynamic processes*

Marine hydrodynamic processes on the shelf and slope can variably influence canyon geomorphology: (i) by their direct effect on sedimentary processes within the canyon itself, and (ii) by exerting control on sediment supply from terrestrial, intra-shelf and slope sources to canyons, which in turn can impact intra-canyon sedimentary processes.

Hydrodynamic processes that have been inferred to facilitate sediment supply to submarine canyons include tides (e.g. Mountjoy et al., 2014), long-lived longshore drifts (e.g. Normark et al., 2009; Smith et al., 2018), slope currents (e.g. Wang et al., 2018), high-energetic waves (e.g., solitary waves, Yin et al., 2019; storm waves, Sequeiros et al., 2019), and dense shelf-water cascading (e.g. Canals et al., 2006; Puig et al., 2014, and references therein; Gales et al., 2021). The processes are highly variable in terms of frequency, magnitude, duration and area of influence, and these factors affect both the volume and grain size of sediment sourced to canyons. Intra-canyon erosion, remobilisation and transport of sediment have been linked to tidal (e.g. Liu and Yin, 2004) and unidirectional oceanic currents (e.g. Itoh et al., 2010) passing through a canyon, and to the focussing of internal waves in both the shallower parts of shelf-incising canyons (e.g. Smith et al., 2018) and at greater water depths in canyons confined within the slope (e.g. Wang et al., 2022). Hence, the influence of marine hydrodynamic processes on

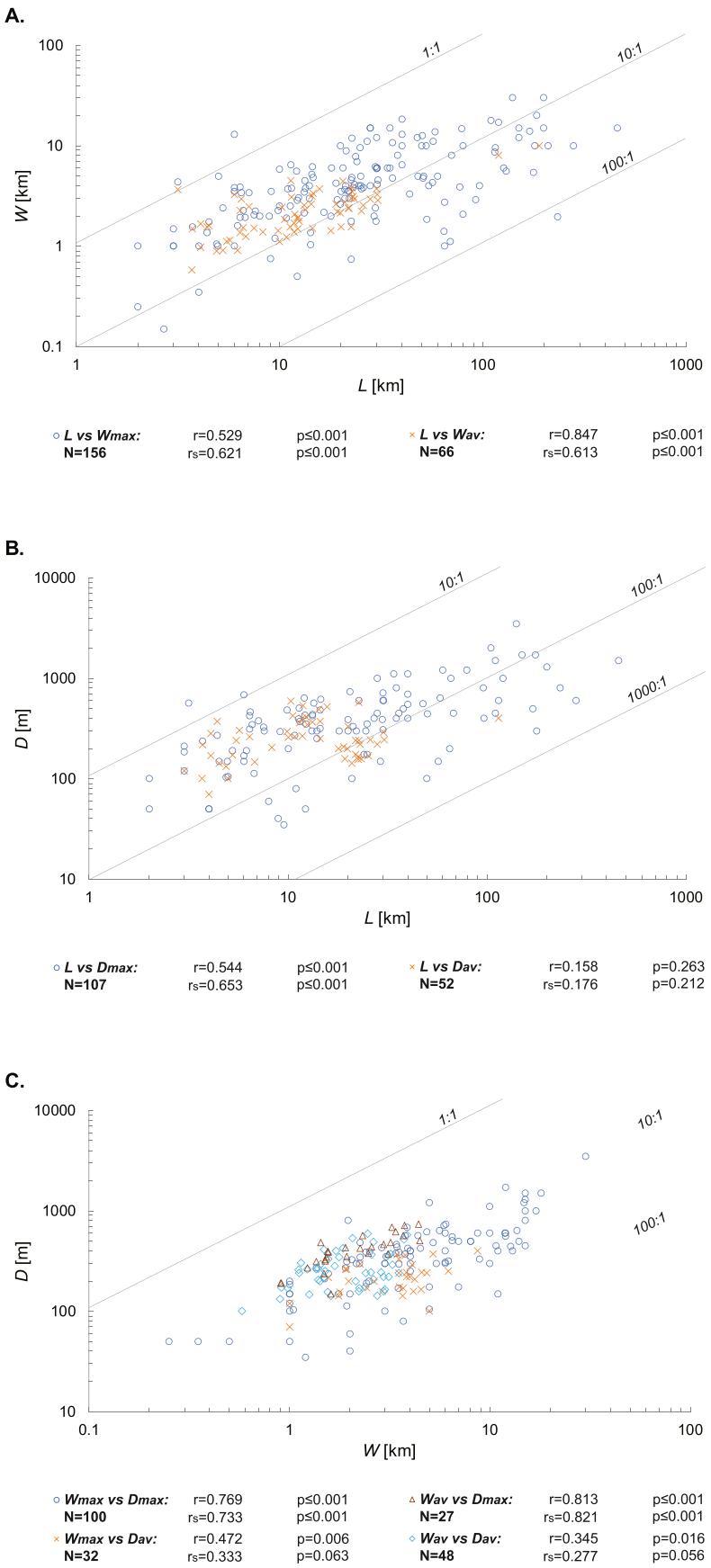

Fig. 4. a-q: A.-O. Scatterplots of morphometric parameters of the studied canyons. P.&Q. Scatterplots of canyon length with width (P) and average depth (Q) plotted from the dataset of Harris et al. (2014) with an overlay of data from this study for comparison. N = number of observations; r = Pearson's correlation coefficient; r_s = Spearman's rank correlation coefficient. See Fig. 3 for key to abbreviations.

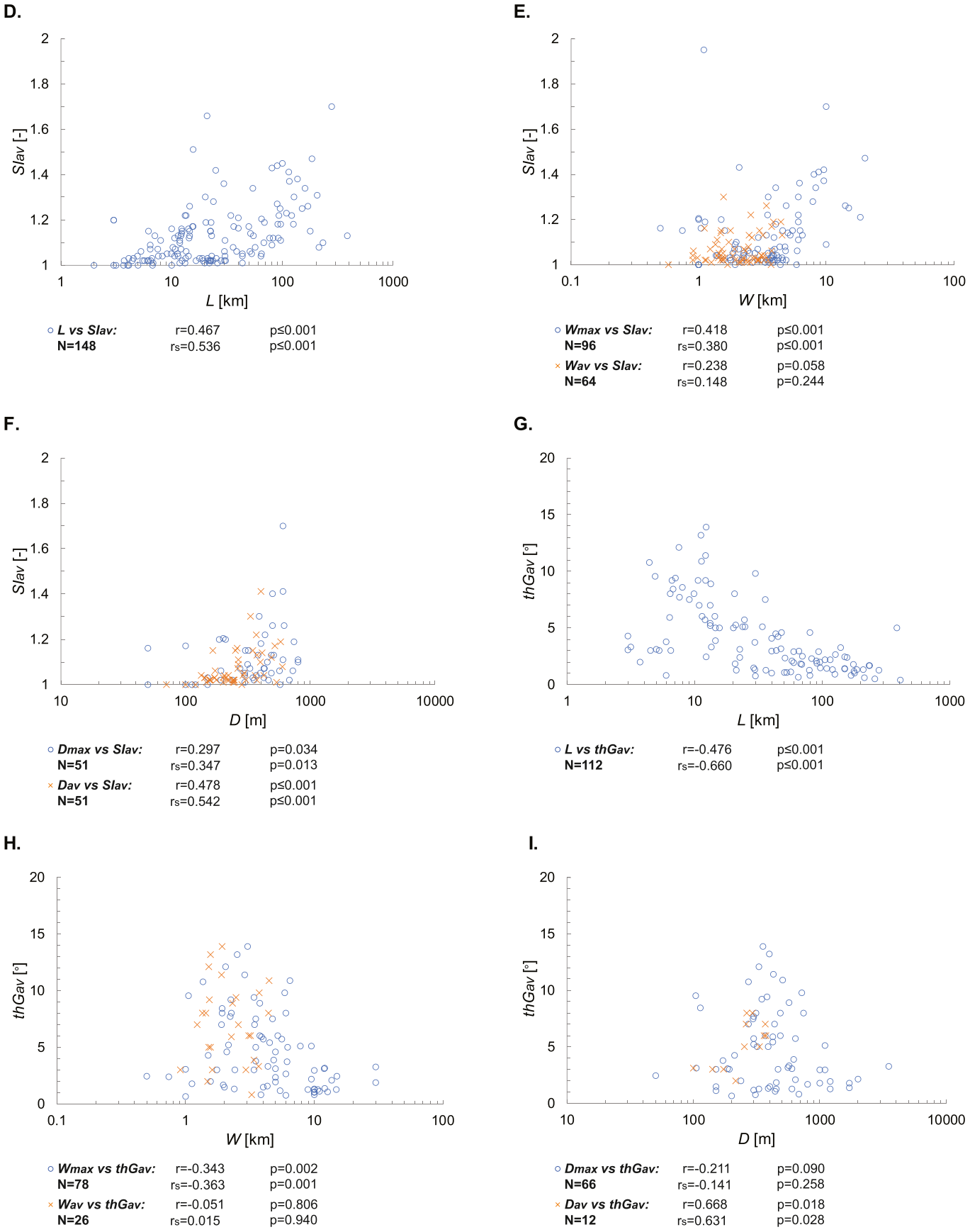

Fig. 4. (*continued*).

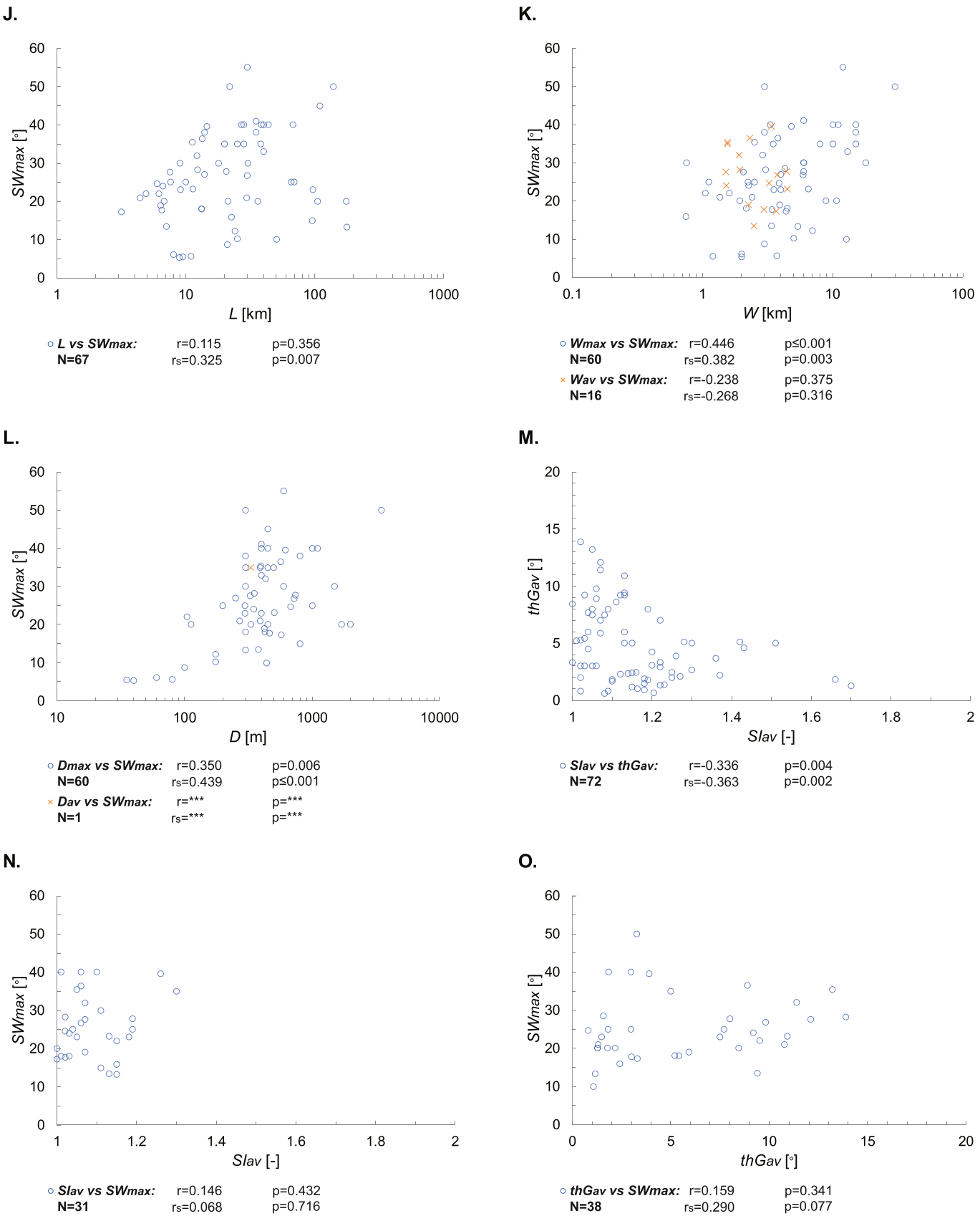

Fig. 4. (*continued*).

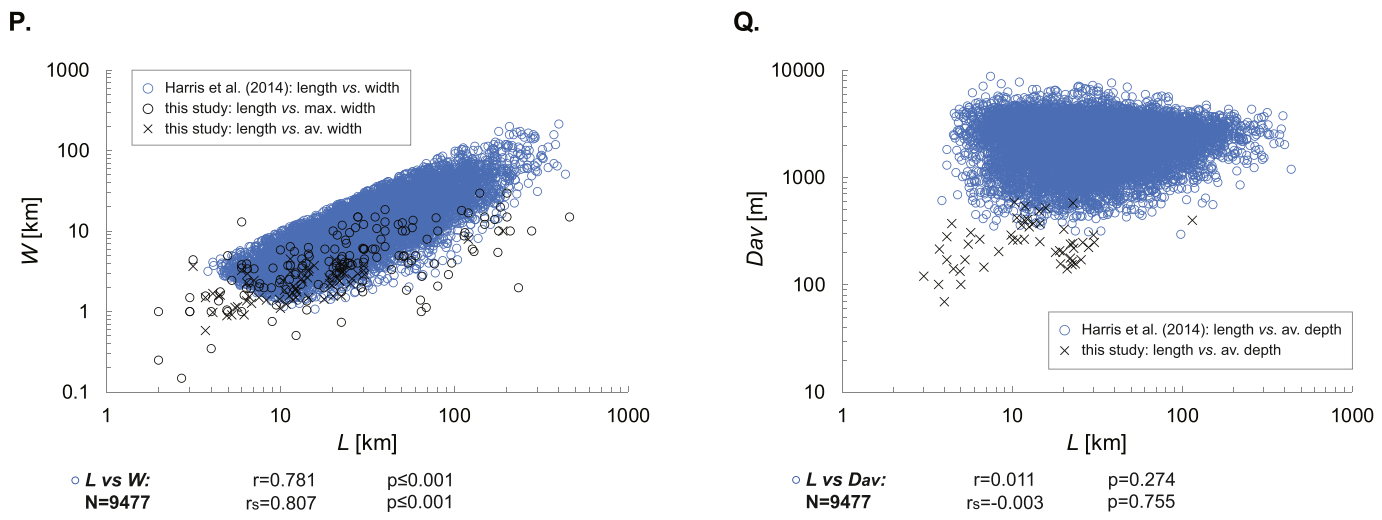

Fig. 4. (*continued*).

canyon geomorphology is complex and might both amplify or weaken the impact of sedimentary processes on the strength of scaling relationships between canyon morphometric attributes.

For example, canyons hosted on continental margins with strong oceanic currents might experience less frequent canyon-margin failures and reduced aggradation, due to the ability of such currents to inhibit sedimentation along canyon margins (e.g. Green, 2011). As a result, the impact of axial sediment gravity flows on scaling in canyons might be, to a lesser degree, overprinted by lateral failure in these canyons. On the contrary, currents that can lead to sediment accumulation along canyon margins may strengthen the scaling between canyon depth, width and margin slopes (see section 4.2.1). Moreover, the complex influence of slope currents and internal tidal waves on canyon geomorphology, related to the co-occurrence of intra-canyon erosional and depositional processes including canyon flushing and canyon-wall failure (see Wang et al., 2022) might variably affect the strength in scaling between canyon morphometrics.

4.2.3. Structural controls

Structural controls might affect canyon geomorphology by their influence on pre-existing and developing seafloor topography, which might have contributed to the weakening of some of the relationships between canyon morphometric attributes. For example, where fault and diapiric structures form part of the canyon walls or are in vicinity of the canyon margin, they can steepen the canyon sidewalls (e.g. Yu and Chang, 2002; Bernhardt et al., 2015), and might overprint the effect of concurrent intra-canyon erosion by down-canyon sediment flows and canyon sidewall failure on canyon width, depth and sidewall steepness and the strength of their mutual scaling. In addition, emerging topography, generated for example by coral reef growth (e.g. Puga-Bernabéu et al., 2011) or diapiric uplift (e.g. Chiang et al., 2012), might cause flow deceleration, flow deflection, flow stripping and/or grain size segregation, which in turn might weaken the erosional effect of flows further down-canyon. Similarly, substrate heterogeneity arising from pre-existing structural features or buried canyons might cause spatial variations in substrate erodibility. In turn, the erodibility of canyon floors or walls might be diminished or enhanced over the affected area, which can promote an overall irregular canyon geometry, and variably impact the average canyon sinuosity and canyon thalweg gradient.

4.2.4. Biogenic processes

The effect of the colonization of canyon walls and margins by marine fauna on canyon-wall stability has received limited attention in the literature (e.g. Shepard, 1981; Eittreim et al., 1982; Carlson and Karl, 1984, and references therein). Depending on factors such as nature of substrate, degree of bioturbation, filling and cementation, the canyon sidewall stability might be increased or decreased by bioturbation. Similarly, vegetation cover in proximal parts of canyons, specifically by marine flora in the photic zone, might reduce the erodibility of canyon slopes. The resulting variability in the erodibility of canyon walls and apices might affect the scaling relationships between canyon length, width and sidewall steepness. Thus, biogenic processes might constitute a controlling factor on scaling in canyon morphology. Future research is needed to enhance our understanding of the impact of biota on canyon geomorphology.

5. Relationships between canyon morphometric parameters and attributes of the physiographic setting

5.1. Distance between canyon and shoreline

5.1.1. Observations

The minimum distance between the canyon apex and the shoreline is not correlated to any of the canyon morphometric parameters except for the average canyon width (Figs. 5 & 6a-f), for which modest but statistically significant positive correlation is seen (Fig. 6b). However, in the assessment of a relationship with average canyon width, the average widths of canyons with a distance to a continent or island of $\leq$ 25 kilometres could not be evaluated.

5.1.2. Interpretations

Although the distance of the canyon to the shoreline plays a role in sediment distribution from fluvial sources across shelves and slopes (section 6.1), the results show that relationships between the distance of the canyon to the shoreline and overall canyon geomorphology are weak. It can thus be inferred that the distance to the shoreline itself is not a major factor, relative to others.

5.2. Canyon bathymetry

5.2.1. Observations

5.2.1.1. Seafloor depth at the canyon apex. Most canyon morphometrics correlate poorly with seafloor depth at the canyon apex (Figs. 5 & 7a-f). Modest negative correlations are seen with average canyon depth, and a weak negative relationship with maximum canyon depth, both of which are statistically significant (Fig. 7c). A weak but significant negative correlation is also displayed with average canyon sinuosity (Fig. 7d).

Pearson's correlation coefficient r

L	0.097	-0.069	0.595	0.142
W max	-0.154	0.143	0.420	0.201
W av	0.171	-0.200	0.135	0.474
D max	-0.068	-0.211	0.750	0.111
D av	-0.330	-0.418	0.707	-0.398
SI av	-0.069	-0.137	0.566	0.176
thG av	-0.218	-0.056	-0.290	-0.352
SW max	-0.334	-0.101	0.364	0.465
	Dis min	*SD min*	*SD max*	*Lat abs*

p-value

L	0.129	0.342	≤0.001	0.021
W max	0.055	0.120	≤0.001	0.010
W av	0.169	0.113	0.317	≤0.001
D max	0.478	0.055	≤0.001	0.240
D av	0.017	0.002	≤0.001	0.003
SI av	0.416	0.128	≤0.001	0.031
thG av	0.021	0.577	0.004	≤0.001
SW max	0.006	0.469	0.008	≤0.001
	Dis min	*SD min*	*SD max*	*Lat abs*

Number of correlations

L	246	194	182	263
W max	155	119	108	164
W av	66	64	57	66
D max	110	83	74	113
D av	52	51	45	52
SI av	143	125	112	151
thG av	111	103	97	120
SW max	67	54	52	69
	Dis min	*SD min*	*SD max*	*Lat abs*

Spearman's rank correlation coefficient rs

L	0.037	-0.172	0.650	0.300
W max	-0.078	-0.096	0.509	0.207
W av	0.420	-0.181	-0.040	0.511
D max	-0.083	-0.353	0.776	0.123
D av	-0.095	-0.381	0.685	-0.421
SI av	-0.273	-0.277	0.460	0.218
thG av	0.011	-0.036	-0.251	-0.324
SW max	0.031	-0.129	0.365	0.415
	Dis min	*SD min*	*SD max*	*Lat abs*

p-value

L	0.566	0.017	≤0.001	≤0.001
W max	0.337	0.300	≤0.001	0.008
W av	≤0.001	0.152	0.766	≤0.001
D max	0.388	0.001	≤0.001	0.196
D av	0.501	0.006	≤0.001	0.002
SI av	0.001	0.002	≤0.001	0.007
thG av	0.905	0.719	0.013	≤0.001
SW max	0.802	0.354	0.008	≤0.001
	Dis min	*SD min*	*SD max*	*Lat abs*

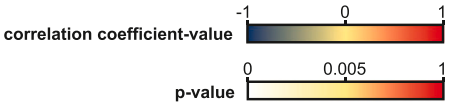

Fig. 5. Heat maps for correlations of canyon morphometrics with the physiographic setting displaying values of Pearson's correlation coefficient r and Spearman's rank correlation coefficient rs, and their respective p-values. L = canyon length; W_{max} = maximum canyon width; W_{av} = average canyon width; D_{max} = maximum canyon depth; Dav = average canyon depth; SI_{av} = average canyon sinuosity index; thG_{av} = average canyon thalweg gradient; SW_{max} = maximum canyon sidewall steepness; Dis_{min} = minimum distance between the canyon and shoreline; SD_{min} = minimum seafloor depth at the canyon apex; SD_{max} = maximum seafloor depth at the canyon mouth; Lat_{abs} = absolute value of the latitude of the canyon apex.

5.2.1.2. Seafloor depth at the canyon mouth. The seafloor depth at the canyon mouth tends to correlate significantly with all investigated canyon morphometric parameters except for average canyon width (Figs. 5 & 8a-f). Moderate positive correlations are seen with canyon length (Fig. 8a), maximum canyon width (Fig. 8b), both maximum and average canyon depth (Fig. 8c), and with average canyon sinuosity (Fig. 8d), whereas correlations with maximum canyon sidewall steepness are weaker (Fig. 8f). In contrast, a weak negative correlation is seen with the average canyon thalweg gradient (Fig. 8e).

5.2.2. Interpretations

5.2.2.1. Seafloor depth at the canyon apex. No clear relationships are seen between canyon geomorphology and the seafloor depth at the apex of the canyon, except for canyon depth. Data on maximum and average canyon dimensions demonstrate that large canyons can develop regardless of the seafloor depth at the canyon apex. The results indicate that the absolute canyon-apex depth does not necessarily relate to controlling factors influencing canyon geomorphology, such as a connection to sediment sources (section 6.1), the hydrodynamic regime (section 4.2.2) or structural controls (section 4.2.3). Although the canyon length increases with retrograde erosion at the canyon head, which leads to progressive shallowing of the canyon apex, the bathymetry of the basin ultimately determines the canyon length (section 6.3). The tendency of canyons to be deeper when their apex is shallower might reflect how canyon deepening may be facilitated by erosive sediment gravity flows linked to the progressive retrogradation of the canyon, which can enhance sediment delivery from terrestrial and intrashelf sources and from sediment remobilisation within the canyon. Weak scaling between canyon morphometric parameters and canyon-apex depth might also reflect how substrate lithology and seafloor gradients, which affect canyon morphodynamics and the magnitude and frequency of mass-wasting processes, vary systematically with depth (e.g. Harris et al., 2014; Diesing, 2020).

5.2.2.2. Seafloor depth at the canyon mouth. The results suggest that canyons reaching greater depths tend to have greater maximum dimensions and average depths, but not average widths. The observed increase in maximum canyon width and depth with increasing seafloor depth at the canyon mouth may be linked to the widening and deepening of canyons by turbidity currents in the region of the canyon mouth as a response to a decrease in slope gradient (e.g. Brunt et al., 2013). In addition, results of physical experiments suggest that, in long canyons, the upwelling of along-slope currents via the canyon mouth creates cyclonic eddies in the mouth region (Waterhouse et al., 2009). This mechanism might cause lateral erosion at the canyon margins and might promote intra-canyon erosion in the canyon-mouth area.

Our results also indicate that canyons reaching into deeper waters tend to be more sinuous, which might reflect an increased impact of seafloor relief on canyon geomorphology with progressive extension of the canyon across the continental slope. For example, canyons might become more sinuous and longer where their pathways are deflected and redirected by topographic highs (e.g. Micallef et al., 2014) and intraslope depressions (e.g. Bourget et al., 2010). The effect of seafloor topographic variability might also in part explain the positive scaling of maximum width with seafloor depth, in view of how longer canyons are more likely to have a larger number of sections displaying local widening in planform, for example where intraslope depressions are incorporated in the canyon.

For maximum canyon sidewall steepness, the positive scaling with seafloor depth at the canyon mouth might in part reflect how the studied canyons located in open seas tend to have steeper canyon margins than those in semi-enclosed and enclosed seas (section 7.4), and continental slopes in open oceanic settings reaching greater depths.

5.3. Latitudinal position of the canyon apex

The canyons in our study cover a latitudinal range between 1° and 72° degrees. However, data on high-latitude canyons is limited to 15 examples from the NW Norwegian continental margin and the Barrow Canyon in the NE Chukchi Sea; polar canyons along the Antarctic margin are notably lacking in the dataset (see section 3.3).

5.3.1. Observations

For absolute values of latitude of the canyon apex and canyon morphometric parameters, correlations are weak to moderate in strength (Figs. 5 & 9a-f). Moderate positive correlation exists between latitude and average canyon width (Fig. 9b), and modest negative correlations between latitude and both average depth (Fig. 9c) and

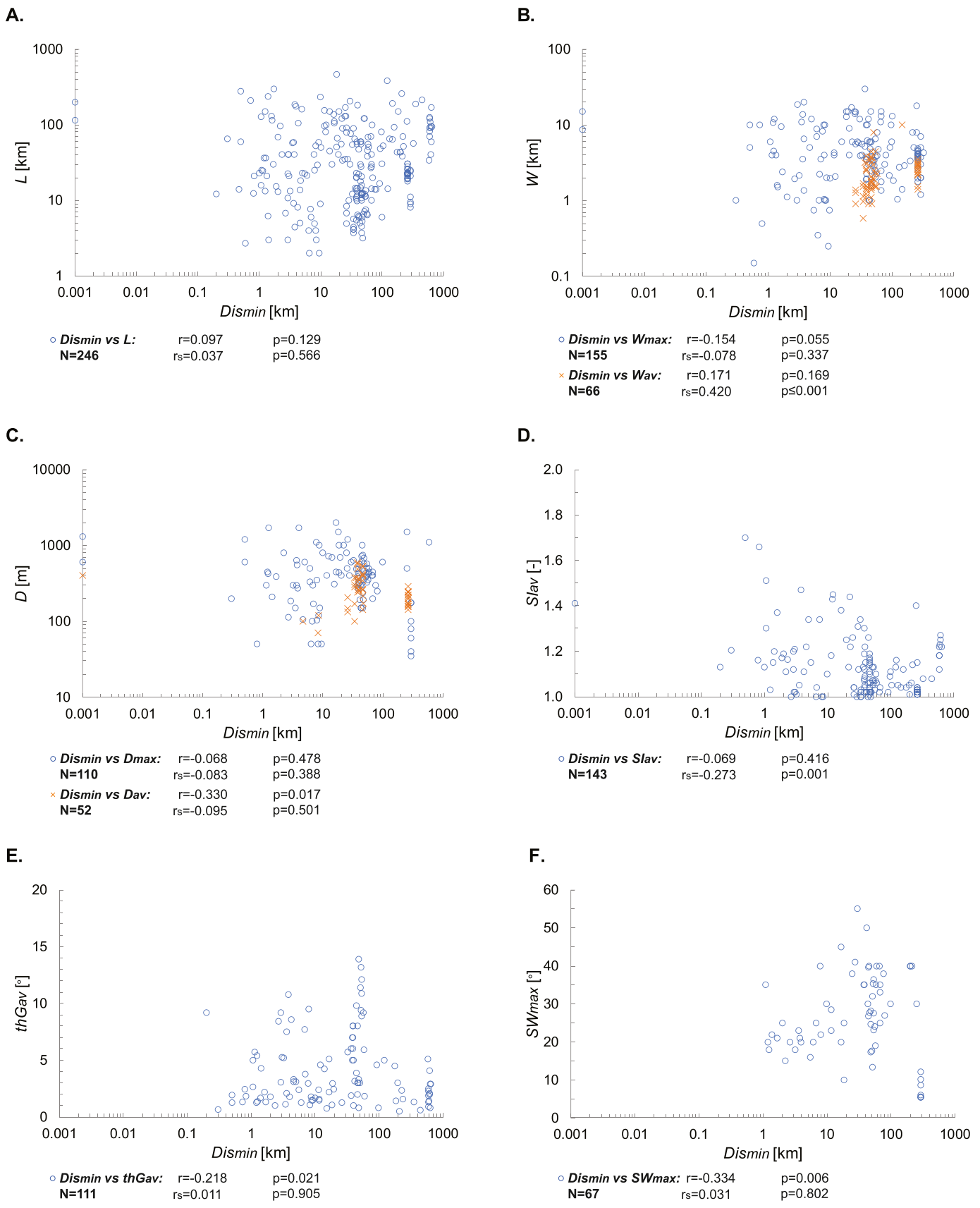

Fig. 6. a-f: Scatterplots of minimum canyon-shoreline distance and canyon morphometric parameters. N = number of observations; r = Pearson's correlation coefficient; r_s = Spearman's rank correlation coefficient. See Fig. 5 for key of abbreviations.

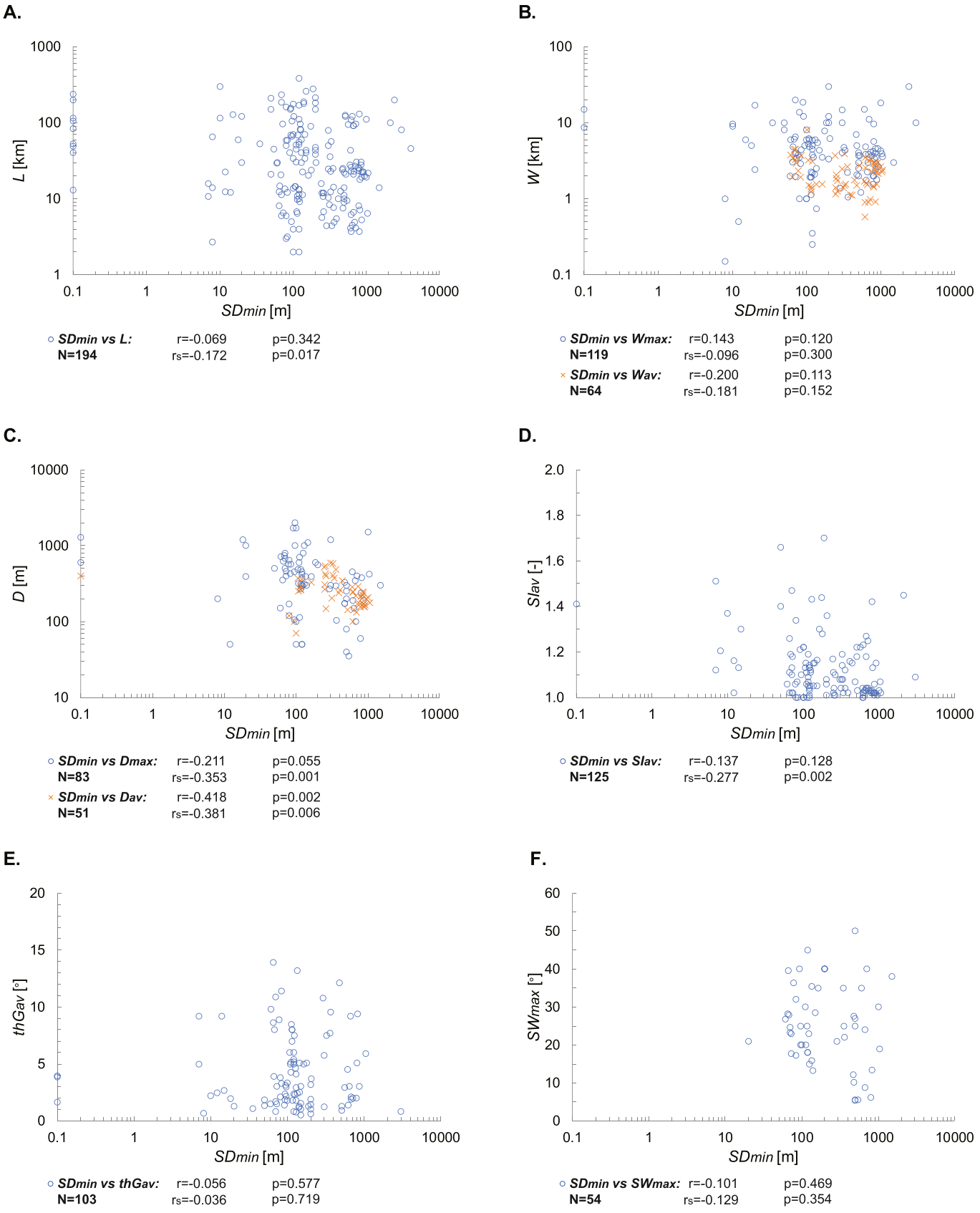

Fig. 7. a-f: Scatterplots of seafloor depth at the top of the canyon and canyon morphometric parameters. N = number of observations; r = Pearson's correlation coefficient; r_s = Spearman's rank correlation coefficient. See Fig. 5 for key of abbreviations.

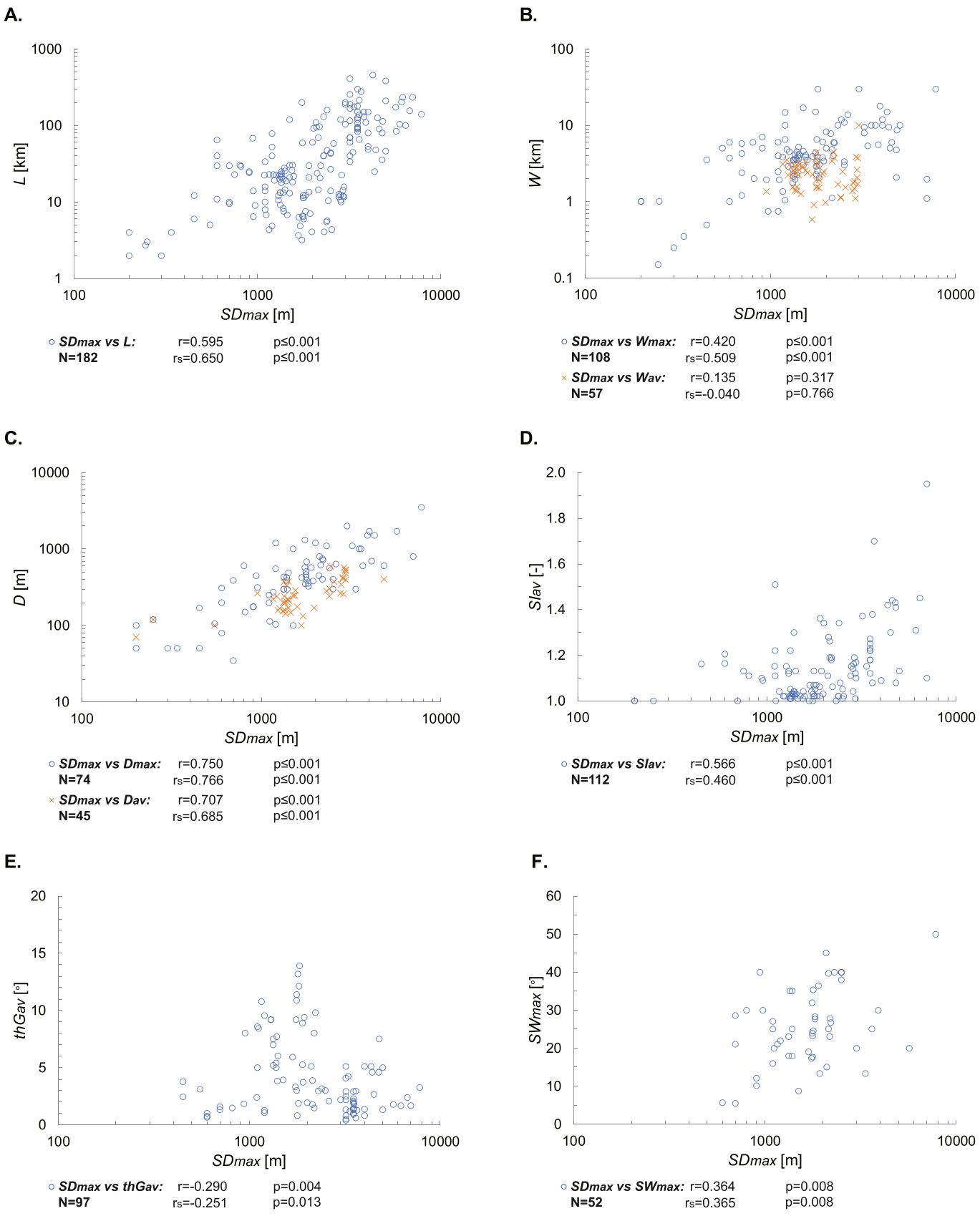

Fig. 8. a-f: Scatterplots of seafloor depth at the canyon mouth and canyon morphometric parameters. N = number of observations; r = Pearson's correlation coefficient; r_s = Spearman's rank correlation coefficient. See Fig. 5 for key of abbreviations.

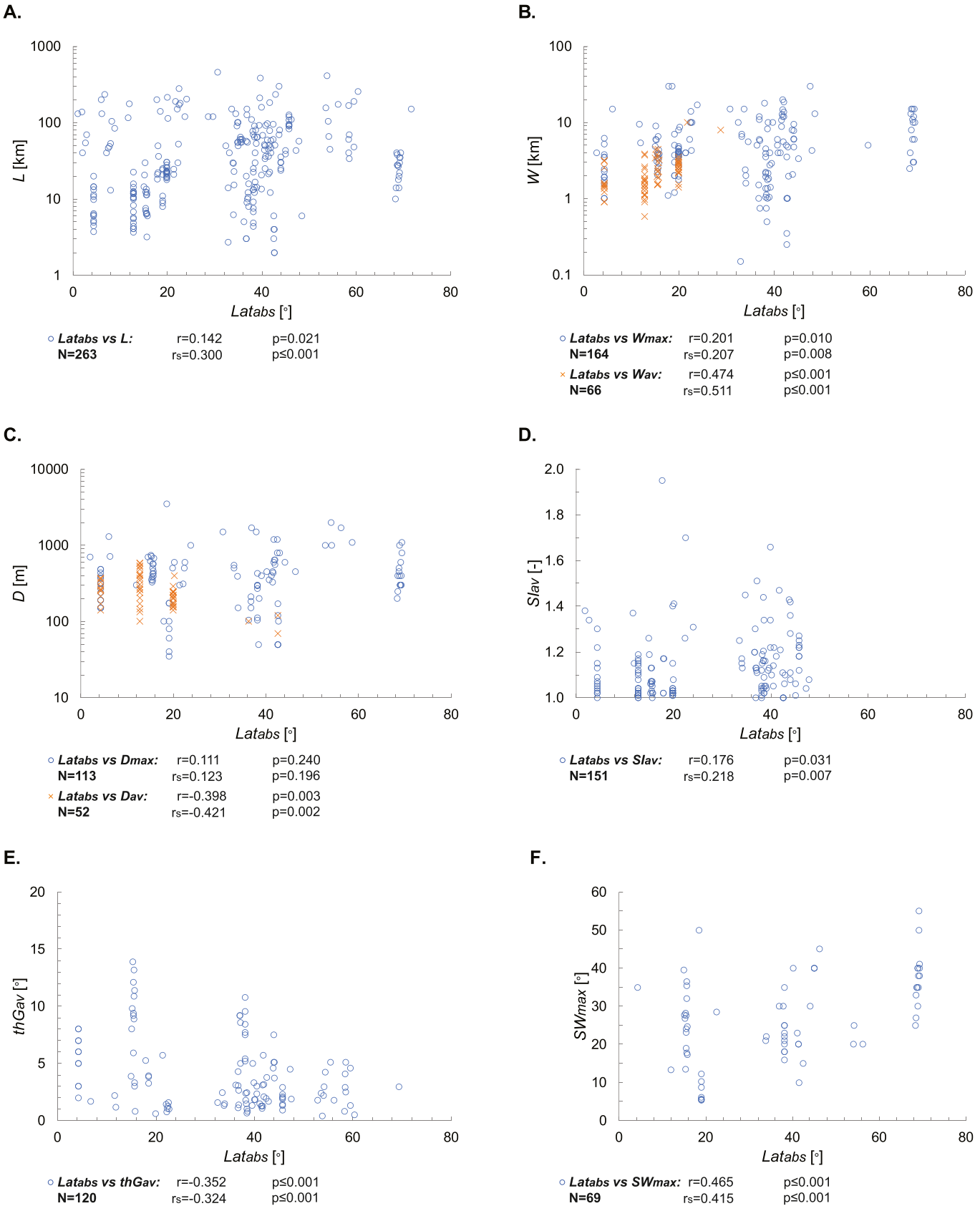

Fig. 9. a-f: Scatterplots of absolute values of latitude of the canyon apex and canyon morphometric parameters. N = number of observations; r = Pearson's correlation coefficient; r_s = Spearman's rank correlation coefficient. See Fig. 5 for key of abbreviations.

maximum canyon sidewall steepness (Fig. 9f). Weaker but statistically significant correlations are seen for canyon length (Fig. 9a), average canyon sinuosity (Fig. 9d) and the average canyon thalweg gradient (Fig. 9e), which are negative for the latter and positive for the first two variables.

5.3.2. Interpretations

The limited correlation between latitude and canyon morphometric parameters is interpreted to (i) arise from the complex ways in which climate can influence processes that can control canyon geomorphology (section 4.2); and (ii) reflect how the occurrence, frequency and magnitude of some processes vary with latitude, or are prevalent in – or even exclusive to – certain latitudinal belts.

Climate can variably influence sediment fluxes to marine environments and submarine canyons, for example by exerting controls on precipitation and subaerial erosion (e.g. Milliman and Farnsworth, 2011; Clift, 2020). Despite marked regional variations, annual precipitation rates decrease with latitude on a global scale (Milliman and Farnsworth, 2011). A general relationship between precipitation and denudation rates has been discussed in the literature (e.g. Fournier, 1949; Langbein and Schumm, 1958; Wilson, 1973; Milliman and Farnsworth, 2011; Zhang et al., 2022). Local and regional erosion rates might vary greatly due to the impact of additional factors such as lithology, tectonic uplift and vegetation cover (e.g. Kober et al., 2015; Torres Acosta et al., 2015; Starke et al., 2020). Hence, the weakness in correlation between latitude and canyon morphometrics might reflect the complex interrelationships between these factors, variability in the degree to which they are controlled by latitude, or that they are not important controls on submarine-canyon geomorphology.

Sediment discharge in rivers tends to peak during extreme weather events (e.g. Mulder and Syvitski, 1995), and to vary in concert with seasonal phenomena like monsoons (e.g. Clift, 2020). For example, cyclones can set the conditions that trigger hyperpycnal flows and turbidity currents at river mouths (e.g. Milliman and Kao, 2005). The passing of such cyclone-driven flows through submarine canyons is known from low-latitudinal regions including the South China Sea (e.g. Milliman and Kao, 2005; Zhang et al., 2018) and the Philippines (e.g. Sequeiros et al., 2019; Porcile et al., 2020), but cyclones also occur at temperate latitudes (e.g. Schultz et al., 2019; Son et al., 2022), and tend to preferentially occur in certain geographic regions in both hemispheres (e.g. Goni et al., 2009; Schultz et al., 2019). Storm-induced intra-canyon flows have been reported from many examples at tropical and temperate latitudes, and can also be linked to the remobilisation of shelf deposits as well as excess pore water pressure facilitating the remobilisation of surface sediments in the vicinity of canyon heads (e.g. Puig et al., 2004, 2014, and references therein).

Thus, climate-related factors that might exert control on canyon geomorphology are in many cases not tied to a certain latitudinal belt and cannot generally be captured by monotonic relationships across tropical and temperate zones.

The potential influence of glacial processes on canyon geomorphology is especially relevant to canyons in polar and mid-latitude regions that were covered by ice sheets during glacial intervals. Sediment can be supplied to slope environments by various glacial processes. The relative predominance of such processes and their importance as sediment sources to submarine canyons can vary over a glacial-interglacial cycle (e.g. Kagami et al., 1991; Gales et al., 2021; Ha et al., 2022). For example, during glacial and interglacial intervals, where ice sheets have prograded across continental shelves, sediment can be distributed to canyon heads via sediment gravity flows fed by subglacial ice streams and meltwater discharge (e.g. Kagami et al., 1991; Dowdeswell et al., 2004; Gales et al., 2021). In contrast, glacioisostatic shelf downwarping and uplift within the shelf might cause disconnection of canyons from sediment sources, by diverting sediment pathways and creating intrashelf sinks (e.g. Kagami et al., 1991). Moreover, ice-sheet loading along shelf margins during glacial maxima and sea-level lowstands is considered a potential trigger to mass failures on continental slopes (e.g. Mulder and Moran, 1995; Gales et al., 2021). This mechanism might contribute to intra-canyon erosion by slope failures that would trigger, or evolve into, sediment gravity flows, and cause mass failures in canyons that have reached or retrograded into glaciated shelves. In addition, sediment can be supplied to slope systems from ice-rafted debris (e.g. Gales et al., 2021; Ha et al., 2022), a process which is influenced by climate but occurs during both glacial and interglacial periods (e.g. Hemming, 2004; Alvarez-Solas et al., 2013; Ha et al., 2022). Sediment can also be transported to canyons via down-canyon cascading of dense shelf water, as seen in the Antarctic Hillary Canyon (see Gales et al., 2021).

In high-latitude settings, sediment connection of canyons to terrestrial catchments might also be affected by glacial isostatic adjustment subsequent to glacial intervals leading to river diversions (e.g. Pico et al., 2018).

An example of steep canyon margins (>40°) is reported for submarine canyons along the Labrador margin (e.g. Dowdeswell et al., 2016). One factor that might contribute to steeper margins in canyons in higher latitudes is the glaciation of continental margins. The prevalence of line sources in glacial margin settings, as opposed to point sources in low-latitudinal settings, has been suggested (e.g. Martinsen, 2005; Armitage et al., 2010): sediment can be discharged rapidly from glaciers and ice streams, and distributed sediment dispersal across the continental slope (Martinsen, 2005) can promote the aggradation of canyon margins and inter-canyon ridges due to background sedimentation and overspill from channelised flows in canyons (e.g. Armitage et al., 2010; Gales et al., 2021), which in turn increase their proneness to slope failure (Armitage et al., 2010).

Although suitable data only include submarine canyons at latitudes up to 45°, the lack of any relationships between latitude and sinuosity is in agreement with findings by Harris and Whiteway (2011) for shelf-incising canyons (see their Fig. 9). The influence of latitude-related processes on submarine-channel sinuosity has been debated: an inverse relationship between channel sinuosity and latitude, linked to influence of the Coriolis force and variations in sediment type and flow type within different latitudinal zones, has been proposed (e.g. Peakall et al., 2012), but its robustness has been subsequently challenged (e.g. Sylvester and Pirmez, 2017). The results indicate that mechanisms invoked as latitudinal controls on sinuosity for submarine channels may not be applicable to submarine canyons. This research area needs further investigation.

Regardless, these considerations must be viewed with reservation due to the limited size of the datasets for arctic and tropical examples, and because of geographic bias. For example, canyons offshore NW Norway are accommodated on a passive margin in an open-sea setting, two environmental conditions that appear to promote steepening of canyon sidewalls; the former by promoting slope failure within canyons (section 7.2) and the latter by favouring canyon margin aggradation related to oceanic currents in open-sea settings (section 7.4).

6. Scaling relationships between canyon morphometric parameters and source-to-sink system attributes

Scaling relationships between canyon morphometric parameters and attributes of related terrestrial catchments, continental shelves and slopes have been evaluated. For 69 submarine canyons, which represent 24% of the studied canyons, scaling relationships between canyon and terrestrial-catchment parameters have been investigated, except for maximum canyon sidewall steepness, average canyon width and depth, due to data paucity. The same applies for correlations of average canyon width and depth with slope characteristics.

An overview of the results is presented in form of heatmaps of correlation (Fig. 10a-c). Furthermore, relationships between attributes of canyon-associated S2S systems (Fig. 11) have been investigated. This has been undertaken to aid in the interpretation of controls on canyon

A. Terrestrial catchment

Pearson's correlation coefficient r

L	0.184	0.244	0.210	0.387
W max	0.358	0.306	0.452	0.633
D max	0.414	***	0.372	***
SI av	-0.075	0.057	-0.089	0.586
thG av	-0.345	***	-0.273	-0.193
SW max	***	***	***	***
	L fls	*Q fls*	*A flsc*	*H flsc*

p-value

L	0.130	0.091	0.091	0.003
W max	0.056	0.232	0.014	0.001
D max	0.098	***	0.117	***
SI av	0.601	0.743	0.539	≤0.001
thG av	0.067	***	0.138	0.402
SW max	***	***	***	***
	L fls	*Q fls*	*A flsc*	*H flsc*

Spearman's rank correlation coefficient rs

L	0.107	0.666	0.137	0.636
W max	0.424	0.123	0.633	0.588
D max	0.736	***	0.737	***
SI av	-0.165	0.510	-0.127	0.602
thG av	-0.171	***	-0.106	-0.286
SW max	***	***	***	***
	L fls	*Q fls*	*A flsc*	*H flsc*

p-value

L	0.381	≤0.001	0.274	≤0.001
W max	0.022	0.639	≤0.001	0.002
D max	0.001	***	≤0.001	***
SI av	0.248	0.002	0.378	≤0.001
thG av	0.375	***	0.572	0.208
SW max	***	***	***	***
	L fls	*Q fls*	*A flsc*	*H flsc*

B. Continental shelf

Pearson's correlation coefficient r

L	0.223	0.382	-0.162
W max	0.071	0.362	-0.133
W av	0.189	0.496	0.692
D max	0.213	0.362	-0.208
D av	-0.346	***	-0.384
SI av	-0.042	0.387	0.249
thG av	-0.244	-0.348	-0.095
SW max	0.552	-0.152	-0.395
	W sh	*D sh*	*G sh*

p-value

L	0.002	≤0.001	0.082
W max	0.440	0.002	0.280
W av	0.128	0.009	≤0.001
D max	0.061	0.004	0.110
D av	0.012	***	0.157
SI av	0.620	0.001	0.035
thG av	0.012	0.002	0.404
SW max	≤0.001	0.439	0.038
	W sh	*D sh*	*G sh*

Spearman's rank correlation coefficient rs

L	0.238	0.537	-0.188
W max	0.164	0.270	-0.028
W av	0.398	0.555	0.592
D max	0.411	0.217	-0.239
D av	-0.227	***	-0.353
SI av	-0.252	0.437	0.150
thG av	-0.155	-0.334	0.005
SW max	0.457	-0.051	-0.408
	W sh	*D sh*	*G sh*

p-value

L	0.001	≤0.001	0.043
W max	0.076	0.025	0.823
W av	0.001	0.003	0.001
D max	≤0.001	0.096	0.066
D av	0.105	***	0.197
SI av	0.002	≤0.001	0.207
thG av	0.116	0.003	0.962
SW max	0.003	0.797	0.031
	W sh	*D sh*	*G sh*

C. Continental slope

Pearson's correlation coefficient r

L	0.439	0.207	-0.099
W max	0.407	0.145	-0.125
W av	***	***	***
D max	0.442	0.601	-0.023
D av	***	***	***
SI av	0.121	0.231	-0.316
thG av	-0.416	-0.002	0.493
SW max	-0.427	-0.150	0.758
	W sl	*D sl*	*G sl*

p-value

L	0.001	0.014	0.370
W max	0.008	0.179	0.340
W av	***	***	***
D max	0.003	≤0.001	0.868
D av	***	***	***
SI av	0.655	0.076	0.053
thG av	0.020	0.983	≤0.001
SW max	0.060	0.367	≤0.001
	W sl	*D sl*	*G sl*

Spearman's rank correlation coefficient rs

L	0.875	0.371	-0.246
W max	0.700	0.032	-0.141
W av	***	***	***
D max	0.637	0.462	0.112
D av	***	***	***
SI av	-0.234	0.208	-0.383
thG av	-0.504	0.062	0.461
SW max	-0.286	-0.628	0.744
	W sl	*D sl*	*G sl*

p-value

L	≤0.001	≤0.001	0.023
W max	≤0.001	0.772	0.284
W av	***	***	***
D max	≤0.001	≤0.001	0.417
D av	***	***	***
SI av	0.383	0.111	0.018
thG av	0.004	0.597	≤0.001
SW max	0.221	≤0.001	≤0.001
	W sl	*D sl*	*G sl*

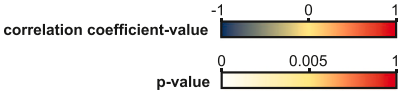

Fig. 10. a-c: Heat maps for correlations of canyon morphometrics with variables of the associated source-to-sink system displaying values of Pearson's correlation coefficient r and Spearman's rank correlation coefficient rs, and their respective p-values. A. Terrestrial catchment. B. Continental shelf. C. Continental slope. L = canyon length; W_{max} = maximum canyon width; W_{av} = average canyon width; D_{max} = maximum canyon depth; D_{av} = average canyon depth; SI_{av} = average canyon sinuosity index; thG_{av} = average canyon thalweg gradient; SW_{max} = maximum canyon sidewall steepness; L_{fls} = fluvial system length; $Qfls$ = average annual fluvial discharge; A_{flsc} = size of the catchment; H_{flsc} = maximum elevation in the catchment area; W_{sh} = shelf width; D_{sh} = shelf-break depth; G_{sh} = average shelf gradient; W_{sl} = slope width; D_{sl} = slope-break depth; G_{sl} = average slope gradient; *** indicates scarcity of data (N<15).

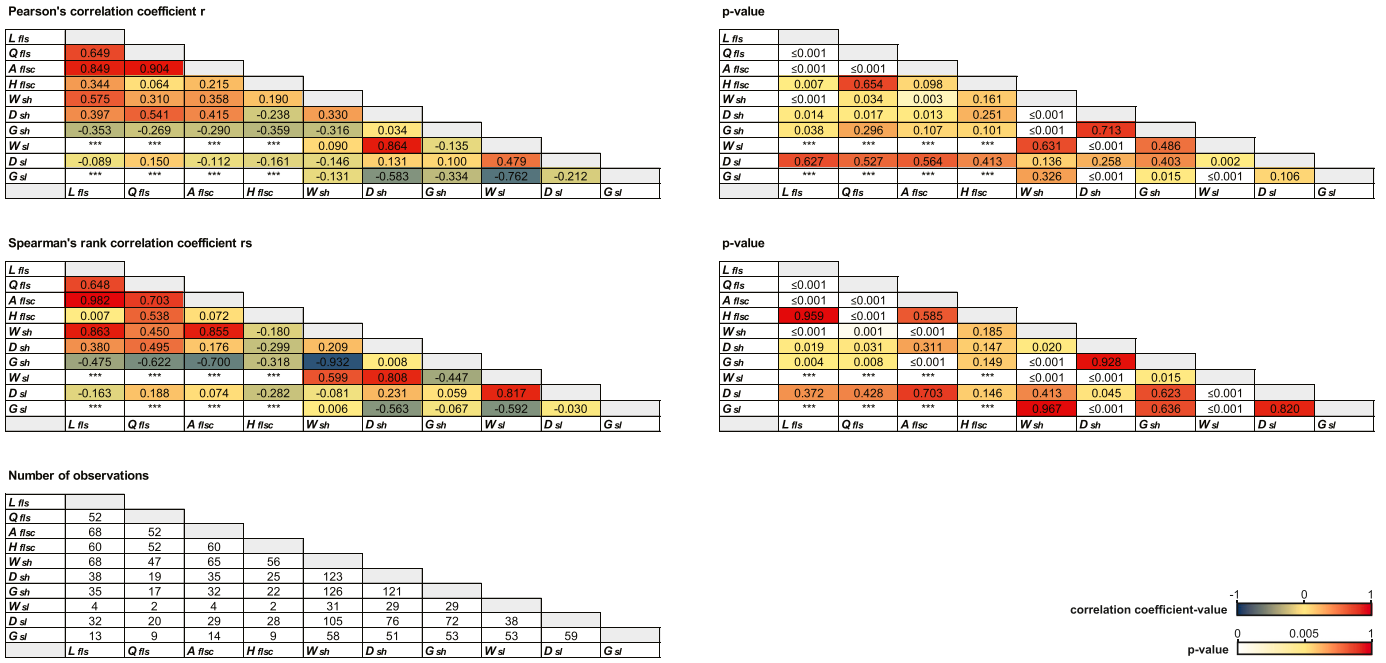

Fig. 11. Heat maps for correlations of variables of the source-to-sink system specific to studied canyons displaying values of Pearson's correlation coefficient r and Spearman's rank correlation coefficient rs, and their respective p-values. L_{fls} = fluvial system length; $Qfls$ = average annual fluvial discharge; A_{flsc} = size of the catchment; H_{flsc} = maximum elevation in the catchment area; W_{sh} = shelf width; D_{sh} = shelf-break depth; G_{sh} = average shelf gradient; W_{sl} = slope width; D_{sl} = slope-break depth; G_{sl} = average slope gradient; *** indicates scarcity of data (N<15).

morphometry by identifying where relationships might in part reflect covariance with one or several other factors. Correlations of canyon morphometrics with attributes of the catchment, shelf and slope are presented as scatterplots in sections 6.1 to 6.3 (Figs. 12–15), in which the findings for the individual S2S segments are discussed. In addition, canyon morphometry has been quantitatively assessed for canyons grouped based on shelf-break thresholds of 120 m and 130 m below present-day sea level at the site of the canyon (Fig. 14a-f).

6.1. Terrestrial catchment

6.1.1. Observations

Fluvial system length displays moderate and statistically significant positive correlation with maximum canyon depth (Fig. 12i), and modest but not significant positive correlation with maximum canyon width (Fig. 12e).

Similarly, moderate significant positive correlations between catchment size and canyon maximum depth and width are seen (Figs. 12 g&k).

Average annual fluvial discharge has moderate direct correlations with canyon length (Fig. 12b) and average canyon sinuosity (Fig. 12n); both relationships are statistically significant.

Moderate statistically significant positive correlations exist between maximum catchment elevation and canyon length (Fig. 12d), maximum width (Fig. 12h) and average sinuosity (Fig. 12p).

6.1.2. Interpretations

The observed relationships between canyon length, maximum canyon depth and average canyon sinuosity with attributes of the terrestrial catchment likely reflect how fluvial sediment discharge can promote intra-canyon erosion by down-canyon flows, e.g. the upslope lengthening of canyons at their apices (e.g. Piper and Normark, 2009), their deepening in the region of canyon mouths, and how the streamwise length of more sinuous canyons is inherently longer (see section 5.2.2.2).

The extent to which the morphology of a submarine canyon is affected by fluvial sediment discharge depends on its erosional versus depositional impact on individual canyon morphometrics, which is determined by many factors and their interplay. The bedrock lithology of terrestrial source areas has been invoked as a control on canyon formation in view of how it can influence the runout distance and erosive strength of submarine flows, e.g. by affecting sediment density, composition and transport mechanisms (Smith et al., 2017). In addition, characteristics of the seafloor substrate can impact its erodibility, which also has an effect on the magnitude of intra-canyon erosion by the flows; for example carbonate cementation can decrease erodibility and stabilise the substrate and canyon walls (e.g. Oiwane et al., 2011), thereby reducing the potential of mass failure on slopes (e.g. Chang et al., 2021) and within canyons. With increasing distance between the river mouth and the submarine canyon head, the sediment transport efficiency decreases as a function of distance and grain size. A global study on sediment delivery to submarine canyons from fluvial systems (Sweet and Blum, 2016) indicates that canyons tend to intercept gravel-sized sediment when their head is within ca. 500 m of a fluvial source, sand-sized sediment when it is within 1 to 5 km, and silt and clay-sized sediment when it is within ca. 40 km. The segregation of grain sizes in shelf-crossing submarine flows can impact canyon evolution; findings from studies of the Monterey Canyon suggest that the presence of unconsolidated sands within a canyon might be a prerequisite for intra-canyon turbidity current generation (Paull et al., 2018), whereas surficial mud deposits on the canyon floor might promote self-acceleration of these flows (Hereema et al., 2020).

The variability of these factors across S2S systems can explain the weakness with which canyon morphometric parameters are scaled with attributes of the terrestrial catchments. Weakness in correlation may also be due to other controls overprinting the effect of fluvial discharge on canyon geomorphology; these controls may include, for example, intra-canyon sedimentary processes (see section 4.2.1), hydrodynamic processes (section 4.2.2), structural controls (section 4.2.3) and biogenic processes (section 4.2.4), as well as sediment remobilisation within the shelf and slope.

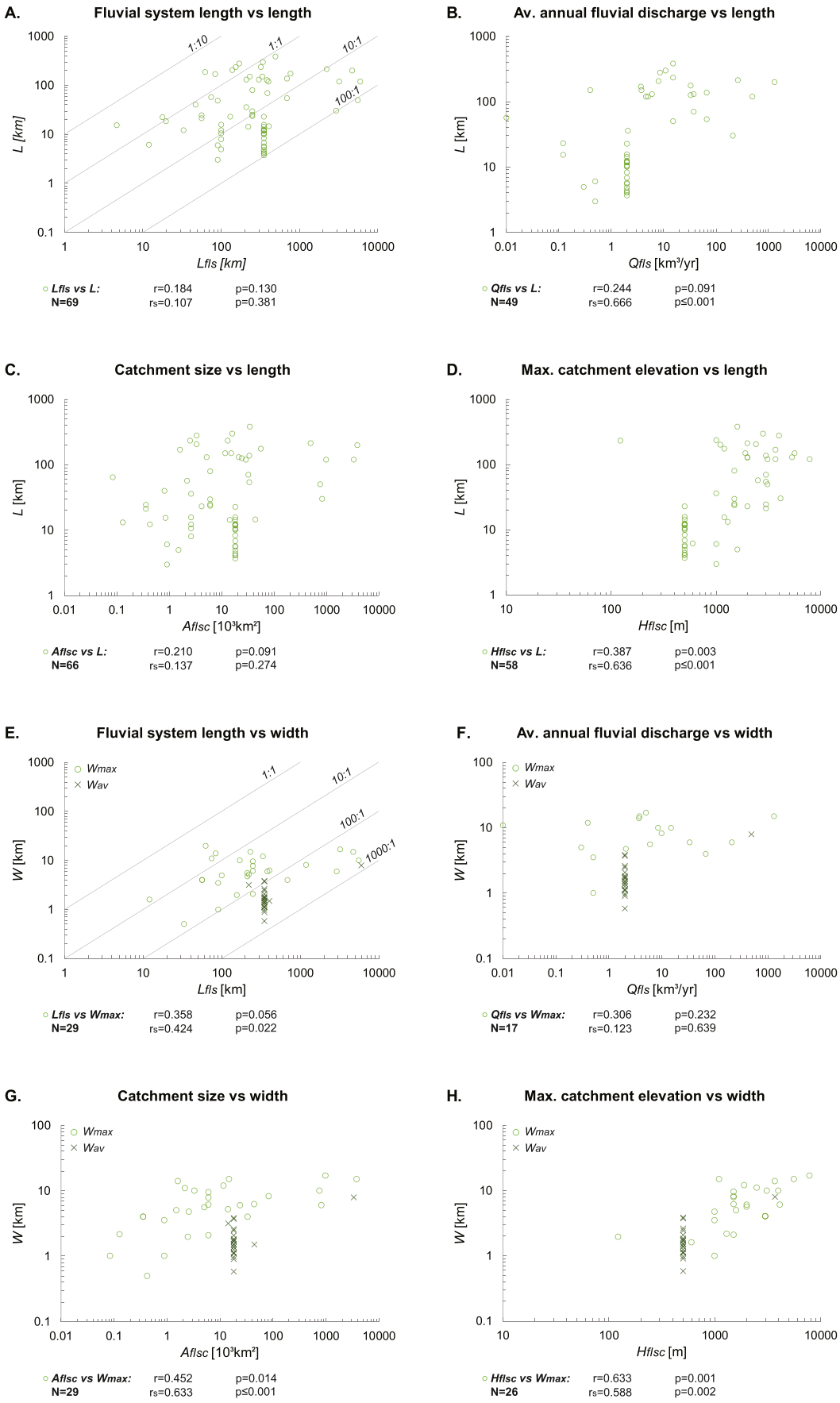

Fig. 12. a-t: Scatterplots between attributes of terrestrial catchments and canyon morphometric parameters. N = number of observations; r = Pearson's correlation coefficient; r_s = Spearman's rank correlation coefficient. See Tab. 2 for key of abbreviations.

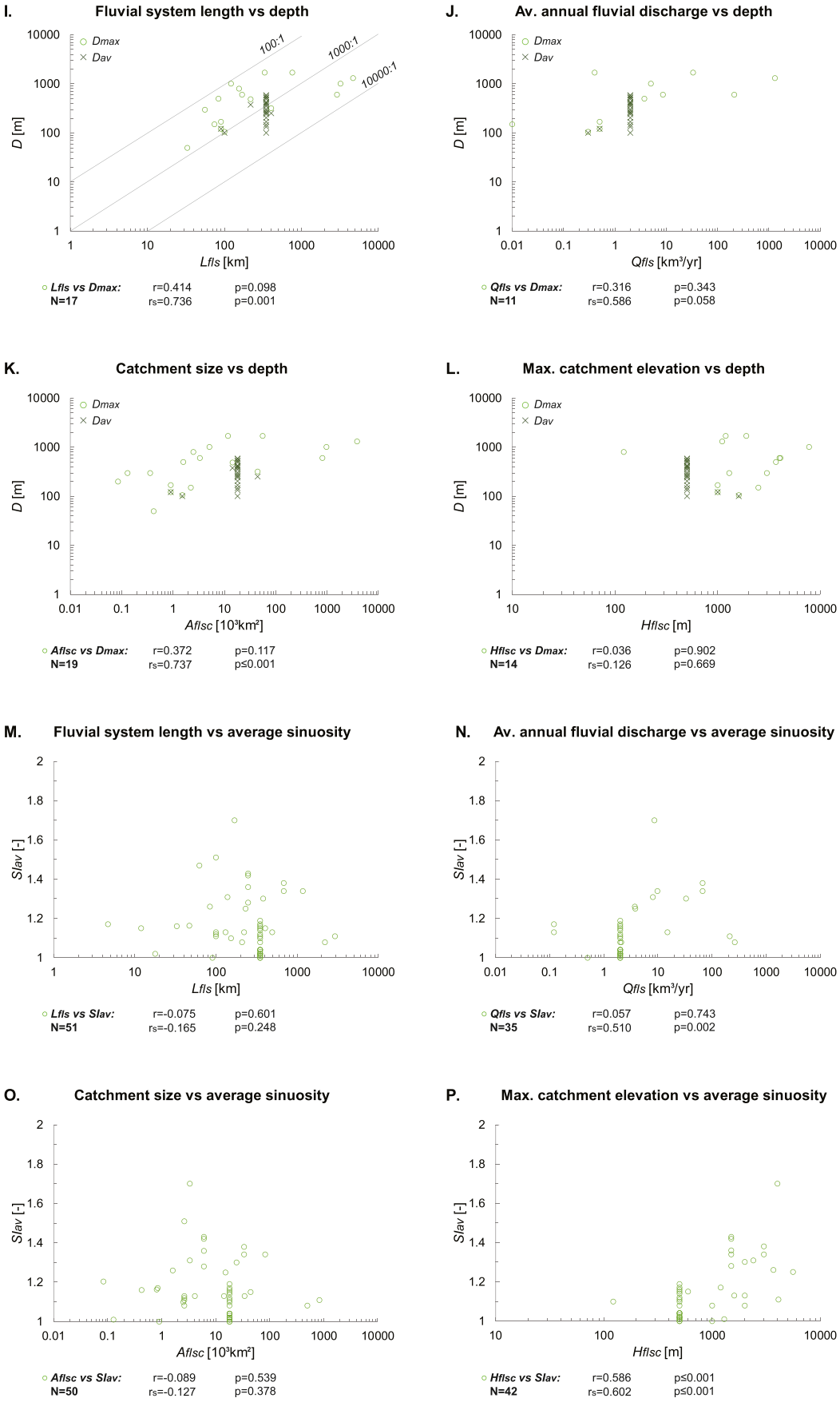

Fig. 12. (*continued*).

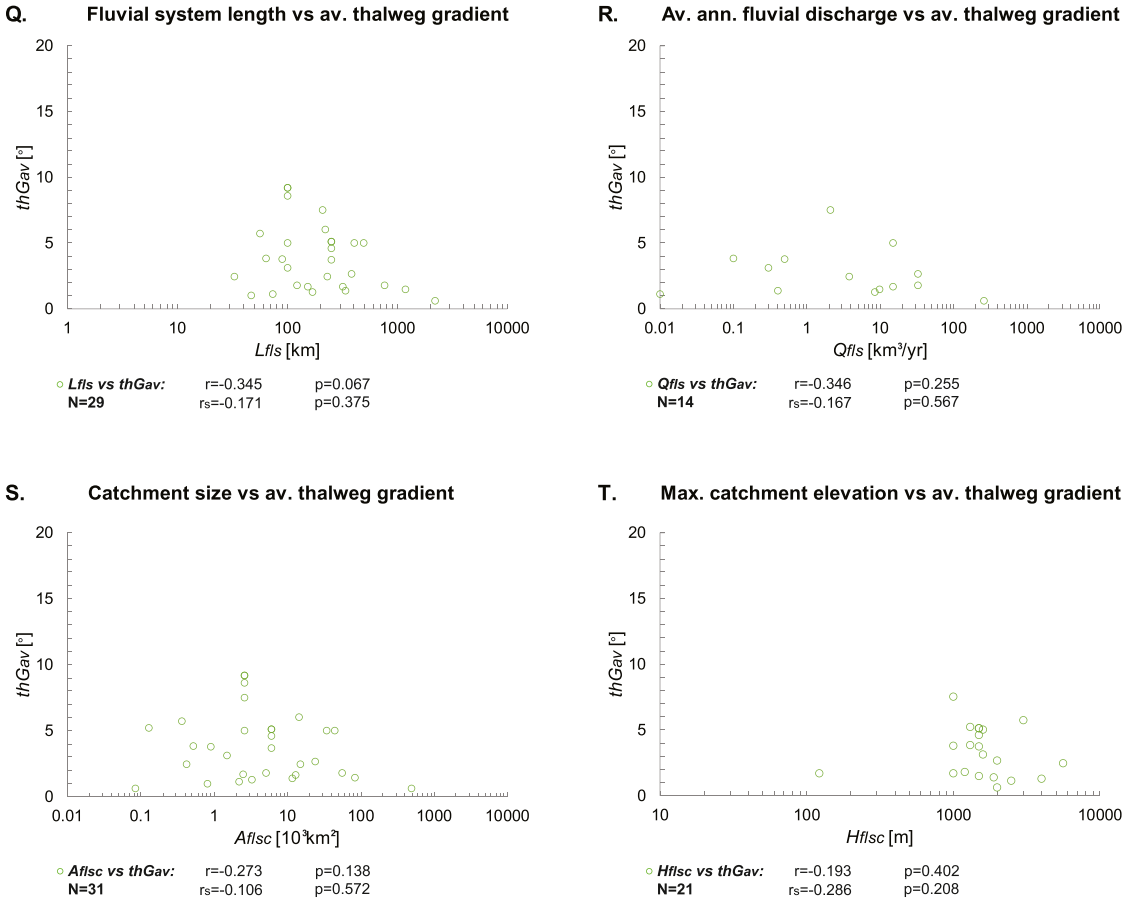

Fig. 12. (*continued*).

6.2. Continental shelf

6.2.1. Observations

The shelf width is moderately directly correlated with the maximum canyon sidewall steepness (Fig. 13p), and only modestly with average canyon width (Fig. 13d) and maximum canyon depth (Fig. 13g). The shelf width is directly correlated with the canyon length (Fig. 13a) and inversely with the average canyon sinuosity (Fig. 13j), but these relationships are weak.

The shelf-break depth correlates significantly with all investigated canyon morphometric parameters except for the maximum canyon sidewall steepness (Fig. 13q), exhibiting moderate positive correlation with the canyon length (Fig. 13b) and modest correlation with the average canyon sinuosity (Fig. 13k); correlations with maximum width (Fig. 13e) and depth (Fig. 13h) are weaker. In contrast, the average canyon thalweg gradient shows weak but significant inverse scaling with the shelf-break depth (Fig. 13n). Moderate scaling exists between the shelf-break depth and the average canyon width, but the data stem from two geographic regions only: offshore NE Australia and NE Brazil, both associated with shallow (70-85 m) shelves (Fig. 13e).

Correlations of canyon morphometric parameters with the average shelf gradient are mostly weak and not significant (Fig. 13a-r). Moderate and significant correlation is observed between shelf gradient and average canyon width (Fig. 13f), but these results are based on data from two geographic regions only. Modest inverse correlation is seen between shelf gradient and maximum canyon sidewall steepness, which is not statistically significant (Fig. 13r).

Submarine canyons with a present-day shelf break deeper than 120 m bsl are on average longer and have greater maximum widths and depths, higher average canyon sinuosities and lower average canyon thalweg gradients than canyons with a shelf-break shallower than 120 m bsl. The same trends are seen for groups of canyons distinguished based on a threshold of shelf-break depth of 130 m (Fig. 14a-f). Although a greater range in maximum canyon sidewall steepness is seen in canyons associated with shelf breaks deeper than 120 m, average values between both canyon groups are very similar. Data on maximum canyon depth and maximum canyon sidewall steepness that can be employed in this analysis are limited, whereas data on average width and depth are only available for canyons installed on slopes with shelf breaks shallower than 120 m.

6.2.2. Interpretations

The width of the shelf plays a role in across-shelf sediment distribution from fluvial outlets to the shelf edge (e.g. Sweet et al., 2020). Narrower shelves are characterised by shorter distances to fluvial outlets that can deliver sediment to canyon heads, and may allow sediment connection of canyons with rivers and littoral cells to be maintained during sea-level highstands (e.g. Covault et al., 2007; Normark et al., 2009; Jipa and Panin, 2020). Steeper shelf gradients might also inhibit deposition by hyperpycnal flows and promote bedload transport of coarse sediment from rivers across shelves (e.g. Jipa and Panin, 2020).

By contrast, the effect of hydroisostasy on continental levering and the ensuing steepening of continental shelves is thought to be stronger for wider shelves, probably by a factor $\leq$0.3 since the Last Glacial Maximum (LGM), relative to narrower shelves (Hutton et al., 2013). Nevertheless, despite being more prone to hydroisostatic flexure, wider shelves tend to have gentler gradients than narrower shelves.

Wider shelves also tend to have resulted from greater shelf-edge progradation, which can occur in response to greater rates of sediment supply to the outer shelf and upper slope from terrestrial catchments and from shelf-internal sources (e.g. Mougenot et al., 1983; Carvajal et al., 2009;

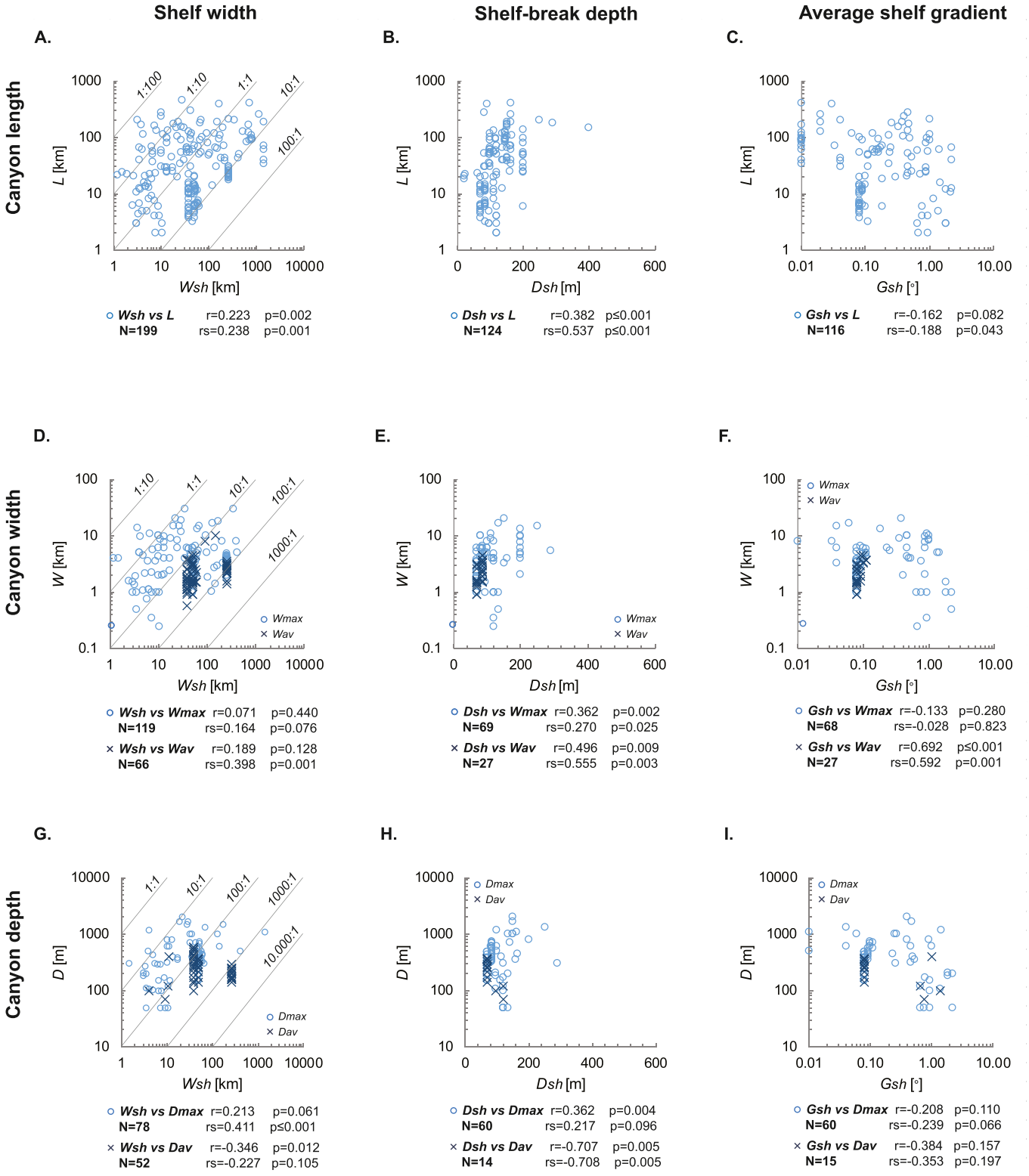

Fig. 13. a-r: Scatterplots between attributes of the continental shelf and canyon morphometric parameters. N = number of observations; r = Pearson's correlation coefficient; r_s = Spearman's rank correlation coefficient. See Tab. 2 for key of abbreviations.

Blum et al., 2013), as well as from the up-building of slope sediment prisms from drifts (e.g. Fulthorpe and Carter, 1991). However, although a wider shelf indicates a more sustained sediment supply to a shelf margin, sediment transport across wide shelves into submarine canyons is most effective for canyons that have significantly retrograded the shelf and/or are connected with a river, either directly or via shelf channels or shelf-edge deltas. With increasing shelf width, the effectiveness of across-shelf sediment transport from fluvial outlets decreases for coarser grained

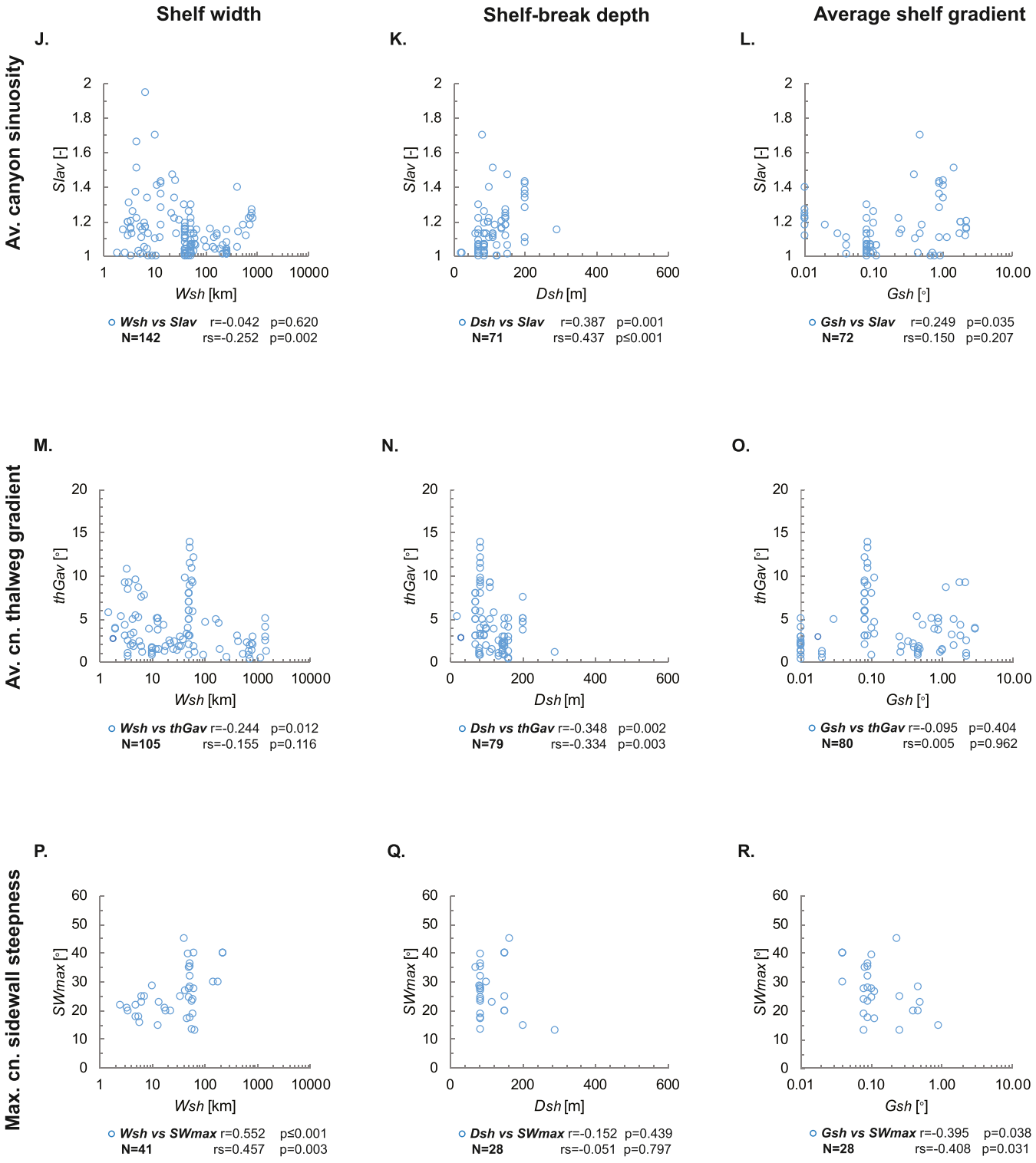

Fig. 13. (*continued*).

sediment, leading to variations in grain-size distribution of sediment discharged from rivers across the shelf. Hence, the importance of erosion by submarine flows linked to rivers on canyon morphology becomes likely less significant on shelves wider than 5 km, given the expected paucity of sand grain-size fractions reaching beyond this boundary (section 6.1). In addition, the frequency and magnitude of hyperpycnal flows can be affected by factors other than the shelf width, such as salinity of the water body, climate and relative sea-level change (e.g. Mulder et al., 2003; Dadson et al., 2005).

The effectiveness of across-shelf sediment transport is also affected by hydrodynamic processes associated with tidal currents, along-shelf currents and waves (Nittrouer and Wright, 1994; Wang et al., 2010). The ability of waves to remobilise sediment is greater at shallower depths (Peters and Loss, 2012); this sediment transport mechanism might have a greater areal effect on wide and shallow shelves with lower gradients.

A. Length

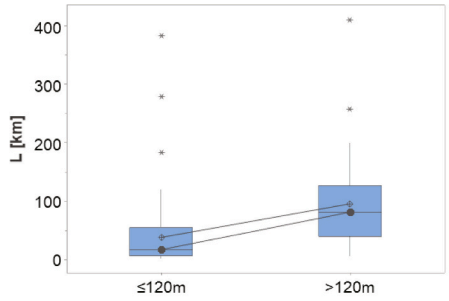

	N	min	mean	StDev	median	max
≤120	**78**	2.00	38.14	58.60	17.02	384.05
>120	**46**	6.00	95.50	74.00	81.30	411.00
T-Value =-7.48 DF = 119 P-Value ≤ 0.001						
≤130	**78**	2.00	37.45	57.15	17.02	384.05
>130	**46**	6.00	96.60	75.00	81.30	411.00
T-Value =-7.55 DF = 119 P-Value ≤ 0.001						

B. Maximum width

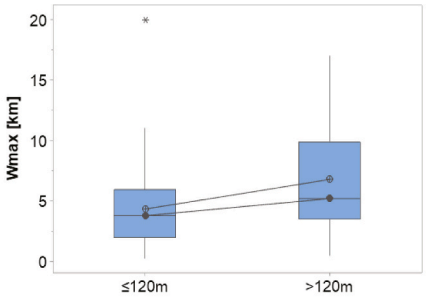

	N	min	mean	StDev	median	max
≤120	**53**	0.25	4.33	3.37	3.78	20.00
>120	**16**	0.50	6.79	4.91	5.20	17.00
T-Value =-1.56 DF = 22 P-Value = 0.134						
≤130	**52**	0.25	4.03	2.58	3.78	11.00
>130	**17**	0.50	7.56	5.73	5.40	20.00
T-Value =-2.46 DF = 18 P-Value = 0.024						

C. Maximum depth

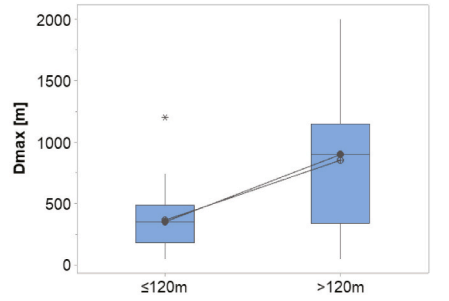

	N	min	mean	StDev	median	max
≤120	**46**	50.00	364.50	225.50	350.00	1200.00
>120	**14**	50.00	854.00	567.00	900.00	2000.00
T-Value =-3.15 DF = 14 P-Value = 0.007						
≤130	**46**	50.00	364.50	225.50	350.00	1200.00
>130	**14**	50.00	854.00	567.00	900.00	2000.00
T-Value =-3.15 DF = 14 P-Value = 0.007						

D. Average canyon sinuosity

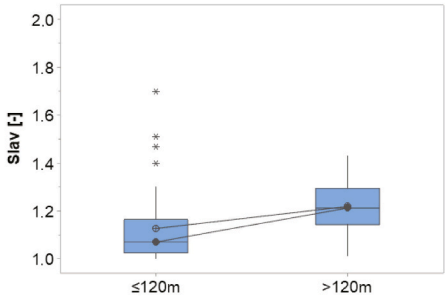

	N	min	mean	StDev	median	max
≤120	**49**	1.00	1.13	0.14	1.07	1.70
>120	**22**	1.01	1.22	0.12	1.21	1.43
T-Value =-3.15 DF = 48 P-Value = 0.003						
≤130	**48**	1.00	1.12	0.14	1.07	1.70
>130	**23**	1.01	1.23	0.12	1.22	1.47
T-Value =-3.66 DF = 46 P-Value = 0.001						

E. Average canyon thalweg gradient

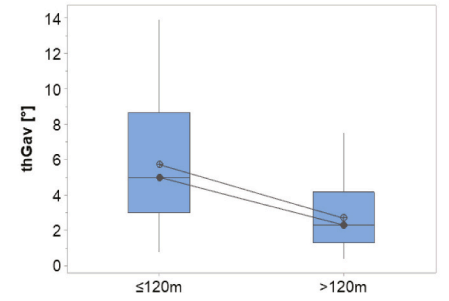

	N	min	mean	StDev	median	max
≤120	**46**	0.78	5.72	3.53	5.00	13.90
>120	**33**	0.40	2.69	1.72	2.30	7.50
T-Value = 5.04 DF = 69 P-Value ≤ 0.001						
≤130	**46**	0.78	5.72	3.53	5.00	13.90
>130	**33**	0.40	2.69	1.72	2.30	7.50
T-Value = 5.04 DF = 69 P-Value ≤ 0.001						

F. Maximum canyon sidewall steepness

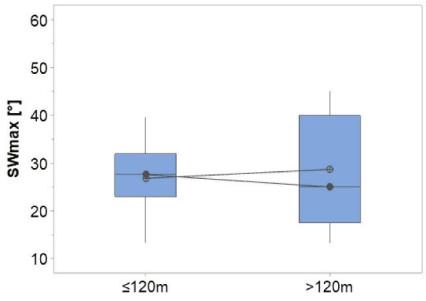

	N	min	mean	StDev	median	max
≤120	**19**	13.40	26.82	7.05	27.60	39.60
>120	**9**	13.30	28.70	12.44	35.00	45.00
T-Value =-0.42 DF = 10 P-Value = 0.681						
≤130	**19**	13.40	26.82	7.05	27.60	39.60
>130	**9**	13.30	28.70	12.44	35.00	45.00
T-Value =-0.42 DF = 10 P-Value = 0.681						

Fig. 14. a-f: Boxplots of frequency distributions of canyon morphometric parameters for studied canyons distinguished based on shelf-break depth thresholds of 120 m at the canyon. Tabulated statistics refer to canyon grouped based on shelf-break thresholds of 120 m and 130 m bsl, respectively. N = number of readings; min = minimum value; mean = mean value; StDev = standard deviation; median = median value; max = maximum value. See Tab. 2 for key of abbreviations.

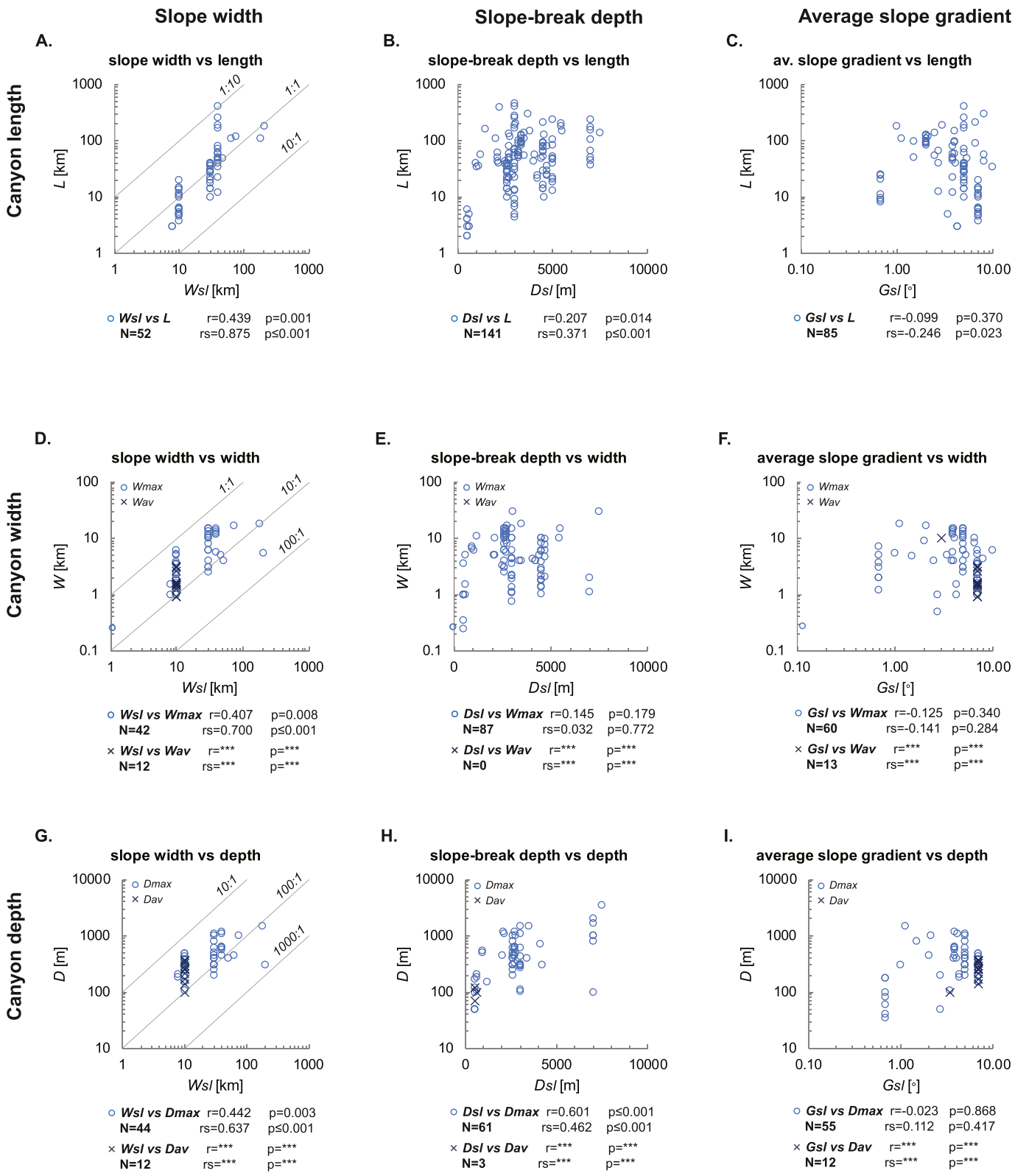

Fig. 15. a-r: Scatterplots between attributes of the slope vs canyon morphometrics. N = number of observations; r = Pearson's correlation coefficient; rs = Spearman's rank correlation coefficient. See Tab. 2 for key of abbreviations.

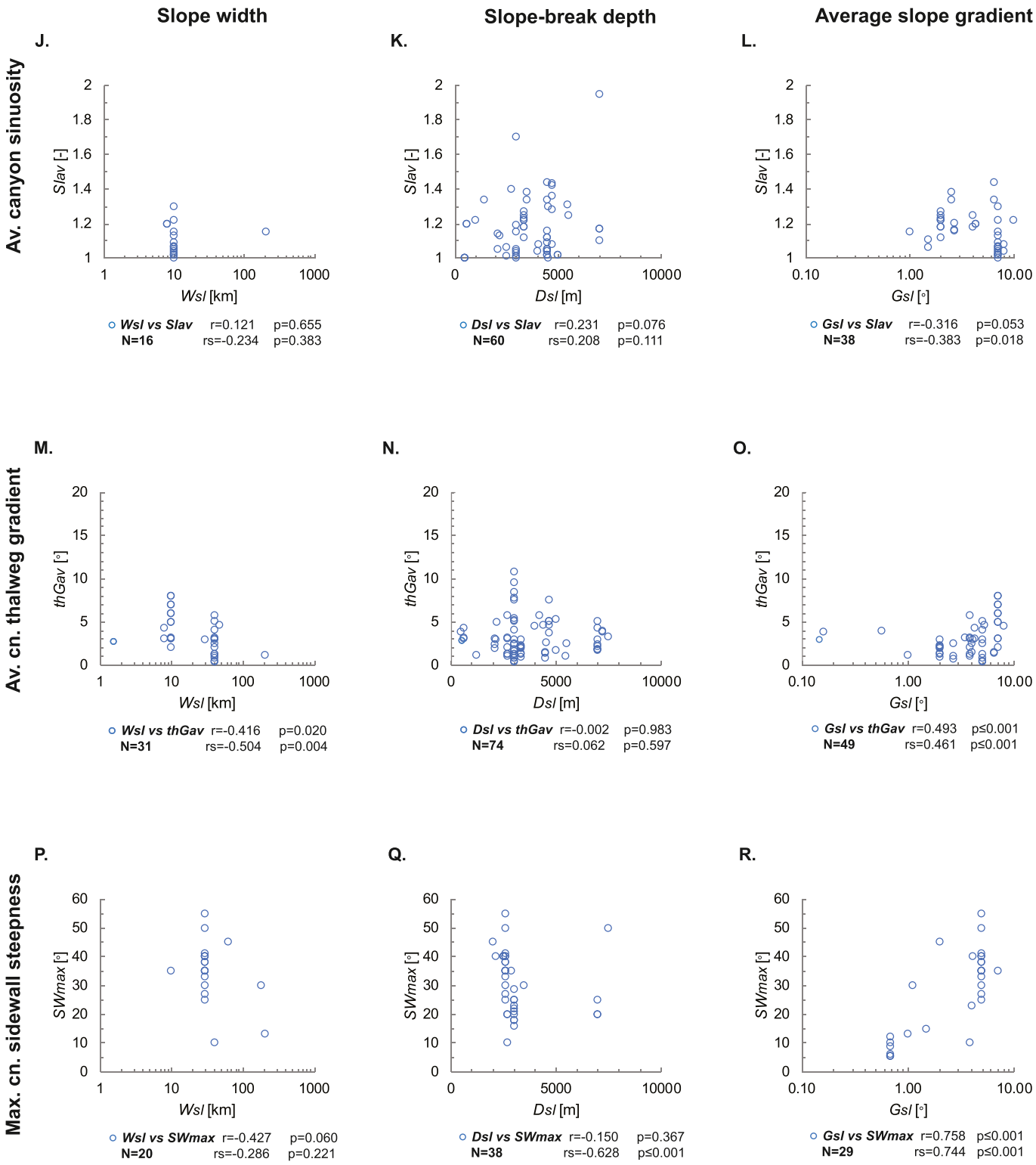

Fig. 15. (*continued*).

Moreover, the shelf topography can variably affect across-shelf sediment dispersal into submarine canyons: shelf uplift and deformation by tectonic activity (e.g. Johnson et al., 2017) and the presence of reefs (see section 4.2.3) can create seafloor topography and modify shelf gradients, which in turn can force sediment transport pathways through shelf valleys and submarine canyons incising the shelf. Currents, waves and flows carrying sediment might also be deflected away from canyons by intrashelf highs of variable origin.

The subaerial exposure of continental shelves at lowstand can lead to the amalgamation of river catchment areas as confluences are established; this might significantly enhance sediment supply to individual fluvial outlets, and in turn to canyons with sediment connectivity to these systems, especially for large fluvial systems that can arise as wide shelves are exposed (Blum et al., 2013). Additional sediment might be

conveyed to canyons from the local erosion of shelf substrate when rivers traverse the exposed shelf (e.g. Sweet et al., 2020).

Some of the scaling relationships between shelf configuration and canyon morphometrics may also be due to covariance with other related parameters. For example, scaling of canyon length with shelf-break depth might in part reflect how deeper shelves are associated with wider slopes, and how shelf-break depths tend to increase for terrestrial catchments associated with larger fluvial systems or multiple fluvial sources, greater average annual discharge and catchment size. However, scaling relationships between shelf-break depth and attributes of the terrestrial catchment are not significant.

During episodes of sea-level lowstand, such as during the LGM, canyons with their heads in vicinity of the shelf-edge could be fed by fluvial systems that had prograded onto the shelves (e.g. Sweet et al., 2020).

In sequence stratigraphic models, routing of significant volumes of sand-sized sediment across continental slopes to basin floors and the development of submarine fans is perceived to be most effective during relative sea-level lowstands (e.g. Posamentier et al., 1991), which would suggest that canyon evolution by down-canyon sediment gravity flows might also be enhanced during these intervals. Reconstructions and estimates for the eustatic fall during the LGM have been variably placed between ca. 120 m to 135 m bsl (e.g. Clark and Mix, 2002; Simms et al., 2019, and references therein), so that most shelves with shelf breaks shallower than 120 m bsl have likely been subaerially exposed during the LGM. Despite this, the studied canyons hosted on shelves with shelf breaks deeper than 120 m bsl tend to be larger, to be more sinuous, and to have lower canyon thalweg gradients than those with shelf breaks at 120 m or less. This indicates that sediment connection of canyons to rivers and littoral cells during phases of sea-level lowstands is not as important a control on canyon geomorphology compared to other controls. The findings might also indicate how deeper shelves tend to be associated with larger terrestrial catchments (Fig. 15; Wang et al., 2019).

The complex role of shelf physiography and across-shelf sediment transport, together with covariance in shelf and canyon characteristics in response to common controls on sediment dispersal, explain the limited value of shelf configuration as a predictor of canyon geomorphology.

6.3. Continental slope

6.3.1. Observations

The slope width exhibits strong and significant correlation with canyon length (Fig. 15a), and moderate significant correlations with maximum width (Fig. 15d), maximum depth (Fig. 15g) and the average canyon thalweg gradient (Fig. 15m).

The slope-break depth shows moderate scaling with maximum canyon depth (Fig. 15h) and maximum canyon sidewall steepness (Fig. 15q), and rather weak but statistically significant correlation with canyon length (Fig. 15b).

For the average slope gradient, moderate correlations are demonstrated with maximum canyon sidewall steepness (Fig. 15r) and average canyon thalweg gradient (Fig. 15o), whereas correlations with other parameters are weak and not significant (Fig. 15a-r).

6.3.2. Interpretations

The canyon length is the only canyon morphometric parameter that is related to the continental-slope width, as reflected in the strong scaling between these two variables and, to a smaller extent, in the relationship between canyon length and slope-break depth.

Positive relationships are seen for slope width with maximum canyon width and depth, and for the latter with slope-break depth; these relationships reflect how intra-canyon erosion is promoted at the canyon mouth (see section 5.2.2.2).

The positive relationship between slope-break depth and maximum canyon depth might also reflect how canyons in open seas tend to be deeper compared to canyons in semi-enclosed and enclosed seas (see section 7.4).

The results show that average canyon sinuosity is not correlated to the slope-break depth or to slope steepness. Additional data are needed to evaluate potential correlation between slope width and average canyon sinuosity.

The modest, positive correlation between the overall slope gradient and average canyon thalweg gradient relates to how the average canyon thalweg gradient is constrained by the average gradient of the continental slope; yet important variability is observed. In this study, as in previous ones (e.g. Harris and Whiteway, 2011), the overall canyon thalweg gradient is determined in part by the position of both canyon apex and mouth, which are themselves related to local seafloor relief. The observed moderate negative relationship between slope width and average canyon thalweg gradient reflects how wider slopes tend to display gentler gradients (Fig. 11; cf. Sømme et al., 2009).

The moderate, positive scaling seen between maximum canyon sidewall steepness and the average slope gradient may reflect how slopes that are steeper on average may be associated with increased erosion in submarine canyons, in relation to steeper slopes promoting processes of mass failure (e.g. McGregor, 1983; Susanth et al., 2021), and potentially driving retrograde slope failure (Lo Iacono et al., 2014), as well as vertical canyon incision (e.g. Susanth et al., 2021). Following this line of interpretation, the negative correlation of slope width with maximum canyon sidewall steepness might be a record of the covariance between average slope gradient and slope width. An inverse moderate relationship is seen between slope-break depth and maximum canyon sidewall steepness, but the dataset does not include slope-break depths between 4,000 and 6,000 m bsl and dominantly includes canyons associated with continental-slope breaks that are 2,000 to 4,000 m bsl. More data are needed to confirm this relationship.

The lack of correlation between the average slope gradient and maximum canyon dimensions indicate that the average slope gradient has no significant influence on canyon size, in spite of how it might affect the magnitude of retrograde erosion and the erosive strength of down-canyon sediment gravity flows. Also, the average slope gradient does not capture local relief along the slope profiles, which can control sediment bypass (e.g. Soutter et al., 2021); further investigation of the role of slope relief and slope profile types as controls on canyon geomorphology is required.

7. Variations in canyon morphometric parameters across classes of environments

Descriptive statistics of frequency distributions of canyon morphometric parameters have been evaluated for the entire dataset (Fig. 16 a-f), as well as for separate groups of canyons reflecting categories of canyon-apex location relative to the shelf-break, continental-margin type, source-to-sink setting, oceanographic environment, and latitudinal zones (sections 7.1 to 7.5). This was done to investigate whether and how factors associated with the environmental setting may control canyon geomorphology. Meaningful comparisons of average canyon width and depth as a function of S2S system setting and latitudinal zone, and for average canyon depth relative to canyon-head location, were not possible due to limited data availability.

In addition, ratios of maximum width to maximum depth across the different environmental settings have been assessed (section 7.6).

The distributions of each canyon morphometric parameter are graphically presented in form of boxplots (Figs. 16–22) and are discussed in sections 7.1 to 7.6 below.

7.1. Canyon-apex location relative to the shelf break

7.1.1. Observations

The studied shelf-incising canyons tend to be longer (Fig. 17a), more

A. Length

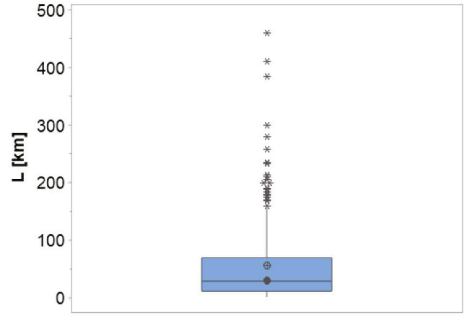

	N	min	mean	StDev	median	max
L	**263**	2.00	56.52	69.15	29.79	460.00

B. Width

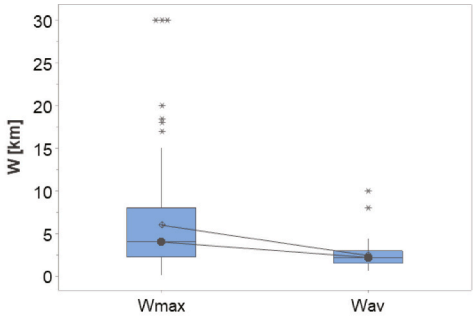

	N	min	mean	StDev	median	max
Wmax	**164**	0.15	5.97	5.43	4.00	30.00
Wav	**66**	0.58	2.41	1.50	2.18	10.00

C. Depth

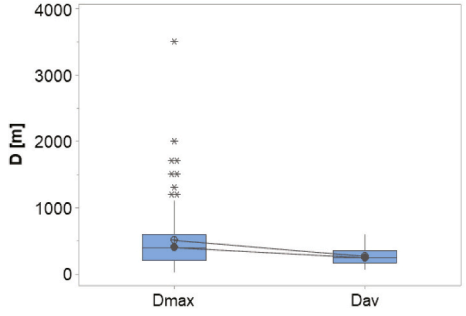

	N	min	mean	StDev	median	max
Dmax	**113**	35.00	508.00	475.10	400.00	3500.00
Dav	**52**	70.00	268.10	126.30	244.00	594.00

D. Average canyon sinuosity

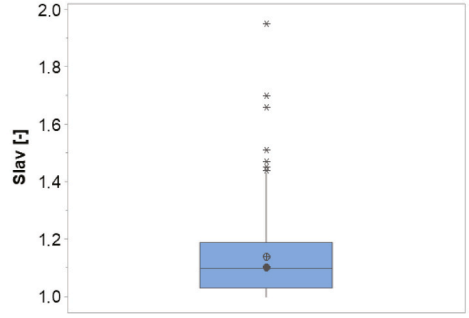

	N	min	mean	StDev	median	max
Slav	**151**	1.00	1.14	0.15	1.1	1.95

E. Average canyon thalweg gradient

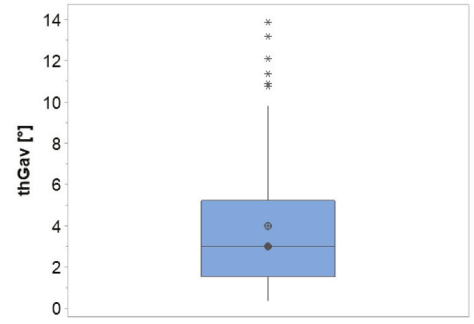

	N	min	mean	StDev	median	max
thGav	**120**	0.40	3.98	3.09	3.00	13.90

F. Maximum canyon sidewall steepness

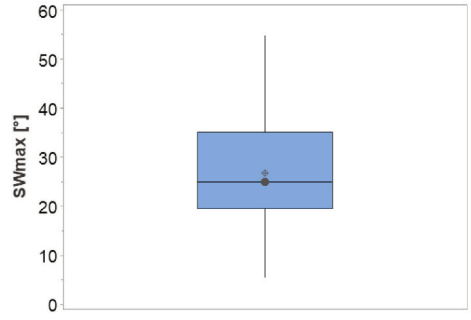

	N	min	mean	StDev	median	max
SWmax	**69**	5.40	26.80	11.48	25.00	55.00

Fig. 16. a-f: Boxplots of frequency distributions of the investigated canyon morphometric parameters. L = canyon length; W_{max} = maximum canyon width; W_{av} = average canyon width; D_{max} = maximum canyon depth; D_{av} = average canyon depth; SI_{av} = average canyon sinuosity index; thG_{av} = average canyon thalweg gradient; SW_{max} = maximum canyon sidewall steepness. N = number of readings; min = minimum value; mean = mean value; StDev = standard deviation; median = median value; max = maximum value.

sinuous (Fig. 17f), and with larger average widths (Fig. 17c) than slope-confined canyons, on average by factors of 2.25, 1.09 and 1.52, respectively. Across these two groups, these are the morphometric parameters whose mean values differ significantly; differences are also seen in maximum canyon depth that are associated with p values that are just above the defined threshold of statistical significance. Although canyons incising the shelf display on average slightly greater maximum and overall widths, slope-confined canyons reach the same values (Fig. 17b&c), and the largest value of average width is associated with a slope-confined canyon (Fig. 17c). Although greater maximum depths (Fig. 17d), and lower overall thalweg gradients (Fig. 17g) are seen in canyons incising the shelf, differences in their average values are not statistically significant. The data on average canyon depth are limited, but the results show very similar ranges in values across the two groups (Fig. 17e). On average, the maximum sidewall steepness is similar between groups of canyons classified on the location of the canyon apex relative to the shelf break, but slope-confined canyons display a greater range (Fig. 17h).

A. Length

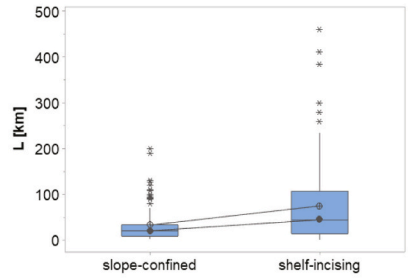

	N	min	mean	StDev	median	max
slope	**98**	3.70	33.37	39.32	21.00	200.00
shelf	**137**	2.00	75.13	84.69	45.00	460.00
T-Value =-4.53 DF = 230 P-Value ≤ 0.001						

B. Maximum width

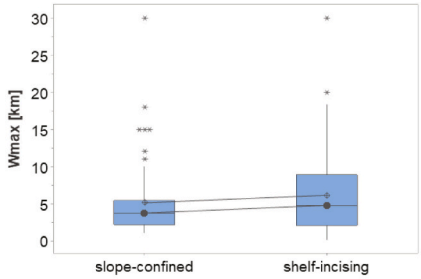

	N	min	mean	StDev	median	max
slope	**64**	1.00	5.12	4.96	3.74	30.00
shelf	**87**	0.15	6.14	5.32	4.79	30.00
T-Value =-0.44 DF = 148 P-Value = 0.658						

C. Average width

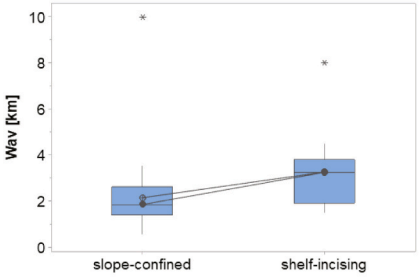

	N	min	mean	StDev	median	max
slope	**45**	0.58	2.15	1.41	1.85	10.00
shelf	**17**	1.51	3.26	1.58	3.25	8.00
T-Value =-3.42 DF = 31 P-Value = 0.002						

D. Maximum depth

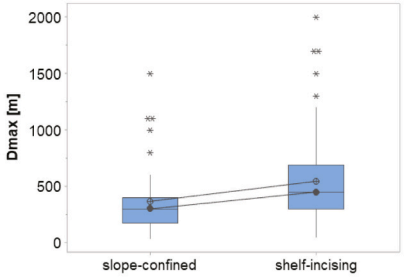

	N	min	mean	StDev	median	max
slope	**39**	35.00	367.30	322.10	300.00	1500.00
shelf	**65**	50.00	545.10	410.10	450.00	2000.00
T-Value =-2.45 DF = 80 P-Value = 0.016						

E. Average depth

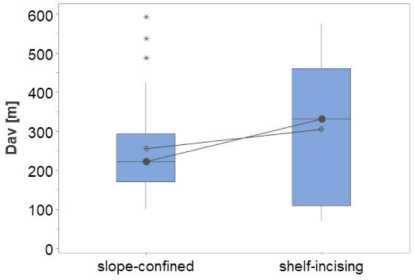

	N	min	mean	StDev	median	max
slope	**39**	100.00	255.30	115.70	222.00	594.00
shelf	**9**	70.00	304.90	183.40	331.00	576.00
T-Value =-0.17 DF = 9 P-Value = 0.868						

F. Average canyon sinuosity

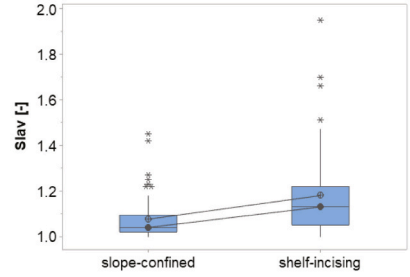

	N	min	mean	StDev	median	max
slope	**61**	1.00	1.08	0.09	1.04	1.45
shelf	**79**	1.00	1.18	0.17	1.13	1.95
T-Value =-4.70 DF = 131 P-Value ≤ 0.001						

G. Average canyon thalweg gradient

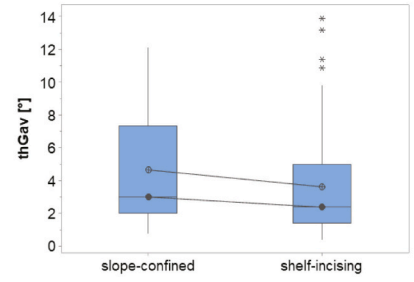

	N	min	mean	StDev	median	max
slope	**29**	0.78	4.65	3.29	3.00	12.10
shelf	**77**	0.40	3.62	3.14	2.37	13.90
T-Value = 1.73 DF = 51 P-Value = 0.090						

H. Maximum canyon sidewall steepness

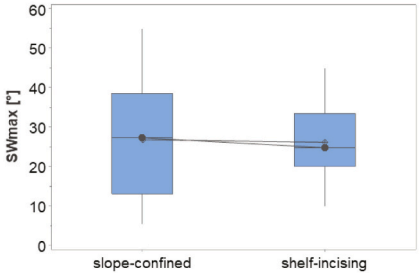

	N	min	mean	StDev	median	max
slope	**30**	5.40	26.82	13.92	27.30	55.00
shelf	**38**	10.00	26.18	8.68	24.80	45.00
T-Value = 0.22 DF = 46 P-Value = 0.825						

Fig. 17. a-j: Boxplots of frequency distributions of canyon morphometric parameters for studied canyons classified on the location of the canyon apex relative to the shelf break into slope-confined (N=99) and shelf-incising canyons (N=154). I.&J. Boxplots of canyon length (I) and average depth (J) and results of statistical analyses plotted from the dataset of Harris et al. (2014) for calibration. L = canyon length; W_{max} = maximum canyon width; W_{av} = average canyon width; D_{max} =

maximum canyon depth; D_{av} = average canyon depth; SI_{av} = average canyon sinuosity index; thG_{av} = average canyon thalweg gradient; SW_{max} = maximum canyon sidewall steepness. N = number of readings; min = minimum value; mean = mean value; StDev = standard deviation; median = median value; max = maximum value. Results of Two-Sample T-test: DF = degrees of freedom.

I. Length (Harris et al., 2014)

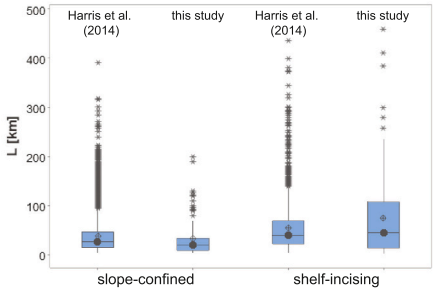

	N	min	mean	StDev	median	max
slope	**7401**	4.10	37.29	33.38	26.92	391.34
shelf	**2076**	3.84	54.82	50.27	39.76	436.33
T-Value =-18.16 DF = 3191 P-Value ≤ 0.001						

J. Average depth (Harris et al., 2014)

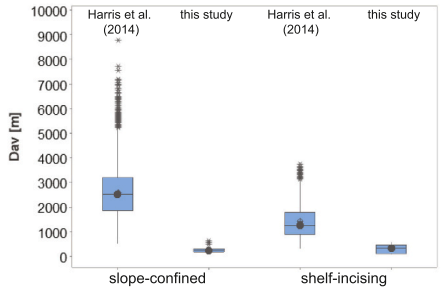

	N	min	mean	StDev	median	max
slope	**7401**	507.20	2563.50	978.40	2506.90	8770.30
shelf	**2076**	294.10	1395.00	657.60	1260.10	3746.00
T-Value =55.26 DF = 2972 P-Value ≤ 0.001						

Fig. 17. (*continued*).

For the canyons studied by Harris et al. (2014), statistical tests reveal significant differences in mean values of length (Fig. 17i) and average depth (Fig. 17j) across the two groups. As in the canyons considered in our study, shelf-incising canyons are on average longer than their slope-confined counterparts, by a factor of 1.47, which is lower than what found in our study (2.25). Harris and Whiteway (2011) also reported mean values of canyon length; studied shelf-incising canyons with and without a river connection were on average 2.07 and 1.29 times longer, respectively, than canyons with their apex below the shelf break.

7.1.2. Interpretations

The greater lengths of shelf-incising canyons may reflect how retrograde incision of the shelf and the promotion of canyon progradation by sediment gravity flows originating on the shelf and in the terrestrial catchment constitute primary controls on the length of submarine canyons. Sediment is supplied to the canyons via coupling with fluvial outlets or littoral cells and locally from within the shelf (sections 6.1 & 6.2). In addition, canyon heads placed above the storm wave-base can intercept sediment mobilised and transported during storm events (e.g. Sequeiros et al., 2019) (section 4.2.2). Our finding that shelf-incising canyons are on average longer than their slope-confined counterparts are in agreement with observations by Harris and Whiteway (2011) and Harris et al. (2014).

Harris et al. (2014) also show that shelf-incising canyons are on average twice as large in area compared to slope-confined canyons, whereas canyons of the latter group are on average almost twice as deep. However, for the canyons considered in this study, characteristics like the maximum width, maximum depth, average canyon thalweg gradient and maximum canyon sidewall steepness are not related to whether canyons are incised into the shelf. Thus, overall, the relative position of the canyon apex to the shelf break does not tie to these specific geomorphological characteristics. The results may however also reflect how some of the currently slope-confined canyons had a past connection to the shelf, now lost due to backfilling of their proximal parts (e.g. Pratson et al., 2007) and progradation of their heads (e.g., in relation to high sediment supply; cf. Mauffrey et al., 2015).

Slope-confined canyons can be fed by sands overpassing the shelf edge if their heads are in the range of the run-out distance of turbidity currents linked to fluvial discharge or littoral cells (e.g. Cronin et al., 2005; Yin et al., 2019). Canyons in high-latitude settings affected by glaciation can receive sediment delivered by the progradation of ice sheets onto shelf margins and from floating ice carrying debris (e.g. Gales et al., 2021). Sediment remobilised within the slope can also be distributed to a slope-confined canyon by contour currents if the canyon is coupled with a contourite system (e.g. Wang et al., 2018; Warratz et al., 2019; Serra et al., 2020; Rodrigues et al., 2022, and references therein).

Despite the role of sediment gravity flows in canyon growth and sinuosity increase, mean values of average canyon sinuosity are very similar across the two groups. This indicates that the importance of connections of the canyon to the shelf as a control on its sinuosity might be limited, in contrast with current understanding. Specifically, the process of canyon shelf-breaching, by enabling linkages with shelf and terrestrial sediment sources, has been suggested to lead to distinctively higher sinuosities in shelf-incising canyons compared to slope-confined ones (e.g. Farre et al., 1983; Orange et al., 1994; Wiles et al., 2019). On this basis, the sinuosity of canyons has been utilised to deduct canyon head location relative to the shelf-break on a regional scale in absence of sufficient bathymetric data coverage of proximal parts of canyons (see Wiles et al., 2019). Based on our analyses, it appears that the overall canyon sinuosity is not a suitable predictor of the position of the canyon apex relative to the shelf break.

More generally, considering the findings of this work in light of those of earlier studies (Harris and Whiteway, 2011; Harris et al., 2014; Huang et al., 2014), it is concluded that whether a canyon is incised in the shelf is not a strong predictor of canyon geomorphology overall. Further investigation is necessary to determine the degree to which the volume of a canyon delimited by its 3D surface is related to the relative position of the canyon head on a global scale.

7.2. Continental-margin type

7.2.1. Observations

Submarine canyons located along passive margins tend to be overall deeper (Fig. 18e), have steeper thalwegs (Fig. 18g) and greater maximum sidewall steepness (Fig. 18h), with statistically significant differences in mean values. Groups of canyons associated with active and passive margins exhibit frequency distributions of maximum canyon dimensions (Figs. 18a, b & d) and average canyon sinuosity (Fig. 18f) that are rather similar. Studied active-margin canyons are on average longer (Fig. 18a) and overall wider (Fig. 18c). Average values for maximum canyon width (Fig. 18b) and depth (Fig. 18d) are almost identical across continental-margin types, but canyons from active margins display greater ranges in both morphometric parameters.

On average, continental slopes associated with studied canyons along passive margins tend to be significantly steeper than those along

A. Length

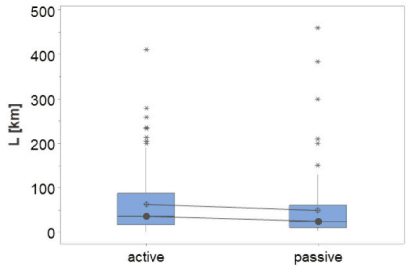

	N	min	mean	StDev	median	max
active	141	2.00	62.90	69.85	36.00	411.00
pass.	122	3.16	49.15	67.87	24.71	460.00
T-Value = 1.93 DF = 258 P-Value = 0.054						

B. Maximum width

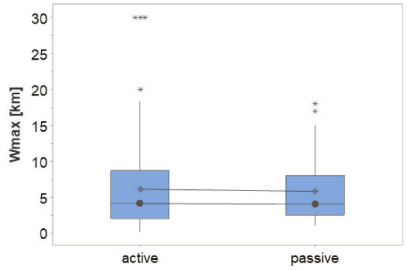

	N	min	mean	StDev	median	max
active	91	0.15	6.11	6.19	4.10	30.00
pass.	73	1.00	5.79	4.33	4.00	18.00
T-Value =-1.02 DF = 159 P-Value = 0.308						

C. Average width

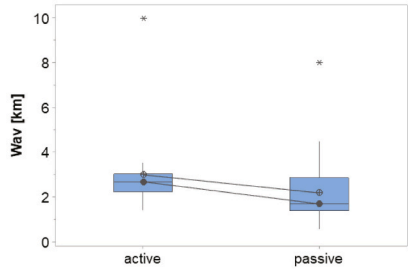

	N	min	mean	StDev	median	max
active	18	1.42	3.00	1.83	2.69	10.00
pass.	48	0.58	2.19	1.31	1.70	8.00
T-Value = 2.96 DF = 39 P-Value = 0.005						

D. Maximum depth

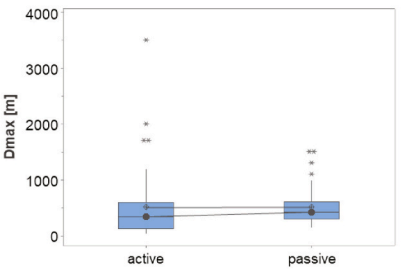

	N	min	mean	StDev	median	max
active	60	35.00	505.40	584.40	340.00	3500.00
pass.	53	150.00	511.00	314.10	422.60	1500.00
T-Value =-2.38 DF = 90 P-Value = 0.019						

E. Average depth

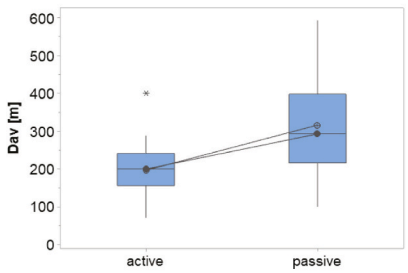

	N	min	mean	StDev	median	max
active	21	70.00	196.70	71.10	200.00	400.00
pass.	31	100.00	316.40	133.20	293.00	594.00
T-Value =-4.20 DF = 47 P-Value ≤ 0.001						

F. Average canyon sinuosity

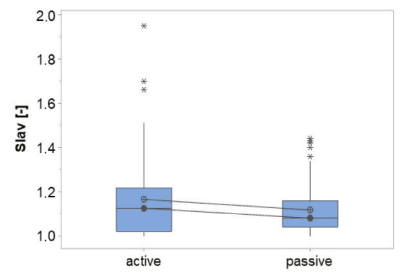

	N	min	mean	StDev	median	max
active	68	1.00	1.17	0.19	1.13	1.95
pass.	83	1.00	1.12	0.11	1.08	1.44
T-Value = 1.79 DF = 109 P-Value = 0.077						

G. Average canyon thalweg gradient

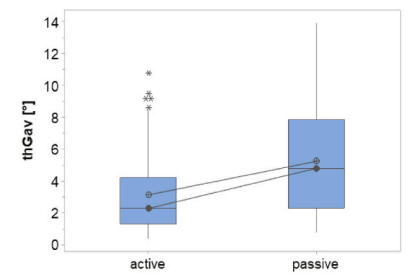

	N	min	mean	StDev	median	max
active	72	0.40	3.13	2.47	2.28	10.773
pass.	48	0.80	5.24	3.50	4.80	13.90
T-Value =-3.80 DF = 100 P-Value ≤ 0.001						

H. Maximum canyon sidewall steepness

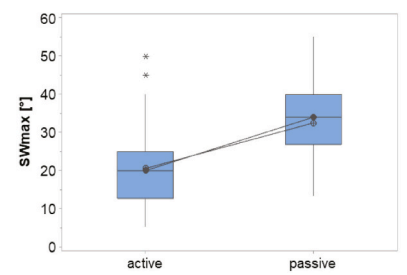

	N	min	mean	StDev	median	max
active	33	5.40	20.60	10.78	20.00	50.00
pass.	36	13.40	32.50	8.95	34.00	55.00
T-Value =-4.97 DF = 62 P-Value ≤ 0.001						

Fig. 18. a-h: Boxplots of frequency distributions of canyon morphometric parameters for studied canyons classified based on the continental-margin type into active-margin (N=153) and passive-margin canyons (N=129) (classification after Harris et al., 2014). See Fig. 17 for legend.

active margins (~3.22° vs. ~5.16°, respectively; Two-sample t-test: T-Value: -4.13 DF= 70 P-Value ≤0.001; N $_{active}$= 44; N $_{passive}$= 47).

7.2.2. Interpretations

The results suggest that the margin type is not a primary predictor of maximum canyon dimensions or canyon sinuosity. Studied canyons along passive margins tend to display larger average depths and steeper canyon thalweg gradients compared to their active-margin counterparts, which tend to have greater average widths. The varied influence of the continental-margin type on different aspects of canyon geomorphology can be explained as follows:

The seafloor relief, which influences sediment transport pathways, hydrodynamic processes and canyon geomorphology, can be sculpted by different processes, which are not limited to one particular continental-margin setting: faulting, although prominent in active-margin environments can also occur along passive margins (e.g. Osmundsen and Redfield, 2011); diapirism can be variably linked to processes acting in both margin types, such as mud and salt movements.

Another aspect to consider is that the physiography of continental margins can vary significantly in both tectonic settings. Although continental shelves along passive margins tend to be wider and with gentler lower-shelf gradients compared to those of active margins (e.g. Inman and Nordstrom, 1971; Blum and Hattier-Womack, 2009; Harris et al., 2014; Harris and Macmillan-Lawler, 2016; Nyberg et al., 2018), other shelf morphotypes exist. For example, shelves associated with passive margins can be as narrow as those associated with active margins (e.g. Harris and Macmillan-Lawler, 2016). The continental slopes of active margins are, on average, 1.28 times narrower (36 km) than those of passive margins (46 km); maximum widths are 368 km and 254 km, respectively (Harris et al., 2014). Given the strong relationship between slope width and canyon length (see section 6.3), similarity in the ranges and mean values of canyon length for the two margin types may be partly related to the limited difference in slope width between active and passive margins. By contrast, the steeper average thalweg gradients of passive-margin canyons likely reflect how the average canyon thalweg gradient is related to the overall slope gradient (cf. section 6.3), and that in the dataset overall gradients of continental slopes associated with canyons along passive margins tend to be higher compared to those along active ones. Considering the observed variability in relationships between aspects of catchment, shelf and slope configuration and canyon morphometric parameters (sections 6.2 & 6.3), contrasting characteristics in margin physiography are not evidently tied to particular geomorphologic characteristics in canyons.

The tendency of canyons from passive margins to have greater maximum sidewall steepness compared to canyons in active-margin settings might be explained by the effect of recurrent seismic activity on the stabilisation of seafloor substrate: although active margins are characterised by recurrent and high-magnitude seismic activity, the occurrence of submarine mass-transport processes can be subdued (e.g. Strozyk et al., 2010). The influence of background seismic activity on slope stability and mass-transport processes is variable and complex: seismic strengthening by recurrent earthquakes has been proposed as an effective mechanism leading to slope stabilisation and a decrease in both scale and occurrence of slope-failure processes (e.g. Strozyk et al., 2010; Nelson et al., 2011; Molenaar et al., 2019). Recurrent seismic activity can decrease the potential oversteepening of slopes by inducing a steady remobilisation and redistribution of slope deposits (Strozyk et al., 2010). However, at the same time the magnitude of earthquakes controls mass-failure processes, whereby higher-magnitude earthquakes tend to trigger larger-scale slope failures (e.g. Strozyk et al., 2010; Molenaar et al., 2019). Thus, slope failure may play a less important role in controlling canyon morphology on active margins compared to passive margins. Furthermore, earthquakes of small to high magnitudes do occur on passive margins (e.g. Stein et al., 1989; Wolin et al., 2012; Katz and Hamiel, 2018) and might act as a trigger of sediment remobilisation (e.g. Katz and Hamiel, 2018).

Our findings suggest that submarine-canyon geomorphology does not differ fundamentally between active and passive margins.

7.3. Source-to-sink system setting

7.3.1. Observations

Submarine canyons in continental and insular settings display similar frequency distributions of canyon morphometric parameters. Between the two groups, mean values only differ by a factor 1.08 or lower, except for the average canyon thalweg gradient, which is on average 1.17 times greater in continental-setting canyons. Frequency distributions of average canyon width and depth could not be evaluated due to lack of data for insular canyons (Fig. 19a-h).

For studied canyons with a sediment connection to one or several fluvial systems, the size of associated terrestrial catchments tends to be markedly greater in continental settings – on average by a factor of ~100 (341.842 km^2 compared to 3071 km^2; Two-sample t-test: T-Value= 4.04 DF= 29 P-Value≤0.001; N $_{continental}$= 31 and N $_{insular}$= 10). Whereas more data is needed to corroborate this finding, the results demonstrate that continental catchments display a great variability in size; studied catchments vary from 84 km^2 to 3,800,000 km^2. Insular shelves tend to be narrower and steeper than shelves offshore continental landmasses. The shelves of continental settings are on average 4.51 times wider than those of insular settings (108 km compared to 24 km; Two-sample t-test: T-Value=8.20 DF=56 P-Value≤0.001; N $_{continental}$= 166 and N $_{insular}$= 37). Mean overall shelf gradients of insular shelves at the canyon location are 1.8 times greater (0.756° compared to 0.420°; Two-sample t-test: T-Value=-3.21 DF= 33 P-Value= 0.003; N $_{continental}$= 96 and N $_{insular}$= 21).

7.3.2. Interpretations

The results indicate that the association of a submarine canyon with a continental landmass or an island is not reflected in important differences in canyon geomorphology, with the caveat that relationships between S2S system setting and average canyon dimensions remain to be assessed. The similarity in frequency distributions and mean values for individual canyon morphometric parameters across the two groups might reflect how controlling factors are not significantly impacted by the S2S system setting, but also that different controls can generate similar geomorphologic characteristics in canyons across different S2S system settings.

The inherently limited extent of the terrestrial catchment in insular S2S systems compared to continental S2S systems does not appear to be a major factor for submarine canyon geomorphology. In part, this may be linked to the variability of the scale of islands, with large islands having potentially sizable catchments, and smaller catchments also occurring on continental landmasses.

For canyons associated with volcanic islands (97% of the investigated insular canyons in the study), volcanic activity may be the dominant source of sediment (e.g. Aiello et al., 2020). In such case, uplift and denudation rates are of lesser importance as controlling factors on sediment fluxes to canyons.

In addition, findings from the regional canyon study by Smith et al. (2017) indicate that the prevalence of igneous bedrock lithology in terrestrial source areas might inhibit canyon formation. In volcanic rocks, weathered clay minerals might enhance seafloor cohesion, whereas the lack of mud in plutonic bedrock might inhibit the development of turbidity currents (Smith et al., 2017, and references therein). Hence, the transitioning of hyperpycnal flows (e.g. Zhao et al., 2018), dilute surface river plumes (e.g. Hizzet et al., 2018) and submarine mass failures (e.g. Puig et al., 2014) into turbidity currents might constitute a subordinate evolutionary process in canyons located in front of islands of a volcanic origin. On the other hand, the tendency of volcanic islands to experience slope failures along their flanks (e.g. Le Bas et al., 2007; Chang et al., 2021) and shelf margins (e.g. Quartau et al., 2015) can supply sediment to a canyon by both individual large-scale failures (e.g.

A. Length

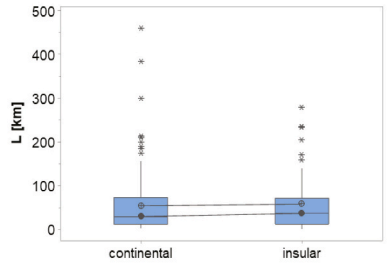

	N	min	mean	StDev	median	max
cont.	177	2.70	54.07	65.22	29.62	460.00
insular	50	2.00	58.36	67.80	37.28	279.67
T-Value = 0.01 DF = 72 P-Value = 0.992						

B. Maximum width

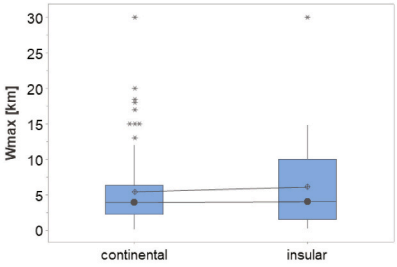

	N	min	mean	StDev	median	max
cont.	101	0.15	5.41	4.89	3.91	30.00
insular	36	0.25	6.06	6.08	4.00	30.00
T-Value = 0.31 DF = 50 P-Value = 0.758						

C. Average width

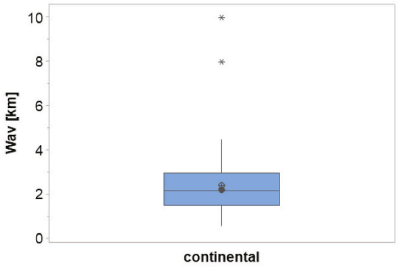

	N	min	mean	StDev	median	max
cont.	66	0.58	2.41	1.50	2.18	10.00
insular	0	***	***	***	***	***
T-Value =*** DF =*** P-Value =***						

D. Maximum depth

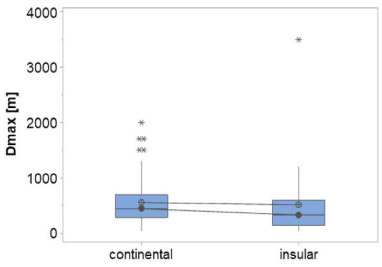

	N	min	mean	StDev	median	max
cont.	60	50.00	553.70	426.40	442.50	2000.00
insular	29	50.00	511.00	648.00	330.00	3500.00
T-Value = 1.39 DF = 43 P-Value = 0.173						

E. Average depth

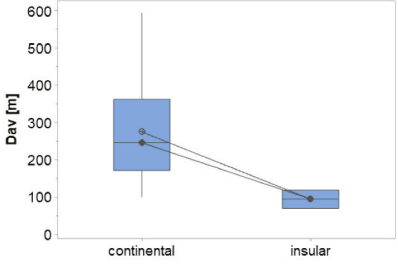

	N	min	mean	StDev	median	max
cont.	50	100.00	275.00	123.70	246.00	594.00
insular	2	70.00	95.00	35.40	95.00	120.00
T-Value =*** DF =*** P-Value =***						

F. Average canyon sinuosity

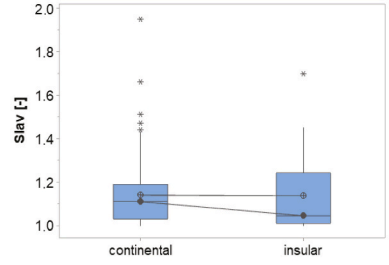

	N	min	mean	StDev	median	max
cont.	129	1.00	1.14	0.15	1.11	1.95
insular	20	1.00	1.14	0.19	1.05	1.70
T-Value = 0.20 DF = 22 P-Value = 0.846						

G. Average canyon thalweg gradient

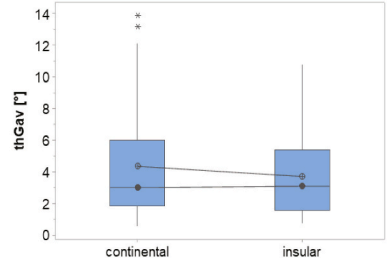

	N	min	mean	StDev	median	max
cont.	77	0.60	4.35	3.31	3.00	13.90
insular	31	0.78	3.71	2.76	3.09	10.77
T-Value = 0.83 DF = 58 P-Value = 0.408						

H. Maximum canyon sidewall steepness

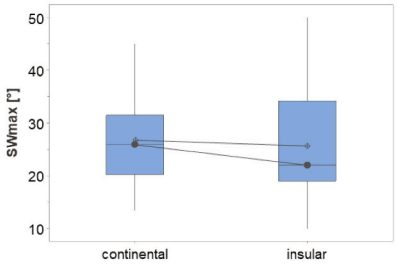

	N	min	mean	StDev	median	max
cont.	28	13.40	26.75	7.96	25.90	45.00
insular	17	10.00	25.67	10.65	22.00	50.00
T-Value = 0.66 DF = 27 P-Value = 0.517						

Fig. 19. a-h: Boxplots of frequency distributions of canyon morphometric parameters for studied canyons classified based on the source-to-sink setting into continental-margin (N=189) and insular canyons (N=57). *** denotes data paucity. See Fig. 17 for legend.

Le Bas et al., 2007) and high-frequency smaller failures (e.g. Chang et al., 2021). The importance of volcanic activity as a trigger for submarine slope failures, however, might be subordinate where other factors prevail, as storm events and onshore failure (Clare et al., 2018). Additionally, sediment transported by oceanic currents can represent a sustained source of sediment to insular canyons, independently of their origin.

Narrow and steep insular shelves promote sediment dispersal to the shelf margin, increased shear stress of sediment gravity flows, and shelfal sediment remobilisation (e.g. Hale et al., 2012; Babonneau et al., 2013). These factors may facilitate canyon activity, countering the effects of the reduced size of terrestrial catchments and limited seafloor erodibility.

7.4. Oceanographic environment

7.4.1. Observations

Distributions of canyon length (Fig. 20a), maximum width (Fig. 20b), average sinuosity (Fig. 20f) and average thalweg gradient (Fig. 20g) for open-sea canyons and canyons from semi-enclosed or enclosed seas are similar: apart from the thalweg gradient, the mean values of these parameters do not differ to a statistically significant level across the two groups. The average canyon width is greater for canyons located in semi-enclosed and enclosed seas compared to those in open seas, but this observation is based on a small dataset (Fig. 20c); conversely, the average depth of open-sea canyons is higher. The differences in mean values of average canyon depth and width across the two groups are only statistically significant for the former. In contrast, marked differences in distributions of maximum canyon depth are seen across the two groups: on average, the maximum canyon depth is 1.91 times higher in open-sea canyons (Fig. 20d). Open-sea canyons also tend to have steeper sidewalls than canyons from semi-enclosed and enclosed seas, by a factor of 1.73 on average (Fig. 20h). These differences are statistically significant.

Continental slopes located in open-sea settings have on average greater slope-break depths than continental slopes associated with semi-enclosed and enclosed seas (3959 m compared to 3072 m, respectively; T-Value=3.92 DF=98 P-Value$\leq$0.001; $N_{\text{open sea}} = 85$; $N_{\text{se\&e seas}} = 70$).

7.4.2. Interpretations

The results suggest that conditions associated with the oceanographic environment may exert an influence on maximum canyon depth, the average canyon gradient and the steepness of canyon margins, but not on canyon length, maximum width and overall sinuosity.

Fundamental differences between the two environments lie in the scale of the water body, in its degree of confinement, and in the presence of thermohaline circulation and major oceanic currents in oceans (e.g. Rahmstorf, 2006; Faugères and Mulder, 2011). In contrast, upwelling and internal waves can affect canyons in both open-oceanic (e.g. Hickey, 1997; Smith et al., 2018) and semi-enclosed seas (e.g. Flexas et al., 2008; Li et al., 2022). Our findings might indicate that controlling factors that predominantly affect canyon geomorphology by acting along directions that are transverse to the canyon axis, like slope-parallel currents and lateral slope failures, might have a greater impact on canyon geomorphology in open seas. Oceanic currents might transport greater volumes of sand-sized sediment due to their greater extent and great depth range (e.g. Faugères and Mulder, 2011) compared to those in semi-enclosed and enclosed seas, which can be deposited onto intra-canyon ridges and canyon margins thereby increasing canyon depths and steepening canyon sidewalls by aggradation. Oversteepened margins are in turn more prone to collapse, which can lead to steeper margins over the affected area of the canyon.

The greater sidewall steepness of open-sea canyons might also reflect how the studied high-latitude (sections 5.3 & 7.5) and passive-margin canyons (section 7.2), which tend to have steeper margins, are dominantly located in open-sea settings.

It must be recognised, additionally, that the findings may emerge not because of causal relationships with processes associated with the oceanographic environment, but merely because of positive scaling between canyon depth and sidewall steepness (section 4).

7.5. Latitudinal zones

Variations in canyon morphometric parameters are evaluated for latitudinal belts assigned to tropical (0-23.5°), temperate (23.5°-66.5°), and polar (>66.5°) zones. The dataset contains fewer data from canyons from polar latitudes compared to canyons in tropical and temperate zones; this reflects the paucity of investigations of high-latitude submarine canyons, despite the large number of canyons in the Arctic and Antarctic regions (see Harris and Whiteway, 2011; Harris et al., 2014). The arctic canyons in this study are from only two regions: the NW Norwegian margin (N=15) and the Barrow Canyon from the N Alaskan margin. Thus, the representativeness of the data is likely to be limited. Because of this geographic bias, differences in mean values of canyon morphometric parameters from tropical and temperate latitudes have been tested separately.

7.5.1. Observations

Results of one-way ANOVA for canyons grouped by latitude range show statistically significant differences in mean values of length (Fig. 21a), maximum canyon width (Fig. 21b) and maximum canyon sidewall steepness (Fig. 21h), but not for maximum canyon depth (Fig. 21d).

Based on two-sample t-tests, statistically significant differences are seen for mean values of length (Fig. 21a) and average canyon sinuosity (Fig. 21f) between canyons of tropical and temperate latitudes. The difference in mean values of average canyon thalweg gradient is associated with a p value that is just above the threshold of statistical significance (Fig. 21g).

7.5.2. Interpretations

The observed significant differences in canyon morphometrics may represent a record of latitude-related controls on aspects of canyon geomorphology. Considering the relationship between continental-slope gradient and average canyon thalweg gradient (section 6.3.2), the typically steeper thalwegs of tropical canyons, compared to temperate ones, might be related to the known latitudinal control on carbonate distribution to deep-marine environments (see Figure 3 of O'Mara and Dunne, 2019), in light of how carbonate can act to stabilise the slope substrate by binding and cementation (e.g. Adams and Kenter, 2013, and references therein).

Based on the results of the statistical analyses, submarine canyons do not vary markedly across tropical and temperate latitudinal zones with regards to their maximum width and depth, maximum sidewall steepness, or average sinuosity. Limited latitudinal variations in canyon sinuosity are also documented in the geographic regions examined by Harris and Whiteway (2011).

In contrast, both oversteepening of canyon margins related to high and dispersed sediment supply from glaciated margins (e.g. Martinsen, 2005; Armitage et al., 2010; Gales et al., 2021) and gravitational slope failure from ice loading (Mulder and Moran, 1995) may cause canyon sidewalls to be steeper in high-latitude settings compared to low- and mid-latitude ones. Yet any such inference has to be viewed with caution (see section 5.3 for a more detailed discussion).

7.6. Width-to-depth ratios

To investigate potential relationships between the ratio between maximum canyon width to maximum canyon depth (wd_{max}) and environmental factors, 100 submarine canyons of the study for which both maximum width and depth values have been obtained have been considered; aspect ratios have been evaluated for canyons across classes

A. Length

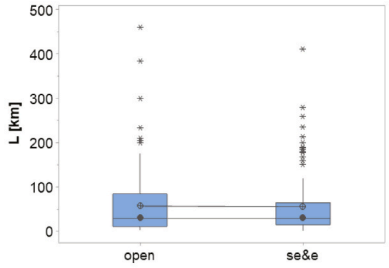

	N	min	mean	StDev	median	max
open	146	2.70	57.10	70.36	29.85	460.00
se&e	117	2.00	55.80	67.91	29.79	411.00
T-Value =-0.23 DF = 253 P-Value = 0.816						

B. Maximum width

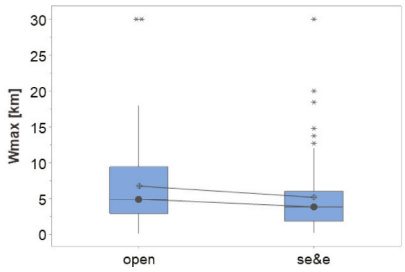

	N	min	mean	StDev	median	max
open	84	0.15	6.73	5.72	4.92	30.00
se&e	80	0.25	5.16	5.02	3.83	30.00
T-Value = 2.34 DF = 159 P-Value = 0.020						

C. Average width

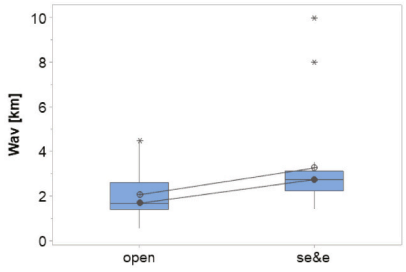

	N	min	mean	StDev	median	max
open	47	0.58	2.06	1.00	1.68	4.48
se&e	19	1.42	3.26	2.12	2.74	10
T-Value =-3.50 DF = 34 P-Value =0.001						

D. Maximum depth

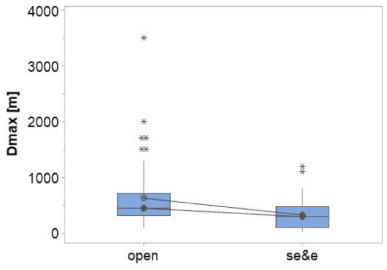

	N	min	mean	StDev	median	max
open	68	100.00	627.50	540.70	450.00	3500.00
se&e	45	35.00	327.40	271.90	297.00	1200.00
T-Value = 4.74 DF = 74 P-Value ≤ 0.001						

E. Average depth

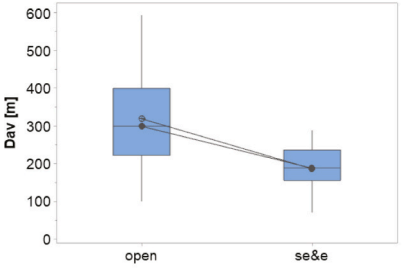

	N	min	mean	StDev	median	max
open	32	100.00	319.00	131.90	299.00	594.00
se&e	20	70.00	186.50	55.20	188.00	289.00
T-Value = 5.03 DF = 45 P-Value ≤ 0.001						

F. Average canyon sinuosity

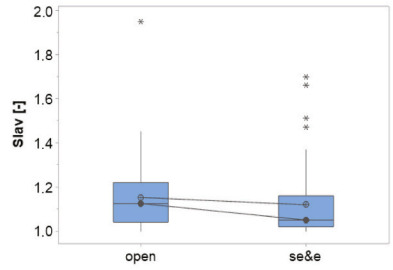

	N	min	mean	StDev	median	max
open	88	1.00	1.15	0.15	1.13	1.95
se&e	63	1.00	1.12	0.15	1.05	1.70
T-Value = 1.49 DF = 133 P-Value = 0.139						

G. Average canyon thalweg gradient

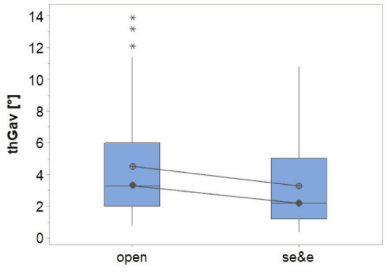

	N	min	mean	StDev	median	max
open	67	0.80	4.53	3.22	3.30	13.90
se&e	53	0.40	3.28	2.79	2.19	10.77
T-Value = 2.95 DF = 99 P-Value = 0.004						

H. Maximum canyon sidewall steepness

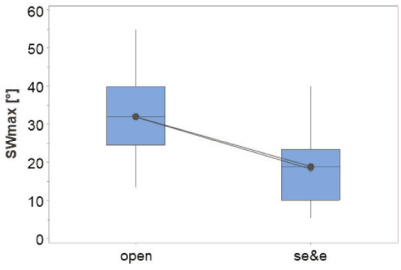

	N	min	mean	StDev	median	max
open	43	13.40	31.93	9.59	32.00	55.00
se&e	26	5.40	18.32	9.17	19.00	40.00
T-Value = 5.87 DF = 54 P-Value ≤ 0.001						

Fig. 20. a-h: Boxplots of frequency distributions of canyon morphometric parameters for studied canyons classified based on the oceanographic environment into canyons associated with open seas (N=162) and semi-enclosed and enclosed seas (N=120). See Fig. 17 for legend.

A. Length

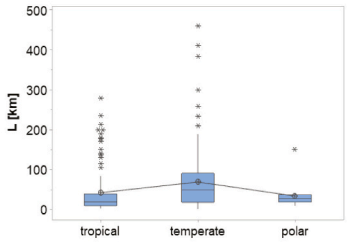

	N	min	mean	StDev	median	max
tropical	108	3.16	42.48	59.48	19.57	279.67
temper.	139	2.00	69.99	76.34	50.93	460.00
polar	16	10.00	34.31	32.30	28.00	150.00
F-Value = 9.62	DF1 = 2 DF2 =53.2955				P-Value ≤ 0.001	
T-Value*=-4.39	DF = 234				P-Value ≤ 0.001	

B. Maximum width

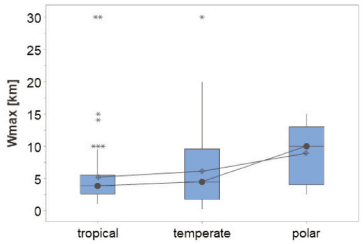

	N	min	mean	StDev	median	max
tropical	70	1.00	5.19	5.12	3.85	30.00
temper.	79	0.15	6.09	5.70	4.49	30.00
polar	15	2.50	8.90	4.61	10.00	15.00
F-Value = 6.86	DF1 = 2 DF2 = 43.3839				P-Value = 0.003	
T-Value*=0.42	DF = 132				P-Value = 0.675	

C. Average width

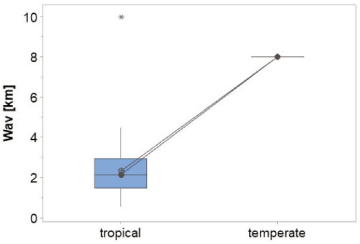

	N	min	mean	StDev	median	max
tropical	65	0.58	2.32	1.339	2.14	10.00
temper.	1	8.00	8.00	***	8.00	8.00
polar	0	***	***	***	***	***
F-Value = ***	DF1 = *** DF2 = ***				P-Value = ***	
T-Value*= ***	DF = ***				P-Value = ***	

D. Maximum depth

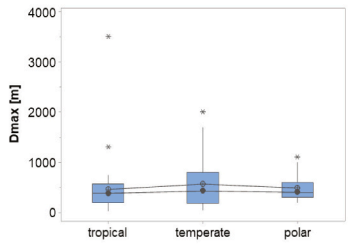

	N	min	mean	StDev	median	max
tropical	49	35.00	458.30	504.20	380.40	3500.00
temper.	49	50.00	564.20	494.60	425.00	2000.00
polar	15	200.00	486.70	274.20	400.00	1100.00
F-Value = 1.14	DF1 = 2 DF2 = 53.2580				P-Value = 0.328	
T-Value*=-0.65	DF = 93				P-Value = 0.518	

E. Average depth

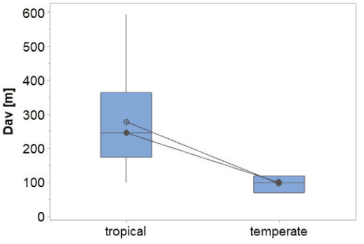

	N	min	mean	StDev	median	max
tropical	49	100.00	278.60	122.30	246.00	594.00
temper.	3	70.00	96.70	25.20	100.00	120.00
polar	0	***	***	***	***	***
F-Value = ***	DF1 = *** DF2 = ***				P-Value = ***	
T-Value*= ***	DF = ***				P-Value = ***	

F. Average canyon sinuosity

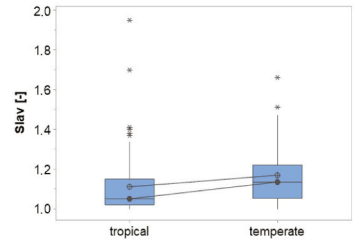

	N	min	mean	StDev	median	max
tropical	79	1.00	1.11	0.16	1.05	1.95
temper.	72	1.00	1.17	0.1395	1.14	1.66
polar	0	***	***	***	***	***
F-Value = ***	DF1 = *** DF2 = ***				P-Value = ***	
T-Value*=-2.77	DF = 148				P-Value = 0.006	

G. Average canyon thalweg gradient

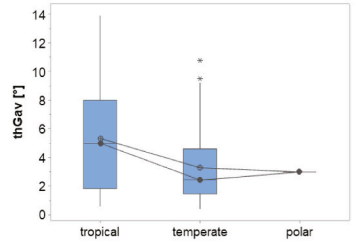

	N	min	mean	StDev	median	max
tropical	41	0.60	5.33	3.78	5.00	13.90
temper.	78	0.40	3.28	2.42	2.42	10.77
polar	1	2.98	2.98	***	2.98	2.98
F-Value = ***	DF1 = *** DF2 = ***				P-Value = ***	
T-Value*= 2.61	DF = 69				P-Value = 0.011	

H. Maximum canyon sidewall steepness

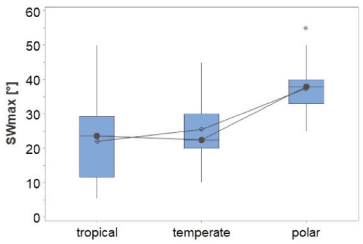

	N	min	mean	StDev	median	max
tropical	26	5.40	22.06	12.02	23.60	50.00
temper.	28	10.00	25.50	8.94	22.50	45.00
polar	15	25.00	37.47	7.82	38.00	55.00
F-Value =19.48	DF1 = 2 DF2 = 42.4993				P-Value ≤ 0.001	
T-Value*=-1.84	DF = 37				P-Value = 0.074	

Fig. 21. a-h: Boxplots of frequency distributions of canyon morphometric parameters for studied canyons classified based on latitudinal zones into tropical (N=117), temperate (N=149) and polar canyons (N=16). * indicates that two-sample-t-tests have been conducted for canyons in tropical versus temperate latitudinal zones. N = number of readings; min = minimum value; mean = mean value; StDev = standard deviation; median = median value; max = maximum value. Results of Welch's ANOVA test: DF 1 = degrees of freedom numerator; DF 2 = degrees of freedom denominator. Results of Two-Sample T-test: DF = degrees of freedom; *** denotes data paucity.

of environments (Fig. 22a-f).

7.6.1. Observations

Although wd_{max} ratios for the studied canyons vary over a broad range (2.45 to 73.33), mean and median values of wd_{max} ratios are in the order of magnitude of 10^1 both for the whole dataset as well as for canyons grouped according to environmental factors. Mean values range between 11 and 20, and only differ significantly from each other for canyons in open seas versus semi-enclosed and enclosed seas (Fig. 22e). For canyons grouped into tropical, temperate and polar latitudinal zones, the difference in mean values yields a p-value of 0.011 (Fig. 22f).

7.6.2. Interpretations

The narrow range in mean and median wd_{max} ratios and the lack of significant differences in mean values for the majority of canyon environmental classes indicate that maximum width-to-maximum depth ratios in canyons are of limited diagnostic value for inferring the environmental settings. This might reflect that width-to-depth ratios in canyons are not particularly sensitive to environmental controls and that they may inherently scale with processes that control canyon geomorphology globally. This would imply that width-to-depth ratios in submarine canyons are predominantly controlled by canyon self-organisation and autogenic processes, from the interplay of canyon-floor and margin aggradation and wall failure with intra-canyon sediment gravity flows, as suggested for submarine channels by Shumaker et al. (2018).

The inferred influence of the oceanographic environment on canyon width-to-depth ratios might reflect the way in which both erosional and depositional processes that operate along canyon margins are more strongly affected by the hydrodynamic regime in open seas than semi-enclosed and enclosed ones (see discussion in section 7.4).

8. Summary and conclusions

To increase understanding of the factors that exert control on canyon geomorphology and their relative importance on a global scale, statistical analyses were conducted to evaluate relationships between canyon morphometric parameters, and between these and attributes describing the physiographic setting of the canyon, including characteristics of elements of the source-to-sink (S2S) system (catchment, shelf and slope), the bathymetric setting of the canyon and its distance to the shoreline, the canyon-apex location relative to the shelf-break, the continental-margin type, the oceanographic environment, and the latitude of the canyon apex. In addition, selected morphometric parameters describing submarine canyons have been quantitatively characterised, both on a global scale and for different environmental settings (canyon-apex location relative to the shelf-break, continental-margin type, source-to-sink system setting, oceanographic environment and climate zones). Certain forms of scaling in attributes of canyon geomorphology are recognisable on a global scale and across different environmental settings and source-to-sink system configurations (Fig. 23a&b and Fig. 24a&b).

Key findings of the study are as follows:

(1) Scaling relationships between canyon morphometric attributes tend to be weak, due to the varied influence of environmental allogenic controls and autogenic processes influencing canyon geomorphology. Nevertheless, despite specific regional or local conditions, some scaling relationships between canyon morphometric attributes are more likely recognisable on a global scale than others; these include, for example, scaling between maximum canyon dimensions, or between maximum sidewall steepness and maximum canyon width and depth.

(2) The tendency of canyons to have greater maximum widths and depths with increasing canyon-mouth seafloor depth, the overall weakness in scaling of canyon morphometry with the terrestrial catchment and continental shelf, and the steeper canyon walls seen in canyons associated with open-sea settings compared to canyons in semi-enclosed or enclosed seas, possibly reflect how hydrodynamic processes such as upwelling, longshore drifts and along-slope currents influence canyon geomorphology.

(3) Canyon morphometric parameters may reflect the interplay of different environmental factors. Hence, controls on canyon geomorphology cannot be described by generic models linking geomorphological characteristics to individual environmental parameters. Potential controls on certain canyon morphometric parameters include: the location of the canyon head relative to the shelf break, the continental-margin type, the oceanographic environment, the absolute latitude of the canyon apex, and the depth of the associated shelf break. Data on canyon length, sinuosity, thalweg gradient and maximum sidewall steepness indicate that these morphometric aspects are likely influenced by several environmental controls.

Key findings regarding relationships between the environmental setting and canyon geomorphology include:

(i) Maximum canyon dimensions and overall canyon sinuosity cannot be used to predict the position of the canyon apex relative to the shelf break and vice versa; this challenges concepts linking higher overall sinuosities in canyons to incision of the canyon into the shelf (e.g. Farre et al., 1983; Jobe et al., 2011; Wiles et al., 2019).

(ii) The tendency of passive-margin canyons to develop steeper sidewalls compared to those of active-margin canyons indicates that slope failure might be generally less important for canyons from active margins compared to passive-margin ones, perhaps due to recurrent seismic strengthening of the seafloor substrate, which might act to inhibit mass failures, with the exception of mass failures triggered by high-magnitude earthquakes (e.g. Strozyk et al., 2010; Molenaar et al., 2019).

(iii) Whether a submarine canyon is associated with a continental or insular setting does not exert control on overall canyon geomorphology. Volcanic sediment sources and narrow and steep insular shelves might compensate for the impact of smaller associated terrestrial catchments on sediment supply to submarine canyons, and for the potential effect igneous bedrock lithology might have on canyon evolution along volcanic islands by affecting seafloor erodibility and the erosive strengths of flows (Smith et al., 2017, and references therein).

(iv) The complex interrelationships between climate-controlled processes are reflected in the weakness of linear and monotonic scaling of latitude with canyon morphometrics and can explain why the latitudinal position of a canyon is not a reliable indicator of overall canyon geomorphology in canyons in tropical and temperate latitudes. The complex role of climate influence on sediment sourcing and dispersal along glaciated continental margins, paired with the effect of ice loading on triggering of mass failures, might explain the observed steeper margins of submarine canyons from higher latitudes. However, in view of geographic bias and the limited sample size, it is possible that the results reflect how the studied higher-latitude canyons are coincidentally associated with passive-margin and open-sea settings, which tend to be associated with distinct distributions in sidewall steepness.

(v) Mean values of maximum width-to-maximum depth ratios in canyons are consistently in the order of magnitude of 10^1 for all investigated canyon classes – regardless of canyon-head location relative to the shelf break, the tectonic-margin type, the S2S setting, the oceanographic environment and the latitudinal zone – albeit with significant global variability in documented values. This might reflect how width-to-depth ratios in submarine

A. Dataset

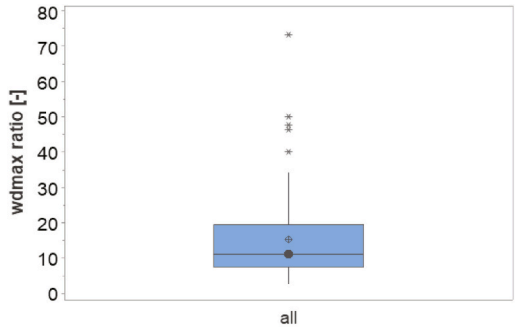

	N	min	mean	StDev	median	max
all	**100**	2.45	15.25	11.62	11.09	73.33

B. Canyon-apex location

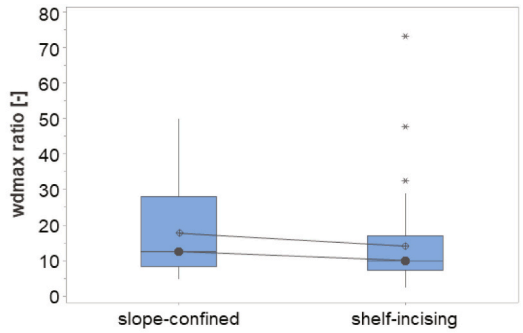

	N	min	mean	StDev	median	max
slope	**37**	4.65	17.67	12.37	12.50	50.00
shelf	**55**	2.45	14.05	11.59	10.00	73.33
T-Value = 1.57			**DF = 73**			**P-Value = 0.120**

C. Continental-margin type

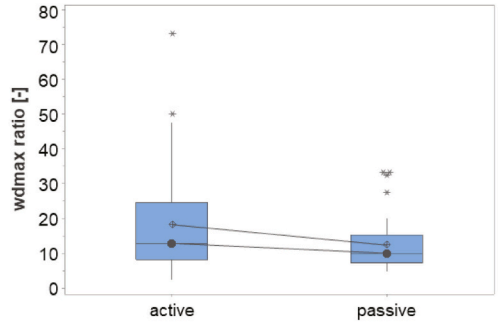

	N	min	mean	StDev	median	max
active	**50**	2.45	18.20	14.31	12.83	73.33
pass.	**50**	4.65	12.30	7.07	10.00	33.33
T-Value = 2.02			**DF = 84**			**P-Value = 0.046**

D. Source-to-sink setting

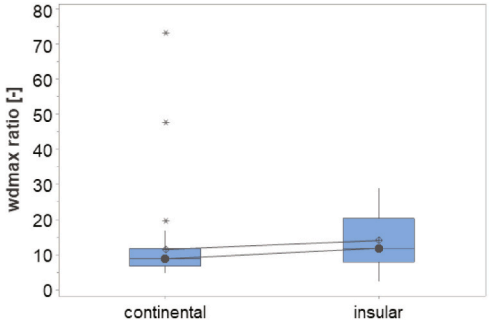

	N	min	mean	StDev	median	max
cont.	**48**	4.65	11.45	11.16	8.78	73.33
insular	**29**	2.45	14.00	7.64	11.82	28.86
T-Value =-1.59			**DF = 50**			**P-Value = 0.119**

E. Oceanographic environment

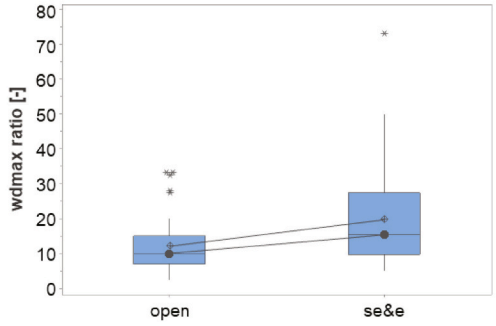

	N	min	mean	StDev	median	max
open	**58**	2.45	12.06	7.19	10.00	33.33
se&e	**42**	5.00	19.66	14.82	15.33	73.33
T-Value =-3.06			**DF = 73**			**P-Value = 0.003**

F. Latitudinal zones

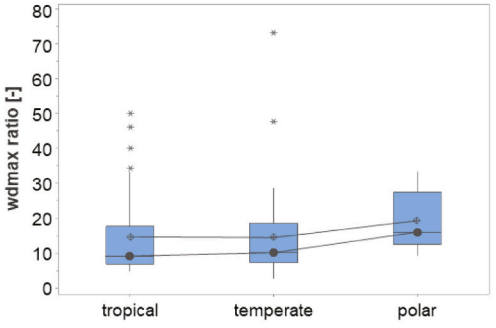

	N	min	mean	StDev	median	max
tropic.	**44**	4.65	14.65	11.45	9.12	50.00
temp.	**41**	2.45	14.43	12.67	10.10	73.33
polar	**15**	9.09	19.27	8.53	16.00	33.33
F-Value = 4.96		**DF1 = 2 DF2 = 46.7627**				**P-Value = 0.011**
T-Value*= 0.21		**DF = 81**				**P-Value = 0.836**

Fig. 22. a-f: Boxplots of frequency distributions of maximum-width-to-maximum-depth (wd_{max}) ratios in studied canyons A. for the dataset and B.-F. across classes of environments. * indicates that two-sample-t-tests have been conducted for canyons in tropical versus temperate latitudinal zones. See Fig. 21 for legend.

A. Relationships between canyon morphometrics

Linear monotonic relationships

	L	Wmax	Wav	Dmax	Dav	Slav	thGav	SWmax
L		0.5	0.8	0.5		0.5	-0.5	
Wmax	0.5		0.8	0.8	0.5	0.4	-0.3	0.4
Wav	0.8	0.8		0.8				
Dmax	0.5	0.8	0.8		1.0			0.4
Dav		0.5		1.0		0.5		***
Slav	0.5	0.4			0.5		-0.3	
thGav	-0.5	-0.3				-0.3		
SWmax		0.4		0.4	***			

Non-linear monotonic relationships

	L	Wmax	Wav	Dmax	Dav	Slav	thGav	SWmax
L		0.6	0.6	0.7		0.5	-0.7	0.3
Wmax	0.6		0.8	0.7		0.4	-0.4	0.4
Wav	0.6	0.8		0.8				
Dmax	0.7	0.7	0.8		1.0			0.4
Dav				1.0		0.5		***
Slav	0.5	0.4			0.5		-0.4	
thGav	-0.7	-0.4				-0.4		
SWmax	0.3	0.4		0.4	***			

B. Relationships between canyon morphometrics and environmental parameters

Linear monotonic relationships & differences between canyon groups

	Lfls	Qfls	Aflsc	Hflsc	Wsh	Dsh	Gsh	Wsl	Dsl	Gsl	Dismin	SDmin	SDmax	Latabs	cnh. location	margin type	S2S setting	ocean. env.	lat. (ANOVA)	lat. (t-test)	sh. depth 120	sh. depth 130
L				0.4	0.2	0.4		0.4					0.6		X				X	X	X	X
Wmax				0.6		0.4		0.4					0.4	0.2					X			
Wav	***	***	***	***		0.5	0.7							0.5	X	X	***	X	***	***	***	***
Dmax		***		***		0.4		0.4	0.6				0.8					X			X	X
Dav	***	***	***	***		***						-0.4	0.7	-0.4	***	X	***	X	***	***	***	***
Slav				0.6		0.4		***					0.6		X				***	X	X	X
thGav		***				-0.3				0.5			-0.3	-0.4		X		X	***		X	X
SWmax	***	***	***	***	0.6					0.8	-0.3		0.4	0.5		X		X	X			

Non-linear monotonic relationships & differences between canyon groups

	Lfls	Qfls	Aflsc	Hflsc	Wsh	Dsh	Gsh	Wsl	Dsl	Gsl	Dismin	SDmin	SDmax	Latabs	cnh. location	margin type	S2S setting	ocean. env.	lat. (ANOVA)	lat. (t-test)	sh. depth 120	sh. depth 130
L		0.7		0.6	0.2	0.5		0.9	0.4				0.7	0.3	X				X	X	X	X
Wmax			0.6	0.6				0.7					0.5	0.2					X			
Wav	***	***	***	***	0.4	0.6	0.6				0.4			0.5	X	X	***	X	***	***	***	***
Dmax	0.7	***	0.7	***	0.4			0.6	0.5			-0.4	0.8					X			X	X
Dav	***	***	***	***		***						-0.4	0.7	-0.4	***	X	***	X	***	***	***	***
Slav		0.5		0.6	-0.3	0.4		***			-0.3	-0.3	0.5	0.2	X				***	X	X	X
thGav		***				-0.3		-0.5		0.5				-0.3		X		X	***		X	X
SWmax	***	***	***	***	0.5				-0.6	0.7			0.4	0.4		X		X	X			

correlation coefficient-value: -1 0 1

X difference in mean values between canyon groups is statistically significant (p≤0.01)

*** not enough data

Fig. 23. a&b: Summary tables displaying relationships of canyon morphometric parameters A. with each other and B. with environmental parameters for results of the correlation analyses and statistical tests with a statistical significance ($p \leq 0.01$) and $N \geq 15$ for each parameter and canyon group. *L* = canyon length; *Wmax* = maximum canyon width; *Wav* = average canyon width; *Dmax* = maximum canyon depth; *Dav* = average canyon depth; *SIav* = average canyon sinuosity index; *thGav* = average canyon thalweg gradient; *Swmax* = maximum canyon sidewall steepness; *Lfls* = fluvial system length; *Qfls* = average annual fluvial discharge; *Aflsc* = size of the catchment; *Hflsc* = maximum elevation in the catchment area; *Wsh* = shelf width; *Dsh* = shelf-break depth; *Gsh* = average shelf gradient; *Wsl* = slope width; *Dsl* = slope-break depth; *Gsl* = average slope gradient; Dis_{min} = minimum distance between the canyon and shoreline; SD_{min} = minimum seafloor depth at the canyon; SD_{max} = maximum seafloor depth at the canyon; Lat_{abs} = absolute value of the latitude of the canyon apex; cnh. location= canyon-apex location relative to the shelf-break; margin type = continental-margin type; ocean. env. = oceanographic environment; lat. = latitude at the canyon apex; sh. Depth = shelf break depth at the canyon. *** denotes datasets that were deemed too small for statistical analyses.

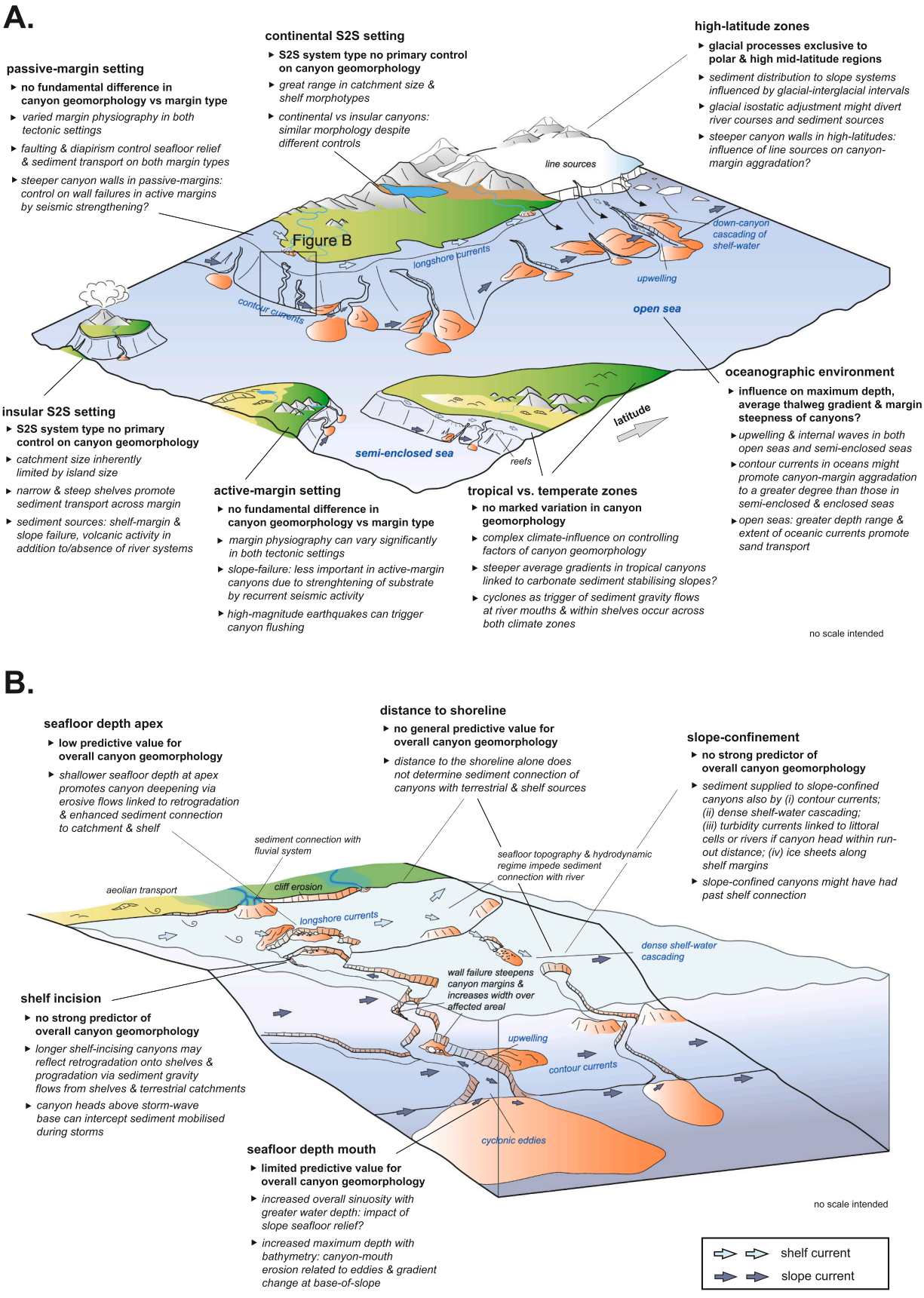

Fig. 24. a&b: Schematic diagrams summarising controlling factors of submarine-canyon geomorphology recognised in the literature and whose statistical signature has been evaluated in this study.

canyons are constrained by the interplay of canyon-margin failure and canyon-floor and canyon-margin aggradation by flows.

Our quantitative characterisation of how canyon morphometric parameters vary as a function of environmental factors demonstrates that the interplay of controls on canyon geomorphology is more complex than hitherto considered in canyon classification schemes (e.g. Jobe et al., 2011), numerical (e.g. Wan et al., 2021) and published conceptual models of canyon evolution (e.g. Chiang and Yu, 2006; Micallef et al., 2014), of deep-water systems and of source-to-sink (S2S) systems (e.g. Sømme et al., 2009; Nyberg et al., 2018). The predictive value of these models can be enhanced by considering the impact of the controlling factors identified in this study – including the hydrodynamic regime of oceans and seas, autogenic canyon processes, characteristics of continental margin physiography and the canyon physiographic setting.

The findings of this study might also aid in estimation of the original geometry of ancient canyons and channel forms whose infills are now preserved in subsurface and outcrop, and in the interpretation of their formative environments, particularly where information on the environmental setting, margin physiography and bathymetry are limited due to scarcity of data (e.g. Martinsen et al., 2010; Helland-Hansen et al., 2016; Xu et al., 2017).

Results of this work will aid analyses of source-to-sink systems, i.e., spanning fluvial, paralic and deep-water domains (e.g. Sømme et al., 2009; Nyberg et al., 2018; Wang et al., 2019), by illuminating the response of slope systems to controlling factors on sedimentary processes from terrestrial hinterlands to deep-water environments. Further research is needed to investigate the relative scaling between features of these clastic environments and those of submarine canyons, and of the relative influence of marine hydrodynamic processes on submarine-canyon geomorphology.

Declaration of Competing Interest

The authors declare that they have no known competing financial interests or personal relationships that could have appeared to influence the work reported in this paper.

Acknowledgements

We thank sponsors and partners of the Fluvial, Eolian & Shallow-Marine Research Group (AkerBP, Areva (now Orano), BHPBilliton (now BHP), Cairn India (Vedanta), Chevron, CNOOC International, ConocoPhillips, Equinor, Murphy Oil, Occidental, Petrotechnical Data Systems, Saudi Aramco, Shell, Tullow Oil, Woodside and YPF) and of the Turbidites Research Group (AkerBP, CNOOC, ConocoPhillips, Harbour, Murphy, Occidental, OMV) at the University of Leeds for financial support that has enabled this research. Financial support to this research was also provided by NERC (NE/P01691X/1). We thank Scott Nichol and two anonymous reviewers for their constructive comments, which helped improve the paper.

References

Acosta, J., Canals, M., López-Martínez Muñoz, A., Herranz, P., Urgeles, R., Palomo, C., Casamor, J.L., 2002. The Balearic promontory geomorphology (western Mediterranean): morphostructure and active processes. Geomorphology 49, 177–204.

Adams, E.W., Kenter, J.A.M., 2013. So different, yet so similar: comparing and contrasting siliciclastic and carbonate slopes. In: Verwer, K., Playton, T.E., Harris, P. M. (Eds.), Deposits, Architecture, and Controls of Carbonate Margin, Slope and Basinal Settings, 115. SEPM Spec. Publ, pp. 14–25. https://doi.org/10.2110/sepmsp.105.14.

Aiello, G., Iorio, M., Molisso, F., Sacchi, M. 2020 Integrated morpho-bathymetric, seismic-stratigraphic, and sedimentological data on the Dohrn Canyon (Naples Bay, Southern Tyrrhenian Sea): Relationships with volcanism and tectonics. Geosciences. 10, 319. https://doi.org/geosciences10080319.

Alford, M.H., MacCready, P., 2014. Flow and mixing in Juan de Fuca Canyon, Washington. Geophys. Res. Lett. 41, 1608–1615. https://doi.org/10.1002/2013GL058967.

Allen, S.E., Vindeirinho, C., Thomson, R.E., Foreman, M.G.G., Mackas, D.L., 2001. Physical and biological processes over a submarine canyon during an upwelling event. Can. J. Fish. Aquat. Sci. 58, 671–684. https://doi.org/10.1139/cjfas-58-4-671.

Allin, J.R., Hunt, J.E., Talling, P.J., Clare, M.A., Pope, E., Masson, D.G., 2016. Different frequencies and triggers of canyon filling and flushing events in Nazaré Canyon, offshore Portugal. Mar. Geol. 371, 89–105. https://doi.org/10.1016/j.margeo.2015.11.005.

Almagor, G., 1993. Continental slope processes off northern Israel and southernmost Lebanon and their relation to onshore tectonics. Mar. Geol. 112, 151–169.

Alonso, B., Ercilla, G., 2003. Small turbidite systems in a complex tectonic setting (SW Mediterranean Sea): morphology and growth patterns. Mar. Pet. Geol. 19, 1225–1240. https://doi.org/10.1016/S0264-8172(03)00036-9.

Alvarez-Solas, J., Robinson, A., Montoya, M., Ritz, C., 2013. Iceberg discharges of the last glacial period driven by oceanic circulation changes. PNAS. 110 (41), 16350–16354. https://doi.org/10.1073/pnas.1306622110.

Amblas, D., Gerber, T.P., De Mol, B., Urgeles, R., Garcia-Castellanos Canals, M., Pratson, L.F., Robb, N., Canning, J., 2012. Survival of a submarine canyon during long-term outbuilding of a continental margin. Geology. 40 (6), 543–546. https://doi.org/10.1130/G33178.1.

Amblas, D., Ceramicola, S., Gerber, T.P., Canals, M., Chiocci, F.L., Dowdeswell, J.A., Harris, P.T., Huvenne, V.A.I., Lai, S.Y.J., Lastras, G., Lo Iacono, C., Micallef, A., Mountjoy, J.J., Paull, C.K., Puig, P., Sanchez-Vidal, A., 2017. Submarine canyons and gullies. In: Micallef, A., Krastel, S., Savini, A. (Eds.), Submarine Geomorphology. Springer, pp. 251–272.

Antobreh, A.A., Krastel, S., 2006. Morphology, seismic characteristics and development of Cap Timiris Canyon, offshore Mauritania: a newly discovered canyon preserved-off a major arid climatic region. Mar. Pet. Geol. 23, 37–59. https://doi.org/10.1016/j.marpetgeo.2005.06.003.

Aranguiz, R., Shibayama, T., 2013. Effect of submarine canyons on tsunami propagation; a case study of the Biobio Canyon. Chile. Coast. Eng. J. 55 (4) https://doi.org/10.1142/S0578563413500162, 1350016-1-1350016-23.

Armitage, D.A., Piper, D.J.W., McGee, D.T., Morris, W.R., 2010. Turbidite deposition on the glacially influenced, canyon-dominated Southwest Grand Banks Slope. Canada. Sedimentology. 57, 1387–1408. https://doi.org/10.1111/j.1365-3091.2010.01149.x.

Arzola, R.G., Wynn, R.B., Lastras, G., Masson, D.G., Weaver, P.P.E., 2008. Sedimentary features and processes in the Nazaré and Setúbal submarine canyons, west Iberian margin. Mar. Geol. 250, 64–88. https://doi.org/10.1016/j.margeo.2007.12.006.

Azaroff, A., Miossec, C., Lanceleur, L., Guyoneaud, R., Monperrus, M., 2020. Priority and emerging micropollutants distribution from coastal to continental slope sediments: a case study of Capbreton Submarine Canyon (North Atlantic Ocean). Sci. Total Environ. 703, 135057 https://doi.org/10.1016/j.scitotenv.2019.135057.

Babonneau, N., Savoye, B., Cremer, M., Klein, B., 2002. Morphology and architecture of the present canyon and channel system of the Zaire deep-sea fan. Mar. Pet. Geo. 19, 445–467.

Babonneau, N., Delacourt, C., Cancouët, R., Sisavath, E., Bachèlery, P., Mazuel, A., Jorry, S.J., Deschamps, A., Ammann, J., Villeneuve., 2013. Direct sediment transfer form land to deep-sea: insights into shallow multibeam bathymetry at La Réunion Island. Mar. Geol. 346, 47–57. https://doi.org/10.1016/j.margeo.2013.08.006.

Bailey, L.P., Clare, M.A., Rosenberger, K.J., Cartigny, M.J.B., Talling, P.J., Paull, C.K., Gwiazda, R., Parsons, D.R., Simmons, S.M., Xu, J., Haigh, I.D., Maier, K.L., McGann, M., Lundstren, E., 2021. Preconditioning by sediment accumulation can produce powerful turbidity currents without major external triggers. Earth Planet. Sci. Lett. 562, 116845 https://doi.org/10.1016/j.epsl.2021.116845.

Baker, E.T., Hickey, B.M., 1986. Contemporary sedimentation processes in and around an active West Coast submarine canyon. Mar. Geol. 71, 15–34.

Baztan, J., Berné, S., Olivet, J.-L., Rabineau, M., Aslanian, D., Gaudin, M., Réhault, J.-P., Canals, m., 2005. Axial incision: The key to understand submarine canyon evolution (in the western Gulf of Lion). Mar. Pet. Geol. 22 (6-7), 805–826. https://doi.org/10.1016/j.marpetgeo.2005.03.011.

Benjamin, U., Huuse, M., Hodgetts, D., 2015. Canyon-confirmed pockmarks on the western Niger Delta slope. J. Afr. Earth Sci. 107, 15–27. https://doi.org/10.1016/j.jafrearsci.2015.03.019.

Bernhardt, A., Melnick, D., Jara-Muñoz, J., Argandoña, B., González, J., Strecker, M.R., 2015. Controls on submarine canyon activity during sea-level highstands. The Bíobío canyon system offshore Chile. Geosphere 11 (4), 1226–1255. https://doi.org/10.1130/GES01063.1.

Bernhardt, A., Schwanghart, W., 2021. Where and why do submarine canyons remain connected to the shore during sea-level rise? Insights from global topographic analysis and Bayesian regression. Geophys. Res. Lett. 48 https://doi.org/10.1029/2020GL092234.

Bhattacharya, J.P., Copeland, P., Lawton, T.F., Holbrook, J., 2016. Estimation of source area, river paleo-discharge, paleoslope, and sediment budgets of linked deep-time depositional systems and implications for hydrocarbon potential. Earth-Sci. Rev. 153, 77–110. https://doi.org/10.1016/j.earscirev.2015.10.013.

Blum, M.D., Hattier-Womack, J., 2009. Climate change, sea-level change, and fluvial sediment supply to deepwater depositional systems. In: Kneller, B., Martinsen, O.J., McCaffrey, B. (Eds.), External Controls on Deep Water Depositional Systems: Climate, Sea-Level, and Sediment Flux. SEPM Spec. Publ. (CD version), 92, pp. 15–39.

Blum, M., Martin, J., Milliken, K., Garvin, M., 2013. Paleovalley systems: insights from Quaternary analogs and experiments. Earth-Sci. Rev. 116, 128–169. https://doi.org/10.1016/j.earscirev.2012.09.003.

Bosley, K.L., Lavelle, J.W., Brodeur, R.D., Wakefield, W.W., Emmet, R.L., Baker, E.T., Rehmke, K.M., 2004. Biological and physical processes in and around Astoria submarine Canyon, Oregon. USA. J. Mar. Syst. 50, 21–37. https://doi.org/10.1016/j.jmarsys.2003.06.006.

Bourget, J., Zaragosi, S., Ellouz-Zimmermann, N., Mouchot, N., Garlan, T., Schneider, J.-L., Lanfumey, V., Lallemant, S., 2010. Turbidite system architecture and sedimentary processes along topographically complex slopes: the Makran convergent margin. Sedimentology. 58 (2), 376–406. https://doi.org/10.1111/j.1365-3091.2010.01168.x.

Brunt, R.L., Hodgson, D.M., Flint, S.S., Pringle, J.K., Di Celma, C.N., Prelat, A., Grecula, M., 2013. Confined to unconfined: Anatomy of a base of slope succession, Karoo Basin, South Africa. Mar. Pet. Geol. 41, 206–221.

Budai, S., Colombera, L., Mountney, N.P., 2021. Quantitative characterization of the sedimentary architecture of Gilbert-type deltas. Sediment. Geol. 426, 106022 https://doi.org/10.1016/j.sedgeo.2021.106022.

Budillon, F., Conforti, A., Tonielli, R., De Falco, G., Di Martino, G., Innangi, S., Marsella, E., 2011. The Bulgheria canyon-fan: a small-scale proximal system in the eastern Tyrrhenian Sea (Italy). Mar. Geophys. Res. 32, 83–97. https://doi.org/10.1007/s11001-011-9138-9.

Çağatay, M.N., Uçarkus, G., Eriş, K.K., Henry, P., Gasperini, L., Polonia, A., 2015. Submarine canyons of the Sea of Marmara. In: Briand, F. (Ed.), Submarine canyon dynamics in the Mediterranean and tributary seas – an integrated geological, oceanographic and biological perspective, 47. CIESM Workshop Monographs, pp. 123–135.

Canals, M., Puig, P., Durrieu de Madron, X., Heussner, S., Palanques, A., Fabres, J., 2006. Flushing submarine canyons. Nature. 444, 354–357. https://doi.org/10.1038/nature05271.

Carlson, P.R., Karl, H.A., 1984. Discovery of two new large submarine canyons in the Bering Sea. Mar. Geol. 56, 159–179.

Carlson, P.R., Karl, H.A., 1988. Development of large submarine canyons in the Bering Sea, indicated by morphologic, seismic, and sedimentologic characteristics. Geol. Soc. Am. Bull. 100, 1594–1615.

Carlson, P.R., Bruns, T.R., Fisher, M.A., 1990. Development of slope valleys in the glacimarine environment of a complex subduction zone, Northern Gulf of Alaska. In: Dowdeswell, J.A., Scourse, J.D. (Eds.), Glacimarine Environments; Processes and Sediments, 53. Geol. Soc. London Spec. Publ, pp. 139–153.

Carson, B., Baker, E.T., Hickey, B.M., Nittrouer, C.A., DeMaster, D.J., Thorbjarnarson, K. W., Snyder, G.W., 1986. Modern sediment dispersal and accumulation in Quinault Submarine Canyon – A summary. Mar. Geol. 71, 1–13.

Carter, L., Gavey, R., Talling, P.J., Liu, J.T., 2014. Insights into submarine geohazards from breaks in subsea telecommunication cables. Oceanography. 27 (2), 58–67. https://doi.org/10.5670/oceanog.2014.40.

Carvajal, C., Steel, R., Petter, A., 2009. Sediment supply: the main driver of shelf-margin growth. Earth-Sci. Rev. 96, 221–248. https://doi.org/10.1016/j.earscirev.2009.06.008.

Casalbore, D., Falcini, F., Martorelli, E., Morelli, E., Bosman, A., Calarco, M., Chiocci, F. L., 2018. Characterization of overbanking features on the lower reach of the Gioia-Mesima canyon-channel system (southern Tyrrhenian Sea) through integration of morpho-stratigraphic data and physical modelling. Prog. Oceanogr. 169, 66–78. https://doi.org/10.1016/j.pocean.2018.02.020.

Chang, Y.-C., Mitchell, N.C., Quartau, R., 2021. Landslides in the upper submarine slopes of volcanic islands: The central Azores. Geochem., Geophys., Geosyst. 22 https://doi.org/10.1029/2021GC009833 e2021GC009833.

Chen, H., Zhan, W., Li, L., Wen, M.-M., 2017. Occurrence of submarine canyons, sediment waves and mass movements along the northern continental slope of the South China Sea. J. Earth Syst. Sci. 126, 73. https://doi.org/10.1007/s12040-017-0844-9.

Chiang, C.-S., Yu, H.-S., 2006. Morphotectonics and incision of the Kaoping submarine canyon, SW Taiwan orogenic wedge. Geomorphology. 80, 199–213. https://doi.org/10.1016/j.geomorph.2006.02.008.

Chiang, C.-S., Yu, H.-S., Noda, A., TuZino, T., Su, C.-C., 2012. Avulsion of the Fangliao submarine canyon off southwestern Taiwan as revealed by morphological analysis and numerical simulation. Geomorphology. 177-178, 26–37. https://doi.org/10.1016/j.geomorph.2012.07.011.

Clare, M.A., Le Bas, T., Price, D.M., Hunt, J.E., Sear, D., Cartigny, M.J.B., Vellinga, A., Symons, W., Firth, C., Cronin, S., 2018. Complex and cascading triggering of submarine landslides and turbidity currents at volcanic islands revealed from integration of high-resolution onshore and offshore surveys. Front. Earth Sci. 6, 223. https://doi.org/10.3389/feart.2018.00223.

Clark, P.U., Mix, A.C., 2002. Ice sheets and sea level of the Last Glacial Maximum. Quat. Sci. Rev. 21, 1–7.

Clift, P.D., 2020. Asian monsoon dynamics and sediment transport in SE Asia. J. Asian Earth Sci. 195, 104352 https://doi.org/10.1016/j.jseaes.2020.104352.

Coleman, J.M., Prior, D.B., Lindsay, J.F., 1982. Formation of the Mississippi Canyon. GCAGS Transactions. 32, 519.

Connolly, T.P., Hickey, B.M., 2014. Regional impact of submarine canyons during seasonal upwelling. J. Geophys. Res. Oceans. 119, 953–975. https://doi.org/10.1002/2013JC009452.

Cosgrove, G.I.E., Colombera, L., Mountney, N.P., 2021. Quantitative analysis of the sedimentary architecture of eolian successions developed under icehouse and greenhouse climatic conditions. Geol. Soc. Am. Bull. 133 (11/12), 2625–2644. https://doi.org/10.1130/B35918.1.

Covault, J.A., Graham, S.A., 2010. Submarine fans at all sea-level stands: tectono-morphologic and climatic controls on terrigenous sediment delivery to the deep sea. Geology. 38 (10), 939–942. https://doi.org/10.1130/G31081.1.

Covault, J.A., Normark, W.R., Romans, B.W., Graham, S.A., 2007. Highstand fans in the California borderland: The overlooked deep-water depositional systems. Geology. 35 (9), 783–786. https://doi.org/10.1130/G23800A.1.

Covault, J.A., Fildani, A., Romans, B.W., McHargue, T., 2011a. The natural range of submarine canyon-and-channel longitudinal profiles. Geosphere. 7 (2), 313–332. https://doi.org/10.1130/GES00610.1.

Covault, J.A., Romans, B.W., Graham, S.A., Fildani, A., Hilley, G.E., 2011b. Terrestrial source to deep-sea sink sediment budgets at high and low sea levels: insights from tectonically active southern California. Geology. 39 (7), 619–622. https://doi.org/10.1130/G31801.1.

Cronin, B.T., Akhmetzhanov, A.M., Mazzini, A., Akhmanov, G., Ivanov, M., Kenyon, N. H., TTR-10 Shipboard Scientists, 2005. Morphology, evolution and fill: implications for sand and mud distribution in filling deep-water canyons and slope channel complexes. Sediment. Geol. 179, 71–97. https://doi.org/10.1016/j.sedgeo.2005.04.013.

Crutchley, G.J., Kroeger, K.F., Pecher, I.A., Mountjoy, J.J., Gorman, A.R., 2017. Gas hydrate formation amid submarine canyon incision: Investigations from New Zealand's Hikurangi Subduction Margin. Geochem., Geophys. Geosyst. 18, 4299–4316. https://doi.org/10.1002/2017GC007021.

Cullis, S., Patacci, M., Colombera, L., Bührig, L., McCaffrey, W.D., 2019. A database solution for the quantitative characterisation and comparison of deep-marine siliciclastic depositional systems. Mar. Pet. Geol. 102, 321–339. https://doi.org/10.1016/j.marpetgeo.2018.12.023.

Dadson, S., Hovius, N., Pegg, S., Dade, W.B., Horng, M.J., Chen, H., 2005. Hyperpycnal river flows from an active mountain belt. J. Geophys. Res. 110, F04016. https://doi.org/10.1029/2004JF000244.

Davies, H.L., Keene, J.B., Hashimoto, K., Joshima, M., Stuart, J.E., Tiffin, D.L., 1987. Bathymetry and canyons of the Western Solomon Sea. Geo-Mar. Lett. 6, 181–191. https://doi.org/10.1007/BF02239579.

Davies, R.J., Thatcher, K.E., Mathias, S.A., Yang, J., 2012. Deepwater canyons: an escape route for methane sealed by methane hydrate. Earth Planet. Sci. Lett. 323-324, 72–78. https://doi.org/10.1016/j.epsl.2011.11.007.

de Almeida, N.M., Vital, H., Gomes, M.P., 2015. Morphology of submarine canyons along the continental margin of the Potiguar Basin, NE Brazil. Mar. Pet. Geol. 68, 307–324. https://doi.org/10.1016/j.marpetgeo.2015.08.035.

De Pippo, T., Ilardi, M., Pennetta, M., 1999. Main observations on genesis and morphological evolution of submarine valleys. Z. Geomorphol. 43 (1), 91–111.

Diesing, M., 2020. Deep-sea sediments of the global ocean. Earth Syst. Sci. Data. 12 (4), 3367–3381. https://doi.org/10.5194/essd-12-3367-2020.

Dietz, R.S., Knebel, H.J., Somers, L.H., 1968. Cayar Submarine Canyon. Geol. Soc. Am. Bull. 79, 1821–1828.

Ding, W., Li, J., Li, J., Fang, Y., Tang, Y., 2013. Morphotectonics and evolutionary controls on the Pearl River Canyon system, South China Sea. Mar. Geophys. Res. 34, 221–238. https://doi.org/10.1007/s11001-013-9173-9.

Dowdeswell, J.A., Cofaigh, Ó., C., Pudsey, C.J., 2004. Continental slope morphology and sedimentary processes at the mouth of an Antarctic palaeo-ice stream. Mar. Geol. 204, 203–214. https://doi.org/10.1016/S0025-3227(03)00338-4.

Dowdeswell, E.K., Todd, B.J., Dowdeswell, J.A., 2016. Canyons and slides on the continental slope seaward of shallow banks, Labrador margin, eastern Canada. In: Dowdeswell, J.A., Canals, M., Jakobsson, M., Todd, B.J. (Eds.), Atlas of Submarine Glacial Landforms: Modern, Quaternary and Ancient, 46. Geological Society, London, pp. 405–406. Memoirs.

Eittreim, S., Grantz, A., Greenberg, J., 1982. Active geologic processes in Barrow Canyon, Northeast Chukchi Sea. Mar. Geol. 50, 61–76.

Ercilla, G., Alonso, B., Perez-Belzuz, F., Estrada, F., Baraza, J., Farran, M., Canals, M., Masson, D., 1998. Origin, sedimentary processes and depositional evolution of the Agadir turbidite system, central eastern Atlantic. J. Geol. Soc. London. 155 (6), 929–939. https://doi.org/10.1144/gsjgs.155.6.0929.

Exon, N.F., Hill, P.J., Mitchell, C., Post, A., 2005. Nature and origin of the submarine Albany canyons off southwest Australia. Aust. J. Earth Sci. 52 (1), 101–115. https://doi.org/10.1080/08120090500100036.

Fanelli, E., Bianchelli, S., Danovaro, R., 2018. Deep-sea mobile megafauna of Mediterranean submarine canyons and open slopes: Analysis of spatial and bathymetric gradients. Prog. Oceanogr. 168, 23–34. https://doi.org/10.1016/j.pocean.2018.09.010.

Farre, J.A., McGregor, B.A., Ryan, W.B.F., Robb, J.M., 1983. Breaching the shelfbreak: passage from youthful to mature phase in submarine canyon evolution. In: Stanley, D.J., Moore, G.T. (Eds.), The Shelfbreak: Critical Interface on Continental Margins, SEPM Spec. Publ., 33, pp. 25–39.

Faugères, J.-C., Mulder, T., 2011. Chapter 3 – Contour currents and contourite drifts. In: Hüneke, H., Mulder, T. (Eds.), Deep-Sea Sediments, Dev. in Sedimentology, 63, pp. 149–214.

Fernane, L., Matougui, R., Amarni, N., Belkessa, R., 2022. Variation in canyon morphology and their relationship with tectonic: the example of the western Algerian margin. Arab. J. Geosci. 15, 254. https://doi.org/10.1007/s12517-022-09566-6.

Ferry, J.-N., Babonneau, N., Mulder, T., Parize, O., Raillard, S., 2004. Morphogenesis of Congo submarine canyon and valley: implications about the theories of the canyons formation. Geodin. Acta. 17, 241–251.

Fiduk, J.C., 1995. Influence of submarine canyon erosion and sedimentation on allochthonous salt body geometry: the pathway of Bryant canyon in garden banks. In: GCSSEPM Foundation 16th Annual Research Conference Salt, Sediment and Hydrocarbons. December 3-6, 1995.

Field, M.E., Gardner, J.V., Prior, D.B., 1999. Geometry and significance of stacked gullies on the northern California slope. Mar. Geol. 154, 271–286. https://doi.org/10.1016/S0025-3227(98)00118-2.

Fildani, A., 2017. Submarine canyons: a brief review looking forward. Geology 45 (4), 383–384. https://doi.org/10.1130/focus042017.1.

Flexas, M.M., Boyer, D.L., Espino, M., Puigdefàbregas, J., Rubio, A., Company, J.B., 2008. Circulation over a submarine canyon in the NW Mediterranean. J. Geophys. Res. 113, C12002. https://doi.org/10.1029/2006JC003998.

Fournier, F., 1949. Les facteur climatiques de l'érosion du sol. Bull. Assoc. Geogr. Fr. 203, 97–103.

Fulthorpe, C.S., Carter, R.M., 1991. Continental-shelf progradation by sediment-drift accretion. Geol. Soc. Am. Bull. 103, 300–309. https://doi.org/10.1130/0016-7606(1991)103<0300:CSPBSD>2.3.CO;2.

Gales, J.A., Forwick, M., Laberg, J.S., Vorren, T.O., Larter, R.D., Graham, A.G.C., beaten, N.J., Amundsen, H.B., 2013. Arctic and Antarctic submarine gullies – A comparison of high latitude continental margins. Geomorphology. 201, 449–461. https://doi.org/10.1016/j.geomorph.2013.07.018.

Gales, J., Rebesco, M., De Santis, L., Bergamasco, A., Colleoni, F., Kim, S., Accettella, D., Kovacevic, V., Liu, Y., Olivo, E., Colizza, E., Florindo-Lopez, C., Zgur, F., McKay, R., 2021. Role of dense shelf water in the development of Antarctic submarine canyon morphology. Geomorphology. 372, 107453 https://doi.org/10.1016/j.geomorph.2020.107453.

Galewsky, J., Silver, E.A., 1997. Tectonic controls on facies transitions in an oblique collision: The western Solomon Sea, Papua New Guinea. Geo. Soc. Am. Bull. 10, 1266–1278. https://doi.org/10.1130/0016-7606(1997)109<1266:TCOFTI>2.3.CO;2.

Gamberi, F., Rovere, M., Marani, M.P., Dykstra, M., 2015. Modern submarine canyon feeder-system and deep-sea fan growth in a tectonically active margin (northern Sicily). Geosphere. 11 (2), 307–319. https://doi.org/10.1130/GES01030.1.

Gardner, W.D., Glover, L.K., Hollister, C.D., 1980. Canyons off Northwest Puerto Rico: studies of their origin and maintenance with the nuclear research submarine NR-1. Mar. Geol. 37, 41–70.

Gardner, J.V., Dartnell, P., Mayer, L.A., Hughes Clarke, J.E., 2003. Mar. Environ. Res. 56, 15–46. https://doi.org/10.1016/S0141-1136(02)00323-9.

Gervais, A., Savoye, B., Piper, D.J.W., Mulder, T., Cremer, M., Pichevin, L., 2004. Present morphology and depositional architecture of a sandy confined submarine system: the Golo turbidite system (eastern margin of Corsica). In: Lomas, S.A., Joseph, P. (Eds.), Confined Turbidite Systems, Geol. Soc. London Spec. Publ., 222, pp. 59–89.

Gervais, A., Mulder, T., Savoye, B., Gonthier, E., 2006. Sediment distribution and evolution of sedimentary processes in a small sandy turbidite system (Golo system, Mediterranean Sea): implications for various geometries based on core framework. Geo-Mar. Lett. 26, 373–395.

Gnibidenko, H.S., Svarichevskaya, L.V., 1984. The submarine canyons of Kamchatka. Mar. Geol. 54, 277–307.

Gómez-Ballesteros, M., Druet, M., Muñoz, A., Arrese, B., Rivera, J., Sánchez, F., Cristobo, J., Parra, S., García-Alegre, A., González-Pola, C., Gallastegui, J., Acosta, J., 2014. Geomorphology of the Avilés Canyon System, Cantabrian Sea (Bay of Biscay). Deep Sea Res. Part II Top. Stud. Oceanogr. 106, 99–117. https://doi.org/10.1016/j.dsr2.2013.09.031.

Goni, G., DeMaria, M., Knaff, J., Sampson, C., Ginis, I., Bringas, F., Mavume, A., Lauer, C., Lin, I.-I., Ali, M.M., Sandery, P., Ramos-Buarque, S., Kang, K., Mehra, A., Chassignet, E., Halliwell, G., 2009. Applications of satellite-derived ocean measurements to tropical cyclone intensity forecasting. Oceanography. 22 (3), 190–197. https://doi.org/10.5670/oceanog.2009.78.

Green, A., 2011. Submarine canyons associated with alternating sediment starvation and shelf-edge wedge development. Northern KwaZulu-Natal continental margin. South Africa. Mar. Geol. 284, 114–126. https://doi.org/10.1016/j.margeo.2011.03.011.

Greene, H.G., Maher, N.M., Paull, C.K., 2002. Physiography of the Montery Bay National Marine Sanctuary and implications about continental margin development. Mar. Geol. 181, 55–82.

Gulliksen, B., 1978. Rocky bottom fauna in a submarine gulley at Loppkalven, Finnmark, Northern Norway. Estuar. Coast. Mar. Sci. 7, 361–372. https://doi.org/10.1016/0302-3524(78)90088-9.

Ha, S., Colizza, E., Torricella, F., Langone, L., Giglio, F., Kuhn, G., Macrì, P., Khim, B.-K., 2022. Glaciomarine sediment deposition on the continental slope and rise of the central Ross Sea since the Last Glacial Maximum. Mar. Geol. 445, 106752 https://doi.org/10.1016/j.margeo.2022.106752.

Hagen, R.A., Bergersen, D.D., Moberly, R., Coulbourn, W.T., 1994. Morphology of a large meandering submarine canyon system on the Peru-Chile forearc. Mar. Geol. 119, 7–38.

Hagen, R.A., Vergara, H., Naar, D.F., 1996. Morphology of San Antonio submarine canyon on the central Chile forearc. Mar. Geol. 129, 197–205.

Hale, R.P., Nittrouer, C.A., Liu, J.T., Keil, R.G., Ogston, A.S., 2012. Effects of a major typhoon on sediment accumulation in Fangliao Submarine Cayon, SW Taiwan. Mar. Geol. 326-328, 116–130. https://doi.org/10.1016/j.margeo.2012.07.008.

Han, X., Li, J., Chu, F., Li, J., Yang, F., 2010. Geomorphology and tectonic interpretation of Zhujiang Submarine Canyon, in the northern South China Sea. In: *OCEANS'10 IEEE SYDNEY*, Conference. May 24-27, 2010. https://doi.org/10.1109/OCEANSSYD.2010.5603638.

Harris, P.T., Macmillan-Lawler, M., 2016. Global overview of continental shelf geomorphology based on the SRTM30_PLUS 30-Arc Second Database. In: Finkl, C., Makowski, C. (Eds.), Seafloor Mapping along Continental Shelves: Research and Techniques for Visualizing Benthic Environments, 13. Coastal Research Library, pp. 169–190. https://doi.org/10.1007/978-3-319-25121-9_7.

Harris, P., Whiteway, T., 2011. Global distribution of large submarine canyons: Geomorphic differences between active and passive continental margins. Mar. Geol. 285, 69–86. https://doi.org/10.1016/j.margeo.2011.05.008.

Harris, P.T., Macmillan-Lawler, M., Rupp, J., Baker, E.K., 2014. Geomorphology of the oceans. Mar. Geol. 352, 4–24. https://doi.org/10.1016/j.margeo.2014.01.011.

Heezen, B.C., Ewing, M., 1952. Turbidity currents and submarine slumps, and the 1929 Grand Banks earthquake. Am. J. Sci. 250, 849–873.

Helland-Hansen, W., Sømme, T.O., Martinsen, O.J., Lunt, I., 2016. Deciphering Earth's natural hourglasses: perspectives on source-to-sink analysis. J. Sediment. Res. 86, 1008–1033. https://doi.org/10.2110/jsr.2016.56.

Hemming, S.R., 2004. Heinrich events: massive late Pleistocene detritus layers of the North Atlantic and their global climate imprint. Rev. Geophys. 42 (1), RG1005. https://doi.org/10.1029/2003RG000128.

Henrich, R., Cherubini, Y., Meggers, H., 2010. Climate and sea level induced turbidite activity in a canyon system offshore the hyperarid Western Sahara (Mauritania): the Timiris Canyon. Mar. Geol. 275, 178–198. https://doi.org/10.1016/j.margeo.2010.05.011.

Hereema, C.J., Talling, P.J., Cartigny, M.J., Paull, C.K., Bailey, L., Simmons, S.M., Parsons, D.R., Clare, M.A., Gwiazda, R., Lundsten, E., Anderson, K., Maier, K.L., Xu, J.P., Sumner, E.J., Rosenberger, K., Gales, J., McGann, M., Carter, L., Pope, E., Monterey Coordinated Canyon Experiment (CCE) Team, 2020. What determines the downstream evolution of turbidity currents? Earth Planet. Sci. Lett. 532, 116023 https://doi.org/10.1016/j.epsl.2019.116023.

Hickey, B.M., 1997. The response of a steep-sided, narrow canyon to time-variable wind forcing. J. Phys. Oceanogr. 27 (5), 697–726.

Higgins, S.A., Overeem, I., Rogers, K.G., Kalina, E.A., 2018. River linking in India: Downstream impacts on water discharge and suspended sediment transport to deltas. Elem. Sci. Anth. 6 (20), 24. https://doi.org/10.1525/elementa.269.

Hizzet, J.L., Hughes Clarke, J.E., Sumner, E.J., Cartigny, M.J.B., Talling, P.J., Clare, M.A., 2018. Which triggers produce the most erosive, frequent, and longest runout turbidity currents on deltas? Geophys. Res. Lett. 45, 855–863. https://doi.org/10.1002/2017GL075751.

Hsiung, K.-H., Yu, H.-S., 2011. Morpho-sedimentary evidence for a canyon-channel-trench interconnection along the Taiwan-Luzon plate margin, South China Sea. Geo-Mar. Lett. 31, 215–226. https://doi.org/10.1007/s00367-010-0226-7.

Hsiung, K.-H., Kanamatsu, T., Ikehara, K., Shiraishi, K., Horng, C.-S., Usami, K., 2017. Morpho-sedimentary features and sediment dispersal systems of the southwest end of the Ryukyu Trench: a source-to-sink approach. Geo-Mar. Lett. 37, 561–577. https://doi.org/10.1007/s00367-017-0509-3.

Hsu, S.-K., Kuo, J., Lo, C.-L., Tsai, C.-H., Doo, W.-B., Ku, C.-Y., Sibuet, J.-C., 2008. Turbidity currents, submarine landslides and the 2006 Pingtung earthquake off SW Taiwan. Terr. Atmos. Ocean. Sci. 19 (6), 767–772. https://doi.org/10.3319/TAO.2008.19.6.767(PT).

https://www.ncei.noaa.gov/maps/bathymetry/ (accessed 20 October 2021).

Huang, Z., Nichol, S.L., Harris, P.T., Caley, M.J., 2014. Classification of submarine canyons of the Australian continental margin. Mar. Geol. 357, 362–383. https://doi.org/10.1016/j.margeo.2014.07.007.

Hutton, E.W.H., Syvitski, J.P.M., Watts, A.B., 2013. Isostatic flexure of a finite slope due to sea-level rise and fall. Comput. Geosci. 53, 58–68. https://doi.org/10.1016/j.cageo.2012.03.020.

Iglesias, O., Lastras, G., Souto, C., Costa, S., Canals, M., 2014. Effects of coastal submarine canyons on tsunami propagation and impact. Mar. Geol. 350, 39–51. https://doi.org/10.1016/j.margeo.2014.01.013.

Inman, D., Nordstrom, C., 1971. On the tectonic and morphologic classification of coasts. J. Geol. 79 (1), 1–21.

Itoh, M., Pickart, R.S., Kikuchi, T., Fukamachi, Y., Oshima, K.I., Simizu, D., Arrigo, K.R., Vagle, S., He, J., Ashjian, C., Mathis, J.T., Nishino, S., Nobre, C., 2010. Water properties, heat and volume fluxes of Pacific water in Barrow Canyon during summer. Deep Sea Res. Part I Oceanogr. Res. Pap. 102, 43–54. https://doi.org/10.1016/j.dsr.2015.04.004.

Jimoh, R.O., Tang, Y., Li, J., Awosika, L.F., Li, H., Akinnigbage, E.A., Adeleye, A.O., 2018. The architecture of the lower parts of submarine canyons on the western Nigerian continental margin. Acta Oceanol. Sin. 37 (7), 28–40. https://doi.org/10.1007/s13131-018-1242-0.

Jipa, D.C., Panin, N., 2020. Narrow shelf canyons vs. wide shelf canyons: Two distinct types of Black Sea submarine canyons. Quat. Int. 540, 120–136. https://doi.org/10.1016/j.quaint.2018.08.006.

Jobe, Z.R., Lowe, D.R., Uchytil, S.J., 2011. Two fundamentally different types of submarine canyons along the continental margin of Equatorial Guinea. Mar. Pet. Geol. 28, 843–860. https://doi.org/10.1016/j.marpetgeo.2010.07.012.

Johnson, S.Y., Hartwell, S.R., Sorlien, C.C., Dartnell, P., Ritchie, A.C., 2017. Shelf evolution along a transpressive transform margin, Santa Barbara Channel. California. Geosphere. 13 (6), 2041–2077. https://doi.org/10.1130/GES01387.1.

Jordi, A., Klinck, J.M., Basterretxea, Orfila, A., Tintoré, J., 2008. Estimation of shelf-slope exchanges induced by frontal instability near submarine canyons. J. Geophys. Res. 113, C05016. https://doi.org/10.1029/2007JC004207.

Kagami, H., Kuramochi, H., Shima, Y., 1991. Submarine canyons in the Bellinghausen and Riiser-Larsen Seas around Antarctica. Proc. NIPR Symp. Antarct. Geosc. 5, 84–98.

Katz, O., Hamiel, Y., 2018. The nature of small to medium earthquakes along the Eastern Mediterranean passive continental margins, and their possible relationships to landslides and submarine salt-tectonic-related shallow faults. In: Lintern, D.G., Mosher, D.C., Moscardelli, L.G., Bobrowsky, P.T., Campbell, C., Chaytor, J.D., Clague, J.J., Georgiopoulou, A., Lajeunesse, P., Normandeau, A., Piper, D.J.W., Scherwath, M., Stacey, C., Turmel, D. (Eds.), Subaqueous Mass Movements. Geol. Soc. London Spec.Publ, 477. https://doi.org/10.1144/SP477.5, 8 p.

Klaus, A., Taylor, B., 1991. Submarine canyon development in the Izu-Bonin Forearc: a SeaMARC II and seismic survey of Aoga Shima Canyon. Mar. Geophys. Res. 13, 131–152.
Kober, F., Zeilinger, G., Hippe, K., Marc, O., Lendzioch, T., Grischott, R., Christl, M., Kubik, P.W., Zola, R., 2015. Tectonic and lithological controls on denudation rates in the central Bolivian Andes. Tectonophysics. 657, 230–244. https://doi.org/10.1016/j.tecto.2015.06.037.
Krastel, S., Hanebuth, T.J.J., Antobreh, A.A., Henrich, R., Holz, C., Kölling, M., Schulz, H. D., Wien, K., 2004. Eos Trans. Am. Geophys. Union 85 (42), 417–432.
Krastel, S., Wefer, G., Hanebuth, T.J.J., Antobreh, A.A., Freudenthal, T., Preu, B., Schwenk, T., Strasser, M., Violante, R., Winkelmann, D., M78/3 shipboard scientific party, 2011. Sediment dynamics and geohazards off Uruguay and the de la Plata River region (northern Argentina and Uruguay). Geo-Mar. Lett. 31, 271–283. https://doi.org/10.1007/s00367-011-0232-4.
Langbein, W.B., Schumm, S.A., 1958. Yield of sediment in relation to mean annual precipitation. Trans.-Am. Geophys. Union. 39 (6), 1076–1084.
Lastras, G., Canals, M., Urgeles, R., Amblas, D., Ivanov, M., Droz, L., Dennielou, B., Fabrés, J., Schoolmeester, T., Akhmetzhanov, A., Orange, D., García-García., 2007. A walk down the Cap de Creus canyon, Northwestern Mediterranean Sea: Recent processes inferred from morphology and sediment bedforms. Mar. Geol. 246, 176–192. https://doi.org/10.1016/j.margeo.2007.09.002.
Lastras, G., Arzola, R.G., Masson, D.G., Wynn, R.B., Huvenne, V.A.I., Hühnerbach, V., Canals, M., 2009. Geomorphology and sedimentary features in the Central Portuguese submarine canyons, Western Iberian margin. Geomorphology. 103, 310–329. https://doi.org/10.1016/j.geomorph.2008.06.013.
Lastras, G., Acosta, J., Muñoz, A., canals, M., 2011a. Submarine canyon formation and evolution in the Argentine Continental Margin between 44°30'S and 48°S. Geomorphology. 128, 116–136. https://doi.org/10.1016/j.geomorph.2010.12.027.
Lastras, G., Canals, M., Amblas, D., Lavoie, C., Church, I., De Mol, B., Duran, R., Calafat, A.M., Hughes-Clarke, J.E., Smith, C.J., Heussner, S., "Euroléon" cruise shipboard party, 2011b. Understanding sediment dynamics of two large submarine valleys from seafloor data: Blanes and La Fonera canyons, northwestern Mediterranean Sea. Mar. Geol. 280, 20–39. https://doi.org/10.1016/j.margeo.2010.11.005.
Laursen, J., Normark, W.R., 2002. Late Quaternary evolution of the San Antonio Submarine Canyon in the central Chile forearc (~33°S). 2002. Mar. Geol. 188, 365–390.
Le Bas, T.P., Masson, R., Holtom, R.T., Grevemeyer, I., 2007. Slope failures of the flanks of the Southern Cape Verde Islands. In: Lykousis, V., Sakellariou, D., Locat, J. (Eds.), Submarine Mass Movements and Their Consequences. Advances in Natural and Technological Hazards Research, 27. Springer, Dordrecht.
Le Dantec, N., Hogarth, L.J., Driscoll, N.W., Babcock, J.M., Barnhardt, W.A., Schwab, W. C., 2010. Tectonic controls on nearshore sediment accumulation and submarine canyon morphology offshore La Jolla, Southern California. Mar. Geol. 268, 115–128. https://doi.org/10.1016/j.margeo.2009.10.026.
Lewis, K.B., Barnes, P.M., 1999. Kaikoura Canyon, New Zealand: active conduit from near-shore sediment zones to trench-axis channel. Mar. Geol. 162, 39–69.
Li, M.Z., Prescott, R.H., Robertson, A.G., 2019. Observation of internal tides and sediment transport processes at the head of Logan Canyon on central Scotian Slope, eastern Canada. J. Mar. Syst. 193, 103–125. https://doi.org/10.1016/j.jmarsys.2019.02.007.
Li, W., Li, S., Alves, T.M., Rebesco, M., Feng, Y., 2021. The role of sediment gravity flows on the morphological development of a large submarine canyon (Taiwan Canyon), north-east South China Sea. Sedimentology. 68, 1091–1108. https://doi.org/10.1111/sed.12818.
Li, S., Alves, T.M., Li, W., Wang, X., Rebesco, M., Li, J., Zhao, F., Yu, K., Wu, S., 2022. Morphology and evolution of submarine canyons on the northwest South China Sea margin. Mar. Geol. 443, 106695 https://doi.org/10.1016/j.margeo.2021.106695.
Liu, J.T., Yin, H.-L., 2004. Sediment dynamics in a submarine canyon: a case of river-sea interaction. Mar. Geol. 207, 55–81.
Liu, J.T., Hsu, R.T., Hung, J.-J., Chang, Y.-P., Wang, Y.-H., Rendle-Bühring, R.H., Lee, C.-L., Huh, C.-A., Yang, R.J., 2016. From the highest to the deepest: The Gaoping River-Gaoping Submarine Canyon dispersal system Earth-Sci. Rev. 153, 274–300. https://doi.org/10.1016/j.earscirev.2015.10.012.
Lo Iacono, C., Sulli, A., Agate, M., Lo Presti, V., Pepe, F., Catalano, R., 2011. Submarine canyon morphologies in the Gulf of Palermo (Southern Tyrrhenian Sea) and possible implications for geo-hazard. Mar. Geophys. Res. 32, 127–138. https://doi.org/10.1007/s11001-011-9118-0.
Lo Iacono, C., Sulli, A., Agate, M., 2014. Submarine canyons of north-western Sicily (Southern Tyrrhenian Sea): variability in morphology, sedimentary processes and evolution on a tectonically active margin. Deep Sea Res. Part II Top. Stud. Oceanogr. 104, 93–105. https://doi.org/10.1016/j.dsr2.2013.06.018.
Lopez-Fernandez, P., Calafat, A., Sanchez-Vidal, A., Canals, M., Flexas, M.M., Cateura, J., Company, J.B., 2013. Multiple drivers of particle fluxes in the Blanes submarine canyon and southern open slope: results of a year round experiment. Prog. Oceanogr. 118, 95–107. https://doi.org/10.1016/j.pocean.2013.07.029.
Maier, K.L., Johnson, S.Y., Hart, P., 2018. Controls on submarine canyon head evolution: Monterey Canyon, offshore central California. Mar. Geol. 404, 24–40. https://doi.org/10.1016/j.margeo.2018.06.014.
Marchès, E., Mulder, T., Cremer, M., Bonnel, C., Hanquiez, V., Gonthier, E., Lecroart, P., 2007. Contourite drift construction influenced by capture of Mediterranean Outflow Water deep-sea current by the Portimão submarine canyon (Gulf of Cadiz, South Portugal). Mar. Geol. 242, 247–260. https://doi.org/10.1016/j.margeo.2007.03.013.
Mart, Y., 1989. Sediment distribution in Akhziv Canyon off Northern Israel. Geo-Mar. Lett. 9, 77–83.
Martín, J., Palanques, A., Puig, P., 2006. Composition and variability of downward particulate matter fluxes in the Palamós submarine canyon (NW Mediterranean). J. Mar. Syst. 60, 75–97. https://doi.org/10.1016/j.jmarsys.2005.09.010.
Martinsen, O.J., 2005. Deep-water sedimentary systems of Arctic and North Atlantic margins: An introduction. Nor. J. Geol. 85, 261–266.
Martinsen, O.J., Sømme, T.O., Thurmond, J.B., Helland-Hansen, W., Lunt, I., 2010. Source-to-sink systems on passive margins: theory and practice with an example from the Norwegian continental margin. In: Vining, B.A., Pickering, S.C. (Eds.), Petroleum Geology: From Mature Basins to New Frontiers – Proceedings of the 7th Petroleum Geology Conference, 7, pp. 913–920. https://doi.org/10.1144/0070913.
Matos, F.L., Ross, S.W., Huvenne, V.A.I., Davies, J.S., Cunha, M.R., 2018. Canyons pride and prejudice: Exploring the submarine canyon research landscape, a history of geographic and thematic bias. Prog. Oceanogr. 169, 6–19. https://doi.org/10.1016/j.pocean.2018.04.010.
Mauffrey, M.A., Berné, S., Jouet, G., Giresse, P., Gaudin, M., 2015. Sea-level control on the connection between shelf-edge deltas and the Bourcart canyon head (western Mediterranean) during the last glacial/interglacial cycle. Mar. Geol. 370, 1–19. https://doi.org/10.1016/j.margeo.2015.09.010.
Mazières, A., Gillet, H., Castelle, B., Mulder, T., Guyot, C., Garlan, T., Mallet, C., 2014. High-resolution morphobathymetric analysis and evolution of Capbreton submarine canyon head (Southeast Bay of Biscay—French Atlantic Coast) over the last decade using descriptive and numerical modelling. Mar. Geol. 351, 1–12. https://doi.org/10.1016/j.margeo.2014.03.001.
McGregor, B.A., 1983. Submarine canyon and slope processes on the U.S. Atlantic continental margin. In: Open-File Report 83-735. U.S. Geological Survey. https://doi.org/10.3133/ofr83735.
Micallef, A., Mountjoy, J.J., Barnes, P.M., Canals, M., Lastras, G., 2014. Geomorphic response of submarine canyons to tectonic activity: insights from the Cook Strait canyon system, New Zealand. Geosphere. 10 (5), 905–929. https://doi.org/10.1130/GES01040.1.
Michaud, F., Proust, J.N., Collot, J.Y., Lebrun, J.F., Witt, C., Ratzov, G., Pouderoux, H., Martillo, C., Hernández, M.J., Loayza, G., Penafiel, L., Schenini, L., Dano, A., Gonzalez, M., Barba, D., De Min, L., Ponce, G., Urresta, A., Calderon, M., 2015. Quaternary sedimentation and active faulting along the Ecuadorian shelf: preliminary results of the ATACAMES Cruise (2012). Mar. Geophys. Res. 36, 81–98. https://doi.org/10.1007/s11001-014-9231-y.
Milia, A., 2000. The Dohrn Canyon: a response to the eustatic fall and tectonic uplift of the outer shelf along the eastern Tyrrhenian Sea margin. Italy. Geo-Mar. Lett. 20, 101–108.
Milliman, J., Farnsworth, K., 2011. River Discharge to the Coastal Ocean: A Global Synthesis. Cambridge University Press, Cambridge. https://doi.org/10.1017/CBO9780511781247.
Milliman, J.D., Kao, S.-J., 2005. Hyperpycnal discharge of fluvial sediment to the ocean: impact of super-typhoon Herb (1996) on Taiwanese rivers. J. Geol. 113, 503–516.
Mitchell, J.K., Holdgate, G.R., Wallace, M.W., Gallagher, S.J., 2007. Marine geology of the Quaternary Bass Canyon system, southeast Australia: a cool-water carbonate system. Mar. Geol. 237, 71–96. https://doi.org/10.1016/j.margeo.2006.10.037.
Molenaar, A., Moernaut, J., Wiemer, G., Dubois, N., Strasser, M., 2019. Earthquake impact on active margins: tracing surficial remobilization and seismic strengthening in a slope sedimentary sequence. Geophys. Res. Lett. 46, 6015–6023. https://doi.org/10.1029/2019GL082350.
Mondziel, S., Grindlay, N., Mann, P., Escalona, A., Abrams, L., 2010. Morphology, structure, and tectonic evolution of the Mona canyon (northern Mona passage) from multibeam bathymetry, side-scan sonar, and seismic reflection profiles. Tectonics. 29, TC2003. https://doi.org/10.1029/2008TC002441.
Morrison, A.K., Hogg, A. McC, England, M.H., Spence, P., 2020. Warm circumpolar deep water transport toward Antarctica driven by local dense water exports in canyons. Sci. Adv. 6, eaav2516.
Mougenot, D., Boillot, G., Rehault, J.-P., 1983. Prograding shelfbreak types on passive continental margins: some European examples. In: Stanley, D.J., Moore, G.T. (Eds.), The Shelfbreak: Critical Interface on Continental Margins, SEPM Spec. Publ., 33, pp. 25–39.
Mountjoy, J.J., Barnes, P.M., Pettinga, J.R., 2009. Morphostructure and evolution of submarine canyons across an active margin: Cook Strait sector of the Hikurangi Margin, New Zealand. Mar. Geol. 260, 45–68. https://doi.org/10.1016/j.margeo.2009.01.006.
Mountjoy, J.J., Micallef, A., Stevens, C.L., Stirling, M.W., 2014. Holocene sedimentary activity in a non-terrestrially coupled submarine canyon: Cook Strait Canyon system, New Zealand. Deep Sea Res. Part II Top. Stud. Oceanogr. 104, 120–133. https://doi.org/10.1016/j.dsr2.2013.09.001.
Mulder, T., Moran, K., 1995. 1995. Relationship among submarine instabilities, sea level variations, and the presence of an ice sheet on the continental shelf: an example from the Verrill Canyon Area, Scotian Shelf. Paleoceanography. 10 (1), 137–154.
Mulder, T., Syvitski, J.P.M., 1995. Turbidity currents generated at river mouths during exceptional discharges to the World oceans. J. Geol. 103, 285–299.
Mulder, T., Syvitski, J.P.M., Migeon, S., Faugères, J.-C., Savoye, B., 2003. Marine hyperpycnal flows: initiation, behavior and related deposits. A review. Mar. Pet. Geol. 20, 861–882. https://doi.org/10.1016/j.marpetgeo.2003.01.003.
Mulder, T., Lecroart, P., Hanquiez, V., Marches, E., Gonthier, E., Guedes, J.-C., Thiébot, E., Jaaidi, B., Kenyon, N., Voisset, M., Perez, C., Sayago, M., Fuchey, Y., Bujan, S., 2006. Geo-Mar. Lett. 26 (1), 31–41. https://doi.org/10.1007/s00367-005-0013-z.
Mulder, T., Ducassou, E., Gillet, H., Hanquiez, V., Tournadour, E., Combes, J., Eberli, G. P., Kindler, P., Gonthier, E., Conesa, G., Robin, C., Sianipar, R., Reijmer, J.J.G., François, A., 2012a. Canyon morphology on a modern carbonate slope of the

Bahamas: evidence of regional tectonic tilting. Geology. 40 (9), 771–774. https://doi.org/10.1130/G33327.1.
Mulder, T., Zaragosi, S., Garlan, T., Mavel, J., Cremer, M., Sottolichio, A., Sénéchal, N., Schmidt, S., 2012b. Present deep-submarine canyons activity in the Bay of Biscay (NE Atlantic). Mar. Geol. 295-298, 113–127. https://doi.org/10.1016/j.margeo.2011.12.005.
Nelson, C.H., Carlson, P.R., Byrne, J.V., Alpha, T.R., 1970. Development of the Astoria Canyon-Fan physiography and comparison with similar systems. Mar. Geol. 8, 259–291.
Nelson, C.H., Escutia, C., Damuth, J.E., Twichell Jr., D.C., 2011. Interplay of mass-transport and turbidite-system deposits in different active tectonic and passive continental margin settings: external and local controlling factors. In: Shipp, R.C., Weimer, P., Posamentier, H.W. (Eds.), Mass-Transport Deposits in Deepwater Settings, SEPM Spec. Publ., 96, pp. 39–66.
Nittrouer, C.A., Wright, L.D., 1994. Transport of particles across continental shelves. Rev. Geophys. 32 (1), 85–113.
Noda, A., TuZino, T., 2010. Shelf-slope sedimentation during the late Quaternary on the southwestern Kuril forearc margin, northern Japan. Sediment. Geol. 232, 35–51. https://doi.org/10.1016/j.sedgeo.2010.09.008.
Noda, A., TuZino, T., Furukawa, R., Joshima, M., Uchida, J., 2008. Physiographical and sedimentological characteristics of submarine canyons developed upon an active forearc slope: the Kushiro Submarine Canyon, northern Japan. Geol. Soc. Am. Bull. 120 (5/6), 750–767. https://doi.org/10.1130/B26155.1.
Normark, W.R., Piper, D.J.W., Romans, B.W., Covault, J.A., Dartnell, P., Sliter, R.W., 2009. Submarine canyon and fan systems of the California Continental Borderland. In: Lee, H.J., Normark, W.R. (Eds.), Earth Science in the Urban Ocean: The Southern California Continental Borderland, Spec. Pap. Geol. Soc. Am., 454, pp. 141–168. https://doi.org/10.1130/2009.2454(2.7).
Nyberg, B., Helland-Hansen, W., Gawthorpe, R.L., Sandbakken, P., Eide, C.H., Sømme, T., Hadler-Jacobsen, F., Leiknes, S., 2018. Revisiting morphological relationships of modern source-to-sink segments as a first-order approach to scale ancient sedimentary systems. Sediment. Geol. 373, 111–133. https://doi.org/10.1016/j.sedgeo.2018.06.007.
Oiwane, H., Tonai, S., Kiyokawa, S., Nakamura, Y., Suganuma, Y., Tokuyama, H., 2011. Geomorphological development of the Goto Submarine Canyon, northeastern East China Sea. Mar. Geol. 288, 49–60. https://doi.org/10.1016/j.margeo.2011.06.013.
O'Mara, N.A., Dunne, J.P., 2019. Hot spots of carbon and alkalinity cycling in the coastal oceans. Sci. Rep. 9, 4434 https://doi.org/10.1038/s41598-019-41064-w.
Orange, D.L., Anderson, R.S., Breen, N.A., 1994. Regular canyon spacing in the submarine environment: the link between hydrology and geomorphology. GSA Today. 4 (2), 35–39.
Osmundsen, P.T., Redfield, T.F., 2011. Crustal taper and topography at passive continental margins. Terra Nova. 23 (6), 349–361. https://doi.org/10.1111/j.1365-3121.2011.01014.x.
Palanques, A., El Khatab, M., Puig, P., Masqué, P., Sánchez-Cabeza, J.A., Isla, E., 2005. Downward particle fluxes in the Guadiaro submarine canyon depositional system (north-western Alboran Sea), a river flood dominated system. Mar. Geol. 220, 23–40. https://doi.org/10.1016/j.margeo.2005.07.004.
Palanques, A., Martín, J., Puig, P., Guillén, J., Company, J.B., Sardá, F., 2006. Evidence of sediment gravity flows induced by trawling in the Palamós (Fonera) submarine canyon (northwestern Mediterranean). Deep Sea Res. Part I Oceanogr. Res. Pap. 53, 201–214.
Paldor, A., Katz, O., Aharonov, E., Weinstein, Y., Roditi-Elasar, M., Lazar, A., Lazar, B., 2020. Deep submarine groundwater discharge—Evidence from Achziv Submarine Canyon at the exposure of the Judea Group confined aquifer, eastern Mediterranean. J. Geophys. Res. Oceans. 125 https://doi.org/10.1029/2019JC015435 e2019JC015435.
Paull, C.K., Caress, D.W., Lundsten, E., Gwiazda, R., Anderson, K., McGann, M., Conrad, J., Edwards, B., Sumner, E.J., 2013. Anatomy of the La Jolla Submarine Canyon system; offshore southern California. Mar. Geol. 335, 16–34. https://doi.org/10.1016/j.margeo.2012.10.003.
Paull, C.K., Talling, P.J., Maier, K.L., Parsons, D., Xu, J., Caress, D.W., Gwiazda, R., Lundsten, E.M., Anderson, K., Barry, J.P., Chaffey, M., O'Reilly, T., Rosenberger, K. J., Gales, J.A., Kieft, B., McGann, M., Simmons, S.M., McCann, M., Sumner, E.J., Clare, M.A., Cartigny, M.J., 2018. Powerful turbidity currents driven by dense basal layers. Nat. Commun. 9, 4114. https://doi.org/10.1038/s41467-018-06254-6.
Peakall, J., Kane, I.A., Masson, D.G., Keevil, G., McCaffrey, W., Corney, R., 2012. Global (latitudinal) variation in submarine channel sinuosity. Geology. 40 (1), 11–14. https://doi.org/10.1130/G32295.1.
Peters, S.E., Loss, D.P., 2012. Storm and fair-weather wave base: a relevant distinction? Geology. 40 (6), 511–514. https://doi.org/10.1130/G32791.1.
Pico, T., Mitrovica, J.X., Braun, J., Ferrier, K.L., 2018. Glacial isostatic adjustment deflects the path of the ancestral Hudson River. Geology. 46 (7), 591–594. https://doi.org/10.1130/G40221.1.
Pierau, R., Hanebuth, T.J.J., Krastel, S., Henrich, R., 2010. Late Quaternary climatic events and sea-level changes recorded by turbidite activity, Dakar Canyon, NW Africa. Quat. Res. 73, 385–392. https://doi.org/10.1016/j.yqres.2009.07.010.
Pierau, R., Henrich, R., Preiß-Daimler, I., Krastel, S., Geersen, J., 2011. Sediment transport and turbidite architecture in the submarine Dakar Canyon off Senegal, NW-Africa. J. African Earth Sci. 60, 196–208. https://doi.org/10.1016/j.jafrearsci.2011.02.010.
Pierdomenico, M., Martorelli, E., Dominguez-Carrío, C., Gili, J.M., Chiocci, F.L., 2016. Seafloor characterization and benthic megafaunal distribution of an active submarine canyon and surrounding sectors: The case of Gioia Canyon (Southern Tyrrhenian Sea). J. Mar. Syst. 157, 101–117. https://doi.org/10.1016/j.jmarsys.2016.01.005.
Pierdomenico, M., Casalbore, D., Latino Chiocci, F., 2019. Massive benthic litter funnelled to deep sea by flash-flood generated hyperpycnal flows. Sci. Rep. 9, 5330. https://doi.org/10.1038/s41598-019-41816-8.
Piper, D.J.W., Normark, W.R., 2009. Processes that initiate turbidity currents and their influence on turbidites: a marine geology perspective. J. Sediment. Res. 79, 347–362. https://doi.org/10.2110/jsr.2009.046.
Piper, D.J.W., Hiscott, R.N., Normark, W.R., 1999. Outcrop-scale acoustic facies analysis and latest Quaternary development of Hueneme and Dume submarine fans, offshore California. Sedimentology. 46, 47–78.
Pisareva, M.N., Pickart, R.S., Lin, P., Fratantoni, P.S., Weingartner, T.J., 2019. On the nature of wind-forced upwelling in Barrow Canyon. Deep Sea Res. Part II Top. Stud. Oceanogr. 162, 63–78. https://doi.org/10.1016/j.dsr2.2019.02.002.
Popescu, I., Lericolais, G., Panin, N., Normand, A., Dinu, C., Le Drezen, E., 2004. The Danube submarine canyon (Black Sea): morphology and sedimentary processes. Mar. Geol. 206, 249–265. https://doi.org/10.1016/j.margeo.2004.03.003.
Porcile, G., Pittaluga, M.B., Frascati, A., Sequeiros, O.E., 2020. Typhoon-induced megarips as triggers of turbidity currents offshore tropical river deltas. Commun. Earth & Environ. 1, 2. https://doi.org/10.1038/s43247-020-0002-1.
Posamentier, H.W., Erskine, R.D., Mitchum Jr., R.M., 1991. Models for submarine-fan deposition within a sequence-stratigraphic framework. In: Weimer, P., Link, M.H. (Eds.), Seismic facies and sedimentary processes of submarine fans and turbidite systems. Frontiers in Sedimentary Geology, Springer, New York, pp. 127–136.
Post, A.L., Przeslawski, R., Nanson, R., Siwabessy, J., Smith, D., Kirkendale, L.A., Wilson, N.G., 2022. Modern dynamics, morphology and habitats of slope-confined canyons on the northwest Australian margin. Mar. Geol. 444, 106694 https://doi.org/10.1016/j.margeo.2021.106694.
Power, W., Mountjoy, J., Lane, E., Popinet, S., Wang, X., 2016. Assessing landslide-tsunami hazard in submarine canyons, using the Cook Strait Canyon System as an example. J. Tsunami Soc. Int. 35 (3), 145–166.
Pratson, L.F., Coakley, B.J., 1996. A model for the headward erosion of submarine canyons induced by downslope-eroding sediment flows. Geol. Soc. Am. Bull. 108 (2), 225–234.
Pratson, L.F., Ryan, W.B.F., Mountain, G.S., Twichell, D.C., 1994. Submarine canyon initiation by downslope-eroding sediment flows: evidence in late Cenozoic strata on the New Jersey continental slope. Geol. Soc. Am. Bull. 106, 395–412.
Pratson, L.F., Nittrouer, C.A., Wiberg, P.L., Steckler, M.S., Swenson, J.B., Cacchione, D. A., Karson, J.A., Murray, A.B., Wolinsky, M.A., Gerber, T.P., Mullenbach, B.L., Spinelli, G.A., Fulthorpe, C.S., O'Grady, D.B., Parker, G., Driscoll, N.W., Burger, R.L., Paola, C., Orange, D.L., Field, M.E., Friedrichs, C.T., Fedele, J.J., 2007. Seascape evolution on clastic continental shelves and slopes. In: Nittrouer, C.A., Austin, J.A., Field, M.E., Kravitz, J.H., Syvitski, J.P.M., Wiberg, P.L. (Eds.), Continental Margin Sedimentation: From Sediment Transport to Sequence Stratigraphy. Blackwell Publishing, Oxford, pp. 339–380.
Puga-Bernabéu, A., Webster, J.M., Beaman, R.J., Guilbaud, V., 2011. Morphology and controls on the evolution of a mixed carbonate–siliciclastic submarine canyon system, Great Barrier Reef margin, north-eastern Australia. Mar. Geol. 289, 100–116. https://doi.org/10.1016/j.margeo.2011.09.013.
Puig, P., Palanques, A., Guillén, J., García-Ladona., 2000. Deep slope currents and suspended particle fluxes in and around the Foix submarine canyon (NW Mediterranean). 47, 343-366. Deep Sea Res. Part I Oceanogr. Res. Pap. 47, 343–366.
Puig, P., Ogston, A.S., Mullenbach, B.L., Nittrouer, C.A., Parsons, J.D., Sternberg, R.W., 2004. Storm-induced sediment gravity flows at the head of the Eel submarine canyon, northern California margin. J. Geophys. Res. 109, c03019. https://doi.org/10.1029/2003JC001918.
Puig, P., Palanques, A., Martín, J., 2014. Contemporary sediment-transport processes in submarine canyons. Annu. Rev. Mar. Sci. 6, 53–77. https://doi.org/10.1146/annurev-marine-010213-135037.
Puig, P., Durán, R., Muñoz, A., Elvira, E., Guillén, J., 2017. Submarine canyon-head morphologies and inferred sediment transport processes in the Alías-Almanzora canyon system (SW Mediterranean): on the role of the sediment supply. Mar. Geol. 393, 21–34. https://doi.org/10.1016/j.margeo.2017.02.009.
Quartau, R., Madeira, J., Mitchell, N.C., Tempera, F., Silva, P.F., Brandão, F., 2015. The insular shelves of the Faial-Pico Ridge (Azores archipelago): A morphological record of its evolution. Geochem., Geophys. Geosyst. 16, 1401–1420. https://doi.org/10.1002/2015GC005733.
Rahmstorf, S., 2006. Thermohaline Ocean Circulation. In: Elias, S.A. (Ed.), Encyclopedia of Quaternary Sciences. Elsevier, Amsterdam, pp. 739–750.
Rasmussen, E.S., 1994. The relationship between submarine canyon fill and sea-level change: an example from Middle Miocene offshore Gabon, West Africa. Sediment. Geol. 90, 61–75.
Ratzov, G., Sosson, M., Collot, J.-Y., Migeon, S., 2012. Late Quaternary geomorphologic evolution of submarine canyons as a marker of active deformation on convergent margins: The example of the South Colombian margin. Mar. Geol. 315-318, 77–97. https://doi.org/10.1016/j.margeo.2012.05.005.
Restrepo-Correa, I.C., Ojeda, G.Y., 2010. Geologic controls on the morphology of La Aguja submarine canyon. J. South. Am. Earth. Sci. 29, 861–870. https://doi.org/10.1016/j.jsames.2010.07.001.
Ridente, D., Martorelli, E., Bosman, A., Chiocci, F.L., 2014. High-resolution morpho-bathymetric imaging of the Messina Strait (Southern Italy). New insights on the 1908 earthquake and tsunami. Geomorphology. 208, 149–159. https://doi.org/10.1016/j.geomorph.2013.11.021.
Rise, L., Bøe, R., Riis, F., Bellec, V.K., Laberg, J.S., Eidvin, T., Elvenes, S., Thorsnes, T., 2013. Mar. Pet. Geol. 45, 134–149. https://doi.org/10.1016/j.marpetgeo.2013.04.021.
Rodrigues, S., Hernández-Molina, F.J., Fonnesu, M., Miramontes, E., Rebesco, M., Campell, D.C., 2022. A new classification system for mixed (turbidite-contourite)

depositional systems: Examples, conceptual models and diagnostic criteria for modern and ancient records. Earth. Sci. Rev. 230, 104030 https://doi.org/10.1016/j.earscirev.2022.104030.
Rona, P.A., 1970. Submarine canyon origin on upper continental slope off cape hatteras. J. Geol. 78 (2), 141–152.
Rona, P., Guida, V., Scranton, M., Gong, D., Macelloni, L., Pierdomenico, M., Diercks, A.-R., Asper, V., Haag, S., 2015. Hudson submarine canyon head offshore New York and New Jersey: a physical and geochemical investigation. Deep Sea Res. Part II Top. Stud. Oceanogr. 121, 213–232. https://doi.org/10.1016/j.dsr2.2015.07.019.
Saldías, G.S., Allen, S.E., 2020. The influence of a submarine canyon on the circulation and cross-shore exchanges around an upwelling front. J. Phy. Oceanogr. 50, 1677–1698. https://doi.org/10.1175/JPO-D-19-0130.1.
Salmanidou, D.M., Heidarzadeh, M., Guillas, S., 2019. Probabilistic landslide-generated tsunamis in the Indus Canyon, NW Indian Ocean, using statistical emulation. Pure Appl. Geophys. 176, 3099–3114. https://doi.org/10.1007/s00024-019-02187-3.
Santora, J.A., Zeno, R., Dorman, J.G., Sydeman, W.J., 2018. Submarine canyons represent an essential habitat network for krill hotspots in a large marine ecosystem. Sci. Rep. 8, 7579. https://doi.org/10.1038/s41598-018-25742-9.
Schnürle, P., Liu, C.-S., Lallemand, S.E., Reed, D., 1998. Structural controls of the Taitung Canyon in the Huatung Basin East of Taiwan. TAO. 9 (3), 453–472.
Schultz, D.M., Bosart, L.F., Colle, B.A., Davies, H.C., Dearden, C., Keyser, D., Martius, O., Roebber, P.J., Steenburgh, W.J., Volkert, H., Winters, A.C., 2019. Extratropical cyclones: a century of research on meteorology's centerpiece. Meteorol. Monogr. 59, 16.1–16.56. https://doi.org/10.1175/AMSMONOGRAPHS-D-18-0015.1.
Sequeiros, O.E., Pittaluga, M.B., Frascati, A., Pirmez, C., Masson, D.G., Weaver, P., Crosby, A.R., Lazzaro, G., Botter, G., Rimmer, J.G., 2019. How typhoons trigger turbidity currents in submarine canyons. Sci. Rep. 9, 9220. https://doi.org/10.1038/s41598-019-45615-z.
Serra, C.S., Martínez-Loriente, S., Gràcia, E., Urgeles, R., Vizcaino, A., Perea, H., Bartolome, R., Pallàs, R., Lo Iacono, C., Diez, S., Dañobeitia, Terrinha, P., Zitellini, N., 2020. Tectonic evolution, geomorphology and influence of bottom currents along a large submarine canyon system: The São Vicente Canyon (SW Iberian margin). Mar. Geol. 426, 106219 https://doi.org/10.1016/j.margeo.2020.106219.
Sheng, H., Gao, J.H., Kettner, A.J., Shi, Y., Wang, Y.P., Chen, Y., 2019. Variations in fluvial discharge of rivers over the last millennium along the eastern coast of the Liaodong Peninsula, China. J Asian Earth Sci. 184, 103993 https://doi.org/10.1016/j.jseaes.2019.103993.
Shepard, F.P., 1936. The underlying causes of submarine canyons. Proc. Natl. Acad. Sci. U.S.A. 22 (8), 496–502.
Shepard, F.P., 1972. Submarine canyons. Earth-Sci. Rev. 8, 1–12.
Shepard, F.P., 1981. Submarine canyons: multiple causes and long-time persistence. Am Assoc. Pet. Geol. Bull. 65 (6), 1062–1077.
Shumaker, L.E., Jobe, Z.R., Johnstone, S.A., Pettinga, L.A., Cai, D.X., Moody, J.D., 2018. Controls on submarine channel-modifying processes identified through morphometric scaling relationships. Geosphere. 14 (5), 2171–2187. https://doi.org/10.1130/GES01674.1.
Simmons, S.M., Azpiroz-Zabala, M., Cartigny, M.J.B., Clare, M.A., Cooper, C., Parsons, D. R., Pope, E.L., Sumner, E.J., Talling, P.J., 2020. Novel Acoustic Method Provides First Detailed Measurements of Sediment Concentration Structure Within Submarine Turbidity Currents. J. Geophys. Res. Oceans 125 (5). https://doi.org/10.1029/2019JC015904 e2019JC015904.
Simms, A.R., Lisiecki, L., Gebbie, G., Whitehouse, P.L., 2019. Balancing the last glacial maximum (LGM) sea-level budget. Quat. Sci. Rev. 205, 143–153. https://doi.org/10.1016/j.quascirev.2018.12.018.
Smith, M.E., Finnegan, N.J., Mueller, E.R., Best, R.J., 2017. Durable terrestrial bedrock predicts submarine canyon formation. Geophys. Res. Lett. 44, 10332–10340. https://doi.org/10.1002/2017GL075139.
Smith, M.E., Werner, S.H., Buscombe, D., Finnegan, N.J., Sumner, E.J., Mueller, E.R., 2018. Seeking the shore: evidence for active submarine canyon head incision due to coarse sediment supply and focusing of wave energy. Geophys. Res. Lett. 45, 12403–12413. https://doi.org/10.1029/2018GL080396.
Soh, W., Tokuyama, H., 2002. Rejuvenation of submarine canyon associated with ridge subduction, Tenryu Canyon, off Tokai, central Japan. Mar. Geol. 187, 203–220.
Soh, W., Tokuyama, H., Fujioka, K., Kato, S., Taira, A., 1990. Morphology and development of a deep-sea meandering canyon (Boso Canyon) on an active plate margin, Sagami Trough. Japan. Mar. Geol. 91, 227–241.
Sømme, T.O., Helland-Hansen, W., Martinsen, O.J., Thurmond, J.B., 2009. Relationships between morphological and sedimentological parameters in source-to-sink systems: a basis for predicting semi-quantitative characteristics in subsurface systems. Basin Res. 21, 361–387. https://doi.org/10.1111/j.1365-2117.2009.00397.x.
Son, J.-H., Heo, K.-Y., Choi, J.-W., Kwon, J.-I., 2022. Long-lasting upper ocean temperature responses induced by intense typhoons in mid-latitude. Sci. Rep. 12, 5752. https://doi.org/10.1038/s41598-022-09833-2.
Soutter, E.L., Kane, I.A., Hodgson, D.M., Flint, S., 2021. The concavity of submarine canyon longitudinal profiles. J. Geophys. Res. Earth. Surf. 126 https://doi.org/10.1029/2021JF006185 e2021JF006185.
Starke, J., Ehlers, T.A., Schaller, M., 2020. Latitudinal effect of vegetation on erosion rates identified along western South America. Science. 367, 1358–1361. https://doi.org/10.1126/science.aaz0840.
Stein, S., Cloetingh, S., Sleep, N.H., Wortel, R., 1989. Passive margin earthquakes, stresses and rheology. In: Gregerssen, S., Basham, P.W. (Eds.), Earthquakes at North-Atlantic Passive Margins: Neotectonics and Postglacial Rebound, 266. Springer, Dordrecht, pp. 231–259.
Straub, K.M., Mohrig, D., 2009. Constructional canyons built by sheet-like turbidity currents: observations from offshore Brunei Darussalam. J. Sediment. Res. 79, 24–39. https://doi.org/10.2110/jsr.2009.006.
Strozyk, F., Strasser, M., Förster, A., Kopf, A., Huhn, K., 2010. Slope failure repetition in active margin environments: constraints from submarine landslides in the Hellenic fore arc, eastern Mediterranean. J. Geophys. Res. Earth. 115, B08103. https://doi.org/10.1029/2009JB006841.
Su, M., Hsiung, K.-H., Zhang, C., Xie, X., Yu, H.-S., Wang, Z., 2015. The linkage between longitudinal sediment routing systems and basin types in the northern South China Sea in perspective of source-to-sink. J. Asian Earth Sci. 111, 1–13. https://doi.org/10.1016/j.jseaes.2015.05.011.
Su, M., Lin, Z., Wang, C., Kuang, Z., Liang, J., Chen, H., Liu, S., Zhang, B., Luo, K., Huang, S., Wu, Q., 2020. Mar. Geol. 424, 106166 https://doi.org/10.1016/j.margeo.2020.106166.
Susanth, S., Kurian, P.J., Bijesh, C.M., Twinkle, D., Tyagi, A., Rajan, S., 2021. Controls on the evolution of submarine canyons in steep continental slopes: geomorphological insights from Palar Basin, southeastern margin of India. Geo-Mar. Lett. 41, 14. https://doi.org/10.1007/s00367-021-00685-9.
Sweet, M.L., Blum, M.D., 2016. Connections between fluvial to shallow marine environments and submarine canyons: implications for sediment transfer to deep water. J. Sediment. Res. 86, 1147–1162. https://doi.org/10.2110/jsr.2016.64.
Sweet, M.L., Gaillot, G.T., Jouet, G., Rittenour, T.M., Toucanne, S., Marsset, T., Blum, M. D., 2020. Sediment routing from shelf to basin floor in the Quaternary Golo System of Eastern Corsica, France, western Mediterranean Sea. Geol. Soc. Am. Bull. 132 (5/6), 1217–1234. https://doi.org/10.1130/B35181.1.
Sylvester, Z., Pirmez, C., 2017. Latitudinal changes in the morphology of submarine channels: reevaluating the evidence for the influence of the Coriolis force. In: Fraticelli, C.M., Markwick, P.J., Martinius, A.W., Suter, J.W. (Eds.), Latitudinal Controls on Stratigraphic Models and Sedimentary Concepts. SEPM Spec. Publ, p. 108, 11 p. https://doi.org/10.2110/sepmsp.108.02.
Torres Acosta, V., Schildgen, T.F., Clarke, B.A., Scherler, D., Bookhagen, B., Wittmann, H., von Blanckenburg, F., Strecker, M.R., 2015. Lithosphere. 7 (4), 408–420. https://doi.org/10.1130/L402.1.
Tournadour, E., Mulder, T., Borgomano, J., Gillet, H., Chabaud, L., Ducassou, E., Hanquiez, V., Etienne, S., 2017. Submarine canyon morphologies and evolution in modern carbonate settings: The northern slope of Little Bahama Bank. Bahamas. Mar. Geol. 391, 76–97. https://doi.org/10.1016/j.margeo.2017.07.014.
Trumbull, J.V.A., Garrison, L.E., 1973. Geology of a system of submarine canyons South of Puerto Rico. J. Res. U.S. Geol. Survey. 1 (3), 293–299.
Tubau, X., Lastras, G., Canals, M., Micallef, A., Amblas, D., 2013. Significance of the fine drainage pattern for submarine canyon evolution: the Foix Canyon System, Northwestern Mediterranean Sea. Geomorphology. 184, 20–37. https://doi.org/10.1016/j.geomorph.2012.11.007.
Tubau, X., Paull, C.K., Lastras, G., Caress, D.W., Canals, M., Lundsten, E., Anderson, K., Gwiazda, R., Amblas, D., 2015. Submarine canyons of Santa Monica Bay, Southern California: variability in morphology and sedimentary processes. Mar. Geol. 365, 61–79. https://doi.org/10.1016/j.margeo.2015.04.004.
TuZino, T., Noda, A., 2010. Architecture and evolution of the Kushiro submarine canyon in the Kurile Trench forearc slope, North-western Pacific. Sedimentology. 57, 611–641. https://doi.org/10.1111/j.1365-3091.2009.01107.x.
Urías Espinosa, J., Bandy, W.L., Mortera Gutiérrez, C.A., Núñez Cornú, F.J., Mitchell, N. C., 2016. Multibeam bathymetric survey of the Ipala Submarine Canyon, Jalisco, Mexico (20°N): The southern boundary of the Banderas Forearc Block? Tectonophysics. 671, 249–263. https://doi.org/10.1016/j.tecto.2015.12.029.
Valentine, P.C., Uzmann, J.R., Cooper, R.A., 1980. Geology and biology of Oceanographer Submarine Canyon. Mar. Geol. 38, 283–312.
Vardar, D., 2019. Morphological definition of the North İmralı Canyon in the Sea of Marmara. Arab. J. Geosci. 12, 76. https://doi.org/10.1007/s12517-019-4257-8.
Voigt, I., Henrich, R., Preu, B.M., Piola, A.R., Hanebuth, T.J.J., Schwenk, T., Chiessi, C. M., 2013. A submarine canyon as a climate archive – Interaction of the Antarctic Intermediate Water with the Mar del Plata Canyon (Southwest Atlantic). Mar. Geol. 341, 46–57. https://doi.org/10.1016/j.margeo.2013.05.002.
von Rad, U., Tahir, M., 1997. Late Quaternary sedimentation on the outer Indus shelf and slope (Pakistan): evidence from high-resolution seismic data and coring. Mar. Geol. 138, 193–236.
Walsh, J.P., Alexander, C.R., Gerber, T., Orpin, A.R., Sumners, B.W., 2007. Demise of a submarine canyon? Evidence for highstand infilling on the Waipaoa River continental margin. New Zealand. Geophys. Res. Lett. 34 (L20606), 2007. https://doi.org/10.1029/2007GL031142.
Wan, L., Bianchi, V., Hurter, S., Salles, T., Zhang, Z., Yuam, X., 2021. Morphological controls on delta-canyon-fan systems: Insights from stratigraphic forward models. Sedimentology. https://doi.org/10.1111/sed.12930.
Wang, H., Bi, N., Wang, Y., Saito, Y., Yang, Z., 2010. Tide-modulated hyperpycnal flows off the Huanghe (Yellow River) mouth. China. Earth Surf. Process. Landf. 35, 1315–1329. https://doi.org/10.1002/esp.2032.
Wang, X., Zhuo, H., Wang, Y., Mao, P., He, M., Chen, W., Zhou, J., Gao, S., Wang, M., 2018. Controls of contour currents on intra-canyon mixed sedimentary processes: Insights from the Pearl River Canyon, northern South China Sea. Mar. Geol. 406, 193–213. https://doi.org/10.1016/j.margeo.2018.09.016.
Wang, R., Colombera, L., Mountney, N.P., 2019. Geological controls on the geometry of incised-valley fills: insights from a global dataset of late-Quaternary examples. Sedimentology. 66 (6), 2134–2168. https://doi.org/10.1111/sed.12596.
Wang, R., Colombera, L., Mountney, N.P., 2020. Quantitative analysis of the stratigraphic architecture of incised-valley fills: A global comparison of Quaternary systems. Earth Sc. Rev. 200, 102988 https://doi.org/10.1016/j.earscirev.2019.102988.
Wang, X., Cai, F., Sun, Z., Li, Q., Li, A., Sun, Y., Wang, H., Sun, Q., 2022. Tectonic and oceanographic controls on the slope-confined dendritic canyon system in the

Dongsha Slope. South China Sea. Geomorphology. 410, 108285 https://doi.org/10.1016/j.geomorph.2022.108285.
Warratz, G., Schwenk, T., Voigt, I., Bozzano, G., Henrich, R., Violante, R., Lantzsch, H., 2019. Interaction of a deep-sea current with a blind submarine canyon (Mar del Plata Canyon, Argentina). Mar. Geol. 417, 106002 https://doi.org/10.1016/j.margeo.2019.106002.
Waterhouse, A.F., Allen, S.E., Bowie, A.W., 2009. Upwelling flow dynamics in long canyons at low Rossby number. J. Geophys. Res. 114, C05004. https://doi.org/10.1029/2008JC004956.
Wiles, E., Green, A., Watkeys, M., Jokat, W., Krocker, R., 2013. The evolution of the Tugela canyon and submarine fan: a complex interaction between margin erosion and bottom current sweeping, southwest Indian Ocean, South Africa. Mar. Pet. Geol. 44, 60–70. https://doi.org/10.1016/j.marpetgeo.2013.03.012.
Wiles, E., Green, A., Watkeys, M., Botes, R., Jokat, W., 2019. Submarine canyons of NW Madagascar: a first geomorphological insight. Deep Sea Res. Part II Top. Stud. Oceanogr. 161, 5–15. https://doi.org/10.1016/j.dsr2.2018.06.003.
Wilson, L., 1973. Variations in mean annual sediment yield as a function of mean annual precipitation. Am. J. Sci. 273, 335–349.
Wolin, E., Stein, S., Pazzaglia, F., Meltzer, A., Kafka, A., Berti, C., 2012. Mineral, Virginia, earthquake illustrates seismicity of a passive-aggressive margin. Geophys. Res. Lett. 39, L02305. https://doi.org/10.1029/2011GL050310.
Wynn, R.B., Weaver, P.P.E., Masson, D.G., Stow, D.A.V., 2002. Turbidite depositional architecture across three interconnected deep-water basins on the north-west African margin. Sedimentology. 49, 669–695.
Xu, J.P., 2011. Measuring currents in submarine canyons: technological and scientific progress in the past 30 years. Geosphere. 7 (4), 868–876. https://doi.org/10.1130/GES00640.1.
Xu, J.P., Noble, M.A., 2009. Currents in monterey submarine canyon. J. Geophys. Res. 114, C03004. https://doi.org/10.1029/2008JC004992.
Xu, S., Wang, Y., Peng, X., Zou, H., Qiu, Y., Gong, C., Zhuo, H., 2014. Origin of Taiwan Canyon and its effects on deepwater sediment. Sci. China Earth Sci. 57 (11), 2769–2780. https://doi.org/10.1007/s11430-014-4942-0.
Xu, J., Snedden, J.W., Galloway, W.E., Milliken, K.T., Blum, M.D., 2017. Channel-belt scaling relationship and application to early Miocene source-to-sink systems in the Gulf of Mexico basin. Geosphere. 13 (1), 179–200. https://doi.org/10.1130/GES01376.1.
Yin, S., Wang, L., Guo, Y., Zhong, G., 2015. Morphology, sedimentary characteristics, and origin of the Dongsha submarine canyon in the northeastern continental slope of the South China Sea. Sci. China Earth Sci. 58, 971–985. https://doi.org/10.1007/s11430-014-5044-8.
Yin, S., Li, J., Ding, W., Gao, J., Ding, W., Wang, Y., 2018. Migration of the lower North Palawan submarine canyon: characteristics and controls. Int. Geol. Rev. 6287-8), 988–1005. https://doi.org/10.1080/00206814.2018.1522519.
Yin, S., Lin, L., Pope, E.L., Li, J., Ding, W., Wu, Z., Ding, W., Gao, J., Zhao, D., 2019. Continental slope-confined canyons in the Pearl River Mouth Basin in the South China Sea dominated by erosion, 2004–2018. Geomorphology. 344, 60–74. https://doi.org/10.1016/j.geomorph.2019.07.016.
Yu, H.-S., Chang, J.-F., 2002. The Penghu Submarine Canyon off Southwestern Taiwan: morphology and origin. TAO. 13 (4), 547–562.
Yu, H.-S., Chiang, C.-S., 1995. Morphology and origin of the Hongtsai Submarine Canyon West of the Hengchun Peninsula. Taiwan. J. Geol. Soc. China. 38 (1), 81–93.
Yu, H.-S., Lu, J.C., 1995. Development of the shale diapir-controlled Fangliao Canyon on the continental slope off southwestern Taiwan. J. Asian Earth Sci. 11 (4), 265–276.
Yu, H.-S., Liu, C.S., Lee, J.-T., 1992. The Kaohsiung Submarine Canyon: a modern aborted canyon and its morphology and echo character. Acta Oceangr. Taiwan. 28, 19–30.
Zhang, Y., Liu, Z., Zhao, Y., Colin, C., Zhang, X., Wang, M., Zhao, S., Kneller, B., 2018. Long-term in situ observations on typhoon-triggered turbidity currents in the deep sea. Geology. 46 (8), 675–678. https://doi.org/10.1130/G45178.1.
Zhang, F., Zeng, C., Wang, G., Wang, L., Shi, X., 2022. Runoff and sediment yield in relation to precipitation, temperature and glaciers on the Tibetan Plateau. Int. Soil Water Conserv. Res. 10, 197–207. https://doi.org/10.1016/j.iswcr.2021.09.004.
Zhao, L., Ouillon, R., Vowinckel, B., Meiburg, E., Kneller, B., He, Z., 2018. Transition of a hyperpycnal flow into a saline turbidity current due to differential diffusivities. *Geophys. Res. Lett.* 45, 11875–11884. https://doi.org/10.1029/2018GL080150.
Zhong, G., Peng, X., 2021. Transport and accumulation of plastic litter in submarine canyons – The role of gravity flows. Geology. 49, 581–586. https://doi.org/10.1130/G48536.1.

frontiers | Frontiers in Earth Science

ORIGINAL RESEARCH
published: 02 June 2022
doi: 10.3389/feart.2022.836823

Tectonic Influence on the Geomorphology of Submarine Canyons: Implications for Deep-Water Sedimentary Systems

Laura H. Bührig[*†], *Luca Colombera*[‡], *Marco Patacci*[‡], *Nigel P. Mountney*[‡] *and William D. McCaffrey*[‡]

School of Earth and Environment, Institute of Applied Geoscience, University of Leeds, Leeds, United Kingdom

OPEN ACCESS

Edited by:
Rosanna Maniscalco, University of Catania, Italy

Reviewed by:
Daniele Casalbore, Sapienza University of Rome, Italy
Andrea Fildani, Deep Time Institute, United States

***Correspondence:**
Laura H. Bührig
lhbuehrig@gmail.com

[†]*This author has first authorship*

[‡]*These authors have contributed equally to this work and share senior authorship*

Specialty section:
This article was submitted to Quaternary Science, Geomorphology and Paleoenvironment, a section of the journal Frontiers in Earth Science

Received: *15 December 2021*
Accepted: *21 April 2022*
Published: *02 June 2022*

Citation:
Bührig LH, Colombera L, Patacci M, Mountney NP and McCaffrey WD (2022) Tectonic Influence on the Geomorphology of Submarine Canyons: Implications for Deep-Water Sedimentary Systems. Front. Earth Sci. 10:836823. doi: 10.3389/feart.2022.836823

A database-informed metastudy of 294 globally distributed submarine canyons has been conducted with the aim of elucidating the role of tectonic setting on submarine-canyon geomorphology. To achieve this, data from seafloor and subsurface studies derived from 136 peer-reviewed publications and from open-source worldwide bathymetry datasets have been statistically analyzed. In particular, relationships between margin type (active vs. passive) or plate-boundary type (convergent vs. transform vs. complex) have been assessed for key morphometric parameters of submarine canyons, including: streamwise length, maximum and average width and depth, canyon sinuosity, average canyon thalweg gradient, and maximum canyon sidewall steepness. In addition, possible scaling relationships between canyon morphometric parameters and characteristics of the associated terrestrial catchment, continental shelf and slope, and of the broader physiographic setting for canyons along both active and passive margins have been evaluated. The following principal findings arise: 1) overall canyon geomorphology is not markedly different across tectonic settings; 2) slope failure might be more important in passive-margin canyons compared to active ones, possibly due to seismic strengthening in the latter; 3) some aspects of canyon geomorphology scale with attributes of the source-to-sink system and environmental setting, but the strength and sign in scaling might differ between active and passive margins, suggesting that the extent to which canyon geomorphology can be predicted depends on the tectonic setting. Insights from our analysis augment and improve conceptual, experimental and numerical models of slope systems at the scale of individual canyons and source-to-sink systems, and increase our understanding of the complex role played by tectonic setting in shaping deep-water systems.

Keywords: global, quantitative analysis, geometry, scaling relationships, source-to-sink, active margin, passive margin

1 INTRODUCTION

As major conduits for the exchange of sediment, organic matter, nutrients, pollutants and water masses across continental margins (e.g., Fildani, 2017; Santora et al., 2018; Maier et al., 2019; Zhong and Peng, 2021), submarine canyons are important components of deep-water environments and of broader source-to-sink (S2S) systems.

Canyon fills and deep-water fans collectively provide a depositional record of the sediment funneled through a connected canyon, and hold valuable information on the long-term evolution of continental margins (e.g., Normark and Carlson, 2003; Hessler and Fildani, 2019). They are more likely preserved when small in size, accommodated on continental crust, and associated with an active-margin setting (e.g., Normark et al., 1993; Normark and Carlson, 2003); this creates bias in the sedimentary record of deep-water systems. As a consequence, insights from ancient systems only provide a selective view on controls on deep-water systems and have limited applicability to modern environments. Moreover, current knowledge of the role of submarine-canyon geomorphology in shaping the configuration of deep-water systems largely relies on insights from a small number of modelling studies based on datasets from passive-margin settings (e.g., Wan et al., 2021) and a small number of comparative global studies with focus on specific aspects of canyon geomorphology (e.g., Normark and Carlson, 2003; Covault et al., 2011a). Furthermore, despite the importance of canyons for the delivery of sediment to deep-water basins, relationships between the geometry of submarine canyons and linked controls have not yet been fully considered in source-to-sink models; previous analyses were limited to the assessment of scaling relationships between canyon morphometric parameters with attributes of terrestrial catchments and continental shelves and slopes, which demonstrate that canyon geomorphology is partially controlled by the configuration of S2S systems (e.g., Sømme et al., 2009; Casalbore et al., 2011; Nyberg et al., 2018; Bührig et al., in review).

The quantitative investigation of modern canyons can increase our understanding of the importance of tectonic controls on their geomorphology, and in turn of the potential role of canyon geomorphology on sediment dispersal to deep-marine sinks. Insights in such relationships may also be useful for the reconstruction and prediction of geometries of deep-water systems and superordinate S2S systems, where these are only partially preserved in outcrop or are partially resolved in surveys of the seafloor and subsurface.

Submarine-canyon geomorphology is governed by multiple environmental factors including their hydrodynamic regime, oceanographic environment, regional climate, and tectonic setting (e.g., Harris and Whiteway, 2011; Huang et al., 2014; Puig et al., 2014; Bührig et al., in review), which control mechanisms of sediment routing from terrestrial source areas to marine sinks. In active-margin settings, relatively steep gradients and short transport distances across terrestrial catchments and the adjoining continental shelf promote rapid delivery of solids from the terrestrial hinterland to the deep-marine environment (e.g., Bouma and Scott, 2003; Sømme et al., 2009; Gamberi et al., 2015; Nyberg et al., 2018; Pierdomenico et al., 2019). In systems with wide shelves along passive margins, sediment routing to slopes and basin floors is facilitated *via* shelf channels, shelf-edge deltas and submarine canyons that have cut across the shelf to connect to a river (e.g., Sylvester et al., 2012; Rona et al., 2015).

Some global studies indicate that the overall geomorphology of canyons might not differ fundamentally between tectonically active and passive margins (e.g., Harris and Whiteway, 2011; Bührig et al., in review). Yet tectonic activity molds the basin topography *via* its control on the distribution and type of faulting and mass-failures, which have been shown to leave characteristic signatures in the morphology of submarine canyons of active continental margins (e.g., Greene et al., 1991; Chiang and Yu, 2006; Micallef et al., 2014; Corradino et al., 2021; Soutter et al., 2021). Moreover, active margins encompass both convergent and strike-slip tectonic domains, and are characterized by variability in sedimentary basin-morphology and sediment generation, transport and dispersal mechanisms (e.g., Ingersoll, 2012; Ju et al., 2020). Although tectonically active margins host over 50% of submarine canyons globally (Harris and Whiteway, 2011), studies of the genesis and evolution of submarine canyons associated with active margins are relatively underrepresented in the scientific literature (Micallef et al., 2014).

The aim of this study is to increase understanding of the influence of tectonic setting on the geomorphology of submarine canyons. To achieve this, the geomorphology of 294 modern canyons has been investigated in their S2S context, considering parameters describing their physiographic and tectonic setting. Specific research objectives are as follows: 1) to quantitatively characterize the variability in selected canyon geomorphologic parameters across active (both convergent and strike-slip) and passive continental-margin types; 2) to evaluate scaling relationships in canyon morphometry and of individual canyon morphometric parameters with attributes describing their environmental setting, discriminating between active and passive margins; 3) to assess the characteristics of canyon-associated terrestrial catchments, shelves and slopes in active- versus passive-margin settings, and their scaling relationships.

2 DATASET AND METHODS

2.1 Dataset

The dataset used in this study has been extracted from a database of submarine canyons collated by Bührig et al. (in review), who have investigated controlling factors on canyon geomorphology in a global metastudy. For the present study, the database has been extended by defining and characterizing new attributes and by integration with additional data to facilitate the analyses. The data presented in this article are made available in the Supplementary Material.

Data on the geomorphology of the canyons have been extracted from high-resolution seabed and subsurface studies from 136 peer-reviewed publications and from open-source worldwide bathymetry (NOAA National Centers for Environmental Information, 2021; Google Earth). The dataset is organized as 97 individual case studies, with each case

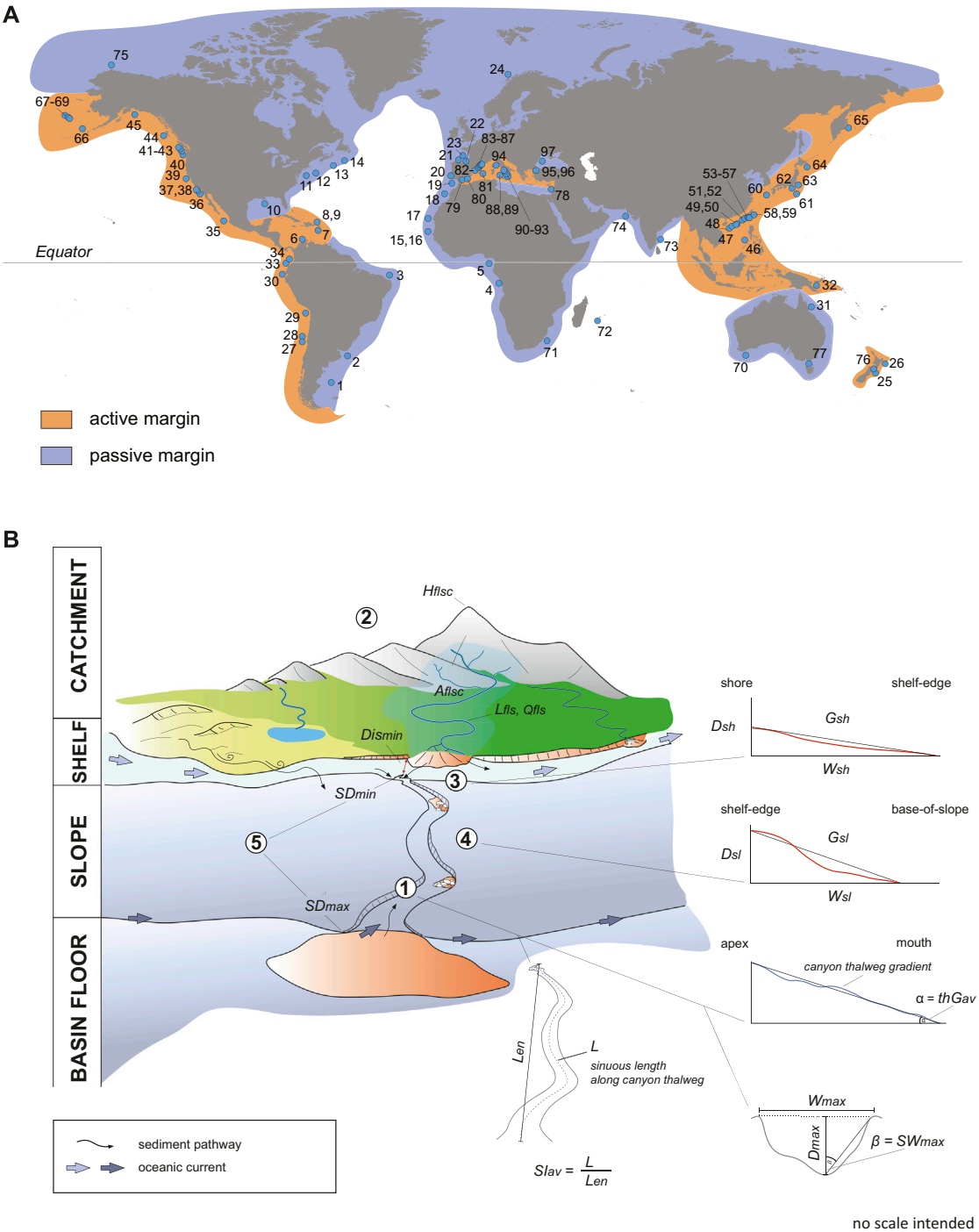

FIGURE 1 | (A) Overview map of the distribution of the 97 case studies and their associated margin-type setting. Continental-margin classification after Harris et al. (2014b) (World map from freevectormaps.com). **(B)** Key parameters investigated in the study: 1) Submarine canyon: L, canyon length along thalweg; L_{en}, canyon length along endpoints; W_{max}, maximum canyon width; D_{max}, maximum canyon depth; SI_{av}, average canyon sinuosity index; thG_{av}, average canyon thalweg gradient; SW_{max}, maximum canyon sidewall steepness. 2) Terrestrial catchment: L_{fls}, fluvial system length; Q_{fls}, average annual fluvial discharge; A_{flsc}, catchment size; H_{flsc}, maximum catchment elevation. 3) Shelf configuration: W_{sh}, shelf width; D_{sh}, shelf-break depth; G_{sh}, average shelf gradient. 4) Slope configuration: W_{sl}, slope width; D_{sl}, slope-break depth; G_{sl}, average slope gradient. 5) Canyon-physiographic setting: SD_{min}, seafloor depth at canyon apex; SD_{max}, seafloor depth at canyon mouth; Dis_{min}, minimum distance of canyon to shoreline.

TABLE 1 | Summary of the 97 case studies considered in this study.

ID	Case study	No. of canyons	Oceanic region	Reference(s)
1	Patagonia canyons, SE Argentina	8	South Atlantic Ocean	Lastras et al. (2011a)
2	Mar del Plata Canyon, E Argentina	1	South Atlantic Ocean	Krastel et al. (2011), Warratz et al. (2019)
3	Potiguar Basin canyons, NE Brazil	14	South Atlantic Ocean	de Almeida et al. (2015)
4	Congo Canyon, W Democratic Republic of Congo	1	South Atlantic Ocean	Babonneau et al. (2002), Ferry et al. (2004)
5	Avon & Mahin canyons, SW Nigeria	2	South Atlantic Ocean	Jimoh et al. (2018)
6	Aguja Canyon, N Colombia	1	North Atlantic Ocean (Caribbean Sea)	Restrepo-Correa and Ojeda (2010)
7	Guayanilla canyon system, S Puerto Rico	4	North Atlantic Ocean (Caribbean Sea)	Trumbull and Garrison (1973)
8	Arecibo & Quebradillas canyons, NW Puerto Rico	2	North Atlantic Ocean	Gardner et al. (1980)
9	Mona Canyon, NW Puerto Rico	1	North Atlantic Ocean	Mondziel et al. (2010)
10	Mississippi Canyon, S United States	1	North Atlantic Ocean (Gulf of Mexico)	Coleman et al. (1982)
11	Hudson Canyon, NE United States	1	North Atlantic Ocean	Rona et al. (2015)
12	Lydonia & Oceanographer canyons, NE United States	2	North Atlantic Ocean	Valentine et al. (1980)
13	Logan Canyon, SE Canada	1	North Atlantic Ocean	Li et al. (2019)
14	SW Grand Banks Slope canyons, SE Canada	3	North Atlantic Ocean	Armitage et al. (2010)
15	Dakar Canyon, W Senegal	1	North Atlantic Ocean	Pierau et al. (2010), Pierau et al. (2011)
16	Cayar Canyon, W Senegal	1	North Atlantic Ocean	Dietz et al. (1968)
17	Timiris Canyon, NW Mauritania	1	North Atlantic Ocean	Krastel et al. (2004), Antobreh and Krastel (2006)
18	Agadir Canyon	1	North Atlantic Ocean	Ercilla et al. (1998), Wynn et al. (2002)
19	Faro & Portimao canyons, SW Portugal	2	North Atlantic Ocean (Gulf of Cadiz)	Mulder et al. (2006)
20	Nazaré, Cascais & Setubal-Lisbon canyons, W Portugal	4	North Atlantic Ocean	Arzola et al. (2008), Lastras et al. (2009), Allin et al. (2016)
21	Aviles Canyon system & Navia canyon, N Spain	5	North Atlantic Ocean (Bay of Biscay)	Goméz-Ballesteros et al. (2014)
22	Capbreton Canyon, SW France	1	North Atlantic Ocean (Bay of Biscay)	Mazières et al. (2014)
23	Audierne & Blackmud canyons, SW France	2	North Atlantic Ocean (Bay of Biscay)	Mulder et al. (2012)
24	Lofoten-Vesterålen canyons (incl. Andøya Canyon), NW Norway	15	North Atlantic Ocean	Rise et al. (2013)
25	Kaikoura Canyon, E New Zealand	1	South Pacific Ocean	Lewis and Barnes (1999)
26	Lachlan Canyon, NE New Zealand	1	South Pacific Ocean	Walsh et al. (2007)
27	Biobío Canyon system, SW Chile	2	South Pacific Ocean	Bernhardt et al. (2015)
28	San Antonio Canyon, NW Chile	1	South Pacific Ocean	Hagen et al. (1996), Laursen and Normark (2002)
29	E Arequipa Basin canyons, NW Chile	3	South Pacific Ocean	Hagen et al. (1994)
30	Guayaquil & Santa Elena canyons, NW Equador	2	South Pacific Ocean	Michaud et al. (2015)
31	N Great Barrier Reef canyons, NE Australia	15	South Pacific Ocean (Coral Sea)	Puga-Bernabéu et al. (2011)
32	Solomon Sea canyons, E & SE Papua New Guinea	8	South Pacific Ocean (Solomon Sea)	Davies et al. (1987), Galewsky and Silver (1997)
33	Esmeraldas Canyon, NW Ecuador	1	North Pacific Ocean	Michaud et al. (2015)
34	Mira & Patia canyons, SW Colombia	2	North Pacific Ocean	Ratzov et al. (2012)
35	Ipala Canyon, W Mexico	1	North Pacific Ocean (South China Sea)	Urías Espinosa et al. (2016)
36	La Jolla, Scripps, Sur, Carmel, Noyo & Eel canyons, SW United States	6	North Pacific Ocean	Le Dantec et al. (2010), Paull et al. (2013)
37	Redondo, Santa Monica & Dume canyons, SW United States	3	North Pacific Ocean	Gardner et al. (2003), Tubau et al. (2015)
38	Mugu & Hueneme canyons, SW United States	2	North Pacific Ocean	Piper et al. (1999)
39	Monterey, Soquel, Año Nuevo & Cabrillo canyons, SW United States	4	North Pacific Ocean	Greene et al. (2002), Xu and Noble (2009)
40	Astoria Canyon, NW United States	1	North Pacific Ocean	Hickey (1997), Bosley et al. (2004)
41	Quinault Canyon, NW United States	1	North Pacific Ocean	Baker and Hickey (1986), Carson et al. (1986)
42	Juan de Fuca Canyon, NW United States	1	North Pacific Ocean (heads in the Juan de Fuca Strait)	Alford and MacCready (2014)
43	Barkley Canyon, SW Canada	1	North Pacific Ocean	Allen et al. (2001)
44	Haida Gwaii canyons, SW Canada	6	North Pacific Ocean	Harris et al. (2014a)
45	Tarr Canyon, NW United States	1	North Pacific Ocean (Gulf of Alaska)	Carlson et al. (1990)
46	North Palawan Canyon, S China	1	North Pacific Ocean (South China Sea)	Yin et al. (2018)
47	Modern Central Canyon, S China	1	North Pacific Ocean (South China Sea)	Su et al. (2015)
48	3 canyons & 4 gullies, S China	3 (4)	North Pacific Ocean (South China Sea)	Chen et al. (2017)
49	Pearl River Mouth Basin canyons, S China	17	North Pacific Ocean (South China Sea)	Han et al. (2010), Su et al. (2020)
50	Zhujiang/Pearl River Canyon, S China	1	North Pacific Ocean (South China Sea)	Han et al. (2010), Ding et al. (2013)
51	Dongsha Canyon, S China	1	North Pacific Ocean (South China Sea)	Yin et al. (2015)
52	Taiwan Canyon, SW Taiwan	1	North Pacific Ocean (South China Sea)	Xu et al. (2014)
53	Hongtsai Canyon, SW Taiwan	1	North Pacific Ocean (South China Sea)	Yu and Chiang (1995)
54	Fangliao Canyon, SW Taiwan	1	North Pacific Ocean (South China Sea)	Yu and Lu (1995), Chiang et al. (2012)
55	Kaoping Canyon, SW Taiwan	1	North Pacific Ocean (South China Sea)	Chiang and Yu (2006), Liu et al. (2016)
56	Kaohsiung Canyon, SW Taiwan	1	North Pacific Ocean (South China Sea)	Yu et al. (1992)

(Continued on following page)

TABLE 1 | (*Continued*) Summary of the 97 case studies considered in this study.

ID	Case study	No. of canyons	Oceanic region	Reference(s)
57	Penghu Canyon, SW Taiwan	1	North Pacific Ocean (South China Sea)	Yu and Chang (2002), Hsiung and Yu (2011), Su et al. (2015)
58	Taitung Canyon, SE Taiwan	1	North Pacific Ocean (Philippine Sea)	Schnürle et al. (1998)
59	Hualien Canyon, SE Taiwan	1	North Pacific Ocean (Philippine Sea)	Hsiung et al. (2017)
60	Goto Canyon, SW Japan	1	North Pacific Ocean (East China Sea)	Oiwane et al. (2011)
61	Aoga Shima Canyon, SE Japan	1	North Pacific Ocean (Philippine Sea)	Klaus and Taylor (1991)
62	Tenryu Canyon, SE Japan	1	North Pacific Ocean	Soh and Tokuyama (2002)
63	Boso Canyon, SE Japan	1	North Pacific Ocean	Soh et al. (1990)
64	Kushiro Canyon, NE Japan	1	North Pacific Ocean	Noda et al. (2008), Noda and Tuzino (2010), Tuzino and Noda (2010)
65	Submarine canyons of Kamchatka, NE Russia	7	North Pacific Ocean	Gnibidenko and Svarichevskaya (1984)
66	Bering Canyon, Bering Sea	1	North Pacific Ocean (Bering Sea)	Carlson and Karl (1988), Harris and Whiteway (2011)
67	Zhemchug, Pervenets & Navarin canyons, Bering Sea	3	North Pacific Ocean (Bering Sea)	Carlson and Karl (1988)
68	Middle canyon system, Bering Sea	2	North Pacific Ocean (Bering Sea)	Carlson and Karl (1984), Carlson and Karl (1988)
69	St. Matthew canyon system, Bering Sea	2	North Pacific Ocean (Bering Sea)	Carlson and Karl (1984), Carlson and Karl (1988)
70	Albany canyons, SW Australia	11	Indian Ocean	Exon et al. (2005)
71	Tugela Canyon, E South Africa	1	Indian Ocean	Wiles et al. (2013)
72	Saint-Etienne & Pierrefonds canyons, SW La Reunion	2	Indian Ocean	Babonneau et al. (2013)
73	Palar Basin canyons, E India	20	Indian Ocean	Susanth et al. (2021)
74	Indus Canyon, SE Pakistan	1	Indian Ocean (Arabian Sea)	Von Rad and Tahir (1997), Salmanidou et al. (2019)
75	Barrow Canyon, NW United States	1	Arctic Ocean	Eittreim et al. (1982), Pisareva et al. (2019)
76	Cook Strait canyons, E New Zealand	9	Cook Strait	Mountjoy et al. (2009), Mountjoy et al. (2014), Micallef et al. (2014)
77	Bass canyon system, SE Australia	10	Bass Strait	Mitchell et al. (2007)
78	Akhviz & Sour canyons, NW Israel	2	Mediterranean Sea	Mart (1989), Almagor (1993)
79	Almeria, Western, Eastern & Guadiaro canyons, S Spain	4	Mediterranean Sea	Alonso and Ercilla (2003), Palanques et al. (2005)
80	Alías-Almanzora canyon system, SE Spain	4	Mediterranean Sea	Puig et al. (2017)
81	Menorca Canyon, SW Menorca, Balearic Islands	1	Mediterranean Sea	Acosta et al. (2002)
82	Orpesa Canyon, NE Spain	1	Mediterranean Sea	Amblas et al. (2012)
83	Foix Canyon system, NE Spain	3	Mediterranean Sea	Puig et al. (2000), Tubau et al. (2013)
84	Blanes Canyon, SE France	1	Mediterranean Sea	Lastras et al. (2011b)
85	Palamós/La Fonera Canyon, NE Spain	1	Mediterranean Sea	Martin et al. (2006), Palanques et al. (2006), Lastras et al. (2011b)
86	Cap de Creus Canyon, NE Spain	1	Mediterranean Sea	Baztan et al. (2005), Lastras et al. (2007), Lastras et al. (2011b)
87	Bourcart Canyon, SE France	1	Mediterranean Sea	Mauffrey et al. (2015)
88	Gulf of Palermo canyons, NW Sicily, Italy	7	Mediterranean Sea	Lo Iacono et al. (2011), Lo Iacono et al. (2014)
89	Gulf of Castellammare canyons, NW Sicily, Italy	2	Mediterranean Sea	Lo Iacono et al. (2014)
90	Messina Canyon, NE Sicily, Italy	1	Mediterranean Sea	Ridente et al. (2014)
91	Petrace, Gioia & Mesima canyons, SW Italy	3	Mediterranean Sea	Pierdomenico et al. (2016), Casalbore et al. (2018)
92	Luna & Infreschi canyons, SW Italy	2	Mediterranean Sea	Budillon et al. (2011)
93	Dohrn Canyon, SW Italy	1	Mediterranean Sea	Milia (2000)
94	Golo system canyons, NE Corsica, France	4 (2)	Mediterranean Sea	Gervais et al. (2004), Gervais et al. (2006)
95	North İmralı Canyon, NW Turkey	1	Sea of Marmara	Vardar (2019)
96	Sarköy & Izmit canyons, NW Turkey	2	Sea of Marmara	Çağatay et al. (2015)
97	Danube/Viteaz Canyon, SE Romania	1	Black Sea	Popescu et al. (2004)

The numbers of canyons reported in brackets indicate channel forms that were termed as "submarine gullies" by the authors of the original data sources.

corresponding to one or several submarine canyons from a geographic location or region, detailed as a self-contained study by the original authors (**Figure 1A**; **Table 1**).

2.2 Methods

Data on individual canyon morphometric parameters, the physiographic setting of the canyon and characteristics of its associated S2S system have been coded in the Deep-Marine Architecture Knowledge Store (DMAKS; Cullis et al., 2019), a relational database storing data on characteristics of deep-water sedimentary systems and their environmental settings (see Cullis et al., 2019).

2.2.1 Canyon Definition

In this study, a submarine canyon is defined as a throughgoing erosional channelform incised into the continental slope; this

TABLE 2 | Overview of the parameters investigated in the study and their definitions.

Study parameter	Definition
Canyon morphometrics	
L (km)**	Streamwise length of the canyon between canyon apex and canyon mouth as measured along the canyon thalweg
W_{max} (km)**	Maximum width of the canyon orthogonal to the canyon length
W_{av} (km)*	Average canyon width over the length of the entire canyon
D_{max} (m)*	Maximum depth of the canyon, i.e., depth of the canyon thalweg relative to the elevation of the canyon margins
D_{av} (m)*	Average canyon thalweg depth over the length of the entire canyon
SI_{av} (–)**	Average canyon sinuosity index, i.e., ratio between the sinuous canyon length measured along its thalweg and the straight distance between canyon apex and canyon mouth
thG_{av} (°)**	Average canyon thalweg gradient, evaluated between canyon apex and canyon mouth
SW_{max} (°)*	Maximum canyon-sidewall steepness, representing the maximum value of gradient between canyon rim and canyon bottom evaluated along the entire length of the canyon
Physiographic setting	
Dis_{min} (km)**	Minimum distance between the canyon and the shoreline
SD_{min} (m)**	Seafloor depth at the top of the canyon
SD_{max} (m)**	Seafloor depth at the mouth of the canyon
Canyon terrestrial catchment	
L_{fls} (km)**	Length of the river with a present-day or previous connection with the canyon, from headwater to river mouth; for canyons connected with several rivers the cumulative length has been considered
Q_{fls} (km^3/yr)*	Mean annual discharge of the fluvial system; for canyons connected with several rivers the cumulative mean annual discharge has been considered
A_{flsc} (km^2)*	Size of the catchment associated with the fluvial system; for canyons connected with several rivers the cumulative catchment area size has been considered
H_{flsc} (m)**	Maximum elevation of the catchment associated with the fluvial system; for canyons connected with several rivers, the elevation of the highest peak in the combined catchments has been considered
Continental shelf	
W_{sh} (km)**	Width of the shelf at the canyon location
G_{sh} (°)**	Average shelf gradient at the canyon location
D_{sh} (m)**	Shelf-break depth at the canyon where the shelf edge is intact and not eroded into by the latter; for shelf edges displaying some degree of variability in their bathymetry the maximum depth of the shelf break has been chosen
Continental slope	
W_{sl} (km)**	Width of the slope at the canyon location
G_{sl} (°)**	Average slope gradient between the shelf break and the slope break
D_{sl} (m)**	Slope-break depth at the canyon
Other parameters	
Continental-margin type	For canyons located along continental margins, including canyons associated with islands: 1) active margin, including transform margins; 2) passive margin [classification after Figure 2 of Harris et al. (2014b)]
Active-margin plate boundary type	Based on the type of plate boundary, active margins are distinguished into 1) convergent, 2) transform, and 3) complex margins. The latter category includes settings which involve more than one plate boundary, and margins which display an additional direction of motion, e.g., convergent margins with a transform component

definition does not therefore consider ancillary criteria that are sometimes used by some authors, such as their origin or minimum size (cf. Harris and Whiteway, 2011). The general definition used herein encompasses smaller channelforms, which are sometimes referred to as "submarine gullies" (e.g., Gervais et al., 2006), "submarine gulleys" (e.g., Normark et al., 2009) or "potential submarine canyons" (e.g., de Almeida et al., 2015), and which might represent forms at the early stage of development of a canyon (e.g., Nelson et al., 2011; Sanchez et al., 2012; Amblas et al., 2017 and references therein). The terms "canyon" and "gully" (or "gulley") are not clearly distinguished in terms of size in the wider literature, and both terms are used when referring to smaller channelforms.

2.2.2 Study Parameters

2.2.2.1 Canyon Morphometrics

Canyon geomorphology has been assessed based on the following morphometric parameters: streamwise canyon length, maximum and average canyon width and depth, canyon sinuosity, average canyon thalweg gradient, and maximum canyon sidewall steepness. Values reported in textual form in the literature sources have only been considered where underpinned by observations on bathymetric surveys with full coverage of the canyon.

2.2.2.2 Physiographic Setting

The physiographic setting of the studied canyons has been characterized by means of attributes describing the bathymetry of the canyon apex and mouth, and the minimum distance of the canyon to the shoreline.

2.2.2.3 Source-to-Sink System Attributes

For canyons with a present or past sediment connection with a fluvial system, the length and average annual water discharge of the river have been recorded, as well as the size and maximum elevation of its catchment. In cases where canyons are linked with several rivers, the sum of the length of the individual rivers, the sum of their mean annual fluvial discharges and catchment areas, and the maximum

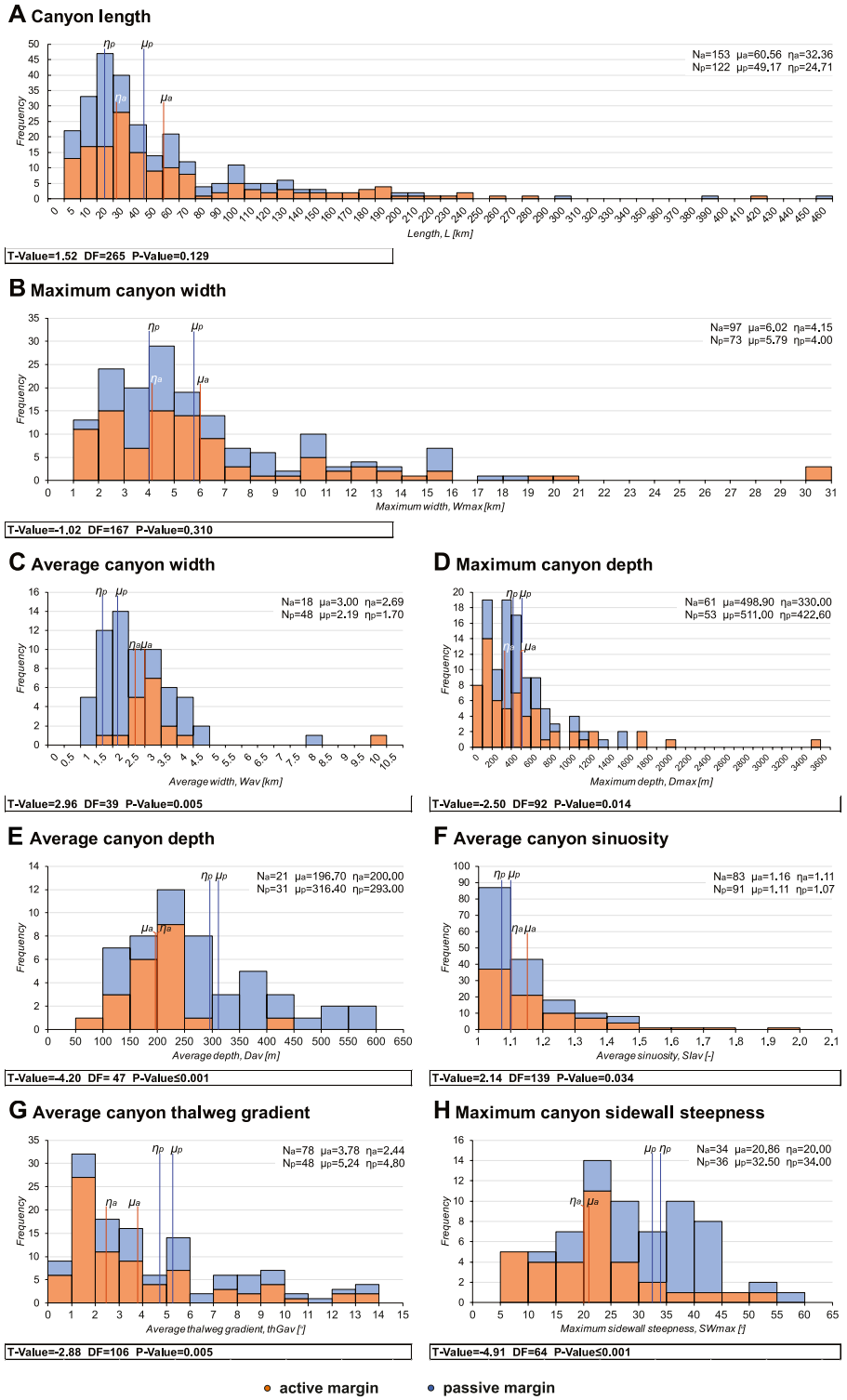

FIGURE 2 | (A–H) Stacked histograms of morphometric values in studied canyons in active (a) vs. passive (p) margins. *N*, number of readings; μ = mean value; η = median value; DF, degrees of freedom.

elevation of the highest peak in the combined catchments have been recorded; this enables comparison with canyons fed by single fluvial systems. The geometric configuration of the continental margin at the canyon location has been characterized in terms of average gradient of shelf and slope, and depth of shelf break and base of slope below present-day mean sea level.

2.2.2.4 Tectonic Setting

Canyon-hosting continental margins have been classified as active or passive following the classification by Harris et al. (2014b) (see **Figure 1A**). Active margins have been further differentiated based on the plate-boundary type with which they are associated, as convergent, transform and complex margins. The term "complex" is used here to refer to settings that involve more than one type of plate boundary and sense of motion (e.g., convergent margins with a transform component).

Definitions of the studied parameters are provided in **Table 2** and illustrated in **Figure 1B**.

2.3 Statistical Analyses

Different types of statistical analyses have been conducted to evaluate scaling relationships within submarine canyons, and between canyon geomorphology and attributes of its environment as a function of the tectonic setting.

1) *Descriptive statistics*: Frequency distributions of the studied canyon morphometric parameters have been summarized in terms of minimum, maximum, mean and median values, to reveal differences across margin types and active-margin plate boundary types.
2) *Hypothesis testing*: Hypothesis testing has been used to evaluate the statistical significance of differences in mean values of canyon morphometric parameters across classes of canyons for different tectonic settings and attributes of the source-to-sink system along active and passive margins. The Welch's two sample t-test (only referred to as "t-test" hereafter) has been used for comparisons between active and passive margins; Welch's ANOVA (only "ANOVA" hereafter) has been used for comparisons between convergent, transform and complex plate-boundary settings of active margins. The chosen tests allow testing of datasets with non-equal variances. For skewed frequency distributions, a logarithmic variable transformation has been conducted prior to the analyses. In these instances, where differences in mean values are reported in the text, they refer to the transformed variables and not the variables themselves. To enable a pairwise comparison of mean values between the three different active-margin settings, ANOVA has been complemented with Games-Howell post-hoc tests. Test statistics (t-test: T-value; ANOVA: F-value; Games-Howell: T-value), p-values and degrees of freedom (DF) are presented for all tests below each individual figure. To limit the number of false positives, the confidence interval has been set at 99%, with results where p-values are ≤0.01 treated as statistically significant.
3) *Correlation analysis*: Correlation analyses have been undertaken to assess pairwise scaling relationships between study parameters. Correlation coefficients quantify the sign and strength of correlation: the Pearson's correlation coefficient (r) describes linear relationships, whereas Spearman's rank correlation coefficient (r_s) describes monotonic relationships. The statistical significance of a correlation between two variables is indicated by p-values. A confidence interval of 99% is employed to indicate significant correlations.

2.4 Limitations of the Study

Data analyses and interpretations are subject to some limitations, including the following:

1) Metastudies might inherit unidentified data errors from the original literature data sources. This has been minimized by exclusively considering data from peer-reviewed publications and government agency sources.
2) Although care has been taken to avoid potential bias in the geographic distribution of case studies (see Matos et al., 2018), some geographic bias may exist for canyons from transform margins specifically, which are only considered for two regions (offshore California, Sea of Marmara), both located at temperate latitudes.
3) Some statistical analyses are based on datasets of limited size. This is the case for data on morphometric parameters of canyons from transform and complex settings, but also for pairs of variables whose correlation is evaluated. Correlation analyses are typically only considered and discussed where the number of observations (N) is equal to or larger than 15, making it explicit when $N < 15$.
4) Some relationships might represent covariance related to factors that were not assessed in this study, but which may influence canyon geomorphology, such as lithology (e.g., Smith et al., 2017) and rate and direction of relative sea-level changes (e.g., Covault et al., 2011b), among others.

3 RESULTS

3.1 Scaling Between Canyon Morphometric Parameters and the Tectonic Setting

3.1.1 Continental-Margin Type

3.1.1.1 Canyon Dimensions and Aspect Ratios

Comparisons of the maximum and average dimensions of submarine canyons along tectonically active and passive margins demonstrate how canyon geometry varies between the two canyon groups.

Canyons in active margins are, on average, longer than those along passive margins—by a factor 1.23—but the difference in mean is not statistically significant. The longest canyon in the study is associated with a passive margin, but lengths of more than 400 km occur in both groups (**Figure 2A**). The deepest and widest canyons are seen on active margins. However, these values of depth and width represent individual outliers; ranges in maximum widths and depths are similar for the vast majority of studied canyons in both margin types, and their mean values are very similar (**Figures 2B,D**).

Canyons in the two margin types exhibit average widths within the same range. On average, mean canyon width is 1.37 times greater in studied active-margin examples, which show a narrower range in values than their counterparts from passive margins (**Figure 2C**). However, average-width data relating to canyons from an active-margin setting are associated with two case studies only, both from the South China Sea, whereas average width data for canyons in passive-margin settings are derived from examples from only three

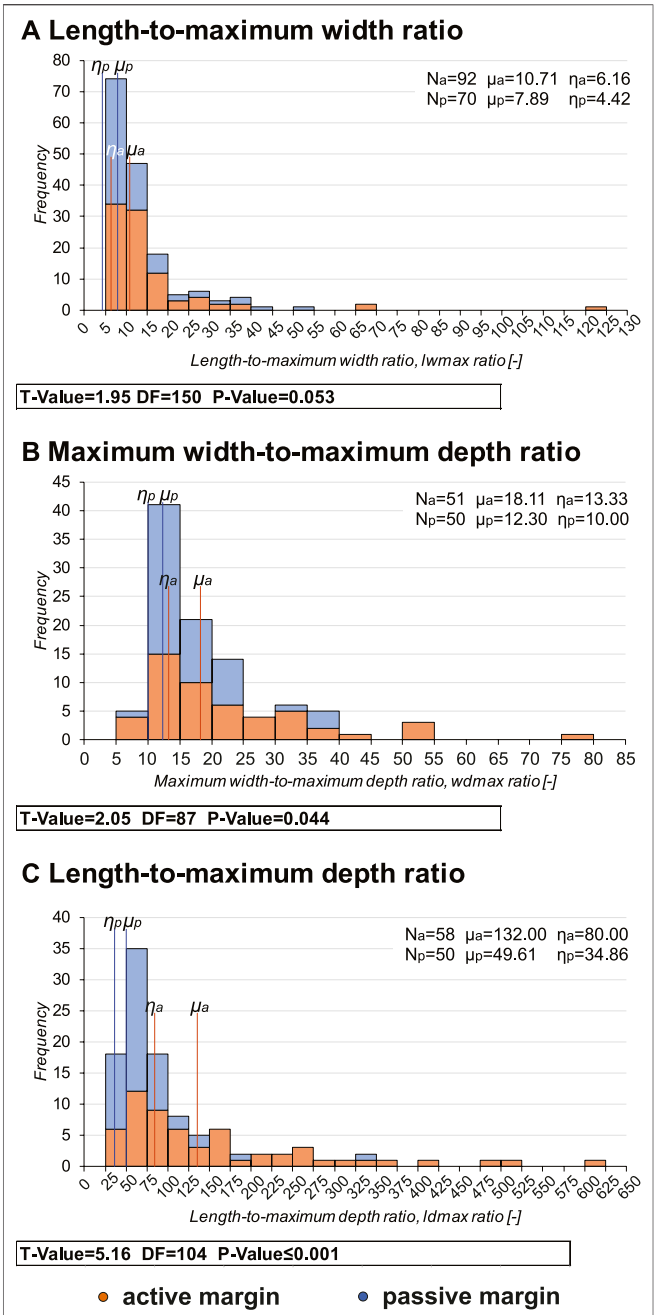

FIGURE 3 | (A–C) Stacked histograms of aspect ratios in studied canyons in active (a) vs. passive (p) margins. *N*, number of readings; μ = mean value; η = median value; DF, degrees of freedom.

geographic regions; therefore, these findings need to be corroborated by additional data in future research. In contrast, the mean average canyon depth is significantly greater for passive margins, by a factor 1.6. The maximum average depth of passive-margin canyons (594 m) is notably higher than that of active-margin ones (400 m) (**Figure 2E**).

Despite a greater range in aspect ratios of maximum canyon dimensions for examples from active margins, the mean values of streamwise length-to-maximum width (lw_{max}) (**Figure 3A**) and maximum width-to-maximum depth (wd_{max}) (**Figure 3B**) ratios are similar for the two margin types. In contrast, a statistically significant difference in the mean value of length-to-maximum depth (ld_{max}) ratio (**Figure 3C**) is seen; this parameter is on average 2.66 times larger for active-margin canyons.

3.1.1.2 Average Canyon Sinuosity, Average Canyon Thalweg Gradient and Maximum Canyon Sidewall Steepness

The studied active-margin canyons show a greater range in average canyon sinuosity than passive-margin ones, but mean average canyon sinuosity is equally low in both margin types, ~1.1 (**Figure 2F**).

The range in average canyon thalweg gradient is very similar for the two margin types; thalwegs are, on average, steeper in the studied passive-margin examples to a statistically significant level (**Figure 2G**).

Canyons situated in passive settings have steeper canyon sidewalls compared to those in tectonically active settings. On average, the maximum sidewall gradient varies significantly between the two canyon groups, and is larger by a factor 1.56 for passive-margin examples (**Figure 2H**).

3.1.2 Active Margin Plate-Boundary Type

3.1.2.1 Canyon Dimensions and Aspect Ratios

Canyons in convergent settings display the highest maximum values of length, maximum width and depth. Yet, on average, maximum canyon dimensions are greater in canyons located at complex plate boundaries (**Figures 4A–C**). The maximum width (**Figure 4B**) and depth (**Figure 4C**) of canyons from this type of setting are on average significantly higher than that of canyons in convergent settings, by a factor of 1.77 and 1.29, respectively.

The length (**Figure 4A**) and maximum width (**Figure 4B**) of canyons along transform plate boundaries are, on average, lower than those of canyons in the other two settings. The mean canyon length does not vary significantly across the three active-margin settings (**Figure 4A**). Instead, the mean maximum canyon width differs at a statistically significant level between transform and complex settings (**Figure 4B**), but this variable could only be constrained for twelve transform-setting canyons. Although data on maximum canyon depth for canyons along transform plate boundaries could only be derived for four examples, the data demonstrate that the depth range of canyons in such settings is similar to that of canyons in convergent settings, and larger than that of canyons from complex settings (**Figure 4C**).

Mean aspect ratios are similar across all three active-margin settings, but relatively few data are available for canyons in transform- and complex-margin settings. Aspect ratios based on maximum canyon dimensions for canyons in convergent settings are highly variable and display the greatest range in values (**Figures 4G–I**).

3.1.2.2 Average Canyon Sinuosity, the Average Canyon Thalweg Gradient and Maximum Canyon Sidewall Steepness

Frequency distributions of average canyon sinuosity for convergent, transform and complex plate boundaries exhibit similar mean and median values. Based on results of Welch's

A Canyon length

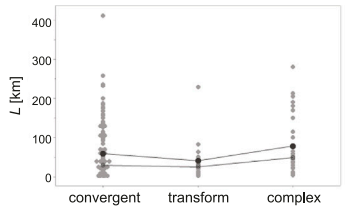

	N	min	mean	StDev	median	max
conv.	108	2.00	59.00	68.47	29.09	411.00
trans.	17	2.50	40.90	52.80	25.10	229.70
comp.	28	3.90	78.50	78.20	48.90	279.70

Welch's ANOVA
F-Value= 1.01 DF Num=2 DF Den=36.7576 P-Value=0.373

Games-Howell

	Dmean	SE	T-Value	adjusted P-Value
conv. vs trans.	-0.100	0.119	-0.84	0.682
conv. vs comp.	0.118	0.119	1.00	0.584
comp. vs trans.	0.218	0.152	1.43	0.335

B Maximum canyon width

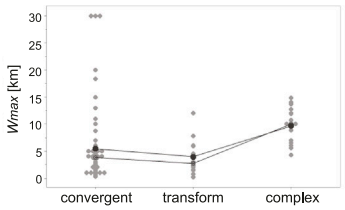

	N	min	mean	StDev	median	max
conv.	67	0.25	5.42	6.60	3.83	30.00
trans.	12	0.15	3.98	3.46	2.73	12.00
comp.	18	4.30	9.62	3.21	10.00	14.80

Welch's ANOVA
F-Value=25.72 DF Num=2 DF Den=27.0868 P-Value≤0.001

Games-Howell

	Dmean	SE	T-Value	adjusted P-Value
conv. vs trans.	-0.124	0.158	-0.78	0.718
conv. vs comp.	0.4356	0.0647	6.73	≤0.001
comp. vs trans.	0.560	0.154	3.64	0.008

C Maximum canyon depth

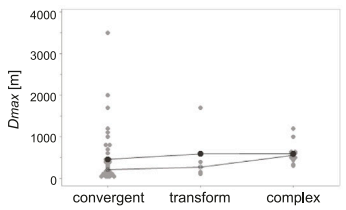

	N	min	mean	StDev	median	max
conv.	43	35.00	459.60	647.90	210.00	3500.00
trans.	4	110.00	588.00	752.00	270.00	1700.00
comp.	15	310.00	594.30	240.50	555.00	1200.00

Welch's ANOVA
F-Value=8.50 DF Num=2 DF Den=7.84612 P-Value=0.011

convergent transform complex

Games-Howell

	Dmean	SE	T-Value	adjusted P-Value
conv. vs trans.	0.133	0.278	0.48	0.886
conv. vs comp.	0.3686	0.0865	4.26	≤0.001
comp. vs trans.	0.236	0.271	0.87	0.690

D Average canyon sinuosity

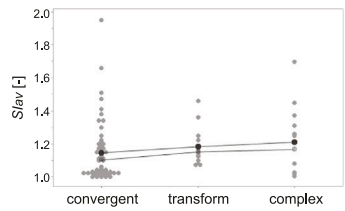

	N	min	mean	StDev	median	max
conv.	58	1.00	1.14	0.18	1.10	1.95
trans.	13	1.07	1.18	0.12	1.15	1.46
comp.	12	1.00	1.21	0.22	1.17	1.70

Welch's ANOVA
F-Value=0.94 DF Num=2 DF Den=22.2231 P-Value=0.405

Games-Howell

	Dmean	SE	T-Value	adjusted P-Value
conv. vs trans.	0.0163	0.0139	1.18	0.477
conv. vs comp.	0.0222	0.0231	0.96	0.613
comp. vs trans.	0.0059	0.0245	0.24	0.969

E Average canyon thalweg gradient

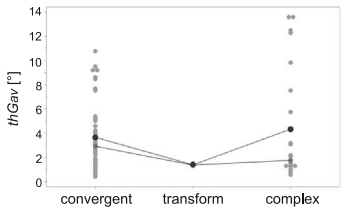

	N	min	mean	StDev	median	max
conv.	52	0.40	3.67	2.63	2.93	10.77
trans.	3	1.30	1.39	0.10	1.38	1.50
comp.	23	0.60	4.34	4.65	1.77	13.60

Welch's ANOVA
F-Value=21.66 DF Num=2 DF Den=37.9576 P-Value≤0.001

Games-Howell

	Dmean	SE	T-Value	adjusted P-Value
conv. vs trans.	-0.3078	0.0498	-6.18	≤0.001
conv. vs comp.	-0.039	0.103	-0.38	0.924
comp. vs trans.	0.2686	0.0943	2.85	0.024

F Maximum canyon sidewall steepness

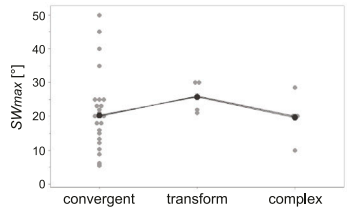

	N	min	mean	StDev	median	max
conv.	26	5.40	20.30	11.75	20.00	50.00
trans.	4	21.00	25.75	4.92	26.00	30.00
comp.	4	10.00	19.63	7.56	20.00	28.50

Welch's ANOVA
F-Value=1.47 DF Num=2 DF Den=7.23013 P-Value=0.291

Games-Howell

	Dmean	SE	T-Value	adjusted P-Value
conv. vs trans.	5.45	3.37	1.62	0.285
conv. vs comp.	-0.68	4.43	-0.15	0.987
comp. vs trans.	-6.12	4.51	-1.36	0.426

G Length-to-maximum width ratio

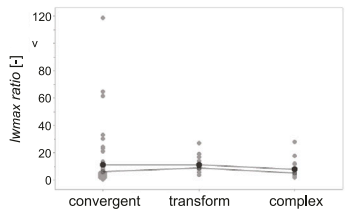

	N	min	mean	StDev	median	max
conv.	64	0.46	11.31	18.06	6.20	118.88
trans.	12	3.88	11.32	6.92	8.94	27.11
comp.	16	1.91	7.85	7.04	5.13	27.97

Welch's ANOVA
F-Value=2.33 DF Num=2 DF Den=28.0361 P-Value=0.116

Games-Howell

	Dmean	SE	T-Value	adjusted P-Value
conv. vs trans.	0.1683	0.0904	1.86	0.172
conv. vs comp.	-0.0525	0.0991	-0.53	0.857
comp. vs trans.	-0.221	0.112	-1.97	0.140

H Maximum width-to-maximum depth ratio

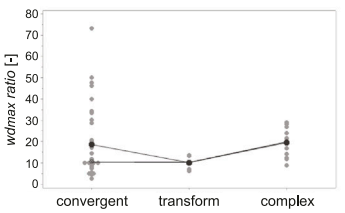

	N	min	mean	StDev	median	max
conv.	34	2.45	18.54	16.71	10.33	73.33
trans.	4	6.15	10.05	3.99	10.20	13.64
comp.	13	8.75	19.48	6.49	19.83	28.86

Welch's ANOVA
F-Value=4.53 DF Num=2 DF Den=9.57062 P-Value=0.041

Games-Howell

	Dmean	SE	T-Value	adjusted P-Value
conv. vs trans.	-0.145	0.110	-1.32	0.434
conv. vs comp.	0.1451	0.0763	1.90	0.150
comp. vs trans.	0.290	0.101	2.87	0.083

I Length-to-maximum depth ratio

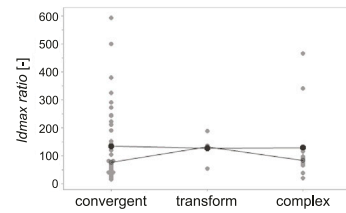

	N	min	mean	StDev	median	max
conv.	42	14.30	133.80	134.4	75.70	593.30
trans.	4	52.60	126.00	56.10	131.20	188.90
comp.	12	18.90	127.70	133.80	82.40	466.10

Welch's ANOVA
F-Value=0.47 DF Num=2 DF Den=9.60212 P-Value=0.641

Games-Howell

	Dmean	SE	T-Value	adjusted P-Value
conv. vs trans.	0.136	0.137	1.00	0.609
conv. vs comp.	0.026	0.126	0.21	0.977
comp. vs trans.	-0.110	0.160	-0.69	0.776

FIGURE 4 | (A–I) Dot plots of morphometric values and aspect ratios for the studied canyons from active margins, classified on plate-boundary type. *N*, number of readings; min, minimum value; mean, mean value; SD, standard deviation; median, median value; max, maximum value. Results of Welch's ANOVA test: DF Num, degrees of freedom numerator; DF Den, degrees of freedom denominator. Games-Howell *post hoc* test: D_{mean}, difference of means; SE, standard error.

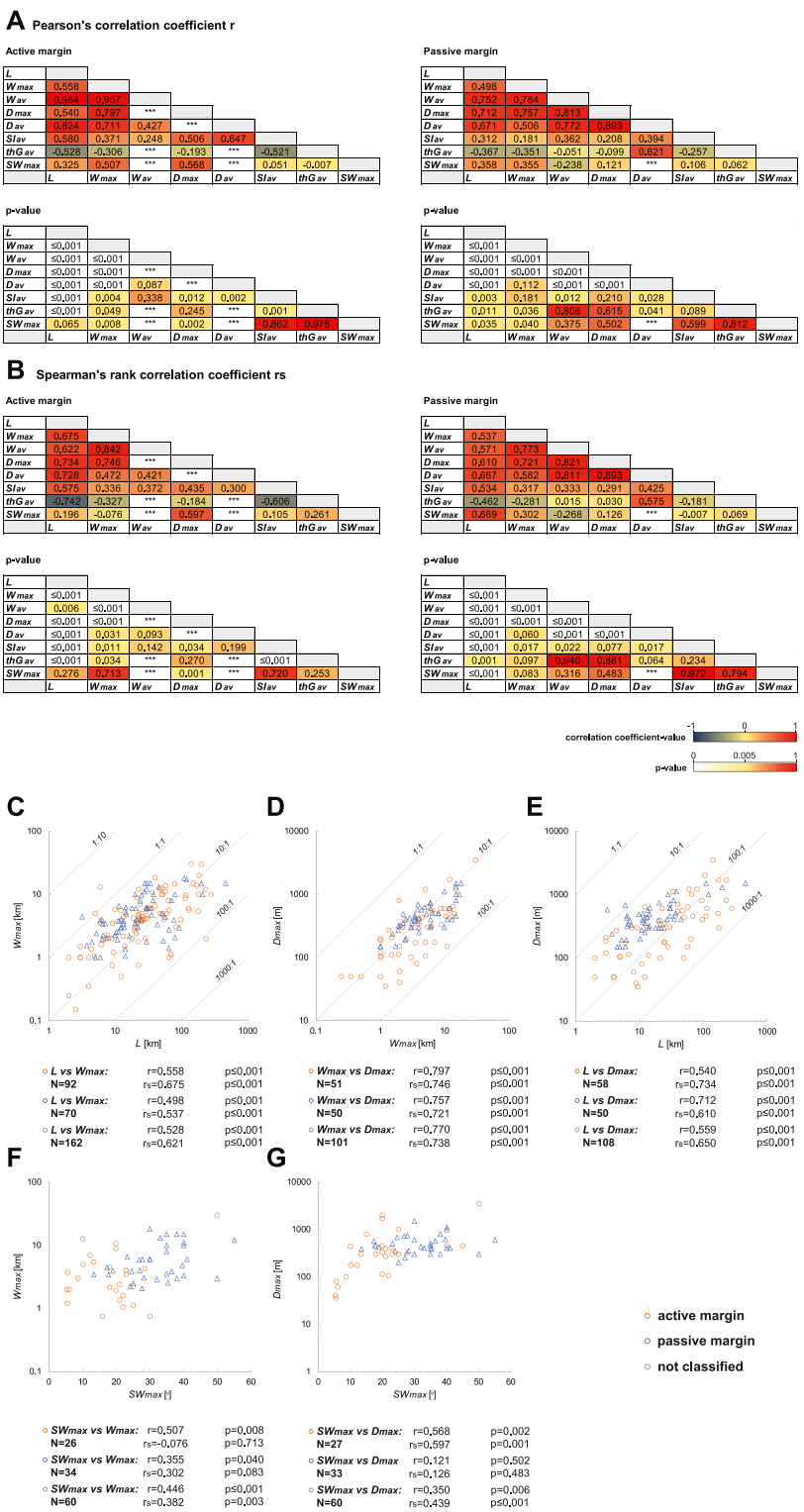

FIGURE 5 | (A–G) Results of the correlation analyses of canyon morphometric parameters with attributes of the physiographic setting at the canyon in active vs. passive margins. **(A,B)** Overview of results presented as heat maps. **(C–G)** Scatter plots of results. *L*, canyon length; W_{max}, maximum canyon width; W_{av}, average canyon width; D_{max}, maximum canyon depth; D_{av}, average canyon depth; SI_{av}, average canyon sinuosity index; thG_{av}, average canyon thalweg gradient; SW_{max}, maximum canyon sidewall steepness; *N*, number of readings; *r*, Pearson's correlation coefficient; r_s, Spearman's rank correlation coefficient.

ANOVA and Games-Howell post-hoc tests, no significant differences are seen for average values across the different active-plate boundary types (**Figure 4D**).

Submarine canyons in complex settings exhibit a greater range in values of the average canyon thalweg gradient than those in convergent margins, but on average, the overall thalweg gradient is only 1.18 times steeper, and not significantly different (**Figure 4E**).

Canyons in convergent settings display a great range in maximum sidewall steepness, which is on average 20.3°. There exists insufficient data on margin steepness in canyons located in transform and complex settings to conduct meaningful analyses on these, but the data available demonstrate that canyons in these settings can reach gradients of 30.0° and 28.5°, respectively; these values are higher than those recorded in the majority of convergent-margin canyons (**Figure 4F**).

3.2 Scaling in Submarine Canyons in Active Versus Passive Margins

Results of the correlation analyses of canyon morphometric parameters with each other are presented as heat maps (**Figures 5A,B**). Additionally, correlations between maximum canyon dimensions and their aspect ratios (**Figures 5C–E**) and between maximum canyon sidewall steepness and maximum width (**Figure 5F**) and depth (**Figure 5G**) are also displayed as scatter plots.

3.2.1 Canyon Dimensions

Moderate and statistically significant scaling between maximum canyon dimensions is seen for submarine canyons along both active and passive margins (**Figures 5A–E**).

3.2.2 Maximum Canyon Sidewall Steepness vs. Maximum Canyon Width and Depth

A moderate linear correlation is seen between maximum sidewall steepness and maximum width in active-margin canyons, whereas the same parameters are weakly correlated in passive-margin canyons (**Figure 5F**).

Correlations of maximum sidewall steepness with maximum depth (**Figure 5G**) are weak and not significant for passive-margin examples. In contrast, maximum sidewall steepness displays moderate correlations with maximum depth in canyons along active margins, which are statistically significant.

3.3 Scaling Between Canyon Morphometric Parameters and Characteristics of Their Physiographic Setting in Active Versus Passive Margins

Results of the correlation analyses of canyon morphometric apex (**Section 3.3.1**) and mouth, and with the distance of the canyon to the nearest shoreline (**Section 3.3.2**) are presented as heat maps (**Figures 6A,B**). In addition, discussed scaling relationships are presented as scatter plots (**Figures 7A–H**).

3.3.1 Seafloor Depth at the Canyon Apex

In canyons from active and passive margins, the seafloor depth at the canyon apex correlates weakly with canyon length, maximum canyon width and average canyon thalweg gradient (**Figures 6A,B**). For average canyon width and seafloor depth at the canyon apex, moderate to modest negative correlations are seen in both active and passive margins, which are only significant for the latter (**Figure 7A**). A negative and significant moderate correlation between seafloor depth and maximum canyon depth is seen for passive-margin canyons; the corresponding relationship is instead weak for canyons along active margins (**Figure 7B**). Average canyon depth displays negative and modest correlations with the seafloor depth at the canyon apex along passive margins, but these are not significant for the chosen alpha value (**Figure 7C**).

Moderate inverse relationships between seafloor depth and both average canyon sinuosity (**Figure 7D**) and maximum canyon sidewall steepness (**Figure 7E**) exist in active margins, which are statistically significant. For canyons in passive margins, the correlations with apex depth are weak for both morphometric parameters (**Figures 7D,E**).

For the investigated aspect ratios, significant and moderate positive scaling exists with wd_{max} ratios of canyons in active settings (**Figure 7F**). The remaining correlations in both margin types are all weak (**Figures 6A,B**).

3.3.2 Minimum Canyon-Shoreline Distance

Correlations between the shortest distance of the canyon to the shoreline with canyon morphometric parameters are weak for all maximum and average canyon dimensions for canyons from both margin types. Relationships with average canyon width in active-margin canyons were not assessed due to insufficient data for the statistical analyses (**Figures 6A,B**).

Average canyon sinuosity demonstrates modest negative scaling with the minimum distance of the canyon to the shoreline in active margins, whereas weak positive scaling is seen for passive margins; correlations are statistically significant for both margins (**Figures 6A,B**).

Inverse scaling between the minimum canyon-shoreline distance and the average canyon thalweg gradient is seen in canyons from both margin types. The correlation is weak for examples from active margins, whereas modest, linear negative correlation is seen for passive-margin settings (**Figures 6A,B**).

With decreasing distance of the canyon to the coastline, the maximum sidewall steepness in active-margin canyons tends to increase, but the strength of this correlation is moderate to modest. Correlation between the two parameters is very weak in examples from passive margins (**Figure 7G**).

Correlations of aspect ratios with minimum distance to the shoreline are weak for maximum canyon dimensions across both margin types (**Figures 6A,B**), with the exception of significant moderate and modest scaling displayed for wd_{max} ratios in active-margin canyons (**Figure 7H**).

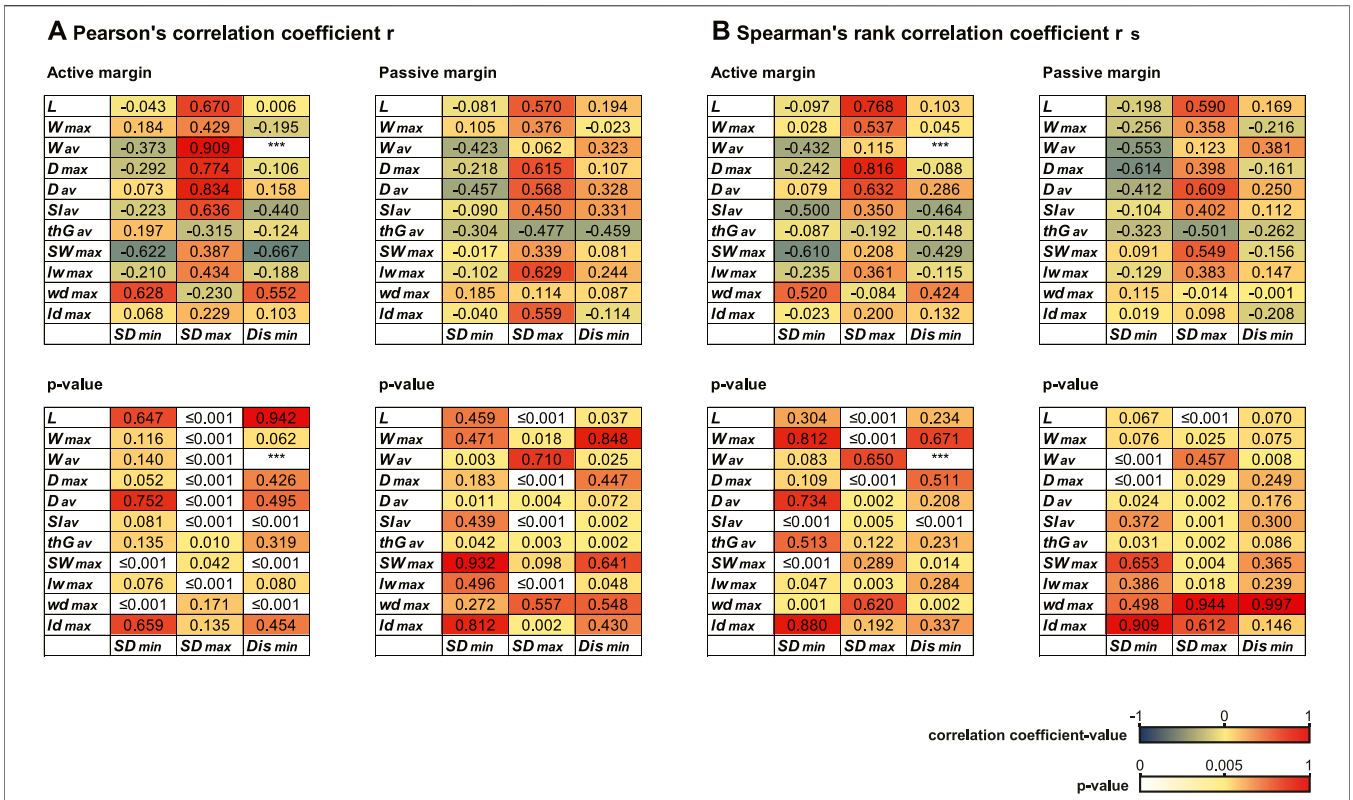

FIGURE 6 | (A,B) Results of the correlation analyses of canyon morphometric parameters and aspect ratios with parameters of the physiographic setting at the canyon in active vs. passive margins presented as heat maps. *L*, canyon length; W_{max}, maximum canyon width; W_{av}, average canyon width; D_{max}, maximum canyon depth; D_{av}, average canyon depth; SI_{av}, average canyon sinuosity index; thG_{av}, average canyon thalweg gradient; SW_{max}, maximum canyon sidewall steepness; lw_{max}, length-to-maximum width ratio; wd_{max}, maximum width-to-maximum depth ratio; ld_{max}, length-to-maximum depth ratio; SD_{min}, seafloor depth at canyon apex; SD_{max}, seafloor depth at canyon mouth; Dis_{min}, minimum distance between canyon and shoreline; *** = correlations not reported due to small dataset size.

3.4 Scaling Between Canyon Morphometry and Characteristics of the Source-to-Sink System

Scaling relationships between canyon morphometric parameters and attributes of the terrestrial catchment (**Figures 8A–L**), shelf (**Figures 8M–Q**, **9A**) and slope (**Figures 8R**, **9B**) have been assessed.

3.4.1 Terrestrial Catchment (Fluvial System Length, Average Annual Fluvial Water Discharge, Catchment Size, Maximum Catchment Elevation)

For the studied canyons with a present and/or past sediment connection with one or several fluvial systems, scaling of canyon length and average canyon sinuosity with attributes of the terrestrial catchment in active and passive margins can be quantified. Statistical analyses on maximum canyon width are limited to active-margin settings in view of data coverage.

3.4.1.1 Fluvial System Length

Correlations of river length with canyon length are weak and not significant for canyons in passive margins. Along active margins, positive and moderate scaling of canyon length with fluvial system length is demonstrated, which is statistically significant (**Figure 8A**). In contrast, maximum width correlates weakly with river length in canyons along active margins, but relatively strongly for canyons located in passive-margin settings. However, findings for the latter group are based on thirteen observations only (**Figure 8E**). For average canyon sinuosity, the correlations are weak and not significant for any margin type (**Figure 8I**).

3.4.1.2 Average Annual Fluvial Water Discharge

The average annual water discharge of the fluvial system displays positive, moderate monotonic correlations with canyon length in canyons of both margin types, as well as overall in the entire dataset; these relationships are statistically significant (**Figure 8B**). Correlations of average annual fluvial discharge and maximum width are weak in active-margin canyons (**Figure 8F**). Positive and monotonic correlations of average canyon sinuosity with this catchment attribute exist for active and passive margins, but these are respectively moderate and weak, and neither is statistically significant (**Figure 8J**).

3.4.1.3 Catchment Size

Scaling of canyon length with catchment size is weak for canyons from passive margins (**Figure 8C**). Moderate, positive monotonic

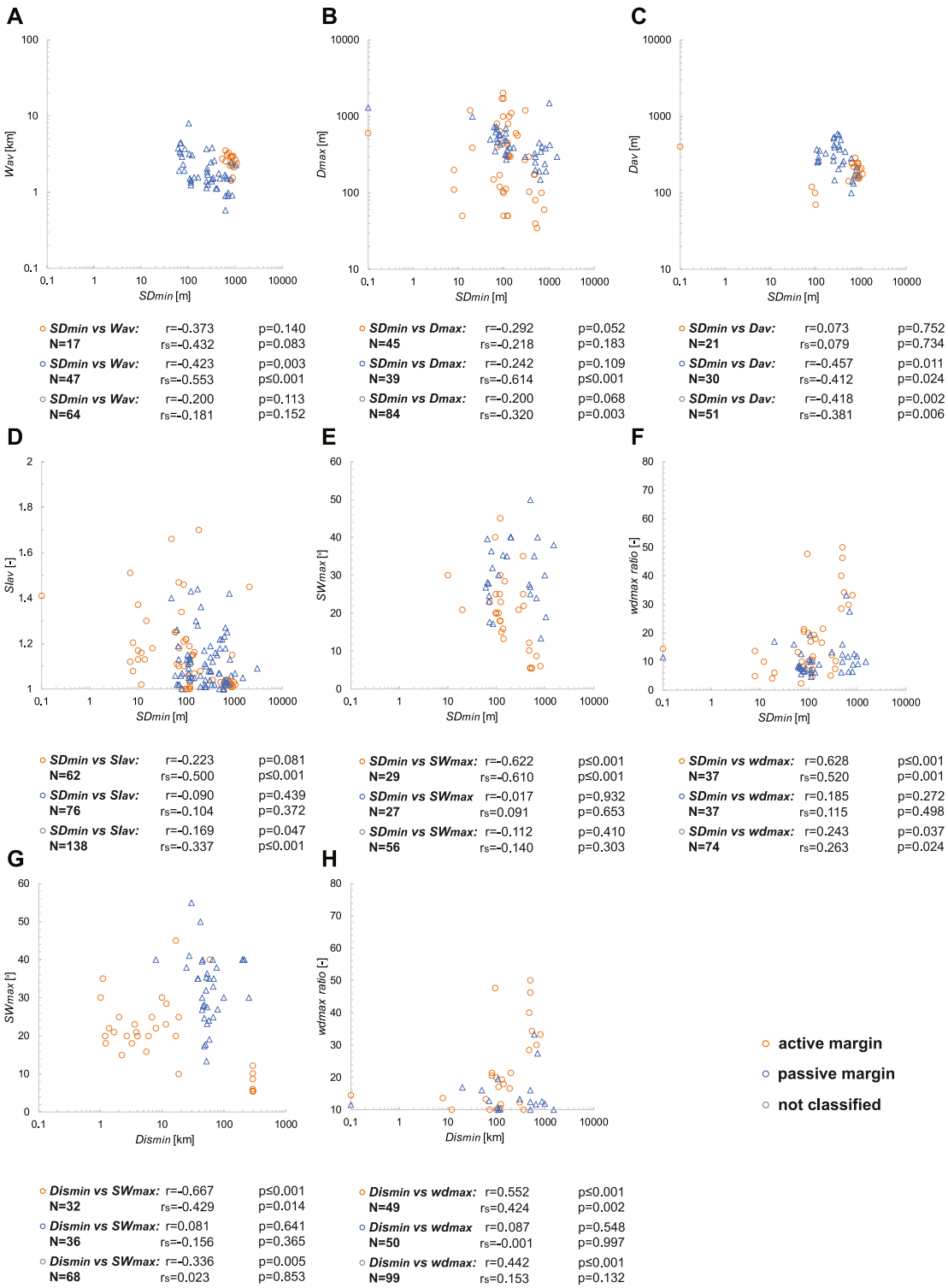

FIGURE 7 | (A–H) Scatterplots of attributes of the canyon-physiographic setting with canyon morphometric parameters for submarine canyons of the study in active vs. passive margins. W_{av}, average canyon width; D_{max}, maximum canyon depth; D_{av}, average canyon depth; Sl_{av}, average canyon sinuosity index; SW_{max}, maximum canyon sidewall steepness; wd_{max} ratio, maximum width-to-maximum depth ratio; SD_{min}, minimum water depth at the canyon apex; Dis_{min}, minimum canyon distance to the shoreline; N, number of readings; r, Pearson's correlation coefficient; r_s, Spearman's rank correlation coefficient.

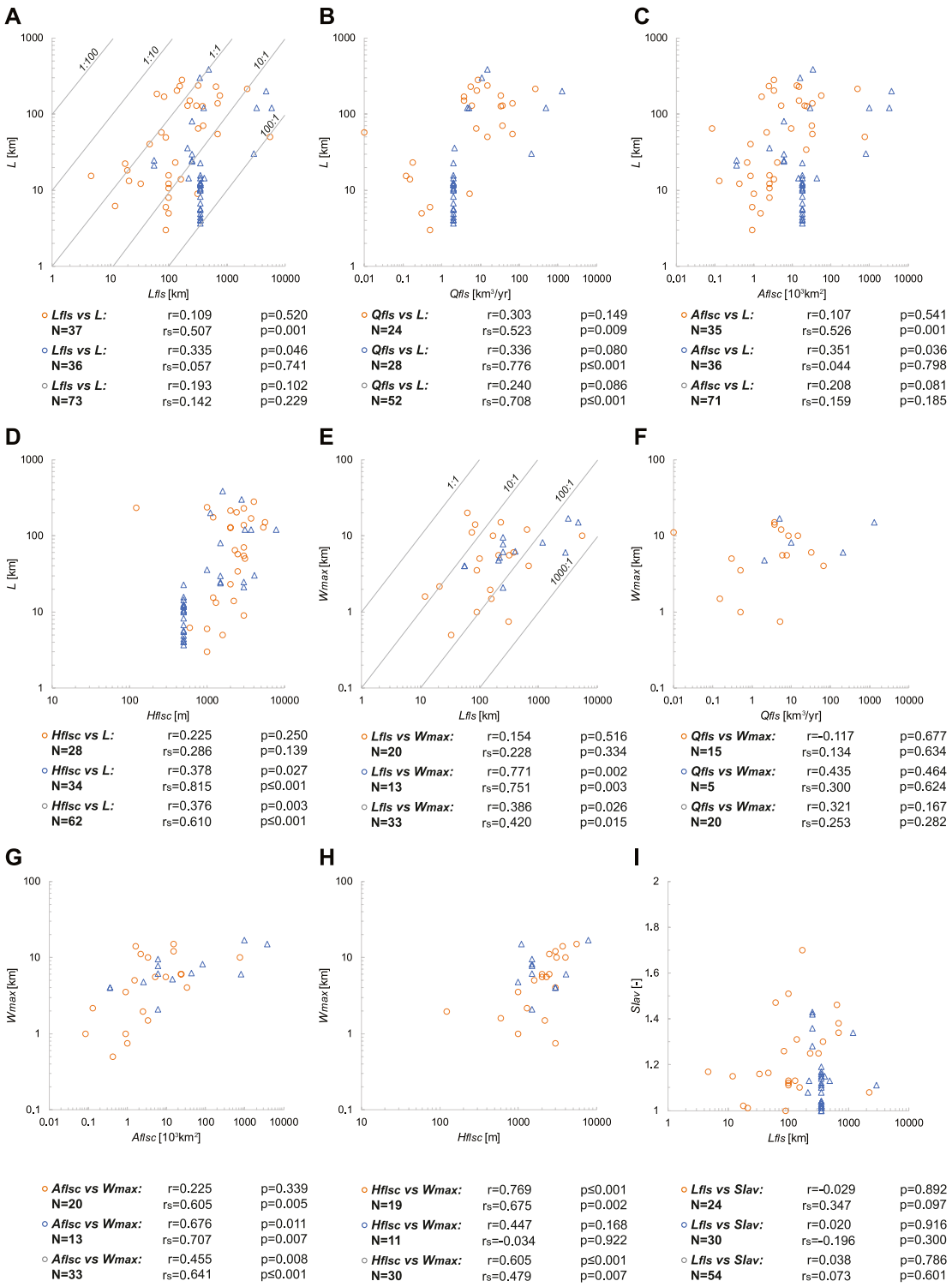

FIGURE 8 | (A–R) Scatterplots of attributes of the terrestrial catchment, shelf and slope with canyon morphometric parameters for submarine canyons of the study in active vs. passive margins. *L*, canyon length; W_{max}, maximum canyon width; SI_{av}, average canyon sinuosity index; SW_{max}, maximum canyon sidewall steeepness; L_{fls}, fluvial system length; Q_{fls}, average annual fluvial discharge; A_{flsc}, catchment size; H_{flsc}, Maximum catchment elevation; D_{sh}, shelf-break depth; W_{sl}, slope width. *N*, number of readings; *r*, Pearson's correlation coefficient; r_s, Spearman's rank correlation coefficient.

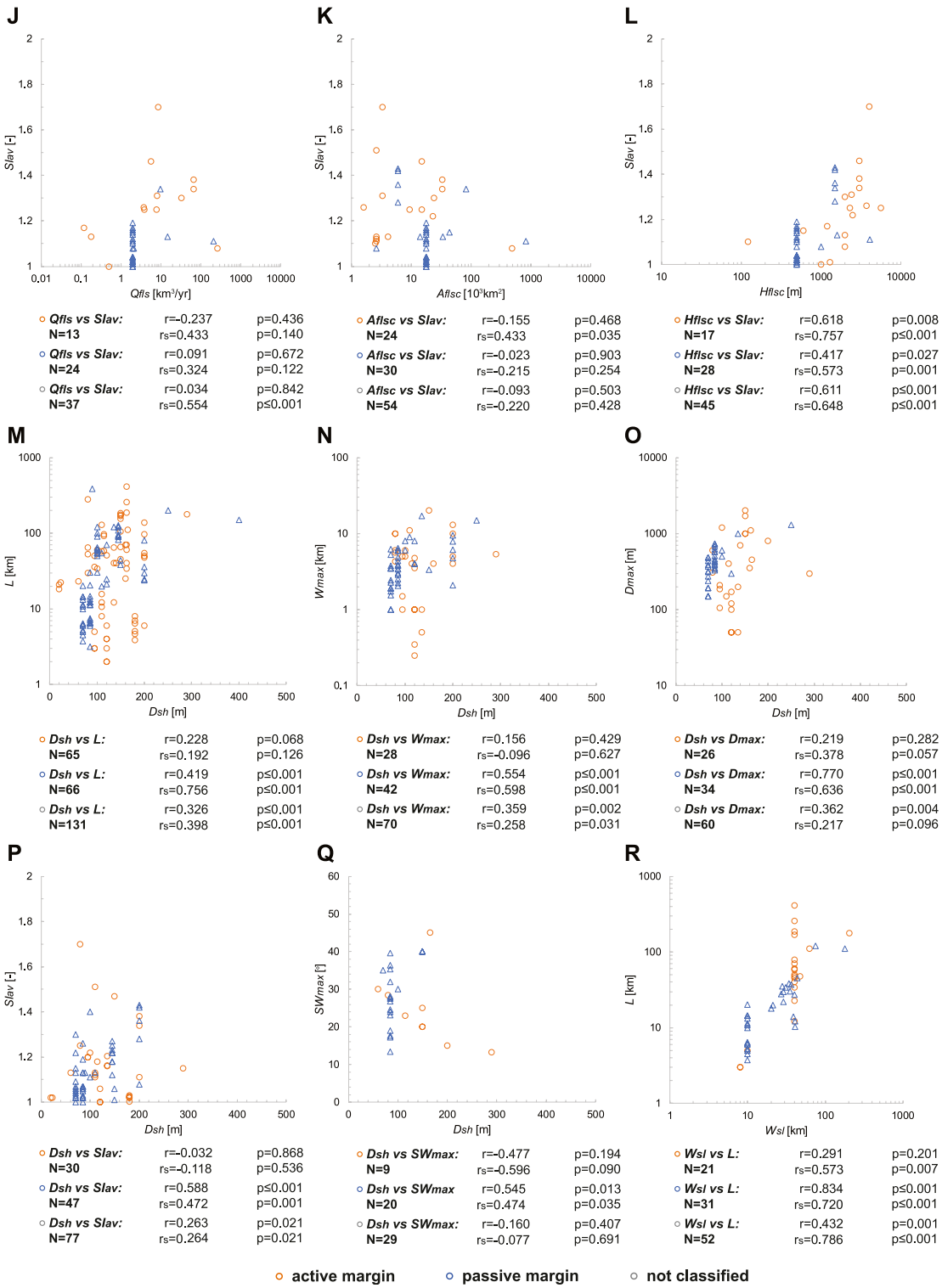

FIGURE 8 | (Continued)

correlations exist for the length (**Figure 8C**) and maximum width (**Figure 8G**) in canyons associated with active margins. No correlation is seen between average canyon sinuosity and catchment area for passive-margin canyons; a modest, positive monotonic correlation is seen for active-margin settings, but this is not significant (**Figure 8K**).

A Shelf

Pearson's correlation coefficient r

Active margin

	Wsh	Dsh	Gsh
L	0.227	0.228	-0.414
Wmax	0.066	0.156	-0.422
Dmax	0.227	0.219	-0.407
SIav	-0.368	-0.032	0.029
thGav	-0.179	0.210	0.180
SWmax	0.373	-0.477	-0.418
lwmax	-0.188	0.207	0.059
wdmax	-0.033	-0.066	-0.095
ldmax	-0.101	0.404	-0.092

Passive margin

	Wsh	Dsh	Gsh
L	0.245	0.419	0.083
Wmax	0.133	0.554	0.283
Dmax	0.198	0.770	-0.193
SIav	0.260	0.588	0.645
thGav	-0.490	-0.343	-0.178
SWmax	0.533	0.545	-0.466
lwmax	0.267	0.515	0.490
wdmax	0.413	0.285	-0.481
ldmax	0.059	0.838	-0.674

Spearman's rank correlation coefficient rs

Active margin

	Wsh	Dsh	Gsh
L	0.365	0.192	-0.537
Wmax	0.339	-0.096	0.283
Dmax	0.525	0.378	-0.525
SIav	-0.344	-0.118	0.089
thGav	-0.339	0.238	0.298
SWmax	0.288	-0.596	-0.370
lwmax	0.013	0.165	-0.086
wdmax	0.093	-0.100	-0.196
ldmax	0.270	0.236	-0.171

Passive margin

	Wsh	Dsh	Gsh
L	0.356	0.756	-0.168
Wmax	-0.052	0.598	0.192
Dmax	0.202	0.636	0.205
SIav	0.049	0.472	0.036
thGav	-0.302	-0.311	0.200
SWmax	0.322	0.474	-0.333
lwmax	0.325	0.377	-0.139
wdmax	0.105	0.234	-0.304
ldmax	-0.080	0.041	-0.281

p-value

Active margin

	Wsh	Dsh	Gsh
L	0.014	0.068	0.001
Wmax	0.572	0.429	0.025
Dmax	0.149	0.282	0.035
SIav	0.001	0.868	0.880
thGav	0.153	0.171	0.242
SWmax	0.087	0.194	0.263
lwmax	0.115	0.299	0.769
wdmax	0.857	0.796	0.689
ldmax	0.535	0.045	0.655

Passive margin

	Wsh	Dsh	Gsh
L	0.016	≤0.001	0.521
Wmax	0.353	≤0.001	0.073
Dmax	0.240	≤0.001	0.281
SIav	0.022	≤0.001	≤0.001
thGav	0.001	0.028	0.265
SWmax	0.013	0.013	0.039
lwmax	0.066	0.001	0.002
wdmax	0.014	0.107	0.005
ldmax	0.735	≤0.001	≤0.001

p-value

Active margin

	Wsh	Dsh	Gsh
L	≤0.001	0.126	≤0.001
Wmax	0.003	0.627	0.073
Dmax	≤0.001	0.057	0.005
SIav	0.002	0.536	0.640
thGav	0.006	0.119	0.050
SWmax	0.193	0.090	0.327
lwmax	0.913	0.409	0.671
wdmax	0.606	0.692	0.408
ldmax	0.092	0.256	0.403

Passive margin

	Wsh	Dsh	Gsh
L	≤0.001	≤0.001	0.192
Wmax	0.715	≤0.001	0.228
Dmax	0.231	≤0.001	0.252
SIav	0.670	0.001	0.810
thGav	0.044	0.047	0.209
SWmax	0.154	0.035	0.152
lwmax	0.024	0.016	0.405
wdmax	0.550	0.190	0.091
ldmax	0.647	0.819	0.119

B Slope

Pearson's correlation coefficient r

Active margin

	Wsl	Dsl	Gsl
L	0.291	0.305	0.221
Wmax	0.018	0.342	0.289
Dmax	-0.034	0.655	0.566
SIav	***	0.244	0.201
thGav	-0.262	-0.066	-0.018
SWmax	***	0.222	0.424
lwmax	0.970	0.438	-0.085
wdmax	-0.038	-0.203	-0.647
ldmax	0.960	0.282	-0.530

Passive margin

	Wsl	Dsl	Gsl
L	0.834	-0.034	-0.327
Wmax	0.639	-0.428	-0.707
Dmax	0.730	0.150	-0.740
SIav	-0.383	0.328	-0.308
thGav	-0.341	0.279	0.638
SWmax	-0.271	-0.344	0.149
lwmax	0.333	0.490	0.089
wdmax	0.170	-0.183	-0.381
ldmax	0.512	0.259	-0.690

Spearman's rank correlation coefficient rs

Active margin

	Wsl	Dsl	Gsl
L	0.573	0.381	0.309
Wmax	0.236	0.244	0.319
Dmax	0.285	0.535	0.652
SIav	***	0.170	0.423
thGav	-0.171	0.161	0.044
SWmax	***	0.118	0.725
lwmax	0.736	0.402	-0.091
wdmax	0.204	-0.082	-0.675
ldmax	0.801	0.214	-0.644

Passive margin

	Wsl	Dsl	Gsl
L	0.720	0.152	-0.578
Wmax	0.671	-0.372	-0.700
Dmax	0.446	0.111	-0.553
SIav	-0.420	0.344	-0.325
thGav	-0.397	0.295	0.742
SWmax	-0.402	-0.598	0.020
lwmax	0.153	0.486	0.017
wdmax	0.564	-0.129	-0.569
ldmax	0.736	0.533	-0.707

p-value

Active margin

	Wsl	Dsl	Gsl
L	0.201	0.005	0.166
Wmax	0.956	0.016	0.152
Dmax	0.911	≤0.001	0.004
SIav	***	0.157	0.511
thGav	0.278	0.623	0.930
SWmax	***	0.360	0.170
lwmax	≤0.001	0.003	0.686
wdmax	0.912	0.256	0.002
ldmax	≤0.001	0.091	0.009

Passive margin

	Wsl	Dsl	Gsl
L	≤0.001	0.788	0.030
Wmax	≤0.001	0.005	≤0.001
Dmax	≤0.001	0.517	≤0.001
SIav	0.087	0.036	0.081
thGav	0.278	0.209	0.001
SWmax	0.293	0.149	0.567
lwmax	0.072	0.002	0.626
wdmax	0.368	0.441	0.038
ldmax	0.003	0.284	≤0.001

p-value

Active margin

	Wsl	Dsl	Gsl
L	0.007	≤0.001	0.049
Wmax	0.460	0.091	0.112
Dmax	0.346	≤0.001	0.001
SIav	***	0.329	0.150
thGav	0.484	0.227	0.831
SWmax	***	0.629	0.008
lwmax	0.010	0.006	0.666
wdmax	0.548	0.650	0.001
ldmax	0.002	0.203	0.001

Passive margin

	Wsl	Dsl	Gsl
L	≤0.001	0.228	≤0.001
Wmax	≤0.001	0.017	≤0.001
Dmax	0.012	0.632	0.001
SIav	0.058	0.028	0.065
thGav	0.202	0.183	≤0.001
SWmax	0.109	0.007	0.938
lwmax	0.419	0.002	0.928
wdmax	0.001	0.588	0.001
ldmax	≤0.001	0.019	≤0.001

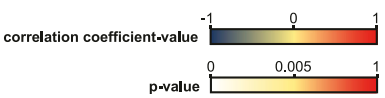

FIGURE 9 | (A,B) Results of the correlation analyses of canyon morphometric parameters with attributes of the **(A)** shelf and **(B)** slope at the canyon in active vs. passive margins presented as heat maps. *L*, canyon length; W_{max}, maximum canyon width; D_{max}, maximum canyon depth; SI_{av}, average canyon sinuosity index; thG_{av}, average canyon thalweg gradient; SW_{max}, maximum canyon sidewall steepness; lw_{max}, length-to-maximum width ratio; wd_{max}, maximum width-to-maximum depth ratio; ld_{max}, length-to-maximum depth ratio; W_{sh}, shelf width; D_{sh}, shelf-break depth; G_{sh}, average shelf gradient; W_{sl}, slope width; D_{sl}, slope-break depth; G_{sl}, average slope gradient; *** = correlations not reported due to small dataset size.

3.4.1.4 Maximum Catchment Elevation

The length of submarine canyons scales positively with the maximum catchment elevation of associated fluvial systems on passive margins. A corresponding relationship is absent for active margins (**Figure 8D**), whereas maximum canyon width shares positive and moderate correlations with maximum catchment elevation in active-margin canyons (**Figure 8H**). Moderate, significant correlations are seen between average canyon

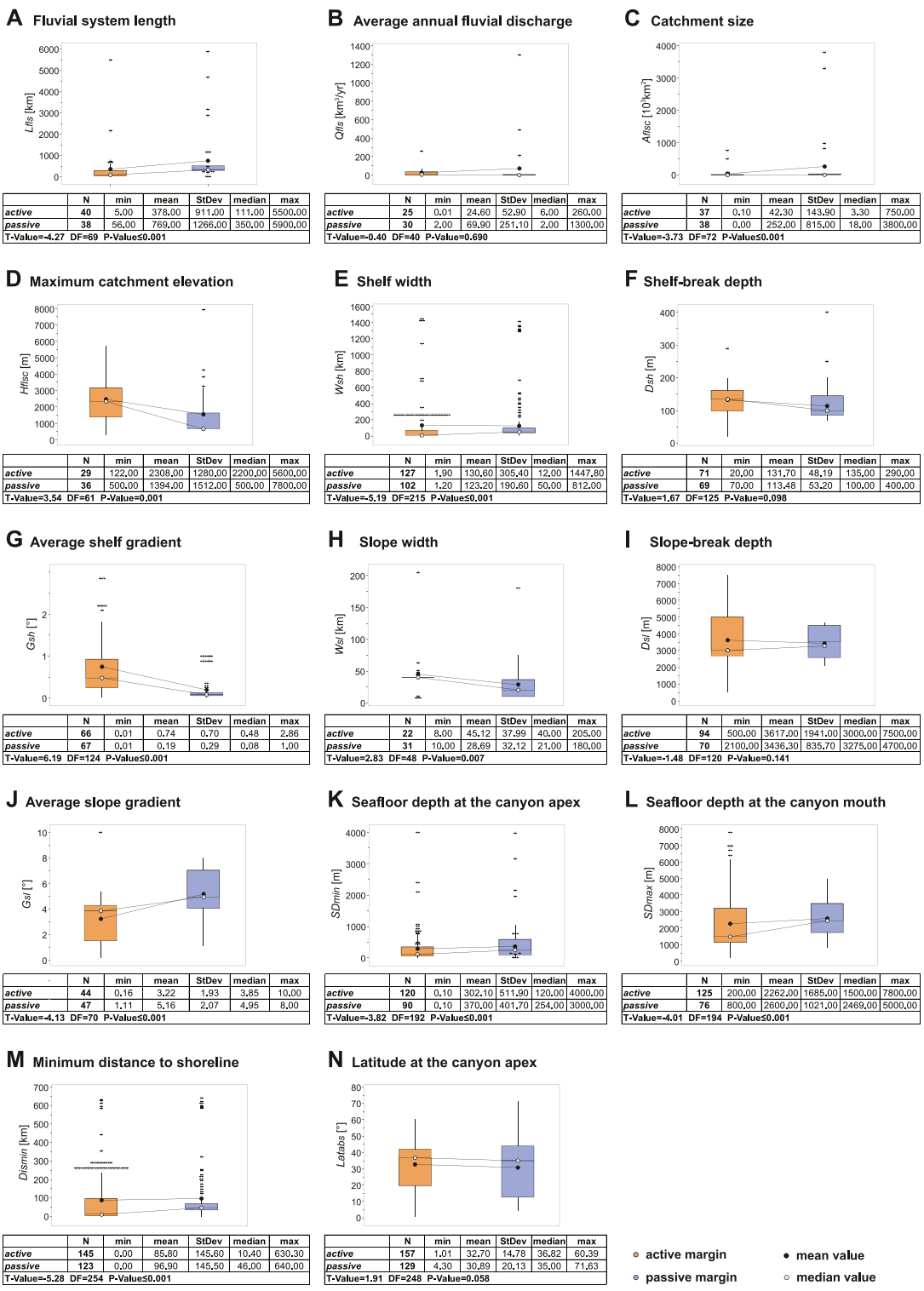

	N	min	mean	StDev	median	max
active	40	5.00	378.00	911.00	111.00	5500.00
passive	38	56.00	769.00	1266.00	350.00	5900.00

T-Value=-4.27 DF=69 P-Value≤0.001

	N	min	mean	StDev	median	max
active	25	0.01	24.60	52.90	6.00	260.00
passive	30	2.00	69.90	251.10	2.00	1300.00

T-Value=-0.40 DF=40 P-Value=0.690

	N	min	mean	StDev	median	max
active	37	0.10	42.30	143.90	3.30	750.00
passive	38	0.00	252.00	815.00	18.00	3800.00

T-Value=-3.73 DF=72 P-Value≤0.001

	N	min	mean	StDev	median	max
active	29	122.00	2308.00	1280.00	2200.00	5600.00
passive	36	500.00	1394.00	1512.00	500.00	7800.00

T-Value=3.54 DF=61 P-Value=0.001

	N	min	mean	StDev	median	max
active	127	1.90	130.60	305.40	12.00	1447.80
passive	102	1.20	123.20	190.60	50.00	812.00

T-Value=-5.19 DF=215 P-Value≤0.001

	N	min	mean	StDev	median	max
active	71	20.00	131.70	48.19	135.00	290.00
passive	69	70.00	113.48	53.20	100.00	400.00

T-Value=1.67 DF=125 P-Value=0.098

	N	min	mean	StDev	median	max
active	66	0.01	0.74	0.70	0.48	2.86
passive	67	0.01	0.19	0.29	0.08	1.00

T-Value=6.19 DF=124 P-Value≤0.001

	N	min	mean	StDev	median	max
active	22	8.00	45.12	37.99	40.00	205.00
passive	31	10.00	28.69	32.12	21.00	180.00

T-Value=2.83 DF=48 P-Value=0.007

	N	min	mean	StDev	median	max
active	94	500.00	3617.00	1941.00	3000.00	7500.00
passive	70	2100.00	3436.30	835.70	3275.00	4700.00

T-Value=-1.48 DF=120 P-Value=0.141

	N	min	mean	StDev	median	max
active	44	0.16	3.22	1.93	3.85	10.00
passive	47	1.11	5.16	2.07	4.95	8.00

T-Value=-4.13 DF=70 P-Value≤0.001

	N	min	mean	StDev	median	max
active	120	0.10	302.10	511.90	120.00	4000.00
passive	90	0.10	370.00	401.70	254.00	3000.00

T-Value=-3.82 DF=192 P-Value≤0.001

	N	min	mean	StDev	median	max
active	125	200.00	2262.00	1685.00	1500.00	7800.00
passive	76	800.00	2600.00	1021.00	2469.00	5000.00

T-Value=-4.01 DF=194 P-Value≤0.001

	N	min	mean	StDev	median	max
active	145	0.00	85.80	145.60	10.40	630.30
passive	123	0.00	96.90	145.50	46.00	640.00

T-Value=-5.28 DF=254 P-Value≤0.001

	N	min	mean	StDev	median	max
active	157	1.01	32.70	14.78	36.82	60.39
passive	129	4.30	30.89	20.13	35.00	71.63

T-Value=1.91 DF=248 P-Value=0.058

FIGURE 10 | (A–N) Boxplots of frequency distributions of attributes of source-to-sink systems and of the canyon-physiographic setting linked to submarine canyons of active and passive margins. *N*, number of readings; min, minimum value; mean, mean value; SD, standard deviation; median, median value; max, maximum value; DF, degrees of freedom.

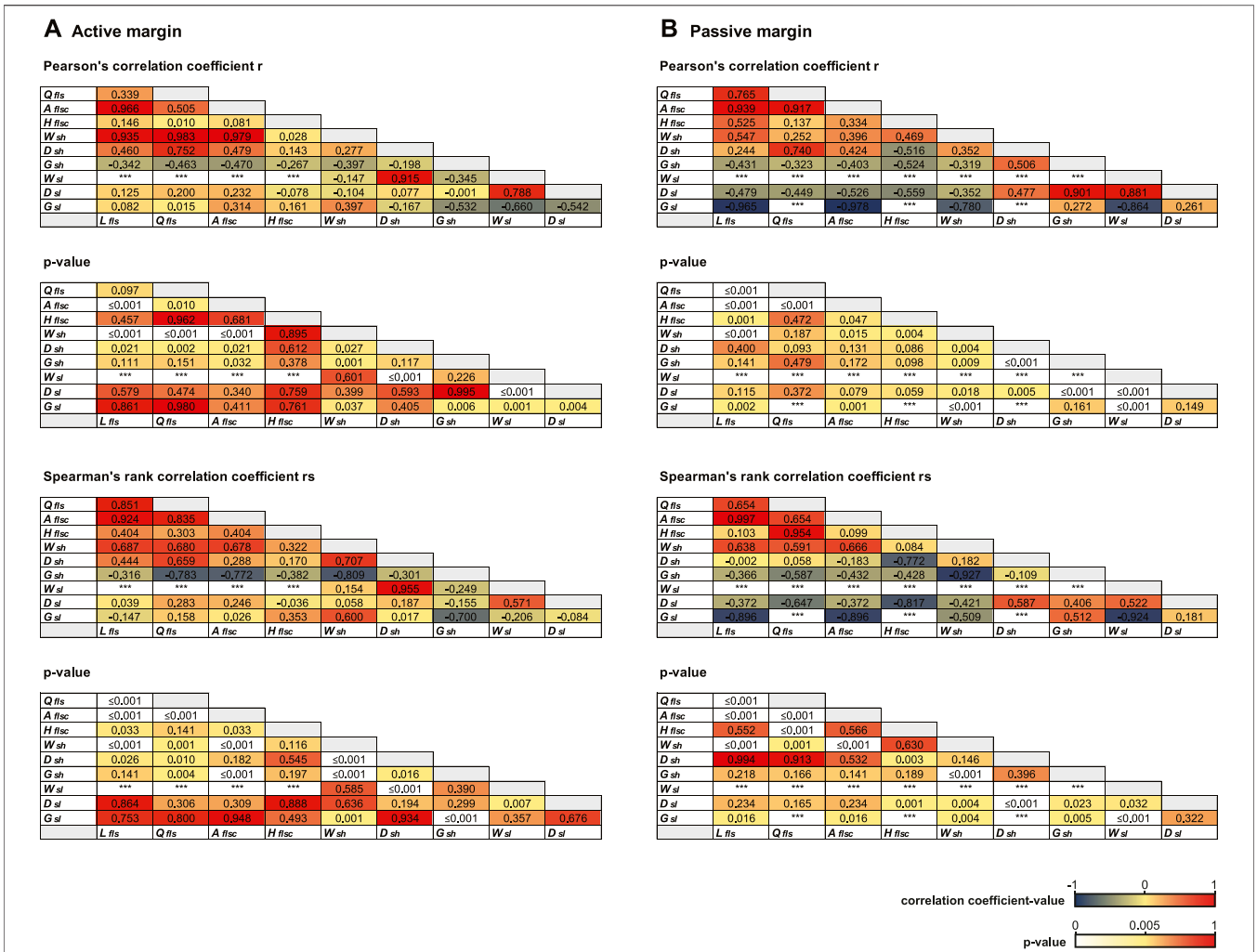

FIGURE 11 | (A,B) Results of the correlation analyses of attributes of the source-to-sink system in active vs. passive margins presented as heat maps. L_{fls}, fluvial system length; Q_{fls}, average annual fluvial discharge; A_{flsc}, catchment size; H_{flsc}, maximum catchment elevation; W_{sh}, shelf width; D_{sh}, shelf-break depth; G_{sh}, average shelf gradient; W_{sl}, slope width; D_{sl}, slope-break depth; G_{sl}, average slope gradient; *** = correlations not reported due to small dataset size.

sinuosity and maximum catchment elevation for both margin types (**Figure 8L**).

3.4.2 Shelf-Break Depth

Correlations of shelf-break depth at the canyon location with attributes of canyon geomorphology are weak and not significant for canyons in active-margin settings; in the studied canyons from passive margins, instead, maximum canyon dimensions (**Figures 8M–O**), average canyon sinuosity (**Figure 8P**) and maximum canyon sidewall steepness (**Figure 8Q**) correlate moderately or strongly with the shelf-break depth (**Figure 9A**).

3.4.3 Slope Width

Canyon length increases with slope width in active and passive margins; the strength of the relationship is moderate in the former and strong in the latter (**Figure 8R**). Maximum canyon width and depth do not correlate with the slope width in active margins, but both variables show moderate correlation with the width of passive-margin slopes. However, more data are needed to support the findings for active-margin canyons (**Figure 9B**).

3.5 Characterization of Canyon Source-to-Sink System and Physiographic Setting by Tectonic Setting

Analyses have been undertaken of 1) attributes of the S2S system and of the physiographic setting, and of how these vary with the margin type (**Section 3.5.1**), and of 2) scaling between attributes of the S2S systems in active and passive margins (**Section 3.5.2**). This has been done for the following reasons: 1) to assess commonalities and differences in characteristics of the two margin types, which can be used to refine existing S2S system models; and 2) to aid recognition of covariance between variables that may be related to the studied canyon morphometric parameters, rendered necessary by data gaps that prevent the application of multivariate techniques.

3.5.1 Attributes of the Canyon Geological Contexts and Their Variations Across Margin Types

Two-sample t-tests undertaken on frequency distributions of the attributes describing canyon terrestrial catchments, continental shelves and slopes (**Figures 10A–N**) demonstrate that significant differences in mean values of the studied variables are seen for all investigated attributes except for average annual fluvial discharge (**Figure 10B**), shelf-break depth (**Figure 10F**), slope-break depth (**Figure 10I**) and latitude at the canyon apex (**Figure 10N**).

On average, the length (**Figure 10A**), average annual water discharge (**Figure 10B**) and catchment size (**Figure 10C**) of fluvial systems supplying sediment to the studied canyons are each greater in terrestrial catchments along passive margins. Although the greatest maximum catchment elevation recorded in the study occurs in a passive-margin drainage basin, terrestrial catchments associated with active margins tend to be higher than along passive margins (**Figure 10D**).

The widest continental shelves in the study are associated with the submarine canyons of the Bering Sea, but the mean shelf widths of the studied active and passive margins are very similar, albeit slightly greater along the former (**Figure 10E**). Shelf-breaks tend to be deeper along active margins, but the results do not indicate a significant difference between the two margin types (**Figure 10F**). The average shelf gradient is on average higher in active-margin systems (**Figure 10G**).

Canyons of the study along active margins are hosted on wider (**Figure 10H**) and deeper (**Figure 10I**) slopes, whereas the average slope gradient tends to be higher in S2S systems associated with the studied passive margins (**Figure 10J**).

With regard to aspects of the physiographic setting, mean values of seafloor depth at the canyon apex and mouth, of the minimum distance of the canyon to the shoreline, and of the latitude of the canyon apex are similar across the two margin types. Active-margin canyons show a greater bathymetric range, and several of the studied canyons in passive margins are located at higher latitudes (**Figures 10K–N**).

3.5.2 Scaling Between Attributes of the Source-to-Sink Systems of Active and Passive Margins

Correlations between attributes of the terrestrial catchment, shelf and slope in canyon-associated S2S systems grouped into active- and passive-margin settings share similarities, yet exhibit differences regarding their sign, strength and statistical significance. For some attributes, the amount of data prevents meaningful analyses to be undertaken (**Figures 11A,B**).

Statistically significant scaling relationships are seen across both margin types, but these vary in strength. Strong and positive significant correlations of catchment area with fluvial-system length and average annual fluvial discharge are seen for both margin types. Also, shelf width correlates positively with catchment area and fluvial system length in both margin types, but the relationship with the latter is stronger in active-margin settings. Strong inverse scaling across both margin types exists between shelf width and the average shelf gradient and between slope width and the average slope gradient in passive margins (**Figures 11A,B**).

For other pairs of attributes, significant relationships may be seen for a particular margin type only. For example, the maximum elevation of passive-margin catchments shows significant and positive scaling with fluvial system length and average annual fluvial discharge, which is moderate for the former and strong for the latter. For active margins, correlations are weak and modest and not statistically significant. Shelf-break depth and the average shelf gradient display linear, moderate and significant positive correlation with each other in passive margins, but along active margins the same trend is weak, negative and not statistically significant (**Figures 11A,B**).

4 DISCUSSION

4.1 Tectonic Influence on Controlling Factors on Submarine-Canyon Geomorphology

Findings from this study suggest that certain aspects of the morphometry of submarine canyons, and some scaling relationships of canyon morphometric parameters mutually and with attributes of their geological setting, are more strongly expressed in a specific margin type (see **Figures 2–9**), indicating a possible tectonic control. Although commonalities seen in scaling across both margin types indicate that a scaling relationship might not be generally sensitive to factors related to tectonic activity, the possibility exists that tectonic influences might be overridden by other controlling factors or that different controls in passive and active margins have led to similar geomorphologic expressions in canyons.

In the following sections, the main findings of the study are discussed in the context of a potential tectonic influence on controlling factors on submarine-canyon geomorphology, including intra-canyon sedimentary processes, sediment connection to fluvial and littoral sources, sediment supply to shelf margins and structural controls.

4.1.1 Intra-Canyon Sedimentary Processes

The contrast in relative importance of intra-canyon processes along active and passive margins may contribute to certain differences seen in scaling relationships between canyons of the two margin types. For example, intra-canyon-wall failure might be less important as a geomorphic agent in canyons from active margins compared to passive-margin ones (Bührig et al., in review). This is because slope failures are thought to occur less commonly along active margins compared to passive margins, due to strengthening of the seafloor from recurrent seismic activity (e.g., Strozyk et al., 2010; Nelson et al., 2011; Sawyer and DeVore, 2015; Molenaar et al., 2019); on active margins, large-scale slope failures tend to be linked to high-magnitude earthquakes (e.g., Strozyk et al., 2010; Molenaar et al., 2019). By contrast, active-margin settings with steep terrestrial catchments and narrow and steep shelf configurations promote maintenance of sediment connection of submarine canyons with fluvial outlets and littoral cells even during periods of sea-level highstand, as at

present (e.g., Gamberi et al., 2015; Bernhardt and Schwanghart, 2021). Hence, moderate correlations of maximum sidewall steepness with maximum canyon width (**Figure 5F**) and depth (**Figure 5G**) in canyons along active margins might reflect the tendency of sediment gravity flows to predominate over intra-canyon slope failure in shaping canyon geomorphology in these settings, *via* their ability to concurrently control canyon width, depth and bank steepness by thalweg erosion (e.g., McHargue et al., 2011; Peakall and Sumner, 2015) and canyon margin aggradation from flow overspilling (e.g., Armitage et al., 2010; Soulet et al., 2016). In contrast, the weaker correlations seen for passive-margin canyons (**Figures 5F,G**) may be linked to the combined effect of a subordinate influence of sediment gravity flows from the disconnection of canyons to fluvial and intrashelf sources during periods of sea-level highstand (e.g., Harris and Whiteway, 2011), paired with the variable impact of canyon-wall failure on canyon-wall slopes, canyon width and canyon depth. As a result, relationships between these morphometrics linked to intracanyon erosion by flows might be overprinted. When deposited near their source, mass failures and their depositional products will lead to lower canyon depths and greater canyon-floor widths over the affected areas, whereas the maximum width between the canyon banks will only increase where the wall collapse extends to the uppermost canyon margin. Intra-canyon slope failures may also have an indirect effect on canyon geomorphology away from the site of failure, particularly when the mass failure transitions into a sediment gravity flow (e.g., Stow, 1986; Hsu et al., 2008), or when the deposit is remobilized at a later point in time and is transported down canyon (e.g., Khripounoff et al., 2012); as a consequence, mass-failure impact on canyon width, depth and sidewall gradients might vary.

Thus, the co-occurrence of wall failure and sediment gravity flows, which is recognized to act as an autogenic control on the variability in width-to-depth ratios of submarine channels (see **Figure 11** and text in Shumaker et al., 2018), may also be effective in controlling maximum width-to-maximum depth (wd_{max}) ratios of submarine canyons (Bührig et al., in review). The smaller mean value and range of wd_{max} ratio seen for passive-margin canyons compared to active-margin ones (**Figures 3B**, **5D**) suggest that width-to-depth aspect ratios in canyons hosted on passive margins tend to be constrained in their magnitude by the way in which wall-collapse may limit canyon-margin aggradation. By contrast, the subordinate role of intra-canyon failure combined with the effect of structural controls on canyon depths and widths (see **Section 4.1.4**) can explain the greater range in wd_{max} ratios seen in active-margin canyons (**Figures 3B**, **5D**).

4.1.2 Sediment Connection to Fluvial and Littoral Sources

4.1.2.1 Sediment Discharge From Rivers

Some geomorphic features of submarine canyons are seen to scale, to some degree, with fluvial system length, average annual water discharge, catchment size and maximum catchment elevation. These observations are interpreted to reflect the importance of sediment discharge from rivers as controls on how canyon geomorphology is shaped by erosional and depositional processes (cf. Casalbore et al., 2011; Bührig et al., in review).

For submarine canyons in active margins, potential causal links between fluvial sediment supply and their length and maximum width are suggested by: 1) moderate scaling of the former with fluvial system length (**Figure 8A**), average annual water discharge (**Figure 8B**) and catchment size (**Figure 8C**), and 2) moderate scaling of the latter with the area (**Figure 8G**) and maximum elevation (**Figure 8H**) of the associated terrestrial catchment. These relationships probably reflect how erosive intracanyon flows related to fluvial discharge promote lengthening at the canyon head (e.g., Piper and Normark, 2009) and mouth (e.g., Hodgson et al., 2016), as well as canyon widening (e.g., Casalbore et al., 2011).

By contrast, weak correlations of passive-margin canyon length with fluvial system length (**Figure 8A**) and catchment size (**Figure 8C**) indicate a lack of control of sediment discharge from rivers on canyon length. This might in part reflect how retrogressive slope failure tends to be a more prominent process along passive margins compared to active ones, and how sediment connection of canyons with fluvial sources in passive-margin settings tend to diminish through time at times of marine transgression (see **Section 4.1.1**). For example, incised valleys along passive margins are thought to be more prone to infill during transgressive and highstand intervals due to their commonly shallower depths compared to those along active margins, promoting the disconnection of canyon heads from fluvial sediment sources in passive-margin settings (Harris and Whiteway, 2011). Also, flooding events are less likely to trigger hyperpycnal flows at the mouth of rivers along passive margins, due to the increased sand-grade sediment segregation in their larger coastal and alluvial floodplains (e.g., Milliman and Syvitski, 1992; Sømme et al., 2009). In addition, larger terrestrial catchments are less affected by extreme weather events, in proportion to their size, compared to smaller ones (e.g., Sømme et al., 2009; Reid and Frostick, 2011).

Despite this, comparably strong scaling of canyon length with average annual fluvial discharge for passive-margin canyons (**Figure 8B**) might reflect that long-lived sediment-laden turbulent flows (*sensu* Zavala, 2020) linked to discharge from rivers are efficient in traversing wide shelves and entire canyons even during periods of sea-level highstand. and are effective in increasing canyon lengths by erosion at the canyon head and at its mouth. Such hyperpycnal flows are thought to be common at the mouths of medium to large rivers associated with low-gradient terrestrial catchments, and to be able to cover distances of up to several hundred kilometers (Zavala, 2020).

4.1.2.2 Seafloor Depth at the Canyon Apex

Inverse relationships of average canyon width (**Figure 7A**) and maximum (**Figure 7B**) and average canyon depth (**Figure 7C**) with seafloor depth at the canyon apex seen for canyons from passive margins might reflect how canyons with apices located at greater water depths are more likely to be disconnected from terrestrial and intrashelf sources, at present and during past sea-level lowstands. Unless such canyons are coupled with a

contouritic system (e.g., Warratz et al., 2019), intra-canyon erosion would be limited to mass-wasting events on the slope proximal to and within the canyon, and to wave erosion.

Active-margin canyons tend to have steeper sidewalls if their canyon apex is closer to the shoreline (**Figure 7G**) and/or at shallower seafloor depth (**Figure 7E**), whereas in passive margins the maximum canyon sidewall steepness does not correlate with either physiographic parameter (**Figures 7E,G**). This finding supports our hypothesis that erosive flows originating from within the shelf and terrestrial catchment may be more important in carving steep canyon walls in active settings compared to passive ones (**Section 4.1.1**). We also find that average canyon sinuosity and wd_{max} ratios of canyons in active settings show moderate scaling with canyon bathymetry at the apex, inverse for the former (**Figure 7D**) and positive for the latter (**Figure 7F**), which can also be ascribed to the influence of such erosive flows.

4.1.3 Sediment Supply to Shelf Margins

The moderate scaling of shelf-break depth with canyon length (**Figure 8M**), maximum width (**Figure 8N**) and depth (**Figure 8O**), and average canyon sinuosity (**Figure 8P**) for passive-margin canyons might reflect to some degree how higher rates of sediment supply from terrestrial source areas promote subsidence along continental margins and act to push the slope break into deeper waters (cf. Sweet and Blum, 2016; Wang et al., 2019). In contrast, relationships between the shelf-break depth and maximum canyon dimensions and overall canyon sinuosity are weak for active-margin canyons (**Figures 8M–P**), even though terrestrial catchments in active margins can be characterized by high rates of sediment supply (see also **Section 4.1.2** and **Section 4.1.4**), which can be associated with narrow shelves promoting sediment routing to canyons (e.g., Blum and Hattier-Womack, 2009). Our observation may reflect, in part, the relative importance of structural controls on geomorphologic evolution in active settings (see **Section 4.1.4**), including the structural control of shelf-break migration (e.g., Han et al., 2016).

4.1.4 Structural Controls

Faulting and diapirism and their effects related to both gravitational failure and tectonic activity (e.g., Rowan et al., 2004; Hudec and Jackson, 2007; Yang et al., 2020) constitute structural controls that might affect canyon geomorphology in different ways through their influence on sediment-transport and canyon pathways (e.g., Chiang et al., 2012; Doo et al., 2015; Urías Espinosa et al., 2016); they can also do so by reshaping canyon walls (e.g., Yu and Chang, 2002; Bernhardt et al., 2015).

The greater impact of faulting and diapirism linked to tectonic activity on margin configuration, seafloor topography and sedimentary processes in active-margin settings compared to passive-margin ones (e.g., Yang et al., 2020) may explain some of the differences in scaling and canyon-morphometric characteristics seen between canyons across different tectonic settings.

The value of slope width for predicting canyon length (Sømme et al., 2009; Bührig et al., in review) is lower in active margins than in passive ones (**Figure 8R**), which is possibly related to a greater and more prolonged impact of tectonic convergence on slope physiography in active margins compared to passive margins (e.g., Pratson et al., 2007; Yang et al., 2020), and its variable influence on canyon length. Canyon pathways can be deflected by positive topography created by faults and diapirs (e.g., Li et al., 2021), or develop along intraslope depressions as transform faults (e.g., Greene et al., 1991), or axes of intraslope basins (e.g., Bourget et al., 2010), thereby increasing canyon length relative to the width of the slope. On the other hand, emerging seafloor topography can lead to canyon abandonment by redirecting sediment pathways (e.g., Chiang et al., 2012), whereas the presence of intraslope basins (e.g., Harris et al., 2014a) and highs (e.g., Hsiung et al., 2014) can inhibit further extension of the canyon across the slope.

Given the general importance of structural controls on canyon length and average canyon sinuosity in active margins, it is unsurprising that our results indicate that both canyon morphometric parameters are not generally different between the different categories of active margins (convergent, transform and complex settings; **Figures 4A,D**).

In contrast, the fact that the maximum width of canyons from complex settings is on average larger compared to that of canyons from convergent and transform ones (**Figure 4B**) suggests that such settings may be inherently more favorable to the development of wide canyons. In tectonically complex settings with strike-slip tectonics, such as the Cook Strait sector, New Zealand, and offshore Taiwan in the East China Sea, a local widening of canyons might be promoted by the concurrence of transform faulting coupled with recurrent sediment gravity flows, where canyons intersect with strike-slip faults (e.g., Schnürle et al., 1998; Micallef et al., 2014).

In case of the SW Taiwan margin canyons, instead, the development of very wide canyons might be explained by the high frequency of hyperpycnal flows at river mouths (e.g., Milliman and Kao, 2005; Liu et al., 2013). The formation of hyperpycnal flows in the region is favored by enhanced erosion rates in terrestrial catchments from earthquake-related landslides (e.g., Dadson et al., 2005), extended periods of precipitation during the monsoonal wet season (e.g., Zhang et al., 2022) and associated with typhoons (e.g., Dadson et al., 2005; Milliman and Kao, 2005; Zhang et al., 2018), as well as from decreased levels of salinity of the ambient oceanic water due to high freshwater discharge along the margin (e.g., Dadson et al., 2005).

Despite the fact that both mean canyon length (**Figure 2A**) and mean maximum canyon depth (**Figure 2D**) are not significantly different in active and passive margins, length-to-maximum depth (ld_{max}) ratios are on average significantly higher in active margins (**Figure 3C**). The findings might reflect how enhanced seafloor relief linked to tectonics tends to increase canyon length, while simultaneously inhibiting canyon deepening. A downcanyon decrease in the erosive power of canyon-traversing flows may be caused by the capture of coarser sediment fractions by intraslope depressions (e.g., Soutter et al., 2021) and by flow deceleration upstream of slope topography leading to deposition of coarser sediment (e.g., Soutter et al., 2020). Although our data on the average

depth of canyons from active and passive margins show that active-margin canyons tend to be significantly shallower (**Figure 2E**), further investigation is needed to corroborate our findings in view of the limited geographic coverage of the dataset.

4.2 Canyon Geomorphology and Associated Characters of Deep-Water Systems

Despite the importance of sediment connection of submarine canyons to sediment sources in terrestrial catchments, shelves and slopes, and the lithological characteristics of source areas for the evolution of deep-water systems (e.g., Normark and Carlson, 2003; Smith et al., 2017; Hessler and Fildani, 2019; Bernhardt and Schwanghart, 2021), the character of a deep-water system is ultimately controlled by the efficiency of sediment transport through canyons to deep-marine sinks (Hessler and Fildani, 2019).

Stratigraphic forward modelling experiments by Wan et al. (2021) for delta-canyon-fan systems in a passive-margin setting suggest that sediment routing to basin floor sinks is promoted for shallow and low-sinuosity canyons.

Results by Wan et al. (2021) suggest that intracanyon basinward transport of coarser grain-size fractions is more efficient in shallower canyons. Canyons along active margins tend to be shallower than passive-margin canyons (**Figure 2E**), but they also tend to exhibit increased intra-canyon relief, which can inhibit the down-canyon erosive strength of flows *via* mass extraction (see **Section 4.1.4**). This suggests that the relationship identified by Wan et al. (2021) might not be applicable for canyons in active-margin settings. Similarly, the impact of canyon depth on grain-size segregation within canyons might be subdued in canyons associated with passive-margin settings where slope relief is increased by gravitational loading.

The rate of thalweg lateral migration, which determines the canyon sinuosity, controls the caliber of sediment transported down-canyon; in more sinuous canyons, a relatively larger proportion of coarse sediment is deposited along the inner bends and the proximal part of the canyon, whereas in canyons with lower sinuosity the coarser sediment can be more effectively transported down-slope (Wan et al., 2021). Given that the average sinuosity of canyons is neither generally different between active and passive margins (**Figure 2F** this study; Harris and Whiteway, 2011; Bührig et al., in review), nor seemingly different across the considered active-margin settings (**Figure 4D**), the control of canyon sinuosity on sediment transport dynamics and grain-size segregation is probably not fundamentally different between active- and passive-margin settings and across active margins with different types of plate boundaries.

However, the influence of canyon geomorphology on sediment connection across deep-water environments might be absent or less prominent for active margins where canyons experience "flushing" initiated by large-magnitude earthquakes (e.g., Goldfinger et al., 2012; Atwater et al., 2014), due to the remobilization of large volumes of sediment, including coarser grain size fractions, and related substrate erosion within the canyon (e.g., Mountjoy et al., 2018).

These aspects highlight the need for modelling studies and conceptual models of S2S and deep-water systems to better consider the wide range of boundary conditions associated with characteristics of continental margins.

4.3 Implications of the Findings and Future Work

Our comparisons of frequency distributions of canyon morphometric parameters for different tectonic settings (**Figures 2A–H**, **4A–I**) corroborate results of earlier quantitative global studies, showing that canyon morphometrics are variably sensitive to factors related to the tectonic-margin type (e.g., Harris and Whiteway, 2011; Bührig et al., in review). These insights suggest that overall canyon geomorphology cannot be predicted from the tectonic setting alone. Our findings that canyons along active margins display a greater variability in aspect ratios of maximum canyon dimensions (**Figures 3A–C**) indicate that the size of canyon fills in the stratigraphic record might be less reliably estimated from outcrop and subsurface data in active-margin settings compared to passive margins. Moreover, aspects of canyon morphometry in canyons associated with convergent settings are not fundamentally different compared to those in complex settings (**Figures 4A–I**), suggesting that canyon geomorphology is not primarily controlled by the complexity of the tectonic regime in active-margin settings. Despite this, complex tectonics may be preferentially associated with canyons with larger maximum widths and depths (**Figures 4B,C**, see also **Section 4.1.4**).

Our analysis also shows that scaling relationships of canyon morphometric parameters with attributes of the physiographic setting (**Figures 6A,B**, **7A–H**) and source-to-sink (S2S) system (**Figures 8A–R**, **9A,B**) might vary between active and passive margins. The same applies for scaling relationships between the different canyon morphometric parameters (**Figures 5A–G**), and for scaling between attributes of S2S systems (**Figures 11A,B**). These findings are important because they demonstrate that the relationships between continental-margin types and the configuration of deep-water systems is more complex than hitherto recognized in conceptual, experimental and numerical models.

The variable and complex influence of the tectonic setting on sediment routing along S2S systems, on canyon geomorphology, and on the degree of confinement of deep-water fans in settings such as intraslope basins (e.g., Budillon et al., 2011; Hsiung et al., 2014), lower slopes with complex seafloor topography (e.g., Hsiung et al., 2018), and trenches (e.g., Thornburg et al., 1990; McArthur and Tek, 2021) raises the question whether scaling relationships between submarine canyons and deep-water fans can be predicted. This needs to be investigated in future work.

5 CONCLUSION

A global metastudy of geomorphic characteristics of submarine canyons as a function of the tectonic setting has been conducted. The key findings of the study are that:

1) Overall canyon geomorphology is not generally different between active and passive margins and across different plate-boundary types in tectonically active settings.
2) The role of slope failure as a mechanism governing the morphology of canyons may be subordinate for canyons associated with active margins, compared to passive-margin examples, possibly due to seismic strengthening of seafloors in the former. This indicates that width-to-depth ratios might be inherently limited in their magnitude in canyons in passive-margin settings due to the interplay of intracanyon sediment flows and canyon-wall failure, with the latter counteracting canyon-margin accretion while promoting canyon widening and aggradation of canyon floors.
3) Scaling relationships of individual canyon morphometric parameters and aspect ratios of maximum canyon dimensions with attributes of the S2S system and the physiographic setting have been demonstrated for 1) active margins, 2) passive margins, and 3) across both margin types. The scaling relationships vary broadly in magnitude of correlation, but are seldom strong; this reflects how canyon geomorphology is shaped by the complex interplay of different controls, which are only in part influenced by the tectonic setting.
4) Our findings suggest that canyon geomorphology can be to some degree predicted in S2S systems in active and passive margins, but that the predictive value of attributes of the environmental setting might vary across different tectonic settings.
5) Insights from this study suggest possible genetic links between aspects of canyon geomorphology and characteristics of the physiographic environment related to the tectonic setting. This finding can be applied to improve and help constrain conceptual, experimental and numerical models of submarine canyons and canyon-associated sedimentary systems at source-to-sink scale by 1) demonstrating how the relative importance of controlling factors on canyon morphometry might vary across different tectonic settings; 2) providing a quantitative characterization of canyon morphometric attributes and associated parameters of the physiographic and environmental setting that can be applied to constrain models in a realistic manner; and 3) illustrating how insights from our analyses can augment existing semi-quantitative models of source-to-sink systems for different tectonic settings, which have not yet expressly considered submarine-canyon morphometry (e.g., Sømme et al., 2009; Nyberg et al., 2018).

DATA AVAILABILITY STATEMENT

The raw data supporting the conclusion of this article will be made available by the authors, without undue reservation.

AUTHOR CONTRIBUTIONS

LB conceptualized and led the investigation, conducted the analyses, drafted the figures and wrote the original draft. LC, MP, NM, and WM supervised the project. LC, MP, NM, and WM provided specialist technical input for the interpretation of geomorphological and geological datasets and the application of statistical analytical techniques; they additionally contributed to the scientific writing of the manuscript and to manuscript revisions.

FUNDING

This research was funded by the sponsors of the Turbidites Research Group (AkerBP, CNOOC, ConocoPhillips, Harbour, Murphy, Occidental, OMV) and of the Fluvial, Eolian & Shallow-Marine Research Group [AkerBP, Areva (now Orano), BHP, Cairn India (Vedanta), Chevron, CNOOC International, ConocoPhillips, Equinor, Murphy Oil, Occidental, Petrotechnical Data Systems, Saudi Aramco, Shell, Tullow Oil, Woodside, YPF], School of Earth and Environment, University of Leeds. Financial support to this research was also provided by NERC (NE/P01691X/1).

ACKNOWLEDGMENTS

We thank the sponsors of the Turbidites Research Group and of the Fluvial, Eolian & Shallow-Marine Research Group for financial support. We thank DC and AF for their constructive comments, which helped improve the paper.

SUPPLEMENTARY MATERIAL

The Supplementary Material for this article can be found online at: https://www.frontiersin.org/articles/10.3389/feart.2022.836823/full#supplementary-material

REFERENCES

Acosta, J., Canals, M., López-MartínezMuñoz, A., Herranz, P., Urgeles, R., et al. (2002). The Balearic Promontory Geomorphology (Western Mediterranean): Morphostructure and Active Processes. *Geomorphology* 49, 177–204.

Alford, M. H., and MacCready, P. (2014). Flow and Mixing in Juan de Fuca Canyon, Washington. *Geophys. Res. Lett.* 41, 1608–1615. doi:10.1002/2013GL058967

Allen, S. E., Vindeirinho, C., Thomson, R. E., Foreman, M. G., and Mackas, D. L. (2001). Physical and Biological Processes Over a Submarine Canyon During an Upwelling Event. *Can. J. Fish. Aquat. Sci.* 58, 671–684. doi:10.1139/cjfas-58-4-67110.1139/f01-008

Allin, J. R., Hunt, J. E., Talling, P. J., Clare, M. A., Pope, E., and Masson, D. G. (2016). Different Frequencies and Triggers of Canyon Filling and Flushing Events in Nazaré Canyon, Offshore Portugal. *Mar. Geol.* 371, 89–105. doi:10.1016/j.margeo.2015.11.005

Almagor, G. (1993). Continental Slope Processes off Northern Israel and Southernmost Lebanon and Their Relation to Onshore Tectonics. *Mar. Geol.* 112, 151–169. doi:10.1016/0025-3227(93)90166-s

Alonso, B., and Ercilla, G. (2003). Small Turbidite Systems in a Complex Tectonic Setting (SW Mediterranean Sea): Morphology and Growth Patterns. *Mar. Pet. Geol.* 19, 1225–1240. doi:10.1016/S0264-8172(03)00036-9

Amblas, D., Ceramicola, S., Gerber, T. P., Canals, M., Chiocci, F. L., Dowdeswell, J. A., et al. (2017). "Submarine Canyons and Gullies," in *Submarine*

Geomorphology. Editors A. Micallef, S. Krastel, and A. Savini (Berlin, Germany: Springer), 251–272. doi:10.1007/978-3-319-57852-1_14

Amblas, D., Gerber, T. P., De Mol, B., Urgeles, R., Garcia-Castellanos, D., Canals, M., et al. (2012). Survival of a Submarine Canyon during Long-Term Outbuilding of a Continental Margin. *Geology* 40 (6), 543–546. doi:10.1130/G33178.1

Antobreh, A. A., and Krastel, S. (2006). Morphology, Seismic Characteristics and Development of Cap Timiris Canyon, Offshore Mauritania: a Newly Discovered Canyon Preserved-Off a Major Arid Climatic Region. *Mar. Petroleum Geol.* 23, 37–59. doi:10.1016/j.marpetgeo.2005.06.003

Armitage, D. A., Piper, D. J. W., McGee, D. T., and Morris, W. R. (2010). Turbidite Deposition on the Glacially Influenced, Canyon-Dominated Southwest Grand Banks Slope, Canada. *Sedimentology* 57, 1387–1408. doi:10.1111/j.1365-3091.2010.01149.x

Arzola, R. G., Wynn, R. B., Lastras, G., Masson, D. G., and Weaver, P. P. E. (2008). Sedimentary Features and Processes in the Nazaré and Setúbal Submarine Canyons, West Iberian Margin. *Mar. Geol.* 250, 64–88. doi:10.1016/j.margeo.2007.12.006

Atwater, B. F., Carson, B., Griggs, G. B., Johnson, H. P., and Salmi, M. S. (2014). Rethinking Turbidite Paleoseismology Along the Cascadia Subduction Zone. *Geology* 42, 827–830. doi:10.1130/G35902.1

Babonneau, N., Delacourt, C., Cancouët, R., Sisavath, E., Bachèlery, P., Mazuel, A., et al. (2013). Direct Sediment Transfer Form Land to Deep-Sea: Insights into Shallow Multibeam Bathymetry at La Réunion Island. *Mar. Geol.* 346, 47–57. doi:10.1016/j.margeo.2013.08.006

Babonneau, N., Savoye, B., Cremer, M., and Klein, B. (2002). Morphology and Architecture of the Present Canyon and Channel System of the Zaire Deep-Sea Fan. *Mar. Petroleum Geol.* 19, 445–467. doi:10.1016/s0264-8172(02)00009-0

Baker, E. T., and Hickey, B. M. (1986). Contemporary Sedimentation Processes in and Around an Active West Coast Submarine Canyon. *Mar. Geol.* 71, 15–34. doi:10.1016/0025-3227(86)90031-9

Baztan, J., Berné, S., Olivet, J.-L., Rabineau, M., Aslanian, D., Gaudin, M., et al. (2005). Axial Incision: The Key to Understand Submarine Canyon Evolution (In the Western Gulf of Lion). *Mar. Pet. Geol.* 22 (6-7), 805–826. doi:10.1016/j.marpetgeo.2005.03.011

Bernhardt, A., Melnick, D., Jara-Muñoz, J., Argandoña, B., González, J., and Strecker, M. R. (2015). Controls on Submarine Canyon Activity during Sea-Level Highstands. The Bíobío Canyon System Offshore Chile. *Geosphere* 11 (4), 1226–1255. doi:10.1130/GES01063.1

Bernhardt, A., and Schwanghart, W. (2021). Where and Why Do Submarine Canyons Remain Connected to the Shore during Sea-Level Rise? Insights from Global Topographic Analysis and Bayesian Regression. *Geophys. Res. Lett.* 48, e2020GL092234. doi:10.1029/2020GL092234

Blum, M. D., and Hattier-Womack, J. (2009). "Climate Change, Sea-Level Change, and Fluvial Sediment Supply to Deepwater Depositional Systems," in *External Controls on Deep Water Depositional Systems: Climate, Sea-Level, and Sediment Flux*. Editors B. Kneller, O. J. Martinsen, and B. McCaffrey (Tulsa, OK: SEPM), 15–40. doi:10.2110/sepmsp.092.015

Bosley, K. L., Lavelle, J. W., Brodeur, R. D., Wakefield, W. W., Emmet, R. L., Baker, E. T., et al. (2004). Biological and Physical Processes in and Around Astoria Submarine Canyon, Oregon, USA. *J. Mar. Syst.* 50, 21–37. doi:10.1016/j.jmarsys.2003.06.006

Bouma, A. H., and Scott, E. D. (2003). "Source-to-sink: the Importance of the Updip Coastal Area in Defining Deep-Water Sand Characteristics," in *Shelf Margin Deltas and Linked Down Slope Petroleum Systems – Global Significance and Future Exploration Potential*. Editors H. H. Roberts, N. C. Rosen, R. H. Fillon, and J. B. Anderson (Houston, TX: GCSSEPM), 597–617. doi:10.5724/gcs.03.23.0597

Bourget, J., Zaragosi, S., Ellouz-Zimmermann, N., Mouchot, N., Garlan, T., Schneider, J.-L., et al. (2010). Turbidite System Architecture and Sedimentary Processes along Topographically Complex Slopes: the Makran Convergent Margin. *Sedimentology* 58 (2), 376–406. doi:10.1111/j.1365-3091.2010.01168.x

Budillon, F., Conforti, A., Tonielli, R., De Falco, G., Di Martino, G., Innangi, S., et al. (2011). The Bulgheria Canyon-Fan: A Small-Scale Proximal System in the Eastern Tyrrhenian Sea (Italy). *Mar. Geophys. Res.* 32, 83–97. doi:10.1007/s11001-011-9138-9

Bührig, L. H., Colombera, L., Patacci, M., Mountney, N. P., and McCaffrey, W. D. (in review). A Global Analysis of Controls on Submarine-Canyon Geomorphology. *arXiv*. doi:10.31223/X5RK9H

Çağatay, M. N., Uçarkus, G., Eriş, K. K., Henry, P., Gasperini, L., and Polonia, A. (2015). "Submarine Canyons of the Sea of Marmara," in *Submarine Canyon Dynamics in the Mediterranean and Tributary Seas – an Integrated Geological, Oceanographic and Biological Perspective*. Editor F. Briand (Monaco:CIESM), 123–135.

Carlson, P. R., Bruns, T. R., and Fisher, M. A. (1990). "Development of Slope Valleys in the Glacimarine Environment of a Complex Subduction Zone, Northern Gulf of Alaska," in *Glacimarine Environments; Processes and Sediments*. Editors J. A. Dowdeswell and J. D. Scourse (London: GEOLOGICAL SOCIETY), 139–153. doi:10.1144/gsl.sp.1990.053.01.08

Carlson, P. R., and Karl, H. A. (1988). Development of Large Submarine Canyons in the Bering Sea, Indicated by Morphologic, Seismic, and Sedimentologic Characteristics. *Geol. Soc. Am. Bull.* 100, 1594–1615. doi:10.1130/0016-7606(1988)100<1594:dolsci>2.3.co;2

Carlson, P. R., and Karl, H. A. (1984). Discovery of Two New Large Submarine Canyons in the Bering Sea. *Mar. Geol.* 56, 159–179. doi:10.1016/0025-3227(84)90011-2

Carson, B., Baker, E. T., Hickey, B. M., Nittrouer, C. A., DeMaster, D. J., Thorbjarnarson, K. W., et al. (1986). Modern Sediment Dispersal and Accumulation in Quinault Submarine Canyon – A Summary. *Mar. Geol.* 71, 1–13. doi:10.1016/0025-3227(86)90030-7

Casalbore, D., Chiocci, F. L., Scarascia Mugnozza, G., Tommasi, P., and Sposato, A. (2011). Flash-flood Hyperpycnal Flows Generating Shallow-Water Landslides at Fiumara Mouths in Western Messina Strait (Italy). *Mar. Geophys. Res.* 32, 257–271. doi:10.1007/s11001-011-9128-y

Casalbore, D., Falcini, F., Martorelli, E., Morelli, E., Bosman, A., Calarco, M., et al. (2018). Characterization of Overbanking Features on the Lower Reach of the Gioia-Mesima Canyon-Channel System (Southern Tyrrhenian Sea) through Integration of Morpho-Stratigraphic Data and Physical Modelling. *Prog. Oceanogr.* 169, 66–78. doi:10.1016/j.pocean.2018.02.020

Chen, H., Zhan, W., Li, L., and Wen, M.-M. (2017). Occurrence of Submarine Canyons, Sediment Waves and Mass Movements along the Northern Continental Slope of the South China Sea. *J. Earth Syst. Sci.* 126, 73. doi:10.1007/s12040-017-0844-9

Chiang, C.-S., and Yu, H.-S. (2006). Morphotectonics and Incision of the Kaoping Submarine Canyon, SW Taiwan Orogenic Wedge. *Geomorphology* 80, 199–213. doi:10.1016/j.geomorph.2006.02.008

Chiang, C.-S., Yu, H.-S., Noda, A., TuZino, T., and Su, C.-C. (2012). Avulsion of the Fangliao Submarine Canyon off Southwestern Taiwan as Revealed by Morphological Analysis and Numerical Simulation. *Geomorphology* 177–178, 26–37. doi:10.1016/j.geomorph.2012.07.011

Coleman, J. M., Prior, D. B., and Lindsay, J. F. (1982). Formation of the Mississippi Canyon. *GCAGS Trans.* 32, 519.

Corradino, M., Pepe, F., Burrato, P., Kanari, M., Parrino, N., Bertotti, G., et al. (2021). An Integrated Multiscale Method for the Characterization of Active Faults in Offshore Areas. The Case of Sant'Eufemia Gulf (Offshore Calabria, Italy). *Front. Earth Sci.* 9, 670557. doi:10.3389/feart.2021.670557

Covault, J. A., Fildani, A., Romans, B. W., and McHargue, T. (2011a). The Natural Range of Submarine Canyon-And-Channel Longitudinal Profiles. *Geosphere* 7 (2), 313–332. doi:10.1130/GES00610.1

Covault, J. A., Romans, B. W., Graham, S. A., Fildani, A., and Hilley, G. E. (2011b). Terrestrial Source to Deep-Sea Sink Sediment Budgets at High and Low Sea Levels: Insights from Tectonically Active Southern California. *Geology* 39 (7), 619–622. doi:10.1130/G31801.1

Cullis, S., Patacci, M., Colombera, L., Bührig, L., and McCaffrey, W. D. (2019). A Database Solution for the Quantitative Characterisation and Comparison of Deep-Marine Siliciclastic Depositional Systems. *Mar. Pet. Geol.* 102, 321–339. doi:10.1016/j.marpetgeo.2018.12.023

Dadson, S., Hovius, N., Pegg, S., Dade, W. B., Horng, M. J., and Chen, H. (2005). Hyperpycnal River Flows from an Active Mountain Belt. *J. Geophys. Res.* 110, F04016. doi:10.1029/2004JF000244

Davies, H. L., Keene, J. B., Hashimoto, K., Joshima, M., Stuart, J. E., and Tiffin, D. L. (1987). Bathymetry and Canyons of the Western Solomon Sea. *Geo-Mar. Lett.* 6, 181–191.

de Almeida, N. M., Vital, H., and Gomes, M. P. (2015). Morphology of Submarine Canyons along the Continental Margin of the Potiguar Basin, NE Brazil. *Mar. Pet. Geol.* 68, 307–324. doi:10.1016/j.marpetgeo.2015.08.035

Dietz, R. S., Knebel, H. J., and Somers, L. H. (1968). Cayar Submarine Canyon. *Geol. Soc. Am. Bull.* 79, 1821–1828. doi:10.1130/0016-7606(1968)79[1821:nadcsc]2.0.co;2

Ding, W., Li, J., Li, J., Fang, Y., and Tang, Y. (2013). Morphotectonics and Evolutionary Controls on the Pearl River Canyon System, South China Sea. *Mar. Geophys. Res.* 34, 221–238. doi:10.1007/s11001-013-9173-9

Doo, W.-B., Hsu, S.-K., Lo, C.-L., Chen, S.-C., Tsai, C.-H., Lin, J.-Y., et al. (2015). Gravity Anomalies of the Active Mud Diapirs off Southwest Taiwan. *Geophys. J. Int.* 203, 2089–2098. doi:10.1093/gji/ggv430

Eittreim, S., Grantz, A., and Greenberg, J. (1982). Active Geologic Processes in Barrow Canyon, Northeast Chukchi Sea. *Mar. Geol.* 50, 61–76. doi:10.1016/0025-3227(82)90061-5

Ercilla, G., Alonso, B., Perez-Belzuz, F., Estrada, F., Baraza, J., Farran, M., et al. (1998). Origin, Sedimentary Processes and Depositional Evolution of the Agadir Turbidite System, Central Eastern Atlantic. *J. Geol. Soc. Lond.* 155 (6), 929–939. doi:10.1144/gsjgs.155.6.0929

Exon, N. F., Hill, P. J., Mitchell, C., and Post, A. (2005). Nature and Origin of the Submarine Albany Canyons off Southwest Australia. *Aust. J. Earth Sci.* 52 (1), 101–115. doi:10.1080/08120090500100036

Ferry, J.-N., Babonneau, N., Mulder, T., Parize, O., and Raillard, S. (2004). Morphogenesis of Congo Submarine Canyon and Valley: Implications about the Theories of the Canyons Formation. *Geodin. Acta.* 17, 241–251. doi:10.3166/ga.17.241-251

Fildani, A. (2017). Submarine Canyons: A Brief Review Looking Forward. *Geology* 45 (4), 383–384. doi:10.1130/focus042017.1

Galewsky, J., and Silver, E. A. (1997). Tectonic Controls on Facies Transitions in an Oblique Collision: The Western Solomon Sea, Papua New Guinea. *Am. Geol. Soc. Bull.* 109 (10), 1266–1278. doi:10.1130/0016-7606(1997)109<1266:tcofti>2.3.co;2

Gamberi, F., Rovere, M., Marani, M. P., and Dykstra, M. (2015). Modern Submarine Canyon Feeder-System and Deep-Sea Fan Growth in a Tectonically Active Margin (Northern Sicily). *Geosphere* 11 (2), 307–319. doi:10.1130/GES01030.1

Gardner, J. V., Dartnell, P., Mayer, L. A., and Hughes Clarke, J. E. (2003). Geomorphology, Acoustic Backscatter, and Processes in Santa Monica Bay from Multibeam Mapping. *Mar. Environ. Res.* 56, 15–46. doi:10.1016/S0141-1136(02)00323-9

Gardner, W. D., Glover, L. K., and Hollister, C. D. (1980). Canyons off Northwest Puerto Rico: Studies of Their Origin and Maintenance with the Nuclear Research Submarine NR-1. *Mar. Geol.* 37, 41–70. doi:10.1016/0025-3227(80)90011-0

Gervais, A., Mulder, T., Savoye, B., and Gonthier, E. (2006). Sediment Distribution and Evolution of Sedimentary Processes in a Small Sandy Turbidite System (Golo System, Mediterranean Sea): Implications for Various Geometries Based on Core Framework. *Geo-Mar. Lett.* 26, 373–395. doi:10.1007/s00367-006-0045-z

Gervais, A., Savoye, B., Piper, D. J. W., Mulder, T., Cremer, M., and Pichevin, L. (2004). "Present Morphology and Depositional Architecture of a Sandy Confined Submarine System: the Golo Turbidite System (Eastern Margin of Corsica)," in *Confined Turbidite Systems*. Editors S. A. Lomas and P. Joseph (London: Geological Society), 59–89. doi:10.1144/gsl.sp.2004.222.01.05

Gnibidenko, H. S., and Svarichevskaya, L. V. (1984). The Submarine Canyons of Kamchatka. *Mar. Geol.* 54, 277–307. doi:10.1016/0025-3227(84)90043-4

Goldfinger, C., Nelson, C. H., Morey, A. E., Johnson, J. R., Patton, J., Karabanov, E., et al. (2012). Turbidite Event History – Methods and Implications for Holocene Paleoseismicity of the Cascadia Subduction Zone. *USGS Prof. Pap.* 1661-F, 170. doi:10.3133/PP1661F

Gómez-Ballesteros, M., Druet, M., Muñoz, A., Arrese, B., Rivera, J., Sánchez, F., et al. (2014). Geomorphology of the Avilés Canyon System, Cantabrian Sea (Bay of Biscay). *Deep Sea Res. Part II Top. Stud. Oceanogr.* 106, 99–117. doi:10.1016/j.dsr2.2013.09.031

Greene, H. G., Clarke, S. H., Jr., and Kennedy, M. P. (1991). "Tectonic Evolution of Submarine Canyons along the California Continental Margin," in *From Shoreline to Abyss: Contributions in Marine Geology in Honor of Francis Parker Shepard*. Editor R. H. Osborne (Tulsa, OK: SEPM), 231–248. doi:10.2110/pec.91.09.0231

Greene, H. G., Maher, N. M., and Paull, C. K. (2002). Physiography of the Monterey Bay National Marine Sanctuary and Implications about Continental Margin Development. *Mar. Geol.* 181, 55–82. doi:10.1016/s0025-3227(01)00261-4

Hagen, R. A., Bergersen, D. D., Moberly, R., and Coulbourn, W. T. (1994). Morphology of a Large Meandering Submarine Canyon System on the Peru-Chile Forearc. *Mar. Geol.* 119, 7–38. doi:10.1016/0025-3227(94)90138-4

Hagen, R. A., Vergara, H., and Naar, D. F. (1996). Morphology of San Antonio Submarine Canyon on the Central Chile Forearc. *Mar. Geol.* 129, 197–205. doi:10.1016/0025-3227(96)83345-7

Han, J., Xu, G., Li, Y., and Zhuo, H. (2016). Evolutionary History and Controlling Factors of the Shelf Breaks in the Pearl River Mouth Basin, Northern South China Sea. *Mar. Pet. Geol.* 77, 179–189. doi:10.1016/j.marpetgeo.2016.06.009

Han, X., Li, J., Chu, F., Li, J., and Yang, F. (2010). "Geomorphology and Tectonic Interpretation of Zhujiang Submarine Canyon, in the Northern South China Sea," in OCEANS'10 IEEE SYDNEY, Sydney, NSW, Australia, May 24-27, 2010. doi:10.1109/OCEANSSYD.2010.5603638

Harris, P. T., Barrie, J. V., Conway, K. W., and Greene, H. G. (2014a). Hanging Canyons of Haida Gwaii, British Columbia, Canada: Fault-Control on Submarine Canyon Geomorphology along Active Continental Margins. *Deep Sea Res. Part II Top. Stud. Oceanogr.* 104, 83–92. doi:10.1016/j.dsr2.2013.06.017

Harris, P. T., Macmillan-Lawler, M., Rupp, J., and Baker, E. K. (2014b). Geomorphology of the Oceans. *Mar. Geol.* 352, 4–24. doi:10.1016/j.margeo.2014.01.011

Harris, P., and Whiteway, T. (2011). Global Distribution of Large Submarine Canyons: Geomorphic Differences between Active and Passive Continental Margins. *Mar. Geol.* 285, 69–86. doi:10.1016/j.margeo.2011.05.008

Hessler, A. M., and Fildani, A. (2019). Deep-sea Fans: Tapping into Earth's Changing Landscapes. *J. Sediment. Res.* 89 (11), 1171–1179. doi:10.2110/jsr.2019.64

Hickey, B. M. (1997). The Response of a Steep-Sided, Narrow Canyon to Time-Variable Wind Forcing. *J. Phys. Oceanogr.* 27 (5), 697–726. doi:10.1175/1520-0485(1997)027<0697:troass>2.0.co;2

Hodgson, D. M., Kane, I. A., Flint, S. S., Brunt, R. L., and Ortiz-Karpf, A. (2016). Time-transgressive Confinement on the Slope and the Progradation of Basin-Floor Fans: Implications for the Sequence Stratigraphy of Deep-Water Deposits. *J. Sediment. Res.* 86, 73–86. doi:10.2110/jsr.2016.3

Hsiung, K.-H., Kanamatsu, T., Ikehara, K., Shiraishi, K., Horng, C.-S., and Usami, K. (2017). Morpho-sedimentary Features and Sediment Dispersal Systems of the Southwest End of the Ryukyu Trench: a Source-To-Sink Approach. *Geo-Mar. Lett.* 37, 561–577. doi:10.1007/s00367-017-0509-3

Hsiung, K.-H., Yu, H.-S., and Chiang, C.-S. (2014). Seismic Characteristics, Morphology and Formation of the Ponded Fangliao Fan off Southwestern Taiwan, Northern South China Sea. *Geo-Mar. Lett.* 34, 59–74. doi:10.1007/s00367-013-0351-1

Hsiung, K.-H., Yu, H.-S., and Chiang, C.-S. (2018). The Modern Kaoping Transient Fan Offshore SW Taiwan: Morphotectonics and Development. *Geomorphology* 300, 151–163. doi:10.1016/j.geomorph.2017.10.013

Hsiung, K.-H., and Yu, H.-S. (2011). Morpho-Sedimentary Evidence for a Canyon-Channel-Trench Interconnection Along the Taiwan-Luzon Plate Margin, South China Sea. *Geo-Mar. Lett.* 31, 215–226. doi:10.1007/s00367-010-0226-7

Hsu, S.-K., Kuo, J., Lo, C.-L., Tsai, C.-H., Doo, W.-B., Ku, C.-Y., et al. (2008). Turbidity Currents, Submarine Landslides and the 2006 Pingtung Earthquake off SW Taiwan. *Terr. Atmos. Ocean. Sci.* 19 (6), 767–772. doi:10.3319/tao.2008.19.6.767(pt)

Huang, z., Nichol, S. L., Harris, P. T., and Caley, M. J. (2014). Classification of Submarine Canyons of the Australian Continental Margin. *Mar. Geol.* 357, 362–383. doi:10.1016/j.margeo.2014.07.007

Hudec, M. R., and Jackson, M. P. A. (2007). Terra Infirma: Understanding Salt Tectonics. *Earth-Sci. Rev.* 82, 1–28. doi:10.1016/j.earscirev.2007.01.001

Ingersoll, R. V. (2012). "Chapter 1: Tectonics of Sedimentary Basins, with Revised Nomenclature," in *Tectonics of Sedimentary Basin: Recent Advances*. Editors C. Busby and A. Azor (Oxford, UK: Blackwell Publishing), 3–43.

Jimoh, R. O., Tang, Y., Li, J., Awosika, L. F., Li, H., Akinnigbage, E. A., et al. (2018). The Architecture of the Lower Parts of Submarine Canyons on the Western

Nigerian Continental Margin. *Acta Oceanol. Sin.* 37 (7), 28–40. doi:10.1007/s13131-018-1242-0

Ju, Y., Wang, G., Li, S., Sun, Y., Suo, Y., Somerville, I., et al. (2020). Geodynamic Mechanism and Classification of Basins in the Earth System. *Gondwana Res.* 2020. In press. doi:10.1016/j.gr.2020.08.017

Khripounoff, A., Crassous, P., Bue, N. L., Dennielou, B., and Jacinto, R. S. (2012). Different Types of Sediment Gravity Flows Detected in the Var Submarine Canyon (Northwestern Mediterranean Sea). *Progr. Oceanogr.* 106, 138–153. doi:10.1016/j.pocean.2012.09.001

Klaus, A., and Taylor, B. (1991). Submarine Canyon Development in the Izu-Bonin Forearc: a SeaMARC II and Seismic Survey of Aoga Shima Canyon. *Mar. Geophys. Res.* 13, 131–152.

Krastel, S., Hanebuth, T. J. J., Antobreh, A. A., Henrich, R., Holz, C., Kölling, M., et al. (2004). Cap Timiris Canyon: a Newly Discovered Channel System Offshore of Mauritania. *Eos Trans. Am. Geophys. Union.* 85 (42), 417–432. doi:10.1029/2004eo420001

Krastel, S., Wefer, G., Hanebuth, T. J. J., Antobreh, A. A., Freudenthal, T., Preu, B., et al. (2011). M78/3 shipboard scientific partySediment dynamics and geohazards off Uruguay and the de la Plata River region (northern Argentina and Uruguay). *Geo-Mar. Lett.* 31, 271–283. doi:10.1007/s00367-011-0232-4

Lastras, G., Acosta, J., Muñoz, A., and Canals, M. (2011a). Submarine Canyon Formation and Evolution in the Argentine Continental Margin Between 44°30′S and 48°S. *Geomorphology* 128, 116–136. doi:10.1016/j.geomorph.2010.12.027

Lastras, G., Arzola, R. G., Masson, D. G., Wynn, R. B., Huvenne, V. A. I., Hühnerbach, V., et al. (2009). Geomorphology and Sedimentary Features in the Central Portuguese Submarine Canyons, Western Iberian Margin. *Geomorphology* 103, 310–329. doi:10.1016/j.geomorph.2008.06.013

Lastras, G., Canals, M., Amblas, D., Lavoie, C., Church, I., De mol, B., et al. (2011b). Understanding Sediment Dynamics of Two Large Submarine Valleys from Seafloor Data: Blanes and La Fonera Canyons, Northwestern Mediterranean Sea. *Mar. Geol.* 280, 20–39. doi:10.1016/j.margeo.2010.11.005

Lastras, G., Canals, M., Urgeles, R., Amblas, D., Ivanov, M., Droz, L., et al. (2007). A Walk Down the Cap de Creus Canyon, Northwestern Mediterranean Sea: Recent processes inferred from morphology and sediment bedforms. *Mar. Geol.* 246, 176–192. doi:10.1016/j.margeo.2007.09.002

Laursen, J., and Normark, W. R. (20022002). Late Quaternary Evolution of the San Antonio Submarine Canyon in the Central Chile Forearc (~33°S). *Mar. Geol.* 188, 365–390. doi:10.1016/s0025-3227(02)00421-8

Le Dantec, N., Hogarth, L. J., Driscoll, N. W., Babcock, J. M., Barnhardt, W. A., and Schwab, W. C. (2010). Tectonic Controls on Nearshore Sediment Accumulation and Submarine Canyon Morphology Offshore La Jolla, Southern California. *Mar. Geol.* 268, 115–128. doi:10.1016/j.margeo.2009.10.026

Lewis, K. B., and Barnes, P. M. (1999). Kaikoura Canyon, New Zealand: Active Conduit from Near-Shore Sediment Zones to Trench-Axis Channel. *Mar. Geol.* 162, 39–69. doi:10.1016/s0025-3227(99)00075-4

Li, M. Z., Prescott, R. H., and Robertson, A. G. (2019). Observation of Internal Tides and Sediment Transport Processes at the Head of Logan Canyon on Central Scotian Slope, Eastern Canada. *J. Mar. Syst.* 193, 103–125. doi:10.1016/j.jmarsys.2019.02.007

Li, W., Li, S., Alves, T. M., Rebesco, M., and Feng, Y. (2021). The Role of Sediment Gravity Flows on the Morphological Development of a Large Submarine Canyon (Taiwan Canyon), North-East South China Sea. *Sedimentology* 68, 1091–1108. doi:10.1111/sed.12818

Liu, J. T., Hsu, R. T., Hung, J.-J., Chang, Y.-P., Wang, Y.-H., Rendle-Bühring, R. H., et al. (2016). From the Highest to the Deepest: The Gaoping River-Gaoping Submarine Canyon Dispersal System Earth-. *Sci. Rev.* 153, 274–300. doi:10.1016/j.earscirev.2015.10.012

Liu, J. T., Kao, S.-J., Huh, C.-A., and Hung, C.-C. (2013). Gravity Flows Associated with Flood Events and Carbon Burial: Taiwan as Instructional Source Area. *Annu. Rev. Mar. Sci.* 5, 47–68. doi:10.1146/annurev-marine-121211-172307

Lo Iacono, C., Sulli, A., Agate, M., Lo Presti, V., Pepe, F., and Catalano, R. (2011). Submarine Canyon Morphologies in the Gulf of Palermo (Southern Tyrrhenian Sea) and Possible Implications for Geo-Hazard. *Mar. Geophys. Res.* 32, 127–138. doi:10.1007/s11001-011-9118-0

Lo Iacono, C., Sulli, A., and Agate, M. (2014). Submarine Canyons of North-Western Sicily (Southern Tyrrhenian Sea): Variability in Morphology, Sedimentary Processes and Evolution on a Tectonically Active Margin. *Deep Sea Res. Part II Top. Stud. Oceanogr.* 104, 93–105. doi:10.1016/j.dsr2.2013.06.018

Maier, K. L., Rosenberger, K. J., Paull, C. K., Gwiazda, R., Gales, J., Lorenson, T., et al. (2019). Sediment and Organic Carbon Transport and Deposition Driven by Internal Tides along Monterey Canyon, Offshore California. *Deep Sea Res. Part I Oceanogr. Res. Pap.* 153, 103108. doi:10.1016/j.dsr.2019.103108

Mart, Y. (1989). Sediment Distribution in Akhziv Canyon off Northern Israel. *Geo-Mar. Lett.* 9, 77–83. doi:10.1007/bf02430427

Martín, J., Palanques, A., and Puig, P. (2006). Composition and Variability of Downward Particulate Matter Fluxes in the Palamós Submarine Canyon (NW Mediterranean). *J. Mar. Syst.* 60, 75–97. doi:10.1016/j.jmarsys.2005.09.010

Matos, F. L., Ross, S. W., Huvenne, V. A. I., Davies, J. S., and Cunha, M. R. (2018). Canyons Pride and Prejudice: Exploring the Submarine Canyon Research Landscape, a History of Geographic and Thematic Bias. *Prog. Oceanogr.* 169, 6–19. doi:10.1016/j.pocean.2018.04.010

Mauffrey, M. A., Berné, S., Jouet, G., Giresse, P., and Gaudin, M. (2015). Sea-level Control on the Connection between Shelf-Edge Deltas and the Bourcart Canyon Head (Western Mediterranean) during the Last Glacial/interglacial Cycle. *Mar. Geol.* 370, 1–19. doi:10.1016/j.margeo.2015.09.010

Mazières, A., Gillet, H., Castelle, B., Mulder, T., Guyot, C., Garlan, T., et al. (2014). High-Resolution Morphobathymetric Analysis and Evolution of Capbreton Submarine Canyon Head (Southeast Bay of Biscay—French Atlantic Coast) over the Last Decade Using Descriptive and Numerical Modelling. *Mar. Geol.* 351, 1–12. doi:10.1016/j.margeo.2014.03.001

McArthur, A. D., and Tek, D. E. (2021). Controls on the Origin and Evolution of Deep-Ocean Trench-Axial Channels. *Geology* 49 (8), 883–888. doi:10.1130/G48612.1

McHargue, T., Pyrcz, M. J., Sullivan, M. D., Clark, J. D., Fildani, A., Romans, B. W., et al. (2011). Architecture of Turbidite Channel Systems on the Continental Slope: Patterns and Predictions. *Mar. Pet. Geol.* 28, 728–743. doi:10.1016/j.marpetgeo.2010.07.008

Micallef, A., Mountjoy, J. J., Barnes, P. M., Canals, M., and Lastras, G. (2014). Geomorphic Response of Submarine Canyons to Tectonic Activity: Insights from the Cook Strait Canyon System, New Zealand. *Geosphere* 10 (5), 905–929. doi:10.1130/GES01040.1

Michaud, F., Proust, J. N., Collot, J. Y., Lebrun, J. F., Witt, C., Ratzov, G., et al. (20152012). Quaternary Sedimentation and Active Faulting along the Ecuadorian Shelf: Preliminary Results of the ATACAMES Cruise. *Mar. Geophys. Res.* 36, 81–98. doi:10.1007/s11001-014-9231-y

Milia, A. (2000). The Dohrn Canyon: A Response to the Eustatic Fall and Tectonic Uplift of the Outer Shelf along the Eastern Tyrrhenian Sea Margin. *Italy. geomar. Lett.* 20, 101–108. doi:10.1007/s003670000044

Milliman, J. D., and Kao, S.-J. (2005). Hyperpycnal Discharge of Fluvial Sediment to the Ocean: Impact of Super-typhoon Herb (1996) on Taiwanese Rivers. *J. Geol.* 113, 503–516. doi:10.1086/431906

Milliman, J. D., and Syvitski, P. M. (1992). Geomorphic/Tectonic Control of Sediment Discharge to the Ocean: The Importance of Small Mountainous Rivers. *J. Geol.* 100, 525–544. doi:10.1086/629606

Mitchell, J. K., Holdgate, G. R., Wallace, M. W., and Gallagher, S. J. (2007). Marine Geology of the Quaternary Bass Canyon System, Southeast Australia: a Cool-Water Carbonate System. *Mar. Geol.* 237, 71–96. doi:10.1016/j.margeo.2006.10.037

Molenaar, A., Moernaut, J., Wiemer, G., Dubois, N., and Strasser, M. (2019). Earthquake Impact on Active Margins: Tracing Surficial Remobilization and Seismic Strengthening in a Slope Sedimentary Sequence. *Geophys. Res. Lett.* 46, 6015–6023. doi:10.1029/2019GL082350

Mondziel, S., Grindlay, N., Mann, P., Escalona, A., and Abrams, L. (2010). Morphology, Structure, and Tectonic Evolution of the Mona Canyon (Northern Mona Passage) from Multibeam Bathymetry, Side-Scan Sonar, and Seismic Reflection Profiles. *Tectonics* 29, TC2003. doi:10.1029/2008TC002441

Mountjoy, J. J., Barnes, P. M., and Pettinga, J. R. (2009). Morphostructure and Evolution of Submarine Canyons across an Active Margin: Cook Strait Sector of the Hikurangi Margin, New Zealand. *Mar. Geol.* 260, 45–68. doi:10.1016/j.margeo.2009.01.006

Mountjoy, J. J., Howarth, J. D., Orpin, A. R., Barnes, P. M., Bowden, D. A., Rowden, A. A., et al. (2018). Earthquakes Drive Large-Scale Submarine Canyon

Development and Sediment Supply to Deep-Ocean Basins. *Sci. Adv.* 4 (3), eaar3748. doi:10.1126/sciadv.aar3748

Mountjoy, J. J., Micallef, A., Stevens, C. L., and Stirling, M. W. (2014). Holocene Sedimentary Activity in a Non-terrestrially Coupled Submarine Canyon: Cook Strait Canyon System, New Zealand. *Deep Sea Res. Part II Top. Stud. Oceanogr.* 104, 120–133. doi:10.1016/j.dsr2.2013.09.001

Mulder, T., Ducassou, E., Gillet, H., Hanquiez, V., Tournadour, E., Combes, J., et al. (2012). Canyon Morphology on a Modern Carbonate Slope of the Bahamas: Evidence of Regional Tectonic Tilting. *Geology* 40 (9), 771–774. doi:10.1130/G33327.1

Mulder, T., Lecroart, P., Hanquiez, V., Marches, E., Gonthier, E., Guedes, J.-C., et al. (2006). The Western Part of the Gulf of Cadiz: Contour Currents and Turbidity Currents Interactions. *Geo-Mar. Lett.* 26 (1), 31–41. doi:10.1007/s00367-005-0013-z

Nelson, C. H., Escutia, C., Damuth, J. E., and Twichell, D. C., Jr. (2011). "Interplay of Mass-Transport and Turbidite-System Deposits in Different Active Tectonic and Passive Continental Margin Settings: External and Local Controlling Factors," in *Mass-Transport Deposits in Deepwater Settings*. Editors R. C. Shipp, P. Weimer, and H. W. Posamentier (Tulsa, OK: SEPM), 39–66. doi:10.2110/sepmsp.096.039

NOAA National Centers for Environmental Information (2021). Available at https://www.ncei.noaa.gov/maps/bathymetry/ [Accessed October 28, 2021]

Noda, A., TuZino, T., Furukawa, R., Joshima, M., and Uchida, J. (2008). Physiographical and Sedimentological Characteristics of Submarine Canyons Developed upon an Active Forearc Slope: the Kushiro Submarine Canyon, Northern Japan. *Geol. Soc. Am. Bull.* 120 (5/6), 750–767. doi:10.1130/B26155.1

Noda, A., and TuZino, T. (2010). Shelf-Slope Sedimentation during the Late Quaternary on the Southwestern Kuril Forearc Margin, Northern Japan. *Sediment. Geol.* 232, 35–51. doi:10.1016/j.sedgeo.2010.09.008

Normark, W. R., and Carlson, P. R. (2003). "Giant Submarine Canyons: Is Size Any Clue to Their Importance in the Rock Record?," in *Extreme depositional Environ. Mega end members Geol. time* Editors M. A. Chan and A. W. Archer (Boulder, CO: GSA), 175–190. doi:10.1130/0-8137-2370-1.175

Normark, W. R., Piper, D. J. W., Romans, B. W., Covault, J. A., Dartnell, P., and Sliter, R. W. (2009). "Submarine Canyon and Fan Systems of the California Continental Borderland," in *Earth Science in the Urban Ocean: The Southern California Continental Borderland*. Editors H. J. Lee and W. R. Normark (Boulder, CO: GSA), 141–168. doi:10.1130/2009.2454(2.7)

Normark, W. R., Posamentier, H., and Mutti, E. (1993). Turbidite Systems: State of the Art and Future Directions. *Rev. Geophys.* 31 (2), 91–116. doi:10.1029/93rg02832

Nyberg, B., Helland-Hansen, W., Gawthorpe, R. L., Sandbakken, P., Eide, C. H., Sømme, T., et al. (2018). Revisiting Morphological Relationships of Modern Source-To-Sink Segments as a First-Order Approach to Scale Ancient Sedimentary Systems. *Sediment. Geol.* 373, 111–133. doi:10.1016/j.sedgeo.2018.06.007

Oiwane, H., Tonai, S., Kiyokawa, S., Nakamura, Y., Suganuma, Y., and Tokuyama, H. (2011). Geomorphological Development of the Goto Submarine Canyon, Northeastern East China Sea. *Mar. Geol.* 288, 49–60. doi:10.1016/j.margeo.2011.06.013

Palanques, A., El Khatab, M., Puig, P., Masqué, P., Sánchez-Cabeza, J. A., and Isla, E. (2005). Downward Particle Fluxes in the Guadiaro Submarine Canyon Depositional System (North-western Alboran Sea), a River Flood Dominated System. *Mar. Geol.* 220, 23–40. doi:10.1016/j.margeo.2005.07.004

Palanques, A., Martín, J., Puig, P., Guillén, J., Company, J. B., and Sardá, F. (2006). Evidence of Sediment Gravity Flows Induced by Trawling in the Palamós (Fonera) Submarine Canyon (Northwestern Mediterranean). *Deep Sea Res. Part I Oceanogr. Res. Pap.* 53, 201–214. doi:10.1016/j.dsr.2005.10.003

Paull, C. K., Caress, D. W., Lundsten, E., Gwiazda, R., Anderson, K., McGann, M., et al. (2013). Anatomy of the La Jolla Submarine Canyon System; Offshore Southern California. *Mar. Geol.* 335, 16–34. doi:10.1016/j.margeo.2012.10.003

Peakall, J., and Sumner, E. J. (2015). Submarine Channel Flow Processes and Deposits: a Process-Product Perspective. *Geomorphology* 244, 95–120. doi:10.1016/j.geomorph.2015.03.005

Pierau, R., Hanebuth, T. J. J., Krastel, S., and Henrich, R. (2010). Late Quaternary Climatic Events and Sea-Level Changes Recorded by Turbidite Activity, Dakar Canyon, NW Africa. *Quat. Res.* 73, 385–392. doi:10.1016/j.yqres.2009.07.010

Pierau, R., Henrich, R., Preiß-Daimler, I., Krastel, S., and Geersen, J. (2011). Sediment Transport and Turbidite Architecture in the Submarine Dakar Canyon off Senegal, NW-Africa. *J. Afr. Earth Sci.* 60, 196–208. doi:10.1016/j.jafrearsci.2011.02.010

Pierdomenico, M., Casalbore, D., and Chiocci, F. L. (2019). Massive Benthic Litter Funnelled to Deep Sea by Flash-Flood Generated Hyperpycnal Flows. *Sci. Rep.* 9, 5530. doi:10.1038/s41598-019-41816-8

Pierdomenico, M., Martorelli, E., Dominguez-Carrío, C., Gili, J. M., and Chiocci, F. L. (2016). Seafloor Characterization and Benthic Megafaunal Distribution of an Active Submarine Canyon and Surrounding Sectors: The Case of Gioia Canyon (Southern Tyrrhenian Sea). *J. Mar. Syst.* 157, 101–117. doi:10.1016/j.jmarsys.2016.01.005

Piper, D. J. W., Hiscott, R. N., and Normark, W. R. (1999). Outcrop-scale Acoustic Facies Analysis and Latest Quaternary Development of Hueneme and Dume Submarine Fans, Offshore California. *Sedimentology* 46, 47–78. doi:10.1046/j.1365-3091.1999.00203.x

Piper, D. J. W., and Normark, W. R. (2009). Processes that Initiate Turbidity Currents and Their Influence on Turbidites: a Marine Geology Perspective. *J. Sediment. Res.* 79, 347–362. doi:10.2110/jsr.2009.046

Pisareva, M. N., Pickart, R. S., Lin, P., Fratantoni, P. S., and Weingartner, T. J. (2019). On the Nature of Wind-Forced Upwelling in Barrow Canyon. *Deep Sea Res. Part II Top. Stud. Oceanogr.* 162, 63–78. doi:10.1016/j.dsr2.2019.02.002

Popescu, I., Lericolais, G., Panin, N., Normand, A., Dinu, C., and Le Drezen, E. (2004). The Danube Submarine Canyon (Black Sea): Morphology and Sedimentary Processes. *Mar. Geol.* 206, 249–265. doi:10.1016/j.margeo.2004.03.003

Pratson, L. F., Nittrouer, C. A., Wiberg, P. L., Steckler, M. S., Swenson, J. B., Cacchione, D. A., et al. (2007). "Seascape Evolution on Clastic Continental Shelves and Slopes," in *Continental Margin Sedimentation: From Sediment Transport to Sequence Stratigraphy*. Editors C. A. Nittrouer, J. A. Austin, M. E. Field, J. H. Kravitz, J. P. M. Syvitski, and P. L. Wiberg (Oxford, UK: Blackwell Publishing), 339–380.

Puga-Bernabéu, A., Webster, J. M., Beaman, R. J., and Guilbaud, V. (2011). Morphology and Controls on the Evolution of a Mixed Carbonate–Siliciclastic Submarine Canyon System, Great Barrier Reef Margin, North-Eastern Australia. *Mar. Geol.* 289, 100–116. doi:10.1016/j.margeo.2011.09.013

Puig, P., Durán, R., Muñoz, A., Elvira, E., and Guillén, J. (2017). Submarine Canyon-Head Morphologies and Inferred Sediment Transport Processes in the Alías-Almanzora Canyon System (SW Mediterranean): on the Role of the Sediment Supply. *Mar. Geol.* 393, 21–34. doi:10.1016/j.margeo.2017.02.009

Puig, P., Palanques, A., Guillén, J., and García-Ladona. (2000). Deep Slope Currents and Suspended Particle Fluxes in and Around the Foix Submarine Canyon (NW Mediterranean). 47. *Deep Sea Res. Part I Oceanogr. Res. Pap.* 47, 343343–366366. doi:10.1016/s0967-0637(99)00062-x

Puig, P., Palanques, A., and Martín, J. (2014). Contemporary Sediment-Transport Processes in Submarine Canyons. *Annu. Rev. Mar. Sci.* 6, 53–77. doi:10.1146/annurev-marine-010213-135037

Ratzov, G., Sosson, M., Collot, J.-Y., and Migeon, S. (2012). Late Quaternary Geomorphologic Evolution of Submarine Canyons as a Marker of Active Deformation on Convergent Margins: The Example of the South Colombian Margin. *Mar. Geol.* 315–318, 77–97. doi:10.1016/j.margeo.2012.05.005

Reid, I., and Frostick, L. E. (2011). "Chapter 13: Channel Form, Flows and Sediments of Endogenous Ephemeral Rivers in Deserts," in *Arid Zone Geomorphology: Process, Form and Change in Drylands*. Editor D. S. G. Thomas (Oxford, UK: John Wiley & Sons), 301–332. doi:10.1002/9780470710777.ch13

Restrepo-Correa, I. C., and Ojeda, G. Y. (2010). Geologic Controls on the Morphology of La Aguja Submarine Canyon. *J. South. Am. Earth. Sci.* 29, 861–870. doi:10.1016/j.jsames.2010.07.001

Ridente, D., Martorelli, E., Bosman, A., and Chiocci, F. L. (2014). High-resolution Morpho-Bathymetric Imaging of the Messina Strait (Southern Italy). New Insights on the 1908 Earthquake and Tsunami. *Geomorphology* 208, 149–159. doi:10.1016/j.geomorph.2013.11.021

Rise, L., Bøe, R., Riis, F., Bellec, V. K., Laberg, J. S., Eidvin, T., et al. (2013). The Lofoten-Vesterålen Continental Margin, North Norway: Canyons and Mass-

Movement Activity. *Mar. Pet. Geol.* 45, 134–149. doi:10.1016/j.marpetgeo.2013.04.021

Rona, P., Guida, V., Scranton, M., Gong, D., Macelloni, L., Pierdomenico, M., et al. (2015). Hudson Submarine Canyon Head Offshore New York and New Jersey: A Physical and Geochemical Investigation. *Deep Sea Res. Part II Top. Stud. Oceanogr.* 121, 213–232. doi:10.1016/j.dsr2.2015.07.019

Rowan, M. G., Peel, F. J., and Vendeville, B. C. (2004). "Gravity-driven Fold Belts on Passive Margins," in *Thrust Tectonics and Hydrocarbon Systems*. Editor K. R. McClay (Tulsa, OK: AAPG), 157–182.

Salmanidou, D. M., Heidarzadeh, M., and Guillas, S. (2019). Probabilistic Landslide-Generated Tsunamis in the Indus Canyon, NW Indian Ocean, Using Statistical Emulation. *Pure Appl. Geophys.* 176, 3099–3114. doi:10.1007/s00024-019-02187-3

Sanchez, C. M., Fulthorpe, C. S., and Steel, R. J. (2012). Miocene Shelf-Edge Deltas and Their Impact on Deepwater Slope Progradation and Morphology, Northwest Shelf of Australia. *Basin Res.* 24, 683–698. doi:10.1111/j.1365-2117.2012.00545.x

Santora, J. A., Zeno, R., Dorman, J. G., and Sydeman, W. J. (2018). Submarine Canyons Represent an Essential Habitat Network for Krill Hotspots in a Large Marine Ecosystem. *Sci. Rep.* 8, 7579. doi:10.1038/s41598-018-25742-9

Sawyer, D. E., and DeVore, J. R. (2015). Elevated Shear Strength of Sediments on Active Margins: Evidence for Seismic Strengthening. *Geophys. Res. Lett.* 42, 10216–10221. doi:10.1002/2015GL066603

Schnürle, P., Liu, C.-S., Lallemand, S. E., and Reed, D. (1998). Structural Controls of the Taitung Canyon in the Huatung Basin East of Taiwan. *TAO* 9 (3), 453–472.

Shumaker, L. E., Jobe, Z. R., Johnstone, S. A., Pettinga, L. A., Cai, D. X., and Moody, J. D. (2018). Controls on Submarine Channel-Modifying Processes Identified through Morphometric Scaling Relationships. *Geosphere* 14 (5), 2171–2187. doi:10.1130/GES01674.1

Shyu, J. B. H., Sieh, K., and Chen, Y.-G. (2005). Tandem Suturing and Disarticulation of the Taiwan Orogen Revealed by its Neotectonics Elements. *Earth Planet. Sci. Lett.* 233, 167–177. doi:10.1016/j.epsl.2005.01.018

Smith, M. E., Finnegan, N. J., Mueller, E. R., and Best, R. J. (2017). Durable Terrestrial Bedrock Predicts Submarine Canyon Formation. *Geophys. Res. Lett.* 44, 10332–10340. doi:10.1002/2017GL075139

Soh, W., Tokuyama, H., Fujioka, K., Kato, S., and Taira, A. (1990). Morphology and Development of a Deep-Sea Meandering Canyon (Boso Canyon) on an Active Plate Margin, Sagami Trough, Japan. *Mar. Geol.* 91, 227–241. doi:10.1016/0025-3227(90)90038-l

Soh, W., and Tokuyama, H. (2002). Rejuvenation of Submarine Canyon Associated with Ridge Subduction, Tenryu Canyon, off Tokai, Central Japan. *Mar. Geol.* 187, 203–220. doi:10.1016/s0025-3227(02)00267-0

Sømme, T. O., Helland-Hansen, W., Martinsen, O. J., and Thurmond, J. B. (2009). Relationships between Morphological and Sedimentological Parameters in Source-to-Sink Systems: A Basis for Predicting Semi-quantitative Characteristics in Subsurface Systems. *Basin Res.* 21, 361–387. doi:10.1111/j.1365-2117.2009.00397.x

Soulet, W., Migeon, S., Gorini, C., Rubino, J.-L., Raisson, F., and Bourges, P. (2016). Erosional versus Aggradational Canyons along a Tectonically-Active Margin: the Northeastern Ligurian Margin (Western Mediterranean Sea). *Mar. Geol.* 382, 17–36. doi:10.1016/j.margeo.2016.09.015

Soutter, E. L., Bell, D., Cumberpatch, Z. A., Ferguson, R. A., Spychala, Y. T., Kane, I. A., et al. (2020). The Influence of Confining Topography Orientation on Experimental Turbidity Currents and Geological Implications. *Earth Sci.* 8, 540633.

Soutter, E. L., Kane, I. A., Hodgson, D. M., and Flint, S. (2021). The Concavity of Submarine Canyon Longitudinal Profiles. *J. Geophys. Res. Earth. Surf.* 126, e2021JF006185. doi:10.1029/2021JF006185

Stow, D. (1986). "Deep Clastic Seas," in *Sedimentary Environments and Facies*. Editor H. G. Reading (Boston, MA: Blackwell), 399–443.

Strozyk, F., Strasser, M., Förster, A., Kopf, A., and Huhn, K. (2010). Slope Failure Repetition in Active Margin Environments: Constraints from Submarine Landslides in the Hellenic Fore Arc, Eastern Mediterranean. *J. Geophys. Res. Earth.* 115, B08103. doi:10.1029/2009JB006841

Su, M., Hsiung, K.-H., Zhang, C., Xie, X., Yu, H.-S., and Wang, Z. (2015). The Linkage between Longitudinal Sediment Routing Systems and Basin Types in the Northern South China Sea in Perspective of Source-To-Sink. *J. Asian Earth Sci.* 111, 1–13. doi:10.1016/j.jseaes.2015.05.011

Su, M., Lin, Z., Wang, C., Kuang, Z., Liang, J., Chen, H., et al. (2020). Geomorphologic and Infilling Characteristics of the Slope-Confined Submarine Canyons in the Pearl River Mouth Basin, Northern South China Sea. *Mar. Geol.* 424, 106166. doi:10.1016/j.margeo.2020.106166

Susanth, S., Kurian, P. J., Bijesh, C. M., Twinkle, D., Tyagi, A., and Rajan, S. (2021). Controls on the Evolution of Submarine Canyons in Steep Continental Slopes: Geomorphological Insights from Palar Basin, Southeastern Margin of India. *Geo-Mar. Lett.* 41, 14. doi:10.1007/s00367-021-00685-9

Sweet, M. L., and Blum, M. D. (2016). Connections between Fluvial to Shallow Marine Environments and Submarine Canyons: Implications for Sediment Transfer to Deep Water. *J. Sediment. Res.* 86, 1147–1162. doi:10.2110/jsr.2016.64

Sylvester, Z., Deptuck, M., Prather, B. E., Pirmez, C., and O'Byrne, C. (2012). "Seismic Stratigraphy of a Shelf-Edge Delta and Linked Submarine Channels in the Northeastern Gulf of Mexico," in *Application of the Principles of Seismic Geomorphology to Continental Slope and Base-Of-Slope Systems: Case Studies from Seafloor and Near-Seafloor Analogues*. Editors B. E. Prather, M. E. Deptuck, D. Mohrig, B. Van Hoorn, and R. B. Wynn (Tulsa, OK:: SEPM), 31–59. doi:10.2110/pec.12.99.0031

Thornburg, T. M., Kulm, L. D., and Hussong, D. M. (1990). Submarine-fan Development in the Southern Chile Trench: A Dynamic Interplay of Tectonics and Sedimentation. *Am. Geol. Soc. Bull.* 102, 1658–1680. doi:10.1130/0016-7606(1990)102<1658:sfdits>2.3.co;2

Trumbull, J. V. A., and Garrison, L. E. (1973). Geology of a System of Submarine Canyons South of Puerto Rico. *J. Res. U.S. Geol. Surv.* 1 (3), 293–299.

Tubau, X., Lastras, G., Canals, M., Micallef, A., and Amblas, D. (2013). Significance of the Fine Drainage Pattern for Submarine Canyon Evolution: the Foix Canyon System, Northwestern Mediterranean Sea. *Geomorphology* 184, 20–37. doi:10.1016/j.geomorph.2012.11.007

Tubau, X., Paull, C. K., Lastras, G., Caress, D. W., Canals, M., Lundsten, E., et al. (2015). Submarine Canyons of Santa Monica Bay, Southern California: Variability in Morphology and Sedimentary Processes. *Mar. Geol.* 365, 61–79. doi:10.1016/j.margeo.2015.04.004

TuZino, T., and Noda, A. (2010). Architecture and Evolution of the Kushiro Submarine Canyon in the Kurile Trench Forearc Slope, North-western Pacific. *Sedimentology* 57, 611–641. doi:10.1111/j.1365-3091.2009.01107.x

Urías Espinosa, J., Bandy, W. L., Mortera Gutiérrez, C. A., Núñez Cornú, F. J., and Mitchell, N. C. (2016). Multibeam Bathymetric Survey of the Ipala Submarine Canyon, Jalisco, Mexico (20°N): The Southern Boundary of the Banderas Forearc Block? *Tectonophysics* 671, 249–263. doi:10.1016/j.tecto.2015.12.029

Valentine, P. C., Uzmann, J. R., and Cooper, R. A. (1980). Geology and Biology of Oceanographer Submarine Canyon. *Mar. Geol.* 38, 283–312. doi:10.1016/0025-3227(80)90004-3

Vardar, D. (2019). Morphological Definition of the North İmralı Canyon in the Sea of Marmara. *Arab. J. Geosci.* 12, 76. doi:10.1007/s12517-019-4257-8

von Rad, U., and Tahir, M. (1997). Late Quaternary Sedimentation on the Outer Indus Shelf and Slope (Pakistan): Evidence from High-Resolution Seismic Data and Coring. *Mar. Geol.* 138, 193–236. doi:10.1016/s0025-3227(96)00090-4

Walsh, J. P., Alexander, C. R., Gerber, T., Orpin, A. R., and Sumners, B. W. (20072007). Demise of a Submarine Canyon? Evidence for Highstand Infilling on the Waipaoa River Continental Margin, New Zealand. *Geophys. Res. Lett.* 34, L20606. doi:10.1029/2007GL031142

Wan, L., Bianchi, V., Hurter, S., Salles, T., Zhang, Z., and Yuan, X. (2021). Morphological Controls on Delta-Canyon-Fan Systems: Insights from Stratigraphic Forward Models. *Sedimentol. Early View* 2021. doi:10.1111/sed.12930

Wang, R., Colombera, L., and Mountney, N. P. (2019). Geological Controls on the Geometry of Incised-Valley Fills: Insights from a Global Dataset of Late-Quaternary Examples. *Sedimentology* 66 (6), 2134–2168. doi:10.1111/sed.12596

Warratz, G., Schwenk, T., Voigt, I., Bozzano, G., Henrich, R., Violante, R., et al. (2019). Interaction of a deep-sea current with a blind submarine canyon (Mar del Plata Canyon, Argentina). *Mar. Geol.* 417, 106002. doi:10.1016/j.margeo.2019.106002

Wiles, E., Green, A., Watkeys, M., Jokat, W., and Krocker, R. (2013). The Evolution of the Tugela Canyon and Submarine Fan: a Complex Interaction between Margin Erosion and Bottom Current Sweeping, Southwest Indian Ocean, South Africa. *Mar. Pet. Geol.* 44, 60–70. doi:10.1016/j.marpetgeo.2013.03.012

Wynn, R. B., Weaver, P. P. E., Masson, D. G., and Stow, D. A. V. (2002). Turbidite Depositional Architecture across Three Interconnected Deep-Water Basins on

the North-West African Margin. *Sedimentology* 49, 669–695. doi:10.1046/j.1365-3091.2002.00471.x

Xu, J. P., and Noble, M. A. (2009). Currents in Monterey Submarine Canyon. *J. Geophys. Res.* 114, C03004. doi:10.1029/2008JC004992

Xu, S., Wang, Y., Peng, X., Zou, H., Qiu, Y., Gong, C., et al. (2014). Origin of Taiwan Canyon and its Effects on Deepwater Sediment. *Sci. China Earth Sci.* 57 (11), 2769–2780. doi:10.1007/s11430-014-4942-0

Yang, X., Peel, F. J., McNeill, L. C., and Sanderson, D. J. (2020). Comparison of Fold-Thrust Belts Driven by Plate Convergence and Gravitational Failure. *Earth-Sci. Rev.* 203, 103136. doi:10.1016/j.earscirev.2020.103136

Yin, S., Li, J., Ding, W., Gao, J., Ding, W., and Wang, Y. (2018). Migration of the Lower North Palawan Submarine Canyon: Characteristics and Controls. *Int. Geol. Rev.* 6287-8, 988–1005. doi:10.1080/00206814.2018.1522519

Yin, S., Wang, L., Guo, Y., and Zhong, G. (2015). Morphology, Sedimentary Characteristics, and Origin of the Dongsha Submarine Canyon in the Northeastern Continental Slope of the South China Sea. *Sci. China Earth Sci.* 58, 971–985. doi:10.1007/s11430-014-5044-8

Yu, H.-S., and Chang, J.-F. (2002). The Penghu Submarine Canyon off Southwestern Taiwan: Morphology and Origin. *Terr. Atmos. Ocean. Sci.* 13 (4), 547–562. doi:10.3319/tao.2002.13.4.547(o)

Yu, H.-S., and Chiang, C.-S. (1995). Morphology and Origin of the Hongtsai Submarine Canyon West of the Hengchun Peninsula, Taiwan. *J. Geol. Soc. China.* 38 (1), 81–93.

Yu, H.-S., Liu, C. S., and Lee, J.-T. (1992). The Kaohsiung Submarine Canyon: a Modern Aborted Canyon and its Morphology and Echo Character. *Acta Ocean. Taiwan* 28, 19–30.

Yu, H.-S., and Lu, J. C. (1995). Development of the Shale Diapir-Controlled Fangliao Canyon on the Continental Slope off Southwestern Taiwan. *J. Asian Earth Sci.* 11 (4), 265–276. doi:10.1016/0743-9547(95)00004-c

Zavala, C. (2020). Hyperpycnal (Over Density) Flows and Deposits. *J. Palaeogeogr.* 9, 17. doi:10.1186/s42501-020-00065-x

Zhang, F., Hu, Y., Fan, X., Yu, W., Liu, X., and Jin, Z. (2022). Controls on Seasonal Erosion Behavior and Potential Increase in Sediment Evacuation in the Warming Tibetan Plateau. *Catena* 209, 105797. doi:10.1016/j.catena.2021.105797

Zhang, Y., Liu, Z., Zhao, Y., Colin, C., Zhang, X., Wang, M., et al. (2018). Long-term *In Situ* Observations on Typhoon-Triggered Turbidity Currents in the Deep Sea. *Geology* 46 (8), 675–678. doi:10.1130/G45178.1

Zhong, G., and Peng, X. (2021). Transport and Accumulation of Plastic Litter in Submarine Canyons – The Role of Gravity Flows. *Geology* 49, 581–586. doi:10.1130/G48536.1

Conflict of Interest: The authors declare that the research was conducted in the absence of any commercial or financial relationships that could be construed as a potential conflict of interest.

Publisher's Note: All claims expressed in this article are solely those of the authors and do not necessarily represent those of their affiliated organizations, or those of the publisher, the editors and the reviewers. Any product that may be evaluated in this article, or claim that may be made by its manufacturer, is not guaranteed or endorsed by the publisher.

Copyright © 2022 Bührig, Colombera, Patacci, Mountney and McCaffrey. This is an open-access article distributed under the terms of the Creative Commons Attribution License (CC BY). The use, distribution or reproduction in other forums is permitted, provided the original author(s) and the copyright owner(s) are credited and that the original publication in this journal is cited, in accordance with accepted academic practice. No use, distribution or reproduction is permitted which does not comply with these terms.